

**INCLUDES**  
ONLINE  
ACCESS TO FULLY  
SEARCHABLE  
TEXT AND  
IMAGES!

# MUSCULOSKELETAL IMAGING *A Teaching File*

Third Edition



**FELIX S. CHEW**  
**HYOJEONG MULCAHY**  
**ALICE S. HA**



Wolters Kluwer  
Health

Lippincott  
Williams & Wilkins





# Musculoskeletal Imaging

A Teaching File

THIRD EDITION



# Musculoskeletal Imaging

## A Teaching File

THIRD EDITION

**Felix S. Chew, M.D., ED.M., M.B.A.**

Professor of Radiology  
Vice-Chair for Academic Innovation  
Section Head of Musculoskeletal Radiology  
University of Washington, Seattle, Washington

**Hyojeong Mulcahy, M.D.**

Assistant Professor of Radiology  
University of Washington, Seattle, Washington

**Alice S. Ha, M.S., M.D.**

Assistant Professor of Radiology  
University of Washington, Seattle, Washington

*Senior Executive Editor:* Jonathan Pine  
*Product Manager:* Ryan Shaw  
*Vendor Manager:* Alicia Jackson  
*Senior Manufacturing Manager:* Benjamin Rivera  
*Senior Marketing Manager:* Caroline Foote  
*Design Coordinator:* Stephen Druding  
*Production Service:* SPi Global

Copyright © 2012 Text and Illustrations by Felix S. Chew, M.D.  
Copyright © 2012 Design and Publication Rights by LIPPINCOTT WILLIAMS & WILKINS,  
a WOLTERS KLUWER business

Two Commerce Square  
2001 Market Street  
Philadelphia, PA 19103 USA  
LWW.com

2<sup>nd</sup> edition Copyright © 2006 Design and Publication Rights by LIPPINCOTT WILLIAMS & WILKINS  
1<sup>st</sup> edition Copyright © 2000 Design and Publication Rights by LIPPINCOTT WILLIAMS & WILKINS

All rights reserved. This book is protected by copyright. No part of this book may be reproduced in any form by any means, including photocopying, or utilized by any information storage and retrieval system without written permission from the copyright owner, except for brief quotations embodied in critical articles and reviews. Materials appearing in this book prepared by individuals as part of their official duties as U.S. government employees are not covered by the above-mentioned copyright.

Printed in China

---

#### **Library of Congress Cataloging-in-Publication Data**

Chew, Felix S.

Musculoskeletal imaging : a teaching file / Felix S. Chew, Hyojeong Mulcahy, Alice S. Ha. — 3rd ed.  
p. ; cm.

Includes bibliographical references and index.

ISBN 978-1-60913-793-9

I. Mulcahy, Hyojeong. II. Ha, Alice S. III. Title.

[DNLN: 1. Musculoskeletal Diseases—radiography—Case Reports. 2. Diagnostic Imaging—Case Reports. WE 141]

LC classification not assigned

616.7'0754—dc23

2011030701

---

Care has been taken to confirm the accuracy of the information presented and to describe generally accepted practices. However, the authors, editors, and publisher are not responsible for errors or omissions or for any consequences from application of the information in this book and make no warranty, expressed or implied, with respect to the currency, completeness, or accuracy of the contents of the publication. Application of the information in a particular situation remains the professional responsibility of the practitioner.

The authors, editors, and publisher have exerted every effort to ensure that drug selection and dosage set forth in this text are in accordance with current recommendations and practice at the time of publication. However, in view of ongoing research, changes in government regulations, and the constant flow of information relating to drug therapy and drug reactions, the reader is urged to check the package insert for each drug for any change in indications and dosage and for added warnings and precautions. This is particularly important when the recommended agent is a new or infrequently employed drug.

Some drugs and medical devices presented in the publication have Food and Drug Administration (FDA) clearance for limited use in restricted research settings. It is the responsibility of the health care provider to ascertain the FDA status of each drug or device planned for use in their clinical practice.

To purchase additional copies of this book, call our customer service department at (800) 638-3030 or fax orders to (301) 223-2320. International customers should call (301) 223-2300.

Visit Lippincott Williams & Wilkins on the Internet: at LWW.com. Lippincott Williams & Wilkins customer service representatives are available from 8:30 am to 6 pm, EST.

10 9 8 7 6 5 4 3 2 1

*We dedicate this work to our families.*



Teaching Files are one of the hallmarks of education in radiology. There has long been a need for a comprehensive series of books, using the Teaching File format that would provide the kind of personal consultation with the experts normally found only in the setting of a teaching hospital. Lippincott Williams & Wilkins is proud to have created such a series; our goal is to provide residents, fellows and practicing radiologists with a useful resource that answers this need.

Actual cases have been culled from extensive teaching files in major medical centers. The discussions presented mimic those performed on a daily basis between residents and faculty members in all radiology departments.

The format of this series is designed so that each case can be studied as an unknown, if desired. A consistent format is used to present each case. A brief clinical history is given, followed by several images. Relevant findings, differential diagnosis, diagnosis, discussion of the case, figure legends and references conclude each case. In this manner, the authors guide the reader through the interpretation of each case, with a strong emphasis on critical thinking.

We hope that this series will become a valuable and trusted teaching tool for radiologists at any stage of training or practice, and that it will also be a benefit to clinicians whose patients undergo these imaging studies.

*The Publisher*

*The third time's a charm!*

The third edition of *Musculoskeletal Imaging: A Teaching File* is new and improved, updated and authoritative, and, indeed, just what you need to upgrade your skills and maintain your competence in musculoskeletal (MSK) imaging. Doctors Chew, Mulcahy, and Ha have maintained the same high-quality standards in the selection and presentation of their material in the third edition as in past editions—no small task.

Advances in MSK imaging have continued apace requiring that older, analogue film based images be removed and replaced with digital images from newly acquired cases as well as necessitating the addition of more timely cases with multidetector CT and MRI. All this has been done to good effect.

The remarkably concise format highlights the principal imaging and clinical characteristics of each case. As in previous editions, every page or two contain a separate case with images; each of the eight chapters contains up to 50 or more cases devoted to a single anatomic region of the skeleton. The cases selected cover the entire spectrum of disease encountered: arthritis, trauma, infection, tumor, metabolic, and congenital diseases. The pertinent imaging findings are discussed, a germane, realistic differential diagnosis is presented, and each case is concluded with a brief review of the pertinent pathophysiology and etiology of the disease.

Are you in need of a quick reference book in MSK imaging? Are you preparing to take the American Board of Radiology examination? Would you like to have an easy way to refresh or periodically reassess your skills in MSK imaging? Do you yearn for a simple, straightforward method of testing your competence in MSK imaging? Then this is the book for you.

Exactly how you use the book is up to you. You could simply read it cover to cover and, as a result, be infinitely more informed about MSK radiology. Or you could test yourself by reviewing the images and coming up with an answer before reading the accompanying text to determine if you noted the important findings and made the correct diagnosis. Or you could go at it until the wee hours of the morning as in cramming for the board examination. Or you could look up cases as you encounter them in your practice to substantiate your diagnoses or to make certain you include the most likely alternative diagnoses. The choice is yours.

Have at it! Read, mark, and inwardly digest! Enjoy! Regardless of your specific needs in MSK imaging, the fruits of Drs. Chew's, Mulcahy's, and Ha's labors are certain to prove both refreshing and informative.

Lee F. Rogers, M.D.  
Tucson, Arizona  
October 5, 2011

This book of teaching file cases is intended to duplicate the learning experience of sitting at the view-box with an expert skeletal radiologist and master teacher. Unlike a comprehensive textbook organized according to pathophysiology, this book is organized by anatomic regions. It provides a broad variety of cases, each intended to teach the nuances of image-based diagnostic reasoning. The cases encompass all imaging modalities, including radiography, CT, MR imaging, nuclear imaging, and sonography, as well as all categories of disease, including trauma, tumors, joint disease, endocrine and metabolic bone disease, infections, congenital and developmental conditions, and musculoskeletal manifestations of systemic disease. The cases are presented as unknowns in a consistent format. Each begins with a brief clinical history and one or more radiologic images. A description of the relevant findings, the diagnosis, and comments regarding the case follow, with emphasis on image-based diagnostic reasoning. The discussions reflect those that typically occur between radiologic consultant and clinician or between a faculty member and radiology trainee. An extensive subject index and lists of diagnoses organized by pathophysiology and anatomic region make the material accessible for use as a reference or as an atlas.

Case selection is not intended to parallel one's daily clinical experience at the workstation, nor to provide an exhaustive subject review. Rather, the cases make specific teaching points, raise clinically relevant issues, satisfy intellectual curiosity, and reflect the particular interests of the authors. By including a number of companion cases, we hope to give the reader an appreciation of the range of radiologic variety in specific diseases. Although the teaching file is organized by anatomic region, in some cases of systemic or polyostotic disease, companion images from other regions are included for convenience. Many diagnoses are represented by more than one case. Some discussions range well beyond the analysis of imaging features and differential diagnosis to include the pathophysiology underlying the images, as well as clinical and management considerations.

Felix S. Chew, M.D.  
Hyojeong Mulcahy, M.D.  
Alice S. Ha, M.D.

Preparation of the first edition of *Musculoskeletal Imaging: A Teaching File*, was begun at Massachusetts General Hospital (MGH), during the time that Susan G. Leffler, M.D., and I were members of the Division of Bone and Joint Radiology. With the help of Catherine Maldjian, M.D., who was on the faculty at Temple University at the time and subsequently at New York University Medical Center, the book was completed while I was Section Head of Musculoskeletal Radiology at Wake Forest. Contributions to the first edition were also made by Michael E. Mulligan, M.D., and Donald J. Flemming, M.D. The preponderance of the case material for the first edition was drawn from MGH, and most of the remaining material was drawn from the personal teaching collections of the authors. I acknowledge the gracious help of my former MGH colleagues, Drs. Daniel I. Rosenthal, Susan V. Kattapuram, and William E. Palmer, for providing me with or guiding me to interesting cases. Preparation of the second and third editions was completed at the University of Washington. My coauthor for the second edition was Catherine C. Roberts, M.D., of the Mayo Clinic in Scottsdale, AZ, with contributions from Anand P. Lalaji, M.D. My former colleagues at Wake Forest University, Drs. Carol A. Boles, Leon Lenchik, and Lee F. Rogers, brought many interesting cases to my attention. Some additional material was developed at the University of Washington with the help of Michael L. Richardson, M.D. I also wish to thank the many residents and fellows whose comments helped shape the final product.

Felix S. Chew, M.D.

## CONTRIBUTORS TO THE FIRST EDITION

**Felix S. Chew, M.D.**

Seattle, Washington

**Donald J. Flemming, M.D.**

Hershey, Pennsylvania

**Susan G. Leffler, M.D.**

Richmond, Virginia

**Catherine Maldjian, M.D.**

West Caldwell, New Jersey

**Michael E. Mulligan, M.D.**

Baltimore, Maryland

**Felix S. Chew, M.D.**  
Seattle, Washington

**Anand P. Lalaji, M.D.**  
Toccoa, Georgia

**Catherine C. Roberts, M.D.**  
Scottsdale, Arizona

<i>Publisher's Foreword</i>	vii
<i>Foreword</i>	viii
<i>Preface</i>	ix
<i>Acknowledgments</i>	x
<i>Contributors to the First Edition</i>	xi
<i>Contributors to the Second Edition</i>	xii
<i>Abbreviations and Acronyms</i>	xx
<i>Figure Credits</i>	xxi

## CHAPTER 1: HAND AND WRIST 1

Case 1.1	Psoriatic Arthritis	2
Case 1.2	Psoriatic Arthritis, Arthritis Mutilans Appearance	3
Case 1.3	Primary Osteoarthritis	4
Case 1.4	Erosive Osteoarthritis	5
Case 1.5	Osteomyelitis	7
Case 1.6	Tuberculous Arthritis	8
Case 1.7	Lytic Metastasis (Lung Carcinoma)	9
Case 1.8	Glomus Tumor	10
Case 1.9	Epidermoid Inclusion Cyst	11
Case 1.10	Sarcoidosis	12
Case 1.11	Burns	13
Case 1.12	Scleroderma	14
Case 1.13	Polyostotic Fibrous Dysplasia	15
Case 1.14	Enchondroma, with Fracture	16
Case 1.15	Tophaceous Gout	17
Case 1.16	Giant Cell Reparative Granuloma	18
Case 1.17	Multicentric Reticulohistiocytosis	19
Case 1.18	Systemic Lupus Erythematosus	20
Case 1.19	Rheumatoid Arthritis	21
Case 1.20	Rheumatoid Arthritis	22
Case 1.21	Rheumatoid Arthritis	23
Case 1.22	Juvenile Idiopathic Arthritis	24
Case 1.23	Thyroid Acropachy	25
Case 1.24	Acromegaly	26
Case 1.25	Hyperparathyroidism, Secondary to Renal Failure	27
Case 1.26	Polymyositis	28
Case 1.27	Embolic Disease (Caused by Neonatal Meningococcemia)	29
Case 1.28	Giant Cell Tumor of Tendon Sheath	30
Case 1.29	A2 Pulley Rupture	31
Case 1.30	Pyrophosphate Arthropathy, with Scapholunate Advanced Collapse (SLAC Wrist)	32
Case 1.31	Hemochromatosis	33
Case 1.32	Hydroxyapatite Deposition Disease (Calcific Tendinosis and Calcific Periarthritis)	34
Case 1.33	Fourth Metacarpal Fracture; Fifth CMC Volar Dislocation	35
Case 1.34	Rotary Subluxation of the Scaphoid (Scapholunate Dissociation)	36
Case 1.35	Lunate Dislocation	37
Case 1.36	Triquetral Fracture	38
Case 1.37	Ganglion Cyst	39
Case 1.38	Chronic Sclerosing Osteomyelitis	40
Case 1.39	Carpal Coalition	41
Case 1.40	Osteonecrosis of the Lunate (Kienböck Disease, Lunate Malacia)	43
Case 1.41	Ulnar Impaction Syndrome	45
Case 1.42	Osteoid Osteoma	47
Case 1.43	Healing Rickets	48
Case 1.44	Growth Plate Fracture (Salter Type I), Healing	49
Case 1.45	Lead Poisoning	50
Case 1.46	De Quervain Tenosynovitis	51
Case 1.47	Foreign Body (Wood Splinter)	52
Case 1.48	Hypertrophic Osteoarthropathy, Secondary	53
Case 1.49	Desmoplastic Fibroma	54
Case 1.50	Nonossifying Fibroma	55
Case 1.51	Congenital Syphilis	56
Case 1.52	Bilateral Madelung Deformity	57
Case 1.53	Extensor Tendon Irritation	59
Case 1.54	Galeazzi Fracture Dislocation	60

**CHAPTER 2: ELBOW, ARM, AND SHOULDER 63**

- Case 2.1 Radial Head Fracture 65
- Case 2.2 Monteggia Fracture Dislocation (Bado Type III) 66
- Case 2.3 Radioulnar Synostosis 67
- Case 2.4 Posterior Elbow Dislocation 68
- Case 2.5 Radial Head Subluxation 69
- Case 2.6 Septic Elbow Joint 70
- Case 2.7 Septic Olecranon Bursitis 71
- Case 2.8 Heterotopic Ossification after Burns 72
- Case 2.9 Supracondylar Fracture 73
- Case 2.10 Osteochondrosis of the Capitellum 74
- Case 2.11 Medial Epicondyle Avulsion Fracture (Salter Type I) 75
- Case 2.12 Posterior elbow dislocation with entrapped medial epicondyle 76
- Case 2.13 Lateral Epicondylitis 77
- Case 2.14 UCL Tear 78
- Case 2.15 Triceps Tendon Tear with Olecranon Bursa Hemorrhage 79
- Case 2.16 Occult Distal Humerus Fracture 81
- Case 2.17 Complete Biceps Tendon Rupture 83
- Case 2.18 Fibromatosis (Extra.abdominal Desmoid Tumor) 85
- Case 2.19 Juxtacortical Chondroma 87
- Case 2.20 Lung Cancer Metastasis, with Pathologic Fracture 88
- Case 2.21 Simple Bone Cyst, with Pathologic Fracture 89
- Case 2.22 Chondrosarcoma 91
- Case 2.23 Telangiectatic Osteosarcoma 92
- Case 2.24 Ewing's Sarcoma 93
- Case 2.25 Chondroblastoma 94
- Case 2.26 Acute Osteomyelitis 95
- Case 2.27 Fracture Nonunion, Surgical Neck of the Humerus 96
- Case 2.28 Osteonecrosis 97
- Case 2.29 Brachial Plexus Palsy (Erb Palsy) 98
- Case 2.30 Parsonage-Turner Syndrome 99
- Case 2.31 Quadrilateral Space Syndrome 101
- Case 2.32 Intramuscular Lipoma 102
- Case 2.33 Ganglion Cyst 103
- Case 2.34 Rotator Cuff Tear Involving Supraspinatus Tendon 105
- Case 2.35 Subscapularis Strain 106
- Case 2.36 Luxatio Erecta (Inferior Glenohumeral Dislocation) 107
- Case 2.37 Anterior (Subcoracoid) Shoulder Dislocation. The Companion Case Shows an Impaction Fracture of the Humeral Head from Previous Anterior Shoulder Dislocation (Hill-Sachs lesion) 109
- Case 2.38 Posterior Shoulder Dislocation 110
- Case 2.39 Seizure Disorder, with Recurrent Bilateral Posterior Shoulder Dislocations 111
- Case 2.40 Neuropathic Arthropathy (Charcot Joint) 112
- Case 2.41 Superior Labral Anterior to Posterior (SLAP) Tear 113
- Case 2.42 Synovial Osteochondromatosis 115
- Case 2.43 Rheumatoid Arthritis 116
- Case 2.44 Pyrophosphate Arthropathy 117
- Case 2.45 Osteolysis of the Distal Clavicle 118
- Case 2.46 Acromioclavicular Separation (Grade 2) 119
- Case 2.47 Calcific Tendinosis 121
- Case 2.48 Supraspinatus Tendon Full-Thickness Tear 122
- Case 2.49 Sternoclavicular Dislocation 123
- Case 2.50 Secondary Tumoral Calcinosis 125
- Case 2.51 Brown Tumor 127
- Case 2.52 Elastofibroma 128

**CHAPTER 3: SPINE 131**

- Case 3.1 Atlanto-Occipital Dislocation 132
- Case 3.2 Hyperflexion Sprain 133
- Case 3.3 Complex C1-C2 Fractures 135
- Case 3.4 Nonunion of Odontoid Fracture (Os Odontoideum) 137
- Case 3.5 Traumatic C2 Spondylolisthesis 139
- Case 3.6 Unilateral Facet Dislocation (Unilateral Locked Facet) 141
- Case 3.7 Klippel-Feil Syndrome 143
- Case 3.8 Hyperflexion Teardrop Fracture 145
- Case 3.9 Hyperextension Sprain at C5-C6 with Teardrop Fragment (Companion Case, Hyperextension Sprain at C2-C3 with Teardrop Fragment) 147
- Case 3.10 Ankylosing Spondylitis, with Fracture 149

Case 3.11	Osteoblastoma	150
Case 3.12	Tuberculous Spondylitis	151
Case 3.13	Rheumatoid Arthritis	153
Case 3.14	Juvenile Idiopathic Arthritis	154
Case 3.15	Bilateral Facet Dislocation (Bilateral Locked Facets)	155
Case 3.16	Morquio Syndrome	156
Case 3.17	Osteopetrosis	157
Case 3.18	Retinoid Toxicity	159
Case 3.19	Hyperflexion Fractures, Thoracic Spine	161
Case 3.20	Pyogenic Diskitis	163
Case 3.21	Tuberculous Spondylitis (Pott Disease)	165
Case 3.22	Metastatic Osteosarcoma	166
Case 3.23	Eosinophilic Granuloma	167
Case 3.24	Scheuermann Disease	168
Case 3.25	Involutional Osteoporosis	169
Case 3.26	Cushing Disease	170
Case 3.27	Sickle Cell Disease	171
Case 3.28	Ochronosis	173
Case 3.29	Congenital Scoliosis	174
Case 3.30	Osteoid Osteoma	175
Case 3.31	Ivory Vertebra from Sclerotic Prostate Metastasis	177
Case 3.32	Osteogenesis Imperfecta	178
Case 3.33	Renal Osteodystrophy with Rugger Jersey Spine	179
Case 3.34	Ivory Vertebra from Paget Disease	180
Case 3.35	Hemangioma	181
Case 3.36	L1 Flexion-Distracton Fracture (Chance Fracture)	183
Case 3.37	Ankylosing Spondylitis with Fracture Dislocation	185
Case 3.38	Hemangioma with Vertebral Collapse	187
Case 3.39	Multiple Myeloma	189
Case 3.40	Paget Disease	190
Case 3.41	Degenerative Disc Disease	191
Case 3.42	Herniated Nucleus Pulposus	193
Case 3.43	Psoriatic Spondyloarthropathy	195
Case 3.44	Coccidioidomycosis	197
Case 3.45	Bilateral L5 Spondylolysis without Anterolisthesis	199
Case 3.46	Traumatic Lumbosacral Spondylolisthesis	201
Case 3.47	Achondroplasia	202

#### CHAPTER 4: **PELVIS 205**

Case 4.1	Chordoma	206
Case 4.2	Radiation Change	207
Case 4.3	Ewing's Sarcoma	209
Case 4.4	Radiation Changes with Insufficiency Fracture	211
Case 4.5	Neurofibroma	213
Case 4.6	Lymphoma (Richter's Syndrome)	214
Case 4.7	Developmental Dysplasia of the Hip (DDH)	215
Case 4.8	Chondrosarcoma	217
Case 4.9	Osteosarcoma	219
Case 4.10	Acetabular Dysplasia	220
Case 4.11	Femoroacetabular Impingement	221
Case 4.12	Intramuscular Myxoma	222
Case 4.13	Fibrodysplasia Ossificans Progressiva	223
Case 4.14	Posterior Hip Dislocation	225
Case 4.15	Anterior Hip Dislocation	226
Case 4.16	Fluorosis	227
Case 4.17	Rickets	228
Case 4.18	Gluteus Medius Tendon Tear	229
Case 4.19	Sarcoma Arising in Paget Disease	230
Case 4.20	Reactive Arthritis	231
Case 4.21	Septic Sacroiliitis	232
Case 4.22	Synovial Osteochondromatosis	233
Case 4.23	Ankylosing Spondylitis	235
Case 4.24	Pigmented Villonodular Synovitis	237
Case 4.25	Osteoarthritis	239
Case 4.26	Rheumatoid Arthritis	240
Case 4.27	Ankylosing Spondylitis	241
Case 4.28	Juvenile Idiopathic Arthritis	242

Case 4.29	Nail-Patella Syndrome (Osteonychodysostosis, Fong's Syndrome)	243
Case 4.30	Myelofibrosis	244
Case 4.31	Hemangiomatosis	245
Case 4.32	Cystic Angiomatosis	246
Case 4.33	Multiple Hereditary Exostoses (MHE) (Osteochondromatosis)	247
Case 4.34	Plasmacytoma	248
Case 4.35	Eosinophilic Granuloma	249
Case 4.36	Insufficiency Fractures	250
Case 4.37	Diffuse Breast Carcinoma Metastases	251
Case 4.38	Tuberculosis	253
Case 4.39	Desmoplastic Fibroma	255
Case 4.40	Dislocated Total Hip Replacement	256
Case 4.41	Total Hip Replacement Failure Caused by Osteolysis	257
Case 4.42	Iliopsoas Bursitis	259
Case 4.43	Metastasis (from Lung Carcinoma)	261
Case 4.44	Abscess from Septic Hip	262
Case 4.45	Hematoma	263
Case 4.46	Sickle Cell Disease	264

## CHAPTER 5: FEMUR AND THIGH 269

Case 5.1	Rectus Femoris Strain, Grade 3	270
Case 5.2	Hamstrings Tear with Associated Hematoma	271
Case 5.3	Dialysis-Related Amyloidosis	273
Case 5.4	Osteonecrosis	274
Case 5.5	Proximal Focal Femoral Deficiency	275
Case 5.6	Osteonecrosis	276
Case 5.7	Transient Bone Marrow Edema	279
Case 5.8	Multiple Epiphyseal Dysplasia (Dysplasia Epiphysealis Multiplex)	280
Case 5.9	Fibrous Dysplasia (with Shepherd's Crook Deformity)	281
Case 5.10	Legg-Calvé-Perthes Disease	282
Case 5.11	Osteopoikilosis	283
Case 5.12	Slipped Capital Femoral Epiphysis	285
Case 5.13	Legg-Calvé-Perthes Disease	286
Case 5.14	Polymyositis	287
Case 5.15	Septic Arthritis, with Secondary Osteonecrosis of the Capital Femoral Epiphysis	289
Case 5.16	Intertrochanteric Femur Fracture	290
Case 5.17	Osteomalacia, with Looser's zones	291
Case 5.18	Stress Fracture	293
Case 5.19	Chronic Osteomyelitis	295
Case 5.20	Chronic Osteomyelitis (Tubercles Bacillus)	297
Case 5.21	Bisphosphonate-Related Fracture	298
Case 5.22	Periarticular Calcinosis (Tumoral Calcinosis, Metastatic Calcification)	299
Case 5.23	Multiple Myeloma	300
Case 5.24	Osteosarcoma with Skip Metastasis	301
Case 5.25	Eosinophilic Granuloma	303
Case 5.26	Ewing Sarcoma	304
Case 5.27	High-Grade Surface Osteosarcoma	305
Case 5.28	Chondrosarcoma	307
Case 5.29	Non-Hodgkin Lymphoma B-Cell Lymphoma, Involving Bone Secondarily	309
Case 5.30	Leukemia	310
Case 5.31	Mixed Connective Tissue Disease (Calcinosis Universalis)	311
Case 5.32	Aneurysmal Bone Cyst	313
Case 5.33	Liposclerosing Myxofibrous Tumor of Bone	315
Case 5.34	Osteoid Osteoma	317
Case 5.35	Soft Tissue Sarcoma (Malignant Fibrous Histiocytoma (MFH))	319
Case 5.36	Myositis Ossificans	320
Case 5.37	Neurofibroma	321
Case 5.38	Glomus Tumor	322
Case 5.39	Camurati-Engelmann Disease (Progressive Diaphyseal Dysplasia)	323
Case 5.40	Synovial Sarcoma	325
Case 5.41	Liposarcoma	327
Case 5.42	Erdheim-Chester Disease	328
Case 5.43	Melorheostosis	329
Case 5.44	MFH, Arising in Bone Infarct	331
Case 5.45	Klippel-Trenaunay Syndrome	333
Case 5.46	Morel-Lavallée Lesion	334

**CHAPTER 6: KNEE 337**

- Case 6.1 Articular Chondroma (Dysplasia Epiphysealis Hemimelica) 339
- Case 6.2 Giant Cell Tumor 341
- Case 6.3 Osteosarcoma, High-Grade Intramedullary Type 342
- Case 6.4 Polycythemia Vera 343
- Case 6.5 Osteosarcoma, High-Grade Intramedullary Type 345
- Case 6.6 Parosteal Osteosarcoma (Juxtacortical Osteosarcoma) 347
- Case 6.7 Osteosarcoma, Low-Grade Intramedullary Type 349
- Case 6.8 MFH of Bone 351
- Case 6.9 Primary Lymphoma of Bone 353
- Case 6.10 Non-Hodgkin Lymphoma 355
- Case 6.11 Hemophiliac Knee 357
- Case 6.12 Rickets 359
- Case 6.13 Gaucher Disease 361
- Case 6.14 Discoid Meniscus with Complex Tear 362
- Case 6.15 Sickle Cell Anemia 363
- Case 6.16 Calcified Medullary Infarcts with Subchondral Collapse of the Tibial Articular Surface 365
- Case 6.17 Radiation Changes 366
- Case 6.18 Chondromalacia Patellae 367
- Case 6.19 Rheumatoid Arthritis 368
- Case 6.20 Calcium Pyrophosphate Dihydrate (CPPD) Crystal Deposition Disease 369
- Case 6.21 PVNS, Diffuse Form 371
- Case 6.22 Juvenile Idiopathic Arthritis 373
- Case 6.23 Juvenile Idiopathic Arthritis 375
- Case 6.24 Secondary Synovial Osteochondromatosis 377
- Case 6.25 Pyrophosphate Arthropathy 378
- Case 6.26 Dermatomyositis 379
- Case 6.27 Poliomyelitis 380
- Case 6.28 Salter Type II Fracture 381
- Case 6.29 Paget Disease of the Femur, with Secondary Osteoarthritis 383
- Case 6.30 ACL Sprain, Grade 3 385
- Case 6.31 Ruptured Baker Cyst 386
- Case 6.32 Lateral Tibia Plateau Fracture 387
- Case 6.33 Medial Meniscal Tear 388
- Case 6.34 Complex Medial Meniscal Tear with Parameniscal Cyst 389
- Case 6.35 Bucket-Handle Tear, Medial Meniscus 390
- Case 6.36 Radial Tear of the Lateral Meniscus 391
- Case 6.37 Acute MCL Sprain. An ACL Sprain is Present. Not Shown But Also Present was a Tear of the Posterior Horn of the Medial Meniscus. The Companion Case is an Old MCL Sprain with Heterotopic Ossification (Pellegrini-Stieda Disease) 393
- Case 6.38 ACL Sprain, Grade 394
- Case 6.39 PCL Sprain, Grade 395
- Case 6.40 Transient Lateral Patellar Dislocation 396
- Case 6.41 SLJ Disease 397
- Case 6.42 Osteochondral Fracture (Osteochondritis Dissecans) 399
- Case 6.43 Horizontal Intercondylar Dislocation of the Patella 400
- Case 6.44 Battered Child 401
- Case 6.45 Lipoma Arborescens 403
- Case 6.46 Pes Anserinus Bursitis 405
- Case 6.47 Subchondral Insufficiency Fracture of the Knee (SIFK) 406
- Case 6.48 Total Knee Replacement with Failure of Tibial Polyethylene 407
- Case 6.49 Metallosis 409
- Case 6.50 Popliteal Artery Entrapment Syndrome 410
- Case 6.51 Arthrofibrosis 412

**CHAPTER 7: LOWER LEG 415**

- Case 7.1 Blount Disease (Tibia Vara) 416
- Case 7.2 Neurofibromatosis (Type I) 417
- Case 7.3 Osteogenesis Imperfecta 418
- Case 7.4 Osteopetrosis, Precocious Form 419
- Case 7.5 Congenital Adrenocortical Hyperplasia with Limb Lengthening 421
- Case 7.6 Physiologic Bowing 422
- Case 7.7 Achondroplasia 423
- Case 7.8 Fibrous Dysplasia 425
- Case 7.9 Mazabraud syndrome 427
- Case 7.10 Neurofibroma 428
- Case 7.11 Simple Bone Cyst 429
- Case 7.12 Osteochondroma 430

Case 7.13	Osteoblastoma 431
Case 7.14	Maisonneuve Fracture 432
Case 7.15	Nonossifying Fibroma (Fibrous Cortical Defect) 433
Case 7.16	Chondromyxoid Fibroma 435
Case 7.17	Adamantinoma 437
Case 7.18	Hemangioma, Soft Tissue 439
Case 7.19	Periosteal Osteosarcoma 441
Case 7.20	Ossifying Fibroma (Osteofibrous Dysplasia) 443
Case 7.21	Clostridia Myonecrosis (Gas Gangrene) 444
Case 7.22	Paget Disease 445
Case 7.23	Ewing Sarcoma 447
Case 7.24	Brodie Abscess 449
Case 7.25	Tuberculous Osteomyelitis 451
Case 7.26	Open Segmental Fracture 452
Case 7.27	Toddler's Fracture 453
Case 7.28	Stress Fracture 455
Case 7.29	Case 1: bilateral Tibial Stress Fractures and Stress Remodeling. Case 2: Anterior Tibial Stress Fracture with Nonunion. Case 3: Longitudinal Anterior Tibial Stress Fracture 456
Case 7.30	Rupture of the Plantaris Tendon with Adjacent Gastrocnemius Strain 457
Case 7.31	Salter Type IV Fracture 458
Case 7.32	Subacute Intramuscular Hematoma in Soleus 459
Case 7.33	Peroneal nerve ganglion cyst, with rupture 461
Case 7.34	Calcific Myonecrosis 462
Case 7.35	Cystic Lymphangiomatosis (Cystic Angiomatosis) 464
Case 7.36	Chronic Recurrent Multifocal Osteomyelitis 465
Case 7.37	Polymyositis 467
Case 7.38	Necrotizing Fasciitis with Abscess Formation and Cellulitis. The Companion Case is Also Necrotizing Fasciitis and Cellulitis, But Without Abscess Formation 469
Case 7.39	Pyomyositis with Abscess 470
Case 7.40	Hypertrophic osteoarthropathy 471
Case 7.41	Aneurysmal Bone Cyst 473
Case 7.42	Intraosseous lipoma 475
Case 7.43	Achilles Tendinosis with Partial Intrastance Tear 477
Case 7.44	Achilles Tendon Rupture 478

## CHAPTER 8: **ANKLE AND FOOT 481**

Case 8.1	PTT Longitudinal Split Tear 482
Case 8.2	Salter Type IV Fracture, Medial Malleolus 483
Case 8.3	Triplane Fracture 485
Case 8.4	Atypical Mycobacterium Osteomyelitis 487
Case 8.5	Extraskeletal Primitive Neuroectodermal Tumor (PNET) 488
Case 8.6	Accessory Soleus Muscle 489
Case 8.7	Lateral Ankle Ligament Tear 491
Case 8.8	Melorheostosis 492
Case 8.9	Hemophilic Pseudotumor 493
Case 8.10	Osteonecrosis in Sickle Cell Disease 494
Case 8.11	Marrow Infarction 495
Case 8.12	Pigmented Villonodular Synovitis (PVNS) 497
Case 8.13	Dermatomyositis 498
Case 8.14	Sinus Tarsi Syndrome 499
Case 8.15	Chondroblastoma with Secondary Aneurysmal Bone Cyst 501
Case 8.16	Osteonecrosis 502
Case 8.17	Subtalar Dislocation 503
Case 8.18	Tarsal Coalition 504
Case 8.19	Classic Clubfoot (Talipes Equinovarus) 505
Case 8.20	Congenital Vertical Talus 506
Case 8.21	Metatarsus Adductus 507
Case 8.22	Systemic Lupus Erythematosus (SLE) 508
Case 8.23	Juvenile Idiopathic Arthritis 509
Case 8.24	Intraosseous Lipoma 511
Case 8.25	Calcaneal Fatigue Fracture 513
Case 8.26	Plantar Fasciitis 514
Case 8.27	Hydroxyapatite Deposition Disease (Calcific Retrocalcaneal Bursitis) 515
Case 8.28	Plantar Fibromatosis 517
Case 8.29	Reactive arthritis 518
Case 8.30	Tophaceous Gout 519
Case 8.31	Neuropathic Osteoarthropathy 521

Case 8.32	Osteochondral Lesion of the Talus	522
Case 8.33	Mueller-Weiss syndrome	523
Case 8.34	Synovial Osteochondromatosis	525
Case 8.35	Giant Cell Tumor of the Tendon Sheath	527
Case 8.36	Lisfranc Fracture-Dislocation, Divergent Type	528
Case 8.37	Peroneus Brevis Tendon Split Tear	529
Case 8.38	Thalassemia	530
Case 8.39	Idiopathic Tumoral Calcinosis	531
Case 8.40	Metatarsal Stress Fracture	532
Case 8.41	Freiberg Infraction	533
Case 8.42	Maffucci Syndrome	535
Case 8.43	Rheumatoid Arthritis	536
Case 8.44	Multiple Enchondromatosis (Ollier Disease)	537
Case 8.45	BPOP (Nora's Lesion)	538
Case 8.46	Hallux Rigidus (Hallux Limitus)	539
Case 8.47	Bunion	541
Case 8.48	Psoriatic Arthritis (Arthritis Mutilans)	542
Case 8.49	Psoriatic Arthritis	543
Case 8.50	Subchondral Fracture	544
Case 8.51	Sesamoid Fracture	545
Case 8.52	Turf Toe (Grade I Plantar Plate Injury)	546
Case 8.53	Sarcoidosis	547

<i>Index</i>	551
--------------	-----

## ABBREVIATIONS AND ACRONYMS

ACL	anterior cruciate ligament	MDP	methylene diphosphonate
AIDS	acquired immunodeficiency syndrome	MFH	malignant fibrous histiocytoma
ANA	antinuclear antibodies	MR imaging	magnetic resonance imaging
AP	anteroposterior	MRI	magnetic resonance imaging
C1, C2, etc.	first cervical vertebra (atlas), second cervical vertebra (axis), etc.	MTP joint	metatarsophalangeal joint
CMC joint	carpometacarpal joint	ORIF	open reduction internal fixation
CPPD	calcium pyrophosphate dihydrate	PA	posteroanterior
CT	computed tomography	PCL	posterior cruciate ligament
DDH	developmental dysplasia of the hip	PD	proton density
DIP joint	distal interphalangeal joint	PIP joint	proximal interphalangeal joint
DISH	diffuse idiopathic skeletal hyperostosis	PMNs	polymorphonuclear leukocytes
DISI	dorsal intercalated segment instability (dorsi-flexion instability)	PVNS	pigmented villonodular synovitis
DPA	dual photon absorptiometry	QCT	quantitative computed tomography
DXA	dual x-ray absorptiometry	RF	rheumatoid factor
FS	fat suppression	S1, S2, etc.	first sacral vertebra, second sacral vertebra, etc.
FSE	fast spin-echo	SCFE	slipped capital femoral epiphysis
GRE	gradient-recalled echo	SI joint	sacroiliac joint
HIV	human immunodeficiency virus	SLE	systemic lupus erythematosus
HLA	human lymphocyte antigens	STIR	short tau inversion recovery
HU	Hounsfield unit (unit of x-ray attenuation on a CT scan)	T1, T2, etc.	first thoracic vertebra, second thoracic vertebra, etc.
IM	rod intramedullary rod	Tc-99m	technetium-99m
IP joint	interphalangeal joint	TFCC	triangular fibrocartilage complex
IR	inversion recovery	THA	total hip arthroplasty
K-wire	Kirschner wire	THR	total hip replacement
L1, L2, etc.	first lumbar vertebra, second lumbar vertebra, etc.	TKA	total knee arthroplasty
LCL	lateral collateral ligament	TKR	total knee replacement
MCL	medial collateral ligament	TMT joint	tarsometatarsal joint
MCP joint	metacarpophalangeal joint	VISI	volar intercalated segment instability (volar flexion instability)
		WBC	white blood cells

Figures 1–24 and 3–26 from Chew FS. Radiologic manifestations in the musculoskeletal system of miscellaneous endocrine disorders. *Radiol Clin North Am* 1991;29(1):135–147.

Figures 2–26A and 2–26B from Chew FS, Schulze ES, Mattia AR. Osteomyelitis. *AJR Am J Roentgenol* 1994; 162:942.

Figures 2–51A, 2–51B, and 2–51C from Chew FS, Huang-Hellinger F. Brown tumor. *AJR Am J Roentgenol* 1993;160:752.

Figures 3–11A and 3–11B from Chew FS, Pena CS, Keel SB. Cervical spine osteoblastoma. *AJR Am J Roentgenol* 1998;171:1244.

Figures 5–41A, 5–41B, and 5–41D from Ramsdell MG, Chew FS, Keel SB. Myxoid liposarcoma of the thigh. *AJR Am J Roentgenol* 1998;170:1242.

Figures 6–49A and 6–49C from Chew FS, Ramsdell MG, Keel SB. Metallosis after total knee replacement. *AJR Am J Roentgenol* 1998;170:1556.

Figures 7–19A, 7–19B, 7–19C, and 7–19D from Chew FS, al-Sinan AA. Periosteal osteosarcoma of the tibia. *AJR Am J Roentgenol* 1977;169:1034.



CHAPTER

1

# Hand and Wrist

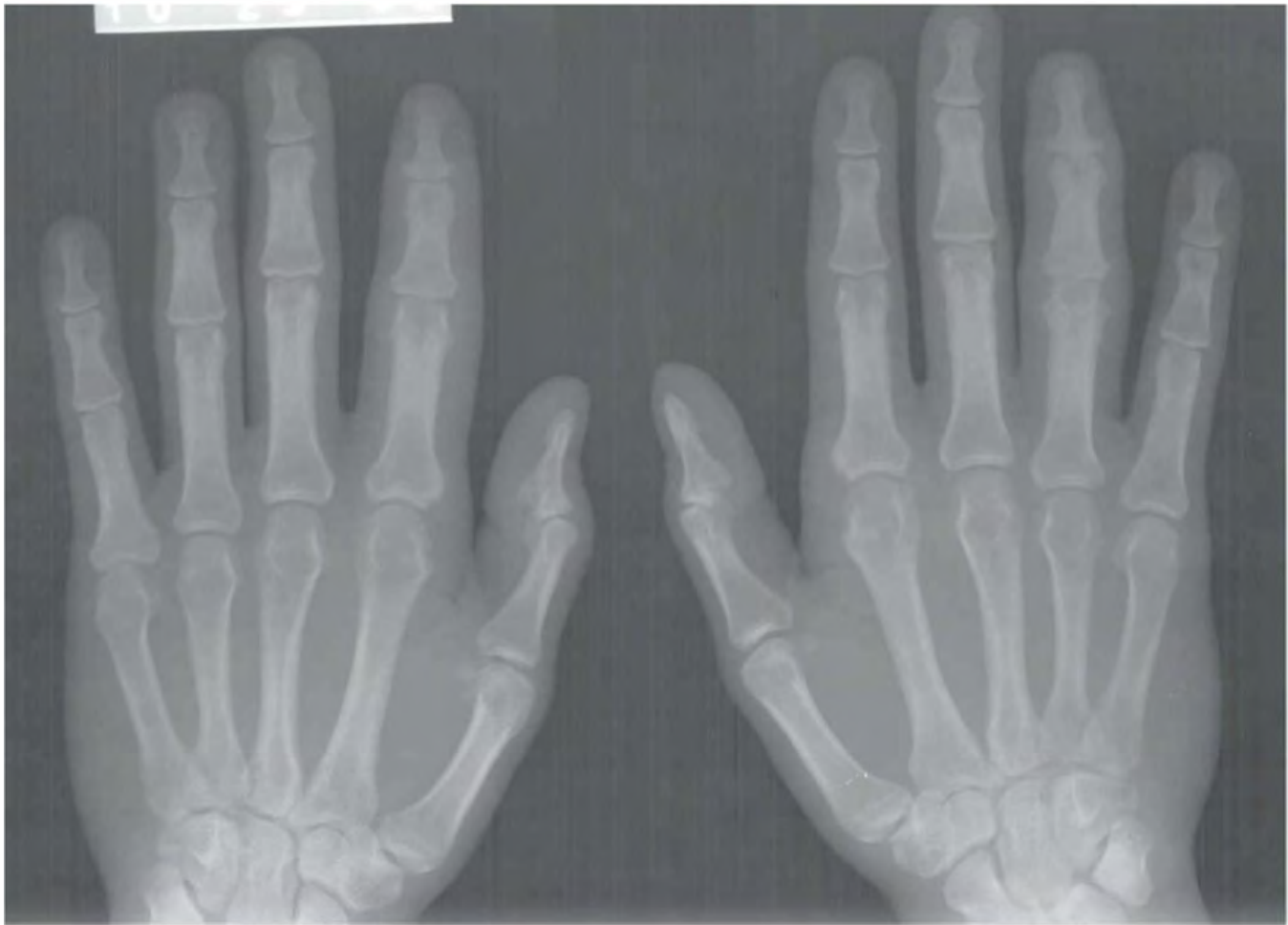


FIGURE 1.1

**FINDINGS** Posteroanterior (PA) radiographs of both hands. On the left side, sausage-digit soft tissue swelling involves the entire index finger. The other fingers are normal. There is a single erosion at the metacarpophalangeal (MCP) joint of the index finger at the radial aspect of the proximal phalanx, and fluffy periostitis is present adjacent to the proximal interphalangeal (PIP) and distal interphalangeal (DIP) joints. Overall bone mineralization is preserved, and there is no abnormality of alignment or narrowing of the cartilage spaces. On the right side, the ring finger shows sausage-digit soft tissue swelling. There are erosions at the PIP and DIP joints and periostitis.

**DIFFERENTIAL DIAGNOSIS** Psoriatic arthritis, erosive osteoarthritis, rheumatoid arthritis, gout.

**DIAGNOSIS** Psoriatic arthritis.

**DISCUSSION** Sausage-digit soft tissue swelling is characteristic of diffuse inflammation, raising the possibility of

cellulitis and underlying osteomyelitis as well as one of the seronegative spondyloarthropathies such as psoriatic arthritis. This pattern of swelling, reflecting involvement of the tendons and ligaments as well as the joint capsules, is different from the fusiform soft tissue swelling that is characteristic of effusion or synovial joint inflammation. The presence of erosions, as well as the fluffy periostitis, is pathognomonic for an inflammatory process. In this case, the periostitis is more evident when the cortex and shapes of the abnormal bones are compared with that of their normal neighbors. The distribution of involvement—a single, entire digit, with normal adjacent digits—is characteristic of psoriatic arthritis. Early changes of psoriatic arthritis may precede or follow dermatologic manifestations of psoriasis, sometimes by many years. Although many patients have relatively indolent arthritic changes, some patients may have a very aggressive, deforming, and disabling arthritis for which early, aggressive treatment is indicated [1].



FIGURE 1.2

**FINDINGS** PA radiograph of the right hand. Polyarticular arthritis is distributed through the entire hand and wrist. The DIP and PIP joints of all the fingers are severely involved, with erosions of the articular ends of the bones resulting in complete loss of cartilage and subarticular bone. Several joints have pencil-in-cup deformities. There is pancompartimental involvement of the wrist, with erosions and mature periosteal new bone. The periosteal bone is best seen at the ulnar styloid processes. The contralateral hand has a similar appearance.

**DIFFERENTIAL DIAGNOSIS** Psoriatic arthritis, erosive osteoarthritis, rheumatoid arthritis, gout.

**DIAGNOSIS** Psoriatic arthritis, arthritis mutilans appearance.

**DISCUSSION** Psoriasis is a common, genetically predisposed skin disease characterized by dry, pink, scaly, nonpruritic lesions. Psoriatic arthritis is an inflammatory arthropathy associated with psoriasis and characterized by the absence of rheumatoid factor [2]. As many as 5% of patients with psoriasis have an associated arthritis. Psoriatic arthritis has five patterns of clinical presentation:

(1) asymmetric oligoarthritis, seen in more than 50% of cases; (2) polyarthritis with predominantly DIP involvement, of which the classic presentation is seen in 5% to 19% of cases; (3) symmetric seronegative polyarthritis simulating rheumatoid arthritis, seen in up to 25% of cases; (4) sacroiliitis and spondylitis resembling ankylosing spondylitis, seen in 20% to 40% of cases; and (5) arthritis mutilans with resorption of phalanges, seen in 5% of cases. Individual patients may progress from one clinical pattern to another. The dominant radiologic features in this case—erosions and periostitis—are those of inflammatory arthritis [3]. The features of degenerative joint disease—osteophytes, subchondral sclerosis, and asymmetric joint space loss—are conspicuously absent. The preservation of normal bone mineralization mitigates against rheumatoid arthritis, in which profound osteoporosis is an invariable feature in chronic, severe disease. The greater severity of interphalangeal (IP) joint involvement, compared with carpal and MCP joint involvement, favors psoriatic arthritis over rheumatoid arthritis. The complete erosions of the articular ends of the phalanges and the involvement of the DIP joints are characteristic of the arthritis mutilans pattern of peripheral psoriatic arthritis.



FIGURE 1.3A



FIGURE 1.3B

**FINDINGS** PA (A) and lateral (B) radiographs of the left hand. Arthritic changes involve the PIP and DIP joints of the fingers and the IP, MCP, and basal joints of the thumb. These changes are characterized by bony hypertrophy, with large osteophytes and subchondral sclerosis. The cartilage spaces are narrowed asymmetrically. Mineralization of the hand is normal. Soft tissue swelling is not prominent, and there are no erosions.

**DIFFERENTIAL DIAGNOSIS** Osteoarthritis, pyrophosphate arthropathy.

**DIAGNOSIS** Primary osteoarthritis.

**DISCUSSION** The presence of hypertrophic degenerative changes at the basal joint of the thumb (first carpometacarpal joint and scaphoid-trapezium-trapezoid joints) is generally seen only in primary osteoarthritis. Involvement of the PIP and DIP joints is also characteristic. Soft

tissue swelling, juxta-articular osteoporosis, erosions, and ankylosis should be absent, unless inflammatory changes are also present. Osteoarthritis is the most common form of polyarticular arthritis. Its prevalence increases with age, so that it is nearly ubiquitous in patients older than 65. In addition to the hand, other common sites of osteoarthritis include the hip, the knee, the first metatarsophalangeal joint, and the synovial joints of the cervical and lumbar spine. The early morphologic abnormality in osteoarthritis is fibrillation of the surface of the articular cartilage, reflecting disruption of the molecular structure of the cartilage. Progressive mechanical erosion of the cartilage, thinning of the cartilage, and formation of fissures will eventually expose the subchondral bone. An adaptive response of osteophyte formation and subchondral sclerosis, combined with asymmetric cartilage space narrowing, results in the characteristic radiographic appearance [4]. In pyrophosphate arthropathy, involvement of the MCP and radial-carpal joints is more typical.



FIGURE 1.4A



FIGURE 1.4B

**FINDINGS** (A, B) PA radiographs of both hands. There is polyarticular disease with asymmetric joint space narrowing, osteophytes, and subchondral sclerosis. The predominant sites of involvement are the IP joints and the basal joints of the thumb, with sparing of the MCP and radiocarpal joints. A seagull appearance is present at the PIP joints of the middle, ring, and little fingers. Bone mineralization is normal.

**DIFFERENTIAL DIAGNOSIS** Osteoarthritis, erosive osteoarthritis, psoriatic arthritis, pyrophosphate arthropathy.

**DIAGNOSIS** Erosive osteoarthritis.

**DISCUSSION** The presence of osteophytes and subchondral sclerosis indicates a degenerative form of arthritis. The particular distribution of involvement is characteristic of osteoarthritis (IP joints, basal joint of the thumb). Although joint degeneration always has some component

of synovial inflammation because of the presence of joint debris and cartilage breakdown products, when the inflammation has erosive changes that dominate the clinical presentation, the condition may be called erosive osteoarthritis [5]. Radiographs show the degenerative features and distribution of primary osteoarthritis, but the acute synovitis causes inflammatory erosions, uniform joint space narrowing, and sometimes ankylosis. A characteristic “gull-wing” appearance may be seen on PA radiographs at the IP joints of the fingers, corresponding to central erosions and bony hypertrophy [6]. The typical patient is a postmenopausal woman (female-to-male ratio of about 12:1). The inflammation usually subsides within a few months to a couple of years, leaving the residual degenerative changes. Although psoriatic arthritis may have a similar distribution, the presence of subchondral sclerosis and osteophytes eliminates psoriatic arthritis as a diagnostic consideration.

**CLINICAL HISTORY** A 33-year-old woman with continued pain, redness, and swelling, Radiographs at presentation, after 2 months, and after 9 months.

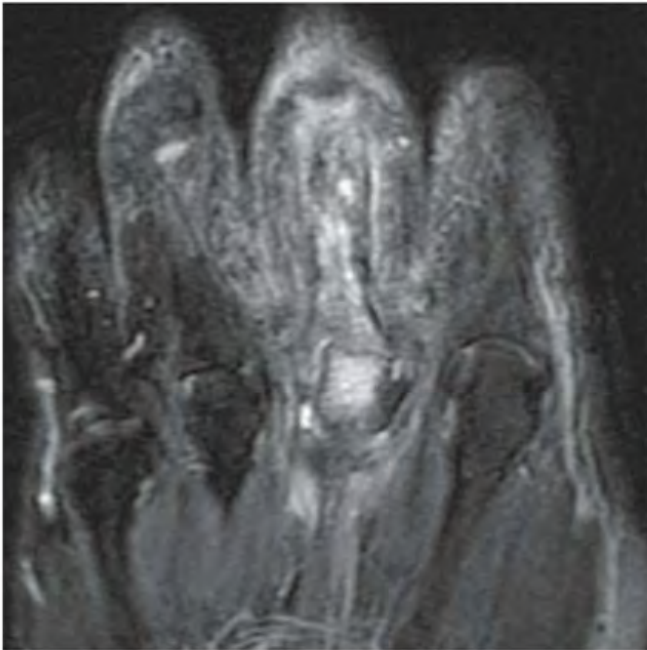


FIGURE 1.5A

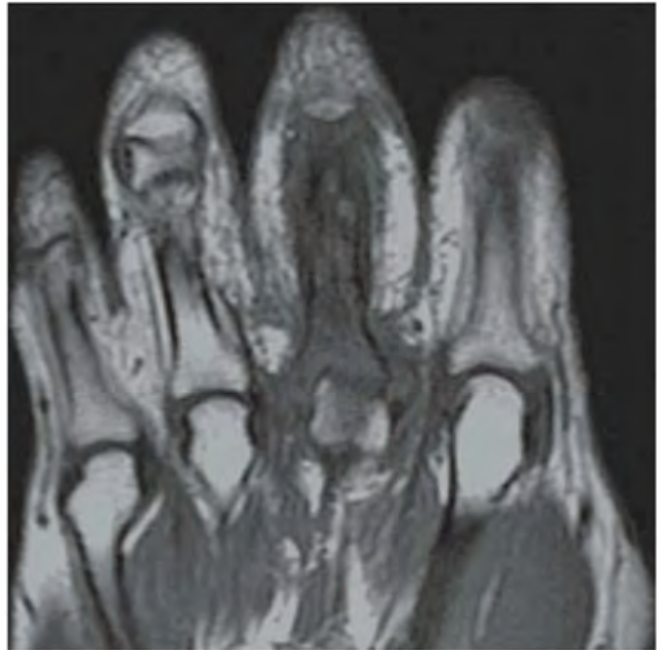


FIGURE 1.5B

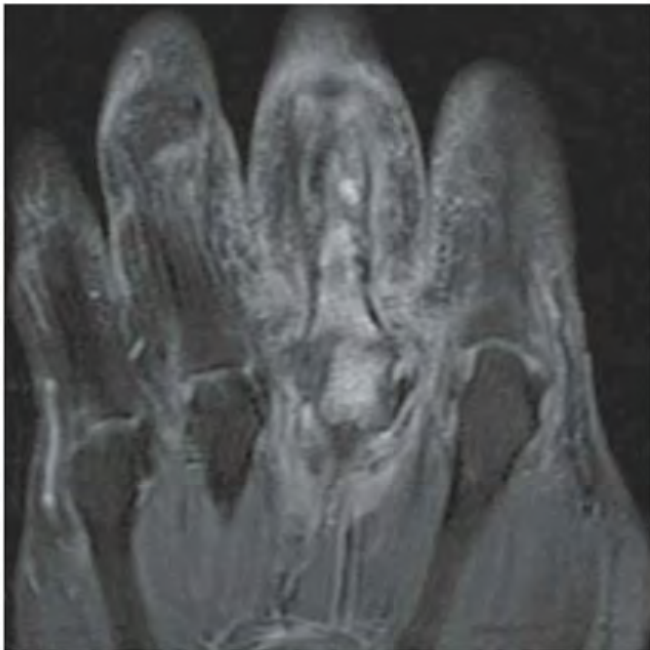


FIGURE 1.5C



FIGURE 1.5D

**FINDINGS**

- A. Coronal T2-weighted fat-suppressed MRI shows fluid signal within the proximal phalanx of the middle finger and head of the third metacarpal and surrounding soft tissue edema.
- B. Coronal T1-weighted MRI shows low marrow signal corresponding to the fluid signal demonstrated on the T2-weighted images, with irregularity of the bony contours of the proximal phalanx of the middle finger.
- C. Coronal T1-weighted fat-suppressed MRI following intravenous gadolinium injection shows enhancement of the involved bones and surrounding soft tissues.
- D. AP radiograph shows destructive and reactive changes in the proximal phalanx of the middle finger and third metacarpal head. A thin layer of periosteal bone surrounding the proximal phalanx represents involucrum; the relatively dense bone within represents sequestrum. The adjacent bones show acute osteoporosis.

**DIFFERENTIAL DIAGNOSIS** Osteomyelitis, fracture healing.

**DIAGNOSIS** Osteomyelitis.

**DISCUSSION** Infection following open fractures is a known and feared complication. The likelihood of infection depends primarily on the degree of tissue damage sustained during the trauma, the size of the open wound, the severity of contamination, and the effectiveness of treatment [7]. On MRI, one generally expects to see low signal within the affected marrow on T1-weighted images, bright signal on T2-weighted or STIR images [8], and enhancement following gadolinium [9]. Features such as involucrum, sequestrum, abscess, and draining sinus may be present. Diagnostic accuracy is greatly improved in the proper clinical setting and decreased in the presence of confounding conditions such as fracture healing [10]. In this case, the clinical setting suggests infection, and the radiographs are confirmatory.

**CLINICAL HISTORY** A 50-year-old immunocompromised man with deformed, tender, swollen thumb. Radiographs at presentation, after 2 months, and after 9 months.



FIGURE 1.6A



FIGURE 1.6B



FIGURE 1.6C

## FINDINGS

- A. Lateral radiograph demonstrates soft tissue swelling and erosion of the articular surfaces of the first MCP joint. The surfaces of the erosions have indistinct margins. Volar subluxation is present.
- B. Oblique radiograph taken 2 months after presentation demonstrates increased reactive bone at the articular erosions and metadiaphyseal periostitis.
- C. Lateral radiograph taken 9 months after initial presentation, following treatment, demonstrates smooth, amputated, well-corticated margins with resolved periostitis.

**DIFFERENTIAL DIAGNOSIS** Osteomyelitis, septic arthritis, tuberculous arthritis, psoriatic arthritis.

**DIAGNOSIS** Tuberculous arthritis.

**DISCUSSION** The images in this case document a slowly destructive arthritis of a single joint that healed without ankylosis. Tuberculous arthritis may be caused by direct extension from tuberculous osteomyelitis of initial seeding of the synovium, generally from a preexisting focus of infection of the lung. The overgrowth of granulation tissue from the synovium extends into the joint, destroying both the articular

cartilage and the subchondral bone. There is virtually no reactive bone formation. Although fibrous ankylosis may result, bony ankylosis ordinarily does not. The process may be protracted and evolve with only mild symptoms occurring over a period of months. Tuberculous arthritis is an unusual form of extrapulmonary tuberculosis, appearing in no more than 1% of patients with tuberculosis. Both *Mycobacterium tuberculosis* as well as atypical mycobacteria may be the infective agents. Often seen in association with human immunodeficiency virus (HIV) infection, patients with tuberculous arthritis who are not infected with HIV are usually adults between 30 and 60 years of age. Predisposing factors for joint involvement include joint trauma, systemic disease such as diabetes mellitus, intravenous drug abuse, intra-articular corticosteroid injection, and HIV infection. HIV specifically eliminates the tissue macrophages and CD4 lymphocytes that provide immunity against tuberculosis; therefore, it is not surprising that tuberculosis, one of the more virulent of opportunistic infections, appears fairly early in HIV disease and is becoming much more common [11]. A large proportion of patients who are infected with tuberculosis will also be seropositive for HIV, and patients with tuberculosis are more likely to have extrapulmonary involvement if they are seropositive for HIV [12].

**CLINICAL HISTORY** A 63-year-old woman with chronic cough.



FIGURE 1.7

**FINDINGS** Detail of thumb reveals mixed lytic and permeative destruction of the distal phalanx with associated soft tissue swelling. The joint space is preserved.

**DIFFERENTIAL DIAGNOSIS** Infection, trauma, squamous cell carcinoma, metastases, melanoma.

**DIAGNOSIS** Lytic metastasis (lung carcinoma).

**DISCUSSION** The radiographic appearance is that of an aggressive bone-destroying lesion. Differential diagnostic considerations might include infection, but one might expect an infection to spread into the joint space and involve the adjacent bone. Metastases to the hands and feet, particularly

the digits, are uncommon. Location in the distal phalanx of a digit, or in a subungual location, is rare [13] and is associated with a poor prognosis. Phalangeal metastases commonly display inflammatory symptoms that may mimic an acute infection [14]. They may also present as onycholysis (detachment of a nail plate from its distal and lateral attachments) [15]. The most common responsible primary sites are lung, kidney, and breast, and in 44% of patients with subungual metastases, this was the presenting symptom [16]. The most common primary malignant lesions of the distal phalanges are epidermoid carcinoma and malignant melanoma. External cortical erosions radiographically characterize primary nail bed lesions, whereas metastatic lesions tend to show extensive permeated destruction [17].

**CLINICAL HISTORY** A 28-year-old woman with slowly enlarging mass at the tip of her index finger; it is painful when she bumps it.



FIGURE 1.8A

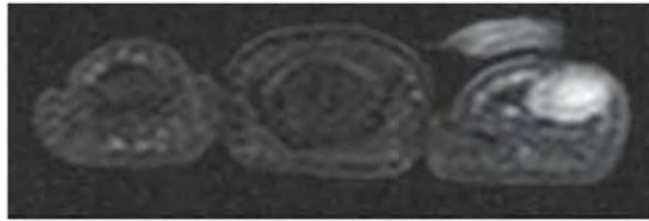


FIGURE 1.8B



FIGURE 1.8C

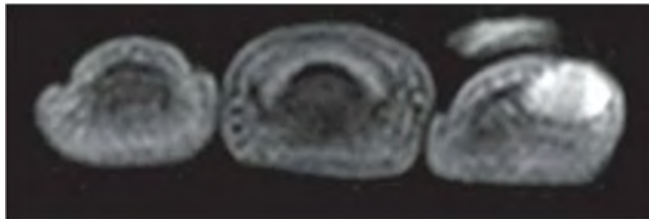


FIGURE 1.8D

## FINDINGS

- A. PA radiograph of the index finger demonstrates soft tissue fullness corresponding to the mass, with smooth erosion of the underlying phalangeal tuft.
- B. Axial STIR MRI shows a soft tissue lesion abutting and eroding the distal phalanx. The lesion has high signal.
- C. Axial T1-weighted MRI shows intermediate signal within the lesion.
- D. Axial T1-weighted fat-suppressed MRI following intravenous gadolinium shows intense enhancement throughout the lesion.

**DIFFERENTIAL DIAGNOSIS** Glomus tumor, epidermoid inclusion cyst, foreign body granuloma, periosteal chondroma, sarcoma.

**DIAGNOSIS** Glomus tumor.

**DISCUSSION** Locating the lesion in the subungual soft tissues rather than within the bone is key to approaching the

diagnosis. Although the differential diagnosis would include foreign body granuloma, epidermoid inclusion cyst, enchondroma, and sarcoidosis, the clinical presentation suggests the correct diagnosis. Glomus tumors are hamartomas that arise from the neuromyoarterial glomus, a normal, specialized vascular anastomotic complex surrounded by nerve elements [18]. Located in diverse internal organs and in the dermis and superficial subcutaneous tissues in the extremities, particularly around the fingertips, the neuromyoarterial glomus functions in the regulation of body temperature. Glomus tumors are typically small, soft tissue lesions that are highly vascular. In the fingers, most are located in the subungual region, with the remaining located in the pulp [19]. Radiographically, they produce shallow erosions in adjacent bone. Direct demonstration by magnetic resonance imaging (MRI) has been described, and multiple lesions may occur [20]. Intraosseous glomus tumors are rare. Complete surgical excision is curative.



FIGURE 1.9A



FIGURE 1.9B

**FINDINGS**

- A. PA radiograph of the finger shows a round lucent lesion in the distal phalanx with a well-defined sclerotic margin. The lesion is slightly eccentric in location.
- B. Lateral radiograph shows a subungual soft tissue mass raising the nail bed and eroding the dorsal surface of the cortex of the distal phalanx.

**DIFFERENTIAL DIAGNOSIS** Glomus tumor, epidermoid inclusion cyst, foreign body granuloma, enchondroma, sarcoidosis.

**DIAGNOSIS** Epidermoid inclusion cyst.

**DISCUSSION** Bone cysts lined with epidermis are uncommon and are found only in the skull and the distal phalanges. Epidermoid inclusion cysts are posttraumatic lesions that result from penetrating trauma in which dermoid elements

are implanted into the bone [21,22]. Growth of these elements results in a slowly enlarging cyst filled with desquamated keratin flakes, sebaceous material, and foreign-body reactive tissue and debris. Nearly all lesions involving the phalanges are reported to be in the hand. In the majority of cases, a definite history of trauma to the affected finger exists. The typical injury is a fairly severe crushing wound to the fingertip. Men are affected more frequently than women by a 2:1 ratio. The episode of trauma may have occurred decades before presentation, often when the patient was a child or young adult. Epidermoid inclusion cysts present clinically with swelling, often with associated redness and tenderness. They may occasionally be asymptomatic. The classic radiologic appearance is a clear-cut, lucent, rounded lesion with a sclerotic rim, causing destruction and expansion of the phalanx. Sometimes a retained foreign body, implanted at the time of trauma, will be visible [23]. Treatment is surgical excision or curettage; amputation is generally not required.

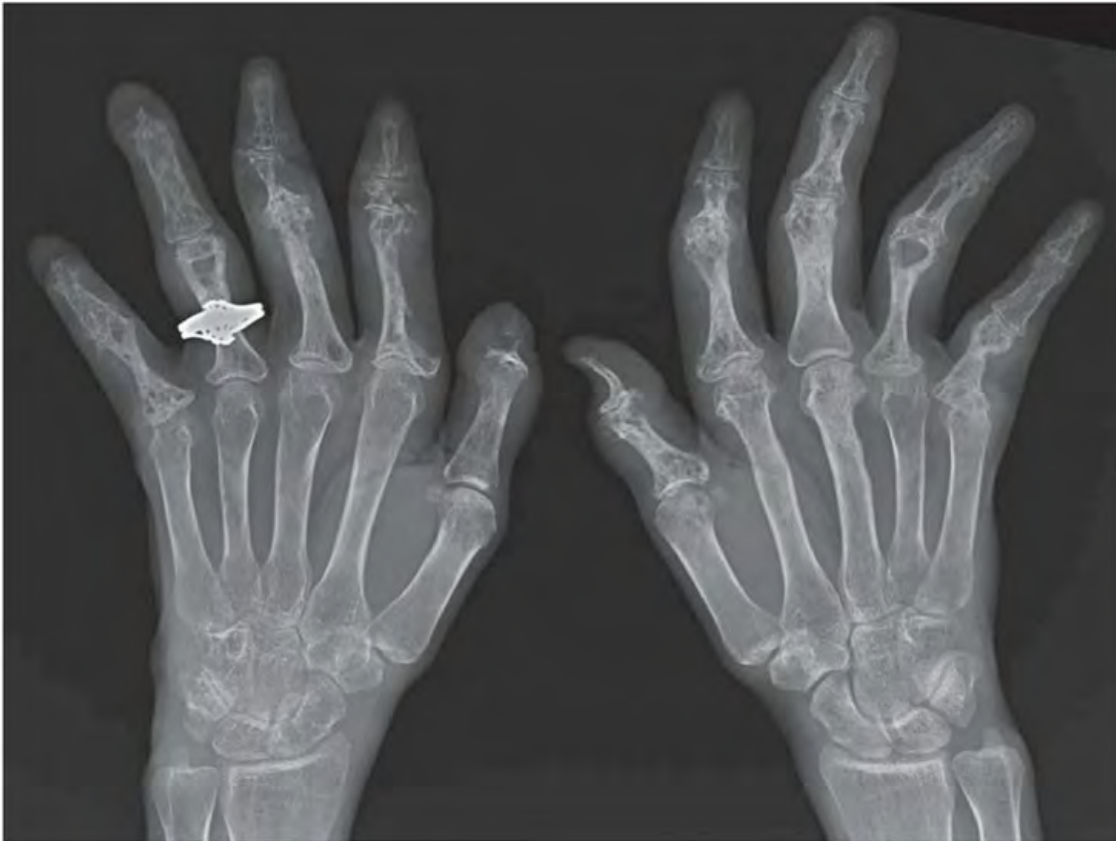


FIGURE 1.10

**FINDINGS** PA radiograph of both hands shows destructive changes involving the phalanges of all the fingers, with a lace-like appearance. The bone has remodeled, and the less involved regions (metacarpals, carpals, and distal forearm) are osteopenic. The soft tissues are not swollen.

**DIFFERENTIAL DIAGNOSIS** Sarcoidosis, hemangiomatosis, enchondromatosis, tophaceous gout.

**DIAGNOSIS** Sarcoidosis.

**DISCUSSION** Sarcoidosis may involve the joints in about 10% of cases, but sarcoidosis most often causes transient migratory polyarticular arthralgias without radiographic findings. A chronic granulomatous arthritis develops in only a few patients, leading to chronic noncaseating granulomatous inflammation of the synovium. Granulomas within or adjacent to the bone may result in punched-out cortical erosions or central lytic lesions with nonaggressive features within the medullary cavity. The process appears not to provoke reactive bone, and the remaining portions of cortex and trabeculae become reinforced and thickened. The middle and distal

phalanges of the fingers are the typical sites of involvement. The characteristic appearance caused by the presence of multiple granulomatous lesions has been described as lace-like, latticework, or honeycomb. The most common radiographic appearance in bone is lace-like or honeycomb involvement of the hands or feet. Cyst-like lesions in bone are, in fact, bone that has been replaced by solid sarcoid granulomas, and are not actually cysts. Soft tissue involvement by sarcoid may occur in one-third of patients. The hand, bone, muscle, tendon, cutaneous or subcutaneous tissue, or synovium may be involved [24,25]. The natural history of sarcoid bone lesions is variable, ranging from rare cases of recovery to gradual progression and eventual autoamputation. Treatment with systemic corticosteroids may result in improvement or stabilization of bone lesions, but bone usually does not return to normal.

Radiologic appearances consist of cyst-like lesions, a lace-like pattern, or extensive bone destruction. Asymmetric soft tissue swelling may be present. Enlargement of the fingertips may result in an appearance on physical examination described as “pseudoclubbing” and reflects phalangeal involvement [26].

**CLINICAL HISTORY** A 29-year-old woman who was in an accident 2 years ago.



FIGURE 1.11

**FINDINGS** PA radiograph of the hand shows loss of the distal portions of the fingers. The margins of the bone loss are corticated and well healed, with some dystrophic calcification at the tips of the index, middle, and ring fingers. The thumb is spared. There is no osteoporosis and there are no joint changes.

**DIFFERENTIAL DIAGNOSIS** Thermal injury (burns, frost-bite), diabetic neuroarthropathy, leprosy, scleroderma, Lesch-Nyhan disease.

**DIAGNOSIS** Burns.

**DISCUSSION** Loss of the distal portions of multiple contiguous fingers, including distal phalanges and DIP joints,

is usually from a trauma. Sparing of the thumb and normal morphology of the more proximal portions of the hand and wrist makes a systemic or vascular disease unlikely. The presence of dense bone distally would not be expected after traumatic mechanical amputation but is common following severe burns. Burns cause coagulative tissue necrosis. The depth of the injury is related to the severity and duration of the applied heat. Initially, one can see soft tissue loss and soft tissue edema. Osteoporosis and periostitis may occur in the weeks that follow. Periarticular osseous excrescences are common after extensive burns and may be seen 2 to 3 months after injury. The exact pathogenesis of these ossifications is unknown and seems not to correlate with the severity of the burn.



FIGURE 1.12A



FIGURE 1.12B

**FINDINGS** PA (A) and lateral (B) radiographs of the right hand show dense, amorphous calcium hydroxyapatite deposits in the distal portions of several digits.

**DIFFERENTIAL DIAGNOSIS** Scleroderma, mixed connective tissue disorder.

**DIAGNOSIS** Scleroderma.

**DISCUSSION** Scleroderma (progressive systemic sclerosis) is a multisystem fibrosing, autoimmune, connective tissue disease of variable clinical course. Characteristically, the skin becomes fibrotic, thickened, and taut. Gastrointestinal and renal involvement is prominent, but radiologic

manifestations in the musculoskeletal system are present in most patients. These abnormalities are usually seen in the hands and consist of soft tissue atrophy, soft tissue calcification, resorption of the phalangeal tufts, and DIP joint erosions. Osseous destruction and bony erosions are common in the phalangeal tufts. The soft tissue atrophy results in cone-shaped fingertips. Subcutaneous calcifications are typically present in multiple digits and elsewhere in the extremities. The calcium deposits are dystrophic, and consist of calcium hydroxyapatite deposits at sites of local tissue damage. Calcification may also occur in tendons and tendon sheaths, in joint capsules, and even within the joint cavity. Synovial fibrosis without inflammation may cause flexion contractures.



FIGURE 1.13A



FIGURE 1.13B

**FINDINGS** (A, B) PA radiographs of both hands show that some of the metacarpals and phalanges are mildly expanded, with thin, osteopenic cortex and no clearly defined trabecular bone pattern within. The involved metacarpals are under-tubulated, resulting in a cylindrical shape. A ground-glass radiolucency can be appreciated. The distribution of abnormalities is bilateral and polyostotic, but not symmetric. Some of the bones appear normal.

**DIFFERENTIAL DIAGNOSIS** Fibrous dysplasia, sickle cell disease, enchondromatosis, Gaucher disease.

**DIAGNOSIS** Polyostotic fibrous dysplasia.

**DISCUSSION** The mild expansion of the long bones and thinning of the cortices suggests a space-occupying process in the marrow, but the asymmetric distribution of

involvement indicates that it is a localized rather than systemic process. Fibrous dysplasia is a nonhereditary condition in which osteoblasts fail to undergo normal morphologic differentiation and maturation, resulting in lesions containing fibro-osseous tissue rather than bone. Lesions may be solitary or multiple, and one or more bones may be involved. Approximately 70% to 80% of cases are monostotic, 20% to 30% are polyostotic, and 2% to 3% are associated with endocrine dysfunction. The typical endocrine abnormality is precocious female sexual development and cutaneous pigmentation (McCune-Albright syndrome). Fibrous dysplasia weakens the structural integrity of the involved bone, predisposing it to fracture or progressive deformity. Such orthopedic complications represent the major morbidity of fibrous dysplasia. Malignant degeneration in fibrous dysplasia is extremely rare, but has been reported in the literature [27].



FIGURE 1.14A



FIGURE 1.14B



FIGURE 1.14C

**FINDINGS** (A–C) PA, oblique, and lateral radiographs of the little finger show a mildly expansile lucent lesion occupying the proximal half of the distal phalanx but not extending to the articular surface. The expanded portion of the cortex is thinned but intact. No definite internal mineralization is seen. There is a transverse fracture through the lesion. The joint is not involved.

**DIFFERENTIAL DIAGNOSIS** None.

**DIAGNOSIS** Enchondroma, with fracture.

**DISCUSSION** The lesion has benign characteristics, with a well-defined sclerotic endosteal margin and an intact, although thinned and mildly expanded, cortex. The lack of cartilaginous matrix mineralization does not exclude an enchondroma.

Solitary enchondromas are benign neoplasms, located within the medullary cavity, that are composed of mature hyaline cartilage. They probably arise from cartilaginous

rests displaced from the growth plate. The incidence in males and females is equal, and most patients are between 10 and 50 years of age. Typically, the lesions are asymptomatic and discovered incidentally, but many patients present with pathologic fractures. The most common locations for solitary enchondromas are the hands (about 50% of cases), the proximal and distal femur, and the proximal humerus. In the hands, the middle and distal portions of the metacarpals and the proximal portions of the phalanges are typically involved. Radiographically, these lesions are lucent from replacement of bone by nonmineralized cartilage, but the typical mineralization patterns of cartilaginous matrix may be present: dense punctate or flocculent calcifications, or ring-shaped or arc-shaped densities from enchondral ossification of lobular cartilage. Slow endosteal enlargement causes an expanded, thinned cortex, but cortical penetration is absent. Healing of pathologic fractures tends to be slow, because the thinned cortex overlying an enchondroma will not have a normal endosteal blood supply. The risk of developing chondrosarcoma in a solitary enchondroma of the hand is exceedingly low [28].



FIGURE 1.15

**FINDINGS** PA radiograph of the left hand demonstrates multiple punched-out erosions in the carpus and index MCP region. The erosions have sclerotic margins, and an overhanging edge may be seen at the scaphoid. Bone mineralization is normal, and there are no alignment deformities. Asymmetric joint space narrowing is seen at several IP joints, at the second MCP joint, and in the carpal and radiocarpal joints.

**DIFFERENTIAL DIAGNOSIS** Gout, xanthomatosis, psoriasis, multicentric reticulohistiocytosis, pyrophosphate arthropathy.

**DIAGNOSIS** Tophaceous gout.

**DISCUSSION** Gout is defined by the presence of hyperuricemia (serum uric acid concentration greater than 7 mg/dL). Hyperuricemia may be idiopathic or secondary to known conditions, including excess ingestion (in protein), intrinsic overproduction, or reduced renal secretion. There is a familial incidence, but it appears to be controlled by multiple genes. Specific mutations with biochemical defects in purine metabolism leading to hyperuricemia have been found in a few cases. Gout is associated with obesity, diabetes, hyperlipidemia, hypertension, atherosclerosis, alcohol consumption,

acute illness, and pregnancy. There is a negative association with rheumatoid arthritis. The prevalence of the symptomatic forms of gout, gouty arthritis, and tophaceous gout has declined dramatically with the increased use of drugs that control hyperuricemia. Gouty arthritis is similar to other crystal-related joint diseases, whereas tophaceous gout has the radiologic appearance of a metabolic deposition disease. Tophaceous gout is the most common metabolic deposition disease. Deposits of monosodium urate crystals are called tophi, and they are generally found in the periarticular soft tissues. The development of tophi requires decades of sustained hyperuricemia and is related to the degree and duration of hyperuricemia. Control of hyperuricemia by drugs has reduced the incidence of tophi in people with gout from over 50% in the 1950s to about 3% today. Deposits near the joints and tendons cause a lumpy-bumpy appearance. These localized areas of swelling may cause the slow development of pressure erosions on adjacent bone. Such erosions will have well-defined sclerotic margins. A shell of new bone may attempt to encompass the deposit, leaving an overhanging edge. The articular spaces may be preserved until late in the disease. Tophaceous gout may occur in combination with episodes of gouty arthritis.

**CLINICAL HISTORY** A 21-year-old man with hand pain after a snowboarding accident, persisting for a year.



FIGURE 1.16

**FINDINGS** PA radiograph of the hand shows an expansile lesion involving the distal third of the index metacarpal, extending into the epiphysis. The lesion is symmetrically expansile but appears contained by a thin expanded shell of bone. The periosteal bone at the interface between the lesion and the normal cortex has not matured, suggesting an actively enlarging process. No appreciable matrix mineralization is present.

**DIFFERENTIAL DIAGNOSIS** Giant cell tumor, giant cell reparative granuloma, aneurysmal bone cyst, enchondroma.

**DIAGNOSIS** Giant cell reparative granuloma.

**DISCUSSION** Giant cell reparative granuloma is a nonneoplastic lesion of bone that is said to be a reactive process (to an unknown stimulus). It is found most commonly in the jaws and in the hands and feet; giant cell tumor of bone is distinctly unusual in these sites (fewer than 1% of the Mayo Clinic series of 671 giant cell tumors [29]). Except for location, giant cell reparative granuloma is virtually indistinguishable from giant cell tumor of bone on imaging [30]. However, giant cell tumor and giant cell reparative granuloma may be distinguished from each other on histologic examination. Giant cell tumors may have a locally aggressive clinical course, whereas giant cell reparative granulomas do not.

**CLINICAL HISTORY** A 70-year-old woman with rapidly progressive pain, swelling and “red bumps” in the skin of both hands.



FIGURE 1.17A



FIGURE 1.17B

### FINDINGS

- A. PA radiograph of the hand. The soft tissues are diffusely thickened. There are erosions with overhanging edges at multiple joints, seen best at the DIP joints.
- B. Detail view of the index finger.

**DIFFERENTIAL DIAGNOSIS** Multicentric reticulohistiocytosis, erosive osteoarthritis, gout, psoriasis.

**DIAGNOSIS** Multicentric reticulohistiocytosis.

**DISCUSSION** Metabolic deposition diseases involving the joints, in which the body accumulates a substance it cannot excrete or metabolize, are relatively uncommon. If focal, mass-like deposits are located in the musculoskeletal system, the result is a clinically indolent disease with randomly distributed, slowly enlarging, space-occupying deposits. Chronic

erosions with overhanging edges are a classic feature of metabolic deposition disease. In this case, the diffuse soft tissue thickening and the absence of a lumpy-bumpy morphology mitigate against tophaceous gout, the only common form of metabolic deposition disease involving the bones and joints. In the rare condition of multicentric reticulohistiocytosis, lipid-containing macrophages are deposited randomly in the soft tissues around joints and tendons. Skin nodules are common. As with gout and other metabolic deposition diseases, normal bone density and normal joint spaces are associated with intraosseous and juxta-articular accumulations. Bone erosions with sclerotic margins and overhanging edges are typical, but sometimes a destructive, erosive arthritis ensues [31]. The origin of the abnormal lipid is unknown. Multicentric reticulohistiocytosis may be associated with the development of malignancies and has been described as a paraneoplastic syndrome [32].



FIGURE 1.18

**FINDINGS** PA radiograph of the left hand shows severe subluxations at the MCP joints, with marked ulnar deviation of the fingers. The carpometacarpal joint of the thumb is dislocated, with proximal retraction of the first metacarpal. The entire carpus is translocated toward the ulna. Boutonniere deformities involve the index and middle fingers, and flexion deformities involve the little finger. Erosions of bone are absent, and there are no hypertrophic changes of bone. Bone density is nearly normal, although perhaps slightly osteopenic.

**DIFFERENTIAL DIAGNOSIS** Systemic lupus erythematosus (SLE), scleroderma, spondyloarthropathy, rheumatoid arthritis.

**DIAGNOSIS** Systemic lupus erythematosus.

**DISCUSSION** SLE is a chronic systemic disease whose pathogenesis is related to immune complex deposition. It is more common in women by an 8:1 ratio, and there is a component of genetic susceptibility. The fluorescent antinuclear antibody

test is virtually always positive at the onset of clinical disease. Manifestations in the musculoskeletal system are common, and may antedate other systemic manifestations by months or years. Nonerosive symmetric polyarthritis with a distribution similar to that of rheumatoid arthritis is present in 75% to 90% of patients with SLE. The early findings on radiographs are fusiform soft tissue swelling and juxta-articular osteoporosis, but there should be no joint space narrowing or erosions. A deforming nonerosive arthropathy is also common in patients with SLE. The hands are typically involved at the MCP and IP joints. Thumb, wrist, and foot involvement is more common than shoulder and knee involvement. Ten percent of patients may develop atlantoaxial subluxation. These deformities are initially reducible, and radiographs may appear normal. Fixed deformities and secondary degenerative changes may develop with time. Osteonecrosis may involve the femoral head, femoral condyle, humeral head, and other sites, and it commonly has a symmetric distribution. Myositis, tendon weakening and spontaneous rupture, and soft tissue calcification are other musculoskeletal manifestations.

**CLINICAL HISTORY** A 45-year-old woman with pain and stiffness in both hands.



FIGURE 1.19

**FINDINGS** PA radiographs of both hands show mild ulnar subluxation of the second and third MCP joints on the right, and the second MCP joint on the left. Marginal erosions involving the metacarpal heads are present at these sites. Secondary degenerative changes are present at the left second MCP joint. The other joints appear relatively spared. Bone mineralization appears normal.

**DIFFERENTIAL DIAGNOSIS** Rheumatoid arthritis, ankylosing spondylitis, psoriatic arthritis, osteoarthritis.

**DIAGNOSIS** Rheumatoid arthritis.

**DISCUSSION** The distribution of disease is that of rheumatoid arthritis in the MCP joints. The marginal erosions are characteristic, and the alignment deformities are suggestive. Although the radiographic manifestations of rheumatoid arthritis are often bilateral and symmetric, bilateral and

asymmetric findings may be present early in the course, and progression may be modified by treatment.

Secondary degenerative changes, such as subchondral sclerosis, may occur if the inflammatory process remits for several years. Both rheumatoid arthritis and primary osteoarthritis are common conditions; patients with both diseases may have confusing radiographic findings. In this case, the distribution of disease is not that of osteoarthritis. The common late radiologic findings of rheumatoid arthritis include chronic generalized osteoporosis, progression of marginal erosions to severe erosions involving subchondral bone, synovial cyst formation, subluxations and abnormalities of alignment, and secondary osteoarthritis. Compressive erosions and remodeling of bone may result from the collapse of osteoporotic bone by muscle tension; this is particularly common at the MCP joints. Malalignment in advanced disease results from the loss of balanced muscular tension and ligamentous involvement by the inflammatory process.

**CLINICAL HISTORY** A 35-year-old woman with morning stiffness of her hands.



FIGURE 1.20

**FINDINGS** PA radiographs of both hands show juxta-articular osteopenia. The cartilage spaces of the carpal, MCP, and PIP joints are diffusely narrowed, and erosions are present, particularly at the MCP joints. There are no hypertrophic bony changes such as osteophytes or subchondral sclerosis.

**DIFFERENTIAL DIAGNOSIS** Rheumatoid arthritis, ankylosing spondylitis, psoriatic arthritis, osteoarthritis.

**DIAGNOSIS** Rheumatoid arthritis.

**DISCUSSION** The underlying pathologic change in rheumatoid arthritis is chronic synovial inflammation with hyperemia, edema, and effusion. Although symmetric clinical

involvement is the rule, the clinical involvement may not correlate with the sites of radiologic involvement. The earliest radiographic changes are demonstrated in this case. The earliest sites of erosions are typically at the MCP joints and are seen best on the supinated oblique “ball catcher’s” views. As the condition progresses, the radiographic features tend to become much more pronounced and differentiated from other forms of polyarticular arthritis. Rheumatoid arthritis has a prevalence of 1% in the general population; women are affected more than men by a 3:1 ratio. The clinical course is progressive in 70% of cases, with rapid or slow clinical deterioration. In 20% of cases, the disease is intermittent, with remissions and exacerbations. In 10% of cases, the remissions may last for several years.



FIGURE 1.21

**FINDINGS** PA radiographs of both hands show fusiform swelling at most of the PIP joints of both hands. Soft tissue swelling is present over the ulnar aspects of both wrists. Juxta-articular osteopenia is present. Diffuse joint space narrowing is present in the intercarpal and radiocarpal joints on both sides, and erosions and subchondral cysts are present in the right CMC, intercarpal, and radiocarpal joints.

**DIFFERENTIAL DIAGNOSIS** Rheumatoid arthritis, ankylosing spondylitis, psoriatic arthritis, osteoarthritis.

**DIAGNOSIS** Rheumatoid arthritis

**DISCUSSION** The diagnosis of an acute, symmetric, inflammatory polyarthritis can be made from these radiographs. The presence and bilaterally symmetric distribution of juxta-articular osteoporosis in the hands and wrists are indicative of hyperemia, suggesting an acute, systemic, inflammatory process. Fusiform periarticular soft tissue swelling, present around the wrists and some of the PIP joints, corresponds to synovial hypertrophy and/or joint effusion, and the diffuse joint space narrowing is typical of joints in which articular cartilage has been dissolved by enzymes released into the joint space. The lack of reactive

bone is characteristic of an inflammatory rather than a degenerative process. The presence of marginal bone erosions would absolutely clinch the diagnosis of rheumatoid arthritis, but early in the clinical course, erosions may not be evident. In this case, the diagnosis is clear without these additional features. Bilaterally symmetric clinical involvement is usual, but the severity of radiologic involvement may not necessarily be symmetric, especially when radiographs are obtained early in the clinical course. In the hand, rheumatoid arthritis classically involves the MCP and PIP joints. In the wrist, it usually involves all the carpal compartments.

Rheumatoid arthritis is a systemic autoimmune disease manifested in the musculoskeletal system by inflammatory polyarthritis of the small synovial joints. The typical age at presentation is 25 to 55 years. In 70% of cases, the onset is insidious and occurs over weeks to months; in 20% of cases, the onset occurs over days to weeks; and in 10% of cases, the onset is acute and occurs over hours to days. The acute onset mimics the onset of septic arthritis. The clinical diagnosis is based on criteria that include morning stiffness, symmetric swelling of the PIP, MCP, or wrist joints, rheumatoid nodules, serum rheumatoid factor, and the specific radiographic findings.

**CLINICAL HISTORY** A 25-year-old woman with long-standing polyarthritis.



FIGURE 1.22A



FIGURE 1.22B

**FINDINGS** (A, B) PA radiographs of both hands show diffuse epiphyseal overgrowth. The carpal bones are small and sclerotic. The remaining bones are osteopenic. The joint spaces appear generally preserved, and there are no erosions.

**DIFFERENTIAL DIAGNOSIS** Juvenile idiopathic arthritis.

**DIAGNOSIS** Juvenile idiopathic arthritis.

**DISCUSSION** The findings in this case are the stigmata of systemic polyarticular disease acquired in childhood. The diffuse, symmetric epiphyseal overgrowth of all of the long bones is indicative of a systemic disease of childhood with hyperemia. The diffuse involvement eliminates more localized processes such as infection, cancer, and hemophilia. The lack of marrow expansion makes anemias unlikely, and the lack of sclerosis and infarcts in the long bones tends to eliminate sickle cell disease. Juvenile idiopathic arthritis is a designation that includes Still disease and juvenile onset of seropositive adult-type rheumatoid arthritis, and the seronegative spondyloarthropathies. The radiologic findings in juvenile idiopathic arthritis reflect the effect of a chronic inflammatory arthritis on a growing skeleton, and generally are not specific for a particular clinical entity. The radiographic findings include soft tissue swelling, osteoporosis, periostitis, erosions, ankylosis, and growth disturbances. The

earlier the age at onset, the more severe the findings are. Not all findings are likely to be present together, but combinations of these findings should point to the diagnosis. The disease may remit in adulthood, but permanent muscle wasting, growth deformities, loss of function from ankylosis, and secondary osteoarthritis are common sequelae.

Approximately 70% of juvenile idiopathic arthritis cases are Still disease. There are three clinical presentations. Classic systemic disease is usually seen before 5 years of age and is associated with severe systemic manifestations, but mild or absent articular disease. Polyarticular disease may occur with systemic disease or may follow it. Sites of involvement are symmetric and may include the MCP and IP joints of the hand, wrist, elbow, hip, knee, ankle, foot, and cervical spine. The prognosis is generally poor. Pauciarticular or monoarticular disease is the most common form of Still disease. It has a female predominance and is associated with iridocyclitis. Monoarticular onset in a knee is the most common presentation, but the ankle, elbow, and wrist are frequent sites. Joint contractures, muscle wasting, bony ankylosis, growth deformities, epiphyseal overgrowth, and early growth plate closure may follow the articular disease. In the hand, common findings include soft tissue swelling, osteoporosis, bony ankylosis, periostitis, growth disturbances, epiphyseal compression fractures, and joint subluxation.



FIGURE 1.23A



FIGURE 1.23B

**FINDINGS** PA (A) and oblique (B) radiographs of the hand demonstrate prominent periosteal reaction along the proximal phalangeal shafts, the radial side of the first and second metacarpal shafts, and the ulnar side of the fifth metacarpal shaft. Diffuse soft tissue swelling is present.

**DIFFERENTIAL DIAGNOSIS** Hypertrophic pulmonary osteoarthropathy, familial pachydermoperiostosis, thyroid acropachy, sarcoid, venous stasis.

**DIAGNOSIS** Thyroid acropachy.

**DISCUSSION** Thyroid acropachy is a rare musculoskeletal manifestation of autoimmune thyroid disease. The characteristic

appearance is periosteal reaction along the diaphyseal regions of the hand and feet metacarpals, metatarsals, and phalanges. The periosteal reaction is classically seen on the radial side of the first through third digits and the ulnar side of the fourth and fifth digits. Diffuse soft tissue swelling and clubbing of the digits may also be present. The joints are uninvolved in this disorder, and it is typically painless. If only a single digit is involved, the appearance can mimic malignancy [33]. Thyroid acropachy is seen in approximately 1% of patients with Grave disease. In Grave disease, acropachy often, but not always, occurs along with dermatopathy and ophthalmopathy. The presence of acropachy and dermatopathy is a marker for severe ophthalmopathy [34].



FIGURE 1.24

**FINDINGS** PA radiograph of the right hand shows diffuse thickening of the soft tissues. The phalangeal tufts and the shafts of the long bones, particularly the proximal phalanges, are widened. Alignment, mineralization, and cartilage spaces are normal, but prominent hooks are present at the MCP joints.

**DIFFERENTIAL DIAGNOSIS** Osteoarthritis, acromegaly, diffuse idiopathic skeletal hyperostosis, hypervitaminosis A, fluorosis.

**DIAGNOSIS** Acromegaly.

**DISCUSSION** Clinical acromegaly is caused by excess growth hormone in adults. The underlying cause in the vast majority of cases is a pituitary adenoma that produces growth hormone autonomously; however, extrapituitary growth-hormone-secreting tumors, as well as central and peripheral tumors that secrete growth-hormone-releasing hormone also may cause acromegaly. The clinical features

of acromegaly are distinctive and include acromegalic facies, enlargement of the hands and feet, prognathism, and oily skin. Commonly associated conditions include carpal tunnel syndrome, osteoarthritis, hypertension, Raynaud's phenomenon, and diabetes mellitus. Many patients present with the signs and symptoms of a pituitary or hypothalamic mass rather than those of growth hormone excess. Definitive diagnosis is made by direct serum measurements of hormone levels. Growth hormone activates sites of bone remodeling and may increase bone formation more than bone resorption. As a consequence, the bone mass may actually be elevated, with thickened cortex and increased trabecular bone volume. Periosteal bone formation at the insertions of tendons and ligaments, and periarticular hypertrophy at the insertions of joint capsules, contribute to the increase in skeletal mass. Growth hormone increases chondrocytic activity and leads to hypertrophy of the hyaline articular cartilage. This thickened cartilage lacks the normal biomechanical characteristics of articular cartilage and is vulnerable to fissuring, ulceration, denudation, and, ultimately, degenerative changes.



FIGURE 1.25

**FINDINGS** PA radiographs of both hands show advanced subperiosteal bone resorption along the radial and ulnar aspects of all of the phalanges. Advanced resorptive changes involve all of the distal phalanges, with consequent shortening of the bones and clubbing of the soft tissues. There are no alignment deformities. The joint spaces are preserved. Diffuse osteopenia is present. There are no soft tissue calcifications.

**DIFFERENTIAL DIAGNOSIS** Hyperparathyroidism, osteoporosis, rheumatoid arthritis.

**DIAGNOSIS** Hyperparathyroidism, secondary to renal failure.

**DISCUSSION** Hyperparathyroidism stimulates osteoclastic resorption of bone. The excess parathyroid hormone can be a result of primary or secondary hyperparathyroidism.

Secondary hyperparathyroidism is a response to sustained hypocalcemia that is typically caused by chronic renal failure, as in this case, or gastrointestinal malabsorption. Radiographic changes, including bone resorption, brown tumors, bone sclerosis, and chondrocalcinosis, are seen best in the hands. Bone resorption occurs at all surfaces, including subperiosteal, intracortical (along haversian systems), endosteal, trabecular, subchondral, and subligamentous locations. Subperiosteal bone resorption is virtually diagnostic of hyperparathyroidism. It is seen best and most frequently along the radial aspect of the phalanges of the hands, especially the middle phalanges of the index and middle fingers. Subperiosteal bone resorption may also be evident at the phalangeal tufts. Vascular and soft tissue calcification is common in secondary hyperparathyroidism.



FIGURE 1.26A



FIGURE 1.26B

**FINDINGS** (A, B) Lateral and PA radiographs of the right hand demonstrate severe flexion deformity of the index finger, with conglomerate soft tissue calcifications and erosions at the MCP joint. The bones are osteoporotic.

**DIFFERENTIAL DIAGNOSIS** Polymyositis, dermatomyositis, scleroderma, calcific tendinitis.

**DIAGNOSIS** Polymyositis.

**DISCUSSION** Polymyositis is a disorder of unknown cause characterized by inflammation and degeneration of muscle [35]. In the most common clinical form of polymyositis, gradually increasing proximal limb weakness, and a later effect on the laryngeal and pharyngeal muscles, may be accompanied by joint manifestations in 20% to 50% of

patients. These joint manifestations include arthralgias and arthritis [36,37], and the clinical and radiographic appearance may be confused with SLE and rheumatoid arthritis. In this particular case, the presence of soft tissue calcification rules out SLE and rheumatoid arthritis as diagnostic possibilities, and suggests scleroderma or related connective tissue diseases, including dermatomyositis or polymyositis. Hydroxyapatite crystal deposition disease (calcific tendinitis) is eliminated by the specific location and distribution of the calcifications—they are not in the expected location of tendons. Calcification in scleroderma and polymyositis may not be distinguishable from each other, but the flexion deformity, MCP erosion, and osteoporosis would be unusual in scleroderma. Moreover, the soft tissue resorptive changes and skin-tightening characteristic of scleroderma are absent.



FIGURE 1.27

**FINDINGS** PA radiograph of both hands shows asymmetric absence of the distal portions of the fingers and thumb. The distal bones are smooth. Both wrists have cone-shaped epiphyses and consequent deformities of the distal radioulnar joints. The radius is short relative to the ulna on the left, and the distal right ulna has a tethered physis on the radial side, leading to a slant-like deformity.

**DIFFERENTIAL DIAGNOSIS** Trauma, burns, frostbite, embolic disease, infection, Lesch-Nyhan syndrome, congenital indifference to pain, child abuse, Munchausen disease by proxy.

**DIAGNOSIS** Embolic disease (caused by neonatal meningococcemia).

**DISCUSSION** Loss of fingers is most often the result of mechanical or thermal trauma, and the trauma may be accidental or

intentional. In this case, however, the presence of coned epiphyses cannot be accounted for by trauma. A coned epiphysis can be the result of premature closure of the central portion of the physis, following which the peripheral portions of the physis continue to grow. As a result, the metaphysis lengthens around the tethered portion of the epiphysis, and the epiphysis develops into a cone shape. The situation may also be called a cupped metaphysis. This impairment to longitudinal growth also leads to a relative shortening of the affected bone. Because the growth impairment is central, there is no angular deformity. Both loss of fingertips and coned epiphyses may result from vascular infarcts caused by embolic disease [38,39]. Premature closure of the peripheral portion of a growth plate will lead to tethering and asymmetric longitudinal growth. Disseminated intravascular coagulopathy is one complication of neonatal meningococcemia. These long-term sequelae of meningococcemia do not reflect sites of actual infection.

**CLINICAL HISTORY** A 42-year-old man with slowly enlarging thumb mass.

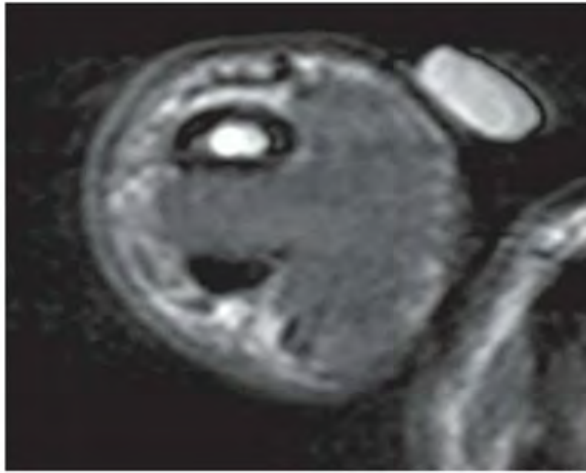


FIGURE 1.28A

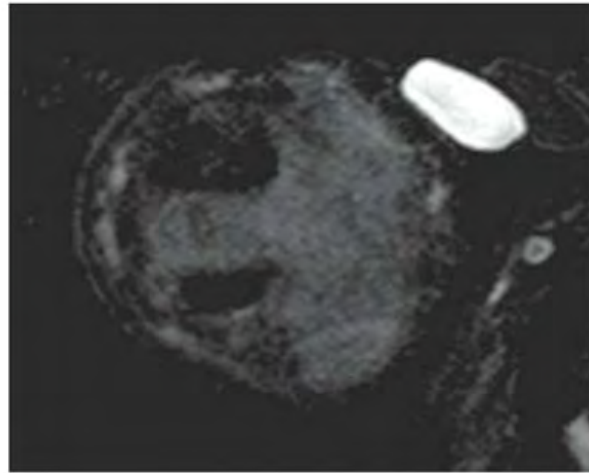


FIGURE 1.28B

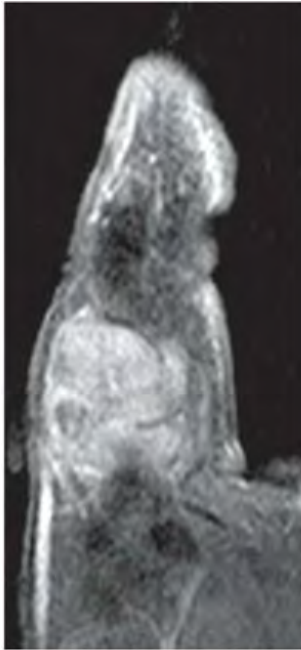


FIGURE 1.28C



FIGURE 1.28D



FIGURE 1.28E

## FINDINGS

- A. Axial T1-weighted MRI of the thumb shows a mass of intermediate signal interposed between the shaft of the proximal phalanx and the flexor tendons, extending into the medial soft tissues like a mushroom.
- B. Axial STIR MRI shows intermediate signal within the mass. There is no edema in the adjacent bone or fluid in the tendon sheath.
- C-E. Sagittal T1-weighted fat-suppressed MRI following intravenous gadolinium (medial to lateral) shows enhancement throughout the lesion.

**DIFFERENTIAL DIAGNOSIS** Giant cell tumor of tendon sheath, soft tissue sarcoma, nerve sheath tumor.

**DIAGNOSIS** Giant cell tumor of tendon sheath.

**DISCUSSION** Localized giant cell tumor of tendon sheath is the most common solid tumor in the hands [40]. Giant cell tumor of tendon sheath is a benign synovial proliferative disorder, histologically indistinguishable from PVNS, that typically presents as a slowly growing mass in an adult. On MRI, it is easily distinguished from ganglion cysts by the absence of fluid. The MRI features are otherwise nonspecific for a solid tumor, with intermediate signal on T1-weighted images, intermediate signal on T2-weighted images, and moderate-to-intense enhancement following gadolinium infusion [41]. Most of these lesions involve the volar aspect of the hand and are intimately associated with the tendon. Pressure erosions of the adjacent bone are found occasionally.



FIGURE 1.29A

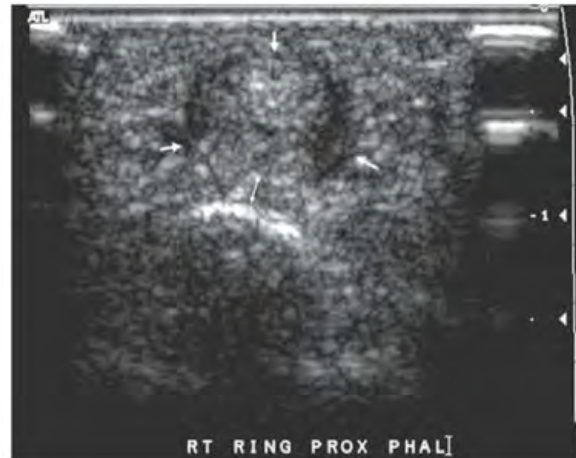


FIGURE 1.29B



FIGURE 1.29C

**FINDINGS** (A) Longitudinal and (B) transverse volar sonograms of the ring finger at the proximal phalanx show intact but slightly thickened flexor tendons (*arrows*). Along the proximal phalanx, however, the flexor tendons are displaced from the surface of the bone by approximately 5 mm (*double headed arrows*), consistent with bowstringing of the flexor tendons. This appearance is indicative of rupture of the A2 pulley. (C) Sagittal STIR MR image of the right ring finger shows the flexor tendons (*arrows*) separated from the underlying proximal phalanx (*double-headed arrow*).

**DIFFERENTIAL DIAGNOSIS** None.

**DIAGNOSIS** A2 pulley rupture.

**DISCUSSION** The pulley system of the fingers refers to a ligamentous tunnel that stabilizes the flexor tendons in close apposition to the volar surface of the fingers during flexion [w]. Several ligaments form this system, including five annular pulleys (A1–A5) and three cruciform pulleys

(C1–C3). The A2 and A4 annular pulleys, located along the shafts of the proximal and middle phalanges, respectively, are the longest and the most functionally important of the annular pulleys. Pulley disruption may result in radial displacement or volar bowstringing of the flexor tendons, with pain and loss of strength [42]. During sport climbing, the pulley system is exposed to high grip-specific loads. Pulley ruptures related to climbing are most commonly seen in the ring and middle fingers. Sonography may be used to identify the normal annular pulleys as very thin (thickness 0.3 to 0.5 mm) anisotropic bands covering the flexor tendons. On transverse planes, the superficial portion of the pulleys has a hyperechoic, fibrillar appearance related to the perpendicular incidence of the US beam, whereas its lateral portions are hypoechoic as a result of anisotropy. Dynamic scanning during flexion and extension movements of the fingers can help to distinguish the fixed pulleys from the underlying gliding tendons. The sonographic diagnosis of a pulley tear is based on demonstration of subluxation of the flexor tendons that, instead of coursing along the concavity of the phalanges, lie at a variable distance from the bone. Establishing which pulley is the ruptured one can be achieved by referring to the site of maximal volar bowstringing: in A2 pulley rupture, maximal volar displacement occurs over the proximal phalanx, whereas in A4 pulley tears, bowstringing is observed over the middle phalanx [43]. Early diagnosis of pulley ruptures is mandatory to prevent fixed contractures of the PIP joint. However, limited clinical examination, due to pain, soft tissue swelling, and restricted range of motion, may create difficulty in obtaining the diagnosis of a pulley rupture.

**CLINICAL HISTORY** A 56-year-old man with chronic wrist pain and instability.



FIGURE 1.30A



FIGURE 1.30B

### FINDINGS

- A. PA radiograph of the left wrist shows that the scapholunate joint is grossly widened, and the capitate has migrated proximally into the gap. Joint space narrowing and subchondral sclerosis has developed at the articulation between the scaphoid and radius, and the lunate is slightly rotated.
- B. The lateral radiograph shows mild dorsal tilt of the lunate articular surface. Chondrocalcinosis is not visible. There are no erosions. Bone mineralization is normal.

**DIFFERENTIAL DIAGNOSIS** Pyrophosphate arthropathy, rheumatoid arthritis, osteoarthritis, trauma.

**DIAGNOSIS** Pyrophosphate arthropathy, with scapholunate advanced collapse (SLAC wrist).

**DISCUSSION** Calcium pyrophosphate dihydrate (CPPD) crystal deposition disease is a polyarticular arthritis with deposition of CPPD crystals in articular tissues. CPPD crystals are generated locally in the articular tissues, where asymptomatic deposits may accumulate in cartilage, joint capsules, intervertebral discs, tendons, and ligaments.

In cartilage, these deposits may be evident radiographically as chondrocalcinosis. Pyrophosphate arthropathy is the degenerative result of structural joint damage, caused by chronic CPPD crystal deposition and irreversible destruction of the articular cartilage. The degenerative changes can be identical to those of osteoarthritis, but the distribution of involvement is different. In the wrist, the radiocarpal joint is characteristically involved, whereas in osteoarthritis, the scaphoid-trapezoid-trapezium–first metacarpal articulations are characteristically involved. In severe cases, the process causes gross scapholunate dissociation, in association with degenerative radiocarpal changes. The scaphoid and lunate separate, and the capitate migrates proximally into the resulting gap. This syndrome is called the SLAC wrist. It usually includes pancompartmental degenerative involvement. The shoulder (glenohumeral), knee (especially patellofemoral), elbow, ankle, and foot (talonavicular) are the other common sites of involvement. Chondrocalcinosis need not be present and will be absent if there is no remaining cartilage. Pyrophosphate arthropathy is often, but not necessarily, combined with acute episodes of crystal-induced synovitis. Very severe degenerative changes may lead to an appearance that resembles neuropathic osteoarthropathy.



FIGURE 1.31A



FIGURE 1.31B

**FINDINGS** (A, B) PA and oblique radiographs of the metacarpals demonstrate flattening of all metacarpal heads, with subchondral sclerosis and joint space loss. Beak-type osteophytes are present on the medial aspects of the second through fifth metacarpals. The IP joints are spared, but there are changes at the basal joints of the thumb and radiocarpal joints. Bone mineralization is mildly decreased. The opposite hand has a similar appearance.

**DIFFERENTIAL DIAGNOSIS** Hemochromatosis, pyrophosphate arthropathy, osteoarthritis, gout.

**DIAGNOSIS** Hemochromatosis.

**DISCUSSION** The predominant articular changes are those of a degenerative process, but the distribution is not that of primary osteoarthritis. Pyrophosphate arthropathy, the

chronic degenerative form of CPPD deposition disease, may have an identical appearance, but the clinical features suggest hemochromatosis as the underlying cause. As a differential diagnostic point, osteoporosis is usually a feature of hemochromatosis, but typically is not present in pyrophosphate arthropathy. Hemochromatosis results from deposition of iron in various tissues, caused by increased absorption of dietary iron from the gastrointestinal tract (primary), or by increased intake from blood transfusions, alcoholism, or ingestion (secondary). As many as 50% of patients with hemochromatosis may develop arthropathy; the arthropathy is caused by accumulation of iron and/or CPPD crystals in the joints. Arthritis may be the sole manifestation of hereditary hemochromatosis [44]. The classic clinical triad is bronze skin, cirrhosis, and diabetes. Laboratory tests will show an increased serum iron and iron-binding capacity. Phlebotomy does not help the symptoms of advanced arthropathy.

**CLINICAL HISTORY** A 70-year-old man with acute pain and swelling over the dorsal and ulnar aspects of the wrist.



FIGURE 1.32A



FIGURE 1.32B

### FINDINGS

- A. Lateral radiograph of the wrist shows amorphous calcification located along the extensor tendons with soft tissue swelling.
- B. PA radiograph shows a distended distal radioulnar joint capsule that is made partially visible by calcification. Incidental osteoporosis and osteoarthritis are present.

**DIFFERENTIAL DIAGNOSIS** Hydroxyapatite deposition disease, synovial chondromatosis, calcium pyrophosphate dihydrate (CPPD) deposition disease, scleroderma, tumoral calcinosis.

**DIAGNOSIS** Hydroxyapatite deposition disease (calcific tendinosis and calcific peri-arthritis).

**DISCUSSION** Amorphous calcification in the soft tissues is characteristic of calcium in the form of hydroxyapatite crystals. Each collection of calcium is more or less uniform in density from the edge to the center, with no evident structural features, and a somewhat irregular shape. The calcifications

are distributed along the expected location of the extensor tendons of the wrist and hand. The distal radioulnar joint capsule is similarly involved, where crystals may be grossly visible in the form of milk of calcium. Hydroxyapatite crystal deposition may be related to chronic minor trauma and deposition in localized necrotic tissue and may be associated with a painful inflammatory reaction of acute onset. Generally seen in patients over the age of 40, it affects men and women equally. It is most commonly seen around the shoulder. The main differential diagnostic consideration is synovial chondromatosis. If the calcification represented bone fragments or heterotopic ossification, one would expect a cortical and trabecular structure. Calcification in cartilage may have a punctate, flocculent, or rings-and-arcs morphology if enchondral ossification is occurring, but in this location, the cartilage would be heterotopic. Dystrophic calcification in cartilage may have a lamellated appearance. CPPD crystal deposition occurs in articular cartilage, which would not be expected within tendons. When CPPD crystals are free within the joint capsule, they are generally not visible on radiographs.

**CLINICAL HISTORY** A 69-year-old woman with hand injury, possibly from a fall.



FIGURE 1.33A



FIGURE 1.33B

**FINDINGS** PA (A) and lateral (B) radiographs of metacarpals demonstrate there is a fracture of the proximal third of the shaft of the fourth metacarpal with shortening and apex radial angulation. There is subluxation of the fourth CMC joint. There is also complete dislocation of the fifth CMC joint with the fifth metacarpal displaced volarly into the hypothenar eminence and proximally.

**DIFFERENTIAL DIAGNOSIS** None.

**DIAGNOSIS** Fourth metacarpal fracture; fifth CMC volar dislocation.

**DISCUSSION** The fourth metacarpal is typically protected by the third and fifth metacarpals, which flank it. In this

case, the dislocation of the fifth metacarpal base left the fourth metacarpal vulnerable to fracture. Volar dislocation at the fifth CMC is a rare injury, with the fifth metatarsal more typically dislocating dorsally. In the few reported cases in the literature, authors reported patients as doing better when open reduction and internal fixation was performed [45]. On physical exam, volar dislocations may be challenging to detect because the overlying hypothenar eminence may obscure the deformity. With strict attention to the M-shaped CMC articulations, this injury should not be missed on radiographs [46]. Confirmation by CT may be obtained in equivocal cases.



FIGURE 1.34A



FIGURE 1.34B

**FINDINGS**

- A. PA wrist radiograph shows foreshortening of the scaphoid with a cortical ring sign over its distal pole. The interval between the scaphoid and the lunate is minimally abnormally wide (compare with other carpal bone articulations).
- B. Lateral wrist radiograph shows an abnormal scapholunate angle of about 90 degrees.

**DIFFERENTIAL DIAGNOSIS** None.

**DIAGNOSIS** Rotary subluxation of the scaphoid (scapholunate dissociation).

**DISCUSSION** The scaphoid bridges the proximal and distal carpal rows, and its long axis is normally oriented

approximately 45 degrees on the lateral view from the plane of the carpus, allowing the thumb to be opposed to the fingers. When the ligamentous sling that suspends the scaphoid from the carpus is disrupted, muscle tension from the flexors and extensors of the thumb that cross the carpus brings it proximally, rotating the scaphoid on its short axis. On PA radiographs, the scaphoid will appear as a small round bone. On lateral radiographs, the angle between the long axis of the scaphoid and the long axis of the wrist will be increased to approximately 90 degrees. The injury may be sustained when the hand is extended to break a backward fall. On impact, the hand and wrist undergo hyperextension, ulnar deviation, and intercarpal supination (rotary motion between the proximal and distal carpal rows), loading the ligamentous sling of the carpus in tension from the radial side and causing it to tear.



FIGURE 1.35A



FIGURE 1.35B

**FINDINGS**

- A. PA radiograph shows the lunate as an overlapping triangular structure.
- B. Lateral radiograph of the wrist shows volar dislocation of the lunate with 90-degree rotary displacement. The capitate occupies the normal position of the lunate.

**DIFFERENTIAL DIAGNOSIS** None.

**DIAGNOSIS** Lunate dislocation.

**DISCUSSION** On the PA radiograph, one should recognize that the radiographic overlapping of the lunate over the other carpal bones indicates that it is not in the same spatial plane, and the triangular rather than trapezoidal shape indicates that the lunate has rotated out of its normal orientation. The lateral view confirms these findings. Volar dislocation of the lunate is the most severe of the group of perilunate injuries, a consistent pattern of injuries sustained around the lunate when the hand is extended to break a backward fall. On impact, the hand and wrist undergo hyperextension, ulnar deviation, and

intercarpal supination. The ligamentous sling of the carpus is loaded in tension from the radial side, and a sequence of injuries may ensue. In stage 1 (scapholunate dissociation or rotary subluxation), there is rupture of the proximal ligamentous attachments of the scaphoid; alternatively, the scaphoid may fracture. In stage 2 (perilunate dislocation), the capitate dislocates from the lunate dorsally, taking with it the hand and the scaphoid. In stage 3 (midcarpal dissociation or triquetral dislocation), the triquetral ligaments fail by tear or avulsion of insertions, separating the triquetrum from the lunate. Although the lunate remains in place, the rest of the carpus is dislocated dorsally, coming to rest on the dorsal surface of the lunate. The lunate is subluxated and tilted volarly, but is not completely dislocated. In stage 4 (lunate dislocation), the dorsal radiocarpal ligament tears, allowing the dorsally dislocated carpus to eject the lunate from the radius volarly. The capitate comes to rest in the radial articular surface. The dislocated lunate is also rotated 90 degrees volarly, still held to the radius by its volar ligaments. The radiologic signs of reduced perilunate injuries may be subtle, particularly in the absence of fractures.

**CLINICAL HISTORY** A 57-year-old woman who fell on an outstretched hand.



FIGURE 1.36A

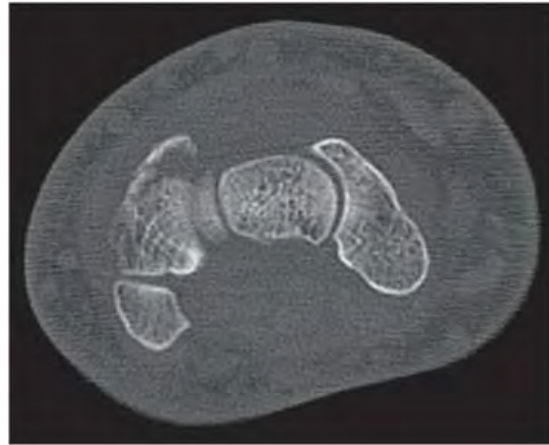


FIGURE 1.36B



FIGURE 1.36C

### FINDINGS

- A. Lateral wrist radiograph shows soft tissue swelling and a subtle bony fragment at the dorsal aspect of the proximal carpal row.
- B, C. Contiguous axial computed tomography (CT) images demonstrate a minimally displaced fracture of the dorsal triquetral bone.

**DIFFERENTIAL DIAGNOSIS** None.

**DIAGNOSIS** Triquetral fracture.

**DISCUSSION** Fractures of the triquetral bone are typically due to a direct blow or to forced dorsiflexion, usually from

a fall on the outstretched hand. The mechanism is compressive force from either the hamate or ulnar styloid process. The most common appearance is a “chip” fracture off the dorsal aspect of the bone, which can be treated with immobilization. Displaced fractures of the triquetral body are surgically repaired. The lateral view of the wrist is best to visualize chip fractures. Patients with point tenderness of the triquetral bone, but with no abnormality on standard radiographs, may require CT or MR imaging to delineate the fracture. Fractures off the volar aspect of the triquetral bone have a high association with perilunate ligament injuries [47].

**CLINICAL HISTORY** A mature woman with soft tissue nodule at the radial aspect of the wrist.

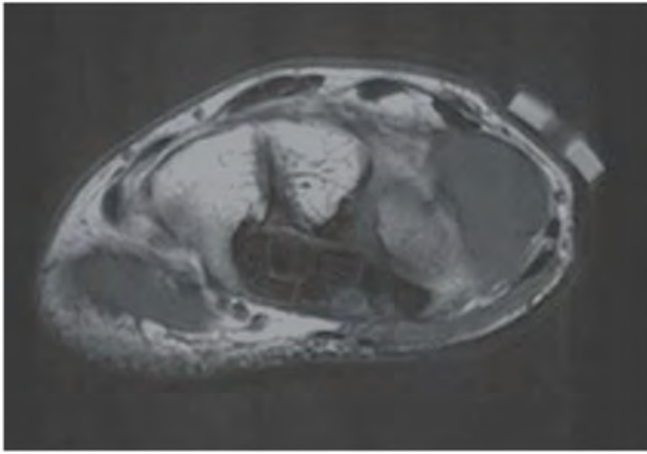


FIGURE 1.37A

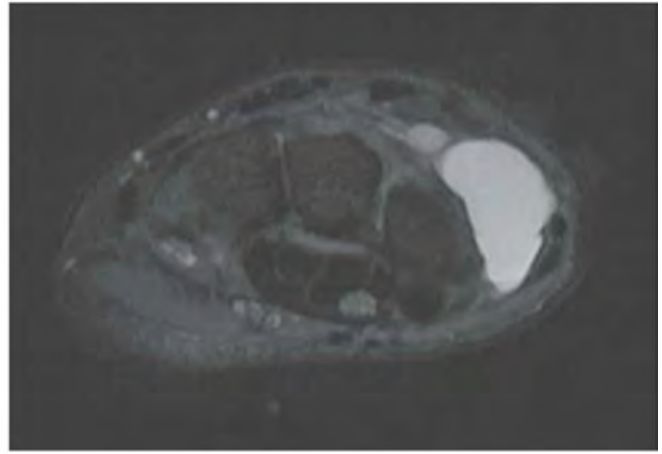


FIGURE 1.37B

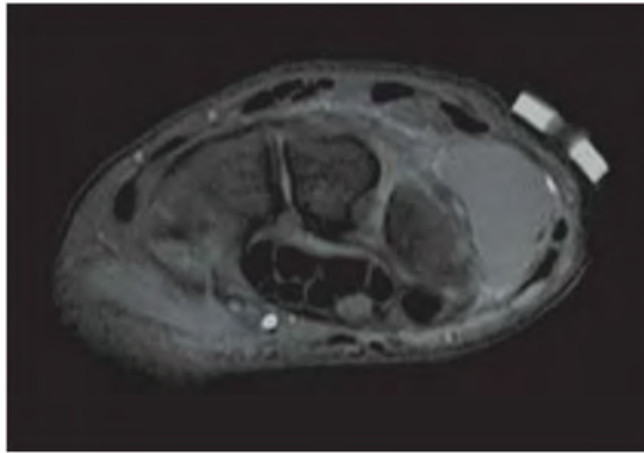


FIGURE 1.37C

**FINDINGS** (A) Axial T1-weighted, (B) T2-weighted fat-suppressed, and (C) T1-weighted fat-suppressed postgadolinium images show a multilobulated, low T1 and high T2 signal mass dorsal aspect of the hand at the level of the carpal tunnel. The mass demonstrates no significant enhancement on postcontrast sequences. The mass has interposed itself into the carpal tunnel adjacent to the median nerve.

**DIFFERENTIAL DIAGNOSIS** Ganglion cyst, schwannoma, abscess, giant cell tumor of tendon sheath, synovial cyst.

**DIAGNOSIS** Ganglion cyst.

**DISCUSSION** A ganglion cyst develops along a tendon sheath. It most likely forms due to a herniation of synovial lining in a joint, a tendon sheath, or even a nerve covering. The connection with the original site of formation can be lost as the cyst migrates toward the subcutaneous tissue.

A ganglion cyst often contains simple fluid (high T2, low T1 signal). It can also contain hemorrhagic fluid and therefore have heterogeneous signal characteristics. Ganglion cysts can be associated with internal derangement (triangular fibrocartilage complex and ligament tears) [48]. It is important to differentiate ganglion cysts from a solid mass. Administering gadolinium helps to make this differentiation. Ganglion cysts will not have central enhancement, whereas solid masses do. Most ganglion cysts demonstrate rim-like enhancement. Because gadolinium diffuses in the extracellular spaces, if there is a long delay between injection and imaging, a cyst may appear to have a thick, enhancing wall, or may even enhance homogeneously. On sonography, ganglion cysts appear as anechoic structures with posterior acoustic enhancement. Connection to a joint capsule or tendon sheath is sometimes demonstrable. Chronic ganglia may have internal echoes from debris. Color Doppler should show a lack of flow.

**CLINICAL HISTORY** A 34-year-old man who developed multifocal bone pain over a 1-year period.



FIGURE 1.38A



FIGURE 1.38B

## FINDINGS

- A. Gamma camera views of the hands from delayed images of radionuclide bone scan. Radionuclide accumulation is noted in the right distal ulna and second metacarpal, left radius, ulna, trapezium, and first and third metacarpal heads.
- B. PA radiograph of the left wrist show dense sclerosis of the distal radius and ulna, scaphoid, trapezoid, trapezium, and first metacarpal. The differentiation between cortex and medullary space is absent, and very little remaining trabecular bone pattern is seen. However, the bones are not enlarged, and their shape is normal. The remaining bones that are visible have a normal appearance.

**DIFFERENTIAL DIAGNOSIS** Chronic sclerosing osteomyelitis, osteoblastic lymphoma, osteomyelitis, Paget disease, sclerosing bone dysplasias.

**DIAGNOSIS** Chronic sclerosing osteomyelitis.

**DISCUSSION** The abnormal bone scan and corresponding sclerosis raise the differential diagnosis of osteoblastic neoplasm, osteomyelitis, Paget disease, and sclerosing bone

dysplasias. Paget disease can be eliminated by the lack of bone enlargement and cortical thickening, and sclerosing bone dysplasias can be eliminated by the otherwise normal bone morphology and clinical history. Given the patient's age, lymphoma and osteomyelitis were the primary considerations, and *Staphylococcus aureus* was cultured from a biopsy specimen of the radius. Hematogenous osteomyelitis is caused most frequently in adults by *S. aureus*. Cortical destruction and periostitis with involucrum formation dominates the early radiographic appearance. In the subacute and chronic stages of osteomyelitis, reactive bone formation may result in dense sclerosis [49], with low-grade clinical symptoms. Foci of bacteria persist within bone cavities that are filled with granulation tissue, and dense reactive bone surrounds the site. The cortex may be thickened as a result of long-term deposition of reactive medullary and periosteal bone. Serpiginous sinus tracts may extend to the skin surface. Chronic osteomyelitis may exist many years after acute osteomyelitis, even if the acute infection was treated appropriately. Systemic antibiotics will be ineffective against organisms sequestered in necrotic bone. Blood cultures are almost always negative, and cultures of the lesions are frequently negative as well.

**CLINICAL HISTORY** A 31-year-old woman who fell on her outstretched hand.



FIGURE 1.39A



FIGURE 1.39B

### FINDINGS

- A. Lateral radiograph of the wrist shows an abnormal appearance to the lunate, with slight volar angulation. The scapholunate angle is actually decreased. No fracture is evident.
- B. PA radiograph of the wrist shows an incompletely segmented lunate and triquetrum. There is no fracture.

**DIFFERENTIAL DIAGNOSIS** None.

**DIAGNOSIS** Carpal coalition.

**DISCUSSION** Carpal coalitions are relatively common anomalies in which two or more carpal bones fail to segment during development, resulting in a congenital fusion. The anomaly results from incomplete cavitation of a

common embryologic carpal precursor during the fifth to eighth weeks of intrauterine life [50]. The fusion can be bony, cartilaginous, or fibrous. Carpal coalitions are usually isolated anomalies that involve bones of the same row. The most common coalition is between the lunate and triquetrum. The prevalence of this abnormality is approximately 1%, and it is bilateral in 60%. Carpal coalitions are usually incidental findings, but carpal coalition and associated degenerative arthritis of the incompletely involved joints has been proven as a cause of occult wrist pain [51]. Multiple carpal coalitions or coalitions between bones of the proximal and distal rows are frequently associated with other anomalies, including tarsal coalitions, arthrogryposis, Ellis-van Creveld syndrome, Holt-Oram syndrome, Turner's syndrome, and symphalangism. These coalitions may be familial.

**CLINICAL HISTORY** A 52-year-old male with chronic wrist pain.



FIGURE 1.40A



FIGURE 1.40B



FIGURE 1.40C



FIGURE 1.40D



FIGURE 1.40E

**FINDINGS**

- A. PA radiograph of the wrist shows that the lunate is dense, with tiny fragments visible at the proximal articulation with the scaphoid, and perhaps with the triquetrum.
- B. Coronal T1-weighted MRI shows mostly low signal in the lunate.
- C. Coronal T2-weighted MRI shows effusion in the radiocarpal compartment and focal area of high signal within the lunate.
- D. Coronal CT reformation shows sclerosis of the lunate with fragmentation adjacent to the triquetral articulation.
- E. Sagittal CT reformation shows sclerosis and flattening of the proximal surface of the lunate.

**DIFFERENTIAL DIAGNOSIS** Osteonecrosis, fracture.

**DIAGNOSIS** Osteonecrosis of the lunate (Kienböck disease, lunate malacia).

**DISCUSSION** In the normal wrist, loading of the hand is transmitted to the forearm through the radiocarpal joint, with approximately one-third of the force passing through each articulating proximal row carpal bone (scaphoid, lunate, and triquetrum). When the ulna is abnormally short with respect to the radius—the so-called ulnar minus variance—loading that would have passed through the triquetrum is passed instead through the lunate. This may result in stress-related osteonecrosis of the lunate [52,53]. A similar process may occur as a result of trauma, as perhaps in this case. It is rare for Kienböck disease to occur bilaterally [54]. On CT, sclerosis, deformation, and fragmentation are typically seen. On MRI, the lunate tends to be dark on all sequences, presumably as a result of sclerosis. Because the natural history of Kienböck disease is progressive deformation and fragmentation, high T2 signal is more likely to reflect cystic degenerative change rather than revascularization and remodeling.

**CLINICAL HISTORY** A 45-year-old construction worker with chronic ulnar-sided wrist pain.



FIGURE 1.41A

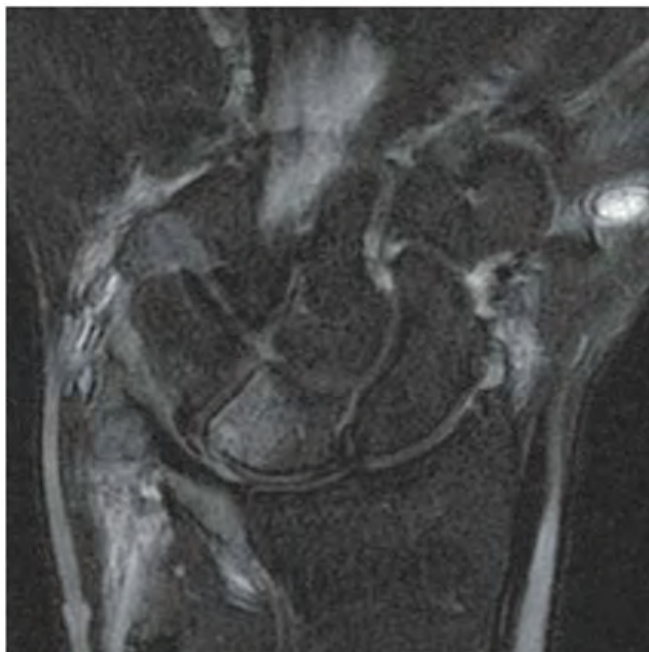


FIGURE 1.41B



FIGURE 1.41C

**FINDINGS**

MRI following three-compartment wrist injection.

- A. Coronal T1-weighted fat-suppressed MRI shows distal bulging of the triangular fibrocartilage complex (TFCC) over the ulnar head and subchondral bone changes in the proximal aspect of the lunate. The lunotriquetral ligament was intact (not shown).
- B. Coronal T2-weighted fat-suppressed MRI shows marrow edema in the lunate.
- C. Coronal GRE MRI shows sclerosis and cyst formation in the lunate.

**DIFFERENTIAL DIAGNOSIS** Ulnar impaction syndrome, Kienböck disease, lunate contusion or fracture.

**DIAGNOSIS** Ulnar impaction syndrome.

**DISCUSSION** Ulnar impaction syndrome (also called ulnar abutment syndrome) may occur as a result of chronic

impaction between the ulnar head and the lunate, with the TFCC trapped in between. Patients may complain of chronic ulnar-sided wrist pain, swelling, and limitation of motion. Protrusion of the ulnar head beyond the adjacent radial articular surface is a common predisposing factor, and may be the result of anatomic variation (positive ulnar variance) or shortening of the radius from causes such as trauma. Firm grip, pronation, and ulnar deviation of the wrist tend to dynamically increase ulnar variance, and may be associated with worsening symptoms. Radiologic correlates of ulnar impaction syndrome include positive ulnar variance or relative shortening of the radius, articular and subchondral changes of the ulnar head and proximal lunate, and perforations of the TFCC [55]. Regarding the differential diagnosis, Kienböck disease would typically be associated with negative ulnar variance (radius protruding beyond ulnar head) that causes increased loading of the lunate, not present in this case; fracture or bone contusion would not be a consideration without previous trauma.

**CLINICAL HISTORY** *A 16-year-old with wrist pain and swelling.*

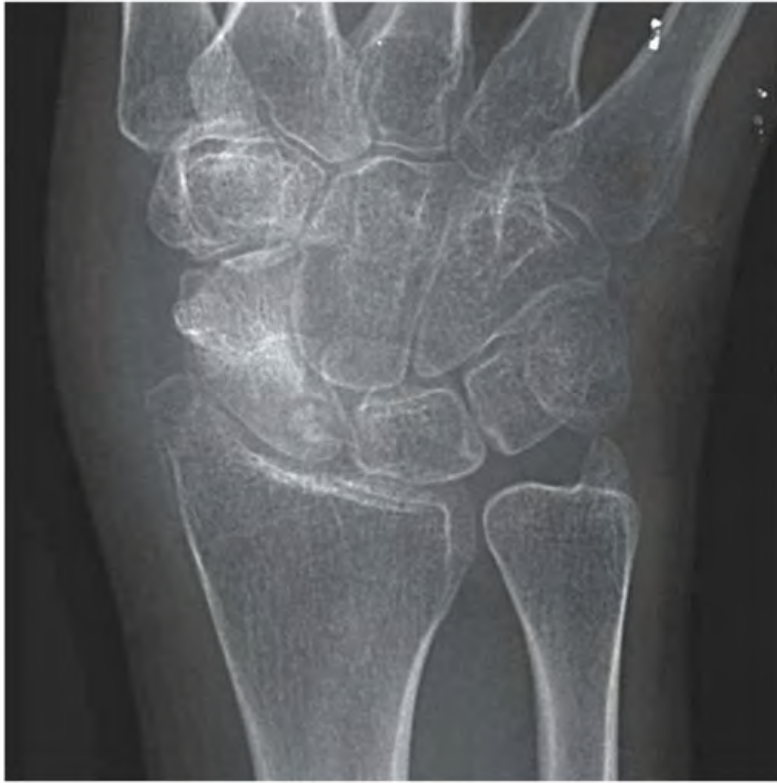


FIGURE 1.42A



FIGURE 1.42B



FIGURE 1.42C

**FINDINGS**

- A. PA radiograph of the wrist shows diffuse soft tissue swelling and osteopenia. However, the scaphoid appears relatively dense. There is a lucent region in the proximal pole of the scaphoid with central sclerosis.
- B, C. Axial CT (B) and coronal CT (C) reformation show a round lesion occupying the proximal pole of the scaphoid. The lesion has a thin, sclerotic margin and a dense, irregularly calcified center. The adjacent portions of the scaphoid are sclerotic, but the surrounding bones are osteopenic.

**DIFFERENTIAL DIAGNOSIS** Osteonecrosis, enchondroma, osteomyelitis, osteoid osteoma, lymphoma, eosinophilic granuloma.

**DIAGNOSIS** Osteoid osteoma.

**DISCUSSION** The differential diagnosis revolves around the finding in the proximal pole of the scaphoid; it could be seen

as a lytic lesion with a sequestrum or a lucent lesion with a mineralized center. Osteonecrosis, osteomyelitis, lymphoma, and eosinophilic granuloma are reasonable possibilities for sequestrum formation [56], and the latter three lesions might be associated with soft tissue swelling and surrounding osteopenia. The CT scan clarifies the radiographic finding as a lesion with mineralized center. The sclerosis of the scaphoid, soft tissue swelling, and surrounding osteopenia would fit well with the inflammatory reaction that typically accompanies osteoid osteomas in subarticular locations, but not with enchondroma. Osteoid osteoma is a benign neoplasm of bone that appears on radiographs and CT as a small (1 cm or smaller) lucent lesion with a densely mineralized center. There is often extensive surrounding reactive bone, particularly when located in the cortex. When located in subarticular bone, patients may present with synovitis; the classical presentation is an adolescent or young adult male with gradually worsening pain, worse at night, dramatically relieved by aspirin. The carpus is an unusual location for osteoid osteoma [57].



FIGURE 1.43

**FINDINGS** PA radiograph of the wrist. The growth plates of the distal radius and ulna are thick and wide. Dense sclerosis is present at the distal metaphyses. The metaphyses have a frayed appearance.

**DIFFERENTIAL DIAGNOSIS** Healing rickets, hypophosphatasia, renal disease, metaphyseal chondrodysplasia.

**DIAGNOSIS** Healing rickets.

**DISCUSSION** Rickets is the childhood manifestation of a systemic disease in which the calcification of osteoid is deficient. The final common pathway is the lack of available calcium or phosphorus (or both) for mineralization of osteoid, but a number of different abnormalities in the availability, synthesis, or biologic action of vitamin D and its hormonally active metabolites may be responsible. Because there is continued cartilage growth in the absence of normal mineralization and ossification, the growth plates become widened.

This defining radiographic finding will be most apparent in the most active regions of growth. Uncalcified cartilage may become quite bulky and evident on clinical examination. Frequent sites of radiographic abnormalities include the costochondral junctions of the ribs, the distal femur, both ends of the tibia, the proximal humerus, the distal radius, and the distal ulna. Irregular, disorganized mineralization of the zone of provisional calcification creates a frayed appearance. Mechanical stress on the thickened growth plate may lead to widening, cupping, and bowing deformity. The bone texture (trabecular pattern) may appear smudged or coarsened, and there is a delayed appearance of ossification centers. Rachitic bone is less resistant to bending and shearing loads, and insufficiency fractures and bowing deformities are common. Following the initiation of successful treatment of rickets, the uncalcified osteoid calcifies, so that the zone of provisional calcification appears as a wide band that narrows the growth plate to its normal thickness. Ossification of nonmineralized subperiosteal osteoid is apparent as new periosteal bone.



FIGURE 1.44

**FINDINGS** PA radiograph of the wrist. There is widening and irregularity of the zone of provisional calcification of the growth plate of the radius, but the growth plates of the distal ulna and first metacarpal are normal.

**DIFFERENTIAL DIAGNOSIS** Trauma, rickets.

**DIAGNOSIS** Growth plate fracture (Salter type I), healing.

**DISCUSSION** The abnormality of the growth plate of the distal radius has a superficial resemblance to rickets—it is widened and there is irregular sclerosis on the metaphyseal side—but the presence of normal growth plates elsewhere (distal ulna, proximal first metacarpal) eliminates systemic or metabolic bone disease as a diagnostic consideration. The growth plate is attached to the metaphysis internally by the interdigitation of bone with the zone of calcified cartilage,

and externally by the periosteum. The growth plate is relatively weak when loaded in torsion or shear, but is resistant to tension and compression. When the epiphysis is separated from the metaphysis, the plane of separation through the growth plate is in the zone of cartilage transformation between the calcified and uncalcified layers of cartilage, leaving the germinal cell layers with the epiphysis and the calcified cartilage with the metaphysis. Displacement does not occur unless the periosteum is also torn. The production of growing cartilage by the germinal layers may be uninterrupted by a fracture if the blood supply to the separated epiphysis remains intact. However, the newly formed cartilage will not ossify until vascular ingrowth from the metaphyseal side is reestablished. Thus, after a fracture, the growth plate becomes wider until the normal zone of cartilage transformation is reestablished; once ossification of the widened growth plate begins, its thickness returns to normal.



FIGURE 1.45

**FINDINGS** PA radiograph of the wrist. There are dense transverse metaphyseal lines at the distal radius and ulna. The growth plate is of normal thickness, and there is no periosteal bone reaction.

**DIFFERENTIAL DIAGNOSIS** Heavy metal poisoning, physiologic lines.

**DIAGNOSIS** Lead poisoning.

**DISCUSSION** Chronic lead poisoning (plumbism) in children results in dense transverse lines across the growing metaphysis, so-called *lead lines* or *lead bands*. Lead interferes with the resorption of the primary spongiosa during growth. New bone is laid down on top of the primary

spongiosa, but because normal resorption of the primary spongiosa does not occur during the period of exposure, a dense line becomes evident on radiographs, even if lead is present in only minute amounts. Lead lines are a late manifestation of chronic lead poisoning and are best seen at the knee or distal radius, where growth is the most rapid. Lead lines do not appear until blood lead attains a concentration of 70 to 80 g/dL. Lead lines are not affected by treatment of the underlying lead poisoning; they disappear spontaneously within 4 years [58,59]. Lead toxicity has been reported following retention of lead fragments after a gunshot wound. Chronic exposure during growth to other heavy metals, including phosphorus and bismuth, may result in transverse lines similar to those seen with chronic lead poisoning.

**CLINICAL HISTORY** A 51-year-old woman with pain along the radial side of the wrist.



FIGURE 1.46A

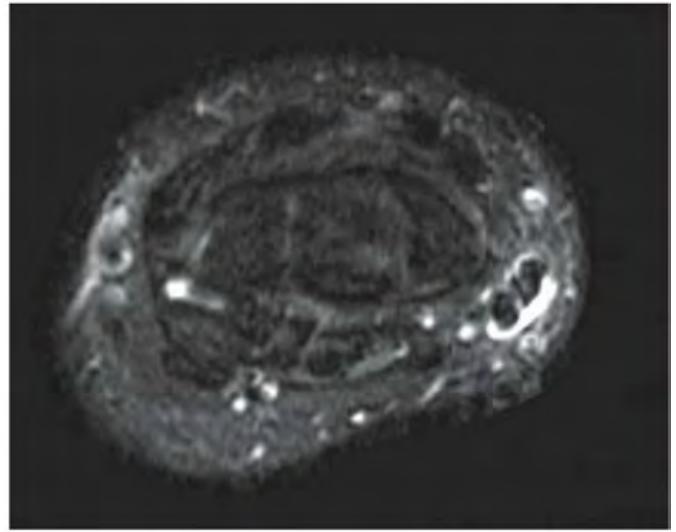


FIGURE 1.46B

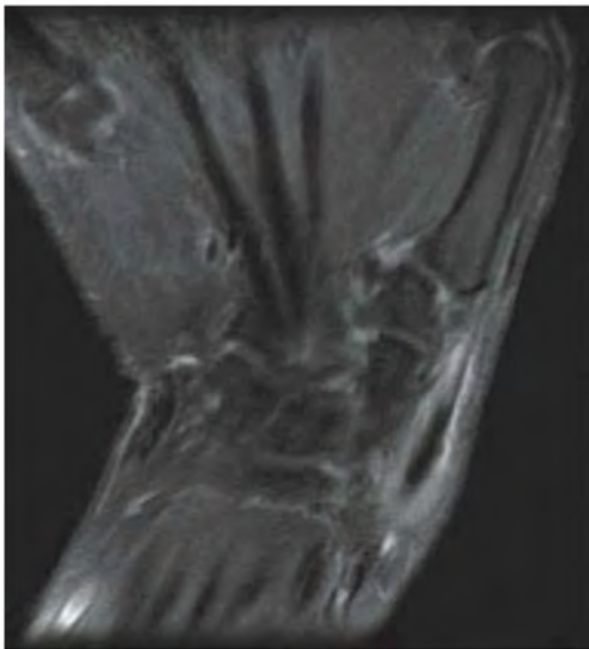


FIGURE 1.46C

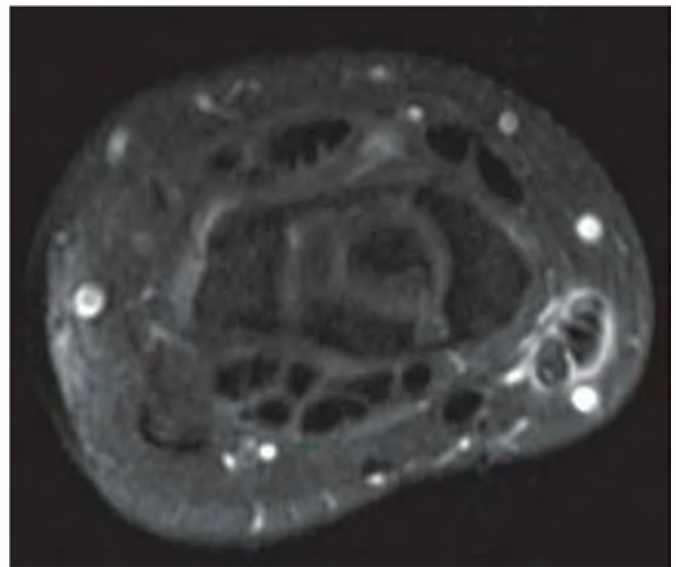


FIGURE 1.46D

**FINDINGS** Axial T1-weighted (A), axial T2-weighted fat-suppressed (B) post-gadolinium coronal (C), and axial T1-weighted fat-suppressed (D) images of the wrist show thickening and irregularity of the abductor pollicis longus (APL) and the extensor pollicis brevis (EPB). High T2-weighted signal is present around and within these tendons.

**DIFFERENTIAL DIAGNOSIS** None.

**DIAGNOSIS** De Quervain tenosynovitis.

**DISCUSSION** De Quervain tenosynovitis describes a clinical entity involving abnormal thickening of the APL and EPB tendon sheaths. These tendons travel through the first dorsal compartment of the wrist. This syndrome is most common in women between the ages of 35 and 55, though it has been reported in new mothers due to overuse [60]. Patients complain of gradual onset of pain over the radial styloid when they abduct or extend the thumb. Clinically, this condition may be difficult to differentiate from osteoarthritis at the base of the thumb. If left untreated, patients may develop fibrosis within the tendon sheath with subsequent limited motion.

**CLINICAL HISTORY** A 38-year-old male with persistent thenar eminence pain, a couple of weeks after crashing a Jet Ski into a wooden dock. Radiographs (not shown) at the time of the incident were normal.

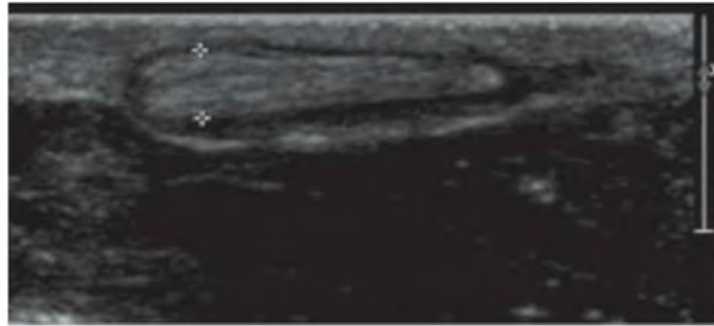


FIGURE 1.47A

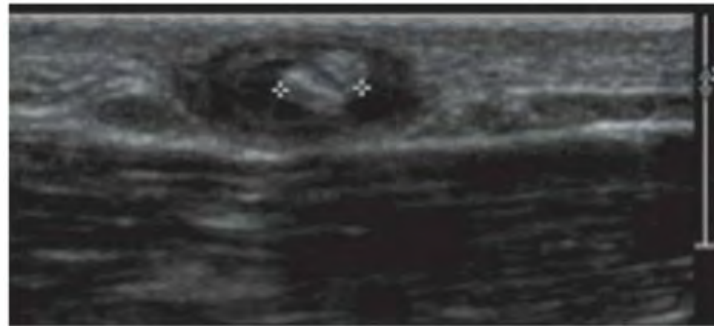


FIGURE 1.47B

**FINDINGS** Sonography shows a linear hyperechoic object in subcutaneous tissues adjacent to first metacarpal on longitudinal (A) and transverse (B) scans. The object is surrounded by a hypoechoic rim. This lesion corresponded to the site of the patient's pain.

**DIFFERENTIAL DIAGNOSIS** None.

**DIAGNOSIS** Foreign body (wood splinter).

**DISCUSSION** Sonography has been an invaluable tool in detecting small foreign bodies in the superficial soft

tissues, particularly when they are radiolucent. Wood splinters appear as linear hyperechoic lesions. Foreign bodies may be associated with surrounding foreign body granuloma formation or by abscess. Sonography has multiple advantages from static imaging modalities such as MRI or CT [61,62]. First, with interaction with the patient pointing out the exact site of pain, small foreign bodies are more likely to be found on a directed search. Second, if a foreign body is near a neurovascular bundle, its integrity and location can be mapped out for the surgeons. Third, adjacent tendons can be studied dynamically to determine whether they are involved.

**CLINICAL HISTORY** A 56-year-old man with swollen, painful joints and chronic cough.



FIGURE 1.48

**FINDINGS** Oblique radiograph of the wrist demonstrates undulating periosteal reaction along the metadiaphysis of the distal radius and distal ulna. The contralateral side (not shown) has similar findings.

**DIFFERENTIAL DIAGNOSIS** Hypertrophic osteoarthropathy, melorheostosis, hypervitaminosis A.

**DIAGNOSIS** Hypertrophic osteoarthropathy, secondary.

**DISCUSSION** Hypertrophic osteoarthropathy is a syndrome characterized by digital clubbing and periostitis of the tubular bones [63]. There are primary and secondary forms of the condition, and there may be incomplete manifestations. Secondary forms may be localized and associated with hemiplegia, aneurysm, infective arteritis, and patent ductus arteriosus, or they may be generalized and associated with a wide variety of conditions, including various chronic and neoplastic pulmonary, cardiac, hepatic, intestinal, and mediastinal diseases, as well as a diverse variety of other malignancies. Hypertrophic osteoarthropathy may occur as one of a number of paraneoplastic syndromes in which the clinical manifestations may precede, coincide

with, or follow the diagnosis of the malignancy [64,65]. The clinical presentation as joint disease and the isolated radiographic finding of periosteal reactive bone are typical for hypertrophic osteoarthropathy. Involvement of the diaphysis and metaphysis (but not the epiphysis) is characteristic, and location in the leg and forearm is more common than in the femur, humerus, hands, or feet [66]. In an older patient, the condition is most commonly secondary to bronchogenic carcinoma, although it may also occur in other malignant, benign, or chronic suppurative diseases of the lung; cyanotic heart disease; liver or biliary cirrhosis; or inflammatory bowel disease. The mechanism of the reaction is unknown. In an adolescent or young adult, the condition may be pachydermoperiostosis (primary hypertrophic osteoarthropathy), a condition of unknown etiology that may also include thickening of the skin of the face and hands, and clubbed digits. The primary form of hypertrophic osteoarthropathy represents approximately 3% to 5% of cases. The distinction between primary and secondary hypertrophic osteoarthropathy may be difficult to make radiographically, but findings in the primary form may be more florid, may involve the epiphyses, and may be located in the ribs, pelvis, and skull.



FIGURE 1.49

**FINDINGS** PA radiograph of the wrist. There is a lesion with geographic bone destruction in the distal radius. The lesion extends from the distal shaft to the articular surfaces, both radiocarpal and the distal radioulnar. The cortex is thinned and mildly expanded. Prominent bony ridges or struts are seen traversing the lesion. There is no apparent matrix mineralization. The transition between lesion and normal bone is sharp, but with a definite sclerotic rim distally. The cortex appears thin, but intact and mildly expanded on the ulnar side.

**DIFFERENTIAL DIAGNOSIS** Desmoplastic fibroma, hemophilic pseudotumor, aneurysmal bone cyst, geode, giant cell tumor.

**DIAGNOSIS** Desmoplastic fibroma.

**DISCUSSION** The presence of the reinforced ridges or struts of bone suggests that the lesion is indolent and that the bone has remodeled to accommodate the geographic destruction. Large lesions of low aggressiveness located in the

metaphysis but extending to the articular surface in adults are few and include subchondral cyst, hemophilic pseudotumor, osteonecrosis, and this lesion, desmoplastic fibroma. Giant cell tumor, although occurring at this site, would tend to have more aggressive characteristics and generally not a sclerotic margin or reinforced trabeculae. Desmoplastic fibroma is a rare intraosseous fibrous lesion that is histologically identical to soft tissue fibromatosis (extra-abdominal desmoid tumor of soft tissues). They are seen mostly in adolescents and young adults. Their location is typically central in the metaphysis of a long bone, and radiographic characteristics are typically benign [67]. They are geographic, lytic lesions, with a narrow zone of transition but often not a sclerotic rim. There is no matrix mineralization. Endosteal erosion and modest cortical expansion are present, but usually cortical breakthrough is not. The endosteal margins characteristically have thick ridges of bone that may suggest the diagnosis. They may be infiltrative and occasionally locally aggressive, but they have no metastatic potential. Local recurrence is common after intralesional curettage, so en bloc excision is the treatment of choice [68].



FIGURE 1.50

**FINDINGS** PA radiograph of the forearm. There is a long lesion in the distal radial shaft. The lesion has a bubbly appearance, with a sclerotic margin, mildly expanded cortical shell, and no matrix mineralization.

**DIFFERENTIAL DIAGNOSIS** Nonossifying fibroma, fibrous dysplasia, aneurysmal bone cyst.

**DIAGNOSIS** Nonossifying fibroma.

**DISCUSSION** The lesion has nonaggressive characteristics: the well-defined sclerotic margin, the mild cortical expansion without cortical thinning, and the lack of cortical penetration or periosteal reaction. The long shape and bubbly appearance are characteristic of nonossifying fibroma (fibroxanthomas).

Nonossifying fibromas are nonneoplastic lesions thought to be the result of faulty ossification at the growth plate. A causal relationship with stress or trauma has been suggested but not proven. These lesions are self-limited, with no potential for growth or spread, and regress spontaneously by filling in with bone from the periphery. They are histologically identical to fibrous cortical defects (metaphyseal fibrous defects). Nonossifying fibromas are less common than fibrous cortical defects and occur in older children or adolescents. Located eccentrically within the medullary cavity but still within an expanded cortex, nonossifying fibromas are lucent with a sclerotic margin. Some lesions have a trabeculated, scalloped, multilocular, or bubbly appearance. They range in size from 1 to 7 cm, and the larger ones may fracture or cause pain.

**CLINICAL HISTORY** A 2-week-old infant born to a mother with poor prenatal care, and seen again 3 months later.



FIGURE 1.51A



FIGURE 1.51B

### FINDINGS

- A. PA radiograph of the forearm demonstrates mild periostitis of the metadiaphyseal regions.
- B. PA radiograph of the forearm performed 3 months later demonstrates a marked increase in the amount of periostitis, as well as irregularity and widening of the metaphysis, an increase in soft tissue swelling, and a possible focal lucency in the proximal ulna.

**DIFFERENTIAL DIAGNOSIS** Congenital infections by toxoplasmosis, syphilis, rubella, Cytomegalovirus, or herpes simplex; hypervitaminosis A.

**DIAGNOSIS** Congenital syphilis.

**DISCUSSION** Syphilis is a chronic infection caused by the spirochete bacterium *Treponema pallidum*. Congenital syphilis is acquired by transplacental migration of the organism, usually in women who are infected during pregnancy. Heavy

infection of the fetus may cause abortion or death shortly after birth. In survivors, invasion of the developing skeleton, particularly sites of active enchondral ossification, result in the stigmata of congenital syphilis. In the neonate and very young infant, bony abnormalities include osteochondritis, diaphyseal osteomyelitis, and periostitis. Syphilitic osteochondritis is typically seen as symmetric involvement of the sites of enchondral ossification, including the growth plates of long bones, costochondral regions, and sometimes the flat bones and spine. Lucency and osseous irregularity may be seen. In diaphyseal osteomyelitis, focal regions of osteolysis and exuberant periostitis involve the shafts of the long bones. Periostitis may be a manifestation of subperiosteal infection, or may be a reactive process associated with osteomyelitis or healing osteochondritis. These lesions heal promptly with appropriate antibiotic therapy. Although reliable serologic methods for detecting syphilis exist, several epidemiologic factors have contributed to its reemergence as a significant potential cause of congenital infection [69].

**CLINICAL HISTORY** A 40-year-old woman with chronic bilateral wrist pain.



FIGURE 1.52A



FIGURE 1.52B

**FINDINGS** (A, B) PA radiographs of both wrists.

**DIFFERENTIAL DIAGNOSIS** None.

**DIAGNOSIS** Bilateral Madelung deformity.

**DISCUSSION** Madelung deformity refers to ulnar and volar subluxation of the carpus on the radius, with undergrowth of the radius relative to the ulna. Madelung deformity results from a growth disturbance in the ulnar-volar portion of the distal radial physis and has a genetic origin. The distal radial articular surface develops with a volar and ulnar tilt and in consequence, there is volar translation of the carpus. Because the ulna is unaffected, it becomes prominent and contributes to the clinical presentation of pain, decreased range of motion, and deformity. Although Madelung deformity may occur in association with dysplasias such as multiple

hereditary exostoses, Ollier disease, and multiple epiphyseal dysplasia, its most important association is with Leri-Weill dyschondrosteosis, a type of mesomelic dwarfism. Madelung deformity may also occur in isolation in an autosomal dominant fashion with 50% penetrance and variable expression [70]. It is seen most commonly in girls who present during their growth spurt (typically ages 10 to 14). So-called secondary Madelung deformity may follow trauma, infection, infarction, or other injury to the growing distal radial physis. On radiographs and CT, the angular deformity of the distal radius, the subluxation of the carpus, and the prominence of the ulna should be recognizable. On MRI, a thickened dorsal ligament tethering the lunate and the triangular fibrocartilage complex to the dorsal ulnar aspect of the radial metaphysis (Vickers ligament) may be seen [71]. The site of Vickers ligament may be evident on radiographs as a flame-shaped radiolucency along the ulnar aspect of the distal radial metaphysis.

**CLINICAL HISTORY** A 35-year-old man with catching sensation in the dorsal wrist, 7 months after ORIF for distal radius fracture.



FIGURE 1.53A

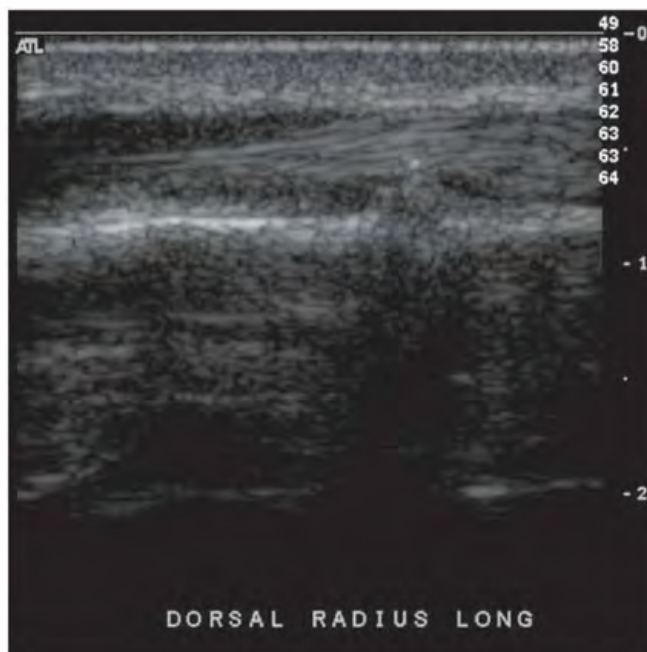


FIGURE 1.53B

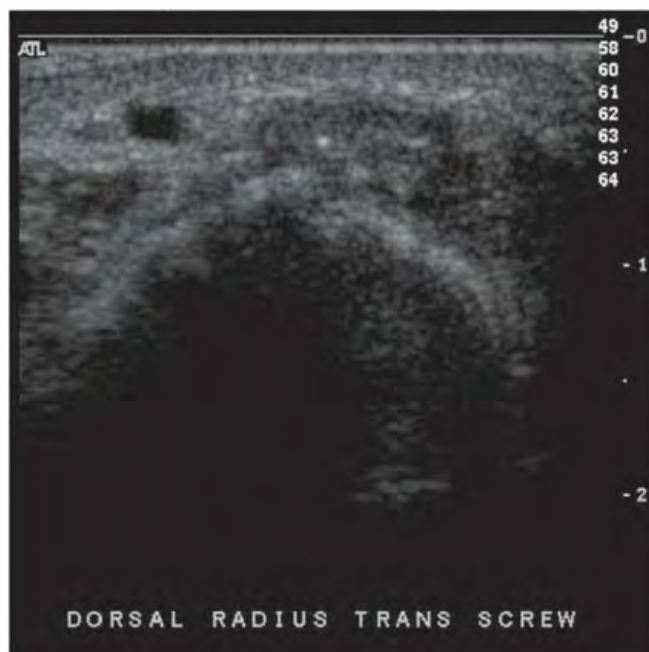


FIGURE 1.53C

## FINDINGS

- A. Lateral radiograph of the wrist. There is a healed fracture of the distal radius with a volar plate and multiple screws. One screw protrudes through the dorsal cortex.
- B. Longitudinal sonogram of the dorsal wrist shows the tip of the screw as a bright echogenic focus with shadowing. The overlying extensor tendon is directly apposed to the tip of the screw. Real-time imaging showed normal motion of the tendon within its tendon sheath, but impingement by the screw tip that reproduced the symptoms.
- C. Transverse sonogram shows the tip of the screw impinging on the deep surface of the extensor digitorum communis tendon.

**DIFFERENTIAL DIAGNOSIS** Tendon irritation, tenosynovitis, tenosynovial adhesions.

**DIAGNOSIS** Extensor tendon irritation.

**DISCUSSION** Protrusion of a screw through the surface of a bone is not infrequently seen on radiographs, but only occasionally appears to cause problems. In this case, the protruding screw tip had the misfortune to be directly underneath the extensor digitorum communis tendon, so that the patient felt a catching sensation as the screw tip snagged the tendon as it moved back and forth over it. Complications involving prominent hardware at the distal radius that have been reported by others include tendon irritation and delayed tendon rupture [72,73]. In one study of screw prominence following treatment of unstable distal radius fractures by palmar locking plates, 26% of the screws protruded from the dorsal cortex by at least 0.5 mm, and 24% of these caused symptomatic tenosynovitis [74]. The ability to demonstrate anatomic structures while dynamically reproducing the patient's symptoms, even in the presence of metal, makes sonography is an excellent method for problem solving in the postoperative wrist. In other anatomic sites, reported complications of protruding screw tips include pseudoaneurysm formation and nerve injury.



FIGURE 1.54A



FIGURE 1.54B

**FINDINGS** (A, B) Lateral and PA radiographs of the wrist. There is a comminuted fracture of the distal radial shaft at the junction of the middle and distal thirds, with volar angulation of the distal fragment and dorsal dislocation of the distal radioulnar joint.

**DIFFERENTIAL DIAGNOSIS** None.

**DIAGNOSIS** Galeazzi fracture dislocation.

**DISCUSSION** A fracture of the radial shaft with dislocation of the distal radioulnar joint is called a Galeazzi fracture dislocation. It accounts for approximately 7% of adult forearm fractures [75]. Isolated fractures of the radial shaft in adults are almost always associated with disruption of the distal

radioulnar joint. The injury is believed to occur during a fall on an outstretched hand combined with extreme pronation of the forearm. In this case, the distal radioulnar joint dislocation is grossly displaced. In less severe cases, the distal radioulnar joint may only be subluxated or dynamically unstable. CT with the wrist pronated may be required to document the abnormality; in supination, the unstable distal radioulnar joint tends to reduce itself. Treatment typically requires open reduction and internal fixation of the radial shaft fracture, and often direct repair of the distal radioulnar joint [76]. In children, a so-called Galeazzi-equivalent injury may occur as a fracture of the distal radial shaft with displaced epiphyseal separation of the distal ulna (Salter type I); however, unlike the adult injury, the distal ligamentous stabilizers at the distal radioulnar joint will remain intact [77].

## SOURCES AND READINGS

- Pipitone N, Kingsley GH, Manzo A, Scott DL, Pitzalis C. Current concepts and new developments in the treatment of psoriatic arthritis. *Rheumatology (Oxford)*. 2003;42(10):1138–1148.
- Gladman DD. Current concepts in psoriatic arthritis. *Curr Opin Rheumatol*. 2002;14(4):361–366.
- Bennett DL, Ohashi K, El-Khoury GY. Spondyloarthropathies: ankylosing spondylitis and psoriatic arthritis. *Radiol Clin North Am*. 2004;42(1):121–134.
- Gupta KB, Duryea J, Weissman BN. Radiographic evaluation of osteoarthritis. *Radiol Clin North Am*. 2004;42(1):11–41.
- Belhorn LR, Hess EV. Erosive osteoarthritis. *Semin Arthritis Rheum*. 1993;22:298–306.
- Greenspan A. Erosive osteoarthritis. *Semin Musculoskelet Radiol*. 2003;7(2):155–159.
- Zalavras CG, Marcus RE, Levin LS, Patzakis MJ. Management of open fractures and subsequent complications. *Instr Course Lect*. 2008;57:51–63.
- Erdman WA, Tamburro F, Jayson HT, Weatherall PT, Ferry KB, Peshock RM. Osteomyelitis: characteristics and pitfalls of diagnosis with MR imaging. *Radiology*. 1991;180(2):533–539.
- Hopkins KL, Li KC, Bergman G. Gadolinium-DTPA-enhanced magnetic resonance imaging of musculoskeletal infectious processes. *Skeletal Radiol*. 1995;24(5):325–330.
- Pineda C, Vargas A, Rodríguez AV. Imaging of osteomyelitis: current concepts. *Infect Dis Clin North Am*. 2006;20(4):789–825.
- Biviji AA, Paiement GD, Steinbach LS. Musculoskeletal manifestations of human immunodeficiency virus infection. *J Am Acad Orthop Surg*. 2002;10(5):312–320.
- Alpert PL, Munsiff SS, Gourevitch MN, Greenberg B, Klein RS. A prospective study of tuberculosis and human immunodeficiency virus infection: clinical manifestations and factors associated with survival. *Clin Infect Dis*. 1997;24:661–668.
- Vine JE, Cohen PR. Renal cell carcinoma metastatic to the thumb: a case report and review of subungual metastases from all primary sites. *Clin Exp Dermatol*. 1996;21:377–380.
- Baran R, Tosti A. Metastatic carcinoma to the terminal phalanx of the big toe: report of two cases and review of the literature. *J Am Acad Dermatol*. 1994;31:259–263.
- Lambert D, Escallier F, Collet E, et al. Distal phalangeal metastasis of a chondrosarcoma presenting initially as bilateral onycholysis. *Clin Exp Dermatol*. 1992;17:463–465.
- Cohen PR. Metastatic tumors to the nail unit: subungual metastases. *Dermatol Surg*. 2001;27(3):280–293.
- Pantoja E, Cross VF, Vitale P, Wendth AJ. Neoplastic involvement of terminal digits masquerading clinically as benign disease. *Rev Interam Radiol*. 1976;1:9–13.
- Heys SD, Brittenden J, Atkinson P, Eremin O. Glomus tumour: an analysis of 43 patients and review of the literature. *Br J Surg*. 1992;79:345–347.
- Dumont J. Glomus tumour of the fingers. *Can J Surg*. 1975;18:542–544.
- Bhaskaranand K, Naradgi BC. Glomus tumour of the hand. *J Hand Surg Br*. 2002;27:229–231.
- Byers P, Mantle J, Salm R. Epidermal cysts of phalanges. *J Bone Joint Surg Br*. 1966;48:577–581.
- Davids JR, Graner KA, Mubarak SJ. Post-fracture lipid inclusion cyst. A case report. *J Bone Joint Surg Am*. 1993;75:1528–1532.
- Samlaska CP, Hansen MF. Intraosseous epidermoid cysts. *J Am Acad Dermatol*. 1992;27:454–455.
- Rivera-Sanfeliz G, Resnick D, Haghighi P. Sarcoidosis of hands. *Skeletal Radiol*. 1996;25:786–788.
- Gonzalez del Pino J, Diez Ulloa A, Lovic A, Relea MF. Sarcoidosis of the hand and wrist: a report of two cases. *J Hand Surg Am*. 1997;22:942–945.
- Lieberman J, Krauthammer M. Pseudoclubbing in a patient with sarcoidosis of the phalangeal bones. *Arch Intern Med*. 1983;143:1017–1019.
- Yabut SM Jr, Kenan S, Sissons HA, Lewis MM. Malignant transformation of fibrous dysplasia. A case report and review of the literature. *Clin Orthop*. 1988;(228):281–289.
- Peiper M, Zornig C. Chondrosarcoma of the thumb arising from a solitary enchondroma. *Arch Orthop Trauma Surg*. 1997;166:246–248.
- Unni KK, Inwards CY. *Dahlin's Bone Tumors: General Aspects and Data on 10,165 Cases*. 6th ed. Philadelphia, PA: Lippincott Williams & Wilkins; 2010:226.
- Murphy MD, Nomikos GC, Flemming DJ, Gannon FH, Temple HT, Kransdorf MJ. Imaging of giant cell tumor and giant cell reparative granuloma of bone: radiologic-pathologic correlation. *Radiographics*. 2001;21(5):1283–1309.
- Nakajima Y, Sato K, Morita H, et al. Severe progressive erosive arthritis in multicentric reticulohistiocytosis: possible involvement of cytokines in synovial proliferation. *J Rheumatol*. 1992;19:1643–1646.
- Snow JL, Muller SA. Malignancy-associated multicentric reticulohistiocytosis: a clinical, histological and immunophenotypic study. *Br J Dermatol*. 1995;133:71–76.
- Chapman ME, Beggs I, Wu PS. Case report: thyroid acropachy in a single digit. *Clin Radiol*. 1993;47(1):58–59.
- Fatourechi V, Bartley GB, Eghbali-Fatourechi GZ, Powell CC, Ahmed DD, Garrity JA. Graves' dermopathy and acropachy are markers of severe Graves' ophthalmopathy. *Thyroid*. 2003;13(12):1141–1144.
- Resnick D. Dermatomyositis and polymyositis. In: Resnick D, Niwayama G, eds. *Diagnosis of Bone and Joint Disorders*. 3rd ed. Philadelphia, PA: WB Saunders; 1995:1218–1231.
- Bunch TW, O'Duffy JD, McLeod RA. Deforming arthritis of the hands in polymyositis. *Arthritis Rheum*. 1976;19:243–248.
- Schumacher HR, Schimmer B, Gordon GV, Bookspan MA, Brogadir S, Dowart BB. Articular manifestations of polymyositis and dermatomyositis. *Am J Med*. 1979;67:287–292.
- Hyszcak R, Bartold KP, Eggleston D. Gangrene associated with meningococcemia. *AJR Am J Roentgenol*. 1988;151:203–204.
- Lowenthal MN. Peripheral gangrene in infancy and childhood. *Br Med J*. 1967;2:700–701.
- Kransdorf MJ, Murphy MD. *Imaging of Soft Tissue Tumors*. 2nd ed. Philadelphia, PA: Lippincott Williams & Wilkins; 2006:381–388.
- Kitagawa Y, Ito H, Amano Y, Sawaizumi T, Takeuchi T. MR imaging for preoperative diagnosis and assessment of local tumor extent on localized giant cell tumor of tendon sheath. *Skeletal Radiol*. 2003;32:633–638.
- Klauser A, Frauscher F, Bodner G, et al. Finger pulley injuries in extreme rock climbers: depiction with dynamic US. *Radiology*. 2002;222(3):755–761.
- Martinoli C, Bianchi S, Cotten A. Imaging of rock climbing injuries. *Semin Musculoskelet Radiol*. 2005;9(4):334–345.
- Askari AD, Muir WA, Rosner IA, Moskowitz RW, McLaren GD, Braun WE. Arthritis of hemochromatosis. Clinical spectrum, relation to histocompatibility antigens, and effectiveness of early phlebotomy. *Am J Med*. 1983;75:957–965.
- Prokopia PM, Weiland AJ. Volar dislocation of the fourth and fifth carpometacarpal joints: a case report and review of the literature. *HSSJ*. 2008;4(2):138–142.
- Fisher MR, Rogers LF, Hendrix RW. Systematic approach to identifying fourth and fifth carpometacarpal joint dislocations. *AJR Am J Roentgenol*. 1983;140:319–324.
- Smith DK, Murray PM. Avulsion fractures of the volar aspect of triquetral bone of the wrist: a subtle sign of carpal ligament injury. *AJR Am J Roentgenol*. 1996;166(3):609–614.
- el-Noueam KI, Schweitzer ME, Blasbalg R, et al. Is a subset of wrist ganglia the sequela of internal derangements of the wrist joint? MR imaging findings. *Radiology*. 1999;212(2):537–540.
- Collert S, Isacson J. Chronic sclerosing osteomyelitis (Garre). *Clin Orthop*. 1982;164:136–140.
- Delaney TJ, Eswar S. Carpal coalitions. *J Hand Surg Am*. 1992;17:28–31.
- Marburger R, Burgess RC. Symptomatic lunate-triquetral coalition. *J South Orthop Assoc*. 1995;4:307–310.

52. Gelberman RH, Salamon PB, Jurist JM, Posch JL. Ulnar variance in Kienbock's disease. *J Bone Joint Surg Am.* 1975;57:674–676.
53. Gerwin M. The history of Kienbock's disease. *Hand Clin.* 1993;9:385–390.
54. Morgan RF, McCue FC III. Bilateral Kienbock's disease. *J Hand Surg Am.* 1983;8:928–932.
55. Cerezal L, del Piñal F, Abascal F, García-Valtuille R, Pereda T, Canga A. Imaging findings in ulnar-sided wrist impaction syndromes. *Radiographics.* 2002;22(1):105–121.
56. Jennin F, Bousson V, Parlier C, Jomaah N, Khanine V, Laredo JD. Bony sequestrum: a radiologic review. *Skeletal Radiol.* 2011;40:963–975.
57. Unni KK, Inwards CY. *Dahlin's Bone Tumors: General Aspects and Data on 10,165 Cases.* 6th ed. Philadelphia, PA: Lippincott Williams & Wilkins; 2010:103.
58. Sachs HK. The evolution of the radiologic lead line. *Radiology.* 1981;139:81–85.
59. Blickman JG, Wilkinson RH, Graef JW. The radiologic "lead band" revisited. *AJR Am J Roentgenol.* 1986;146:245–247.
60. Anderson SE, Steinbach LS, De Monaco D, Bonel HM, Hurtienne Y, Voegelin E. "Baby wrist": MRI of an overuse syndrome in mothers. *AJR Am J Roentgenol.* 2004;182(3):719–724.
61. Peterson JJ, Bancroft LW, Kransdorf MJ. Wooden foreign bodies: imaging appearance. *AJR Am J Roentgenol.* 2002;178:557–562.
62. Jacobson JA. *Fundamentals of Musculoskeletal Ultrasound.* Philadelphia, PA: Saunders/Elsevier; 2007.
63. Martinez-Lavin M, Matucci-Cerinic M, Jajic I, Pineda C. Hypertrophic osteoarthropathy: consensus on its definition, classification, assessment and diagnostic criteria. *J Rheumatol.* 1993;20:1386–1387.
64. Kurrock R, Cohen PR. Cutaneous paraneoplastic syndromes in solid tumors. *Am J Med.* 1995;99:662–671.
65. Nashitz JE, Rosner I, Rozenbaum M, Elias N, Yeshurun D. Cancer-associated rheumatic disorders: clues to occult neoplasia. *Semin Arthritis Rheum.* 1995;24:231–241.
66. Pineda C. Diagnostic imaging in hypertrophic osteoarthropathy. *Clin Exp Rheumatol.* 1992;10(suppl 7):27–33.
67. Taconis WK, Schutte HE, van der Heul RO. Desmoplastic fibroma of bone: a report of 18 cases. *Skeletal Radiol.* 1994;23:283–288.
68. Inwards CY, Unni KK, Beabout JW, Sim FH. Desmoplastic fibroma of bone. *Cancer.* 1991;68:1978–1983.
69. Murph JR. Rubella and syphilis: continuing causes of congenital infection in the 1990s. *Semin Pediatr Neurol.* 1994;1:26–35.
70. Lamberti PM, Light TR. Madelung deformity. eMedicine (10 Aug 2010). <http://emedicine.medscape.com/article/1260002-overview>.
71. Kim HK. Madelung deformity with Vickers ligament. *Pediatr Radiol.* 2009;39:1251.
72. Rampoldi M, Marsico S. Complications of volar plating of distal radius fractures. *Acta Orthop Belg.* 2007;73(6):714–719.
73. Hattori Y, Doi K, Sakamoto S, Yukata K. Delayed rupture of extensor digitorum communis tendon following volar plating of distal radius fracture. *Hand Surg.* 2008;13(3):183–185.
74. Sügün TS, Karabay N, Gürbüz Y, Ozaksar K, Toros T, Kayalar M. Screw prominences related to palmar locking plating of distal radius. *J Hand Surg Eur.* 2011;36(4):320–324.
75. Bruckner JD, Alexander AH, Lichtman DM. Acute dislocations of the distal radio-ulnar joint. *J Bone Joint Surg Am.* 1995;77:958–968.
76. Strehle J, Gerber C. Distal radioulnar joint function after Galeazzi fracture-dislocations treated by open reduction and internal plate fixation. *Clin Orthop.* 1993;293:240–245.
77. Imatani J, Hashizume H, Nishida K, Morito Y, Inoue H. The Galeazzi-equivalent lesion in children revisited. *J Hand Surg Br.* 1996;21:455–457.

CHAPTER

# 2

## **Elbow, Arm, and Shoulder**

**CLINICAL HISTORY** A 55-year-old woman who fell off a curb while trying to hail a taxi.



FIGURE 2.1A



FIGURE 2.1B



FIGURE 2.1C

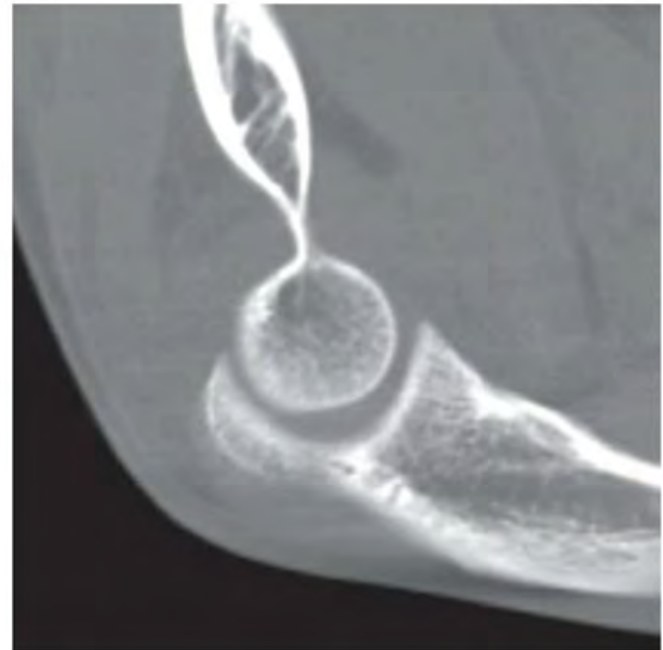


FIGURE 2.1D

**FINDINGS**

- A. Lateral radiograph shows elevated anterior and posterior fat pads, indicative of joint effusion. There is an intra-articular fracture of the radial head.
- B. Axial CT shows the fracture traversing the articular surface of the radial head.
- C. Sagittal CT reformation through the radiocapitellar joint shows slight depression of the radial head fragment.
- D. Sagittal CT reformation through the ulnar-trochlear joint shows the elevated anterior and posterior fat pads.

**DIFFERENTIAL DIAGNOSIS** None.

**DIAGNOSIS** Radial head fracture.

**DISCUSSION** The fat pad sign at the elbow indicates an elbow effusion. Distention of the elbow capsule by fluid lifts up the anterior and posterior fat pads at the superior

aspect of the elbow joint, displacing them from their normal positions and rendering them visible radiographically on the lateral view. The displaced anterior fat pad has been likened to a spinnaker sail, so the anterior fat pad is also called the “*spinnaker sail sign*.” A small portion of the anterior fat pad is normally visible as a thin, triangular radiolucency with a short base facing the elbow joint. The posterior fat pad is normally fully contained within the olecranon fossa and is not visible. In the setting of acute trauma, the fat pad sign is indicative of fracture, but an effusion from any cause may result in a fat pad sign. Radial head and neck fractures are sustained by younger adults during falls onto an outstretched hand, impacting the radial head against the capitellum. Two types of fractures result: the intra-articular radial head fracture, as in this case, and the radial neck fracture. Many radial head fractures may be treated by closed means or internal fixation, but comminuted displaced fractures have a high risk for osteonecrosis and resection with prosthetic implant may be performed [1].



FIGURE 2.2A



FIGURE 2.2B

**FINDINGS** (A, B) AP and lateral radiographs of the elbow demonstrate lateral dislocation of the radius and displaced fractures of the midshaft of the ulna.

**DIFFERENTIAL DIAGNOSIS** None.

**DIAGNOSIS** Monteggia fracture dislocation (Bado type III).

**DISCUSSION** A Monteggia fracture dislocation [2] is composed of a fracture of the ulna and a dislocation of the radial head. Various types are based on the site of the fracture and the associated direction of angulation and dislocation (Bado

classification). The types are as follows: (I) proximal ulnar fracture with anterior angulation and anterior dislocation of the radial head (65%); (II) proximal ulnar fracture with posterior angulation and posterior dislocation of the radial head (18%); (III) ulnar fracture just distal to coronoid process with lateral dislocation of the radial head (16%); and (IV) proximal ulnar fracture and fracture of the proximal radius distal to the bicipital tuberosity with anterior dislocation of the radial head (1%). This injury should be sought vigorously in adults with a demonstrated proximal ulnar shaft fracture. The radial head should intersect the capitellum on any view obtained. The radial nerve is damaged in 20% of cases, but most nerve injuries are transient.



FIGURE 2.3A



FIGURE 2.3B

**FINDINGS** (A, B) Lateral and oblique radiographs of the elbow. There is abnormal fusion of the proximal radius and ulna, with continuity of medullary space and cortical margins.

**DIFFERENTIAL DIAGNOSIS** None.

**DIAGNOSIS** Radioulnar synostosis.

**DISCUSSION** Two types of radioulnar synostosis have been described [3]. This is a case of “true” or proximal synostosis, where there is smooth fusion along a 2- to 6-cm length of the proximal radius and ulna. The other type is typified by congenital dislocation of the radial head. Both types result from a failure of longitudinal segmentation of the proximal forearm, leading to bony or fibrous synostosis. Both types of synostosis

may be bilateral in 60% of cases. Sporadic and familial forms are described, but sporadic forms are more common [4]. Associated findings include clubfoot deformities, developmental dysplasia of the hip, thumb hypoplasia, Madelung’s deformity, and other segmentation anomalies (including carpal coalition and symphalangism). Associated syndromes include arthrogryposis, multiple hereditary exostoses, and Holt-Oram syndrome, to mention a few. Acquired synostosis can result from trauma, osteomyelitis, or Caffey disease. Before the osseous bridge is obvious, careful observation for the lateral radial bowing or ulnar tethering may help make an early diagnosis. Although some cases may be treated surgically, a longitudinal study of the natural history of congenital proximal radioulnar synostosis showed that most patients had few or no functional limitations, and were often employed in jobs that demanded extensive use of the forearm [5].



FIGURE 2.4A



FIGURE 2.4B

**FINDINGS** (A, B) AP and lateral radiographs of the elbow. Posterior dislocation of the elbow is present, without fractures.

**DIFFERENTIAL DIAGNOSIS** None.

**DIAGNOSIS** Posterior elbow dislocation.

**DISCUSSION** The elbow is the most common site of dislocation in a skeletally immature patient and the third most common site of dislocation in an adult (after shoulder and interphalangeal dislocations). Acute dislocations of the elbow result from falls or sports-related mishaps, with the forces transmitted to a hyperextended elbow. Typically, the ulna dislocates posteriorly relative to the humerus, taking the radius with it. There

are frequently no associated fractures, although the coronoid process and radial head in an adult and medial epicondyle in a child should be scrutinized. In children, both the medial epicondyle and the median nerve can become entrapped, preventing a closed reduction. Although posterior elbow dislocations are the most common, dislocation in other directions may occur. There is a rare variant known as a divergent dislocation, in which the radius and ulna separate in different directions. Recurrent dislocations imply instability, usually attributed to rupture of the medial collateral ligaments, avulsion of the brachialis attachment, damage to the anterior capsule, or some combination. Complications associated with elbow dislocations include compromise of the brachial artery, damage to the median or ulnar nerves, and heterotopic ossification (most commonly in the brachialis muscle, anterior to the elbow).



FIGURE 2.5A



FIGURE 2.5B

**FINDINGS**

A, B. AP and oblique radiographs of the left elbow demonstrate subtle subluxation of the radius with respect to the capitellum. A line drawn through the short segment of the radial shaft that is proximal to the radial tuberosity should intersect the center of the capitellum on all radiographic projections, but in this case it does not.

**DIFFERENTIAL DIAGNOSIS** Subluxation of the radial head, dislocation of the radial head, normal.

**DIAGNOSIS** Radial head subluxation.

**DISCUSSION** Subluxation of the radial head (nursemaid's elbow, pulled elbow) is usually a temporary condition with spontaneous reduction. The usual history is a sudden pull on a forearm held in the pronated position, as might occur when a small child, who is being led by the hand by an adult, stumbles and falls. The adult will pull suddenly on the hand

and forearm to prevent the child from striking the ground. The radial head slips under the lax annular ligament. Some authors state that the radiographs are normal, whereas other authors note that there may be subtle signs that indicate subluxation. If the radial head does not intersect the capitellum on all views, it is subluxated or dislocated [6]. The method of reduction involves a combination of flexion and supination (usually against an unhappy, resisting child). A palpable click is felt when the radial head relocates into its normal position. Offering a lollipop to the child and noting the ease of motion at the elbow joint can test the success of the maneuver. Occasionally, the annular ligament can become entrapped and prevent reduction [7]. The orthopedist will cast the child who fails to reduce or has a recurrent subluxation. Isolated radial head dislocation is a rare occurrence, limited to children. One is obligated to search for an associated fracture. Hereditary causes of radial head dislocation exist in, for example, the nail-patella syndrome, but are even more unusual than isolated dislocations. Injuries similar to pulled elbow have been described in adults [8,9].

**CLINICAL HISTORY** A 5-year-old boy with elbow swelling. Radiographs at presentation and 4 months later.



FIGURE 2.6A



FIGURE 2.6B

## FINDINGS

- A. Oblique elbow radiograph at presentation reveals soft tissue swelling about the olecranon. Faint periosteal reaction is noted about the proximal olecranon metaphysis, and there is juxta-articular osteoporosis at the elbow joint.
- B. Oblique radiograph taken 4 months later demonstrates a marked increase in the periosteal reaction about the distal humerus and proximal ulna. Juxta-articular osteoporosis is still present and is most marked in the proximal olecranon.

**DIFFERENTIAL DIAGNOSIS** Septic joint, juvenile chronic arthritis, trauma, Lyme arthritis.

**DIAGNOSIS** Septic elbow joint.

**DISCUSSION** The recovery of an organism from the joint is the only reliable method for distinguishing a septic elbow joint from an aseptic joint. Examples of conditions associated with aseptic monoarticular inflammatory arthritis include rheumatic fever, hepatitis, and reactive arthritis. These immunologic entities commonly occur 2 to 3 weeks after the initial symptoms. Similarly, sterile synovitis can occur secondary to an

inflammatory process in the adjacent bone or bursa. Potential sources of infection include the blood, adjacent bones or soft tissues, and direct penetration (accidental or iatrogenic). The classic radiologic sequence of events is as follows: joint effusion and soft tissue swelling (edema and hypertrophy of synovium, with leaky membranes), osteoporosis (hyperemia), joint space loss (chondral loss from inflamed pannus), marginal and central erosions (osseous destruction from inflamed pannus), sclerotic host bone formation (periostitis in this case), and late bony ankylosis (either fibrous or true osseous ankylosis). Bacterial septic arthritis is usually due to *Staphylococcus aureus* or a streptococcus species. In children, *Haemophilus influenzae* is an important causative organism. Polyarticular involvement is usually secondary to encapsulated organisms such as pneumococcus or *H. influenzae*.

When septic arthritis is secondary to tuberculosis or fungi, the radiographic findings differ in that there is little or no reparative bone, and the process is more indolent in nature. The hips and knees are more commonly involved than the wrist and elbow. Complications include synovial cyst formation, soft tissue and tendon injury (especially rotator cuff rupture in the shoulder) or abscesses, osteomyelitis, ankylosis, overgrowth of epiphyses from regional hyperemia (if physes are still open), and osteoarthritis.

**CLINICAL HISTORY** A 70-year-old man with painful swelling over the elbow for several days.



FIGURE 2.7A

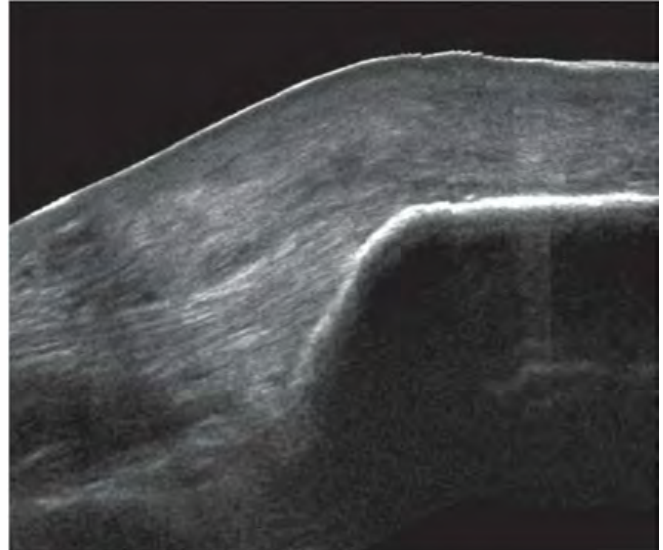


FIGURE 2.7B

### FINDINGS

- A. Lateral radiograph of the elbow shows focal soft tissue swelling over the olecranon process. There is no soft tissue calcification and there are no changes in the underlying bone.
- B. Longitudinal sonogram with the transducer over the region of swelling shows a collection with heterogeneous echotexture and small central anechoic region. There are no calcifications. Color Doppler (not shown) revealed internal flow.

**DIFFERENTIAL DIAGNOSIS** Olecranon bursitis, septic or nonseptic; rheumatoid arthritis.

**DIAGNOSIS** Septic olecranon bursitis.

**DISCUSSION** Olecranon bursitis is a common lesion [10]. Beyond location, the imaging appearance is nonspecific, and aspiration with culture and gram stain may be required for definitive diagnosis. However, patients with septic bursitis may have systemic features of infection and tend to present earlier and with more severe symptoms than patients with non-septic bursitis. If calcification is present, tophaceous gout is a strong consideration. Patients with rheumatoid arthritis are also predisposed to developing olecranon bursitis. Swelling of the olecranon bursa may also follow falls onto the elbow, and if accompanied by an open injury, infection may follow.



FIGURE 2.8A



FIGURE 2.8B

**FINDINGS** (A, B) AP and lateral elbow radiographs show extensive soft tissue ossification at the elbow, enveloping the elbow joint. Flexion and extension at the elbow joint are severely limited. The overlying surgical staples indicate sites of skin grafting.

**DIFFERENTIAL DIAGNOSIS** Posttraumatic changes, thermal injury, collagen vascular disease.

**DIAGNOSIS** Heterotopic ossification after burns.

**DISCUSSION** Thermal burns cause coagulative tissue necrosis. The depth of the injury is related to the severity and duration of the applied heat. Initially, one can see soft tissue loss and soft tissue edema. Osteoporosis (30% of cases) may be localized or diffuse, and is explained on the basis of hyperemia, reflex sympathetic response, or alteration in local

metabolism. Periostitis may also occur in the weeks that follow, and is thought to be secondary to a local periosteal irritation. Periarticular osseous excrescences, osteophytes, or soft tissue calcification or ossification (23% of cases) are common after extensive burns, and may be seen 2 to 3 months after injury [11,12]. They typically occur in adults along the preexisting connective tissue framework, most commonly around the elbow. The range of motion of involved joints will be limited mechanically. The exact pathogenesis of these ossifications is unknown and does not seem to correlate with the severity of the burn. The hyperemic response seen with burns can elicit bone growth. Contractures are most common about the elbow and within the hand. Articular abnormalities can be local or remote and result from hyperemia, compression, infection, or thermal injury. Differential considerations of ankylosis from heterotopic ossification include posttraumatic [13], neurogenic, and other etiologies [14].



FIGURE 2.9

**FINDINGS** Lateral elbow radiograph. Anterior and posterior fat pad signs are prominent. There is slight posterior angulation of the distal humerus. A line drawn along the anterior cortex of the humerus (anterior humeral line) should intersect the capitellum in its posterior third, but in this case, the line intersects the capitellum in its anterior third. An actual fracture line is not visible on this radiograph.

**DIFFERENTIAL DIAGNOSIS** None.

**DIAGNOSIS** Supracondylar fracture.

**DISCUSSION** The fat pad sign is the clue to the presence of a fracture about the elbow. More than 90% of children or adolescents with a posterior fat pad sign will have a demonstrable

fracture, and absence of the fat pad sign in these age groups virtually excludes an intra-articular fracture, unless the injury is so severe that there is disruption of the elbow joint capsule. The supracondylar fracture constitutes 60% of fractures around the elbow in children. Radial head and neck fractures, common in adults, are generally not seen in children. Supracondylar fractures occur with hyperextension of the elbow, usually from a fall. The fracture extends transversely across the distal humerus through the coronoid and olecranon fossae, above the level of the condyles. The distal fragment is angulated posteriorly, so that the anterior humeral line passes anterior to the capitellum. A posterior fat pad sign is almost always present. The fracture is usually complete, but greenstick fractures, torus fractures, or plastic bowing are possible. The typical treatment is closed reduction with casting.

**CLINICAL HISTORY** An 8-year-old little league pitcher with right elbow pain. Radiographs of right and left elbows.



FIGURE 2.10A



FIGURE 2.10B

### FINDINGS

- A. AP radiograph of the right elbow (symptomatic). There is an irregular horizontal lucent defect through the ossification center of the capitellum.
- B. Radiograph of the left elbow (asymptomatic) is normal.

**DIFFERENTIAL DIAGNOSIS** Osteochondrosis of the capitellum, osteochondritis dissecans, acute trauma.

**DIAGNOSIS** Osteochondrosis of the capitellum.

**DISCUSSION** Osteochondrosis of the capitellum, or Panner disease, is better known as “little leaguer’s elbow.” The condition is an osteochondrosis of the humeral capitellum that is seen principally in boys between the ages of 5 and 10 years. An osteochondrosis is a general term that has come to refer to the condition resulting from ischemia of a growing epiphysis. The capitellum is the rounded protuberance at the distal humerus that articulates with the proximal radius and is covered with articular cartilage. The blood supply enters from

its posterior aspect and is vulnerable to traumatic disruption by indirect repetitive valgus stress or direct compression, sometimes leading to vascular compromise. Although most lesions revascularize and heal without consequence, deformity, bony resorption, or frank fragmentation of the capitellum may occur. Pain and stiffness may limit full extension of the elbow, and a commonly associated clinical finding is joint swelling from effusion and/or synovial hypertrophy. Radiographic findings at the capitellum include the crescentic fissure through the ossification center (as noted in this case), increased density, decreased size, resorption, or frank fragmentation. Hyperemia may lead to premature maturation of the radial head. Unilateral involvement is noted in the throwing arm of little league baseball players, and the condition has also been noted in gymnasts. The main differential consideration is osteochondritis dissecans, a traumatic osteochondral injury seen in an older age group, after the capitellum has essentially stopped growing [15]. Computed tomography (CT) or magnetic resonance imaging (MRI) may be helpful when there is a question of fragmentation.



FIGURE 2.11A



FIGURE 2.11B

**FINDINGS**

- A. AP elbow radiograph shows that the medial epicondyle has been avulsed from the distal humerus, with the fracture plane passing through the apophyseal plate. Soft tissue swelling is present at the site.
- B. Lateral elbow radiograph does not show a fat pad sign.

**DIFFERENTIAL DIAGNOSIS** None.

**DIAGNOSIS** Medial epicondyle avulsion fracture (Salter type I).

**DISCUSSION** The medial epicondylar ossification center appears around the age of 5 years. It is the site of origin of

the common tendon of the flexor pronator muscle group, and can be avulsed by muscular contraction. This often results in a fracture fragment that is displaced distally or anteriorly. Medial epicondylar injuries are usually seen in the 5-to-15-year age group; after the medial epicondyle fuses in late adolescence, this injury no longer occurs. Medial epicondylar injuries are far more common than lateral epicondyle injuries. An important association to recognize with medial epicondylar injury is damage to the ulnar nerve as it passes the elbow. Injury of the ulnar nerve may result in motor weakness of the flexor carpi ulnaris, flexor digitorum profundus muscle of the fourth and fifth fingers, and intrinsic hand muscles of the fourth and fifth digits, as well as sensory deficits of the fourth and fifth fingers.



FIGURE 2.12A



FIGURE 2.12B

**FINDINGS** (A, B) AP and lateral elbow radiographs. The medial epicondyle has been avulsed from the distal humerus during posterior dislocation of the elbow. The fracture plane passes through the apophyseal plate, and the fragment has interposed itself between the trochlea and ulna, preventing reduction of the dislocation.

**DIFFERENTIAL DIAGNOSIS** None.

**DIAGNOSIS** Posterior elbow dislocation with entrapped medial epicondyle.

**DISCUSSION** Dislocation of the elbow may separate the medial epicondyle from the distal humerus by stress applied

through the medial ulnar collateral ligament (UCL). The medial epicondylar fragment may then become entrapped in the elbow joint as it opens with valgus stress, requiring surgical reduction. For review, the order of ossification of the epiphyses and apophyses of the elbow can be remembered by the mnemonic CRITOE: Capitellum (less than 1 year), Radial head (5 years), Internal humeral epicondyle (7 years), Trochlea (10 years), Olecranon (10 years), and External humeral epicondyle (12 years). The age at which these centers begin to ossify is variable, but the order in which they close is generally not.

**CLINICAL HISTORY** A 57-year-old woman with pain at the lateral aspect of the elbow.

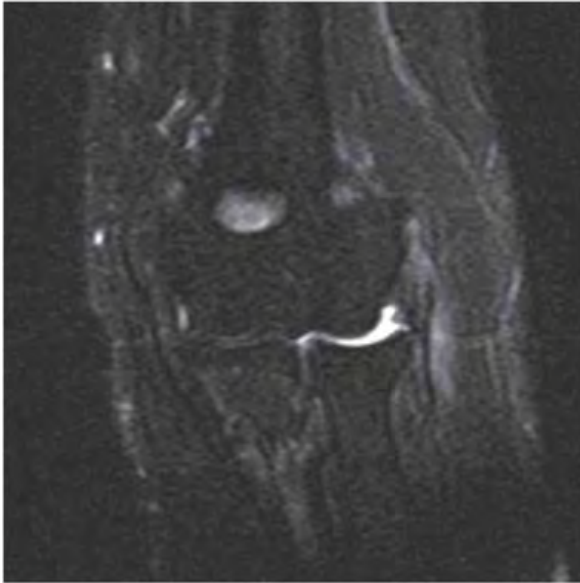


FIGURE 2.13A



FIGURE 2.13B

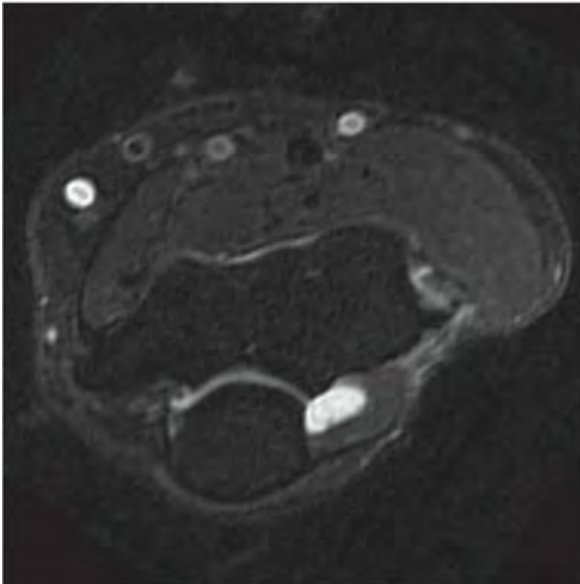


FIGURE 2.13C

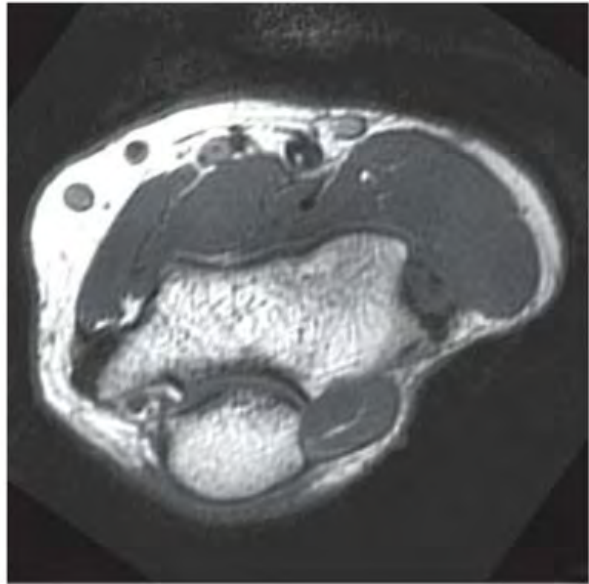


FIGURE 2.13D

**FINDINGS** Coronal (A) and axial (C) T2-weighted fat-suppressed and coronal (B) and axial (D) T1-weighted MRI of the elbow show increased signal and thickening within the normally very low signal intensity common extensor tendon.

**DIFFERENTIAL DIAGNOSIS** Common extensor tendon full-thickness tear, lateral epicondylitis.

**DIAGNOSIS** Lateral epicondylitis.

**DISCUSSION** Lateral epicondylitis presents as lateral elbow pain that has an insidious onset, beginning gradually after vigorous activity and progressing to pain with activity.

Radiographs are frequently normal, although some patients may have evidence of a spur at the lateral epicondyle or calcification of the common extensor tendon. MRI is useful in assessing the degree of tendon damage and associated ligament abnormality. Increased T1-weighted and T2-weighted signal is seen within the tendon with epicondylitis. The tendon is usually thickened, and edema can be present in the adjacent soft tissues. Using both the axial and coronal planes is helpful in assessing these lateral tendons. Additionally, MRI is useful in evaluating additional structures that may explain the lack of response to therapy (e.g., ligamentous injury) [16]. Ultrasonography may also be used to assess for epicondylitis, although it has been found to be less specific than MRI [17].

**CLINICAL HISTORY** A 21-year-old college baseball player with medial elbow pain.

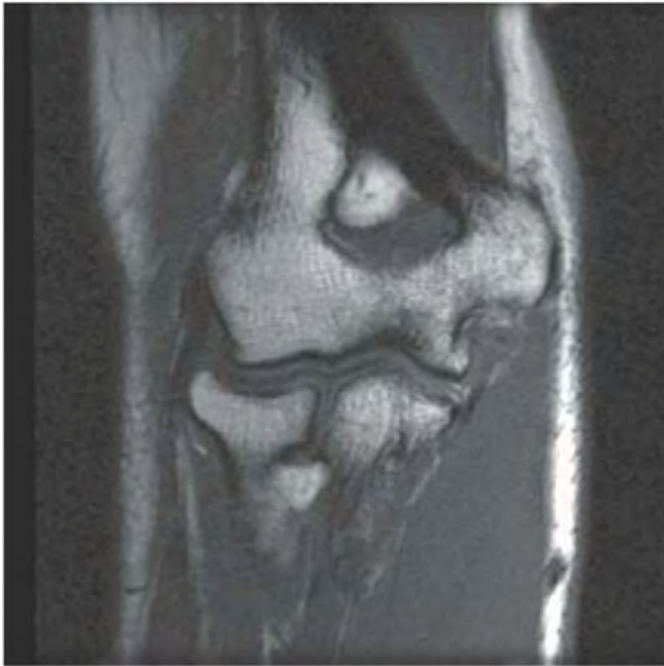


FIGURE 2.14A

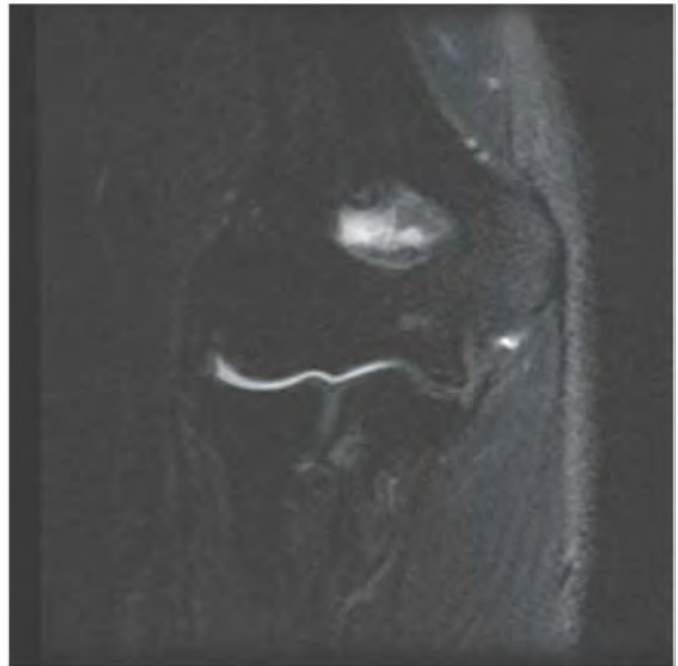


FIGURE 2.14B

### FINDINGS

- A. Coronal T1-weighted MRI shows globular signal isointense to muscle at the expected humeral origin of the UCL. The distal portion of the ligament may be seen as a dark, linear structure attaching to the ulna. The overlying common flexor tendon origin is intact at the medial epicondyle.
- B. Coronal T2-weighted fat-suppressed MRI shows high signal where the UCL is torn at its proximal origin.

**DIFFERENTIAL DIAGNOSIS** UCL tear, medial epicondylitis.

**DIAGNOSIS** UCL tear.

**DISCUSSION** The ulnar collateral ligament (UCL, also called medial collateral ligament) originates from the inferior

aspect of the medial epicondyle, deep to the common flexor tendon origin, and does not have an attachment to the adjacent medial condyle. The UCL has an important anterior band that inserts at the sublime tubercle at the medial aspect of the coronoid process and a clinically less important posterior band that inserts along the supinator crest at the lateral aspect of the ulna. Tears of the UCL typically result from repetitive valgus stress, as may occur with pitching a baseball overhand, and may involve the proximal origin, the mid-substance, or the distal insertion. Avulsion fractures of the sublime tubercle may occur through the same mechanism. A tear of the UCL is a much more common injury than medial epicondylitis.

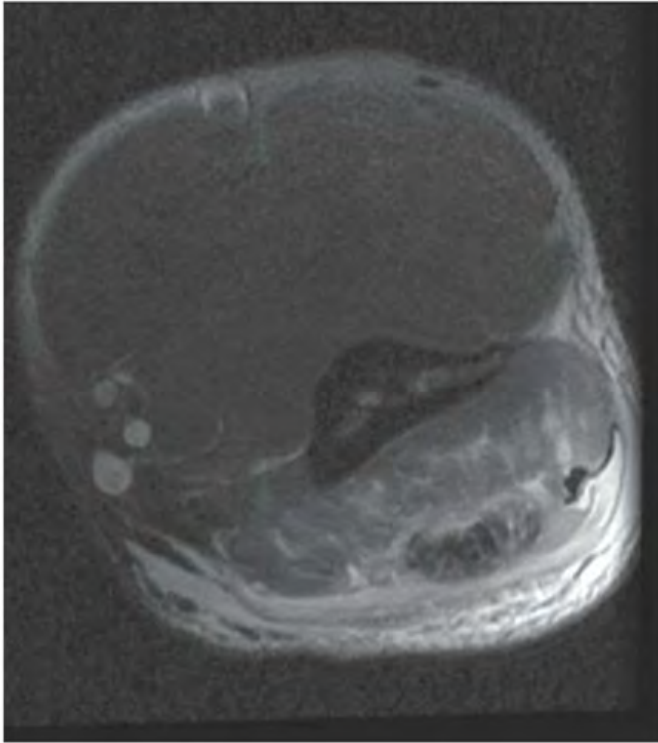


FIGURE 2.15A



FIGURE 2.15B

**FINDINGS**

- A. Axial proton-density fat-suppressed MRI shows high signal in the triceps compartment, corresponding to edema and hemorrhage in and around the posterior aspect of the muscle. The triceps tendon is thickened and has high signal within it.
- B. Sagittal T2-weighted fat-suppressed MRI shows retraction of the triceps tendon, and surrounding edema and hemorrhage. The muscular portion of the triceps insertion has some high signal, but is not detached. Hemorrhage also involves olecranon bursa, with a hematocrit effect.

**DIFFERENTIAL DIAGNOSIS** None.

**DIAGNOSIS** Triceps tendon tear with olecranon bursa hemorrhage.

**DISCUSSION** Triceps tendon ruptures are uncommon injuries caused by decelerating counterforce during active extension of the elbow. These injuries are seen mostly in participants of sports that require upper body strength training. Although tears at the musculotendinous junction may occur, in most cases there is a catastrophic failure at the distal insertion. Distal triceps tears are frequently associated with avulsion fractures at the olecranon. On MRI, the detachment of the tendon can be seen directly, with proximal retraction that is best demonstrated on sagittal images. Surrounding hemorrhage and edema will be seen in acute injuries, but clinical diagnosis in the acute phase may be challenging, and many patients will not be imaged until the injuries are subacute or chronic. Treatment in most cases will be surgical repair.

**CLINICAL HISTORY** A 45-year-old woman with elbow pain following a fall.



FIGURE 2.16A

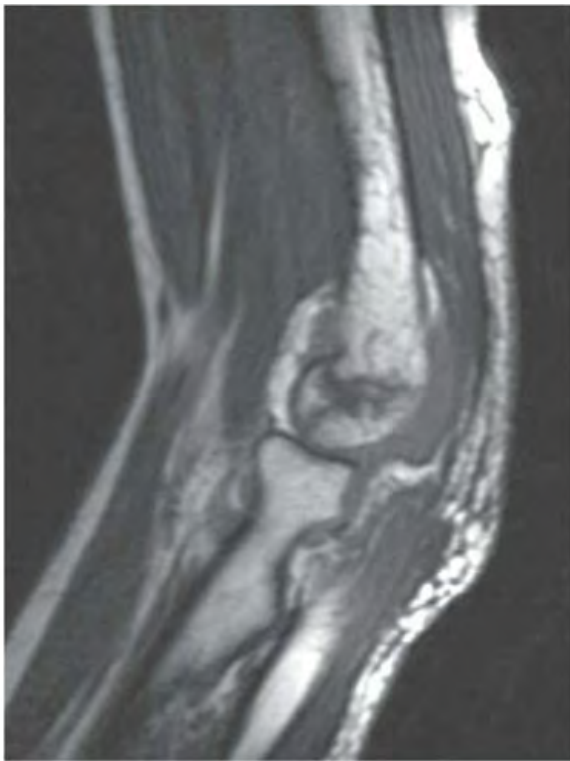


FIGURE 2.16B

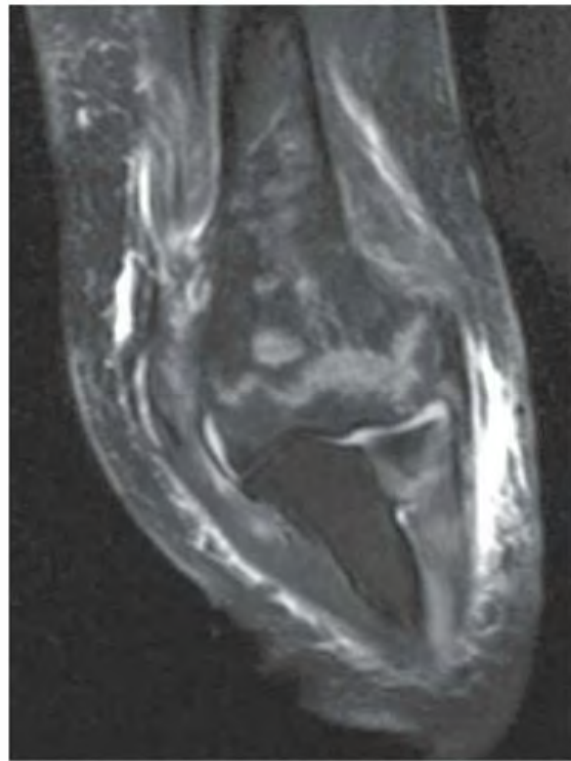


FIGURE 2.16C

**FINDINGS**

- A. Lateral radiograph of the elbow shows anterior and posterior fat pad signs. No fracture was visualized on the AP and oblique views.
- B. Sagittal T1-weighted MRI shows a complex intra-articular fracture involving the capitellum. An effusion lifting up the posterior fat pad can be seen.
- C. Coronal T2-weighted fat-saturated MRI shows a jagged fracture line traversing the distal humerus, from epicondyle to epicondyle.

**DIFFERENTIAL DIAGNOSIS** None.

**DIAGNOSIS** Occult distal humerus fracture.

**DISCUSSION** The value of the fat pad sign in identifying patients with elbow fractures has been proven time and

again, but it is not perfect. In a recent study, 20 adult elbow trauma cases, with positive fat pad signs but no identified fractures, underwent MRI scans within 0 to 12 days [18]. The authors found that 75% of their patients had identifiable fractures, mostly involving the radial head, but they also noted that actual management was not changed by the additional information in any of the cases. The issues raised by studies like this have been discussed in an editorial by Rogers [19]. If the cost and convenience of MRI in the acute setting were the same as that of radiography, it would clearly be the diagnostic modality of choice, and although management might not change, the diagnostic certainty would have some value to patients and their families, physicians and other providers, insurance companies and other payors, and so forth. Thus, Rogers argues that cost and convenience are the true barriers to the better diagnosis of musculoskeletal trauma.

**CLINICAL HISTORY** A 75-year-old man with injury sustained while pulling cactus out of his yard.

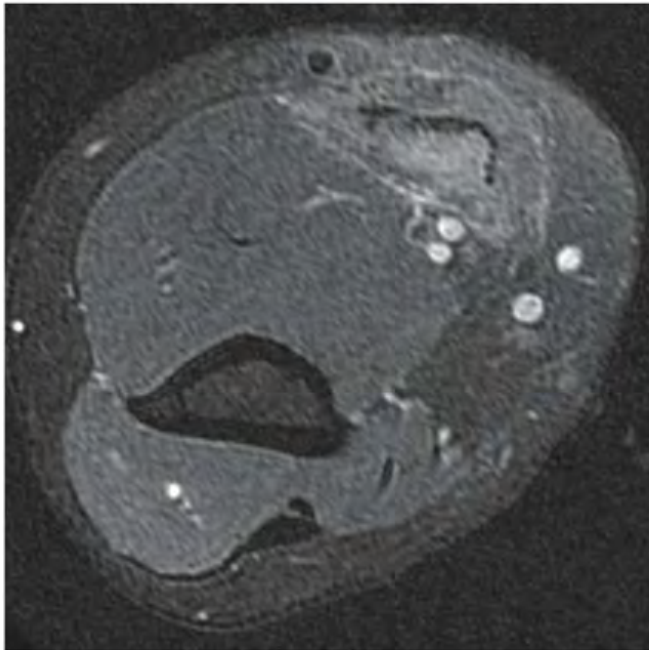


FIGURE 2.17A

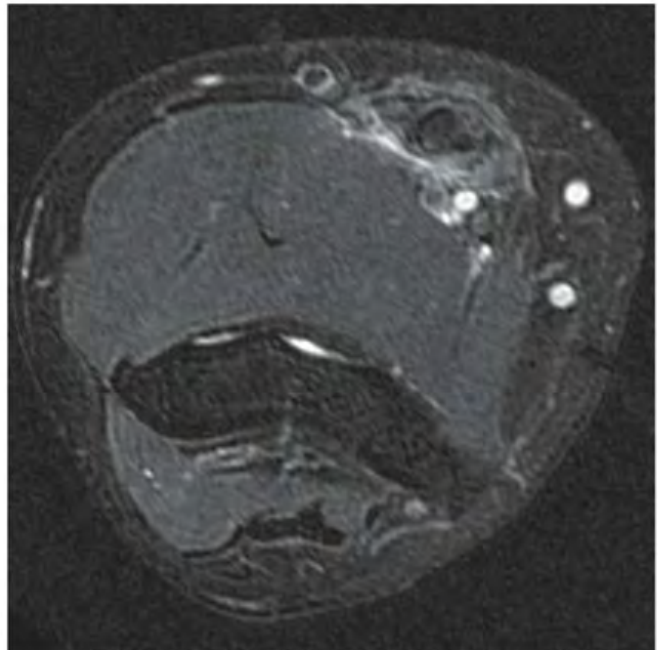


FIGURE 2.17B

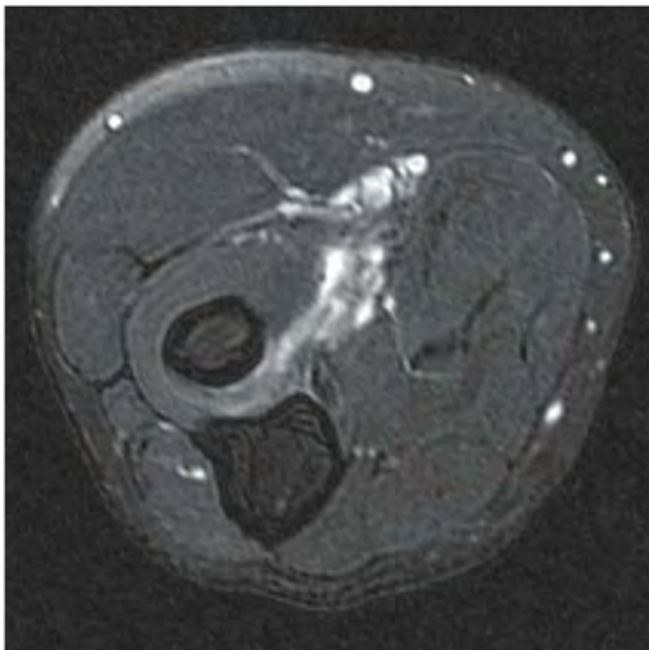


FIGURE 2.17C

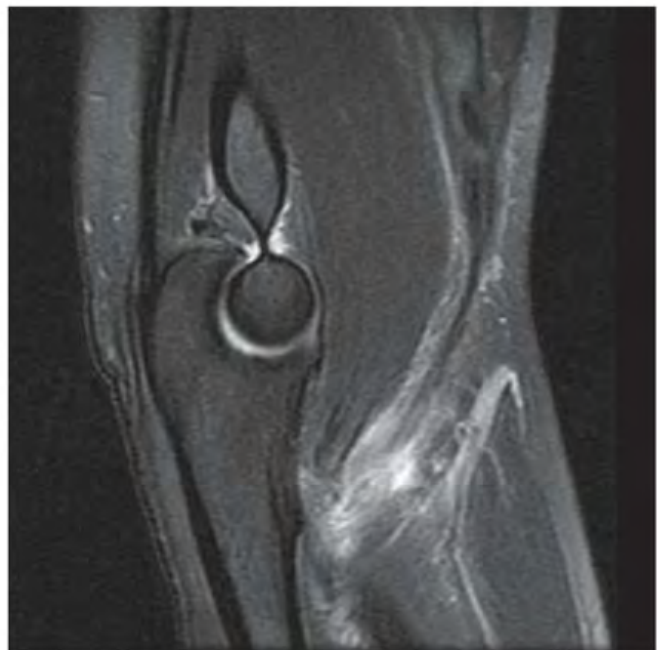


FIGURE 2.17D

**FINDINGS**

- A. Axial STIR MRI at the level of the distal humeral shaft shows swelling of the biceps muscle with high signal in the muscle and tendon.
- B. Axial STIR MRI at the level of the humeral condyles shows a retracted biceps tendon with thickening and high signal.
- C. Axial STIR MRI at the level of the bicipital tuberosity of the radius shows absence of the biceps tendon with high signal tracking along its expected course.
- D. Sagittal proton density MRI with fat-suppression shows the retracted biceps tendon and muscle belly.

**DIFFERENTIAL DIAGNOSIS** High-grade partial-thickness or full-thickness tear of the biceps tendon.

**DIAGNOSIS** Complete biceps tendon rupture.

**DISCUSSION** Biceps tendon tears occur during flexion against strong resistance. These are most commonly seen in

the dominant arm of middle-aged males who smoke tobacco [20]. The complete tear typically occurs at its insertion at the bicipital tuberosity of the proximal radius. In complete tears, proximal retraction of the tendon by muscle action results in a mass or bulbous swelling of the proximal arm; swelling at the distal arm may be minimal because of the tense antecubital fascia. Degenerative thickening of the biceps tendon may be present. MRI of complete biceps tendon ruptures will always show the absence of the tendon distally and nearly always shows a fluid-filled tendon sheath. Less common findings include an antecubital fossa mass, muscle edema, and atrophy [21]. Partial tears show high signal intensity within the tendon, fluid in the biceps tendon sheath, and thinning or thickening of the distal tendon, but the tendon will remain in continuity with its insertion. Biceps tendon ruptures are treated surgically, but some loss of function, particularly with activities requiring repetitive supination, is common [22].

**CLINICAL HISTORY** A 45-year-old woman with progressive difficulty in rotating her shoulder after an injury. She had previously undergone surgical repair of her rotator cuff.

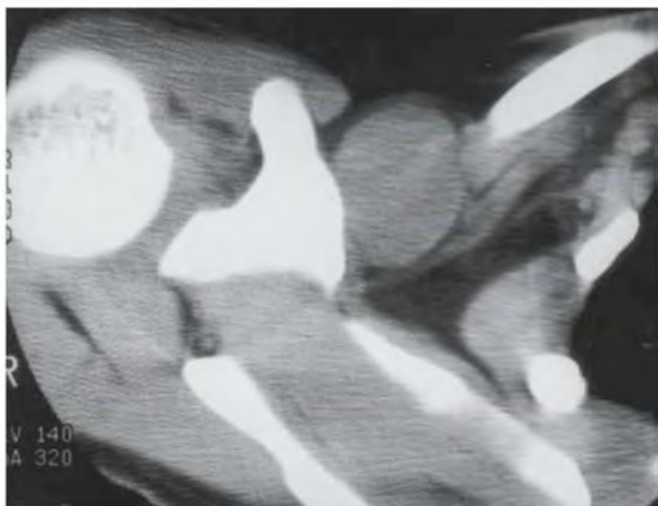


FIGURE 2.18A



FIGURE 2.18B

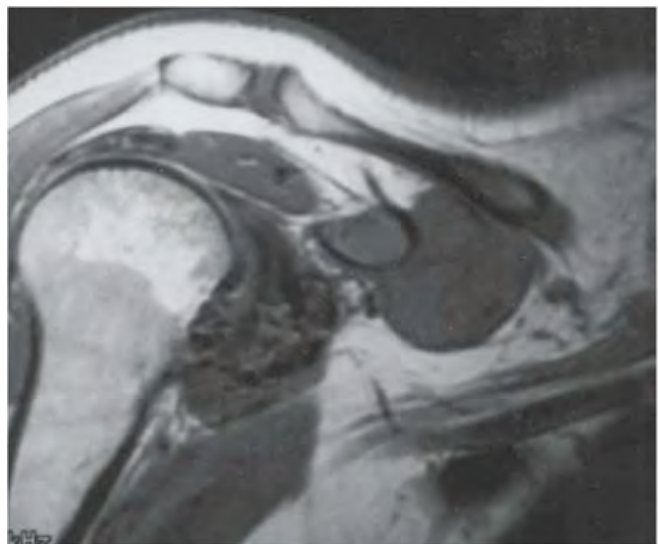


FIGURE 2.18C

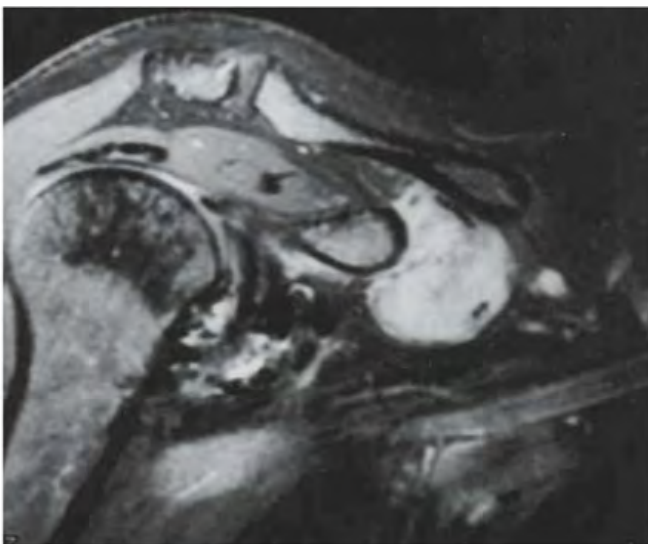


FIGURE 2.18D

**FINDINGS**

- A. Axial CT scan (soft tissue windows) shows a globular 3-cm mass, isodense to muscle, in the infraclavicular region, medial to the coracoid process. The lesion is not calcified.
- B. Axial T2-weighted MRI demonstrates the rounded lesion located medial to the coracoid process and inferior to the clavicle. The lesion has high signal intensity.
- C, D. Coronal T1-weighted MRI before and after intravenous injection of gadolinium shows avid enhancement in the lesion. The abnormal appearance of the epiphysis is related to prior surgery.

**DIFFERENTIAL DIAGNOSIS** Ganglion cyst, fibromatosis, postsurgical scarring, soft tissue sarcoma.

**DIAGNOSIS** Fibromatosis (extra-abdominal desmoid tumor).

**DISCUSSION** Fibromatosis is a neoplastic process that arises in fascial and musculoaponeurotic coverings, sometimes at a site of previous trauma or surgery [23]. Described initially in the abdominal wall, it is commonly divided into

superficial and deep forms [24]. Deep forms include extra-abdominal, abdominal, and intra-abdominal, which refer to their location relative to the abdominal wall. The extra-abdominal form of deep fibromatosis is of concern in this case. The age of peak incidence is between 25 and 35 years, and there is no clear sex predominance. The tumors are usually solitary, but as many as 15% of patients have synchronous multicentric lesions in the same extremity. Commonly involved sites include the shoulder area, upper arm, thigh, neck, pelvis, forearm, and popliteal fossa, in decreasing order of prevalence. Fibromatosis is nonencapsulated and has an infiltrative growth pattern that may be locally invasive. Lesions may grow to large size and become adherent to adjacent structures such as bone or neurovascular bundles. Fibromatosis is composed of well-differentiated fibroblasts embedded in an abundant collagenous matrix. Because of variable degrees of cellularity, matrix water content, and infiltration, attenuation on CT scans and signal intensity on MRI may be variable [25]. Enhancement may be heterogeneous. Associated osseous findings can include periostitis and pressure erosion. Treatment is surgical resection, but local recurrence is frequent unless wide margins can be obtained.

**CLINICAL HISTORY** *An 11-year-old boy with lumpy arm.*



FIGURE 2.19A



FIGURE 2.19B

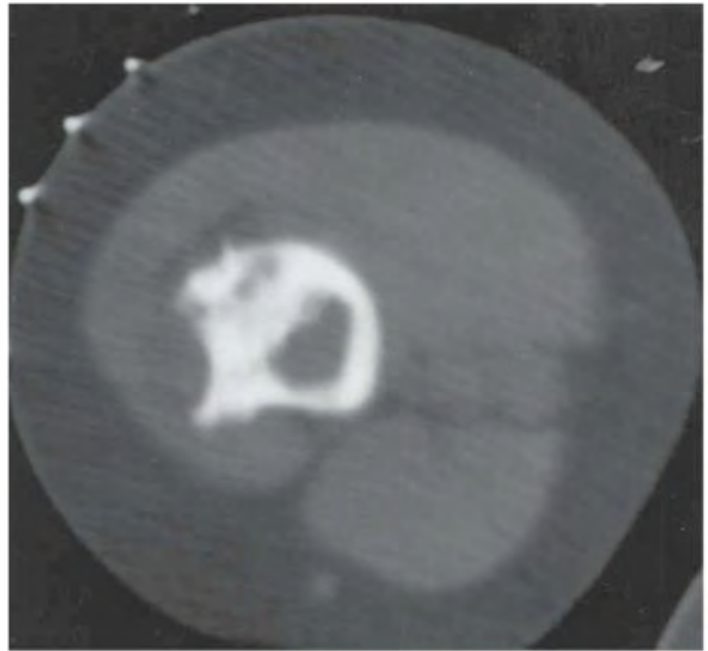


FIGURE 2.19C

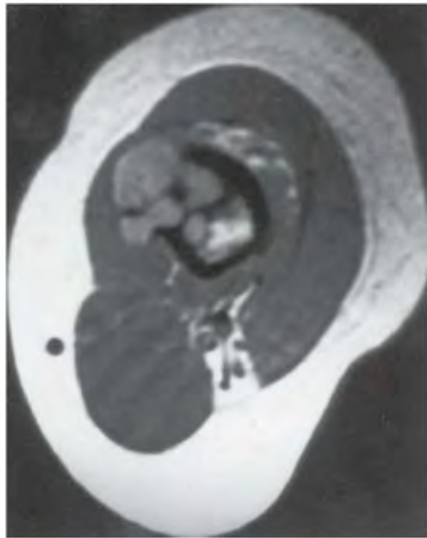


FIGURE 2.19D

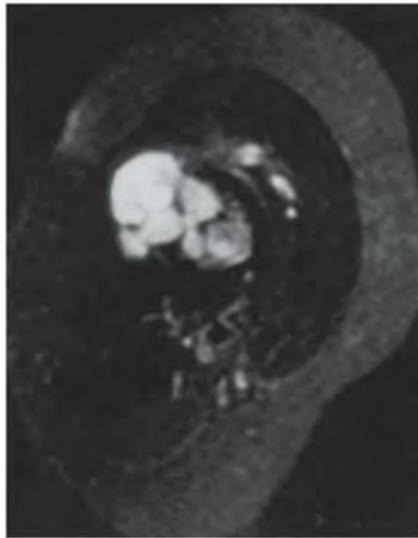


FIGURE 2.19E

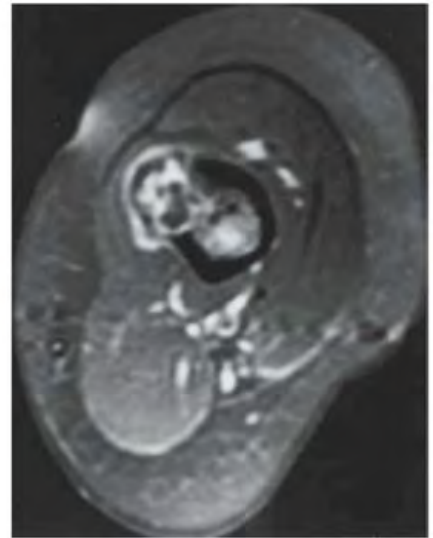


FIGURE 2.19F

## FINDINGS

- A, B. AP and lateral radiographs demonstrate a cortically based lesion at the humeral diaphysis. The lesion involves the posterolateral cortex and is characterized by lobulated lucency surrounded by thickened cortex.
- C. Axial CT image shows the marked cortical thickening associated with the sessile, cortically based lesion. A lower-density soft tissue component surrounds the thickened cortex.
- D, E. Axial T1-weighted and axial T2-weighted MRI shows T1 hypointensity and T2 hyperintensity within the lobules of the lesion. The bulk of the lesion is on the cortical surface, but a portion of it projects into the medullary space.
- F. Axial T1-weighted MRI obtained after gadolinium injection shows enhancement of portions of the lesion.

**DIFFERENTIAL DIAGNOSIS** Juxtacortical (periosteal) chondroma, chondrosarcoma, osteochondroma, surface osteosarcoma, posttraumatic deformity, aneurysmal bone cyst.

**DIAGNOSIS** Juxtacortical chondroma.

**DISCUSSION** Juxtacortical (periosteal) chondroma is a benign, cortically based cartilage lesion that is similar to an enchondroma except for its location on the surface of bone [26]. The lesions consist of mature cartilage, and they are

covered with periosteum. On pathologic examination, juxtacortical chondroma can be more cellular than enchondroma and contain double-nucleated chondrocytes, which can lead to a diagnosis of a low-grade chondrosarcoma if the findings are not correlated with the benign radiologic appearance [27]. Most lesions are found in adolescents or young adults, with a male predominance [28]. The most common sites are the proximal humerus and femur, with two-thirds of lesions involving the metaphysis and the remainder involving the diaphysis. The presenting symptom is usually pain and/or swelling, but many juxtacortical chondromas are discovered incidentally on radiographs obtained for other reasons. The radiographic appearance of a calcified soft tissue mass eroding the associated cortex is classic. Solid periosteal bone formation at the margins of the lesion may produce buttresses and form a cup-like appearance. Calcification of matrix is seen in only one-half of cases and, therefore, need not be present for the diagnosis. Markedly elongated lesions with irregular cortical thickening are not atypical. Reactive medullary sclerosis and periostitis can be identified, and do not necessarily imply malignant degeneration or pathologic fracture; these features are probably a response to the peripheral vascularity. MRI is useful to show the lobulated morphology and T2 hyperintensity that is characteristic of chondroid lesions. Size greater than 4 cm, medullary involvement, cortical destruction, and an associated soft tissue mass are features suggestive of chondrosarcoma. Treatment is surgical, and lesions should not recur.



FIGURE 2.20A



FIGURE 2.20B



FIGURE 2.20C

**FINDINGS**

- A, B. AP (A) and axillary (B) radiographs of the left shoulder show a large mass in the left lung apex, and a lytic lesion in the midhumeral shaft. The humeral lesion is centered in the cortex and has provoked little, if any, reactive bone formation. Incidental degenerative changes at the glenohumeral joint are advanced.
- C. Radionuclide bone scan demonstrates abnormal radiotracer uptake within the midshaft of the left humerus, right iliac crest, and right acetabulum, which is suspicious for bone metastasis. Increased uptake within the shoulder joints is related to osteoarthritis.

**DIFFERENTIAL DIAGNOSIS** Metastases, myeloma, lymphoma.

**DIAGNOSIS** Lung cancer metastasis, with pathologic fracture.

**DISCUSSION** Pathologic fractures through bones involved by metastases are common. The most common sites of pathologic fracture are the vertebral bodies, ribs, proximal

femur, and proximal humerus. Metastases of lytic, blastic, and mixed radiographic appearance all cause weakening of the bone.

In the long bones, destructive lesions with full-thickness cortical penetration lead to pathologic fractures. Gaps in the cortex weaken the bone by causing uneven and aberrant distribution of the stresses of loading, impeding the normal biomechanical dispersion of force. Weakening is gradual as cortical bone is infiltrated, eroded, and destroyed. Blastic lesions also destroy cortex, and the reactive and the stromal bone that gives blastic lesions their radiodensity is structurally unsound. The bone may fracture under the stresses of normal activity. Cortical weakening makes bone most vulnerable to tensile forces; therefore, in the long bones, pathologic fractures are usually transverse. The onset of pain at a site of metastatic involvement may indicate the presence of microfractures in a weakened cortex. Median survival after discovery of a pathologic fracture through an osseous metastasis is only about 18 months (combined for all primary sites).



FIGURE 2.21A



FIGURE 2.21B

**FINDINGS** AP radiograph of the humerus (A, B). There is a pathologic fracture through a lucent lesion in the metadiaphysis of the humerus. The lesion has a faintly sclerotic border and is centrally located.

**DIFFERENTIAL DIAGNOSIS** Simple bone cyst, aneurysmal bone cyst, fibrous dysplasia.

**DIAGNOSIS** Simple bone cyst, with pathologic fracture.

**DISCUSSION** The pathogenesis of a simple bone cyst is not known; the most favored theory is that it results from venous obstruction. Boys are affected more than twice as frequently as girls. Cysts are typically noted in the metaphysis of long bones before the age of 20, and in the pelvis or calcaneus thereafter. Eighty-five percent of humeral or femoral cysts are noted in the proximal metaphysis. Diaphyseal involvement is identified in 4% to 12% of the long bone lesions. Although some authors consider the diaphyseal lesions to be latent, having grown away from the growth plate, an age of less than 10 years is more predictive of a higher recurrence rate (i.e., activity) than is location within bone. Other poor prognostic factors include large size and large numbers of loculations [29]. Simple bone cysts tend to be geographic lucent lesions

with a central location, mild cortical thinning, and gentle expansion. In addition, the lesion tends to elongate along the long axis of the bone. CT or MRI may show fluid-fluid levels, septations not seen on radiography, soft tissue changes, and nodular enhancement [30]. A fallen-fragment sign is diagnostic of this entity, but it is reported in only 20% of patients who present with pathologic fractures, and only in those with open physes [31]. The fallen fragment results from a pathologic fracture of the cyst wall, with displacement of a fragment into the cyst itself. Change of position of the fragment within the lesion to the dependent portion indicates that the cyst is fluid-filled rather than solid. A variant of the fallen fragment is the trapdoor fragment, in which a periosteal hinge keeps the fragment from falling dependently, but allows it to change position with the patient. Traumatic transformation to aneurysmal bone cyst has been reported [32]. Differential diagnostic considerations in the metaphysis include enchondroma, fibrous lesions, and aneurysmal bone cyst. In the diaphysis, the appearance can be similar to fibrous dysplasia, eosinophilic granuloma, and chondromyxoid fibroma. In the calcaneus, intraosseous lipoma or pseudocyst from rarefied trabeculae should be considered. Complications of simple bone cysts are related to fractures and resultant deformities and/or growth disturbances. Bone cysts have no malignant potential.

**CLINICAL HISTORY** *An 86-year-old man with right shoulder pain.*



FIGURE 2.22A



FIGURE 2.22B

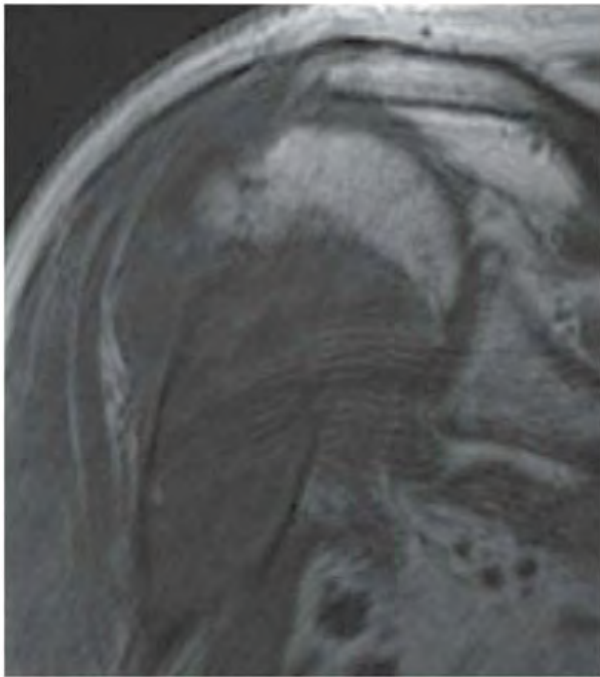


FIGURE 2.22C



FIGURE 2.22D

## FINDINGS

- A. Magnified portion of posteroanterior (PA) chest radiograph 6 years prior to presentation shows a chondroid matrix lesion in the proximal humerus.
- B. AP shoulder radiograph shows destruction of the medial aspect of the humeral neck, and calcifications with a rings-and-arcs configuration.
- C, D. Coronal oblique T1-weighted and T2-weighted fat-suppressed MRI shows a heterogeneous mass involving the entire medullary space, eroding through the medial bone cortex and extending into the shoulder joint.

**DIFFERENTIAL DIAGNOSIS** Chondrosarcoma, metastasis, lymphoma, malignant fibrous histiocytoma.

**DIAGNOSIS** Chondrosarcoma.

**DISCUSSION** In this case, the patient had what appeared to be either an enchondroma or low-grade chondrosarcoma for many years prior to presentation. Malignant transformation of an enchondroma into a chondrosarcoma is rare. Pain is the most suggestive symptom for chondrosarcoma in a

lesion with cartilaginous calcification. Typical worrisome radiographic features of chondrosarcoma include prominent endosteal scalloping, any degree of cortical thickening or cortical destruction, or an area of lucency in an otherwise mineralized lesion. Associated soft tissue masses are noted more commonly in the flat bones or peripheral lesions. Sixty to seventy percent of the time, the tumor contains punctate or flocculent calcification, and ring-shaped ossification characteristic of cartilage tissue. The lucent appearance is due to replacement of normal bone by noncalcified cartilage. On CT, the nonmineralized regions have a myxoid appearance, with attenuation in the range of 10 to 30 Hounsfield units; a high proportion of myxoid material is correlated with a higher histologic grade. On MRI, these regions have very high signal intensity on T2-weighted images and variable signal on T1-weighted images. A lobular growth pattern is often evident on CT or MRI and is characteristic of this entity. The bone scan will show increased tracer accumulation. The treatment of chondrosarcoma is surgical. The incidence of metastasis and the prognosis are related to the histologic grade, with 10-year survival ranging from 85% for low-grade lesions to 28% for high-grade lesions. Recurrent lesions will be of a higher grade 10% of the time.

**CLINICAL HISTORY** An 11-year-old boy with shoulder pain and swelling.



FIGURE 2.23A

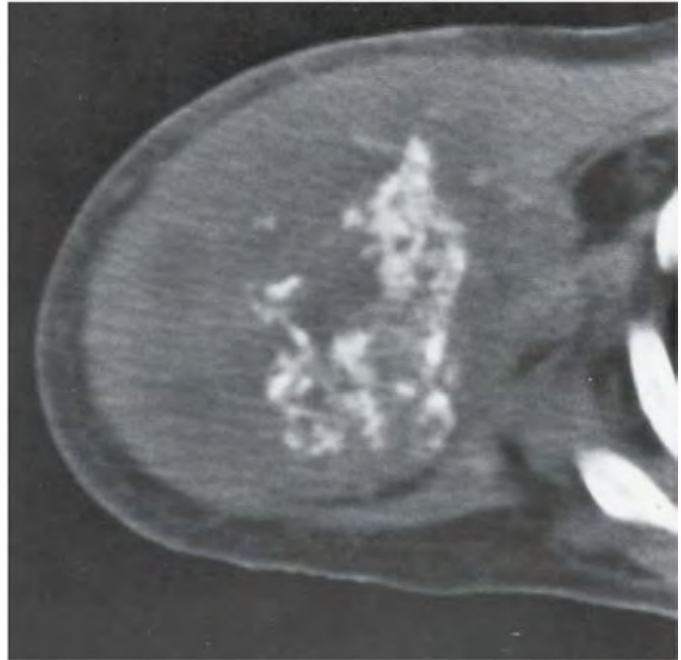


FIGURE 2.23B

### FINDINGS

- A. AP radiograph of the right shoulder shows an expansile, destructive lesion in the proximal humerus with cortical penetration (blow-out). Focal regions of sclerosis are present. The lesion does not appear to cross the growth plate.
- B. CT at the level of the central portion of the lesion shows the circumferential cortical penetration and soft tissue extension, with neoplastic and reactive ossification.

**DIFFERENTIAL DIAGNOSIS** Osteosarcoma, Ewing's sarcoma, lymphoma, aneurysmal bone cyst, giant cell tumor, angiosarcoma.

**DIAGNOSIS** Telangiectatic osteosarcoma.

**DISCUSSION** Telangiectatic osteosarcomas represent approximately 4% of all osteosarcomas, and display the distinctive

pathologic feature of cystic areas filled with hemorrhage in various stages of evolution. They are lined by giant cells and tumor cells, not endothelial cells that would be typical of an aneurysmal bone cyst. The amount of osteoid is quite small. The lesions are destructive and lytic, with large extraosseous masses incompletely surrounded by thin shells of bone [33]. Approximately 25% to 30% of cases have a pathologic fracture at presentation. They grow rapidly and elicit relatively little bone reaction; therefore, their appearance is very similar to that of an aneurysmal bone cyst, giant cell tumor, or angiosarcoma. Fluid levels may be demonstrated on CT or MRI. The distribution of telangiectatic osteosarcoma is similar to that of conventional osteosarcomas. Most arise in the metaphysis; 10% arise in the diaphysis. The femur is involved most frequently, followed by the tibia and humerus. The prognosis is generally considered poorer than that of conventional osteosarcoma, but this has been debated in the recent literature.



FIGURE 2.24A



FIGURE 2.24B

**FINDINGS**

- A. AP radiograph of the shoulder at presentation shows an oblique pathologic fracture through the proximal humerus. Marked soft tissue swelling is seen around the shoulder, and the humerus itself is osteopenic.
- B. Follow-up examination 2 months after the completion of radiotherapy shows marked diminution in the size of the soft tissue mass, with periosteal bone formation and healing of the fracture.

**DIFFERENTIAL DIAGNOSIS** Ewing's sarcoma or other round cell malignancy, lymphoma, eosinophilic granuloma, metastasis, infection.

**DIAGNOSIS** Ewing's sarcoma.

**DISCUSSION** Ewing's sarcoma belongs to the category of small round cell tumors, sometimes referred to as the

Ewing's sarcoma family of tumors. Ewing's sarcoma is commonly seen before the age of 20, and presents with pain. One-third of patients will have symptoms simulating infection, including fever, elevated white count, and elevated erythrocyte sedimentation rate. It is commonly found in the femoral metadiaphysis or flat bones as an osteolytic or permeative lesion, with an associated soft tissue mass and periosteal reaction. Sclerotic reactive bone may be present at the periphery, but there is no tumor matrix. Lack of any reactive bone in the soft tissue mass sometimes distinguishes Ewing's sarcoma from osteosarcoma on imaging. Primitive neuroectodermal tumors differ histologically from Ewing's sarcoma, but usually not radiologically. Approximately 15% to 30% of Ewing's sarcoma cases have lung and osseous metastases at presentation. Local recurrences occur in 12% to 25% of cases. Treatment consists of chemotherapy combined with radiation therapy or surgery.



FIGURE 2.25A

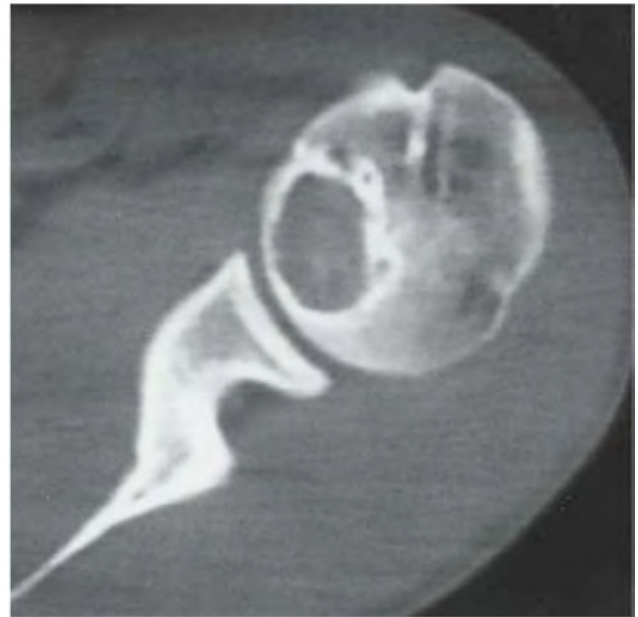


FIGURE 2.25B

### FINDINGS

- A. AP radiograph of the shoulder shows a lucent lesion with a thin but dense sclerotic margin in the humeral epiphysis, extending into the metaphysis.
- B. CT scan of the proximal humerus. The lesion is round in shape and has a well-defined sclerotic margin. Faint matrix mineralization is noted in the lesion.

**DIFFERENTIAL DIAGNOSIS** Chondroblastoma, Brodie's abscess, eosinophilic granuloma.

**DIAGNOSIS** Chondroblastoma.

**DISCUSSION** Chondroblastoma (Codman's tumor) is an uncommon benign neoplasm that consists of chondroid tissue mixed with more cellular tissue. Location in the epiphysis or apophysis is characteristic (about 98%), often with extension into the metaphysis. Two-thirds arise in the lower extremities, and half around the knee. Most patients are young: 80% are between 5 and 25 years old. Males are affected twice as often as females. When chondroblastomas occur outside the usual age group, they arise in unusual locations. The presentation is nonspecific, typically consisting of pain. Articular symptoms are commonly encountered, and sterile effusions are noted in up to one-third of cases. The

radiographic appearance is an ovoid or rounded lucent epiphyseal lesion that is eccentrically or centrally located. The margins are geographic, usually with a thin, reactive bony rim. Scattered mottled or stippled calcifications, like those of other cartilage tumors, may be present. Extension can occur into the subarticular bone or metaphysis (25% to 50% of cases). Calcification can occur in up to half of the cases, but is commonly subtle enough to require CT for documentation. The associated metaphyseal periosteal reaction is seen in up to 50% of cases distinguishes it from the other etiologies of epiphyseal lucent lesions. Cystic or hemorrhagic components are recognized and may be prominent enough to suggest the alternate diagnoses of simple bone cysts or aneurysmal bone cysts (but the location of the lesion should redirect one toward the correct diagnosis). Chondroblastomas treated by curettage usually do not recur, but some are aggressive locally.

The classic differential of an epiphyseal lucent lesion is that of chondroblastoma and a Brodie's abscess. Epiphyseal eosinophilic granuloma is a rare enough entity to be excluded from a general differential. Giant cell tumors can also extend into the epiphysis and contain giant cells but are distinguished from chondroblastomas by their lack of a sclerotic border. After physeal closure, other differential considerations would include enchondroma, osteoblastoma, and clear cell chondrosarcoma.



FIGURE 2.26A



FIGURE 2.26B

**FINDINGS**

- A. AP radiograph of the shoulder. There is permeated destruction of the proximal humeral metaphysis extending into the shaft, with a single layer of periosteal reaction enveloping the region of abnormality. Penetration of the cortex is present along the medial aspect of the metaphysis.
- B. Coronal T2-weighted MRI shows marrow edema, permeated cortical destruction, and subperiosteal fluid medially. Note the well-defined dark line of enveloping periosteal new bone surrounding the proximal humerus. There is a small amount of fluid in the glenohumeral joint capsule.

**DIFFERENTIAL DIAGNOSIS** Infection, Ewing's sarcoma, osteosarcoma, lymphoma.

**DIAGNOSIS** Acute osteomyelitis.

**DISCUSSION** Acute hematogenous osteomyelitis is generally a disease of children that occurs when the physes are open. Bacteria from a remote source of infection are

carried into the bone via the nutrient artery and become deposited in the metaphysis, where blood flow slows as arterial branches loop in a hairpin turn and enter large sinusoidal veins. Once colonies begin to grow, they may spread across the physis into the epiphysis and throughout the medullary cavity. As the acute inflammatory reaction proceeds, edema and accumulated pus increase the intramedullary pressure, leading to decreased blood flow, thrombosis, and necrosis. Pus may extrude through the cortex into the subperiosteal space via haversian and Volkmann's canals, elevating the periosteum and stripping away the cortical blood supply. Reactive periosteal bone forms a shell around the necrotic cortex. The most common pathogen is *S. aureus*. Radiographic changes tend to occur late in the pathophysiologic process, but MRI is sensitive very early in the course and precise in delineating the anatomic extent [34]. Osteomyelitis usually responds to systemic antibiotics, but collections of pus must be drained surgically. Pathogenic bacteria may remain sequestered for decades within avascular pockets of necrotic bone, where they are inaccessible to systemic antibiotics.

**CLINICAL HISTORY** A 62-year-old woman with chronic shoulder deformity several weeks after trauma.



FIGURE 2.27

**FINDINGS** There is a fracture of the humeral neck with medial rotation of the humeral head. Sclerotic, sharp borders are noted. Diffuse osteoporosis is present.

**DIFFERENTIAL DIAGNOSIS** None.

**DIAGNOSIS** Fracture nonunion, surgical neck of the humerus.

**DISCUSSION** The three phases of bone healing (inflammatory, reparative, and remodeling) can be modified or arrested by an alteration in the local environment. The inflammatory phase is elicited by the hematoma and necrotic material in the fracture bed. An influx of plasma cells and leukocytes is the result. The reparative phase ensues, with fibrovascular ingrowth into the clot, which establishes an organized framework for mineralization. Callus formation stabilizes the fracture fragments for the next stage, remodeling. The remodeling phase is characterized by resorption of the

excess callus according to the principles of the piezoelectric effect.

Cortical bone heals with callus, whereas cancellous bone heals by endosteal apposition. Local factors that slow the progression through the sequence include severe trauma, poor immobilization, infection, osteonecrosis, contact with synovial fluid (which contains fibrinolysins), interposed tissue, underlying pathology, and prior radiation. Systemic factors that slow the progression include old age, malnutrition, steroid use, and metabolic derangements. If the healing process is delayed, the fracture has *delayed union*. If healing fails to progress, the diagnosis of nonunion is raised. Usually a fibrous union or pseudoarthrosis is present. A pseudoarthrosis is defined by a synovial-lined cavity, perpetuated by motion at the fracture site. A pseudoarthrosis need not be present to suggest a nonunion. Radiographically, the ends of the fracture site are osteoporotic, with atrophic or sclerotic margins. Pseudoarthroses are commonly present at the humeral diaphysis or femoral neck, both of which are subjected to considerable motion.

**CLINICAL HISTORY** (A) A 58-year-old man with chronic right shoulder pain but no history of trauma. (B) Companion case of patient with left shoulder pain.



FIGURE 2.28A

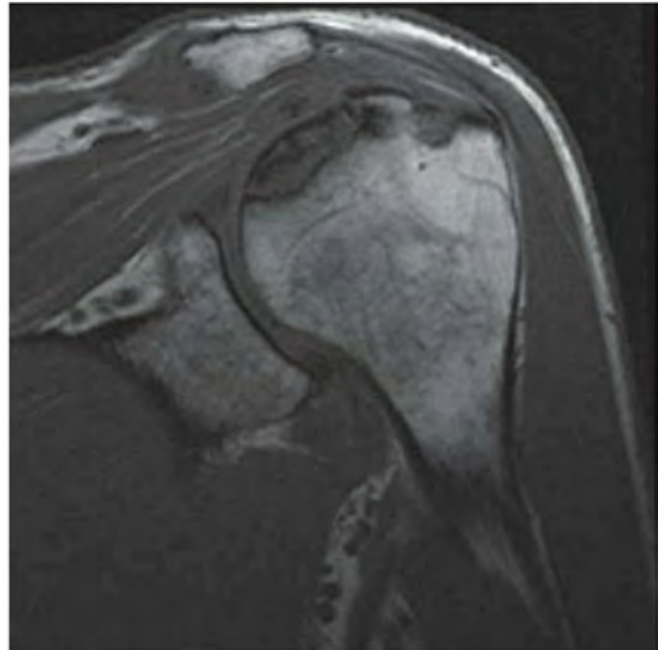


FIGURE 2.28B

### FINDINGS

- A. AP radiograph shows discrete region of irregular sclerosis and lucency along the superior central portion of the articular surface of the humeral head. A portion of the articular surface is slightly depressed. There is no abnormality in the surrounding bones.
- B. Coronal T1-weighted MRI shows abnormality in the superior articular surface of the humeral head. The subcortical region has heterogeneous intermediate-to-dark signal, and there is a surrounding zone of dark signal. T2-weighted MRI (not shown) demonstrated low signal within the abnormal region and surrounding marrow edema.

**DIFFERENTIAL DIAGNOSIS** Osteonecrosis, fracture.

**DIAGNOSIS** Osteonecrosis.

**DISCUSSION** The diagnosis is made by the characteristic subchondral location of the lesion and the absence of a history of trauma. Arthritis is not a consideration because the joint space and the glenoid are normal. The humeral head is a common site for osteonecrosis or the in situ death of a

segment of bone [35]. The risk factors for osteonecrosis of the humeral head are similar to those for osteonecrosis of the femoral head, and include corticosteroid use, sickle cell disease and other hemoglobinopathies, dysbarism (caisson disease), Gaucher disease, alcoholism, and systemic lupus erythematosus. The principal arterial supply to the humeral head consists of a branch of the anterior humeral circumflex artery that has a tortuous intraosseous course and few anastomoses, leaving the bone vulnerable to ischemia following the interruption of blood flow. Healing of the site through bone remodeling may lead to subchondral fracture and displacement of fragments, typically years after the onset. Patients often present with advanced disease because patients are able to compensate for loss of glenohumeral function; this is unlike the hip, where patients often present with early disease. The progression of disease may be staged as follows: stage I, normal radiographs but abnormal MRI; stage II, sclerosis on radiographs without fracture or subchondral collapse; stage III, crescent sign and subchondral collapse, indicating gross subchondral fracture; stage IV, widespread collapse and secondary degenerative change; and stage V, end-stage with secondary degenerative change also involving the glenoid.

**CLINICAL HISTORY** A 12-year-old boy with right arm weakness. Radiographs of right and left shoulders.



FIGURE 2.29A



FIGURE 2.29B

### FINDINGS

- A. AP radiograph of the right shoulder. Hypoplasia and underdevelopment of the humeral head are noted. The concavity of the glenoid is larger than expected. The humeral head is high riding.
- B. AP radiograph of the left shoulder. The left shoulder is normal.

**DIFFERENTIAL DIAGNOSIS** None.

**DIAGNOSIS** Brachial plexus palsy (Erb palsy).

**DISCUSSION** Two common forms of obstetrical trauma—clavicle fracture and Erb palsy—both result in refusal of a newborn to move his arm. Erb palsy is the result of excessive trauma on the arm, resulting in damage to the C5 and C6 roots. A less common injury is Klumpke paralysis, which results from damage to the C7, C8, and T1 nerve roots. Spontaneous, complete recovery is noted in 90% of cases, representing

instances of reversible stretch injury to the nerve roots. Those that completely avulse eventually result in hypoplasia and elevation of the scapula, underdevelopment of the glenoid, and an abnormal coracoid and acromion. Additionally, there is underdevelopment of the remainder of the extremity, including the osseous and soft tissue elements. CT measurements of the amount of humeral torsion (comparable to measurements for tibial torsion) can be undertaken in surgical planning for tendon transfer procedures. Similar to clavicular fractures, brachial plexus palsy in the newborn [36–38] may be the result of difficulties during delivery, particularly in infants with shoulder dystocia and macrosomia [39]. Clavicular fractures, however, are a far more common complication, with an incidence of about 2% compared to a mere 0.4% incidence of Erb palsy. Similar conditions also appear to occur through another mechanism, possibly in utero. The prognosis when no predisposing factor can be identified is worse, with a lengthy recovery time in those cases in which resolution occurred, and a greater proportion with permanent palsy.

**CLINICAL HISTORY** A 48-year-old woman with abrupt onset of shoulder pain and weakness. No history of trauma. Symptoms and imaging findings resolved 6 months later.

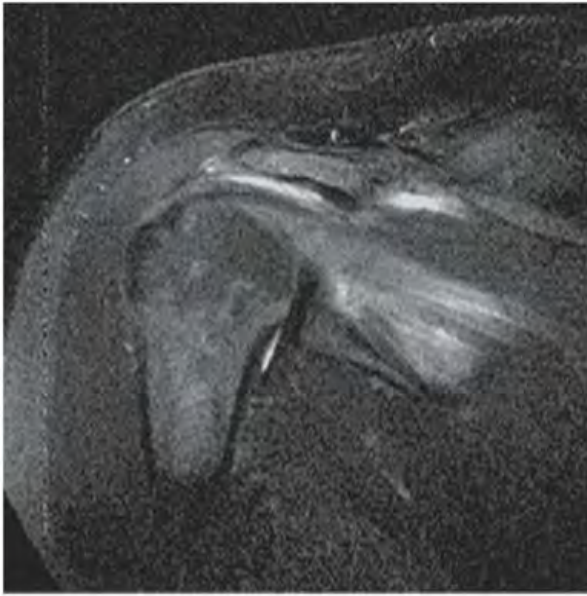


FIGURE 2.30A

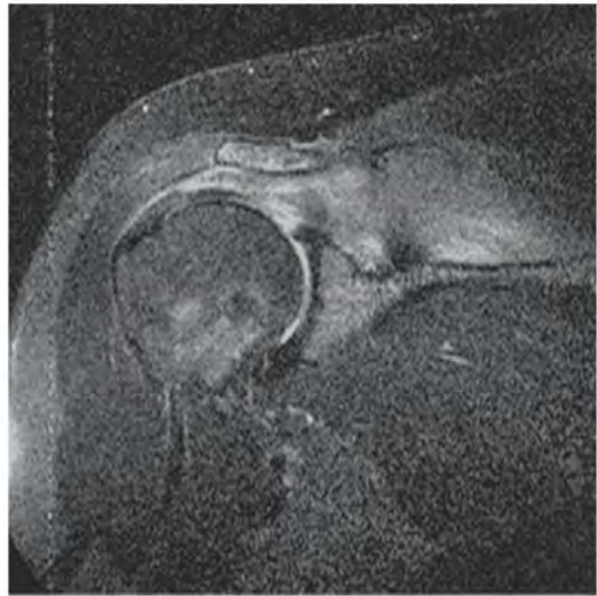


FIGURE 2.30B

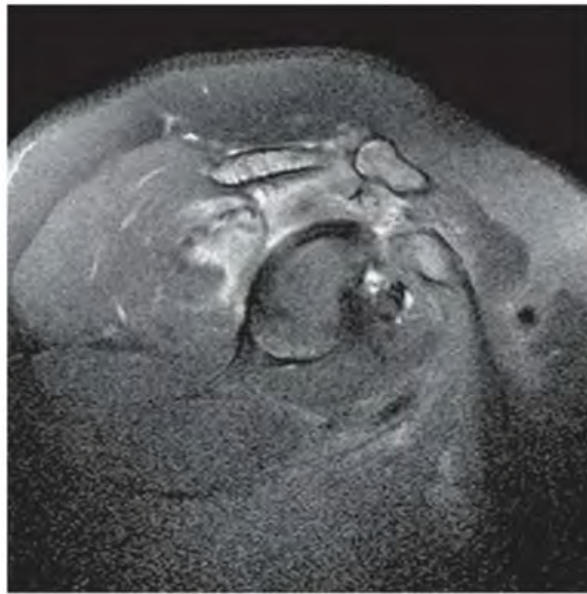


FIGURE 2.30C

**FINDINGS** (A, B) Coronal oblique and (C) sagittal oblique T2-weighted fat-suppressed images demonstrate edema in the supraspinatus and infraspinatus muscles.

**DIFFERENTIAL DIAGNOSIS** Parsonage-Turner syndrome, myositis, neuropathy, rotator cuff tear.

**DIAGNOSIS** Parsonage-Turner Syndrome.

**DISCUSSION** Parsonage-Turner syndrome, also known as acute brachial neuritis, refers to an idiopathic denervation

of the shoulder [40]. This can be seen in patients ranging from infants to the elderly and is more common in men. Up to half of patients had a viral illness or vaccination in the 2 weeks prior to symptom onset. On MRI, increased signal is seen within the shoulder musculature on T2-weighted and inversion recovery images [41]. Muscle enlargement can be present acutely. Muscle atrophy can occur in chronic cases. The muscle edema may or may not follow the nerve distribution, as individual nerves or nerve branches may be involved. The majority of cases resolve spontaneously within a year.

**CLINICAL HISTORY** *A 70-year-old man with shoulder pain and weakness.*

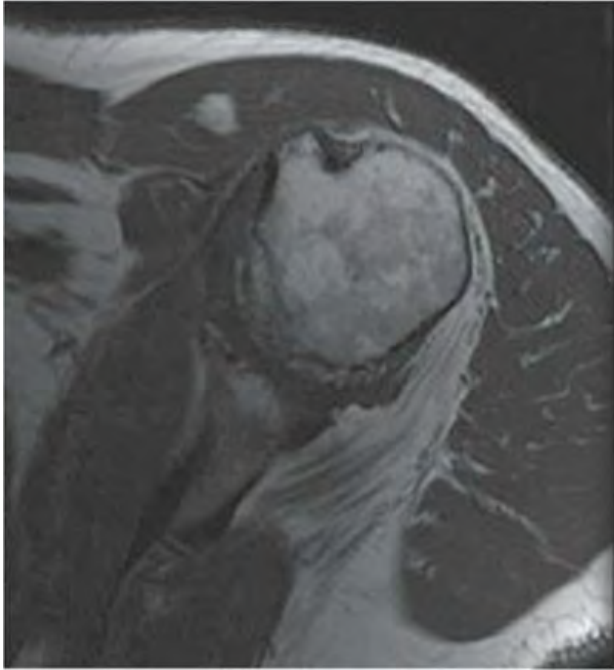


FIGURE 2.31A

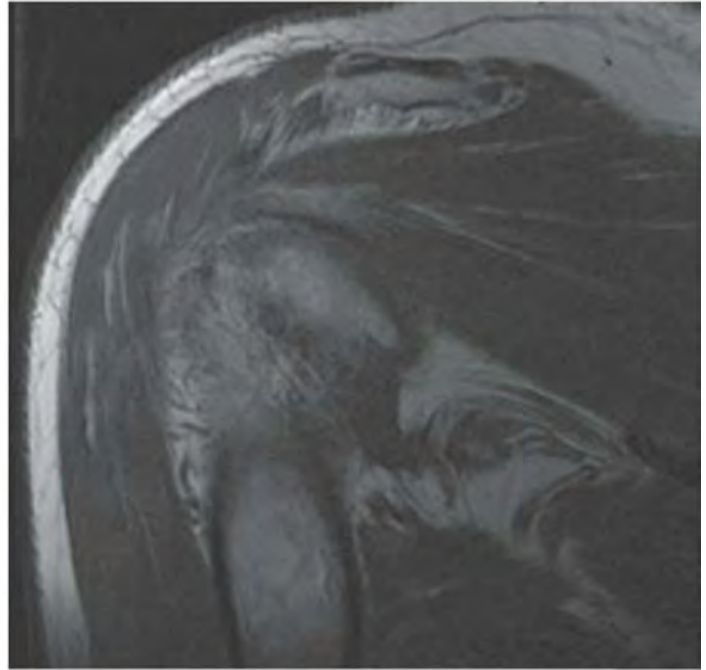


FIGURE 2.31B

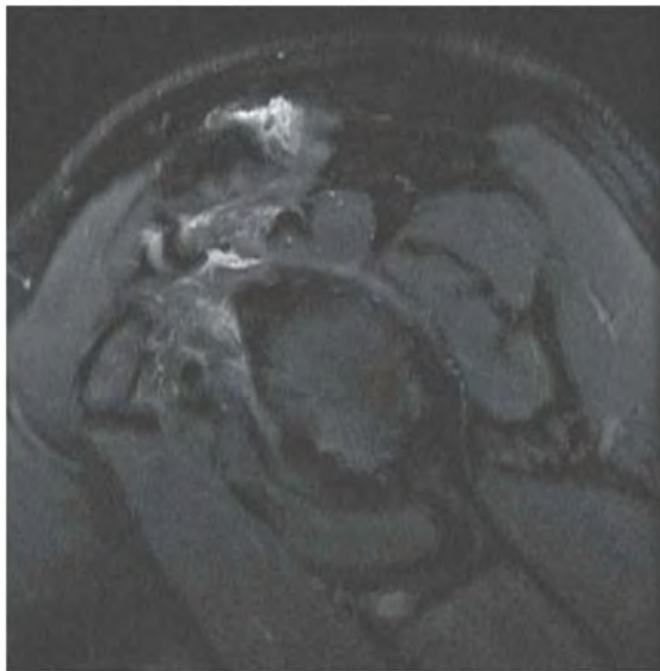


FIGURE 2.31C

**FINDINGS** (A) Axial and (B) coronal oblique T1-weighted and (C) sagittal oblique T2-weighted fat-suppressed MRI images demonstrate disproportionate fatty atrophy of the teres minor, without tendon tear.

**DIFFERENTIAL DIAGNOSIS** Full-thickness teres minor tendon tear, quadrilateral space syndrome, Parsonage-Turner syndrome.

**DIAGNOSIS** Quadrilateral space syndrome.

**DISCUSSION** The teres minor muscle is innervated by a distal branch of the axillary nerve that passes posteriorly underneath

the teres minor through a space that is also bounded by the teres major muscle (inferiorly), the humerus (laterally), and the long head of the triceps muscle (medially). The posterior humeral circumflex artery also passes through this so-called quadrilateral space [42]. Compression of the nerve within the quadrilateral space causes painful denervation and may lead to focal atrophy of the teres minor muscle. The deltoid muscle may be involved sometimes. Nerve compression is thought to result most often from posttraumatic fibrous bands [43]. On MRI, early changes include muscle edema and swelling. Chronic changes include muscle atrophy and fatty infiltration. Most patients are treated conservatively, but some require surgical decompression of the quadrilateral space [44].

**CLINICAL HISTORY** An 87-year-old man with an enlarging shoulder mass.

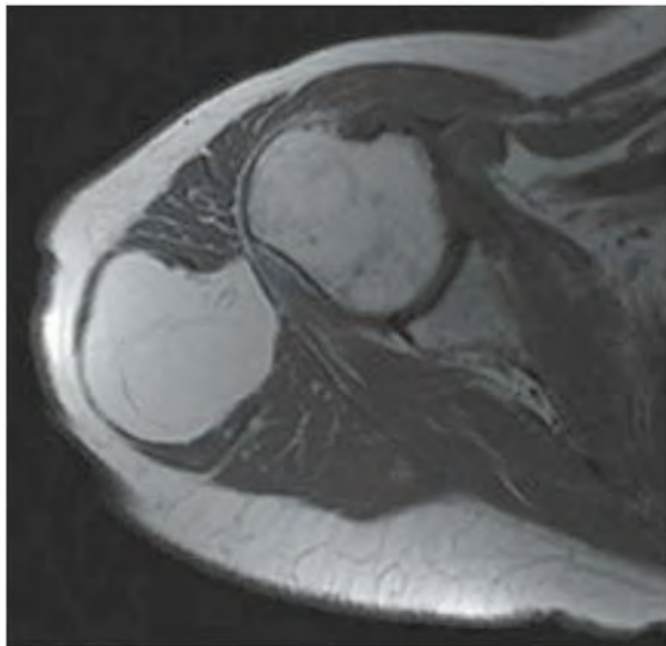


FIGURE 2.32A

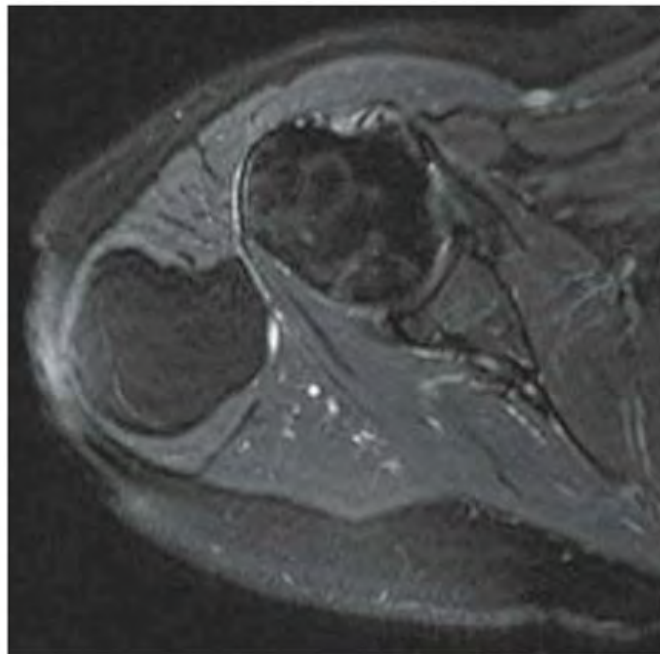


FIGURE 2.32B

**FINDINGS** Axial T1-weighted (A) and T2-weighted fat-suppressed (B) MRI of the shoulder demonstrates a well-defined rounded mass within the deltoid muscle. The mass follows the signal intensity of subcutaneous fat on both imaging sequences. Thin septa traverse the lesion, but it is otherwise homogeneous.

**DIFFERENTIAL DIAGNOSIS** None.

**DIAGNOSIS** Intramuscular lipoma.

**DISCUSSION** Lipomas are very common, benign tumors of mesenchymal origin that are most frequent in the subcutaneous soft tissues of the extremities in women. They are usually painless, freely moveable soft tissue masses that can be distorted easily by mild pressure. Painful lipomas are known by the term “*lipoma dolorosa*,” and are characterized by a migratory pain syndrome associated with multiple lipomas.

The general classification is by site (subcutaneous or deep). Deep lipomas within a limited fascial compartment can sometimes be hard on physical examination due to local infiltration and distention of the compartment. Subcutaneous lipomas may be indistinguishable from the native fat on imaging [45].

Both osseous and cartilaginous elements can be seen radiographically and pathologically in benign lipomas, but increase the likelihood that the lesion is actually a liposarcoma. A Hounsfield unit measurement with negative value is diagnostic of a fatty constituent. On MRI, T1-weighted hyperintensity and fat-suppressed sequence hypointensity are suggestive, but they can also be seen with the presence of intracellular methemoglobin. An uncomplicated lipoma should not enhance on CT or MRI and appears avascular at angiography. Periosteal and synovial lipomas are uncommon. Within the joint, a discrete round or oval fat-containing lesion is noted, and should be distinguished from lipoma arborescens, a form of synovial metaplasia seen in osteoarthritis, rheumatoid arthritis, or after trauma. Treatment is surgical resection.

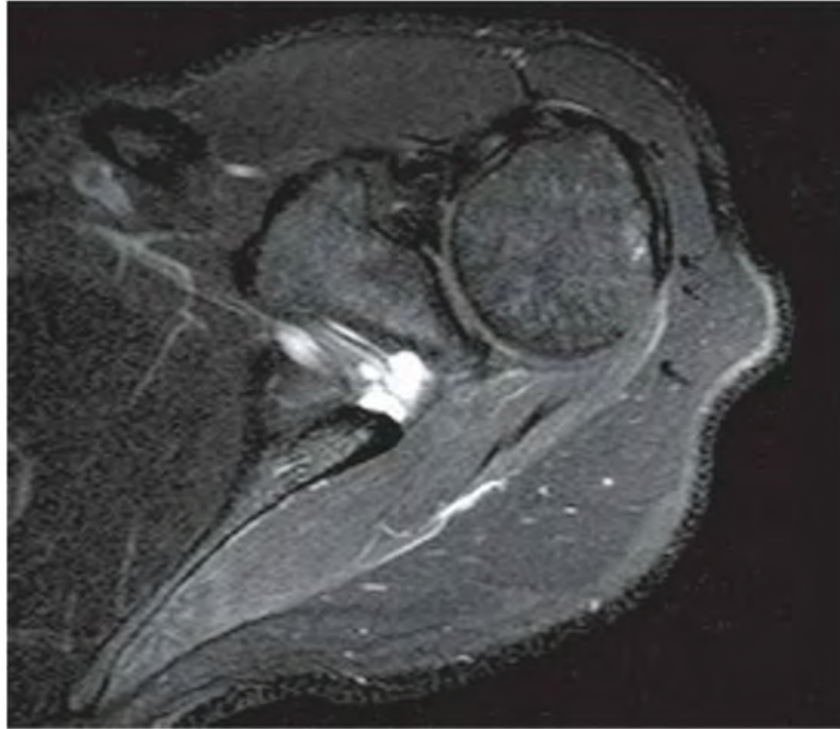


FIGURE 2.33

**FINDINGS** Axial T2-weighted fat-suppressed MRI shows a multiloculated, hyperintense mass in the spinoglenoid notch, with extension into the suprascapular notch. There is increased signal in the teres minor muscle.

**DIFFERENTIAL DIAGNOSIS** Ganglion cyst, synovial cyst, schwannoma, neurofibroma.

**DIAGNOSIS** Ganglion cyst.

**DISCUSSION** Suprascapular nerve entrapment occurs most commonly in the suprascapular notch [46]. In this location, the nerve carries fibers to the supraspinatus muscle, infraspinatus muscle, glenohumeral joint, acromioclavicular joint, and anterior two-thirds of the shoulder joint capsule. The second most common location for impingement, as illustrated in this case, would be the spinoglenoid notch, adjacent to the infraspinatus muscle. Clinical features include shoulder pain and weakness, with limited external rotation and abduction of the humerus. Radiographic features in chronic cases include fatty atrophy of the infraspinatus muscle, with or without involvement of the supraspinatus muscle. Etiologies for entrapment include scapular fracture, ligamentous hypertrophy, glenohumeral dislocation, ganglia, tumors, developmental notch abnormalities, and excessive traction on the suprascapular, inferior transverse, or spinoglenoid ligaments, as seen in manual laborers or weight lifters.

If the ganglion occurs in the suprascapular notch, then both the supraspinatus and infraspinatus muscles are usually involved. If the ganglion occurs more distally in the spinoglenoid notch, then the infraspinatus alone is typically involved.

These lesions are typically hypointense or isointense on T1-weighted MRI, and hyperintense on T2-weighted MRI. They are multiloculated but are typically discrete. The lesion in this case had a neck communicating with a torn glenoid labrum, thought to be the etiology of these cysts.

Ganglion cysts are benign cystic lesions that are attached to a tendon sheath, tendon, muscle, or cartilage. They are typically found in the hands, feet, or wrists. Ganglion cysts are thought to develop as a result of tissue degeneration or synovial herniation. They may or may not communicate with the associated joint or tendon sheath. Ganglion cysts are commonly considered by patients to be unsightly, and this may lead to treatment by surgical excision. Depending on location, their physical mass also may cause significant neurologic impairment. Well-documented conditions include ganglion cysts at the region of the proximal tibiofibular articulation causing footdrop, and ganglion cysts in the suprascapular notch causing atrophy of the infraspinatus muscle. Ganglion cysts that are associated with the cruciate ligaments may cause limitation of motion in the knee, and meniscal cysts may cause swelling, pain, and limitation of motion. If the ganglion cyst is adjacent to a bone, it can erode or elicit a periosteal reaction.

**CLINICAL HISTORY** A 55-year-old man who crashed on a motorbike.



FIGURE 2.34A

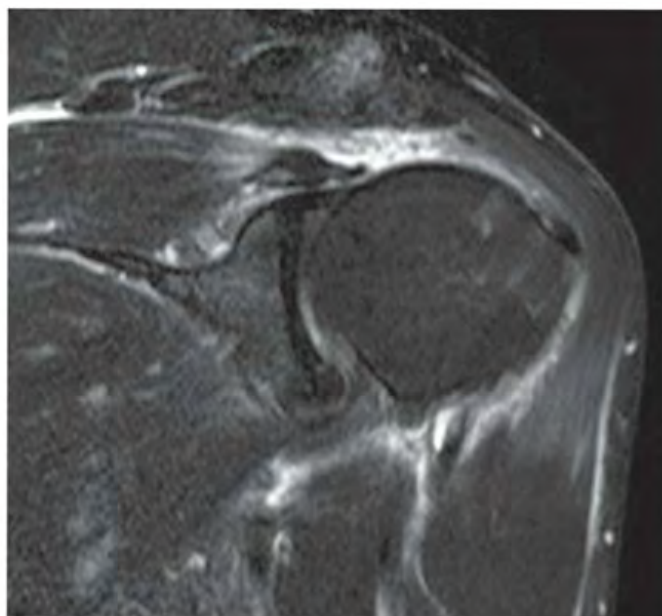


FIGURE 2.34B

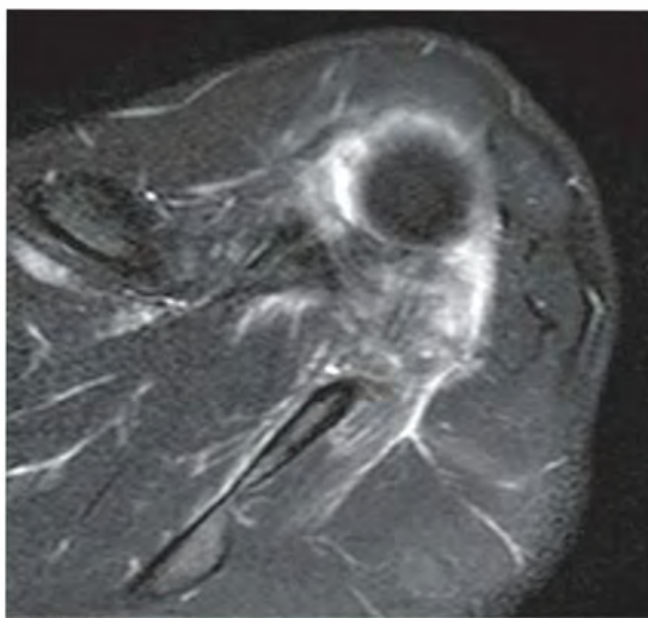


FIGURE 2.34C

**FINDINGS**

- A. AP arthrogram shows extravasation of contrast into the subdeltoid-subacromial bursa.
- B. Oblique coronal T2-weighted fat-suppressed MRI shows fluid in the expected location of the supraspinatus tendon and 4 cm of medial retraction of the tendon stump.
- C. Axial T2-weighted fat-suppressed MRI through the upper humeral head shows fluid where normal dark-signal tendon should be.

**DIFFERENTIAL DIAGNOSIS** None.

**DIAGNOSIS** Rotator cuff tear involving supraspinatus tendon.

**DISCUSSION** The tendons of the rotator cuff may tear as a result of acute or repetitive trauma, mechanical impingement, degeneration, focal ischemia, or some combination of these. More than 90% of rotator cuff tears are spontaneous ruptures through an abnormal tendon and present as chronic weakness and pain.

Patte [47] has introduced the following grading system: Partial-thickness and full-thickness tears that measure less than 1 cm in sagittal dimension.

Full-thickness supraspinatus tears that measure less than 2 cm in sagittal dimension.

Full-thickness supraspinatus (and infraspinatus or subscapularis) tears that measure greater than 4 cm in sagittal dimension.

Massive full-thickness tears with secondary glenohumeral osteoarthritis.

Partial tears are more common than complete tears, tendon insertion articular side tears are more common than bursal side tears at the myotendinous junction, and intrasubstance tears are the least common. Rotator cuff tears can be demonstrated by arthrography, sonography, or MRI. On arthrography, contrast medium leaks through full-thickness tears into the subdeltoid-subacromial bursa. On MRI or sonography, tears result in a discontinuity that may fill with fluid or granulation tissue. The involved muscle belly, most often the supraspinatus muscle, may retract, and the humeral head may subluxate superiorly. Partial-thickness tears may involve either the inferior or superior surfaces of the cuff, or they may be entirely within the substance of the tendons. Chronic tears can be identified by narrowing of the acromiohumeral distance to less than 0.6 cm, reversal of the normal inferior acromial convexity secondary to repeated impaction, and cystic changes and sclerosis of both the humeral head and acromion undersurface.

**CLINICAL HISTORY** 27-year-old woman with acute anterior shoulder pain following injury while performing a break dancing maneuver (the worm).

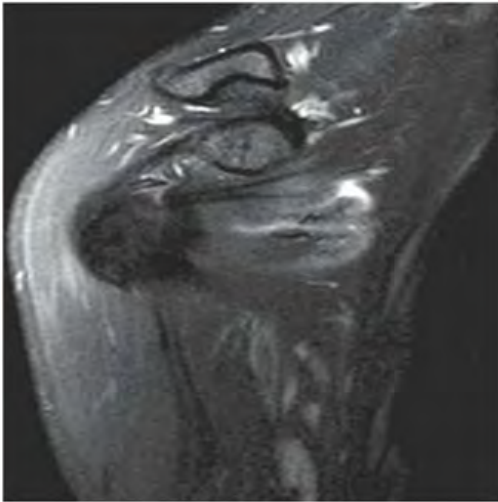


FIGURE 2.35A

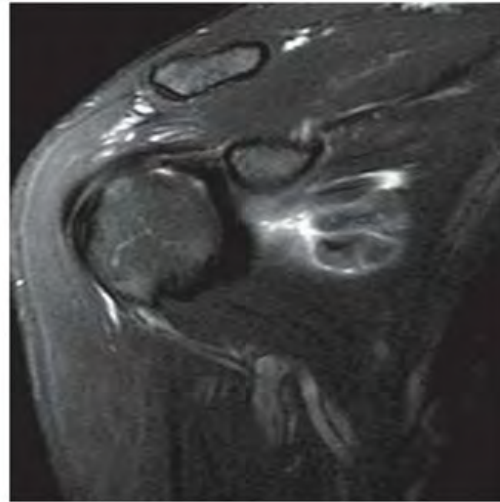


FIGURE 2.35B

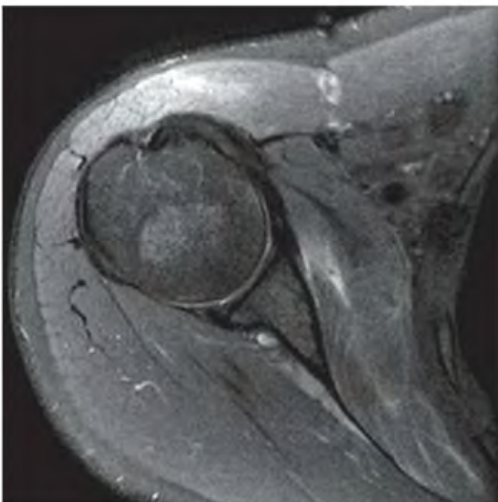


FIGURE 2.35C

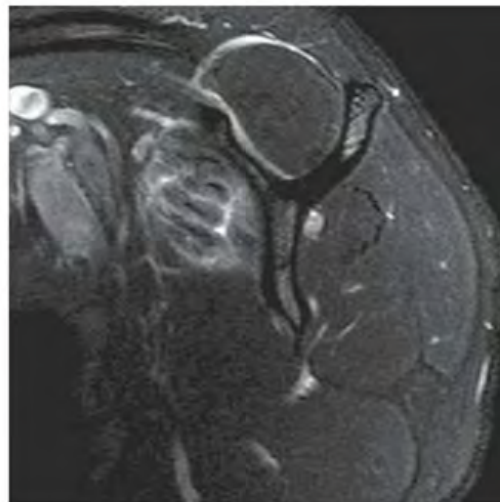


FIGURE 2.35D

**FINDINGS** Oblique coronal (A, B), axial (C), and oblique sagittal (D) T2-weighted fat-suppressed MRI of the shoulder show increased signal along the myotendinous junctions of the multiple heads of the subscapularis muscle. The subscapularis tendon itself (A) is intact.

**DIFFERENTIAL DIAGNOSIS** None.

**DIAGNOSIS** Subscapularis strain

**DISCUSSION** Most subscapularis ruptures occur in the setting of gross rotator cuff tears and follow rupture of the supraspinatus or infraspinatus tendons; isolated injury is uncommon but well documented [48]. Clinical signs suggestive of isolated subscapularis tendon tears include increased external rotation and decreased strength of internal rotation. Patients will complain of anterior pain and weakness, particularly when the arm is used above or below the shoulder level. Patients generally do not experience instability. The mechanism of injury is usually a discrete episode of trauma, with traumatic hyperextension

or external rotation of the abducted arm. The axial images on CT arthrography or MRI are most sensitive in detecting subscapularis tendon abnormalities. A partial tear is manifest as thickening or fraying of the tendon. A complete tear is typically associated with tendon retraction and fluid intravasation into the prior tendon site. After partial tear, fatty infiltration is common in the subscapularis muscle. The MRI appearance of subscapularis tendon tears will show the subscapularis tendon to have poorly defined contours and abnormal high signal on T2-weighted images [49]. Most cases will show discontinuity and frank retraction of the tendon, whereas a few may show thickening of the distal portion of the tendon or calcification. Tears of the subscapularis muscle belly, like muscle tears in other body parts, generally occur along the muscle-tendon interfaces, and on MRI will show high signal on T2-weighted or STIR pulse sequences. An important association with subscapularis rupture is dislocation of the biceps tendon from its groove, particularly intralaminar or medial dislocation of the tendon. Associated bony abnormalities are uncommon.

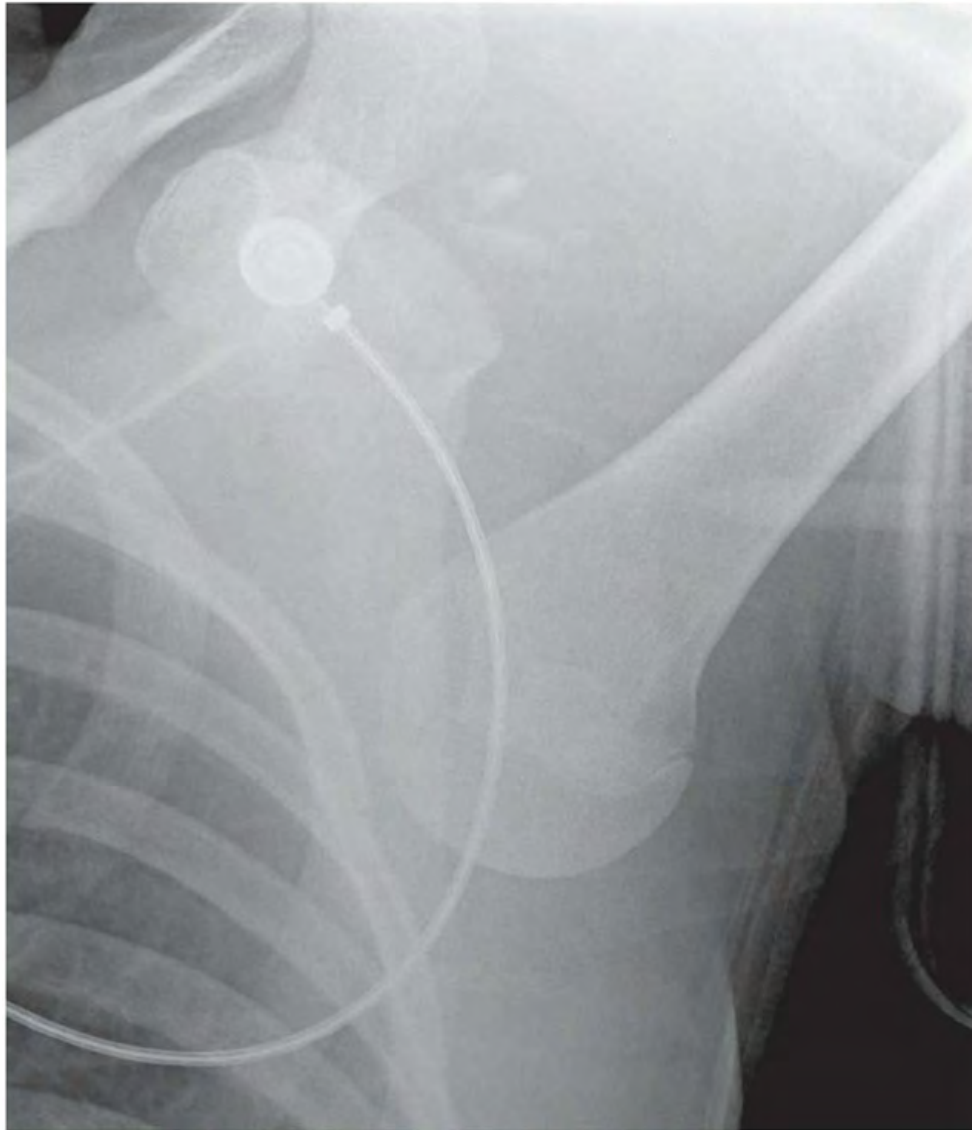


FIGURE 2.36

**FINDINGS** AP radiograph of the right shoulder. The humeral head is located in a subcoracoid position, with the humeral shaft extended superiorly. There are small avulsion fragments from the greater tuberosity. She was unable to bring the arm down.

**DIFFERENTIAL DIAGNOSIS** None.

**DIAGNOSIS** Luxatio erecta (inferior glenohumeral dislocation).

**DISCUSSION** Dislocation of the glenohumeral joint should be immediately obvious; however, the location of the humeral head and the mechanism of injury may require a little more consideration. This patient arrived in the emergency room with

her forearm resting on the top of her head, and could not be coaxed by the radiologic technologist to bring it down to her side for proper positioning. Luxatio erecta, or inferior glenohumeral dislocation, is a rare form of shoulder dislocation [54]. It is caused by hyperabduction of the arm while in the overhead position. As with the common anterior dislocation, the humeral head comes to rest in an anterior subcoracoid position, but the humeral shaft will be extended superiorly or parallel to the scapular spine, rather than inferiorly and parallel to the chest wall. Either a fracture of the greater tuberosity or a tear of the rotator cuff is associated with this injury in 80% of patients. Sixty percent may have some degree of neurologic compromise, most commonly to the axillary nerve, and three percent may have significant vascular compromise to the limb [55].

**CLINICAL HISTORY** A 27-year-old man with rugby injury and a companion case.



FIGURE 2.37A



FIGURE 2.37B



FIGURE 2.37C

**FINDINGS**

- A. AP radiograph of the shoulder. The humeral head is located in a subcoracoid position.
- B. Axillary lateral shoulder radiograph. The humeral head is located anterior to the glenoid process.
- C. Companion case. AP radiograph of the shoulder in internal rotation shows a defect in the posterolateral aspect of the humeral head.

**DIFFERENTIAL DIAGNOSIS** None.

**DIAGNOSIS** Anterior (subcoracoid) shoulder dislocation. The companion case shows an impaction fracture of the humeral head from previous anterior shoulder dislocation (Hill-Sachs lesion).

**DISCUSSION** The stability of the glenohumeral joint depends on the surrounding capsule and ligaments; the glenohumeral contact surface area is only one-third the cross-sectional area of the humeral head, similar to the relationship of a golf ball to a tee. Therefore, shoulder dislocation is a common injury in adults. In about 95% of cases of glenohumeral dislocation, the humeral head dislocates anteriorly and ends up anterior, inferior, and medial to the glenoid process, in a subcoracoid location. Impaction of the anterior inferior

surface of the glenoid labrum on the posterolateral aspect of the humeral head after it dislocates may cause a depressed humeral head fracture called the Hill-Sachs lesion. A large Hill-Sachs lesion may cause the glenoid process to catch during rotation of the shoulder, and result in recurrent dislocations. Visualization of the defect is optimized with internal rotation, positioning the lesion in profile. Less dramatic, but perhaps more important than the dislocation itself, is the concomitant soft tissue injury, anterior capsulolabral tears, in which the glenoid labrum and shoulder capsule becomes detached from the glenoid process (Bankart lesion). This injury is present in over 90% of young patients [50,51], and is sometimes associated with an avulsion fracture of the anterior inferior margin of the glenoid process (Bankart fracture). If not repaired, these injuries usually result in posttraumatic anterior shoulder instability or recurrent dislocations. Concomitant rotator cuff disruption occurs in about one-third of patients over the age of 40 who suffer a traumatic anterior shoulder dislocation for the first time [52]. These rotator cuff tears may result in prolonged morbidity or the need for surgical repair. A brachial plexus injury together with rotator cuff tear has also been recognized as a concurrent injury combination [53]. Acute dislocations are treated with closed reduction. The most common surgical repair for anterior dislocations is the Bankart repair, in which the anterior capsular mechanism is reattached to the glenoid process.



FIGURE 2.38A



FIGURE 2.38B

**FINDINGS**

- A. AP radiograph of the shoulder. The humeral head is in extreme internal rotation, and the humeral head is positioned too far laterally relative to the glenoid process. There is a fine cortical line along the medial aspect of the humeral head that parallels the medial cortex.
- B. Axillary lateral view. The humeral head is impacted on the posterior aspect of the glenoid process.

**DIFFERENTIAL DIAGNOSIS** None.

**DIAGNOSIS** Posterior shoulder dislocation.

**DISCUSSION** Size incongruity between the glenoid fossa and the humeral head predisposes this joint to dislocation. The surrounding capsular structures, in large measure, are responsible for maintaining the stability of this articulation. Anterior dislocations are by far the most common variety

of dislocation. Posterior dislocations are uncommon and constitute no more than 5% of all cases. The radiographic findings may be subtle. Axillary or Y-views are diagnostic and demonstrate posterior displacement of the humeral head relative to the glenoid fossa. The humeral head tends to be fixed in internal rotation. This may be detected on the frontal views. The glenohumeral joint space is widened (greater than 6 mm) [56]. A reverse Hill-Sachs deformity should be sought and, when present, provides further evidence to support acute or prior posterior dislocation. More than 50% of posterior dislocations of the shoulder are not recognized initially. In 75% of cases, two parallel lines of cortical bone may be recognized on the medial aspect of the humeral head. One line represents the medial cortex of the humeral head, but the other represents the margin of a trough-like impaction fracture of the anterior aspect of the humeral head [57], where the posterior margin of the glenoid impinges on it.

**CLINICAL HISTORY** A 17-year-old boarding school student with bilateral shoulder pain and nocturnal episodes.



FIGURE 2.39A

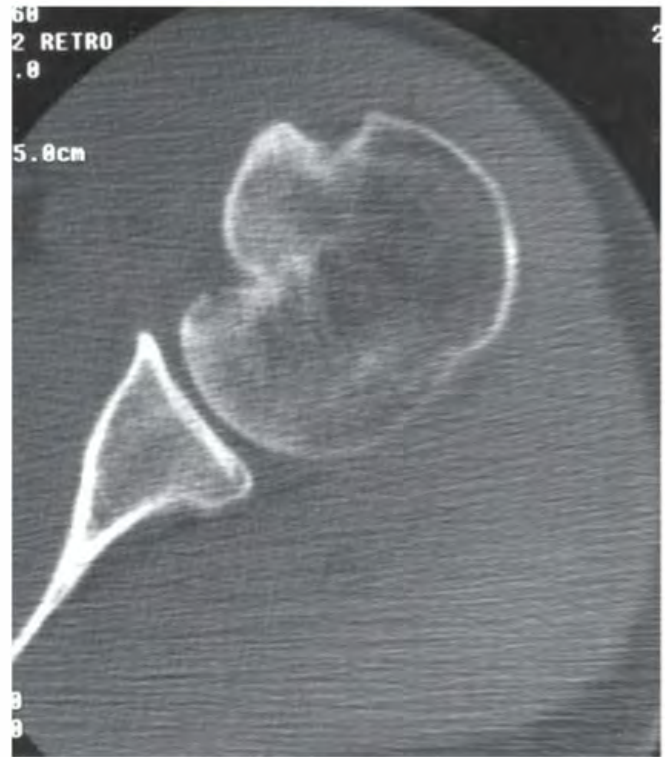


FIGURE 2.39B

**FINDINGS** (A, B) Axial CT scans of each shoulder at the level of the midglenohumeral joints. Both glenohumeral joints are normally located. There are bilateral, symmetric, impaction fractures of the anterior aspects of the humeral heads. There is a nondisplaced avulsion fracture of the lesser tuberosity on the right.

**DIFFERENTIAL DIAGNOSIS** Bilateral shoulder dislocation, secondary to seizures or trauma.

**DIAGNOSIS** Seizure disorder, with recurrent bilateral posterior shoulder dislocations.

**DISCUSSION** The anterior humeral head impaction fracture is known as a reverse Hill-Sachs lesion, or a trough fracture. Posterior dislocation of the glenohumeral joint allows the posterior rim of the glenoid process to impact

into the softer cancellous bone of the humeral head. Trough fracture deformities are seen much better on CT than radiography, as are associated fractures such as avulsions of the lesser tuberosity that otherwise may not be apparent [58]. In this case, the student was having unwitnessed grand mal seizures during the night, resulting in recurrent bilateral posterior shoulder dislocations. Bilateral posterior shoulder dislocation is an uncommon complication of seizure activity [59]. Other orthopedic injuries associated with seizures include dislocations of the hip [60], central fractures of the acetabulum [61], thoracic burst fractures [62], anterior shoulder dislocations, manubriosternal fracture dislocation, and fractures of the proximal femur and humerus. Other causes of uncontrolled myoclonus may cause injuries similar to those sustained during seizures. Posterior shoulder dislocations may also be caused by trauma, most commonly falls.

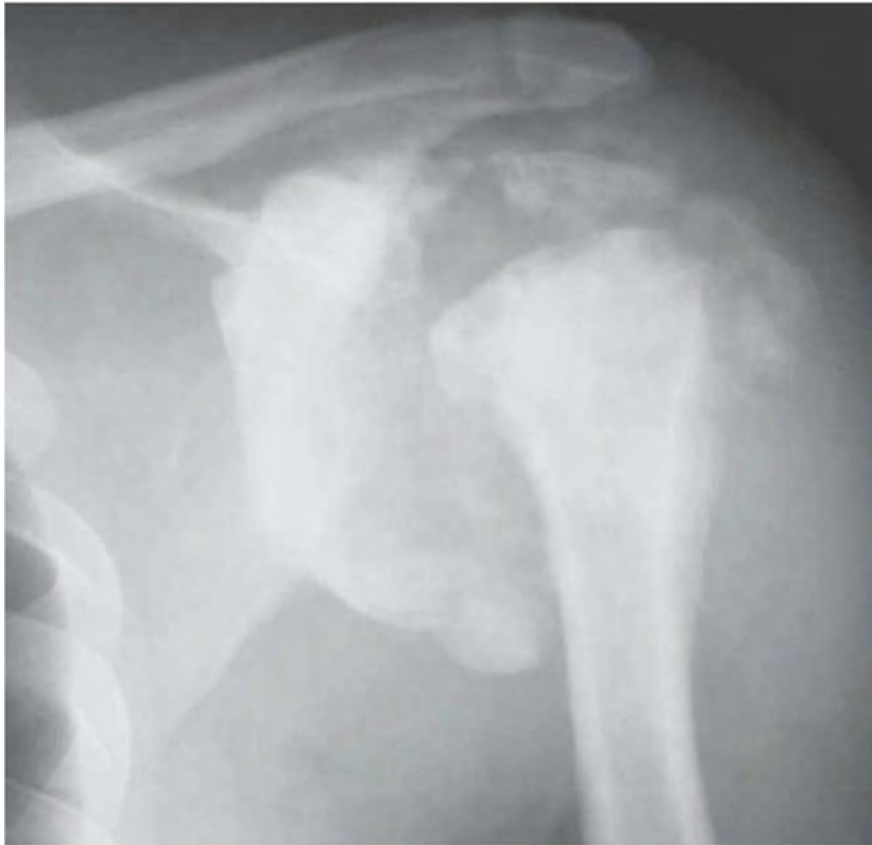


FIGURE 2.40

**FINDINGS** AP radiograph of the left shoulder shows marked deformity of the glenoid with osteolysis, marked productive change, extensive soft tissue calcification, and fragmentation with periosteal reaction about the proximal humerus. The humeral head is missing. There is no destructive change in the adjacent bones.

**DIFFERENTIAL DIAGNOSIS** Neuropathic arthropathy, septic arthritis, tuberculosis, metastasis, primary bone malignancy.

**DIAGNOSIS** Neuropathic arthropathy (Charcot joint).

**DISCUSSION** Destruction of the glenohumeral joint may result from infection, tumor, and neuropathic arthropathy. Septic arthritis would typically be accompanied by osteomyelitis of the adjacent bone, and tumors that cause this degree

of joint resorption might be expected to show destructive changes in the adjacent bones. Tuberculosis could have a similar appearance, but in this case, the clinical history suggests neurologic disease. Although the most common cause of neuropathic arthropathy in the upper extremities is syringomyelia, other causes include multiple sclerosis, myelomeningocele, spinal cord injury, Charcot-Marie-Tooth disease, alcoholism, amyloidosis, congenital indifference to pain, dysautonomia, and iatrogenic steroid injection. Neuropathic arthropathy may be considered an end-stage degenerative arthropathy, with characteristic findings of debris, increased density, disorganization, joint distension, and dislocation (or more concisely, the five Ds). While the hypertrophic form of this condition is more common in the lower extremities, the atrophic form, as in this case, is more common in the upper extremities.

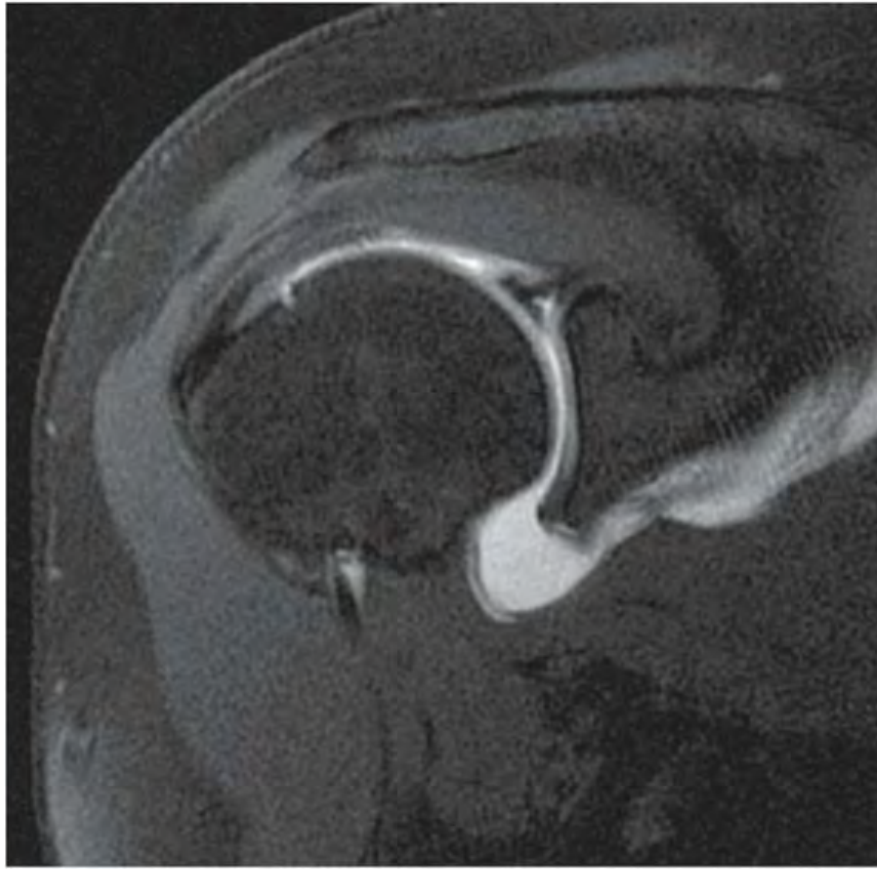


FIGURE 2.41

**FINDINGS** Coronal oblique T1-weighted fat-suppressed MRI after intra-articular administration of dilute gadolinium shows extension of contrast into the superior glenoid labrum.

**DIFFERENTIAL DIAGNOSIS** None.

**DIAGNOSIS** Superior labral anterior to posterior (SLAP) tear.

**DISCUSSION** Injuries of the labrum and associated capsular structures are often related to sports activities. The SLAP tear consists of detachment of the labral-capsular-bicipital tendon complex from the superior aspect of the glenoid process. The mechanism of injury consists of traction on the long head of the biceps tendon during sudden arm abduction (e.g., sports that require throwing). This injury does not necessarily result in instability. Pain and clicking are usually the reported symptoms.

One classification system for SLAP lesions is as follows [63]:

1. (Type I) Irregularity of the superior labrum with an intact biceps tendon (10%).
  2. (Type II) Avulsion of the labral-biceps-capsular complex (40%).
  3. (Type III) Bucket-handle tear of the superior labrum with an intact labral-biceps-capsular complex seen by arthrography as grouped tissue surrounded by contrast (“cheerio sign”) (30%).
  - (Type IV) Bucket-handle tear of the superior labrum with extension into the proximal biceps tendon (20%).
- Since the initial four types were described, at least a half dozen other types have been described [64]. Labral and capsular injuries are best shown by MRI arthrography or CT arthrography. A major diagnostic differential is between a SLAP lesion and isolated injury to the biceps tendon. Treatment consists of excision of part of the glenoid labrum and associated ganglia or cysts, which can insinuate as far as the suprascapular notch or spinoglenoid notch and cause entrapment neuropathies.

**CLINICAL HISTORY** A 58-year-old woman with shoulder pain for many years.

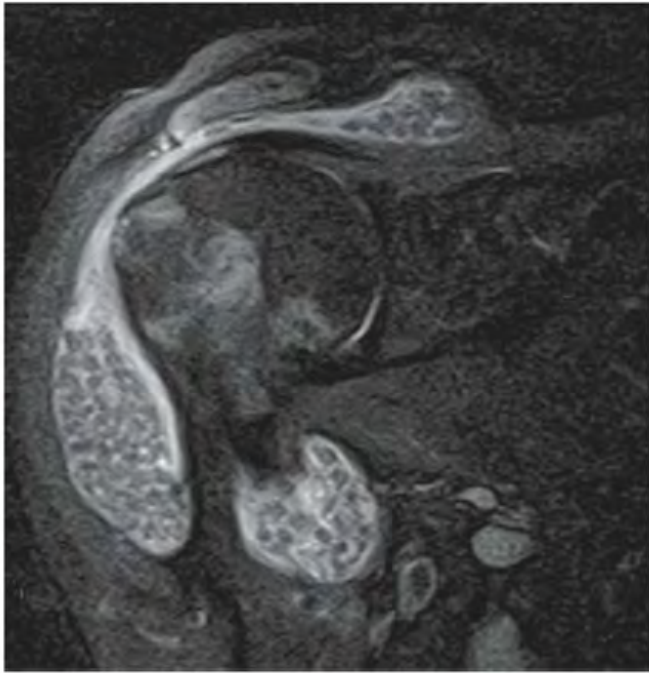


FIGURE 2.42A

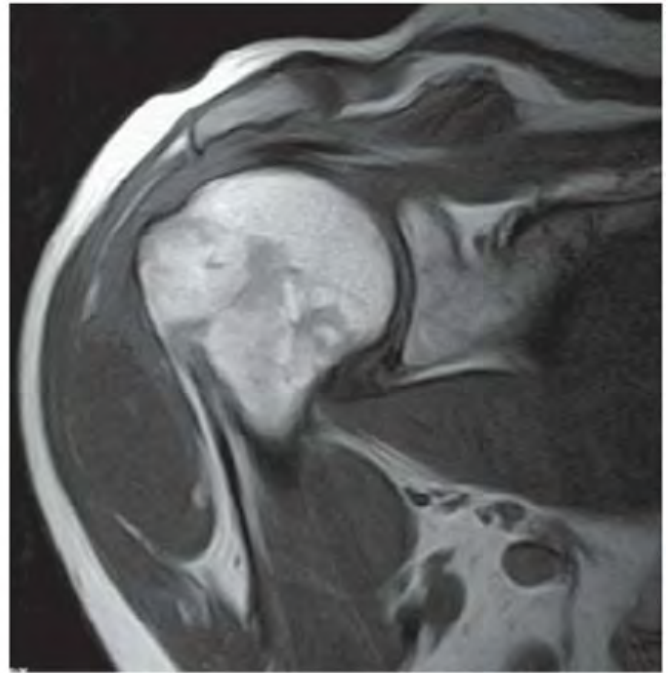


FIGURE 2.42B

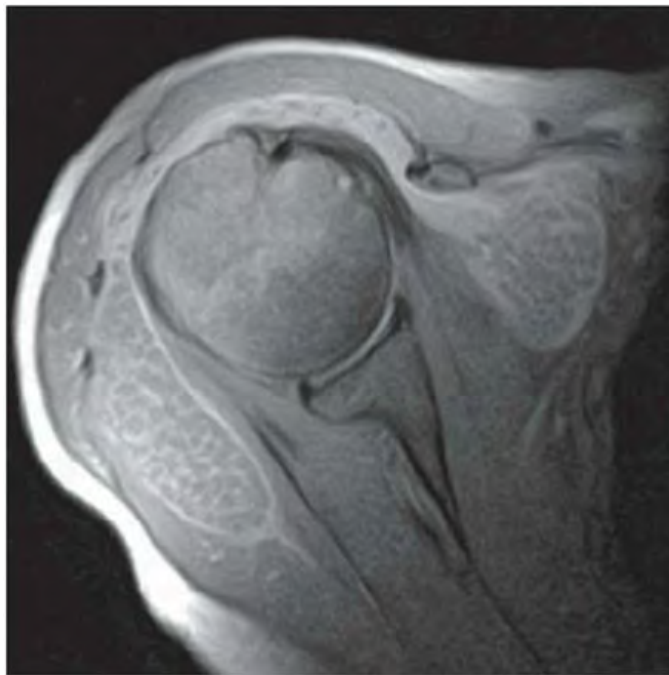


FIGURE 2.42C

**FINDINGS** Coronal oblique T2-weighted fat-suppressed (A), coronal oblique T1-weighted (B) and axial T2-weighted (C) MRI demonstrates numerous, tiny, intermediate signal intensity masses within the subacromial-subdeltoid bursa.

**DIFFERENTIAL DIAGNOSIS** None.

**DIAGNOSIS** Synovial osteochondromatosis.

**DISCUSSION** Synovial metaplasia occurs most commonly in the joints, but also in the tendon sheaths and bursae. Typically, this is a monoarticular process seen in men between the ages of 20 and 50. Commonly involved joints include the knee, hip, and elbow, but the shoulder is depicted in this case. The patient complains of a chronic history of

joint locking. Joint effusion is typically not seen, but, when present, aspiration will yield bloody material. Secondary osteoarthritis is very common. These bodies can extrude outside the joint and persist in a periarticular location. After surgical debridement, recurrences are not uncommon, though malignant degeneration is rare [65–67]. The cartilaginous nodules begin their life cycle as synovial villonodular projections that become pedunculated, break off, and ossify. Growth may continue by nourishment through the synovial fluid, but individual bodies do not typically exceed 3 cm in size. Radiography may reveal soft tissue prominence, specks of calcification, peripherally dense lesions, or mature central ossific trabeculations. In the 15% that do not calcify or ossify, arthrography or MRI is most useful for their demonstration.

**CLINICAL HISTORY** A 43-year-old woman with polyarticular arthritis and a companion case.



FIGURE 2.43A



FIGURE 2.43B

### FINDINGS

- A. AP shoulder radiograph. The bones are diffusely osteoporotic. The humeral head is subluxated superiorly, with adaptive change at the inferior surface of the acromion. Bony hypertrophy is virtually absent, but there are no erosions. There are no soft tissue calcifications.
- B. Companion case. AP radiograph of the shoulder of a different patient shows more marked subchondral cyst formation and bony eburnation on both sides of the glenohumeral joint. Elevation of the humerus is secondary evidence of a chronic rotator cuff tear.

**DIFFERENTIAL DIAGNOSIS** None.

**DIAGNOSIS** Rheumatoid arthritis.

**DISCUSSION** Involvement of the shoulder in rheumatoid arthritis is common [68]. The shoulder capsule surrounds the articular surfaces of the humeral head and glenoid process, and extends medially beneath the coracoid process and inferiorly well below the glenoid process. Chronic inflammation of the synovium may lead to extensive involvement of the

adjacent structures, including the glenohumeral joint itself, the rotator cuff, the acromioclavicular joint, and the adjacent thoracic cage. Inflammatory changes of the subdeltoid-subacromial bursa, the subcoracoid bursa, and the extensive tendon sheaths around the shoulder may contribute to the process. At the glenohumeral joint, the presence of inflamed synovium results in progressive destruction of the cartilage surfaces, and marginal and subchondral erosions. Erosions of the humerus tend to be more prominent than erosions of the glenoid process and are particularly characteristic of advanced disease. Inflamed synovial tissue may eventually damage adjacent tendons, so that rotator cuff tear or atrophy is common. The result is superior subluxation of the humeral head relative to the glenoid process and the development of adaptive change at the inferior surface of the acromion process. This surface develops a concavity to fit the top of the humeral head, along with sclerosis, subchondral cyst formation, and osteophyte formation. Unlike most joints that are involved by rheumatoid arthritis, secondary degenerative changes with sclerosis and osteophyte formation are not unusual at the shoulder. When medical therapy fails, total shoulder replacement is an option.



FIGURE 2.44

**FINDINGS** AP radiograph of the shoulder. Arthritic changes are present at the glenohumeral joint with cartilage space narrowing, subchondral sclerosis, and prominent osteophyte formation. The joint surface is enlarged and remodeled, but the humeral head is not subluxated and there are no erosions or soft tissue calcifications. The acromioclavicular joint is not involved.

**DIFFERENTIAL DIAGNOSIS** Pyrophosphate arthropathy, neuropathic arthropathy, posttraumatic arthropathy.

**DIAGNOSIS** Pyrophosphate arthropathy.

**DISCUSSION** The radiographic findings are those of degenerative joint disease; however, osteoarthritis at the glenohumeral

joint is unusual except in the setting of preexisting disease. Pyrophosphate arthropathy is the end-stage degenerative joint disease associated with calcium pyrophosphate dihydrate crystal deposition disease. Abnormalities that may be seen in this condition at the glenohumeral joint include chondrocalcinosis, cartilage space narrowing, subchondral sclerosis, subchondral cyst formation, and osteophyte formation. Osteophytes are characteristically florid on the humeral side, as in this case, with a drooping appearance on the AP projection. If the articular cartilage has been destroyed, chondrocalcinosis will be absent. Rotator cuff tears and calcific deposits in the joint capsule, tendons, and bursae may be associated abnormalities. Occasionally, destructive bone changes may be severe and progressive, resembling neuropathic arthropathy.

**CLINICAL HISTORY** A 48-year-old man with chronic renal failure, and two companion cases.



FIGURE 2.45A

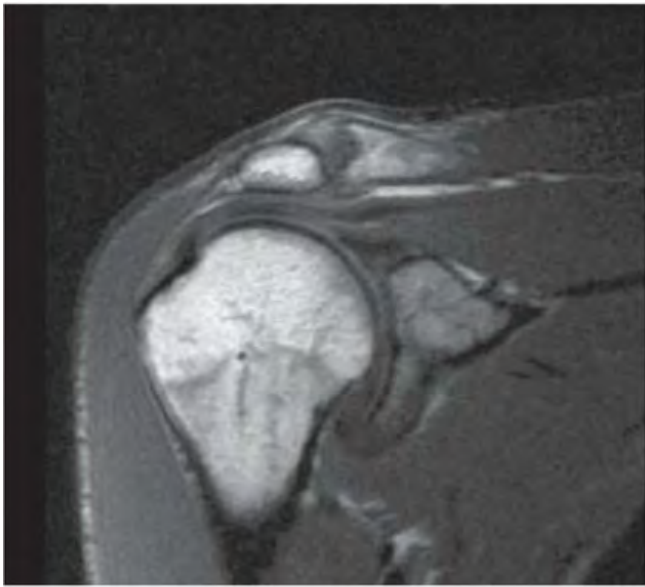


FIGURE 2.45B

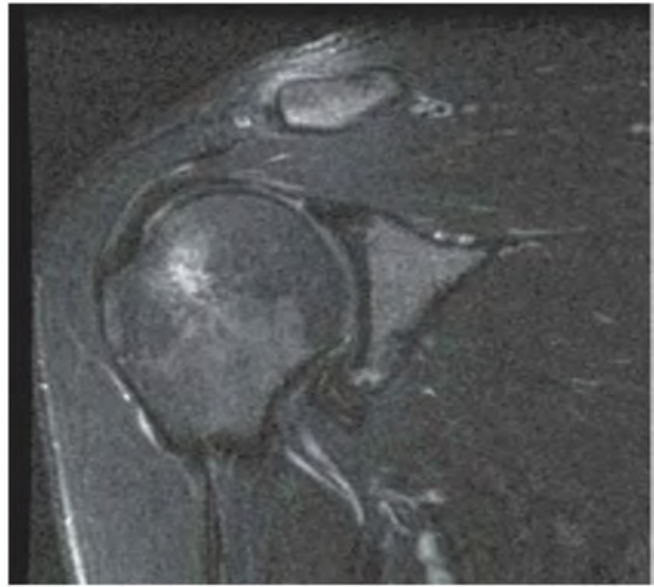


FIGURE 2.45C

### FINDINGS

- A. AP view of the clavicles demonstrates widening of the acromioclavicular joints, with bony resorption of the distal clavicles.
- B. First companion case. Oblique coronal T1-weighted MRI shows bony loss at the distal clavicle and capsular hypertrophy.
- C. Second companion case. Oblique coronal T2-weighted MRI with fat saturation shows increased T2 signal in the distal clavicle and surrounding soft tissues.

**DIFFERENTIAL DIAGNOSIS** Osteolysis of the distal clavicle, acromioclavicular joint separation, acromioclavicular arthritis.

**DIAGNOSIS** Osteolysis of the distal clavicle.

**DISCUSSION** Osteolysis of the distal clavicle refers to subchondral bony resorption of the distal clavicle. Originally described following direct shoulder trauma, this condition has many etiologies besides posttraumatic, including overuse or repetitive stress (especially weight lifters), metabolic (hyperparathyroidism), inflammatory (rheumatoid arthritis, infection), collagen vascular disorders, multiple myeloma, and massive essential osteolysis [69]. Radiographs can be normal early in the clinical course. Later changes include irregularity and osteopenia of the distal clavicles, and widening of the acromioclavicular joints. MRI can demonstrate the bone loss and increased T2-weighted signal in the distal clavicle. However, the increased T2 signal is a nonspecific and relatively frequent finding in asymptomatic patients as well [70].



FIGURE 2.46

**FINDINGS** AP radiograph of the right acromioclavicular joint shows superior subluxation of the distal clavicle relative to the acromion process. No fracture is seen.

**DIFFERENTIAL DIAGNOSIS** None.

**DIAGNOSIS** Acromioclavicular separation (grade 2).

**DISCUSSION** Acromioclavicular injuries involve disruption of the acromioclavicular and coracoclavicular ligaments. Acromioclavicular subluxation can result from a direct blow if the arm is adducted at the time of injury, or from an indirect transmission of the forces through the glenohumeral joint to the acromion if the shoulder is in the protected stance of flexion and abduction. The inferior surfaces of the acromion process and the distal clavicle are normally at the same level on AP radiographs. In a grade 1 injury, the acromioclavicular ligaments are stretched but not disrupted; radiographs are normal or show a slight increase in the joint space and associated soft tissue swelling. When the acromioclavicular ligaments (and usually the trapezius and deltoid

aponeuroses as well) are completely torn (grade 2), the distal clavicle subluxates superiorly. If the coracoclavicular ligaments are also torn, or the coracoid avulses (grade 3), the clavicle dislocates and the space between clavicle and coracoid process widens. Stress views may be needed to elicit the subluxation and are obtained with angled frontal radiographs while the patient holds hand weights. It is recommended that both acromioclavicular joints be included on the radiographs because there may be normal joint laxity in asymptomatic patients. If the distance between the superior aspect of the coracoid and the inferior aspect of the clavicle differs by more than 2 to 4 mm relative to the opposite comparison side, the diagnosis is made. Rarely, the clavicle will dislocate inferiorly, entrap superiorly, or dislocate in association with the sternoclavicular joint (floating clavicle). Posttraumatic coracoclavicular ligament calcification or ossification is common and is usually asymptomatic. The most common complication is osteoarthritis. The most problematic complication is posttraumatic osteolysis of the distal clavicle, which can have an active lytic phase for up to 18 months and mimic infection.

**CLINICAL HISTORY** A 39-year-old woman with shoulder pain.



FIGURE 2.47A



FIGURE 2.47B



FIGURE 2.47C

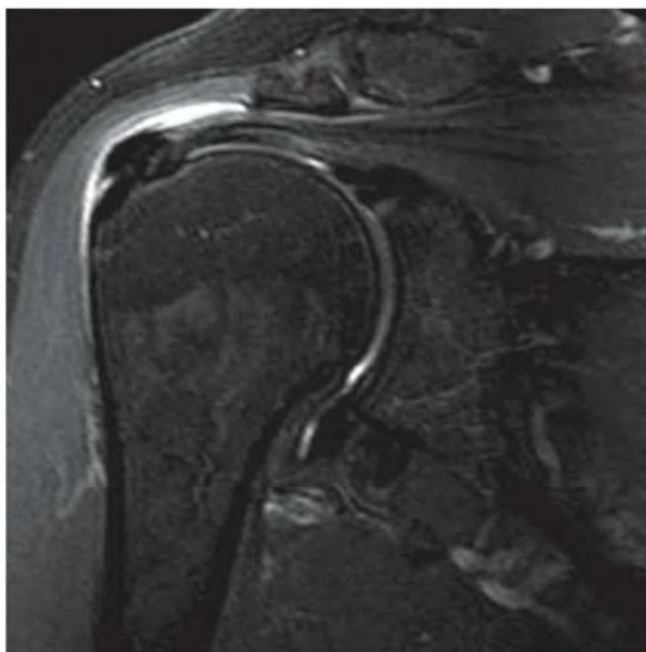


FIGURE 2.47D

**FINDINGS** External rotation radiograph (A), axial proton density fat-suppressed MRI (B), coronal oblique T1-weighted MRI (C), and coronal oblique T2-weighted fat-suppressed MRI (D) of the right shoulder demonstrate calcium hydroxyapatite deposit in the supraspinatus tendon of the rotator cuff. Calcium deposits have low T1-weighted and T2-weighted signal on MRI. A mild amount of high signal is seen surrounding the calcium deposit on the T2-weighted MRI, indicating inflammation or edema.

**DIFFERENTIAL DIAGNOSIS** calcific tendinitis, calcific bursitis, intra-articular loose body.

**DIAGNOSIS** calcific tendinitis.

**DISCUSSION** Soft tissue calcium deposits appear on radiographs as amorphous densities, often sharply defined or angular in shape, and never having a cortex or a trabecular bone pattern, or a calcification pattern of cartilage. Recurrent episodes

of calcific tendinitis or calcific bursitis are commonly associated with hydroxyapatite deposits. Most patients are adults in their 40s and 50s who present with acute pain, swelling, and tenderness. Symptoms respond rapidly to nonsteroidal anti-inflammatory agents. The shoulder is a common site of involvement, usually at the supraspinatus tendon. Tendons may go on to atrophy and rupture, but it is unclear whether the deposits initially caused the local tissue damage, or whether preexisting tissue damage allowed the deposits to accumulate. The calcific deposits around the shoulder are bilateral in about half the cases, and they may migrate to contiguous structures. After clinical resolution, the deposits may disappear. The process is usually monoarticular, but multiple joints may be involved at the same time or in succession. Other common sites of involvement include the long head of the biceps tendon, the extensors of the wrist, the myotendinous attachments along the linea aspera of the femur (thigh adductors), at the medial border of the proximal tibia (pes anserinus), the olecranon bursa, the trochanteric bursa, and the ischial bursa.

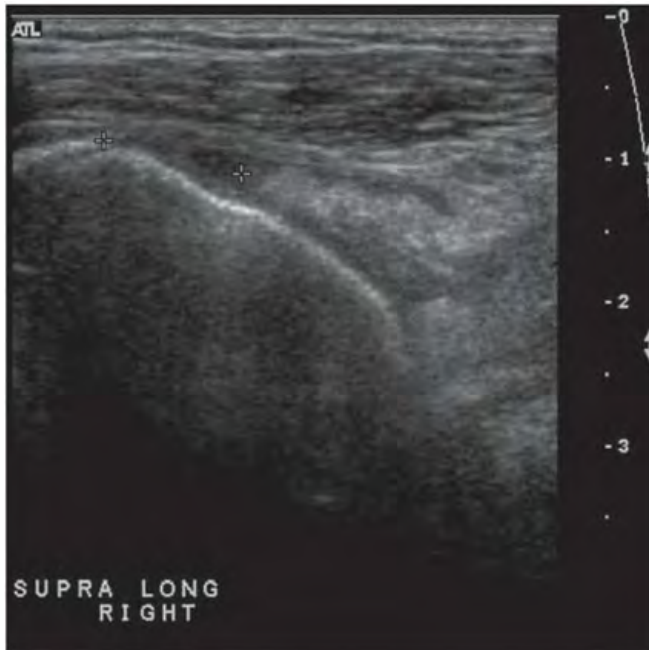


FIGURE 2.48A

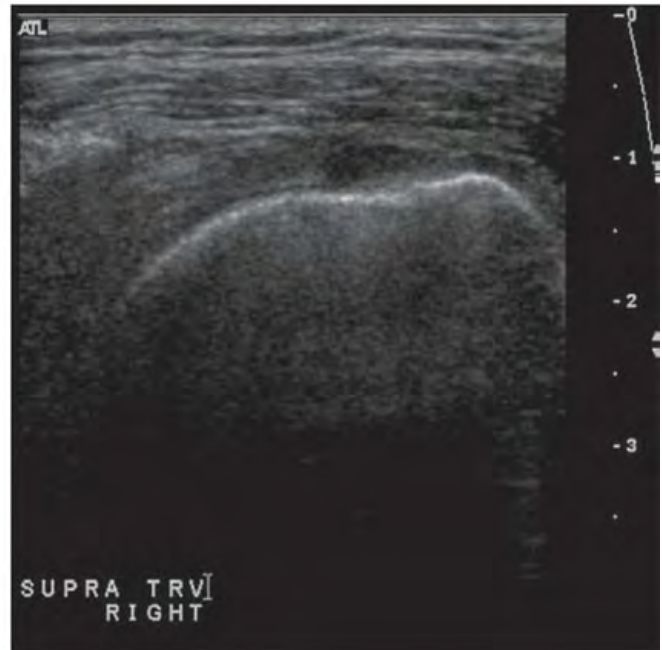


FIGURE 2.48B

**FINDINGS**

- A. Longitudinal sonogram of the distal supraspinatus tendon shows a focal defect where it has detached from the greater tuberosity and retracted medially by 1 cm. The gap is filled with material of mixed echogenicity that exhibits increased through-transmission.
- B. Transverse sonogram through the level of the tear shows an intact infraspinatus tendon adjacent to the gap left by the retracted supraspinatus tendon.

**DIFFERENTIAL DIAGNOSIS** None.

**DIAGNOSIS** Supraspinatus tendon full-thickness tear.

**DISCUSSION** The supraspinatus tendon is the most commonly torn tendon of the rotator cuff. Most full-thickness tears occur at the insertion of the tendon on the greater

tuberosity, frequently beginning at the anterior portion and extending posteriorly across the width of the tendon, but tears may have different morphologies. The sonographic criteria for a full-thickness supraspinatus tendon tear include (a) nonvisualization of the tendon in its expected location or (b) focal defect created by retraction of the torn ends of the tendon ends, with filling of the defect by fluid, debris, or dipping of the deltoid muscle [71]. A number of studies have shown sensitivity and specificity of greater than 90% for detection of full-thickness and partial-thickness rotator cuff tears, including studies performed by nonradiologists [72]. As stated by van Holsbeeck et al, the criteria for detection of partial-thickness supraspinatus tendon tears are (a) a mixed hyperechogenic and hypoechogenic focus in the crucial zone, or (b) a hypoechoic lesion visualized in orthogonal planes with articular or bursal extension [73].

**CLINICAL HISTORY** A 52-year-old man in a high-speed automobile accident.



FIGURE 2.49A

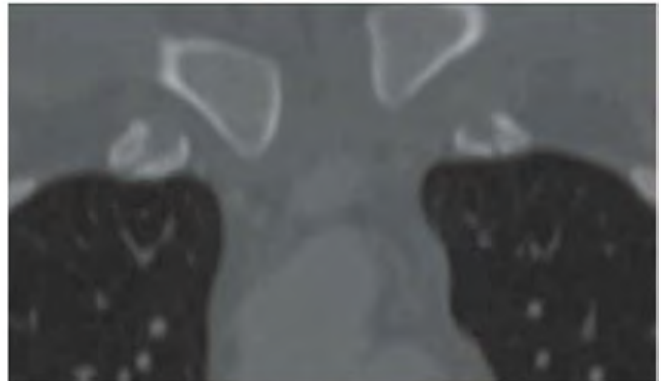


FIGURE 2.49B

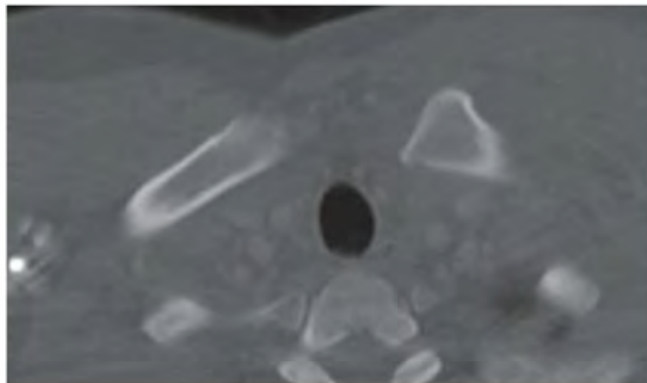


FIGURE 2.49C

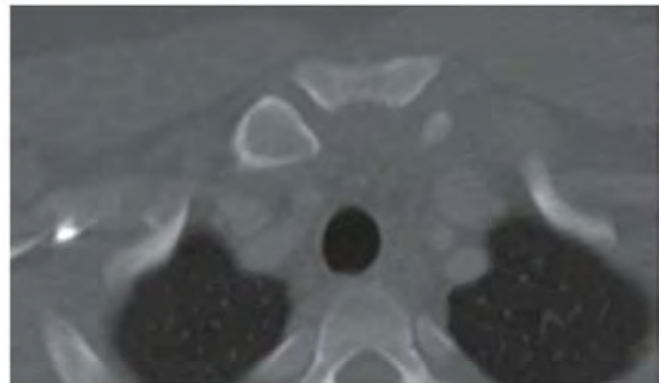


FIGURE 2.49D

### FINDINGS

- A. AP chest radiograph (detail). The medial clavicles are asymmetric, with the left being superior to the right in position.
- B. Coronal CT reformation. The left sternoclavicular joint is dislocated superiorly.
- C, D. Axial CT scan. The left sternoclavicular joint is much wider than the right.

**DIFFERENTIAL DIAGNOSIS** None.

**DIAGNOSIS** Sternoclavicular dislocation.

**DISCUSSION** Sternoclavicular dislocations are exceedingly rare. Indirect trauma propagated along the clavicular

long axis can result in anterior or posterior dislocation of the joint. Direct trauma to the sternoclavicular joint results in posterior dislocation. Reduction of a posterior dislocation is an orthopedic emergency, because the dislocated medial head of the clavicle can impinge on the great vessels, phrenic nerve, esophagus, or trachea. Pneumothorax or hemothorax may also be associated with this condition. Anterior dislocations of the sternoclavicular joint result from a forcible backward traction on the scapula, which torques the clavicle and exceeds the tolerance of the joint capsule and ligaments. Complications are unusual. Dislocation needs to be distinguished from avulsion of the medial clavicular epiphysis [74,75], which is the last growth plate to fuse at about 25 years of age. Both result in pain and a prominent soft tissue bump. CT may be required for definitive diagnosis.

**CLINICAL HISTORY** (A) A 39-year-old man with chronic renal failure. (B–D) A 58-year-old female on hemodialysis with enlarging posterior shoulder and back mass.



FIGURE 2.50A

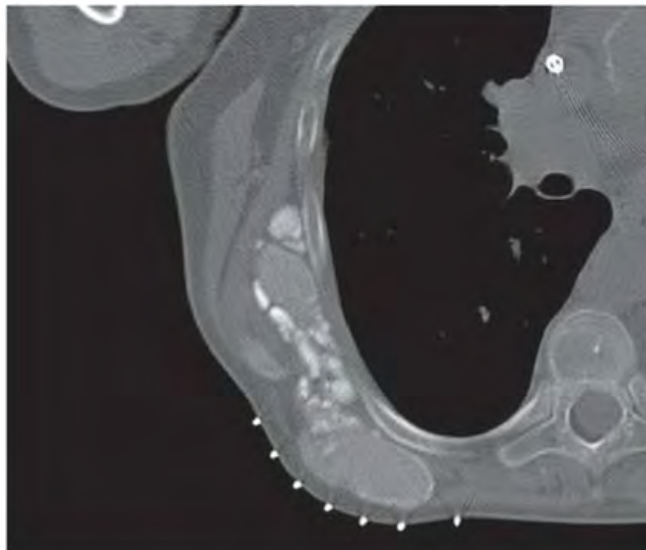


FIGURE 2.50B

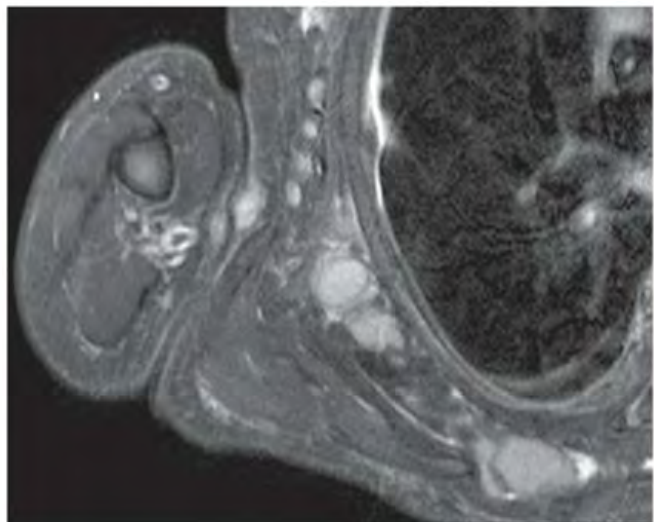


FIGURE 2.50C

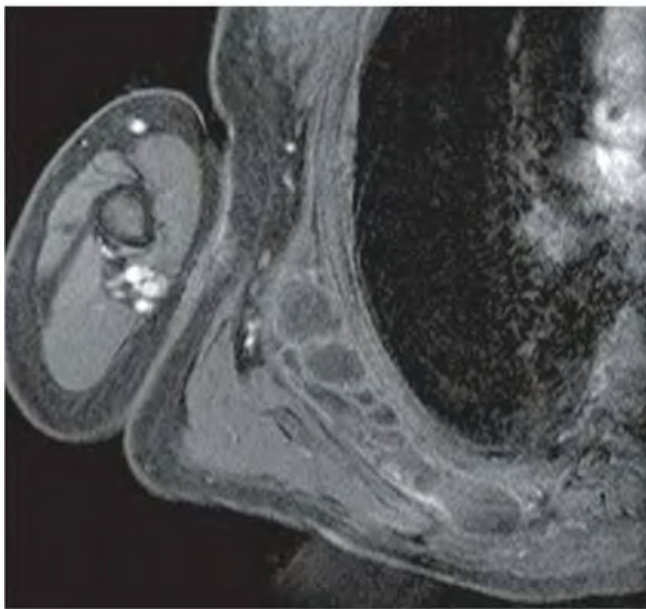


FIGURE 2.50D

**FINDINGS** (A) AP radiograph of left shoulder shows calcific densities overlying the region of the shoulder. The calcifications are rounded and amorphous. The underlying bone appears intact. A few fluid levels are present. Companion case: (B) Axial unenhanced CT in preparation for a CT-guided biopsy demonstrates multiloculated calcific collections of varying density. (C) Axial inversion recovery MRI shows some of the loculations to have fluid signal intensity. (D) Axial gadolinium-enhanced T1-weighted, fat-suppressed MRI shows no enhancement.

**DIFFERENTIAL DIAGNOSIS** None.

**DIAGNOSIS** Secondary tumoral calcinosis.

**DISCUSSION** The key to the diagnosis is the recognition that the soft tissue densities represent calcification rather

than ossification, and that sedimentation levels are present. Metastatic soft tissue deposits of calcium hydroxyapatite crystals around joints may be found in patients with chronic renal failure who are managed on hemodialysis or continuous ambulatory peritoneal dialysis [76]. The particular condition that appears to result in the deposition of calcium is a combination of hyperphosphatemia, hypercalcemia, and increased calcium-phosphorus product. On radionuclide bone scans, the deposits of calcium will show tracer accumulation, often before visualization on radiographs [77]. Because the crystals are often in an aqueous suspension (milk of calcium), CT and upright radiographs may demonstrate fluid-sediment levels [78]. Other dialysis-related bone conditions include aluminum toxicity, which has the appearance of osteomalacia, and amyloid arthropathy.

**CLINICAL HISTORY** A 52-year-old man with chest pain and history of smoking.



FIGURE 2.51A

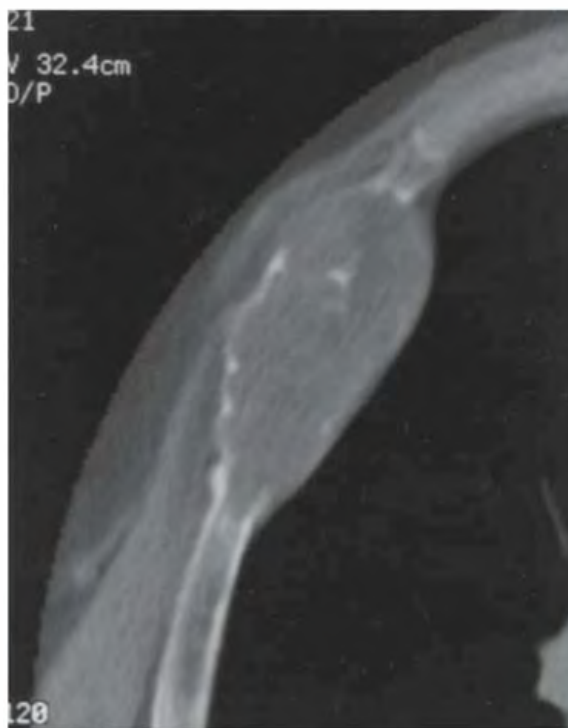


FIGURE 2.51B

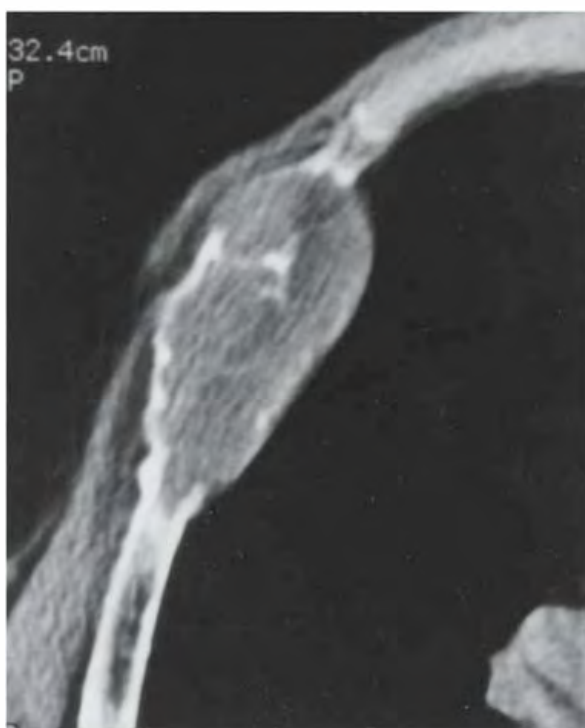


FIGURE 2.51C

## FINDINGS

- A. AP radiograph (detail) of the right ribs demonstrates a pleural-based mass (smooth, well-defined superior margins, indistinct inferior margins) with a loss of the normal anterior right fifth rib.
- B, C. Axial CT (bone and soft tissue settings) shows an expansile soft tissue mass in the rib that has largely destroyed the normal cortical margin. The lesion does not involve the costal cartilage.

**DIFFERENTIAL DIAGNOSIS** Metastasis, myeloma, lymphoma, Ewing's sarcoma, plasmacytoma, eosinophilic granuloma, hemophilic pseudotumor, giant cell tumor, brown tumor.

**DIAGNOSIS** Brown tumor.

**DISCUSSION** A focal, destructive lesion of bone with cortical breakthrough suggests an aggressive process. In this

clinical setting, metastasis or marrow element malignancy would be the leading consideration. If the underlying disorder of hyperparathyroidism is known, then brown tumor would be a leading diagnosis. Brown tumors are typically solitary, expansile, eccentric or cortical lucent lesions that can cause pain due to a pressure phenomenon or pathologic fracture. The lesions provoke little, if any, reactive bone and consist of hemorrhage, multinucleated giant cells, and proliferating fibrous tissue. With successful treatment of the underlying metabolic condition, the lesions can be observed to become sclerotic and heal. Although brown tumors are more common in primary hyperparathyroidism, secondary hyperparathyroidism is more prevalent than primary hyperparathyroidism [79]. Therefore, brown tumors are seen more commonly in conjunction with secondary hyperparathyroidism.

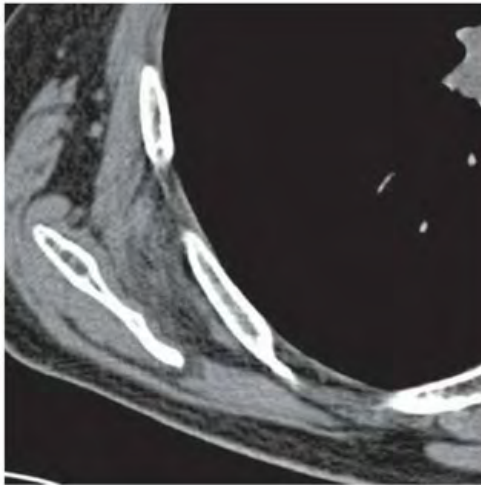


FIGURE 2.52A

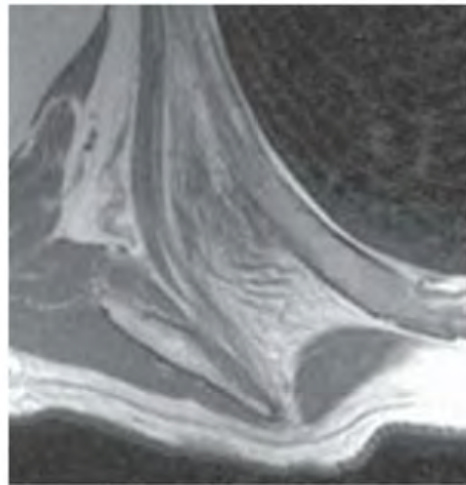


FIGURE 2.52B

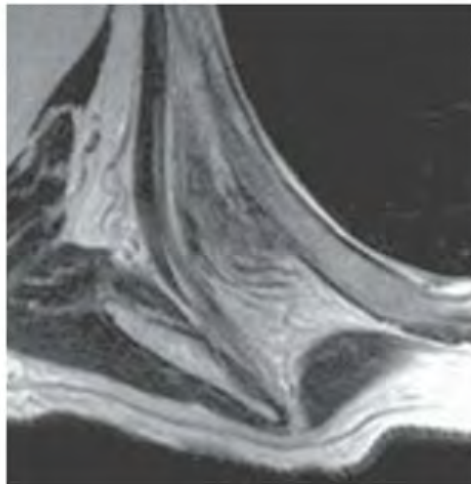


FIGURE 2.52C

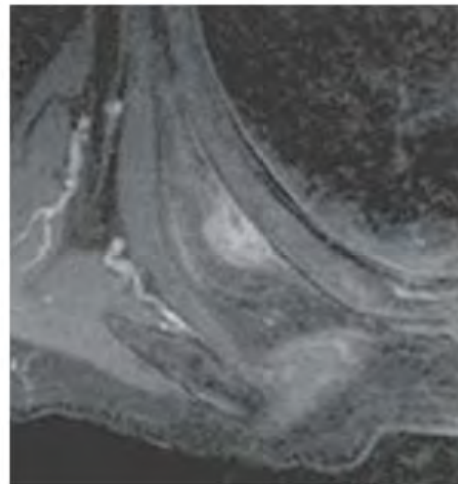


FIGURE 2.52D

## FINDINGS

- A. Axial CT image demonstrates a semicircular mass deep to the scapula. The lesion abuts the chest wall, but does not erode the bone or involve the subpleural space. The lesion is predominantly fatty, but also has strands of soft tissue attenuation.
- B–D. Axial T1-weighted, T2-weighted, and T1-weighted fat-suppressed gadolinium-enhanced MRI demonstrates heterogenous signal and enhancement, arranged in bands.

**DIFFERENTIAL DIAGNOSIS** Liposarcoma, atypical lipoma, elastofibroma, hemangioma, fibromatosis.

**DIAGNOSIS** Elastofibroma.

**DISCUSSION** The appearance and location is characteristic of an elastofibroma. An elastofibroma is a benign fibrous proliferation of adulthood [80]. Other lesions in this category include nodular fasciitis, proliferative fasciitis, proliferative

myositis, and keloid formation. The etiology is thought to be a degenerative response to chronic, repetitive trauma in the upper limb girdle, and the lesion is seen most commonly in weight lifters or laborers who require strong upper body strength. Although they tend to be unilateral, when they occur bilaterally the appearance is virtually diagnostic. Elastofibromas have many of the imaging characteristics of fat-containing tumors, including liposarcoma and hemangioma. The radiologic appearance is that of semicircular, heterogeneous, low-attenuation mass that respects the normal contours of the chest wall or scapula. On MRI, the lesion tends to be heterogeneous, but always has portions with the signal intensity of fat. Enhancement is the rule for all fibromatosis or fibrous proliferative lesions, benign or malignant [81]. On sonography, the fibroelastic strands are hypoechoic, and the characteristic location between the serratus anterior muscles and the chest wall may be identified. Occasionally, biopsy must be used in unilateral lesions to exclude liposarcoma. The prevalence of elastofibroma on autopsy series is 11% to 24%. In one large CT series of adults, the prevalence was 2% [82].

## SOURCES AND READINGS

- Pike JM, Athwal GS, Faber KJ, King GJ. Radial head fractures—an update. *J Hand Surg Am.* 2009;34(3):557–565.
- Ring D, Jupiter JB, Waters PM. Monteggia fractures in children and adults. *J Am Acad Orthop Surg.* 1998;6(4):215–224.
- Sachar K, Akelman E, Ehrlich MG. Radioulnar synostosis. *Hand Clin.* 1994;10:399–404.
- Spritz RA. Familial radioulnar synostosis. *J Med Genet.* 1978;15:160–162.
- Cleary JE, Omer GE Jr. Congenital proximal radio-ulnar synostosis. Natural history and functional assessment. *J Bone Joint Surg Am.* 1985;67:539–545.
- Frumkin K. Nursemaid's elbow: a radiographic demonstration. *Ann Emerg Med.* 1985;14:690–693.
- Triantafyllou SJ, Wilson SC, Rychak JS. Irreducible “pulled elbow” in a child. A case report. *Clin Orthop.* 1992;284:153–155.
- Adeniran A, Merriam WF. Pulled elbow in an adult patient. *J Bone Joint Surg Br.* 1994;76:848–849.
- Prendergast M. Hysteria or pulled elbow. *Lancet.* 1994;343:926.
- Stell IM. Septic and non-septic olecranon bursitis in the accident and emergency department—an approach to management. *J Accid Emerg Med.* 1996;13(5):351–353.
- Holguin PH, Rico AA, Garcia JP, Del Rio JL. Elbow ankylosis due to postburn heterotopic ossification. *J Burn Care Rehabil.* 1996;17:150–154.
- Richards AM, Klaassen MF. Heterotopic ossification after severe burns: a report of three cases and review of the literature. *Burns.* 1997;23:64–68.
- Ilahi OA, Strausser DW, Gabel GT. Posttraumatic heterotopic ossification about the elbow. *Orthopedics.* 1998;21:265–268.
- Goodman TA, Merkel PA, Perlmutter G, Doyle MK, Krane SM, Polisson RP. Heterotopic ossification in the setting of neuromuscular blockade. *Arthritis Rheum.* 1997;40:1619–1627.
- Kobayashi K, Burton KJ, Rodner C, Smith B, Caputo AE. Lateral compression injuries in the pediatric elbow: Panner's disease and osteochondritis dissecans of the capitellum. *J Am Acad Orthop Surg.* 2004;12(4):246–254.
- Fritz RC. MR imaging of sports injuries of the elbow. *Magn Reson Imaging Clin N Am.* 1999;7(1):51–72.
- Miller TT, Shapiro MA, Schultz E, Kalish PE. Comparison of sonography and MRI for diagnosing epicondylitis. *J Clin Ultrasound.* 2002;30(4):193–202.
- O'Dwyer H, O'Sullivan P, Fitzgerald D, Lee MJ, McGrath F, Logan PM. The fat pad sign following elbow trauma in adults: its usefulness and reliability in suspecting occult fracture. *J Comput Assist Tomogr.* 2004;28:562–565.
- Rogers LF. To see or not to see, that is the question: MR imaging of acute musculoskeletal trauma. *AJR Am J Roentgenol.* 2001;176:1.
- Safran MR, Graham SM. Distal biceps tendon ruptures: incidence, demographics, and the effect of smoking. *Clin Orthop.* 2002;404:275–283.
- Falchhook FS, Zlatkin MB, Erbacher GE, Moulton JS, Bisset GS, Murphy BJ. Rupture of the distal biceps tendon: evaluation with MR imaging. *Radiology.* 1994;190:659–663.
- Davison BL, Engber WD, Tigert LJ. Long term evaluation of repaired distal biceps brachii tendon ruptures. *Clin Orthop.* 1996;333:186–191.
- Satsuma S, Yamamoto T, Kobayashi D, et al. Extraabdominal desmoid tumor in a surgical scar of a patient with Sprengel's deformity. *J Pediatr Surg.* 2003;38(10):1540–1542.
- Edmonds LD, Ly JQ, LaGatta LM, Lusk JD, Beall DP. Quiz case. Extraabdominal desmoid tumor of the upper arm. *Eur J Radiol.* 2003;48(3):312–315.
- Robbin MR, Murphey MD, Temple HT, Kransdorf MJ, Choi JJ. Imaging of musculoskeletal fibromatosis. *Radiographics.* 2001;21(3):585–600.
- Fechner RE, Mills SE. *Tumors of the Bones and Joints.* Washington, DC: Armed Forces Institute of Pathology; 1993:84–85.
- Brien EW, Mirra JM, Luck JV Jr. Benign and malignant cartilage tumors of bone and joint: their anatomic and theoretical basis with an emphasis on radiology, pathology and clinical biology: II. Juxtacortical cartilage tumors. *Skeletal Radiol.* 1999;28(1):1–20.
- Unni KK, Inwards CY. *Dahlin's Bone Tumors: General Aspects and Data on 10,165 Cases.* 6th ed. Philadelphia, PA: Lippincott Williams & Wilkins; 2010:22–40.
- Capanna R, Dal Monte A, Gitelis S, Campanacci M. The natural history of unicameral bone cyst after steroid injection. *Clin Orthop.* 1982;166:204–211.
- Margau R, Babyn P, Cole W, Smith C, Lee F. MR imaging of simple bone cysts in children: not so simple. *Pediatr Radiol.* 2000;30(8):551–557.
- Struhl S, Edelson C, Pritzker H, Seimon LP, Dorfman HD. Solitary (unicameral) bone cyst. The fallen fragment sign revisited. *Skeletal Radiol.* 1989;18:261–265.
- Johnston CE II, Fletcher RR. Traumatic transformation of unicameral bone cyst into aneurysmal bone cyst. *Orthopedics.* 1986;9:1441–1447.
- Murphey MD, Robbin MR, McRae GA, Flemming DJ, Temple HT, Kransdorf MJ. The many faces of osteosarcoma. *Radiographics.* 1997;17:1205–1231.
- Schweitzer ME, Morrison WB. MR imaging of the diabetic foot. *Radiol Clin North Am.* 2004;42(1):61–71.
- Hasan SS, Romeo AA. Nontraumatic osteonecrosis of the humeral head. *J Shoulder Elbow Surg.* 2002;11(3):281–298.
- Gherman RB, Ouzounian JG, Miller DA, Kwock L, Goodwin TM. Spontaneous vaginal delivery: a risk factor for Erb's palsy? *Am J Obstet Gynecol.* 1998;178:423–427.
- Ouzounian JG, Korst LM, Phelan JP. Permanent Erb palsy: a traction-related injury? *Obstet Gynecol.* 1997;89:139–141.
- Jennett RJ, Tarby TJ, Kreinick CJ. Brachial plexus palsy: an old problem revisited. *Am J Obstet Gynecol.* 1992;166:1673–1676.
- Peleg D, Hasnin J, Shalev E. Fractured clavicle and Erb's palsy unrelated to birth trauma. *Am J Obstet Gynecol.* 1997;177:1038–1040.
- Miller JD, Pruitt S, McDonald TJ. Acute brachial plexus neuritis: an uncommon cause of shoulder pain. *Am Fam Physician.* 2000;62:2067–2072.
- Helms CA, Martinez S, Speer KP. Acute brachial neuritis (Parsonage-Turner syndrome): MR imaging appearance—report of three cases. *Radiology.* 1998;207(1):255–259.
- Chautems RC, Glauser T, Waeber-Fey MC, Rostan O, Barraud GE. Quadrilateral space syndrome: case report and review of the literature. *Ann Vasc Surg.* 2000;14(6):673–676.
- Helms CA. The impact of MR imaging in sports medicine. *Radiology.* 2002;224(3):631–635.
- Lester B, Jeong GK, Weiland AJ, Wickiewicz TL. Quadrilateral space syndrome: diagnosis, pathology, and treatment. *Am J Orthop.* 1999;28(12):718–722, 725.
- Roberts CC, Liu PT, Colby TV. Encapsulated versus nonencapsulated superficial fatty masses: a proposed MR imaging classification. *Am J Roentgenol.* 2003;180(5):1419–1422.
- Zehetgruber H, Noske H, Lang T, Wurnig C. Suprascapular nerve entrapment. A meta-analysis. *Int Orthop.* 2002;26(6):339–343.
- Patte D. Classification of rotator cuff lesions. *Clin Orthop.* 1990;254:639–645.
- Mansat P, Frankle MA, Cofield RH. Tears in the subscapularis tendon: descriptive analysis and results of surgical repair. *Joint Bone Spine.* 2003;70(5):342–347.
- Tung GA, Yoo DC, Levine SM, Brody JM, Green A. Subscapularis tendon tear: primary and associated signs on MRI. *J Comput Assist Tomogr.* 2001;25(3):417–424.
- Taylor DC, Arciero RA. Pathologic changes associated with shoulder dislocations. Arthroscopic and physical examination findings in first-time, traumatic anterior dislocations. *Am J Sports Med.* 1997;25:306–311.
- Suder PA, Frich LH, Hougaard K, Lundorf E, Wulff Jakobsen B. Magnetic resonance imaging evaluation of capsulolabral tears after traumatic primary anterior shoulder dislocation. A prospective comparison with arthroscopy of 25 cases. *J Shoulder Elbow Surg.* 1995;4:419–428.

52. Pevny T, Hunter RE, Freeman JR. Primary traumatic anterior shoulder dislocation in patients 40 years of age and older. *Arthroscopy*. 1998;14:289–294.
53. Gonzalez D, Lopez R. Concurrent rotator-cuff tear and brachial plexus palsy associated with anterior dislocation of the shoulder. A report of two cases. *J Bone Joint Surg Am*. 1991;73:620–621.
54. Yamamoto T, Yoshiya S, Kurosaka M, Nagira K, Nabeshima Y. Luxatio erecta (inferior dislocation of the shoulder): a report of 5 cases and a review of the literature. *Am J Orthop*. 2003;32(12):601–603.
55. Karaoglu S, Guney A, Ozturk M, Kecec Z. Bilateral luxatio erecta humeri. *Arch Orthop Trauma Surg*. 2003;123(6):308–310.
56. Arndt JH, Sears AD. Posterior dislocation of the shoulder. *AJR Am J Roentgenol*. 1965;94:81–86.
57. Cisternino SJ, Rogers LF, Stuffelbam BC, Kruglik GD. The trough line: a radiographic sign of posterior shoulder dislocation. *AJR Am J Roentgenol*. 1978;130:951–954.
58. Wadlington VR, Hendrix RW, Rogers LF. Computed tomography of posterior fracture-dislocations of the shoulder: case reports. *J Trauma*. 1992;32:113–115.
59. Elberger ST, Brody G. Bilateral posterior shoulder dislocations. *Am J Emerg Med*. 1995;13:331–332.
60. Rath E, Levy O, Liberman N, Atar D. Bilateral dislocation of the hip during convulsions: a case report. *J Bone Joint Surg Br*. 1997;79:304–306.
61. Van Heest A, Vorlicky L, Thompson RC Jr. Bilateral central acetabular fracture dislocations secondary to sustained myoclonus. *Clin Orthop*. 1996;324:210–213.
62. McCullen GM, Brown CC. Seizure-induced thoracic burst fractures. A case report. *Spine*. 1994;19:77–79.
63. Snyder SJ, Karzel RP, Del Pizzo W, et al. SLAP lesions of the shoulder. *Arthroscopy*. 1990;6:274–279.
64. Modarresi S, Motamedi D, Jude CM. Superior labral anteroposterior lesions of the shoulder: part 2, mechanisms and classification. *AJR Am J Roentgenol*. 2011 Sep;197(3):604–11.
65. Hermann G, Klein MJ, Abdelwahab IF, Kenan S. Synovial chondrosarcoma arising in synovial chondromatosis of the right hip. *Skeletal Radiol*. 1997;26:366–369.
66. De Ferm A, Lagae K, Bunker T. Synovial osteochondromatosis: an unusual cause for subacromial impingement. *Acta Orthop Belg*. 1997;63:218–220.
67. Buess E, Friedrich B. Synovial chondromatosis of the glenohumeral joint: a rare condition. *Arch Orthop Trauma Surg*. 2001;121(1-2):109–111.
68. Resnick D. *Diagnosis of Bone and Joint Disorders*. 4th ed. Philadelphia, PA: WB Saunders; 2002:917–921.
69. Gordon BH, Chew FS. Isolated acromioclavicular joint pathology in the symptomatic shoulder on magnetic resonance imaging: a pictorial essay. *J Comput Assist Tomogr*. 2004;28:215–222.
70. Fiorella D, Helms CA, Speer KP. Increased T2 signal intensity in the distal clavicle: incidence and clinical implications. *Skeletal Radiol*. 2000;29(12):697–702.
71. Teefey SA, Hasan SA, Middleton WD, Patel M, Wright RW, Yamaguchi K. Ultrasonography of the rotator cuff: a comparison of ultrasonographic and arthroscopic findings in one hundred consecutive cases. *J Bone Joint Surg Am*. 2000;82:498–450.
72. Ziegler DW. The use of in-office, orthopaedist-performed ultrasound of the shoulder to evaluate and manage rotator cuff disorders. *J Shoulder Elbow Surg*. 2004;13:291–297.
73. van Holsbeeck MT, Kolowich PA, Eyler WR, et al. US depiction of partial-thickness tear of the rotator cuff. *Radiology*. 1995;197:443–446.
74. Cope R. Dislocations of the sternoclavicular joint. *Skeletal Radiol*. 1993;22:233–238.
75. Lewonowski K, Bassett GS. Complete posterior sternoclavicular epiphyseal separation. A case report and review of the literature. *Clin Orthop*. 1992;281:84–88.
76. Kuriyama S, Tomonari H, Nakayama M, Kawaguchi Y, Sakai O. Successful treatment of tumoral calcinosis using CAPD combined with hemodialysis with low-calcium dialysate. *Blood Purif*. 1998;16:43–48.
77. Ejaz AA, Nisar N, Ghandhi VC, Eilers DB, Shirazi PH, Ing TS. Metastatic soft tissue calcification in chronic renal failure detected by radionuclide imaging. *Clin Nucl Med*. 1995;20:505–507.
78. Gordon LF, Arger PH, Dalinka MK, Coleman BG. Computed tomography in soft tissue calcification layering. *J Comput Assist Tomogr*. 1984;8:71–73.
79. Pai M, Park CH, Kim BS, Chung YS, Park HB. Multiple brown tumors in parathyroid carcinoma mimicking metastatic bone disease. *Clin Nucl Med*. 1997;22:691–694.
80. Kudo S. Elastofibroma dorsi: CT and MR imaging findings. *Semin Musculoskelet Radiol*. 2001;5(2):103–105.
81. Schick S, Zembsch A, Gahleitner A, et al. Atypical appearance of elastofibroma dorsi on MRI: case reports and review of the literature. *J Comput Assist Tomogr*. 2000;24(2):288–292.
82. Brandser EA, Goree JC, El-Khoury GY. Elastofibroma dorsi: prevalence in an elderly patient population as revealed by CT. *AJR Am J Roentgenol*. 1998;171:977–980.

CHAPTER

# 3

## Spine

**CLINICAL HISTORY** *An unconscious 13-year-old girl after a motor vehicle accident, and a companion case.*



FIGURE 3.1A

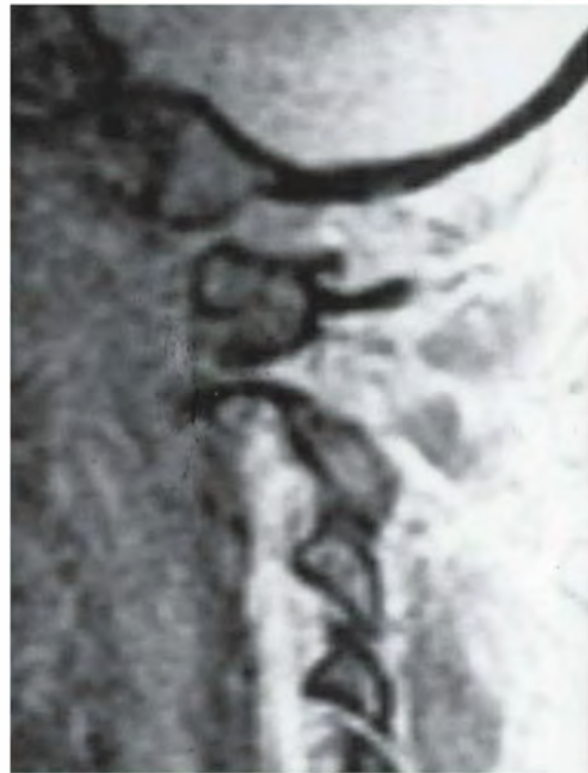


FIGURE 3.1B

## FINDINGS

- A. Lateral radiograph of the cervical spine. The prevertebral soft tissues are massively enlarged, even with intubation of the patient. The integrity of the craniocervical junction is difficult to assess, but the upper cervical spine appears intact.
- B. Companion case: A 42-year-old woman ejected from rollover motor vehicle accident. Sagittal T2-weighted magnetic resonance imaging (MRI) through the left atlanto-occipital joint demonstrates marked forward subluxation of the occipital condyle. The appearance of the right atlanto-occipital joint (not shown) is similar.

**DIFFERENTIAL DIAGNOSIS** None.

**DIAGNOSIS** Atlanto-occipital dislocation.

**DISCUSSION** The craniocervical junction is evaluated on radiographs with lateral and open mouth views. Soft tissue swelling is an invariable finding in the acute presentation, as seen here. The superior facets of the lateral masses of C1 should articulate with the occipital condyles. Although there are several indirect radiographic methods for assessing the craniocervical junction, they depend on accurately

positioned radiographs, which are often difficult to obtain in the acute setting with multiple injuries. When injury is suspected by the mechanism of trauma and the presence of soft tissue swelling, even if the relationship of the occipital condyles to the superior facets of the atlas appears normal on radiographs, direct imaging with cross-sectional methods (computed tomography [CT] or MRI) is still indicated.

Traumatic atlanto-occipital dislocation has generally been considered to be incompatible with life, but many patients have survived this injury [1–4]. As CT is being used more frequently to screen for cervical spine injuries, less severe forms of atlanto-occipital dislocation are being recognized. Early diagnosis is crucial in order to avoid life-threatening diagnostic manipulations, such as attempts at flexion-extension views, and to provide adequate treatment. This is a particular concern in patients with multiple traumas. Unrecognized traumatic atlanto-occipital dislocation may contribute to deterioration and rapid demise of patients who arrive from the scene alert and neurologically intact. Patients who survive these injuries often have severe spinal cord injury, but there are reports of recovery with good neurologic outcome [5]. Cerebral trauma is frequently associated. Treatment is halo immobilization and surgical fusion of the occiput to C1 and C2.

**CLINICAL HISTORY** *An adult female automobile accident victim, acute presentation; companion case, man who fell off roof.*



FIGURE 3.2A

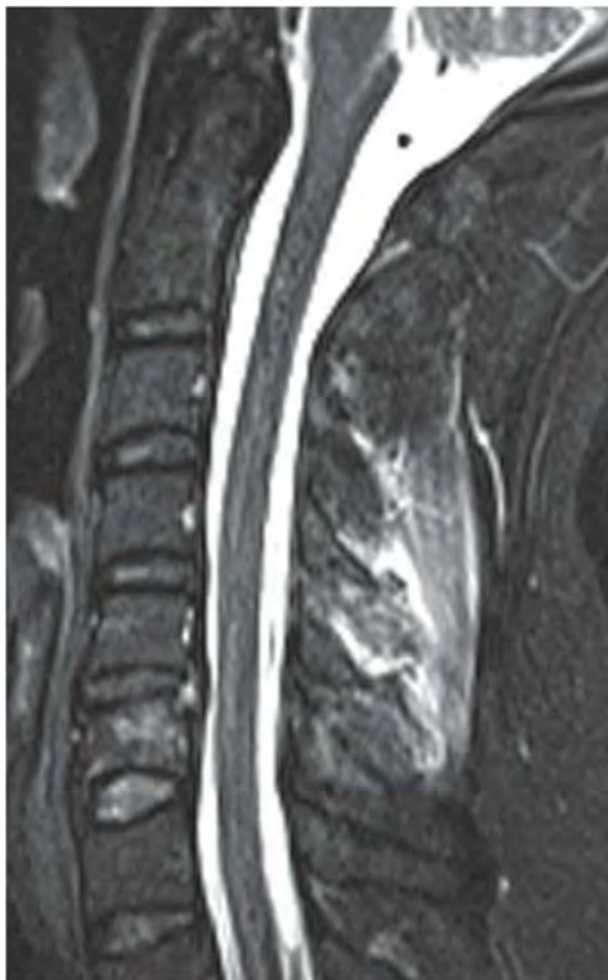


FIGURE 3.2B

## FINDINGS

- A. Lateral radiograph of the cervical spine. There is narrowing of the C5–C6 anterior disc space and widening of the posterior disc space. Marked widening is present between the C5 and C6 spinous processes. Mild prevertebral soft tissue swelling is present. No fracture is identified.
- B. Companion case. Sagittal T2-weighted MRI shows high signal in the posterior soft tissues at the C3–C5 levels indicative of hyperflexion sprain. There is also a fracture of the body of C6.

**DIFFERENTIAL DIAGNOSIS** None.

**DIAGNOSIS** Hyperflexion sprain.

**DISCUSSION** When the neck is forcibly flexed, the cervical spine is distracted posteriorly and compressed anteriorly. If the forces are relatively small, the injury may consist of a posterior ligamentous sprain (hyperflexion sprain) and

possibly a compression fracture of the vertebral body. The radiographic hallmarks of a hyperflexion injury are a focal kyphosis in conjunction with narrowing of the anterior disc space, widening of the posterior disc space, and splaying of the spinous processes [25]. Hyperflexion sprain results in a tear of the posterior longitudinal ligament complex (including the posterior longitudinal ligament, supraspinous and interspinous ligaments, joint capsule, and ligamentum flavum). This disruption allows anterior subluxation of the vertebral body by 1 to 3 mm in conjunction with mild subluxation of the facet joints. The radiographic findings may be subtle. Straightening of the cervical spine in the acute setting may be secondary to muscular trauma, and a focal kyphosis may ensue at a later time. Fluid-sensitive sequences on MRI may show high signal in the posterior soft tissues, corresponding to tears of the posterior ligaments. Injury may occur at more than one level, as demonstrated in the companion case presented here. If untreated, this type of injury may be associated with delayed instability [26].

**CLINICAL HISTORY** *A 70-year-old man who fell.*



FIGURE 3.3A

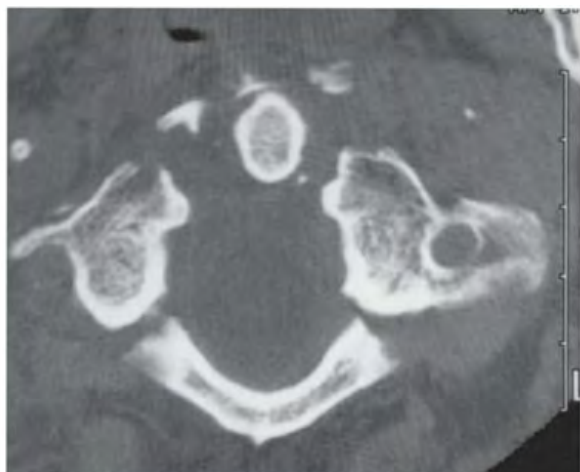


FIGURE 3.3B



FIGURE 3.3C

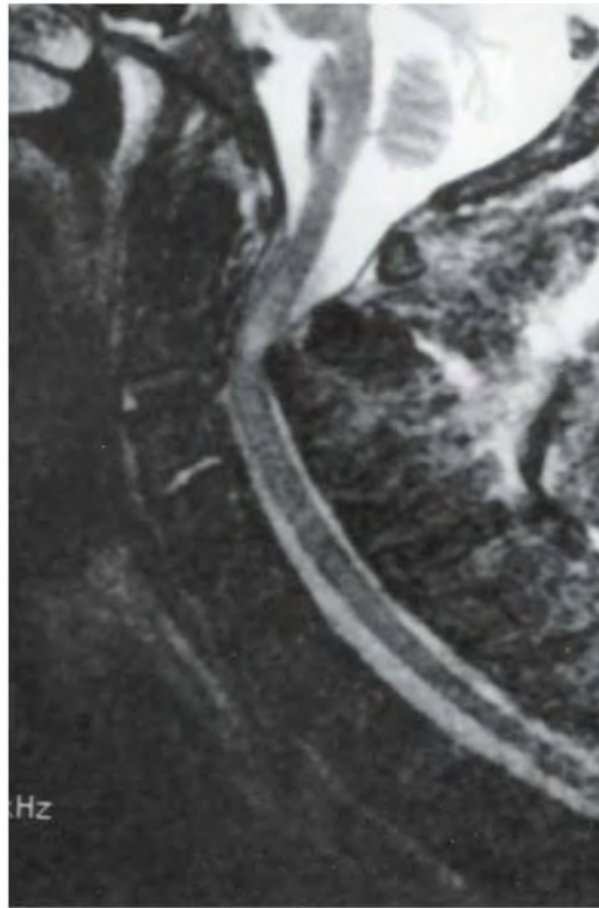


FIGURE 3.3D

**FINDINGS**

- A. Lateral radiograph of the cervical spine demonstrates widening of the C1 ring. Increased distraction of the C2–C3 disc space is noted, with an accentuated, focal lordosis. There are incidental findings of diffuse idiopathic skeletal hyperostosis (DISH).
- B. Axial CT demonstrates Jefferson burst fracture at C1.
- C. Detail of sagittally reformatted CT image shows the increased distraction and lordosis at C2–C3 and the displacement of the posterior arch of C1.
- D. Sagittal T2-weighted MRI at the midline demonstrates mechanical impingement on the posterior aspect of the cervical spinal cord at the C2–C3 level. High signal in the cord itself indicates contusion.

**DIFFERENTIAL DIAGNOSIS** None.

**DIAGNOSIS** Complex C1–C2 fractures.

**DISCUSSION** Mimics of a Jefferson fracture include the isolated posterior C1 arch fracture (which can be distinguished by the lack of prevertebral soft tissue swelling) and the

congenital fusion failure of posterior C1 arch. These can be differentiated by CT. This case illustrates the importance of careful screening after identifying one injury [6]. Distraction of the C2–C3 disc space is most suggestive of a concurrent hyperextension injury. The classic axial load injury is the Jefferson fracture, which consists of a disruption of the anterior and posterior arches of C1. The fractures can be unilateral or bilateral. The transverse ligament can be intact or disrupted, resulting in widening of the anterior or lateral atlantodental interval. If there is a vertical fracture through one of the articular masses, the medial fragment may maintain its normal relationship with the dens while the lateral fragment migrates laterally. Cervical spine fractures in the elderly are relatively common, comprising 23% of cervical spine fractures in one study [7]. Virtually all fractures in the elderly age group involve the atlantoaxial complex [8], with the most common lesion being a fracture of the odontoid process or a combination of fractures of both C1 and C2, as in this case. The injuries are associated with considerable morbidity and mortality, mostly from coexisting respiratory disease [9]. Treatment with a rigid collar, a halo brace, or surgical stabilization may be successful according to circumstance.

## 3.4

**CLINICAL HISTORY** A 54-year-old man with chronic neck pain. He was involved in an automobile accident at age 20.



FIGURE 3.4A



FIGURE 3.4B



FIGURE 3.4C

## FINDINGS

- A, B. Lateral cervical spine flexion-extension series. There is gross instability of C1 over C2 in both flexion and extension, resulting from an ununited odontoid fracture. Sclerotic, remodeled fracture margins with pseudoarthrosis are evidence of the chronicity of the lesion. The margins of the spinal canal at C1 and C2 are malaligned.
- C. Sagittal T2-weighted MRI demonstrates a neutral position of the dens at the time of imaging, with T2 hyperintense fluid interposed between the C2 body and the dens. Extensive ligamentous edema is noted in the posterior neck musculature.

**DIFFERENTIAL DIAGNOSIS** None.

**DIAGNOSIS** Nonunion of odontoid fracture (os odontoideum).

**DISCUSSION** Fractures of the odontoid process of C2 (dens) occur transversely across the base, probably as a result of hyperextension, hyperflexion, or lateral flexion [10]. The Anderson classification for fractures of the dens is as follows: (type I) superolateral odontoid, avulsed by the intact

alar ligament, an exceedingly rare lesion; (type II) base of dens, “high dens fracture;” (type III) superior axis, caudal to the odontoid base, “low dens fracture.”

The odontoid is composed primarily of cortical bone, so this fracture heals less well than fractures through portions of the vertebra that are primarily cancellous. Schatzker et al. [11] report nonunion in 64% of type II fractures, and 100% of those with 5 mm or more of distraction.

An odontoid fracture that has progressed to atrophic nonunion is called an os odontoideum. Like nonunions elsewhere, the margins of the fracture line become corticated; a fibrous union or a pseudoarthrosis may be present. Although some authorities argue that the os odontoideum is a developmental variant in which the odontoid process does not fuse to the body of C2, the site of the synchondrosis between the odontoid process and the body of C2 is not located here. Because of present or potential mechanical instability, surgical fusion of C1 and C2 is the common method of management.

This is a complex case because the sclerotic dens margin suggests chronicity, whereas the posterior soft tissue swelling indicates a superimposed acute injury. The instability of the upper cervical spine leaves the spine vulnerable to catastrophic injury with relatively minor trauma.

**CLINICAL HISTORY** A 23-year-old man who was the front seat passenger in a high-speed automobile crash. There was no neurologic deficit.



FIGURE 3.5A



FIGURE 3.5B

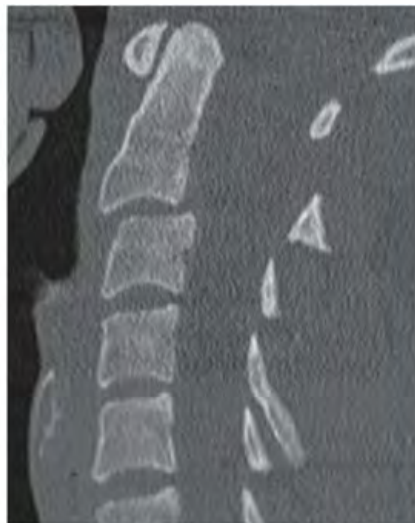


FIGURE 3.5C



FIGURE 3.5D

## FINDINGS

- A. Lateral radiograph of the cervical spine. Horizontal fractures through the bilateral pars interarticularis have allowed the anterior portion of C2 to translate anteriorly. The posterior arch fragment of C2 is displaced posteriorly, resulting in segmental widening of the spinal canal.
- B–D. Sagittal CT reformations of the cervical spine (left to right). There is mild distraction at the fracture sites. The fractures have an oblique coronal morphology from tensile loading. There is approximately 3 mm anterolisthesis of C2 over C3, pulling the left vertebral artery forward. The C2–C3 disc space may be minimally narrowed.

**DIFFERENTIAL DIAGNOSIS** None.

**DIAGNOSIS** Traumatic C2 spondylolisthesis.

**DISCUSSION** In traumatic C2 spondylolisthesis (hangman's fracture), there are bilateral pars interarticularis fractures with forward subluxation of C2 over C3 [12]. The pars interarticularis is the bridge of bone that occupies the position in the articular mass between the superior and inferior articular facets.

An individual subjected to judicial hanging drops feet first through a trap door with a rope secured around the neck and the hangman's knot located under the chin. When he or she

reaches the end of the rope, the upper cervical spine is pulled violently into hyperextension and simultaneously subjected to massive distractive forces from the downward inertia of the body. The ligaments of the anterior column are torn at the C2–C3 level, and the posterior elements are fractured at the pars interarticularis, as C2 is grossly distracted from C3. Similar fractures of the C2 posterior elements may also occur when an axial load (compressive rather than distractive) is applied with the neck hyperextended, but the gross distraction of C2 from C3 does not occur. This mechanism of injury may occur in a motor vehicle accident in which the passenger slides forward and strikes the forehead, forcing the neck into hyperextension.

The Levine and Edwards modification of the Effendi classification for traumatic C2 spondylolisthesis is as follows [13]: (type I) less than 3-mm anterior C2 body translation and no angulation; (type II) greater than 3-mm anterior C2 body translation and angulation; (type IIA) minimal C2 body translation but severe angulation; (type III) severe displacement and severe angulation.

There are associated injuries in 14% of cases, half of which involve the C1 posterior arch or dens. With the exception of the type III variant, the resulting neurologic deficits are often absent or minimal because of the typically capacious spinal canal at the C2 level and the fact that the fragments spread circumferentially. Depending on the severity of the injury, treatment may be conservative or surgical [14].

**CLINICAL HISTORY** *A 35-year-old woman in an automobile accident.*



FIGURE 3.6A

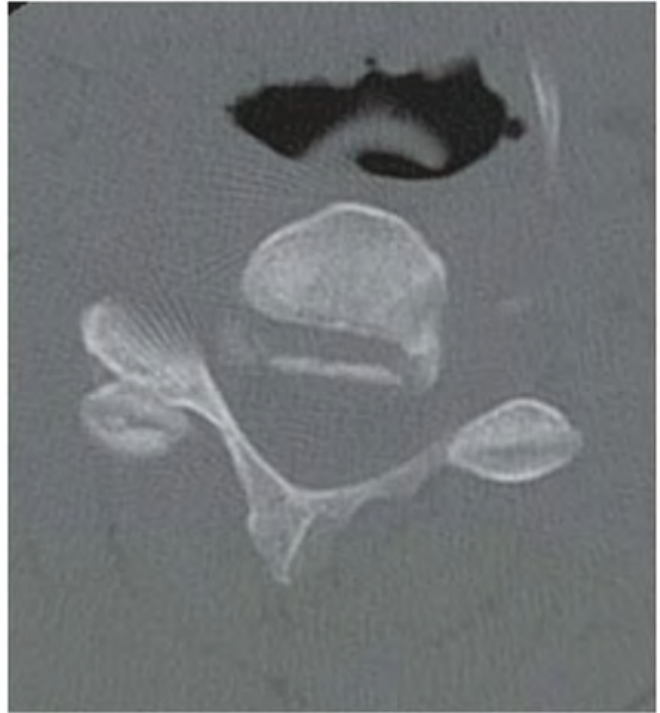


FIGURE 3.6B



FIGURE 3.6C

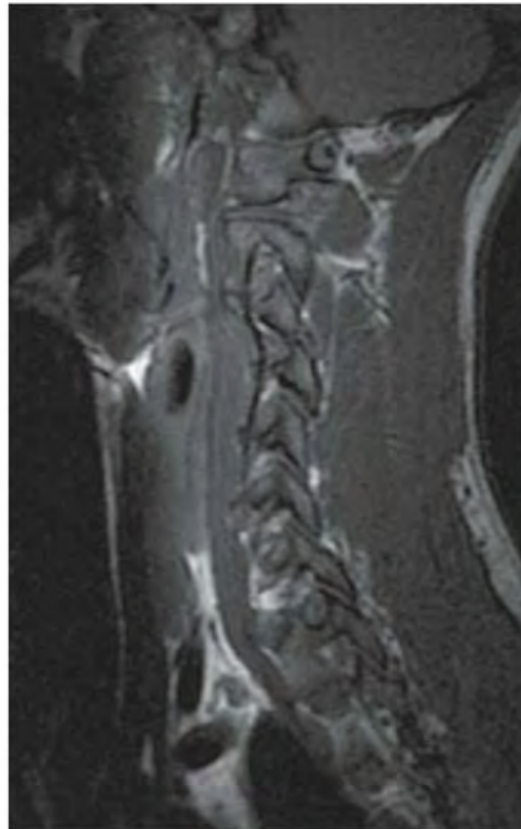


FIGURE 3.6D

## FINDINGS

- A. Lateral radiograph of the cervical spine. There is 25% forward subluxation of C3 over C4. The inferior facet of C3 is dislocated over the superior facet of C4, leaving it partially uncovered. Rotatory displacement is evident by the differences in the radiographic overlap of the facets above and below the level of injury. A focal kyphosis is present, and there is soft tissue swelling.
- B. CT (bone windows) at the C3–C4 level shows the right inferior articular process of C3 is anterior to the right superior articular process of C4, but a normal relationship is present on the left.
- C. Sagittal proton density (PD) MRI in the midline shows forward subluxation of C3 over C4 with a widening of the disc space.
- D. MRI on the right shows the C3 facet dislocated over C4.

**DIFFERENTIAL DIAGNOSIS** None.

**DIAGNOSIS** Unilateral facet dislocation (unilateral locked facet).

**DISCUSSION** The plain film is diagnostic in this case. C3 is anteriorly subluxated approximately 25% of a vertebral body width in conjunction with minimal distraction of the C3–C4 disc space and a solitary “jumped” facet (the more superior facet is anterior to its articulating inferior facet). These findings are corroborated on CT and MRI. Unilateral

facet dislocation occurs with hyperflexion and rotation [15]. Axial rotation and lateral bending are normally coupled in the middle and lower cervical spine because of the angle of the facet joints. With lateral bending, the facet joint on the concave side of the bend is compressed and essentially fixed, and the contralateral articular mass rides forward and up and dislocates into the intervertebral foramen. The superior portion of the inferior facet is frequently fractured, presumably from impaction. The ligaments are disrupted on the side of the dislocation. Unilateral facet dislocation is recognized by forward subluxation of the vertebral body, as shown here, combined with the dislocation of the facet. Sometimes the dislocated inferior facet can be seen projecting into the vertebral foramen (not shown), and the superior facet of the level below is uncovered or “naked” (shown on the plain radiographs). Soft tissue swelling is often present. The fanning of the spinous processes and widening of the disc space are indicative of the hyperflexion component of the injury. The CT can show the clockwise rotation of one vertebral body relative to the level below. In addition, the “reverse hamburger bun” sign can be demonstrated as replacement of the normal, flat, articulating surfaces with the convex surfaces in apposition [16]. CT can also define an associated articular process fracture, seen in up to 73% of cases. MRI would show the associated hemorrhage tracking along the anterior and posterior longitudinal ligaments. MRI can also identify associated soft tissue injuries [17] and serve as a screen to identify intimal injury of the vertebral artery.

**CLINICAL HISTORY** A 22-year-old woman in a motor vehicle crash, and a companion case.



FIGURE 3.7A



FIGURE 3.7B



FIGURE 3.7C



FIGURE 3.7D

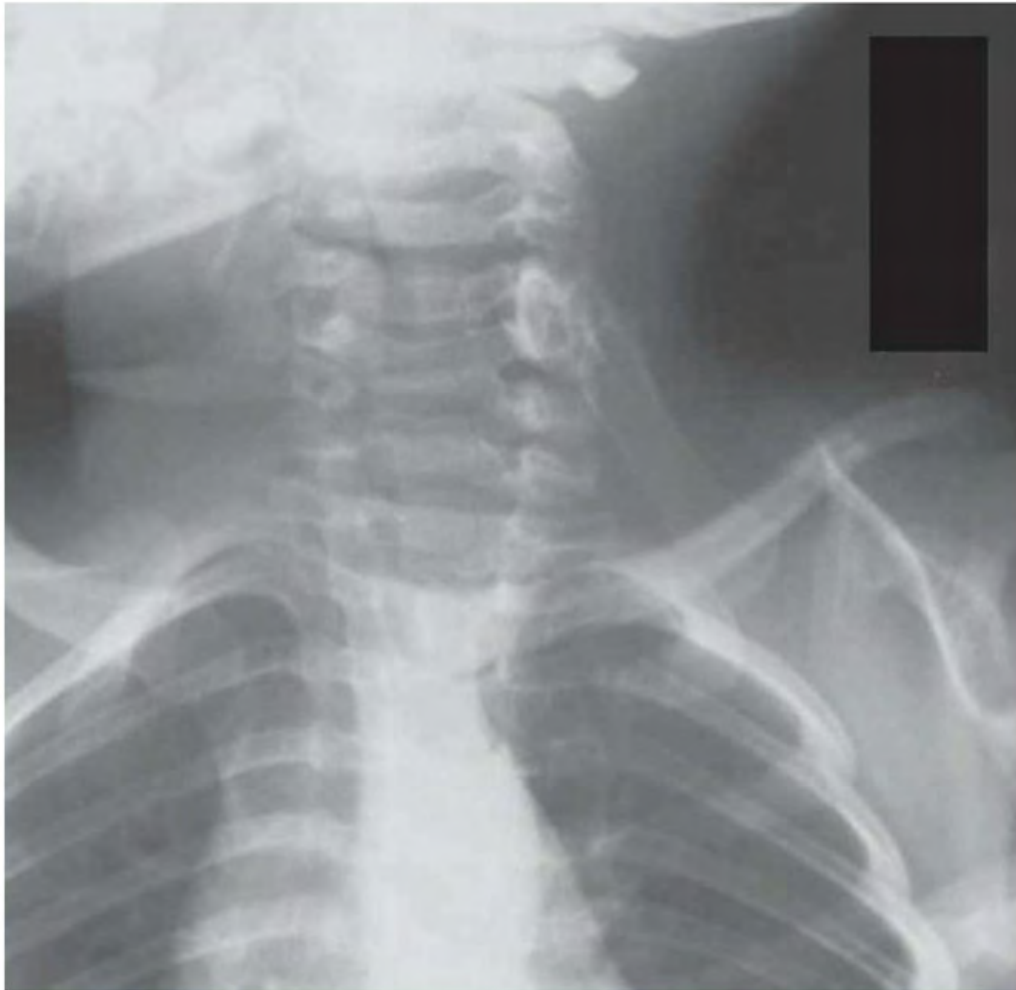


FIGURE 3.7E

**FINDINGS**

- A. Lateral cervical spine. Congenital fusion of C4–C5 is present.
- B–D. Sagittal CT reformations of the cervical spine (left to right). The fusion includes the C4 and C5 bodies and posterior elements.
- E. Companion case: 2-year-old girl. Anteroposterior (AP) view of the cervical spine shows dysplasia of the cervical vertebral bodies and an omovertebral bone.

**DIFFERENTIAL DIAGNOSIS** Klippel-Feil syndrome, juvenile chronic arthritis.

**DIAGNOSIS** Klippel-Feil syndrome.

**DISCUSSION** Klippel-Feil syndrome is a congenital condition of unknown cause [18]. Most patients present with a

short neck and a decreased range of motion in the cervical region. Klippel-Feil syndrome may be associated with many other anomalies (cardiovascular, renal, and limb) and is not clearly genetic; it likely results from an insult to the circulatory system in the 6th week of embryologic development. Common findings are fusion of the cervical spine vertebral bodies and congenital scoliosis. Deformities of the cranio-cervical junction may cause severe neurologic impairment. Approximately one-third of patients will have an elevated and rotated scapula, known as a Sprengel deformity. An accessory bone extending from the medial border of the scapula to the spine—an omovertebral bone—is also commonly seen [19]. One classification system is based on the levels of fusion: type I, single-level fusion; type II, multiple noncontiguous fused segments; type III, multiple, contiguous fused segments [20].

**CLINICAL HISTORY** A 27-year-old man with quadriplegia after rescue from an automobile accident, and a companion case.



FIGURE 3.8A

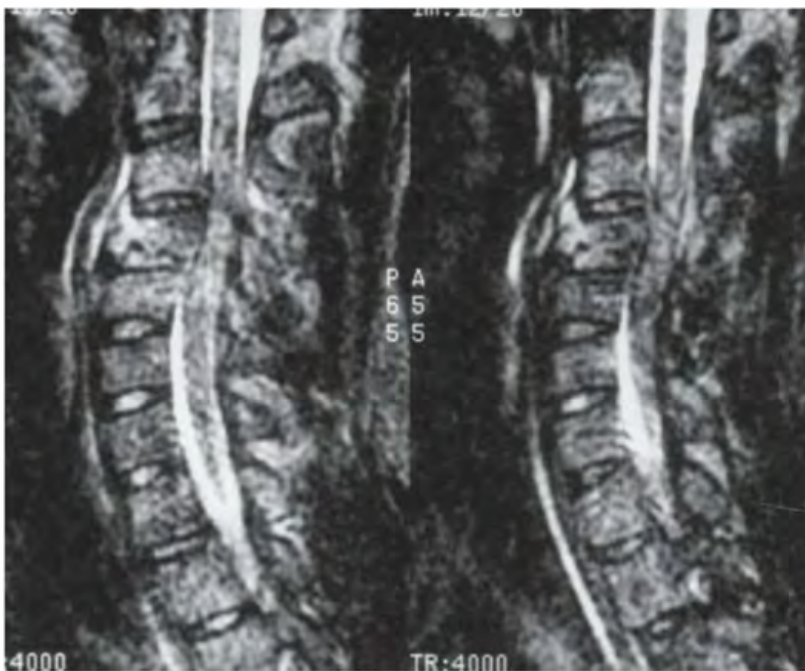


FIGURE 3.8B



FIGURE 3.8C

## FINDINGS

- A. Lateral radiograph of the cervical spine. A fracture of the body of C4 is present with anterior soft tissue swelling. The major portion of the C4 vertebra remains in normal alignment, whereas the anteroinferior teardrop fragment is rotated anteriorly. Mild soft tissue swelling is evident by a contour abnormality of the anterior prevertebral soft tissues.
- B. Sagittal T2-weighted MRI at the midline shows the fracture at C4. The spinal canal is narrowed, with impingement on the spinal cord.
- C. Companion case. Lateral radiograph of the cervical spine shows a displaced teardrop fragment of the body of C6, which is also compressed.

**DIFFERENTIAL DIAGNOSIS** None.

**DIAGNOSIS** Hyperflexion teardrop fracture.

**DISCUSSION** The hyperflexion teardrop injury is the result of axial compression with hyperflexion caused by large forces, leading to a fracture dislocation [21]. An example of this type of loading might be diving into shallow water with the chin tucked, flexing the neck [22]. Massive posterior distractive forces disrupt the posterior ligament complex and dislocate the facet joints. The anterior and middle columns

are disrupted, with tears of the longitudinal ligaments and the intervertebral disc. A triangular fragment (teardrop fragment) is sheared off the anteroinferior corner of the dislocating vertebral body. The result is complete disruption of the cervical spine, with the superior portion displaced posteriorly and angulated anteriorly. The injury is recognized radiographically by focal kyphosis, posterior dislocation, distraction of the posterior elements, and wedging deformity of the vertebral body with teardrop fragment off the anteroinferior corner. The teardrop fragment usually remains aligned with the vertebral column inferior to the level of injury, whereas the remainder of the vertebral body and the vertebral column superior to the injury will be displaced posteriorly. This retrolisthesis may result in widening of the facet joints and disruption of the spinolaminar line. Sagittal fractures of the vertebral body and laminae, caused by the axial loading, are commonly associated. Diffuse, marked, anterior prevertebral soft tissue swelling is always present. The most common site of involvement is C5. The hyperflexion teardrop fracture dislocation is a highly unstable injury, and the spinal cord is always injured. Although paraplegia or quadriplegia can result, the characteristic injury associated with this fracture is the anterior cord syndrome, which consists of complete motor paralysis coupled with a loss of pain, temperature, and touch, but preservation of the posterior column functions of vibration and position.

**CLINICAL HISTORY** *A 36-year-old man in an automobile accident, and a companion case.*



FIGURE 3.9A



FIGURE 3.9B



FIGURE 3.9C

**FINDINGS**

- A. Lateral radiograph of the cervical spine. Anterior soft tissue swelling is present. At the C5–C6 level, the intervertebral disc space is widened anteriorly and narrowed posteriorly. There is retrolisthesis of C5 relative to C6. A small fragment of the C5 body remains aligned with the anterior aspect of C6.
- B. Sagittal CT reformation shows the misalignment of C5 over C6.
- C. Companion case. Lateral radiograph of the cervical spine shows anterior soft tissue swelling and a nondisplaced fracture of the anteroinferior corner of the body of C2. Alignment is normal.

**DIFFERENTIAL DIAGNOSIS** None.

**DIAGNOSIS** Hyperextension sprain at C5–C6 with teardrop fragment (companion case, hyperextension sprain at C2–C3 with teardrop fragment).

**DISCUSSION** Widening of the anterior disc space and narrowing of the posterior disc space is the hallmark for a hyperextension injury. Axial loading with hyperextension places the anterior column under tension, and the posterior column under

compression [23]. Structures of the spine fail in sequence, depending on the magnitude of the loading: tear of the anterior longitudinal ligament, disruption of the intervertebral disc, and tear of the posterior longitudinal ligament. A tension fracture of the anterior inferior corner of the vertebral body may occur instead of disc disruption, as in this case. If present, the triangular fracture fragment may be called a teardrop fragment, and the injury may be called a hyperextension teardrop fracture, but the significance of this fragment is the accompanying ligamentous injury. The anteroinferior avulsion may remain undisplaced, or may be rotated anteriorly from the vertebral body on an intact hinge of anterior longitudinal ligament. If the spine reduces after the injury, the teardrop fragment may be the best radiographic clue to the presence of the more serious injury. Compression fractures of the posterior elements are common, including fractures of the lamina and lateral masses. One or both facet joints may become dislocated. If only ligaments are disrupted and the spine relocates on the rebound, radiographs may show a normally aligned spine without fracture in an acutely quadriplegic patient. Marked prespinal soft tissue swelling should be present.

This injury is most commonly seen in older patients with osteopenia or cervical spondylosis [24]. The prevertebral soft tissue swelling can be minimal in older patients.

**CLINICAL HISTORY** *A 57-year-old man with a stiff, painful neck.*



FIGURE 3.10A



FIGURE 3.10B



FIGURE 3.10C

## FINDINGS

- A. Lateral radiograph of the cervical spine shows severe cervical kyphosis, but vertebral heights are normal. There is ankylosis of the facet joints and intervertebral disc joints, and the anterior corners of the vertebral bodies are squared off. The bones are osteoporotic. In addition, there is a minimally displaced fracture that extends through the entire vertebral column at the C4–C5 level.
- B, C. Sagittal reformatted images from CT show the fracture plane extending through the upper portion of the body of C5 and then through the fused posterior elements of C4 and C5.

**DIFFERENTIAL DIAGNOSIS** Ankylosing spondylitis, juvenile idiopathic arthritis, DISH.

**DIAGNOSIS** Ankylosing spondylitis, with fracture.

**DISCUSSION** The combination of ankyloses of the facet joints and syndesmophytes is diagnostic of this disorder. The delicacy of the syndesmophytes and the presence of osteopenia are key differential features relative to DISH. Preservation of vertebral body height and intervertebral

disc spaces are key differential features relative to juvenile idiopathic arthritis. Syndesmophyte formation in ankylosing spondylitis is the result of inflammation that leads to ossification of the outer layers of the annulus fibrosis. The resulting bridges of bone that fuse the adjacent vertebral bodies should not extend beyond the endplates. Ankylosing spondylitis affects the synovial articulations, cartilaginous articulations, and entheses. In synovial joints, the inflammatory process is a synovitis that is pathologically similar to rheumatoid arthritis, but less intense. Inflammatory fibroplasia of synovium can transform into chondroid metaplasia that then ossifies, resulting in ankylosis; this is a major feature of this disease, unlike rheumatoid arthritis.

Similar pathologic abnormalities occur in cartilaginous articulations. Swollen fibrocytes in the outer annulus fibrosis layers at the attachment of Sharpey's fibers undergo chondroid metaplasia and ossify, resulting in the smooth, flowing appearance of syndesmophyte formation. Pain diminishes or disappears as the spine fuses, but the fused spine becomes osteoporotic and fragile and is subject to insufficiency fractures. Fusion usually begins at the lumbosacral junction and extends superiorly. The ankylosed spine is much more vulnerable to traumatic injuries than the normal spine; furthermore, these patients are at high risk for complications and death [27].

**CLINICAL HISTORY** A 25-year-old man with back pain in the upper cervical region for several months.

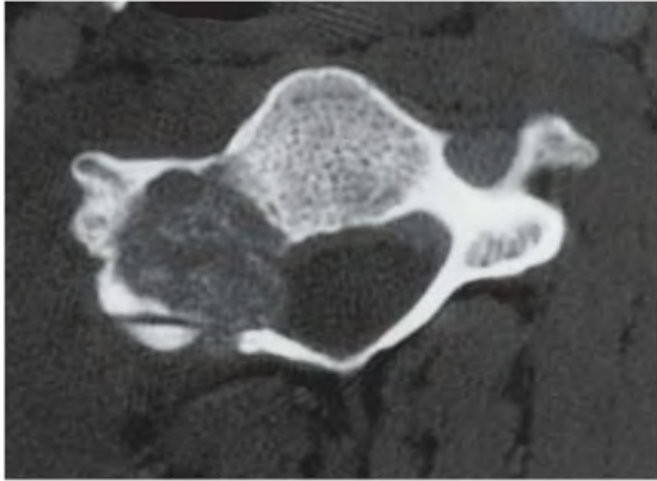


FIGURE 3.11A

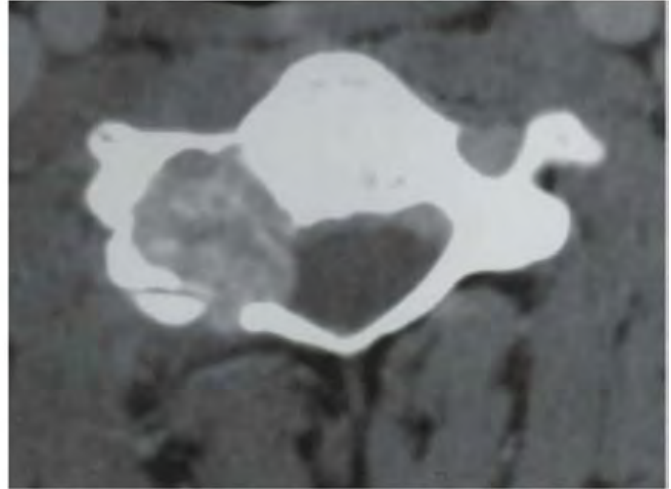


FIGURE 3.11B

**FINDINGS** (A, B) CT (bone and soft tissue windows). CT shows an expansile lesion in the right lateral mass of a cervical vertebra (C4), extending into the spinal canal, transverse foramen, and vertebral body. Focal destruction of the cortex is present. The lesion is well circumscribed, but does not have reactive margin of bone. The lesion is mineralized.

**DIFFERENTIAL DIAGNOSIS** Osteoblastoma, aneurysmal bone cyst, osteosarcoma, brown tumor, fibrous dysplasia.

**DIAGNOSIS** Osteoblastoma.

**DISCUSSION** Differential considerations in this case include osteoid osteoma (if the lesion were less than 2 cm), osteosarcoma (if the lesion had a more aggressive appearance or associated soft tissue mass), aneurysmal bone cyst (which can be seen in conjunction with an osteoblastoma; therefore, the pathologist ultimately distinguishes between the two), giant cell tumor (if the lesion were less well defined), and a brown tumor (if the patient had other clinical evidence for hyperparathyroidism).

Osteoblastomas are uncommon lesions considered by some to be giant osteoid osteomas because of their histologic resemblance [28]. They affect young people—80% occur

in patients younger than 30 years old—and there is a male predominance. About half are located in the spine and most of the remainder in the femur and tibia; 9% are located in the cervical spine [29,30]. Of those in the spine, most are in the posterior elements, but a few also involve the vertebral body, and very few involve the vertebral body alone.

The radiographic appearance is a partially lucent expansile lesion, with well-defined thin sclerotic margins and a variable amount of matrix mineralization. The lucent area of geographic bone destruction corresponds to replacement of bone by nonmineralized tumor tissue. The tumor osteoid may have densely solid or ground-glass mineralization. Large lesions may have an expanded cortical shell from slow endosteal cortical erosion, balanced against an enlarging layer of periosteal new bone. Cortical penetration into the soft tissues is absent, but tomography may be required to demonstrate the cortical shell. The tumor tissue may have high attenuation on CT from the diffuse mineralization. Osteoblastomas are hot on bone scan. They usually grow slowly and respond well to excision; radiation is useful when the lesion is difficult to excise. Very few have been reported to become locally aggressive. In the cervical spine, lesions in close proximity to the vertebral artery require complex therapeutic solutions [31].

**CLINICAL HISTORY** A 53-year-old man with neck pain for several weeks.



FIGURE 3.12A

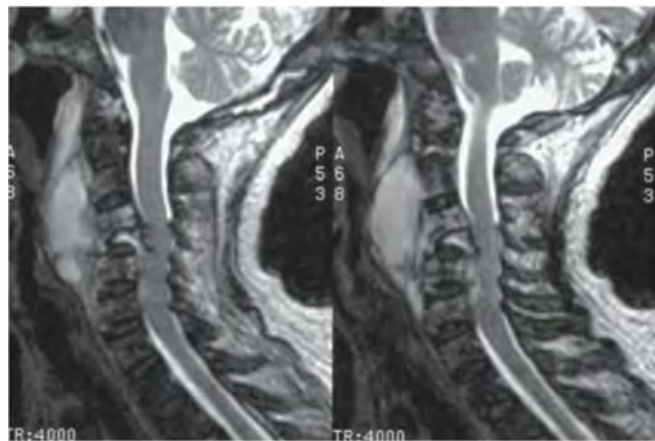


FIGURE 3.12B

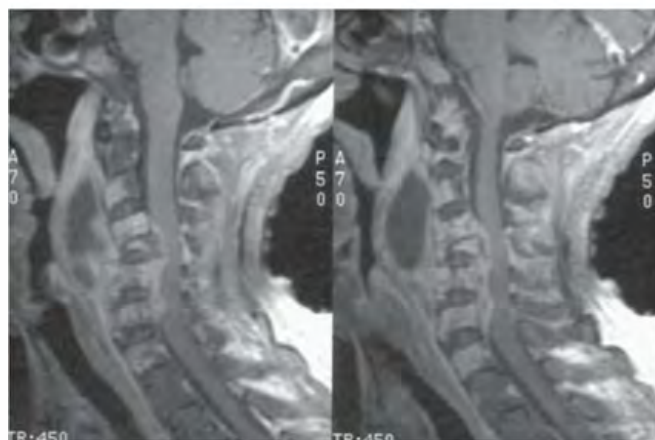


FIGURE 3.12C

### FINDINGS

- Lateral radiograph of the cervical spine through a cervical collar. The C4 vertebral body has dissolved, and the C3–C4 and C4–C5 disc spaces are narrowed. Marked prevertebral soft tissue swelling is identified.
- Sagittal T2-weighted MRI shows partial collapse of C4 and C5, with prevertebral fluid collection and posterior mass effect on the spinal cord. The abnormality extends along several levels.
- Sagittal T1-weighted MRI after gadolinium shows enhancement involving most of the cervical spine, with no enhancement of the prevertebral collection.

**DIFFERENTIAL DIAGNOSIS** Pyogenic diskitis, tuberculous spondylitis, metastasis, lymphoma, massive vertebral osteolysis (Gorham disease), trauma.

**DIAGNOSIS** Tuberculous spondylitis.

**DISCUSSION** At first glance, one might suspect osteolytic destruction secondary to tumor or Gorham disease, but the

large prevertebral fluid collection would be expected only with infection. Pyogenic infections typically arise in the disc space and provoke reactive bone formation, whereas tuberculosis tends to provoke little, if any, reactive bone formation. The large retropharyngeal abscess and the multilevel involvement would also be very unusual in pyogenic diskitis. Although tuberculosis is becoming more common in North America, involvement of the cervical spine remains rare, comprising only 3% to 5% of cases of tuberculosis of the spine. Patients present with neck pain and may have a kyphotic deformity. In children, the disease is frequently extensive, with paraspinal abscess formation [32], while in adults it is more commonly localized to one or two segments. Cord compression is common, and patients may develop reversible quadriparesis as a result [33]. The treatment of tuberculous spondylitis in the cervical spine is similar to treatment of tuberculosis elsewhere in the spine, and consists of antituberculous chemotherapy and, when necessary, surgical resection of abscesses and mechanical stabilization.

**CLINICAL HISTORY** A 43-year-old woman with polyarticular arthritis, and a companion case.



FIGURE 3.13A



FIGURE 3.13B



FIGURE 3.13C

## FINDINGS

- A. Lateral cervical spine (neutral position). The atlantoaxial distance is difficult to assess since there is marked irregularity of the odontoid. Generalized osteoporosis is present. The visualized facets are fused.
- B. Sagittal T1-weighted MRI with gadolinium demonstrates marked erosion of the odontoid, with an effective increase in the atlantoaxial distance. Marked enhancement of pannus is identified.
- C. Companion case. Lateral cervical spine. There is axial migration of the C2 vertebral body with absence of the dens. Subluxation is most prominent at C5–C6. Whittling of the C3, C4, and C5 spinous processes is noted. Disc space narrowing with associated endplate is present at C6–C7, but also at the uncommon C3–C4 level.

**DIFFERENTIAL DIAGNOSIS** Rheumatoid arthritis, ankylosing spondylitis, juvenile idiopathic arthritis.

**DIAGNOSIS** Rheumatoid arthritis.

**DISCUSSION** In the cervical spine, multilevel subluxation, osteopenia, and erosions at sites of ligamentous attachments without evidence for reparative bone is characteristic of rheumatoid arthritis. Erosion of the odontoid and instability of the atlantoaxial articulation is a classic presentation for

rheumatoid arthritis. Other etiologies for these two findings might include congenital hypoplasia of the odontoid with ligamentous instability, amyloid, or perhaps an atypical infection. Atlantoaxial subluxation is the dominant and the first cervical spine finding, and may occur without radiographic evidence for erosions [34]. A measurement of greater than 2.5 mm between the inferior aspect of the posterior C1 arch and anterior dens is diagnostic. It typically results from disruption of the transverse ligament by pannus formation, as demonstrated here by MRI. Axial migration of the C2 vertebral body is not uncommon as the odontoid dissolves and a potential space is created.

In the lower cervical spine, subluxations are most prominent at the C3–C4 and C4–C5 levels. Anterior subluxation is most common, and the levels of involvement are commonly discontinuous. Apophyseal joint space narrowing and erosions can lead to instability or fibrous union. Discovertebral narrowing, erosion, and late subchondral sclerosis without osteophyte formation can be seen. Whittling of the spinous processes at the insertion of the supraspinous ligaments may be identified. Generalized osteoporosis may be secondary to the disease process or the use of steroids. Compared with other patients with rheumatoid arthritis, those with cervical involvement tend to have a positive rheumatoid factor, higher C-reactive protein level, and progression of peripheral joint disease.



FIGURE 3.14A

**FINDINGS** Lateral radiograph of the cervical spine demonstrates fusion of the C3, C4, and C5 facets, with hypoplasia of the respective vertebral bodies and calcification of the intervertebral discs.

**DIFFERENTIAL DIAGNOSIS** Ankylosing spondylitis, juvenile chronic arthritis, DISH.

**DIAGNOSIS** Juvenile idiopathic arthritis.

**DISCUSSION** Diffuse ankylosis of the facet joints in the cervical spine is associated with two conditions: ankylosing spondylitis and juvenile idiopathic arthritis. Distinguishing between the two on radiographs is often possible because ankylosing spondylitis is a disease that involves the mature skeleton, whereas juvenile idiopathic arthritis, by definition, involves the immature, growing skeleton. In the latter, stigmata of the disease process itself and of the effects of the disease on skeletal development should be evident. Thus, diffuse ankylosis of the facet joints in combination with hypoplasia of the vertebral bodies and intervertebral discs is virtually diagnostic for juvenile idiopathic arthritis. In ankylosing spondylitis, the vertebral body and intervertebral disc

heights remain normal, even in the presence of ankylosis of the facet joints and syndesmophyte formation, because the spine has already developed fully at the time the disease process affects it.

The cervical spine is more commonly involved with juvenile idiopathic arthritis than other spinal levels [35]. The most common finding is that of atlantoaxial instability; however, other considerations for this finding in a child would include Down's syndrome, odontoid hypoplasia, and Grisel's syndrome (infectious laxity as an extension of a peripharyngeal process).

The apophyseal joint fusion is most common at the C2–C3 and C3–C4 levels, as seen in this case. Because this occurs before full growth potential, the constellation of ankylosis and vertebral body and disc hypoplasia is diagnostic.

Other etiologies of apophyseal joint fusion can be excluded by their secondary findings. In addition, enthesopathy and tarsal disease within the first year of presentation is diagnostic of juvenile ankylosing spondylitis, with or without the presence of axial disease. Klippel-Feil syndrome (congenital fusion anomaly) may be difficult to distinguish unless posterior element fusion is a dominant feature. Fibrodysplasia ossificans progressiva should have an element of soft tissue ossification.

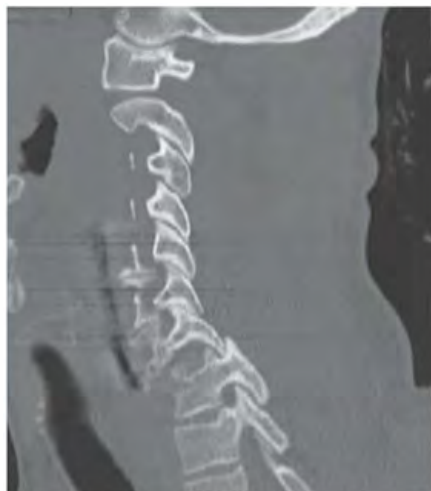


FIGURE 3.15A



FIGURE 3.15B



FIGURE 3.15C

**FINDINGS** A–C. Sagittal CT reformations of the cervical spine (left to right). There has been previous anterior cervical discectomy and fusion, with anterior plate and screws fixing the C4 through C7 vertebral bodies. There is bilateral inter-facet dislocation at C7–T1, with approximately 50% of the body of C7 displaced anteriorly relative to T1. The inferior facets of C7 are dislocated anteriorly over the superior facets of T1. The superior articular facets of T1 are uncovered by the inferior articular facets of C7 (naked facet sign). There is a displaced avulsion fracture of the anterior superior corner of T1. There is a displaced fracture of the spinous process of C7. There is no rotatory displacement.

**DIFFERENTIAL DIAGNOSIS** None.

**DIAGNOSIS** Bilateral facet dislocation (bilateral locked facets).

**DISCUSSION** The major injury vector in bilateral facet dislocation is hyperflexion of large magnitude without axial compression [36]. Bilateral facet dislocation is a tension injury that propagates from posterior to anterior. Complete

disruption of the ligaments and forward displacement of one involved vertebra over another allows the inferior articular facets of the superjacent vertebra to dislocate into the inter-vertebral foramen. In addition to disruption of the posterior longitudinal complex, seen in unilateral facet dislocation, the disc and anterior longitudinal ligament are disrupted, allowing the superior vertebra to be subluxated anteriorly by about 50% of the width of its body. When the facets are subluxated (perched) but not completely dislocated (“partial dislocation”), the anterior subluxation is greater than the 3 mm seen in a flexion sprain, but less than the 50% seen in the complete dislocation. There may be accompanying fractures of the articular processes of the subjacent vertebra. The spine is unstable, and there is a high association with cord contusion, of variable severity. MRI is better than CT for demonstrating possible cord injury and other soft tissue abnormalities [37].

Traumatic injuries to a previously surgically fused spine usually occur at a level adjacent to the fusion [38], presumably due to the concentration of stress by the lever arm formed by the fused segments [39]. Fracture through the fused segment itself appears to be a rare event [40].



FIGURE 3.16A

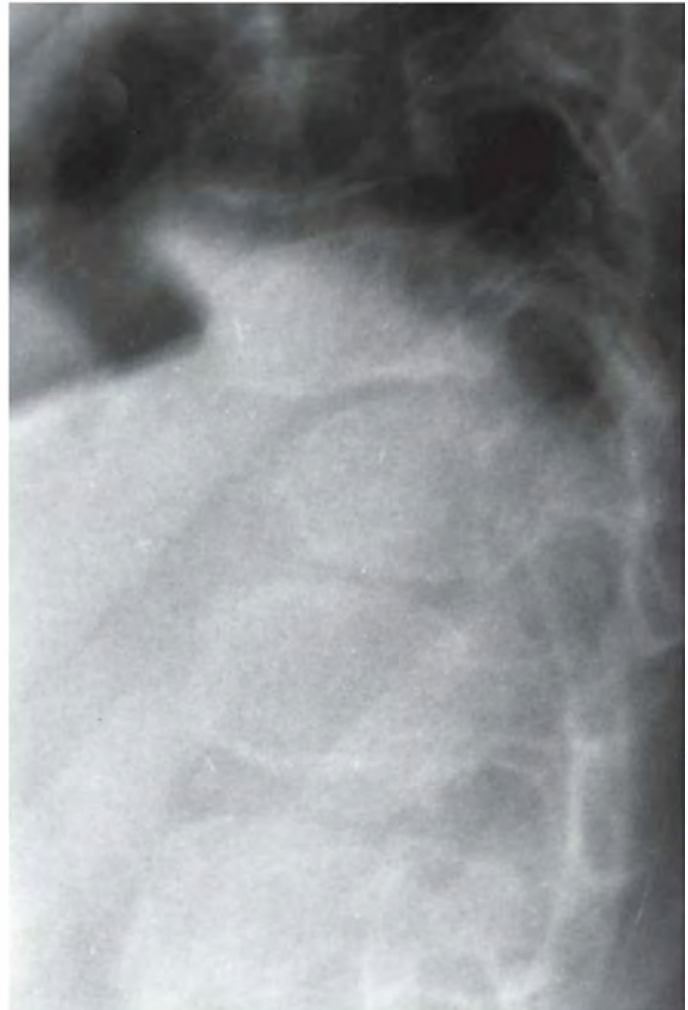


FIGURE 3.16B

### FINDINGS

- A. Lateral radiograph of the cervical spine. There is flattening of the visualized cervical vertebral bodies and hypoplasia of the odontoid process.
- B. Lateral radiograph of the thoracic spine. There is hypoplasia of the T11 vertebral body with a central beak deformity.

**DIFFERENTIAL DIAGNOSIS** Mucopolysaccharidoses (dysostosis multiplex), spondyloepiphyseal dysplasia.

**DIAGNOSIS** Morquio syndrome.

**DISCUSSION** Morquio syndrome, or mucopolysaccharidosis IV A, is an autosomal recessive deficiency of the enzyme N-acetylgalactosamine-6-sulfatase and has a frequency of 1 in 100,000 births [41]. The key radiologic feature in this case is flattening of the cervical vertebral bodies at every level (universal platyspondyly). In addition, the findings of

hypoplastic odontoid with secondary atlantoaxial instability are common in this condition. Although it would be unrealistic for a radiologist to make a specific biochemical and genetic diagnosis from these radiographs, one should recognize that a systemic, congenital disease is present. Morquio syndrome is one of the mucopolysaccharidoses, or diseases caused by inborn errors of complex carbohydrate metabolism. The skeletal features of all these conditions have been collectively called dysostosis multiplex, and are the manifestation of storage of abnormal complex carbohydrate substances that cannot be metabolized further because of enzyme deficiencies. The mucopolysaccharidoses share the findings of macrocephaly; “canoe paddle-shaped” ribs; focal kyphosis with distinctive centrally beaked, diminutive retro-listhesed L1 or L2 vertebral body; flared pelvis; and shortened, broadened long bones [42]. In Morquio syndrome, the platyspondyly tends to be more widespread and marked than in the other mucopolysaccharidoses, which is a possible clue to the specific diagnosis.



FIGURE 3.17A

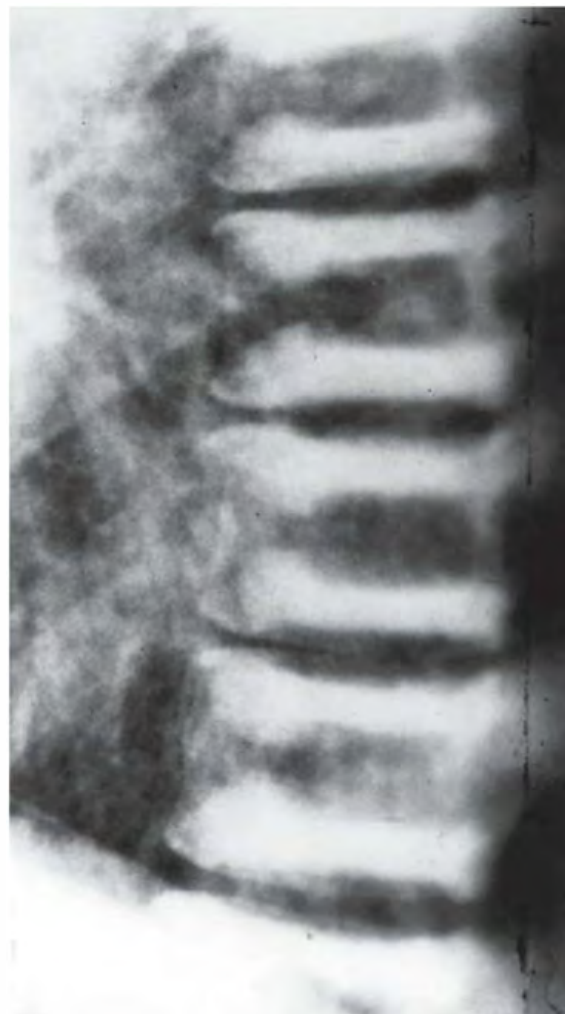


FIGURE 3.17B

**FINDINGS** (A) AP and (B) lateral radiograph of the thoracic spine shows that the vertebral bodies have a uniform “sandwich” appearance, with sharply demarcated sclerosis abutting the endplates. The vertebral body heights and alignment are normal.

**DIFFERENTIAL DIAGNOSIS** Osteopetrosis, renal osteodystrophy, degenerative disc disease.

**DIAGNOSIS** Osteopetrosis.

**DISCUSSION** The sandwich appearance of vertebral bodies results from horizontal layers of increased bony density involving the upper and lower ends of the vertebral body, with a less dense central portion. This appearance is distinguished from the rugger jersey spine of renal osteodystrophy by the sharpness of the margin between sclerotic and less sclerotic bone and, of course, by the absence of other features of renal osteodystrophy. Discogenic sclerosis

may also have the appearance of horizontal stripes of sclerosis, but is seen only in combination with degenerative disc disease in older patients. The exact pathogenesis of the layers of sclerotic bone in osteopetrosis is unknown, but this appearance is classic for the autosomal dominant osteopetrosis with delayed manifestations that was originally described by Albers-Schoenberg [43]. The sandwich appearance may also be thought of as a variation of the bone-in-bone appearance that may be seen in the pelvis or the long bones. A central core of more primitive, coarsely fibrillar, and cellular osseous tissue becomes surrounded by dense new bone during growth that is not able to remodel into normal trabecular and cortical bone. Osteopetrosis is a group of heritable diseases characterized by reduced bone resorption from osteoclast failure [44]. Many genetic defects may cause osteoclast failure, and each has different underlying biochemical and histopathologic abnormalities. The final common effect is that bone remodels incompletely or not at all.

**CLINICAL HISTORY** A 26-year-old patient with congenital ichthyosis.



FIGURE 3.18A



FIGURE 3.18B



FIGURE 3.18C



FIGURE 3.18D

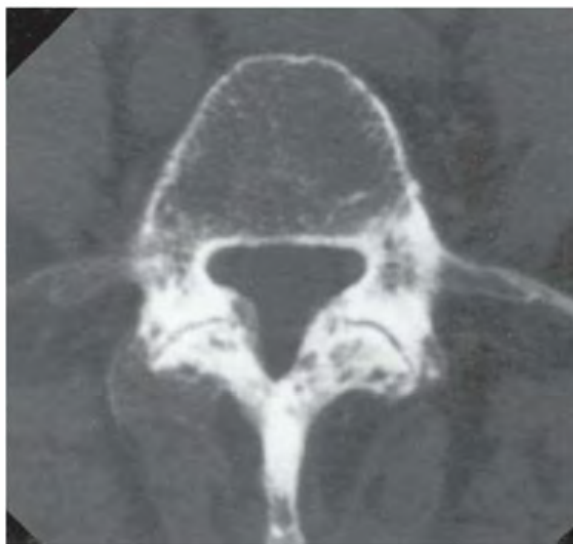


FIGURE 3.18E

## FINDINGS

- A, B. Lateral radiographs of the cervical and thoracic spine demonstrate flowing ossification of the anterior longitudinal ligament at multiple contiguous levels.
- C, D. Lateral and AP radiographs of the lumbar spine demonstrate mild anterior longitudinal ligament ossification, but severe facet arthropathy. Ankylosis of the interspinous ligament of the lower lumbar vertebrae is present.
- E. Axial CT through the L4–L5 facet joint shows severe facet arthropathy with dominant hyperostotic changes.

**DIFFERENTIAL DIAGNOSIS** DISH, degenerative joint disease, spondyloarthropathy, hypertrophic osteoarthropathy, retinoid toxicity, fluorosis.

**DIAGNOSIS** Retinoid toxicity.

**DISCUSSION** Congenital ichthyosis is a severe disorder of skin keratinization that responds to treatment by oral retinoids. Retinoids, a class of pharmaceutical agents derived from vitamin A, are highly effective in various dermatologic

conditions, including acne, severe psoriasis, and severe disorders of keratinization [45]. Although ichthyosis itself has no skeletal manifestations, the retinoids used to treat it may have adverse effects on the skeleton. Retinoid-induced changes in bone are similar to those described in hypervitaminosis A. Retinoids may also have a severe teratogenic effect, thus limiting their use in females of childbearing potential. Chronic use of retinoids in children may cause premature closure of growth plates, which inhibits growth [46,47]. Isotretinoin is among the more commonly used retinoids for oral use. Isotretinoin (13-cis-retinoic acid [Accutane]) in high doses given over prolonged periods, such as for treatment of congenital ichthyosis, may result in various skeletal changes. Some of these findings are similar to those of DISH. Although ligamentous calcifications are seen in both conditions, they are less dramatic with isotretinoin therapy. Additional findings with long-term isotretinoin therapy include osteoporosis, osteophytosis, and growth arrest. The osteophytosis is more pronounced in the lumbar spine. The mechanism of action may be related to effects on preosteoclasts via cytokines. Bone scintigraphy may play a useful role in identifying patients with early bone changes [48].

**CLINICAL HISTORY** A 24-year-old man in a high-speed automobile accident.

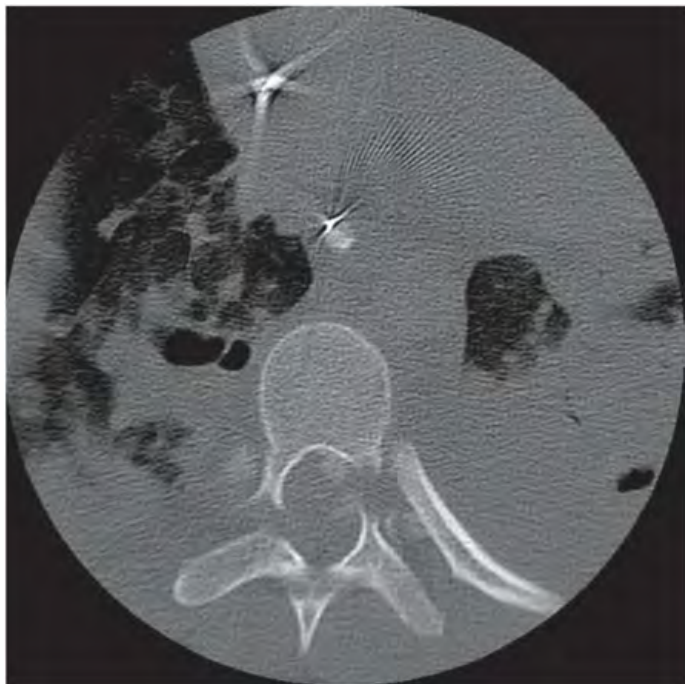


FIGURE 3.19A

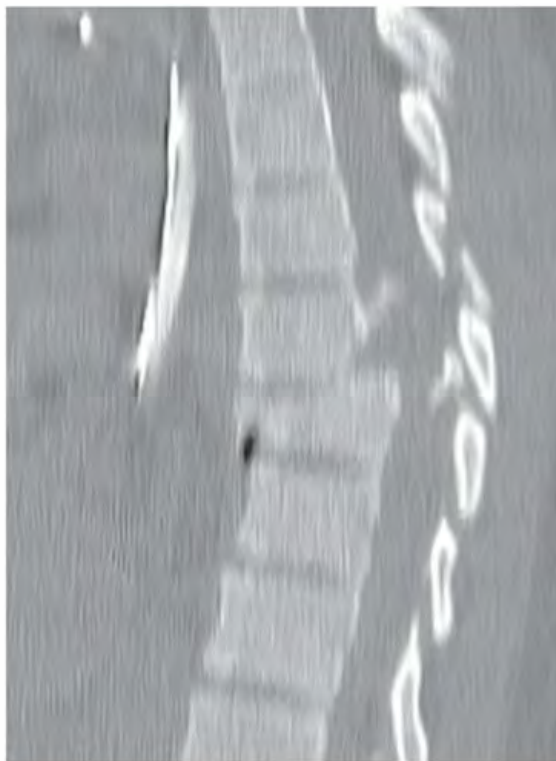


FIGURE 3.19B



FIGURE 3.19C



FIGURE 3.19D

## FINDINGS

- A. Axial CT scan at the level of T8–T9. The T8 vertebral body is translated forward over the T9 vertebra, and the posterior elements of T8 are fractured. Extensive pleural and pulmonary disease is present.
- B. Sagittal reformatted CT scan through the midline. The extent of the forward translation of T8 over T9 is clearly shown. There are tension fractures of the posterior elements of T8 and an anterior wedging deformity of T9. Fragments of bone have been displaced into the spinal canal.
- C. Sagittal T2-weighted MRI through the midline. Edema and hemorrhage involve the spinal cord extensively. Disruption of the posterior longitudinal ligament and the posterior elements at T8 is visible, along with the T8 translation and the T9 fractures.
- D. Lateral radiograph following reduction and internal fixation of the injury. The fusion construct involves multiple levels above and below the lesion.

**DIFFERENTIAL DIAGNOSIS** None.

**DIAGNOSIS** Hyperflexion fractures, thoracic spine.

**DISCUSSION** The typical initial emergency trauma series of radiographs in patients with polytrauma is a lateral cervical spine, an AP chest, and an AP pelvis, all obtained without moving the patient for positioning. Injuries to the spine should be recognized from these limited radiographs before the patient is moved. In this case, the diagnosis of thoracic spine injury was difficult to make from the AP radiograph

of the chest because of the extensive pleural and pulmonary disease and limiting technical factors. Key radiographic features of thoracic spine injuries would include focal soft tissue swelling of the paravertebral region, misalignment of the vertebral bodies or posterior elements, and loss of vertebral height. CT is considered the imaging method of choice for identifying and characterizing traumatic injuries of the thoracic and lumbar spine. Reformatted images from CT of the chest, abdomen, and pelvis using protocols designed to identify blunt injuries of the viscera have been shown to be superior to radiographs in screening for thoracic and lumbar spine injuries [49].

The thoracic spine is supported by the rib cage and intercostal muscles and therefore is not very mobile. Fractures are uncommon and require at least four times the force necessary to cause a fracture elsewhere in the spine. Acute traumatic compression fractures are most common at the T6–T7 levels. The vast majority of these injuries are anterior wedge fractures or lateral wedge fractures. Patients complain of localized pain and may have increased kyphosis. On imaging, paraspinal hematoma (lasting up to 1 month), disruption of the cortical surface, and loss of height is present. Severe trauma may cause burst fractures, but these are much more common in the thoracolumbar region. Hyperflexion injuries, uncommon in the midthoracic region, are characterized radiologically by narrowing of the anterior structures, including wedging fractures of the vertebral bodies, narrowing of the disc space, and widening of the posterior structures, including distraction or vertical subluxation of the facet joints and tension fractures of the posterior elements. In this mechanism of injury, the anterior portion is loaded under compression, while the posterior portion is loaded under tension.

**CLINICAL HISTORY** A 52-year-old man with back pain for 3 months, and a companion case.



FIGURE 3.20A



FIGURE 3.20B

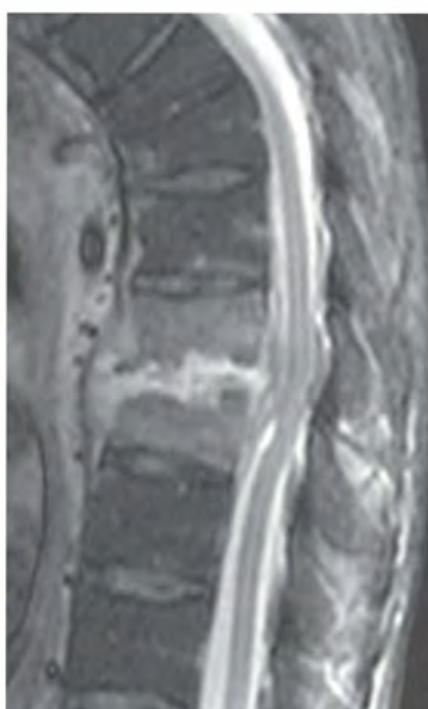


FIGURE 3.20C

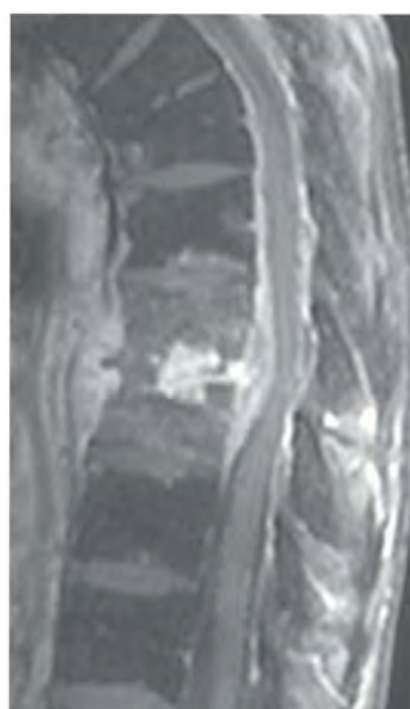


FIGURE 3.20D

## FINDINGS

- A. Lateral radiograph of the thoracic spine shows apparent widening of a lower intervertebral disc space with erosions and sclerosis of the adjacent vertebral endplates.
- B–D. Companion case: A 58-year-old renal transplant patient with back pain. (B) Sagittal T1-weighted MRI shows low signal centered at the T8–T9 interspace, extending into the adjacent vertebral bodies. (C) Sagittal inversion recovery MRI shows the abnormal disc space–centered fluid collection, which causes irregularity of the adjacent endplates and impinges on the epidural space underneath the posterior longitudinal ligament, displacing the thecal sac and cord posteriorly. Abnormal fluid-signal intensity extends anteriorly and tracks cephalad and caudal along the anterior longitudinal ligament. (D) Gadolinium-enhanced sagittal T1-weighted MRI shows enhancement in the central portion of the disc space, as well as in the subligamentous collections anterior and posterior to the disc space.

**DIFFERENTIAL DIAGNOSIS** Pyogenic diskitis, myeloma, metastasis, tuberculosis.

**DIAGNOSIS** Pyogenic diskitis.

**DISCUSSION** This is an aggressive process centered at the disc space, with narrowing and destruction of the facing

vertebral endplates. As the process evolves, increasing reactive sclerosis occurs. Bony ankylosis is one eventual outcome. The clinical presentation is fever, back pain, and stiffness. Diagnosis is often delayed, and radiographic findings may not be apparent until 2 to 8 weeks after onset. A causative organism is often difficult to culture from the patient. In 60% of cases where the agent is recovered, the recovered organism is *Staphylococcus aureus*, and in 30% of cases the organisms are species of *Enterobacteriaceae*. In 40% of cases, a remote source of infection will be known—usually genitourinary tract, skin, or respiratory tract. In the absence of an identified organism, antibiotics are chosen empirically.

Pyogenic vertebral osteomyelitis [50,51] occurs in elderly adults with genitourinary tract infections, patients who are immunocompromised, and intravenous drug abusers. The thoracic spine (50%) is involved more commonly than the lumbar (35%) or cervical spine (15%). Organisms from genitourinary tract infections ascend the vertebral column by way of the vertebral plexus of Batson, a valveless venous bed that allows retrograde blood flow. The initial site of infection is the subcortical bone of the vertebral body, adjacent to the intervertebral disc. The infection typically extends through the endplate, involving the disc and the adjacent vertebral body. Multiple levels of involvement are not uncommon, particularly among immunocompromised or debilitated patients, and the levels may be contiguous or noncontiguous. Lateral extension causes a paraspinal abscess; posterior extension can result in epidural abscess, cord compression, and meningitis.

**CLINICAL HISTORY** A 39-year-old immigrant from rural Mexico with chronic cough and worsening back pain.



FIGURE 3.21A

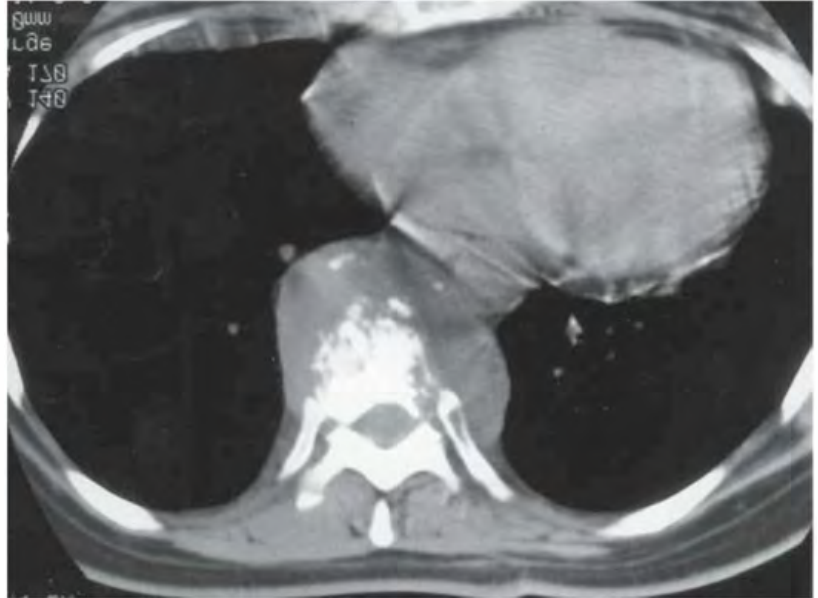


FIGURE 3.21B



FIGURE 3.21C



FIGURE 3.21D

## FINDINGS

- A. AP radiograph of the thoracic spine. There is destruction of the T9–T10 intervertebral disc space and adjacent portions of the T9 and T10 vertebral bodies, with prominent paraspinal soft tissue swelling.
- B. CT through T9. There is destruction and fragmentation of the T9 vertebral body, with paraspinal soft tissue swelling.
- C, D. Sagittal PD and T2-weighted MRI through the midline shows involvement of three contiguous vertebrae. There is an extensive anterior soft tissue inflammatory mass and a smaller, posterior, epidural mass. The posterior mass impinges on the spinal cord.

**DIFFERENTIAL DIAGNOSIS** Pyrogenic infection, tuberculosis, multiple myeloma, metastasis, lymphoma.

**DIAGNOSIS** Tuberculous spondylitis (Pott disease).

**DISCUSSION** The features distinguishing tuberculosis from other infectious agents in the spine are (1) involvement of more than one spinal segment; (2) delay in disc destruction; (3) absence of reparative bone; and (4) large calcified paravertebral masses. It may be difficult to distinguish tuberculosis from

tumors such as metastases, multiple myeloma, and lymphoma, which may have all of these features. Similarly, sarcoid may be included in the differential, depending on the clinical features.

Tuberculous spondylitis is most common at L1 and the contiguous levels [52]. Multilevel (usually three levels) contiguous involvement is characteristic, but separate lesions can be detected in 1% to 4% of cases. Posterior element involvement is seen in 40% of cases, epidural disease in 53% of cases, and disc disease in 73% of cases.

As in pyogenic cases, the lesion begins in the subchondral bone and secondarily spreads to a contiguous vertebral disc, but the process is far more indolent. It also burrows under the anterior longitudinal ligament, allowing spread to additional levels. A kyphosis or scoliosis often results from partial vertebral body collapse. Tuberculosis is unique in that it frequently spills over into the soft tissue and contiguous structures before presentation. Psoas abscesses can develop faint amorphous calcifications or teardrop-shaped calcifications; other soft tissue abscesses typically do not calcify.

Unusual presentations include isolated posterior element involvement, solitary vertebral involvement, “bone-within-bone” appearance due to growth recovery lines, bony ankylosis, ivory vertebrae, atlantoaxial destruction, and intramedullary involvement.

**CLINICAL HISTORY** A 10-year-old girl undergoing treatment for an extremity tumor.

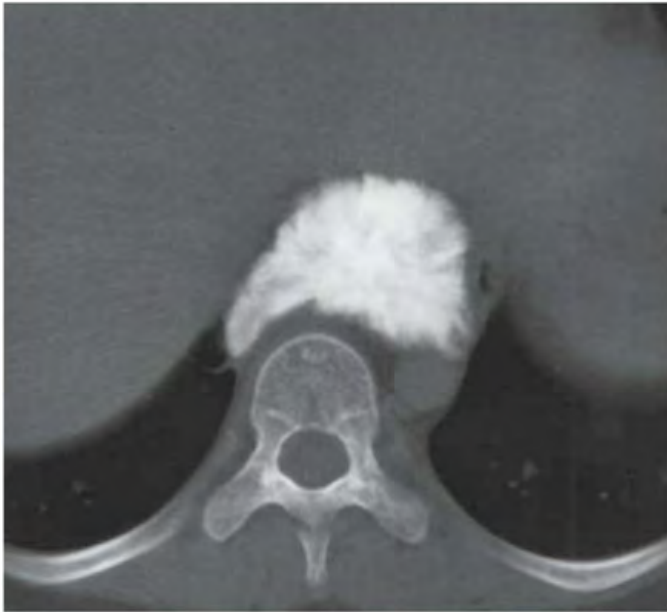


FIGURE 3.22A

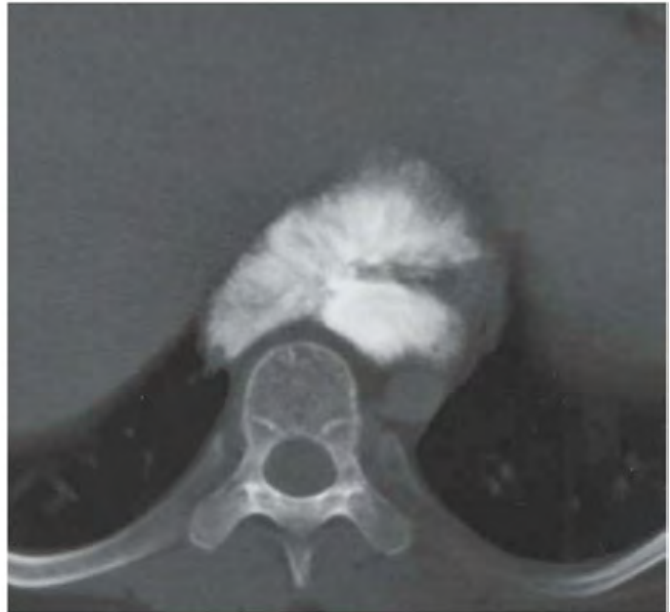


FIGURE 3.22B

**FINDINGS** (A, B) Axial CT images demonstrate an ossified mass anterior to T10, but separate from it, with a spiculated, sunburst appearance.

**DIFFERENTIAL DIAGNOSIS** Osteosarcoma, treated Ewing's sarcoma (or other round cell tumor), treated lymphoma, metastasis.

**DIAGNOSIS** Metastatic osteosarcoma.

**DISCUSSION** This lesion has the cloudlike, spiculated matrix typical of osteosarcoma, but it is located in the soft tissues anterior to the spine. Differential considerations include metastasis, metachronous osteosarcomas, or extraosseous osteosarcoma. Metastases are more common than the latter lesions.

Metachronous osteosarcomas are subtyped into osteosarcomatosis, multiple metachronous osteosarcomas, and unicentric osteosarcoma with metastasis [53]. Osteosarcomatosis

is a rare form that occurs in children. All of the lesions are similar in size and radiographic and histologic appearance; this patient had a dominant lesion in her extremity before this lesion was identified. Similarly, this would not fall into the multiple, metachronous subtype because of the short period of time between the treatment of the original tumor and this site's identification. A unicentric osteosarcoma with a subsequent metastasis is most common if the primary is in a long bone, or a recurrence occurs in the spine or pelvis. Extraosseous primary osteosarcomas are rare.

Conventional osteosarcomas are currently treated with preoperative chemotherapy, followed by resection and prosthetic or allograft placement. Metastasis can appear as ossified or calcified lesions in the lymph nodes, soft tissues, and viscera; these are likewise treated with surgery, chemotherapy, and/or irradiation. Metastases to the lungs can appear quite dense and have a high association with spontaneous pneumothoraces.



FIGURE 3.23A



FIGURE 3.23B



FIGURE 3.23C

**FINDINGS**

- A, B. AP and lateral radiographs of the thoracic spine. There is collapse and flattening of T10 with focal kyphosis.
- C. Sagittal T2-weighted MRI. There is loss of the normal marrow signal from the flattened body and effacement of the anterior spinal cord.

**DIFFERENTIAL DIAGNOSIS** Eosinophilic granuloma, leukemia, metastasis.

**DIAGNOSIS** Eosinophilic granuloma.

**DISCUSSION** Pathologic vertebral body collapse in a child is most commonly due to eosinophilic granuloma [54]. The term *vertebra plana* is used to designate an extremely flat vertebra, as is often the result.

Eosinophilic granuloma is a granulomatous lesion characterized by a focal proliferation of macrophages, eosinophils, and a specific histiocyte (Langerhans cells, which contain

diagnostic cytoplasmic inclusion bodies). Langerhans cell histiocytosis is a process of uncertain etiology that includes Letterer-Siwe disease, Hand-Schuller-Christian disease, and multiple and solitary eosinophilic granuloma of bone. Eosinophilic granuloma of bone presents with skeletal rather than systemic manifestations. Destruction and replacement of bone by eosinophilic granuloma produces a lytic, aggressive-appearing geographic lesion early in the clinical course, sometimes with periosteal reaction. In the spine, asymmetric and symmetric vertebra plana are equally likely to occur. The clinical presentation of eosinophilic granuloma involving the spine is usually localized pain, but lesions may cause neurologic syndromes. The clinical course of both solitary and multiple eosinophilic granuloma of bone is benign, since lesions may regress spontaneously. Therapy is curettage, steroid injection, low-dose radiotherapy, and, rarely, chemotherapy. Lesions heal with sclerosis. After regression of lesions, regrowth of flattened vertebral bodies with reconstitution of vertical height may occur. There is no metastatic potential.

**CLINICAL HISTORY** A 15-year-old girl with increased thoracic kyphosis.



FIGURE 3.24A

### FINDINGS

- A. Standing lateral of the entire spine. The thoracic kyphosis is increased. There are wedging deformities of multiple lower thoracic vertebral bodies with irregular sclerosis at the endplates.
- B. Standing AP of the entire spine. Alignment is straight, without scoliosis.

**DIFFERENTIAL DIAGNOSIS** Scheuermann disease, postural kyphosis, histiocytosis X, osteogenesis imperfecta, trauma.

**DIAGNOSIS** Scheuermann disease.

**DISCUSSION** The normal range of thoracic kyphosis is about 20 to 40 degrees in adolescents, as measured from the superior endplate of T3 or T4 to the inferior endplate of T12 [55]. Most cases of kyphosis in adolescents are postural kyphosis and may simply represent the extremes of



FIGURE 3.24B

normal variation. On radiographs, the morphology of the vertebral bodies is normal and the kyphosis is reduced with hyperextension. Scheuermann disease is a condition with a strong familial tendency [56], which may be diagnosed on standing lateral thoracic spine radiographs when there is increased kyphosis with anterior wedging that involves three or more consecutive vertebrae, by at least 5 degrees each. Additional radiographic features, all demonstrated in this case, include decreased disc space heights, increased AP dimension, endplate irregularity and flattening, and Schmorl's nodes. The underlying abnormality is thought to be mechanical, with increased stress on the anterior portion of the vertebral bodies resulting in abnormal remodeling of the vertebrae during growth. These wedged vertebral bodies are not compression fractures. The kyphosis is accompanied by a scoliosis in up to 75% of patients, usually in the thoracic spine, at either the same level or a higher or lower compensatory level.



FIGURE 3.25

**FINDINGS** Lateral radiograph of the thoracic spine. The bones are severely osteoporotic. Prominent anterior wedge compression fractures are present with 50% vertebral body height loss at T4, T5, and T6. There is a mild anterior wedge compression fracture of T12, and slight superior endplate compression of T7 through T11.

**DIFFERENTIAL DIAGNOSIS** Involutional osteoporosis, osteomalacia, multiple myeloma.

**DIAGNOSIS** Involutional osteoporosis.

### DISCUSSION

Osteopenia, compression fractures, and a resultant kyphosis are typical of this disease. Osteoporosis is characterized by generalized loss of mass from otherwise normal bone [57]. More than 95% of adults with osteoporosis have involutional osteoporosis (also called idiopathic or primary osteoporosis). There are two main clinical types: postmenopausal (also called type I) and senile (type II). Type I involutional osteoporosis is characterized by accelerated bone loss, mainly trabecular, and is caused by factors related to menopause. Type II involutional osteoporosis is characterized by slowly progressive trabecular and cortical bone loss, and is caused by factors related to aging. The pathogenesis of osteoporosis

is incompletely understood, but it seems to involve not only excessive bone resorption but also impaired bone formation. Deteriorating bone strength results in increased vulnerability to traumatic and fatigue fractures. Most fractures of the spine, proximal femur, and distal radius in adults older than 50 are associated with osteoporosis. In type I involutional osteoporosis, vertebral crush fractures and distal radius fractures are the most common. In type II, multiple vertebral wedge fractures and hip fractures are the most common. Fractures are the major cause of morbidity and mortality in osteoporosis.

The radiographic hallmark of osteoporosis is osteopenia, the increased radiolucency of bone. Osteopenia may not be recognizable on plain films until 30% to 50% of the bone mineral has been lost. A coarsened trabecular pattern results from loss of the smaller trabeculae, making the remaining trabeculae more prominent. Cortical thinning is a generalized, uniform, slowly progressive process. Vertebral deformities are related to insufficiency fractures of the endplates. These can have the form of biconcave depressions of contiguous superior and inferior endplates (so-called fish or codfish vertebrae, named for their resemblance to vertebrae in codfish), anterior wedge fractures, crush fractures of entire vertebral bodies, and increased thoracic kyphosis (dowager's hump). The net result is progressive loss of stature.

**FIGURE 3.26**

**FINDINGS** Lateral radiograph of the lumbar spine. The spine is profoundly osteoporotic, with insufficiency fractures of the superior endplates of T12 through L3.

**DIFFERENTIAL DIAGNOSIS** Osteoporosis (from any cause), osteomalacia, multiple myeloma.

**DIAGNOSIS** Cushing disease.

**DISCUSSION** A severely osteoporotic lumbar spine in a man of middle age is distinctly unusual. The presence of shortening of the vertebral body height with uniform biconcave deformities of the endplates at every level suggests a chronic process of gradual onset. The most common cause is iatrogenic, in particular, chronic systemic corticosteroid use. Hypercortisolism, or Cushing disease, is the clinical manifestation of excessive amounts of glucocorticoids from any cause [58]. Cushing disease refers to endogenous, spontaneous hypercortisolism caused by an autonomously functioning pituitary or adrenal lesion, or by nonendocrine adrenocorticotrophic hormone-producing tumors. Demineralization of bone is almost always present if hypercortisolism has been present for a sufficient period

of time. Glucocorticoids inhibit the absorption of calcium from the intestine and increase renal calcium loss, leading to secondary hyperparathyroidism. Glucocorticoids also exert a direct stimulatory effect on osteoclasts. At the same time, glucocorticoids inhibit osteoblastic activity by suppressing the collagen synthesis necessary for the formation of osseous matrix. The net result is continued generalized loss of bone that is prominent in the spine, pelvis, ribs, and cranial vault. In addition to osteopenia, there may be thinning of the cortex, loss of trabecular structure, intracortical tunneling, vertebral central endplate depressions, and insufficiency fractures. Insufficiency fractures characteristically heal with exuberant callus formation. The vertebral endplates may have a sclerotic appearance, resulting from a combination of insufficiency compressive microfractures and subsequent healing. The osteoporosis of hypercortisolism is virtually indistinguishable from involutional osteoporosis. Osteoporosis may persist long after cortisol metabolism has been restored to normal, or synthetic corticosteroid treatment has ended. Patients who chronically take even low doses of systemic corticosteroids are at increased risk for osteoporosis and should undergo routine screening with bone mineral density measurements.

**CLINICAL HISTORY** A 20-year-old man with recurrent bone pain, and two companion cases.



FIGURE 3.27A

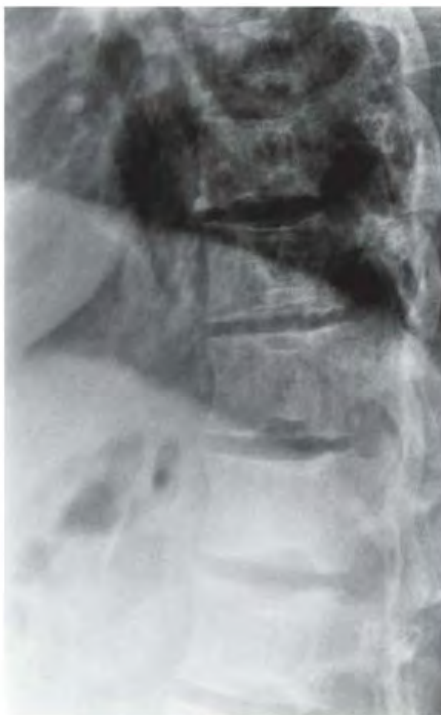


FIGURE 3.27B



FIGURE 3.27C

### FINDINGS

- A. Lateral radiograph of the thoracic spine shows H-shaped or "Lincoln log" vertebral bodies.
- B. Companion case 1. Lateral thoracic spine radiograph shows vertebral bodies with more subtle H shapes.
- C. Companion case 2. AP radiograph of the thoracic spine shows H-shaped vertebral bodies.

**DIFFERENTIAL DIAGNOSIS** Sickle cell disease, Gaucher disease, spherocytosis, thalassemia, osteogenesis imperfecta.

**DIAGNOSIS** Sickle cell disease.

**DISCUSSION** The H-shaped or "Lincoln log" vertebrae are classically described from the AP radiograph but are also seen on the lateral film. They are thought to result from infarction of the central growth plate, which then collapses in a squared-off pattern, but they actually represent a central, focal depression in the endplate [59]. H-shaped vertebrae have been described in thalassemia, osteoporosis, Gaucher

disease, and congenital hereditary spherocytosis, but they are much more common in sickle cell anemia.

The radiographic appearance is that of squared-off defects in the superior and inferior endplates, unlike the biconcave codfish vertebrae seen in osteoporosis.

The additional radiographic features reflect vascular infarctions and marrow hyperplasia in other areas. The marrow hyperplasia results in generalized granular-appearing radiolucency of bone, cortical thinning, and trabecular prominence. Vascular infarction tends to result in dactylitis between the ages of 6 months and 2 years; diaphyseal infarctions of larger, more commonly than smaller, tubular bones; epiphyseal infarction (typically in the hip); and growth disturbances. In addition, the patients are more susceptible to fractures, osteomyelitis, septic arthritis, hemarthrosis, joint effusions, and uric acid deposition.

Companion case 1 is a more subtle case of the H-shaped vertebrae that are classic for sickle cell disease. Companion case 2 is an AP radiograph showing the three-dimensional nature of the vertebral body abnormality.

**CLINICAL HISTORY** A 46-year-old man with spine motion limitation in flexion.



FIGURE 3.28A



FIGURE 3.28B



FIGURE 3.28C

## FINDINGS

- A. Lateral radiograph of the thoracic spine shows marked narrowing of the disc space with ossification. Small marginal disc osteophytes are noted. Diffuse osteopenia is noted.
- B. Lateral radiograph of the lumbar spine shows narrowing and ossification of the disc spaces without significant osteophyte formation.
- C. AP radiograph of the abdomen demonstrates subchondral sclerosis of the sacroiliac joints, without the erosive changes that would be expected in ankylosing spondylitis. Severe subchondral sclerosis and narrowing of the right hip is noted, without osteophyte formation.

**DIFFERENTIAL DIAGNOSIS** Degenerative disc disease, ochronosis, calcium pyrophosphate dihydrate (CPPD) deposition disease, hemochromatosis, hyperparathyroidism, acromegaly, poliomyelitis, amyloidosis.

**DIAGNOSIS** Ochronosis.

**DISCUSSION** Calcification of intervertebral discs may be idiopathic or may be associated with CPPD deposition disease, hemochromatosis, hyperparathyroidism, acromegaly, poliomyelitis, amyloidosis, and spinal fusion. In addition to history, morphology may be useful in making the distinction. The calcification is usually “wafer-like” or dystrophic in ochronosis, and there is marked joint space narrowing [60].

Ochronosis arthropathy results from an absence of the enzyme homogentisic acid oxidase, with resultant accumulation of homogentisic acid in the joints and disc spaces. This is usually inherited as an autosomal recessive trait. Clinical symptoms become evident in patients in their 30s and are usually more severe in men. The clinical presentation is usually similar to rheumatoid arthritis or ankylosing spondylitis.

The basic pathophysiology involves deposition in the articular cartilage, which stiffens it and eventually leads to fragmentation. Secondary osteoarthritic changes then ensue. In the spine, involvement of the hyaline cartilage separating the disc and vertebral body, as well as of the annulus fibrosis, results in premature degeneration. Dystrophic discal calcification thus begins at the margin of the vertebral body, rather than in the center of the disc as seen in idiopathic thoracic disc calcification. The tendency toward collapse of the disc space is more pronounced than in other processes, and may result in a loss of the lumbar lordosis. Ossification of the anterior longitudinal ligament can mimic the syndesmophyte formation seen in ankylosing spondylitis. Osteoporosis quickly ensues after fusion.

Extraspinal involvement is manifest as articular space narrowing with resultant secondary fragmentation (hence, intra-articular loose bodies) and subchondral sclerosis. Osteophytes are not a major finding in this disease. Ligaments and tendons can calcify or ossify, predisposing them to rupture. Involvement is limited largely to the large joints, sacroiliac joints, and symphysis pubis. The peripheral joints are spared. Other organ systems commonly involved by the pigment include the cardiovascular and genitourinary systems, and the upper respiratory tracts.

In large joints, ochronosis looks like degenerative joint disease, but the articular sites are unusual (e.g., shoulder), have an abnormal distribution (e.g., isolated lateral compartment disease in the knee), and are more severe, with more ossified loose bodies and less osteophytosis than is typically seen. Diagnostic considerations include CPPD deposition disease (although the findings are not as marked as seen in ochronosis), calcium hydroxyapatite deposition disease (periarticular calcification may distinguish this), acromegaly (heel pad thickening and widened joints are characteristic), epiphyseal and spondyloepiphyseal dysplasia (history and survey films can distinguish), and neuropathic joints (history distinguishes).

**CLINICAL HISTORY** A young child with abnormal spinal curvature, and a companion case.



FIGURE 3.29A



FIGURE 3.29B



FIGURE 3.29C

### FINDINGS

- A, B. Standing PA and lateral scoliosis study. Multiple segmentation anomalies are present in the lower thoracic and upper lumbar spine, including butterfly vertebrae at T11 and on the left between T9 and T10.
- C. Companion case. Standing PA scoliosis study showing multiple anomalies in the thoracic and lumbar spine, with S-shaped scoliosis.

**DIFFERENTIAL DIAGNOSIS** None.

**DIAGNOSIS** Congenital scoliosis.

**DISCUSSION** The presence of fusion or segmentation anomalies in combination with scoliosis makes this a congenital scoliosis.

The obvious causes of congenital scoliosis relate to failure of normal formation of individual vertebrae [61]. During the embryonic conversion of mesenchymal

vertebrae to cartilaginous vertebrae before week 9 of development, each vertebral body becomes chondrified from two centers of chondrification on either side of the midline. If chondrification fails on only one side, an isolated hemivertebra results. If the centers of chondrification do not fuse at the same level (as they should), but instead fuse across levels, a block vertebra results. Similarly, a pediculate bar or neural arch fusion can result from fusion anomalies. Rarely, a supernumerary hemivertebra can result from partial reduplication. The most common vertebral anomalies causing congenital scoliosis include hemivertebrae, trapezoidal vertebrae, and unilateral neural arch fusions. Combinations of anomalies and multilevel involvement are frequent.

Patients with congenital scoliosis must be carefully examined for the VACTERL syndrome (Vertebral, Anal, Cardiac, Tracheal, Esophageal, Renal, and Limb anomalies). At a minimum beyond physical examination, evaluation of the genitourinary tract is recommended.



FIGURE 3.30A



FIGURE 3.30B

**FINDINGS**

- A. Standing PA radiograph shows a mild left thoracolumbar scoliosis. The right side of the T12 vertebra is densely sclerotic.
- B. CT through T12 shows a 1-cm rounded lesion within the right lateral portion of the vertebral body adjacent to the costovertebral joint. The lesion has a sclerotic central focus, and a zone of surrounding sclerosis that extends well into the vertebral body and right pedicle.

**DIFFERENTIAL DIAGNOSIS** Osteoid osteoma, osteoblastoma, bone island, Brodie's abscess.

**DIAGNOSIS** Osteoid osteoma.

**DISCUSSION** Osteoid osteoma is a benign neoplasm of bone that is distinguished from osteoblastoma principally by size: osteoid osteoma is typically 1 cm or smaller, while osteoblastoma is typically 2 cm or larger. The pain syndrome

associated with osteoid osteoma can be highly suggestive, often as night pain relieved by aspirin. A painful scoliosis may develop due to reflexive splinting in the spine.

This case demonstrates the classic appearance on CT of an osteoid osteoma. Features include the round shape, the dense, central sclerosis, and the surrounding reactive bone formation. The lucent portion of the lesion consists of fibrovascular tissue but is also mineralized, although less so than the central sclerosis. On MRI, osteoid osteomas have high signal on T2-weighted images and enhance following gadolinium injection. They may be less conspicuous than on CT. Bone islands may develop in the vertebral column, but they are painless and are not associated with scoliosis. On CT, they tend to be homogeneously dense, with a spiculated margin where they blend into the surrounding trabecular bone. Although a Brodie's abscess could be expected to be painful, have extensive surrounding sclerosis, and possibly have a round shape, it should not contain mineralization. Current standard treatment of osteoid osteoma is radiofrequency ablation performed under CT guidance [62].

**CLINICAL HISTORY** A 70-year-old man with prostate cancer, and a companion case.

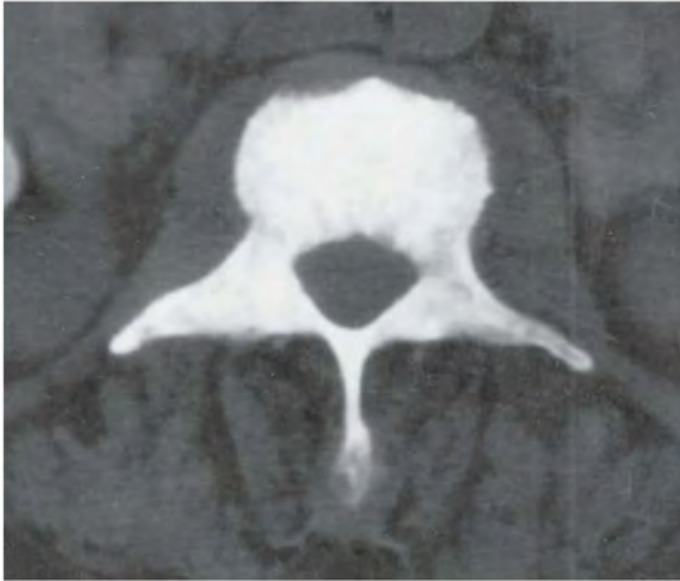


FIGURE 3.31A



FIGURE 3.31B



FIGURE 3.31C



FIGURE 3.31D

**FINDINGS**

- A. Axial CT shows increased sclerosis of a lumbar vertebra, with no increase in the size of the bone.
- B. Companion case: 67-year-old man with prostate cancer. AP view of the lumbar spine and pelvis demonstrates sclerotic lesions throughout the thoracic and lumbar spine, pelvis, and proximal femora.
- C, D. Sagittal T1-weighted and T2-weighted MRI of the lumbar spine reveals multiple bone marrow obliterating masses within the vertebral bodies. A T11 epidural mass extending from the left lamina compresses the adjacent spinal cord.

**DIFFERENTIAL DIAGNOSIS** Metastasis, Paget disease, lymphoma, chordoma, mastocytosis.

**DIAGNOSIS** Ivory vertebra from sclerotic prostate metastasis.

**DISCUSSION**

Sclerosis of the vertebral body in an elderly man is suggestive of prostate carcinoma, but it can also be seen in other metastases, myeloma, Paget disease, lymphoma, and chordomas [63]. Additional etiologies of an ivory vertebrae include sclerosing osteomyelitis (but disc involvement can be documented), mastocytosis, tuberous sclerosis, myelofibrosis, and osteosarcoma.

Lesions that can cause differential vertebral sclerosis include the hemangioma (accentuated vertical striations), renal osteodystrophy (rugger jersey, horizontal radiodense stripes on the bottom and top of the vertebral body), Paget disease (coarsened trabecular pattern with picture frame thickening along the margins of the vertebral body), and osteopetrosis (horizontal, thick, densities along both endplates).

**CLINICAL HISTORY** A 11-year-old girl with short stature, macrocephaly, and dysmorphic features, and a companion case.

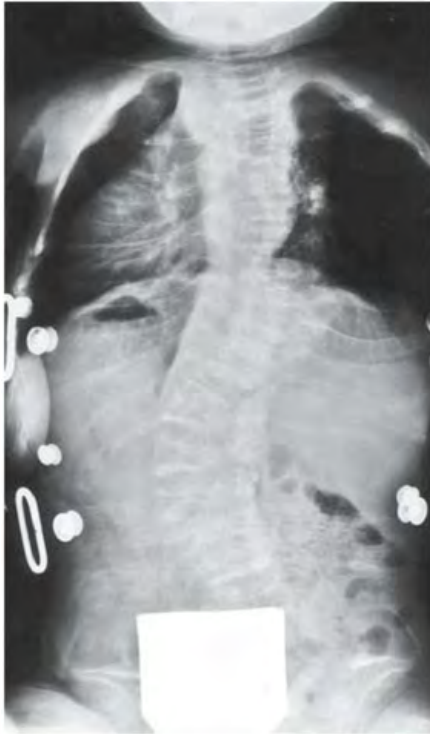


FIGURE 3.32A



FIGURE 3.32B



FIGURE 3.32C

## FINDINGS

- A. Posteroanterior (PA) radiograph of the thoracolumbar spine. There is generalized osteopenia, multiple vertebral body compression fractures, and mild S-shaped scoliosis. The pelvis is symmetrically distorted, with marked protrusio acetabuli.
- B, C. Companion case: A 39-year-old woman. PA and lateral views of the lumbar spine showing multilevel compression deformities and bilateral protrusio acetabuli.

**DIFFERENTIAL DIAGNOSIS** Osteogenesis imperfecta, fibrous dysplasia, juvenile idiopathic arthritis, Cushing syndrome, homocystinuria, idiopathic juvenile osteoporosis, renal osteodystrophy, hypophosphatasia.

**DIAGNOSIS** Osteogenesis imperfecta.

**DISCUSSION** Severe osteoporosis and insufficiency compression fractures of the vertebral bodies in a pediatric patient are uncommon. The diffuse distribution of disease in this case, including the pelvis, would exclude conditions that may cause vertebral compression fractures at

multiple (but not all) levels, such as eosinophilic granuloma and leukemia. Congenital conditions, endocrinopathies, systemic diseases, and iatrogenic forms of osteoporosis (as from treatment with heparin or steroids) may also cause osteoporosis, with resultant compression fractures. In this case, the severity of the changes and the diffuseness of its distribution (all bones) are most consistent with osteogenesis imperfecta. Osteogenesis imperfecta is a generalized connective tissue disorder affecting both collagen and osteoid production [64]. In addition to gracile, osteoporotic, fragile bones, ligamentous laxity and vascular and platelet abnormalities may be seen. Disproportion in stature is caused predominantly by spinal involvement, with a greater decrease in body height than leg length [65]. Platyspondyly, progressive kyphosis, and progressive scoliosis contribute to progressive spinal deformities. Several different specific errors in collagen synthesis may cause osteogenesis imperfecta. Cyclic administration of bisphosphonates, drugs known to reduce bone turnover, have been reported to improve clinical outcomes in patients with severe osteogenesis imperfecta, apparently by reducing bone resorption and increasing bone density [66].



FIGURE 3.33

**FINDINGS**

Lateral radiograph of the lumbar spine. There are sclerotic bands following the superior and inferior vertebral body endplates. The endosteal margins of these bands are irregular. The overall size and shape of the vertebral bodies is preserved, and surgical clips are present.

**DIFFERENTIAL DIAGNOSIS** None.**DIAGNOSIS** Renal osteodystrophy with rugger jersey spine.

**DISCUSSION** The alternating bands of sclerosis and osteoporosis are characteristic of the rugger jersey appearance in

the spine, so called because of the thick horizontal stripes [67]. The surgical clips remain from nephrectomies in this patient on chronic hemodialysis. In renal osteodystrophy, the combination of osteoporosis and osteomalacia is due to secondary hyperparathyroidism, abnormal vitamin D metabolism, and aluminum toxicity (if the patient is on hemodialysis). Osteosclerosis is a common finding that results from an increased volume of abnormal osteoid. The classic site for this finding is in the subchondral location in the spine, giving the rugger jersey appearance with a smudgy transition between normal and dense bone [68]. Other common areas of increased sclerosis in renal osteodystrophy include the pelvis and metaphyses of long bones.



FIGURE 3.34A



FIGURE 3.34B

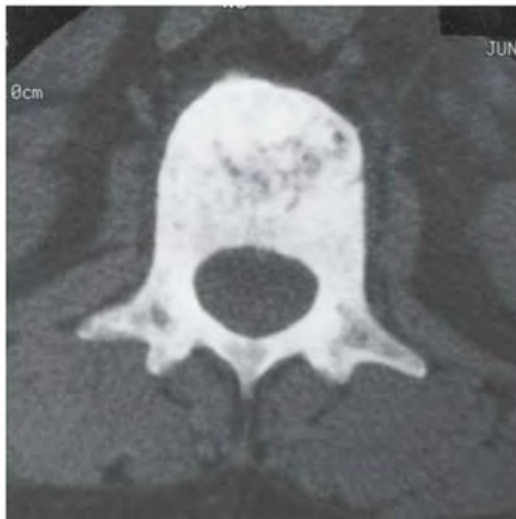


FIGURE 3.34C



FIGURE 3.34D

**FINDINGS**

- A, B. AP and lateral radiographs of the thoracolumbar spine show increased sclerosis of the L1 vertebral body with subtle overall enlargement relative to the vertebra below.
- C, D. CT axial slices show definite increase in the anterior to posterior dimension.

**DIFFERENTIAL DIAGNOSIS** Metastasis, Paget disease, lymphoma, chordoma, mastocytosis.

**DIAGNOSIS** Ivory vertebra from Paget disease.

**DISCUSSION** Paget disease is another etiology for an ivory vertebra. The radiologic findings include a coarsened

trabecular pattern and an overall increase in density [69]. However, it is the vertebral enlargement that distinguishes this from other causes of ivory vertebra. The picture frame appearance secondary to condensation of mineralization at the margins of the vertebral body is another appearance that is diagnostic.

Paget disease most commonly involves the lumbar spine and sacrum. Sacral abnormalities can be detected by a subtle thickening of the arcuate lines, as seen on the AP radiograph. Usually sacral abnormalities are seen in conjunction with other pelvic findings, such as thickening of the iliopectineal or iliopectineal lines. Neurologic symptoms can result from canal or neural foramen mechanical narrowing secondary to ligamentous ossification, vertebral enlargement or collapse, or a vascular steal phenomenon.

**CLINICAL HISTORY** A 40-year-old woman with back pain, and a companion case.

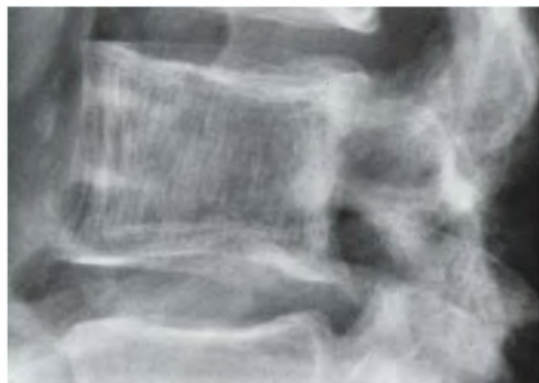


FIGURE 3.35A



FIGURE 3.35B



FIGURE 3.35C



FIGURE 3.35D

### FINDINGS

- A, B. AP and lateral detail radiographs of L2. There are thick vertical striations of the vertebral body. The posterior elements are not affected. The overall vertebral body size is normal. The cortex is of normal thickness.
- C, D. Companion case. Sagittal T1-weighted and T2-weighted MRI of the lumbar spine shows diffusely high signal in the L3 vertebral body. A benign compression fracture of L2 is also present.

**DIFFERENTIAL DIAGNOSIS** Hemangioma, metastasis, lymphoma, myeloma, chordoma, Paget disease, osteoporosis.

**DIAGNOSIS** Hemangioma.

**DISCUSSION** Radiographic features of hemangioma include a coarse reinforcement of the vertical trabecular pattern in response to the horizontal trabeculae that are lost [72]. This “corduroy” pattern is usually identified in the vertebral body, but can extend into the posterior elements. It is more typical to have a focal osseous lesion with a “cartwheel” pattern than involvement of the entire vertebral body. There is usually increased uptake of the radiopharmaceutical on bone scan. T1 hyperintensity results from the fat content, and T2 hyperintensity results from the blood content. Gadolinium enhancement is expected.

Differential considerations include metastatic disease, lymphoma, myeloma, or chordoma, when the lesion extends into the soft tissues. The lesions can usually be differentiated from Paget disease by the lack of cortical thickening.

**CLINICAL HISTORY** A 24-year-old man in a high-speed automobile crash. He was neurologically intact.



FIGURE 3.36A



FIGURE 3.36B



FIGURE 3.36C



FIGURE 3.36D

## FINDINGS

A–C. Sagittal CT reformations of the spine at the thoracolumbar junction. Anterior wedging of the T1 vertebral body is accompanied by a buckle fracture of the anterior cortex. Mildly distracted horizontal fractures extend through both L1 pedicles and the spinous processes. The facets still articulate normally.

D. Coronal CT reformation. The horizontal fractures extend through the transverse processes.

**DIFFERENTIAL DIAGNOSIS** None.

**DIAGNOSIS** L1 flexion-distraction fracture (Chance fracture).

**DISCUSSION** A “seat belt” injury refers to the osseous and ligamentous hyperflexion injuries that commonly occur at the thoracolumbar or upper lumbar levels in adult passengers, or at the midlumbar levels in child passengers.

Because the ligamentous structures withstand the distraction forces better than the vertebral bodies, a horizontal fracture that begins in the posterior elements and propagates anteriorly can result [70]. People with combination shoulder-lap belts incur different types of injuries (compression fractures of the cervicothoracic spine and antero-lateral wedge compressions of the thoracolumbar vertebrae

on the side opposite the shoulder strap) that have a lower incidence of neurologic sequelae, and therefore better prognosis.

There are four subtypes of Chance fractures:

- Type A (47%) is the original description of a horizontal fracture involving all three columns.
- Type B (11%) is restricted to disruption of the ligaments and intervertebral disc.
- Type C (26%) involves the posterior and middle columns, extending into the anterior disc.
- Type D (16%) involves the posterior column, extending then into the disc.

The imaging findings can be quite subtle on a transaxial CT; therefore, sagittal and coronal reformations are necessary. The features on sagittal reformations include a preserved to decreased anterior vertebral body height, a preserved to increased posterior vertebral body height, and rounding of the superior posterior vertebral body. Coronal reformations may demonstrate the extension of the fracture into the pedicles and transverse processes.

Pure posterior ligament disruption results in interspinous widening with subluxation, perching, or distraction of the facets. If there is more than 20 degrees of flexion or 10% lateral bending in the upper lumbar levels (without a fracture), ligamentous disruption must be present.

**CLINICAL HISTORY** A 58-year-old man with paraplegia after a car accident.



FIGURE 3.37A



FIGURE 3.37B

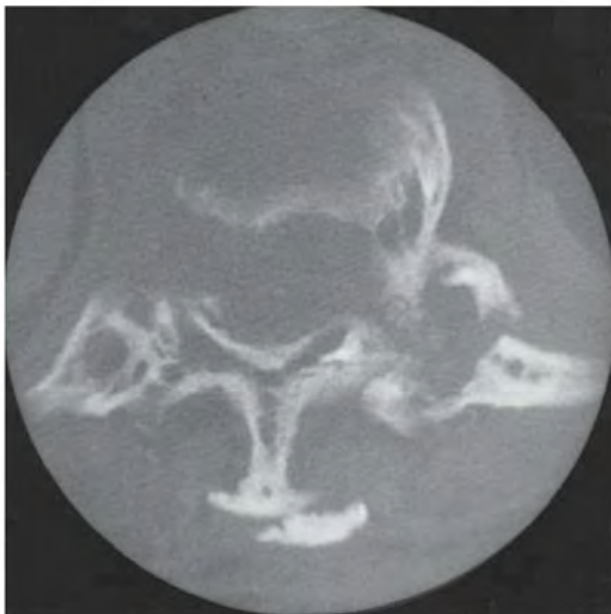


FIGURE 3.37C

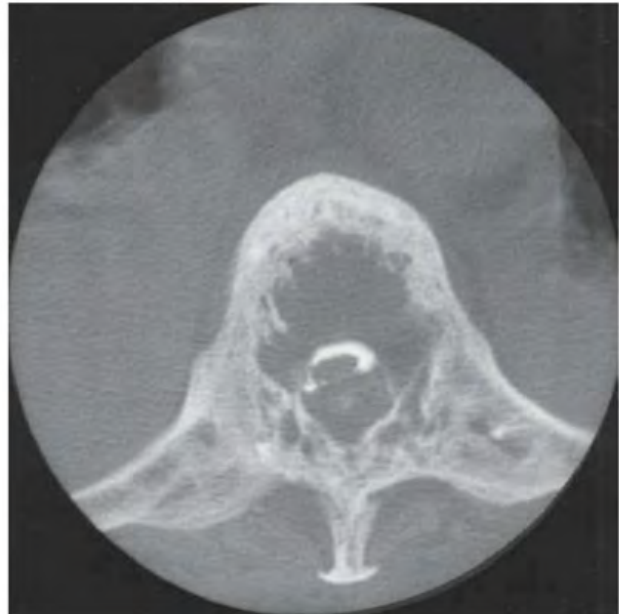


FIGURE 3.37D

## FINDINGS

- A, B. AP and lateral radiographs of the lumbar spine reveal a lateral distraction-dislocation at L1–L2, with an increase in the disc space. Syndesmophyte formation is noted, fusing all other levels. The sacroiliac joints are ankylosed.
- C, D. Axial CT images demonstrate marked narrowing of the spinal canal, with no myelographic contrast seen at the most severe level. The “double spinous process” sign at this level is due to avulsion of the ossification along the spinous process. A second fracture site is noted through the left facet.

**DIFFERENTIAL DIAGNOSIS** Fracture dislocation in ankylosing spondylitis, DISH, or juvenile idiopathic arthritis.

**DIAGNOSIS** Ankylosing spondylitis with fracture dislocation.

**DISCUSSION** A fracture dislocation is one of the most devastating complications of ankylosing spondylitis. The fused

spine in ankylosing spondylitis is much weaker than a normal spine, because its rigidity does not allow it to absorb and dissipate the forces of traumatic loading. In the normal spine, the intervertebral discs, endplates, ligaments, and paravertebral musculature absorb most of these forces. The function of these structures is nullified by ankylosis. In addition, the bone in ankylosing spondylitis is osteoporotic. Relatively minor traumatic loading may cause fractures through syndesmophytes [71]. With greater force, fractures extend through the posterior elements, and the entire spine becomes unstable and may displace. Cord contusion or transection is a significant risk in these patients, a risk made greater by preexisting spinal stenosis that is associated with ossification of the posterior ligamentous complex. In addition to the immediate risk of neurologic catastrophe or even death, delayed neurologic deterioration is a well-recognized complication. Surgical stabilization is the preferred treatment, but the underlying vulnerability of the spine will remain.

**CLINICAL HISTORY** A 23-year-old woman whose back pain became much worse during pregnancy.



FIGURE 3.38A



FIGURE 3.38B



FIGURE 3.38C



FIGURE 3.38D

**FINDINGS**

- A, B. AP and lateral radiographs of the lumbar spine. The L2 vertebral body is compressed and expanded outward circumferentially.
- C, D. Sagittal T2-weighted MRI shows high signal intensity in the L2 body. Posterior expansion impinges on the thecal sac. There is no paravertebral edema, and the cortex appears intact.

**DIFFERENTIAL DIAGNOSIS** Hemangioma with collapse, metastasis with collapse, eosinophilic granuloma with collapse.

**DIAGNOSIS** Hemangioma with vertebral collapse.

**DISCUSSION** Hemangioma is a benign lesion proliferation of vascular channels that can occur in the bone or soft tissues. Typical asymptomatic osseous lesions are often discovered incidentally in adults, and there is a female predominance. Autopsy data suggest that the prevalence of spinal involvement is approximately 10%, but far fewer lesions are of sufficient size to be detected radiographically. Both CT and MRI are more sensitive than radiographs, but the

radionuclide bone scan is typically negative. The thoracic spine is involved more frequently than the lumbar spine, and the cervical spine is not commonly involved. Malignant degeneration does not occur.

Vertebral hemangiomas enlarge during pregnancy and often become symptomatic. The vascular and hemodynamic changes that occur during pregnancy act to enlarge a preexisting hemangioma [73,74]. The average increase in circulatory volume during pregnancy is 40%, with a concomitant increase in venous capacitance. As the gravid uterus enlarges sufficiently to fill the pelvis and begins to extend into the abdominal cavity, its bulk interferes with venous return from the lower extremities into the inferior vena cava. As a collateral pathway, blood engorges the valveless Batson's plexus and flows retrograde in large volume into a preexisting vertebral hemangioma to produce progressive enlargement. Hormonal changes during pregnancy may also produce structural changes. Progesterone increases venous distensibility, and estrogen promotes endothelial growth. Most patients whose vertebral hemangiomas become symptomatic during pregnancy do so in the third trimester, when the gravid uterus begins to redirect blood flow into Batson's plexus. Many patients show spontaneous remission after delivery, but many do not.

**CLINICAL HISTORY** A 43-year-old woman with back pain.



FIGURE 3.39A



FIGURE 3.39B



FIGURE 3.39C



FIGURE 3.39D

**FINDINGS**

- A, B. Lateral and AP radiographs of the lumbar spine. The L3 vertebral body shows destruction along the right cortical margin and superior endplate. The right L3 pedicle is absent, and the vertebral body is mildly compressed. Similar but more severe destruction involves L5, and less severe destruction involves L2 and L4. Widening of the paravertebral soft tissues is evidence of a large associated soft tissue mass.
- C, D. Sagittal and coronal CT reformations. Bone destruction is more extensive than evident on the radiographs, and extends into the L3 spinous process. Soft tissue masses narrow the spinal canal. No reactive bone formation is present.

**DIFFERENTIAL DIAGNOSIS** Metastasis, multiple myeloma, lymphoma, leukemia.

**DIAGNOSIS** Multiple myeloma.

**DISCUSSION** Early destruction of a pedicle is a classic sign of metastatic disease that differentiates it from multiple myeloma [75], but in the presence of extensive disease, distinguishing among the entities in the differential diagnosis ultimately requires a tissue or laboratory diagnosis. The presence of reactive bone formation is more suggestive of metastatic disease rather than marrow cell malignancy. Contiguous tumor involvement within the spine is common in metastatic prostate and breast carcinomas, lymphoma, and multiple myeloma. Extrasosseous extension can sometimes be distinguished from infectious etiologies by the lack of disc involvement. Radiographic demonstration of osteolysis is an insensitive clue to metastatic disease, and radionuclide bone scan, MRI, or positron emission tomography/CT are better imaging methods for early detection. Clinical management of spine metastases may include therapeutic irradiation and surgical decompression and stabilization.

**CLINICAL HISTORY** A 68-year-old woman with newly discovered breast cancer.

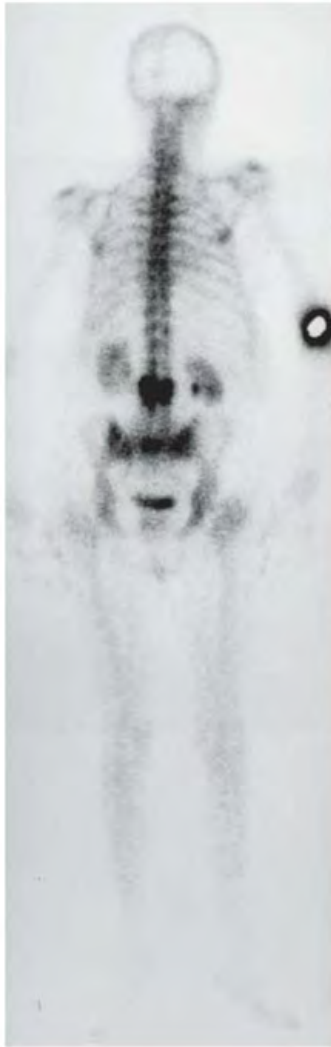


FIGURE 3.40A

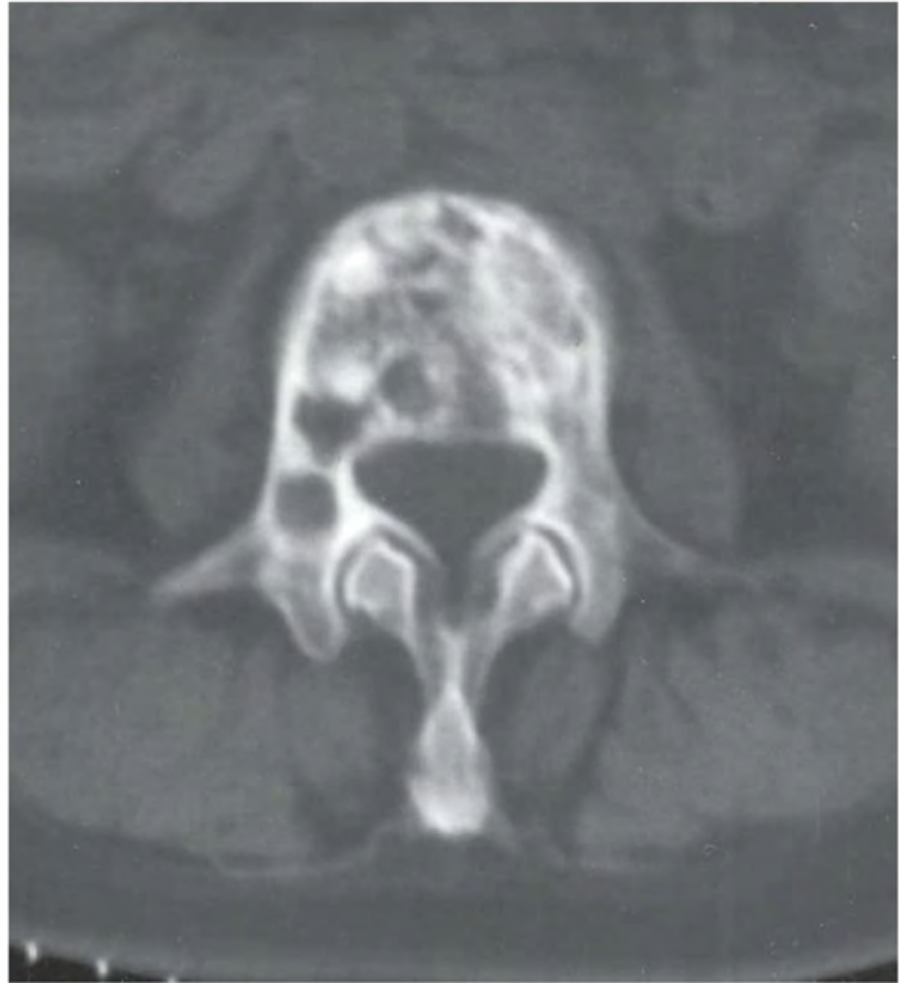


FIGURE 3.40B

### FINDINGS

- A. Radionuclide bone scan. Posterior whole-body view shows intense accumulation of activity in L3.
- B. Axial CT image through the L3 vertebra shows diffuse enlargement. The bone is a mosaic of sclerosis and lucent regions, with a disordered trabecular bone pattern.

**DIFFERENTIAL DIAGNOSIS** Metastasis, Paget disease, lymphoma, chordoma, mastocytosis.

**DIAGNOSIS** Paget disease.

**DISCUSSION** The coarsened trabecular pattern is a prominent feature in this case. However, it is sometimes difficult to arrive at the diagnosis quickly on CT images, because each level is read in isolation. Sagittal CT reformations can be helpful in identifying a subtle increase in vertebral body size.

Because Paget disease leads to weakened bone, biconcave vertebrae can sometimes result, with secondary degenerative changes in the disc. Occasionally, posterior element involvement may be seen in isolation or in conjunction with vertebral body abnormalities. In these cases, sclerosis of the pedicle will usually be accompanied by a subtle, overall increase in interpediculate distance.

Differential considerations of a dense vertebra include blastic metastases, myelofibrosis, fluorosis, mastocytosis, renal osteodystrophy, fibrous dysplasia, and tuberous sclerosis. Two other entities that can be seen in elderly patients include axial osteomalacia and fibrogenesis imperfecta ossium, both of which can be distinguished pathologically. A juvenile form of Paget disease, called familial idiopathic hyperphosphatasia, is recognized as having similar features, except there is sparing of the epiphyses.

**CLINICAL HISTORY** A 56-year-old man with chronic back pain, and a companion case.



FIGURE 3.41A



FIGURE 3.41B

### FINDINGS

- A. Lateral radiograph of the lumbar spine shows disk space narrowing, vertebral body osteophytes, and endplate sclerosis.
- B. Companion case. Lateral radiograph shows vacuum phenomenon in a narrowed disk space.

**DIFFERENTIAL DIAGNOSIS** Degenerative disc disease, infection, posttraumatic deformity.

**DIAGNOSIS** Degenerative disc disease.

**DISCUSSION** Degenerative disease of the spine can be subcategorized into intervertebral osteochondrosis, spondylosis deformans, and osteoarthritis. The primary abnormality in intervertebral osteochondrosis is in the nucleus pulposus, the shock absorber of the spine. Radiographic manifestations include decreased disc height, vacuum phenomenon, and sclerosis of the endplates. In spondylosis deformans, the annulus fibrosis has decreased elasticity and results in

osteophytosis with a normal to slightly decreased disc space. Osteoarthritis is a disease of the facet joints alone, and is manifest by joint space narrowing and sclerosis.

These entities must be differentiated from other processes that cause disc space narrowing [76]. Diskitis will typically show poorly defined endplate sclerosis that graduates into distinct erosive changes, with an associated soft tissue mass. Trauma with herniation of the nucleus pulposus will usually have a visible fracture or secondary signs of ligamentous instability with the appropriate clinical history. In neuropathic osteoarthropathy, the disc space narrowing, sclerosis, and osteophytosis are more pronounced and associated with debris and disorganization. Rheumatoid arthritis is typically seen in the cervical spine, and shows additional evidence of subluxations resulting from apophyseal and ligamentous involvement. The changes of CPPD deposition disease can include fragmentation, subluxation, and calcification, in addition to disc space narrowing and endplate sclerosis. Ochronosis can be suggested if there is prominent disc calcification and osteoporosis.

**CLINICAL HISTORY** A 35-year-old woman with back pain.



FIGURE 3.42A

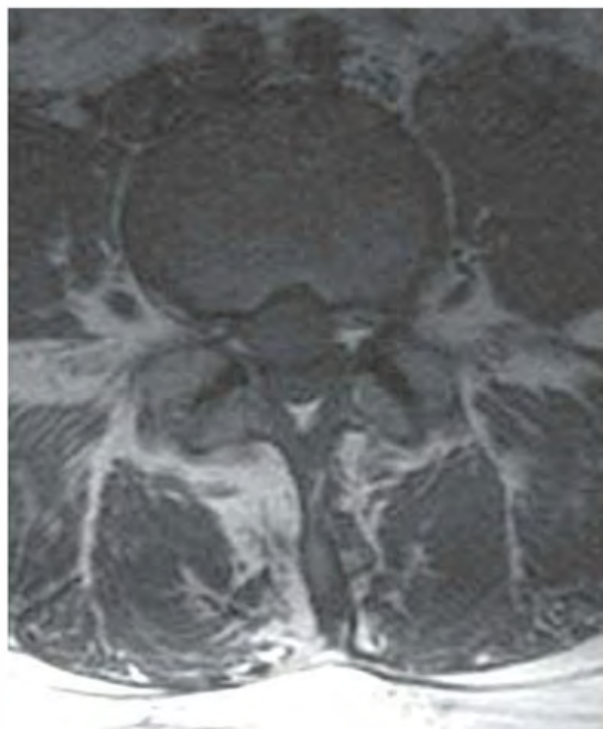


FIGURE 3.42B

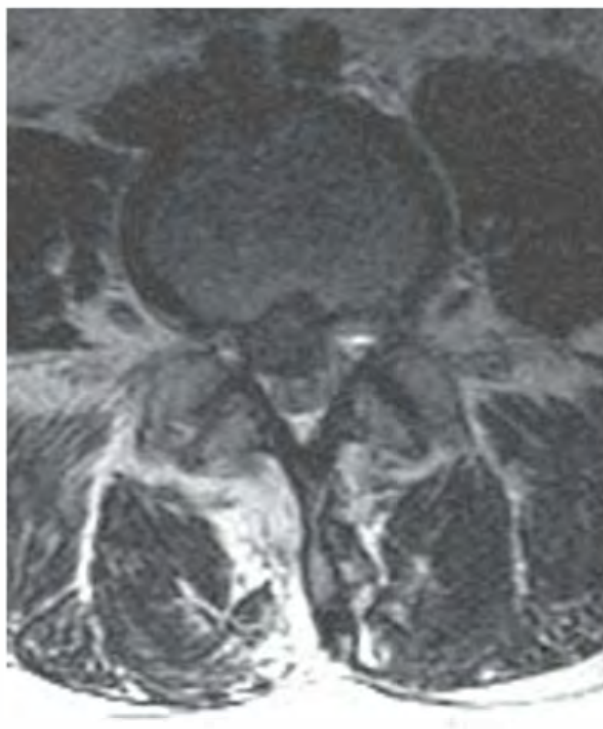


FIGURE 3.42C

**FINDINGS** Sagittal T2-weighted (A), axial T1-weighted (B), and axial T2-weighted (C) MRI demonstrates a bilobed disc extrusion, with a large fragment migrated superiorly lying in the lateral recess behind the L4 vertebral body. The fragment in the lateral recess behind L4 may impinge the right L4 nerve root. There is severe central canal stenosis present due to this lesion. The involved disc space is reduced in height and low in signal.

**DIFFERENTIAL DIAGNOSIS** None.

**DIAGNOSIS** Herniated nucleus pulposus.

**DISCUSSION** The presence of a low signal mass extending from a flattened, degenerated disc into the spinal canal is diagnostic of a herniated nucleus pulposus. Mechanical impingement of the herniated fragment on nerve roots may cause disabling back pain with radiation to the lower limbs.

Low back pain in adults is exceedingly common, affecting the majority of adults at some time during their lives, and it is the most common cause of disability under the age of 45 years. MRI is the study of choice in the setting of acute low back pain complicated by radicular symptoms. Sometimes the distinction between infection and degenerative disc disease can be particularly challenging. However, in discogenic sclerosis, the endplates tend to be uniformly sclerotic, without the focal erosions seen in infection. Defects in the endplates can result from herniated Schmorl's nodes. The presence of a vacuum phenomenon is suggestive of degenerative disc disease; even in the setting of infection superimposed on degenerative disc disease, the bacteria commonly consume the available nitrogen before the patient is imaged.

Other entities that can cause disc space narrowing associated with subchondral sclerosis include the seronegative spondyloarthropathies, CPPD deposition disease, ochronosis, neuropathic disease, and sarcoidosis.

**CLINICAL HISTORY** A 43-year-old man with rash and low back pain for 2 weeks. Radiograph at presentation; radiograph, MRI, and CT 6 weeks later.



FIGURE 3.43A



FIGURE 3.43B

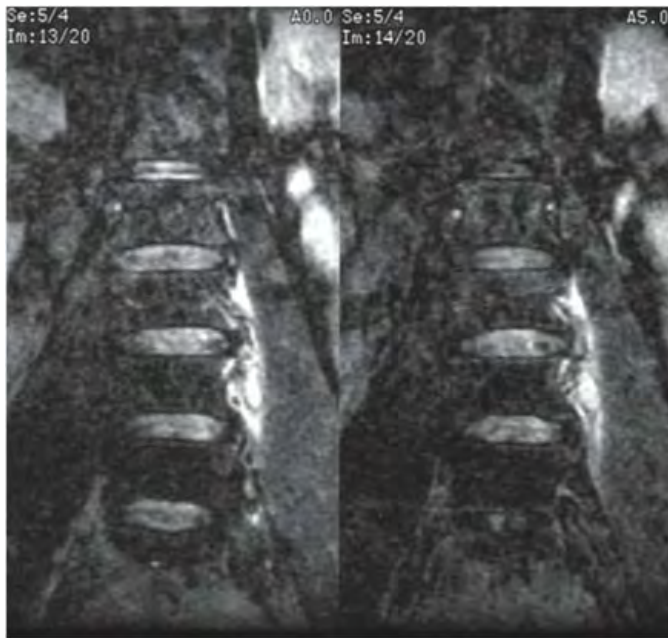


FIGURE 3.43C

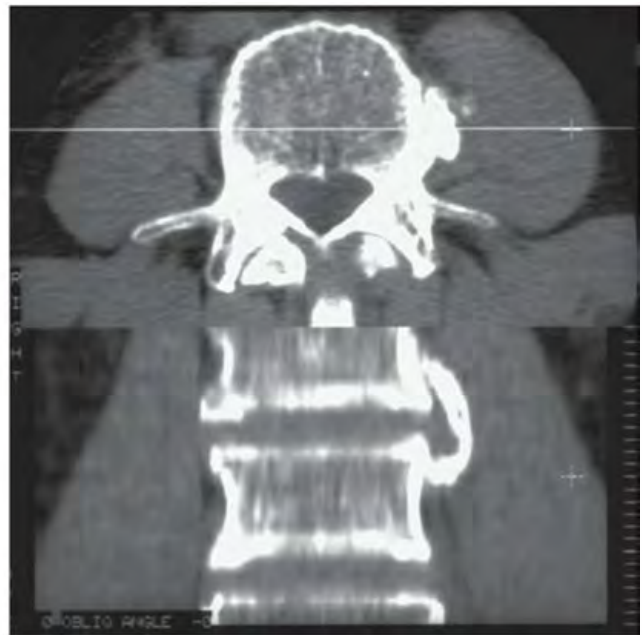


FIGURE 3.43D

## FINDINGS

- A. AP radiograph of the lumbar spine taken at presentation is normal.
- B. Six weeks later. AP radiograph of the lumbar spine taken at 6-week follow-up shows paravertebral ossification along the left lateral aspect at the L3–L4 level.
- C. Coronal short-tau inversion recovery MRI shows high signal in the left L3–L4 paravertebral soft tissues. The intervertebral disc spaces are normal in height and hydration.
- D. Axial CT with coronal reconstruction shows the paravertebral ossification bridging the lateral aspects of the L3–L4 vertebral bodies.

**DIFFERENTIAL DIAGNOSIS** Ankylosing spondylitis, psoriatic arthritis, reactive arthritis, DISH, fluorosis.

**DIAGNOSIS** Psoriatic spondyloarthropathy.

**DISCUSSION** The radiographs demonstrate paravertebral ossification becoming visible after 6 weeks, which is a typical

length of time for bone formation to occur. The MRI shows inflammatory changes surrounding the site of ossification, and the coronal CT reconstruction shows the particular morphology of the bony bridge in relation to the involved vertebral bodies. Paravertebral ossification that bridges adjacent vertebral bodies is a classic radiographic feature of psoriatic arthritis and reactive arthritis. The ossification is typically present at only a few levels—at one level in this case—and extends from the lateral cortex of one vertebral body to the lateral cortex of the next with a curvilinear shape. This particular form of vertebral hyperostosis is distinguishable from spondylosis deformans, in which the bony growth is oriented horizontally from the endplate (osteophytes); from DISH, in which the bony growth flows over multiple contiguous vertebral bodies (ligamentous ossification); and from ankylosing spondylitis, in which the bony growth is vertically oriented from the margins of the vertebral endplates (syndesmophytes). Paravertebral ossification is an early skeletal manifestation of psoriatic arthritis, typically preceding changes in the sacroiliac joints or in the peripheral joints [78]. This patient was not previously known to have psoriatic arthritis.

**CLINICAL HISTORY** A 29-year-old Mexican male farm worker with weight loss and night sweats.



FIGURE 3.44A



FIGURE 3.44B

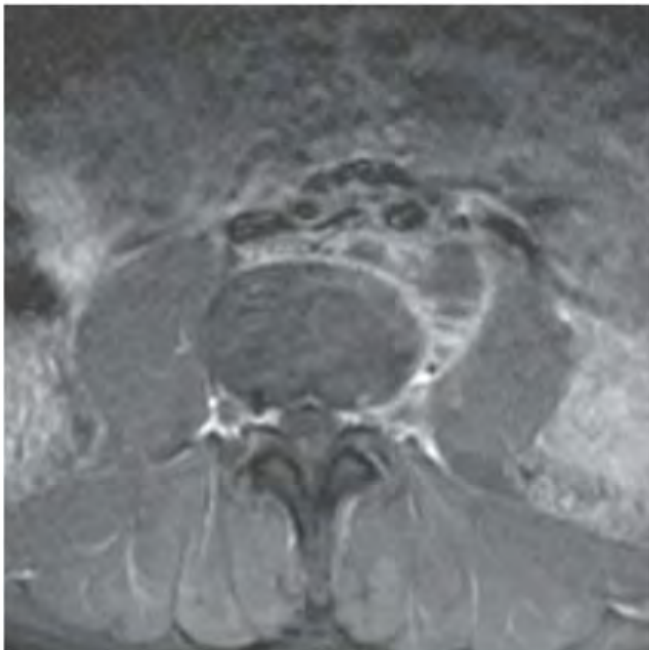


FIGURE 3.44C

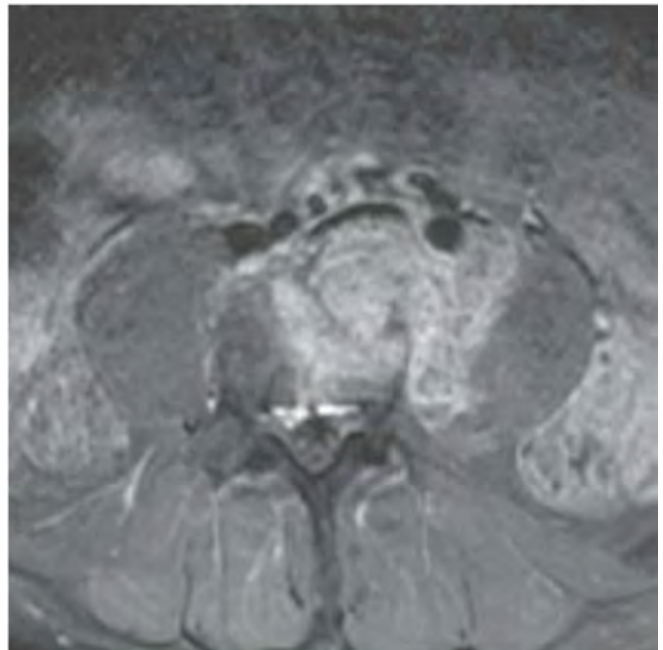


FIGURE 3.44D

## FINDINGS

- A. Sagittal T2-weighted fat-suppressed MRI through the lumbar spine shows a bright lesion in the L4 vertebral body that extends into the anterior paraspinal soft tissues and along the anterior aspects of L3 and the L4–L5 disc.
- B. Sagittal T1-weighted fat-suppressed postgadolinium MRI at the same location shows diffuse enhancement of the intraosseous portion of the lesion but rim enhancement of the soft tissue part.
- C. Axial T1-weighted fat-suppressed postgadolinium MRI at the level of L3 shows rim-enhancing multilocular collection in the left anterolateral paraspinal soft tissues, extending into and displacing the left psoas muscle.
- D. Axial T1-weighted fat-suppressed postgadolinium MRI at the level of L4 shows enhancement of the vertebral body, with a heterogeneously enhancing lesion extending from bone into the soft tissues, displacing the anterior longitudinal ligament.

**DIFFERENTIAL DIAGNOSIS** Mycobacterial infection, pyogenic infection, fungal infection, lymphoma.

## DIAGNOSIS Coccidioidomycosis.

**DISCUSSION** Spinal coccidioidomycosis is a common initial presentation of disseminated coccidioidomycosis, and spine lesions may develop during the course of treatment of coccidioidomycosis in other sites. The disease may be aggressive, and may require surgical debridement and stabilization when medical therapy fails [79]. Unifocal or multifocal spinal involvement may be found on MRI [80]. Involvement of the vertebral bodies and adjacent soft tissues is common. The appearance may resemble that of tuberculous spondylitis, and may be indistinguishable by imaging. Pyogenic infections typically involve a single intervertebral level, centered on the disk and the adjacent superior and inferior vertebral endplates. Lymphoma may involve multiple levels of bone and soft tissue but tends to infiltrate rather than displace and would have diffuse enhancement rather than rim enhancement.

**CLINICAL HISTORY** A 28-year-old woman in motor vehicle accident, but no apparent back pain.



FIGURE 3.45A



FIGURE 3.45B



FIGURE 3.45C



FIGURE 3.45D

## FINDINGS

- A–C. Sagittal reformations of the lumbosacral junction (left to right) from abdomen CT. At the L5 level, there are focal bony defects in the right and left pars interarticularis of the posterior elements. The margins of the lesions are well corticated, but there is no anterolisthesis of L5 over S1.
- D. Axial CT at the L5 level. There are bilateral pars defects with sclerotic margins.

**DIFFERENTIAL DIAGNOSIS** None.

**DIAGNOSIS** Bilateral L5 spondylolysis without anterolisthesis.

**DISCUSSION** The pars interarticularis is the portion of the vertebral body lamina that connects the superior facet to the

inferior facet. When defects are present in this region on both sides of a vertebral body, it may allow the vertebra to slip anteriorly (anterolisthesis or spondylolisthesis). Mechanisms leading to the defect are proposed to be heredity and repetitive microtrauma, leading to completed stress fractures. Spondylolysis is the most common cause of back pain in athletically active adolescents [81]. Conservative treatment with bracing is the favored initial treatment of adolescents, because some will go on to heal [82]. Approximately 95% of spondylolysis defects are found at the L5 level. On CT and MRI, the defects may be directly demonstrated. On lateral radiographs, a focal lucency in the posterior elements can sometimes be seen.

**CLINICAL HISTORY** A 24-year-old man who crashed his all-terrain vehicle (ATV) at high speed.



FIGURE 3.46A

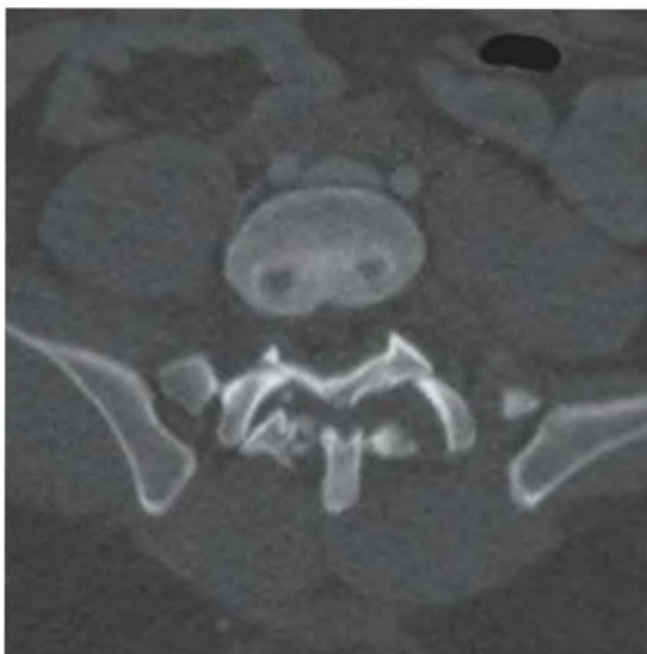


FIGURE 3.46B



FIGURE 3.46C



FIGURE 3.46D

## FINDINGS

- A, B. Axial CT images through the L5 body and inferior endplate. There is anterior dislocation of the left L5–S1 facet joint, with the inferior facet of L5 dislocated anterior to the superior facet of S1; there is fracture dislocation of the right L5–S1 facet joint; there is fracture of the L5 spinous process, with the gap between the posterior fragment and the remainder of the L5 posterior neural arch representing the degree of anterolisthesis of L5 over S1.
- C. Sagittal CT reformat at the lumbosacral junction shows distraction of the L5–S1 intervertebral disc space, anterolisthesis of L5 over S1, and fracture of the L5 spinous process.
- D. Sagittal short tau inversion recovery (STIR) MRI at the lumbosacral junction confirms the CT findings and in addition shows disruption of the L5–S1 disc, and tears of the anterior and posterior longitudinal ligaments. There is extensive surrounding edema and hemorrhage.

**DIFFERENTIAL DIAGNOSIS** None.

**DIAGNOSIS** Traumatic lumbosacral spondylolisthesis.

**DISCUSSION** Traumatic lumbosacral spondylolisthesis (traumatic lumbosacral fracture dislocation) is a rare injury that is described mostly in case reports or very small clinical series. In one series with 11 cases, there was bilateral lumbosacral fracture dislocation in 8 cases, pure lateral dislocation in 2 cases, and unilateral rotatory dislocation in 1 case. Radicular deficits were present in only two cases [83].

Crashes of ATVs during recreational use are a major source of severe vehicular trauma. In one population-based study, the most common mechanism of injury was a rollover, highlighting the instability of these vehicles [84]. Loss of control, separation of rider from vehicle, and collision with stationary or moving objects were other reported mechanisms. Nearly half of all injured patients sustained head and/or spine injuries. Among the spine fractures, there was a preponderance of injuries involving the thoracic (46%) and lumbar (26%) regions, with cervical (24%) and sacral (3%) less common. Drug or alcohol use was rare among injured riders, but 42% were teenagers or younger children. Fewer than 1% of the reported crashes occurred during farm- or work-related activities. Helmets appeared to reduce head injuries, but there is no way to protect the spine.

**CLINICAL HISTORY** A 28-year-old man with short stature, and a companion case.



FIGURE 3.47A



FIGURE 3.47B

### FINDINGS

- A. AP radiograph of the lumbar spine. There is severe developmental spinal stenosis in the lumbar region, with progressive narrowing of the interpediculate distances caudally.
- B. Companion case. AP radiograph of the lumbar spine in a patient with similar findings, but who had laminectomies at multiple levels.

**DIFFERENTIAL DIAGNOSIS** None.

**DIAGNOSIS** Achondroplasia.

**DISCUSSION** Progressive narrowing of the interpediculate distance as one proceeds caudally is seen only in achondroplasia and thanatophoric dwarfism [77]. In an adult, it is only seen in achondroplasia. Achondroplasia is the most common type of dwarfism and has a classic radiologic appearance. It is the result of a generalized defect in enchondral bone formation, leading to underdevelopment of the portions of bones that grow by this mechanism. The result is a symmetric, short-limbed dwarfism in which the proximal segments of the extremities are disproportionately short (rhizomelic micromelia). Because periosteal bone growth is unaffected, the shafts of the long bones are of normal diameter, but there is metaphyseal flaring. The fingers are short and

stubby. The skull base, formed by enchondral bone formation, is abnormally short and has a small foramen magnum. The calvaria, formed by intramembranous bone formation, is appropriately large for the intracranial contents, giving the head a characteristic brachycephaly with frontal bossing and a small face. The spinal canal is narrow in both anteroposterior and lateral dimensions, but the trunk length is nearly normal. This becomes most prominent in the lumbar area, where there is narrowing in the distance between pedicles, as opposed to the maintained or increased distance noted in normal patients as one progresses caudally. There is an exaggerated lumbar lordosis with prominent buttocks. The ribs are likewise shortened, leading to a decrease in intrathoracic volume. These abnormalities are usually evident at birth and become more apparent with age.

Achondroplasia has autosomal dominant genetic transmission, but most cases are sporadic. The classic form is heterozygous, has no associated congenital defects, and may be compatible with a normal life expectancy. Complications of congenital spinal stenosis are common in adulthood. The homozygous condition is lethal in infancy and has a radiologic appearance identical to thanatophoric dwarfism. Thanatophoric (“death bringing”) dwarfism is the most common lethal bone dysplasia. The chromosomal distinction between homozygous achondroplasia and thanatophoric dwarfism is important for genetic counseling of the parents.

## SOURCES AND READINGS

- Nischal K, Chumas P, Sparrow O. Prolonged survival after atlanto-occipital dislocation: two case reports and review. *Br J Neurosurg.* 1993;7:677–682.
- Harmanli O, Koyfman Y. Traumatic atlanto-occipital dislocation with survival: a case report and review of the literature. *Surg Neurol.* 1993;39:324–330.
- Ferrera PC, Bartfield JM. Traumatic atlanto-occipital dislocation: a potentially survivable injury. *Am J Emerg Med.* 1996;14:291–296.
- Henry MB, Angelastrao DB, Gillen JP. Unrecognized traumatic atlanto-occipital dislocation. *Am J Emerg Med.* 1998;16:406–408.
- Guigui P, Milaire M, Morvan G, Lassale B, Deburge A. Traumatic atlanto-occipital dislocation with survival: case report and review of the literature. *Eur Spine J.* 1995;4(4):242–247.
- Harris JH Jr, Edeiken-Monroe B. *The Radiology of Acute Cervical Spine Trauma.* 2nd ed. New York, NY: Williams and Wilkins; 1987:65–91.
- Weller SJ, Malek AM, Rossitch E Jr. Cervical spine fractures in the elderly. *Surg Neurol.* 1997;47:274–280.
- Ryan MD, Henderson JJ. The epidemiology of fractures and fracture-dislocations of the cervical spine. *Injury.* 1992;23:38–40.
- Lieberman IH, Webb JK. Cervical spine injuries in the elderly. *J Bone Joint Surg Br.* 1994;76:877–881.
- Matsui H, Imada K, Tsuji H. Radiographic classification of os odontoides and its clinical significance. *Spine.* 1997;22:1706–1709.
- Schatzker J, Rorabeck CH, Waddell JP. Fractures of the dens (odontoid process): an analysis of 37 cases. *J Bone Joint Surg Br.* 1971;53-B:392–405.
- Jackson RS, Banit DM, Rhyne AL III, Darden BV II. Upper cervical spine injuries. *J Am Acad Orthop Surg.* 2002;10(4):271–280.
- Levine AM, Edwards CC. Traumatic lesions of the occipitoatlanto-axial complex. *Clin Orthop Relat Res.* 1989;53–68.
- Boyarsky I. C2 Fractures. eMedicine 2009 (updated Oct 20, 2009). <http://emedicine.medscape.com/article/1267150-overview>.
- Crawford NR, Duggal N, Chamberlain RH, Park SC, Sonntag VK, Dickman CA. Unilateral cervical facet dislocation: injury mechanism and biomechanical consequences. *Spine.* 2002;27(17):1858–1864.
- Daffner SD, Daffner RH. Computed tomography diagnosis of facet dislocations: the “hamburger bun” and “reverse hamburger bun” signs. *J Emerg Med.* 2002;23(4):387–394.
- Vaccaro AR, Madigan L, Schweitzer ME, Flanders AE, Hilibrand AS, Albert TJ. Magnetic resonance imaging analysis of soft tissue disruption after flexion-distraction injuries of the subaxial cervical spine. *Spine.* 2001;26(17):1866–1872.
- Tracy MR, Dormans JP, Kusumi K. Klippel-Feil syndrome: clinical features and current understanding of etiology. *Clin Orthop.* 2004;424:183–190.
- Ogden JA, Conlogue GJ, Phillips MS, Bronson ML. Sprengel’s deformity. Radiology of the pathologic deformation. *Skeletal Radiol.* 1979;4(4):204–211.
- Sullivan JA. Klippel-Feil Syndrome. eMedicine 2009 (updated June 23, 2009). <http://emedicine.medscape.com/article/1264848-overview>.
- Quencer RM, Nunez D, Green BA. Controversies in imaging acute cervical spine trauma. *AJNR Am J Neuroradiol.* 1997;18:1866–1868.
- Kim KS, Chen HH, Russell EJ, Rogers LF. Flexion tear-drop fracture of the cervical spine: radiographic characteristics. *AJR Am J Roentgenol.* 1989;152:319–326.
- Kathol MH. Cervical spine trauma. What is new? *Radiol Clin North Am.* 1997;35:507–532.
- Kinoshita H. Pathology of hyperextension injury of the cervical spine: a case report. *Spinal Cord.* 1997;35:857–858.
- Green JD, Harle TS, Harris JH Jr. Anterior subluxation of the cervical spine: hyperflexion sprain. *AJNR Am J Neuroradiol.* 1981;2(3):243–250.
- Braakman M, Braakman R. Hyperflexion sprain of the cervical spine. Follow-up of 45 cases. *Acta Orthop Scand.* 1987;58:388–393.
- Caron T, Bransford R, Nguyen Q, Agel J, Chapman J, Bellabarba C. Spine fractures in patients with ankylosing spinal disorders. *Spine (Phila Pa 1976).* 2010;35(11):E458–E464.
- Flemming DJ, Murphey MD, Carmichael BB, Bernard SA. Primary tumors of the spine. *Semin Musculoskelet Radiol.* 2000;4(3):299–320.
- Unni KK, Inwards CY. *Dahlin’s Bone Tumors: General Aspects and Data on 10,165 Cases.* 6th ed. Philadelphia, PA: Lippincott Williams & Wilkins; 2010:112–121.
- Lucas DR, Unni KK, McLeod RA, O’Connor MI, Sim FH. Osteoblastoma: clinicopathologic study of 306 cases. *Hum Pathol.* 1994;25:117–134.
- Zambelli P, Lechevallier J, Bracq H, Carliz H. Osteoid osteoma or osteoblastoma of the cervical spine in relation to the vertebral artery. *J Pediatr Orthop.* 1994;14:788–792.
- Andronikou S, Jadwat S, Douis H. Patterns of disease on MRI in 53 children with tuberculous spondylitis and the role of gadolinium. *Pediatr Radiol.* 2002;32(11):798–805.
- Jain AK. Treatment of tuberculosis of the spine with neurologic complications. *Clin Orthop.* 2002;(398):75–84.
- Rawlins BA, Girardi FP, Boachie-Adjei O. Rheumatoid arthritis of the cervical spine. *Rheum Dis Clin North Am.* 1998;24:55–65.
- Azouz EM. Arthritis in children: conventional and advanced imaging. *Semin Musculoskelet Radiol.* 2003;7(2):95–102.
- Leite CC, Escobar BE, Bazan C III, Jinkins JR. MRI of cervical facet dislocation. *Neuroradiology.* 1997;39:583–588.
- Holmes JF, Mirvis SE, Panacek EA, Hoffman JR, Mower WR, Velmahos GC. For the NEXUS Group. Variability in computed tomography and magnetic resonance imaging in patients with cervical spine injuries. *J Trauma.* 2002;53:524–529.
- Whitehill R, Stowers SF, Ruch WW, Stamp WG. Cervical dislocation adjacent to a fused motion segment: a case report. *Spine.* 1987;12:396–398.
- Gruss P, Tannenbaum H. Stress exertion on adjacent levels after ventral fusion. *Arch Orthop Trauma Surg.* 1983;101:283–286.
- Orndorff DG, Samartzis D, Whitehill R, Shen FH. Traumatic fracture-dislocation of C5 on C6 through previously solid multilevel anterior cervical discectomy and fusion: a case report and review of the literature. *Spine J.* 2006;6(1):55–60.
- Taybi H, Lachman RS. *Radiology of Syndromes, Metabolic Disorders, and Skeletal Dysplasias.* 4th ed. St. Louis, MO: Mosby; 1996:677–679.
- Mikles M, Stanton RP. A review of Morquio syndrome. *Am J Orthop.* 1997;26:533–540.
- McAlister WH, Herman TE. Osteochondrodysplasias, dysostoses, chromosomal aberrations, mucopolysaccharidoses, and mucopolipodioses. In: Resnick D, ed. *Diagnosis of Bone and Joint Disorders.* 4th ed. Philadelphia, PA: WB Saunders; 2001:4489–4491.
- Kovanlikaya A, Loro ML, Gilsanz V. Pathogenesis of osteosclerosis in autosomal dominant osteopetrosis. *AJR Am J Roentgenol.* 1997;168:929–932.
- Ruiz-Maldonado R, Tamayo-Sanchez L, Orozco-Covarrubias ML. The use of retinoids in the pediatric patient. *Dermatol Clin.* 1998;16:553–569.
- DiGiovanna JJ. Isotretinoin effects on bone. *J Am Acad Dermatol.* 2001;45(5):S176–S182.
- David M, Hodak E, Lowe NJ. Adverse effects of retinoids. *Med Toxicol Adverse Drug Exp.* 1988;3:273–288.
- Torok L, Galuska L, Kasa M, Kada L. Bone-scintigraphic examinations in patients treated with retinoids: a prospective study. *Br J Dermatol.* 1989;120:31–36.
- Sheridan R, Peralta R, Rhea J, Ptak T, Novelline R. Reformatted visceral protocol helical computed tomographic scanning allows conventional radiographs of the thoracic and lumbar spine to be eliminated in the evaluation of blunt trauma patients. *J Trauma.* 2003;55(4):665–669.
- Honan M, White GW, Eisenberg GM. Spontaneous infectious discitis in adults. *Am J Med.* 1996;100:85–89.
- Fouquet B, Goupille P, Gobert F, Cotty P, Roulot B, Valat JP. Infectious discitis diagnostic contribution of laboratory tests and percutaneous discovertebral biopsy. *Rev Rhum Engl Ed.* 1996;63:24–29.

52. Loke TK, Ma HT, Chan CS. Magnetic resonance imaging of tuberculous spinal infection. *Australas Radiol.* 1997;41:7–12.
53. Murphey MD, Robbin MR, McRae GA, Flemming DJ, Temple HT, Kransdorf MJ. The many faces of osteosarcoma. *Radiographics.* 1997;17:1205–1231.
54. Floman Y, Bar-On E, Mosheiff R, Mirovsky Y, Robin GC, Ramu N. Eosinophilic granuloma of the spine. *J Pediatr Orthop B.* 1997;6:260–265.
55. Harreby M, Neergaard K, Hesselsoe G, Kjer J. Are radiologic changes in the thoracic and lumbar spine of adolescents risk factors for low back pain in adults? A 25-year prospective cohort study of 640 school children. *Spine.* 1995;20:2298–2302.
56. Gustavel M, Beals RK. Scheuermann's disease of the lumbar spine in identical twins. *AJR Am J Roentgenol.* 2002;179(4):1078–1079.
57. Andersson GB, Bostrom MP, Eyre DR, et al. Consensus summary on the diagnosis and treatment of osteoporosis. *Spine.* 1997;22:63S–65S.
58. Khanine V, Fournier JJ, Requeda E, Luton JP, Simon F, Crouzet J. Osteoporotic fractures at presentation of Cushing's disease: two case reports and a literature review. *Joint Bone Spine.* 2000;67(4):341–345.
59. Kooy A, de Heide LJ, ten Tiji AJ, et al. Vertebral bone destruction in sickle cell disease: infection, infarction, or both. *Neth J Med.* 1996;48:227–231.
60. Mannoni A, Selvi E, Lorenzini S, et al. Alkaptonuria, ochronosis, and ochronotic arthropathy. *Semin Arthritis Rheum.* 2004;33(4):239–248.
61. Arlet V, Odent T, Aebi M. Congenital scoliosis. *Eur Spine J.* 2003;12(5):456–463.
62. Rosenthal DI, Hornicek FJ, Torriani M, Gebhardt MC, Manlin HJ. Osteoid osteoma: percutaneous treatment with radiofrequency energy. *Radiology.* 2003;229:171–175.
63. Carpineta L, Gagne M. The ivory vertebra: an approach to investigation and management based on two case studies. *Spine.* 2002;27(9):E242–E247.
64. Rauch F, Glorieux FH. Osteogenesis imperfecta. *Lancet.* 2004;363(9418):1377–1385.
65. Engelbert RH, Gerver WJ, Breslau-Siderius LJ, et al. Spinal complications in osteogenesis imperfecta: 47 patients 1–16 years of age. *Acta Orthop Scand.* 1998;69:283–286.
66. Arikoski P, Silverwood B, Tillmann V, Bishop NJ. Intravenous pamidronate treatment in children with moderate to severe osteogenesis imperfecta: assessment of indices of dual-energy x-ray absorptiometry and bone metabolic markers during the first year of therapy. *Bone.* 2004;34(3):539–546.
67. Resnick D. The "rugger jersey" vertebral body. *Arthritis Rheum.* 1981;24:1191–1194.
68. Mulligan ME. *Classic Radiologic Signs. An Atlas and History.* New York, NY: Parthenon; 1997:138–139.
69. Whitten CR, Saifuddin A. MRI of Paget's disease of bone. *Clin Radiol.* 2003;58(10):763–769.
70. Saifuddin A, Noordeen H, Taylor BA, Bayley I. The role of imaging in the diagnosis and management of thoracolumbar burst fractures: current concepts and a review of the literature. *Skeletal Radiol.* 1996;25(7):603–613.
71. Hitchon PW, From AM, Brenton MD, Glaser JA, Torner JC. Fractures of the thoracolumbar spine complicating ankylosing spondylitis. *J Neurosurg.* 2002;97(suppl):218–222.
72. Friedman DP. Symptomatic vertebral hemangiomas: MR findings. *AJR Am J Roentgenol.* 1996;167:359–364.
73. Redekop GJ, Del Maestro RF. Vertebral hemangioma causing spinal cord compression during pregnancy. *Surg Neurol.* 1992;38:210–215.
74. Tekkok IH, Acikgoz B, Saglam S, Onol B. Vertebral hemangioma symptomatic during pregnancy—report of a case and review of the literature. *Neurosurgery.* 1993;32:302–306.
75. Resnick D. Skeletal metastases. In: Resnick D, ed. *Diagnosis of Bone and Joint Disorders.* 4th ed. Philadelphia, PA: WB Saunders; 2001:4295.
76. Carragee EJ, Hannibal M. Diagnostic evaluation of low back pain. *Orthop Clin North Am.* 2004;35(1):7–16.
77. Lachman RS. Neurologic abnormalities in the skeletal dysplasias: a clinical and radiological perspective. *Am J Med Genet.* 1997;69:33–43.
78. Sundaram M, Patton JT. Paravertebral ossification in psoriasis and Reiter's disease. *Br J Radiol.* 1975;48:628–633.
79. Wrobel CJ, Chappell ET, Taylor W. Clinical presentation, radiological findings, and treatment results of coccidioidomycosis involving the spine: report on 23 cases. *J Neurosurg.* 2001;95(1 suppl):33–39.
80. Olson EM, Duberg AC, Herron LD, Kissel P, Smilovitz D. Coccidioid spondylitis: MR findings in 15 patients. *AJR Am J Roentgenol.* 1998;171(3):785–789.
81. Lim MR, Yoon SC, Green DW. Symptomatic spondylolysis: diagnosis and treatment. *Curr Opin Pediatr.* 2004;16(1):37–46.
82. Fujii K, Katoh S, Sairyo K, Ikata T, Yasui N. Union of defects in the pars interarticularis of the lumbar spine in children and adolescents. The radiological outcome after conservative treatment. *J Bone Joint Surg Br.* 2004;86(2):225–231.
83. Vialle R, Charosky S, Rillardon L, Levassor N, Court C. Traumatic dislocation of the lumbosacral junction diagnosis, anatomical classification and surgical strategy. *Injury.* 2007;38(2):169–181.
84. Finn MA, MacDonald JD. A population-based study of all-terrain vehicle-related head and spinal injuries. *Neurosurgery.* 2010;67(4):993–997; discussion 997.

CHAPTER

# 4

## **Pelvis**

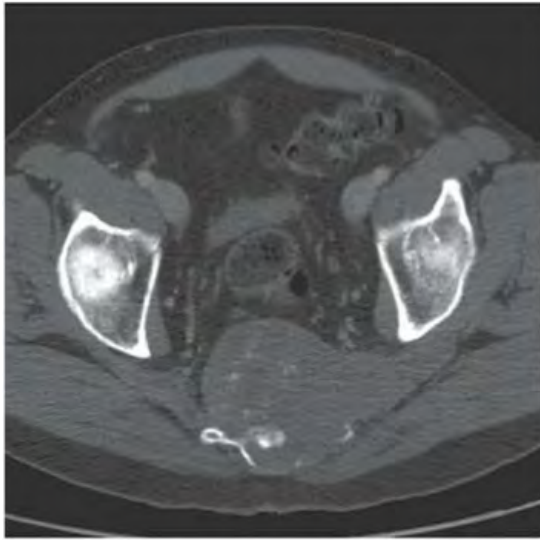


FIGURE 4.1A

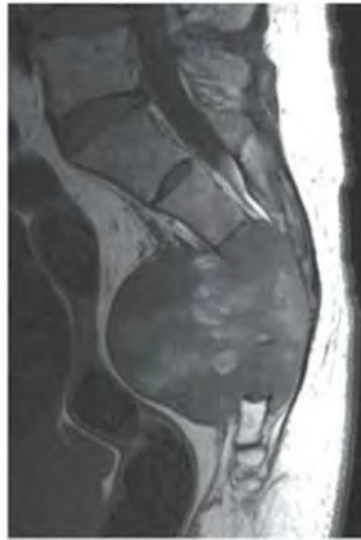


FIGURE 4.1B

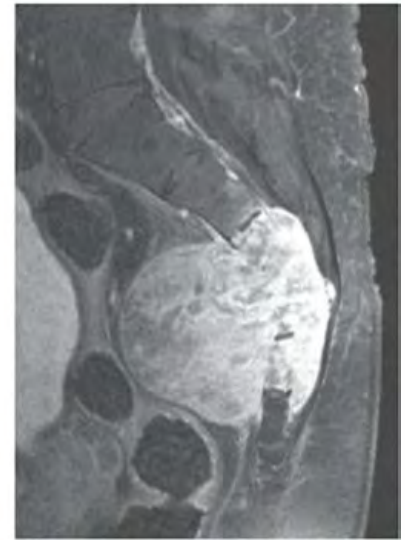


FIGURE 4.1C

### FINDINGS

- A. Axial computed tomography (CT) shows a midline mass causing lytic destruction of inferior sacrum with presacral soft tissue extension. There are small foci of calcifications within the mass.
- B. Sagittal T1-weighted magnetic resonance image (MRI) demonstrates a heterogeneously low signal intensity mass replacing the distal sacrum and extending anteriorly into the pelvis.
- C. Sagittal postcontrast T1-weighted fat-saturated MRI shows diffuse enhancement within the mass.

**DIFFERENTIAL DIAGNOSIS** Chordoma, metastasis, plasmacytoma, lymphoma, sarcoma.

**DIAGNOSIS** Chordoma.

**DISCUSSION** The diagnosis is suggested by the characteristic location in the midline of the sacrococcygeal region, with

asymmetric expansion from the bone into the anterior soft tissues. The radiologic features typical of chordoma in this location are irregular osteolysis and expansion with an associated anterior soft tissue mass. Fifty percent to seventy percent of cases may show amorphous calcification, usually in the periphery of the tumor; some lesions present with sclerosis instead of osteolysis. On T2-weighted MRI, the lesions are typically as bright as hydrated intervertebral discs [1,2]. Chordoma is a locally aggressive lesion of notochordal origin [3]. Chordomas are most common in the sacrococcygeal region (50% to 60% of lesions), in men (2:1 predilection), and between the ages of 40 and 70. Sphenococcygeal lesions account for almost all of the remainder of lesions (25% to 40%). Sacrococcygeal lesions typically present with pain and perineal numbness. The lesions usually arise from the vertebral body, but they can extend into the posterior elements.



FIGURE 4.2

**FINDINGS** Coronal T1-weighted MRI of the pelvis demonstrates a band of increased signal in the inferior sacrum, with a well-defined horizontal border.

**DIFFERENTIAL DIAGNOSIS** Radiation change, insufficiency fracture, imaging artifact.

**DIAGNOSIS** Radiation change.

**DISCUSSION** Therapeutic irradiation has direct effects on the cellular components of bone as well as indirect effects that result from vascular injury. Deleterious effects on bone include growth. MRI is commonly used to study the spine

or pelvis after therapeutic irradiation. On T1-weighted MRI, there is an increased signal in the involved bone due to replacement of the hematopoietic marrow with fat. This alteration can be seen 3 months after initiation of therapy, and may remain indefinitely [5,6]. Radiation can also give rise to marrow fibrosis. Fibrosis should have low signal intensity on both T1-weighted and T2-weighted MRI, whereas tumor typically has increased signal on T2-weighted MRI due to the increased water content. Other effects of radiation therapy include avascular necrosis, insufficiency fractures, and radiation-induced neoplasms. In the growing skeleton, deleterious effects of radiation include inhibition of bone growth, slipped capital epiphyses, and scoliosis.

**CLINICAL HISTORY** A 24-year-old woman with low back pain for several months.

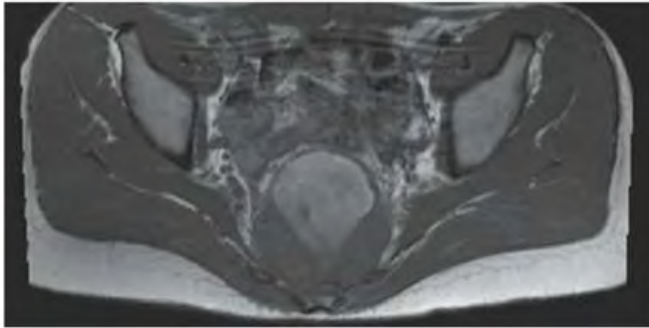


FIGURE 4.3A

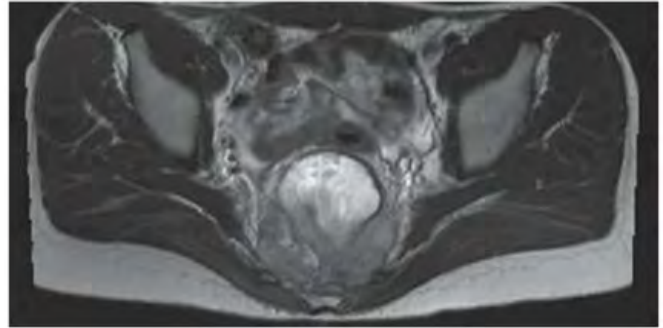


FIGURE 4.3B

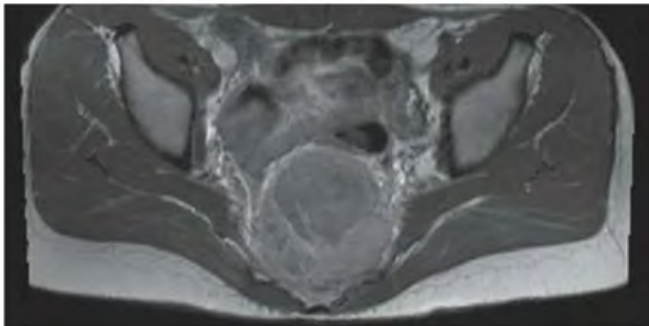


FIGURE 4.3C

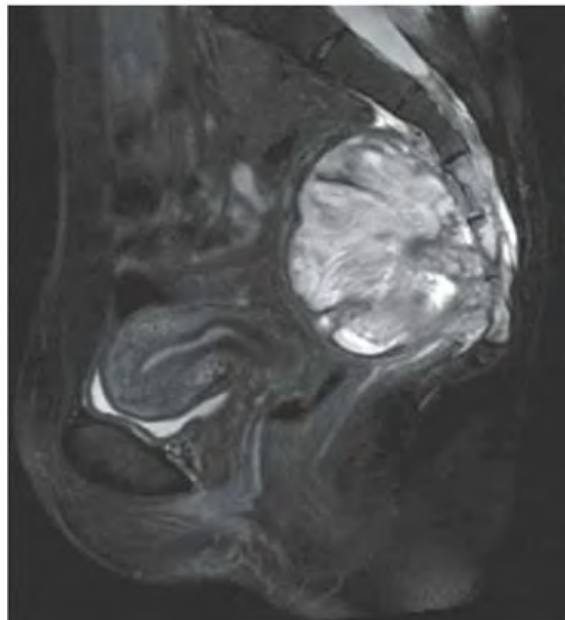


FIGURE 4.3D



FIGURE 4.3E

**FINDINGS**

- A. Axial T1-weighted MRI shows a round mass in the pelvis arising from the lower sacrum in the midline and extending anteriorly into the pelvic cavity. The mass has a large central region of heterogeneous high signal with surrounding rim of low-to-intermediate signal.
- B. Axial T2-weighted fat-suppressed MRI at the same level shows heterogeneous high signal in the central region of the mass with posterior and surrounding regions of low-to-intermediate signal.
- C. Axial postcontrast T1-weighted fat-suppressed MRI shows peripheral enhancement around the mass.
- D. Sagittal T2-weighted fat-suppressed MRI shows the mass protruding into the presacral soft tissues, displacing the visceral structures. The lower sacrum and upper coccyx are enveloped by the lesion.
- E. Anteroposterior (AP) radiograph of the pelvis shows bony destruction of the lower sacrum, largely obscured by bowel contents.

**DIFFERENTIAL DIAGNOSIS** Giant cell tumor, aneurysmal bone cyst, lymphoma, sarcoma, chordoma, metastasis, plasmacytoma/myeloma.

**DIAGNOSIS** Ewing's sarcoma.

**DISCUSSION** An expansile, destructive mass arising in the sacrococcygeal region of a young adult raises a somewhat different differential diagnosis than the same in an older adult. Giant cell tumor of bone and aneurysmal bone cyst are possible diagnoses in young adults that would be much less likely after age 50. Chordoma, metastasis, and plasmacytoma/myeloma are unlikely possibilities in a young adult, but these lesions are more likely after age 50. The aggressive imaging features of the case here are not specific for Ewing's sarcoma, but do indicate the need for a tissue diagnosis. Ewing's sarcoma may occur in virtually any bone, with about 6% in the sacrum and 4% in other regions of the spine [4]. Of primary malignant bone tumors found in the sacrum in the Mayo Clinic series, 45% were chordoma, 12% were myeloma, 11% were lymphoma, 9% were osteosarcoma, 8% were Ewing's sarcoma, and 14% were others [4].

**CLINICAL HISTORY** An 81-year-old woman with left hip pain after left pelvic radiation therapy for non-Hodgkin's lymphoma 2 years earlier.



FIGURE 4.4A

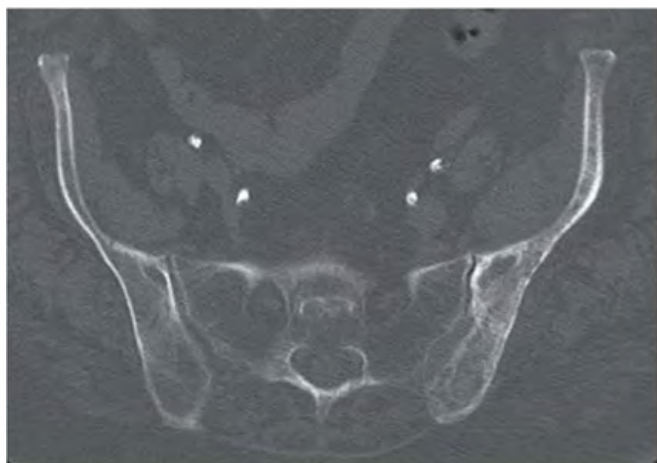


FIGURE 4.4B

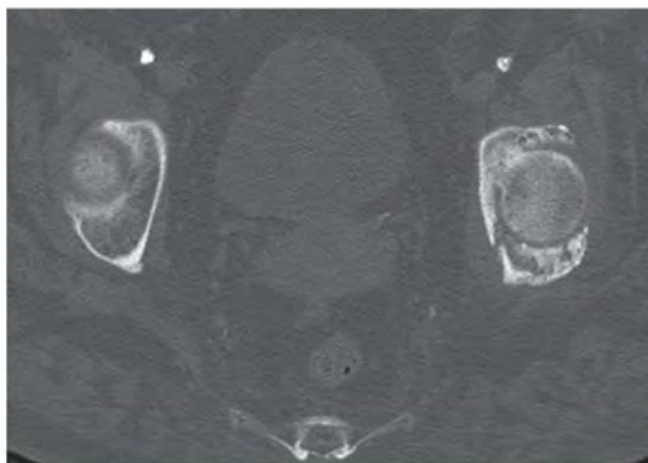


FIGURE 4.4C

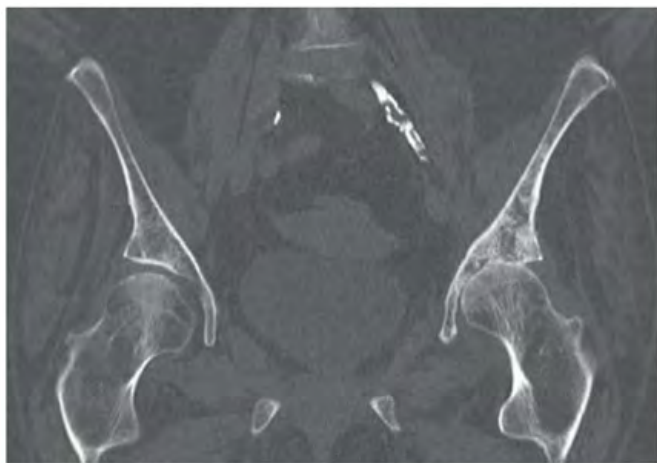


FIGURE 4.4D

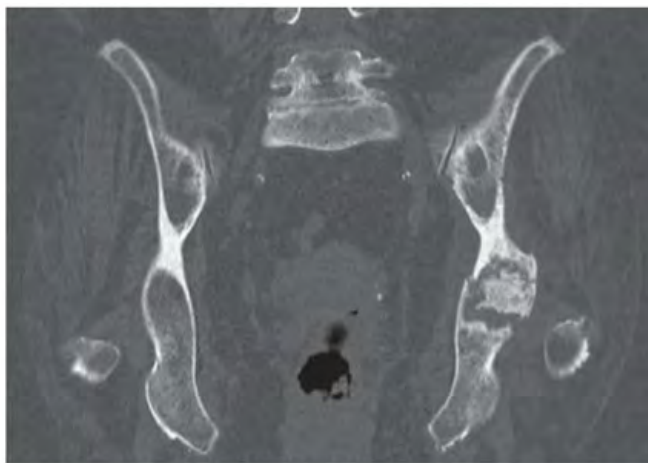


FIGURE 4.4E

**FINDINGS**

- A. AP radiograph shows increased radiodensity over the left hemipelvis and axial joint space narrowing of the left hip.
- B. Axial CT scan through the iliac wings shows irregularly marginated marrow calcifications on the left.
- C. Axial CT scan through the hips shows sclerosis of the left acetabulum and a posterior acetabular wall detached subchondral fracture fragment.
- D. Coronal reformatted CT scan through the hips shows diffuse marrow calcification within the left iliac wing and diffuse loss of cartilage at the left hip. There are no osteophytes. The right hip is normal.
- E. Coronal reformatted CT through the posterior acetabula shows a densely calcified sequestrum on the left.

**DIFFERENTIAL DIAGNOSIS** Radiation changes, insufficiency fracture, Paget disease

**DIAGNOSIS** Radiation changes with insufficiency fracture.

**DISCUSSION** The irregular marrow sclerosis in this case raises the possibility of Paget disease, but the cortex is not thickened and the bone is not enlarged. The subchondral fracture with detached but nondisplaced fragment is characteristic of fractures that occur in osteonecrosis. As bone remodeling occurs around a region of osteonecrosis, trabeculae are removed and then replaced by creeping substitution, leaving the site vulnerable to fracture. In adults, unintended effects of radiation therapy on bone include radiation osteitis and insufficiency fractures. In one study of pelvic bone complications following radiation therapy for uterine cancer, the authors found that the prevalence of insufficiency fractures, as detected by MRI, increased with time after radiation, from approximately 15% after 1 year to 45% after 5 years [6]. The majority of fractures were located in the sacrum, and most of these involved the sacral ala. Radiation may also have a toxic effect on chondrocytes.

**CLINICAL HISTORY** A 24-year-old man with posterior left thigh pain.

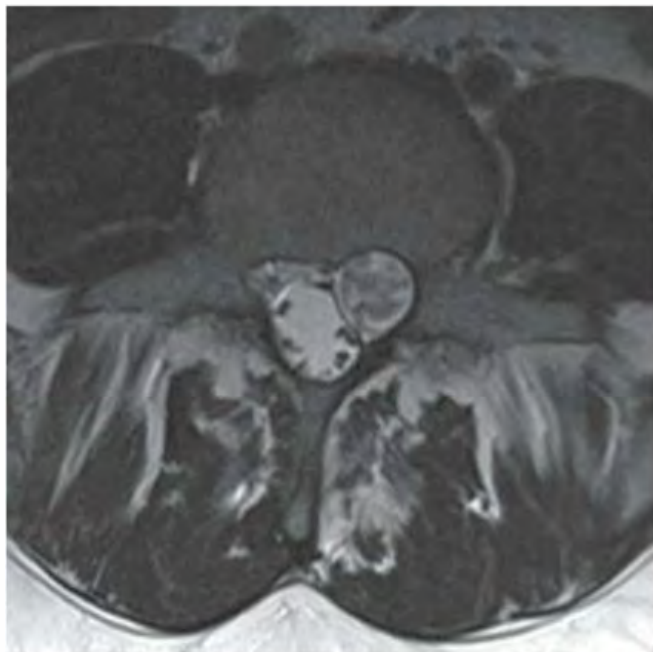


FIGURE 4.5A

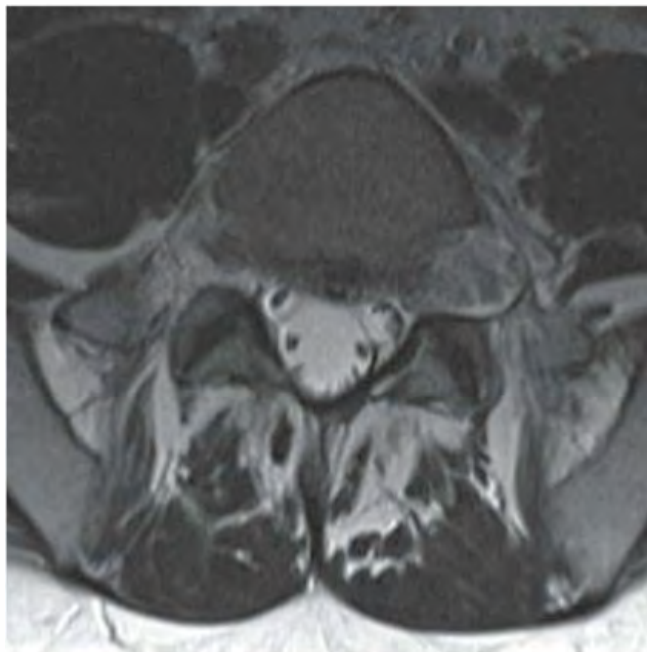


FIGURE 4.5B



FIGURE 4.5C

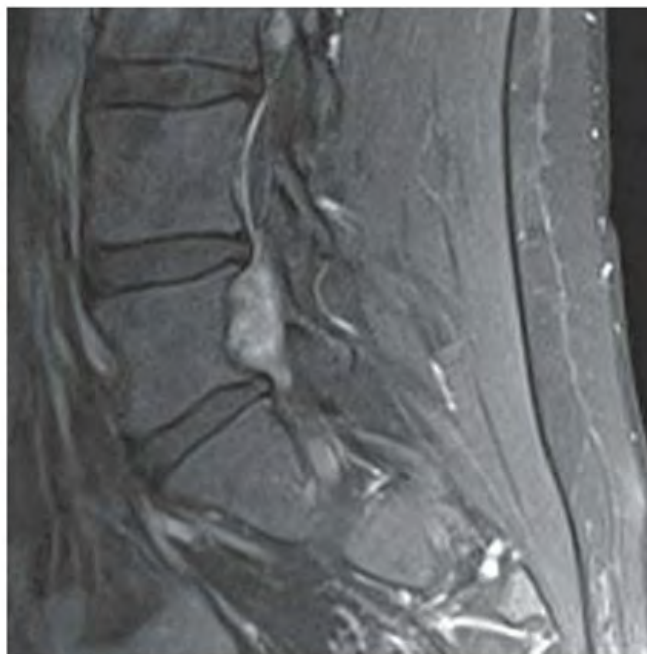


FIGURE 4.5D

**FINDINGS** (A, B) Axial T2-weighted magnetic resonance imaging (MRI) shows a large exiting left L5 nerve root with bony remodeling of the left L5–S1 neural foramen. Pre (C) and post (D) contrast sagittal T1 fat-saturated MRI images on left parasagittal plane show large enhancing mass in the L5–S1 neural foramen. In addition, there is another smaller enhancing focus seen in the L3–L4 foramen.

**DIFFERENTIAL DIAGNOSIS** Neurofibroma, schwannoma, metastasis.

**DIAGNOSIS** Neurofibroma.

**DISCUSSION** The particular location and morphology of this lesion suggests the diagnosis of a nerve sheath tumor. The

remodeling of the bone around the enlarging tumor indicates very slow growth. Neurofibromas are benign fibroblastic neoplasms of peripheral nerves, whose consistency and histologic appearance vary from myxoid to fibrous according to the differentiation of the neoplastic elements [7]. The bulk of the tumor volume consists of intercellular collagen fibrils in an unorganized myxoid matrix. Their imaging characteristics depend on the relative balance of fibrous and myxoid material. On MRI, neurofibromas tend to be isointense to muscle on T1-weighted images and hyperintense on T2-weighted images, and can be inhomogeneous [8]. Neurofibromas in the extremities are a feature of neurofibromatosis type I.

**CLINICAL HISTORY** A 75-year-old man with back pain and history of chronic lymphocytic leukemia (CLL).

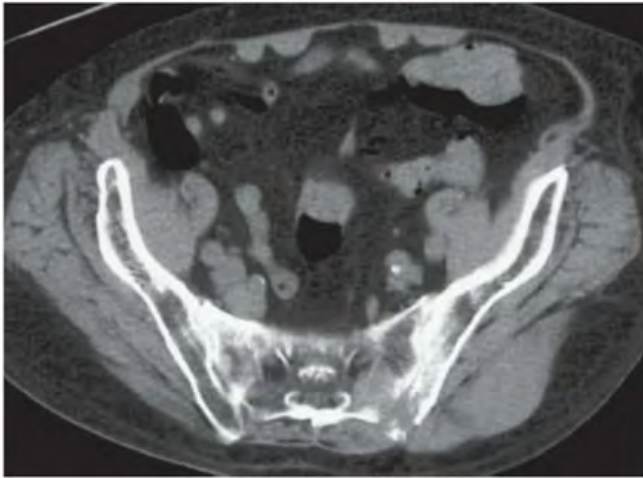


FIGURE 4.6A

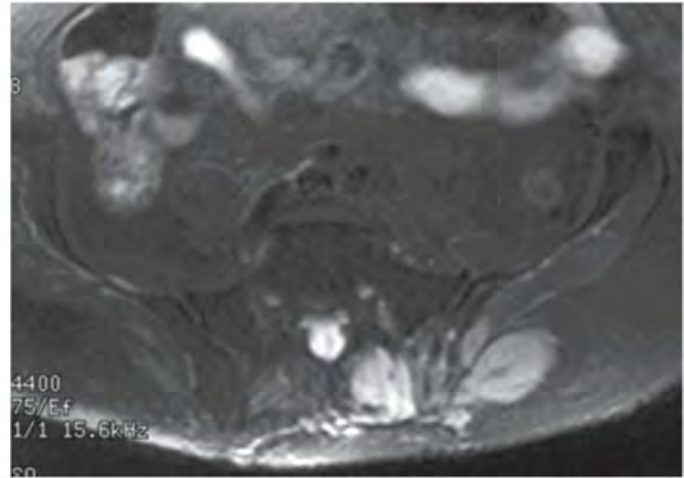


FIGURE 4.6B

### FINDINGS

- A. Axial CT scan shows lytic bone destruction of the sacrum and ilium. The soft tissue masses have no calcification, and there is no reactive bone formation.
- B. Axial T2-weighted MRI with fat saturation at the level of S1 shows masses in the paraspinal musculature and superficial to the gluteus maximus. The lesions have homogeneous high signal, and there is contiguous involvement of the ilium and sacrum.

**DIFFERENTIAL DIAGNOSIS** Lymphoma, leukemia, metastases, infection.

**DIAGNOSIS** Lymphoma (Richter's syndrome).

**DISCUSSION** The images show soft tissue masses involving the paraspinal and gluteus musculature, an appearance that raises the differential diagnosis of lymphoma, leukemia,

metastases, and infection. The presence of bone destruction eliminates hematoma as a possibility, and the lack of a single dominant mass lesion is very uncharacteristic of a connective tissue sarcoma.

The specific diagnosis depends on the clinical situation and must be confirmed by biopsy. Secondary malignancies develop in approximately 5% of patients with CLL, the most common of which is non-Hodgkin's lymphoma, followed by Hodgkin's lymphoma and multiple myeloma [9,10]. The development of non-Hodgkin's lymphoma in CLL is called Richter's syndrome. These lymphomas are high-grade malignancies of B-cell origin, associated with abrupt onset of constitutional symptoms, rapidly progressive lymphadenopathy, and rapid clinical deterioration to a fatal outcome. They are resistant to current therapies and may develop while the CLL is in remission. In approximately 60% of cases, the lymphoma evolves from the original leukemic cell clone, but in the remainder it has a different clonal evolution.

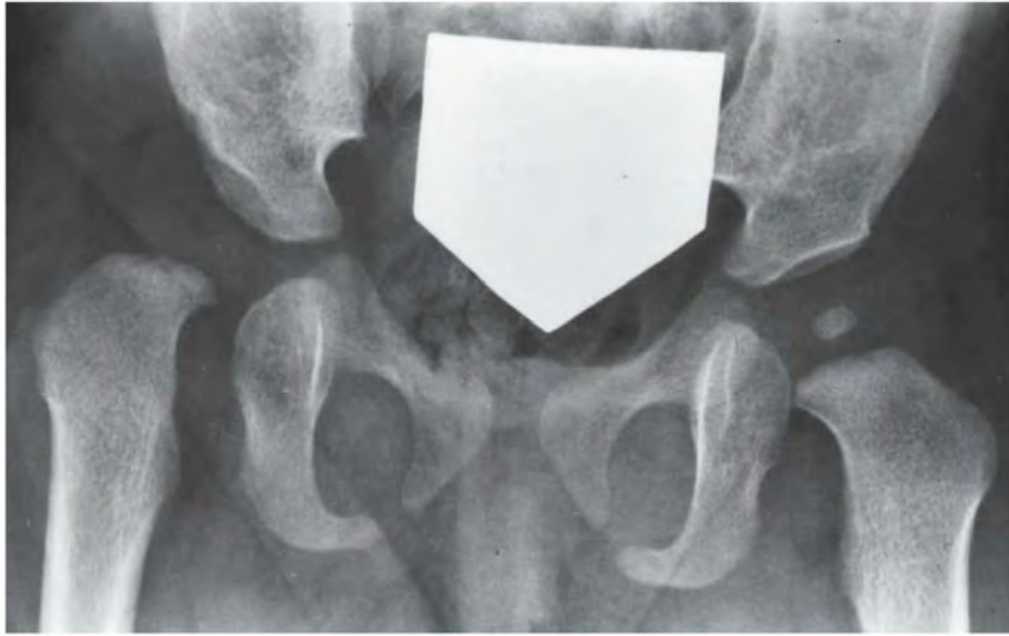


FIGURE 4.7

**FINDINGS** AP pelvis radiograph shows a dysplastic, dislocated right hip. The capital femoral ossification is not yet present, unlike the contralateral side. The acetabular angle is steep and shallow.

**DIFFERENTIAL DIAGNOSIS** None.

**DIAGNOSIS** Developmental dysplasia of the hip (DDH).

**DISCUSSION** In DDH, an abnormally lax joint capsule allows the femoral head to fall out of the acetabulum shortly before or after birth, leading to congenital or postnatal deformation of an initially normal structure. The causes are multifactorial and appear to be related to the effects of restricted intrauterine movement and maternal hormones. Restricted fetal movement during the third trimester may result from conditions such as breech presentation or oligohydramnios, and may partially or completely dislocate the hip. Maternal hormones (such as estrogen) that relax the pelvic ligaments to facilitate childbirth also increase the laxity of the fetal ligaments and joint capsules. This effect is particularly evident in female fetuses and may account for the 6:1 female preponderance of DDH. DDH also has a familial tendency, which is possibly related to an inherited abnormality in estrogen metabolism. Although sonography is the imaging

examination of choice in the neonate and has the advantage of immediate correlation with physical examination, results vary with technical and interpretive factors [16]. In older infants, the AP radiograph becomes more reliable as the capital femoral epiphysis becomes ossified.

Each hip can be divided into quadrants by drawing a horizontal baseline through the triradiate cartilages (Hilgenreiner's horizontal line) and a perpendicular line through the most lateral ossified margin of the roof of the acetabulum (Perkins' line). The normal location of the femoral head is in the lower inner quadrant (down and in). A dislocated femoral head will be in the upper outer quadrant (up and out), and a subluxated femoral head will be in the lower outer quadrant (down and out). The angle between the acetabulum and the horizontal baseline should be less than 40 degrees in a newborn, 33 degrees in a 6-month-old, and 30 degrees in a 1-year-old. In the normal hip, a smooth curve can be drawn along the inferior margin of the superior pubic ramus and the medial femoral cortex (Shenton's line). Other findings include a shallow acetabulum, development of a false acetabulum, and delayed ossification of the involved capital femoral epiphysis. CT scanning may be necessary to confirm anatomic relocation of the hips once the patient has been placed in a cast [17]. MRI may be used to evaluate problematic cases.

**CLINICAL HISTORY** A 36-year-old female with pubic pain.



FIGURE 4.8A



FIGURE 4.8B

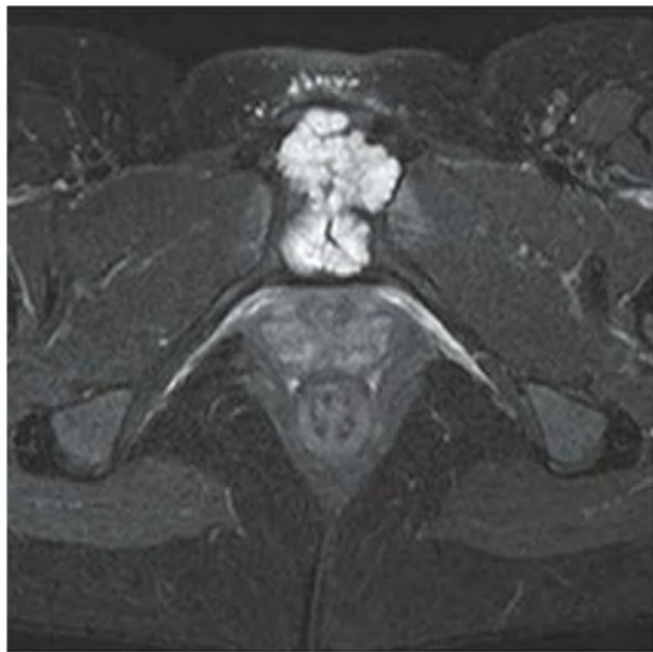


FIGURE 4.8C

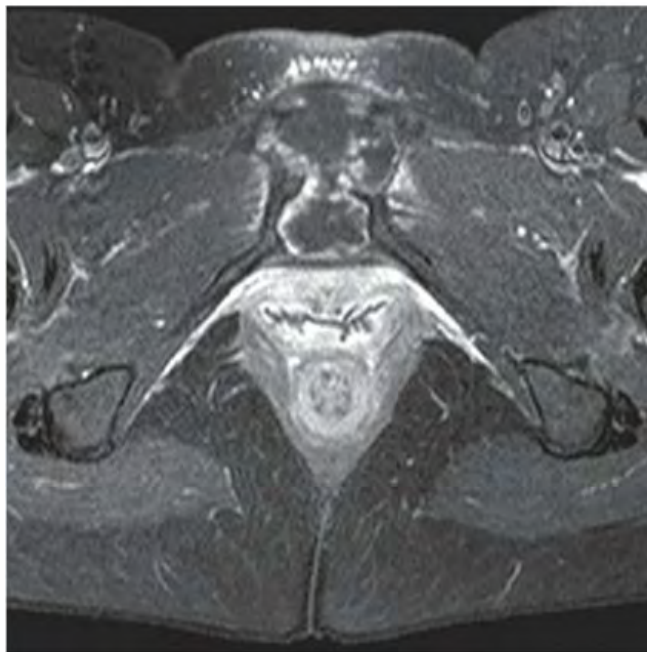


FIGURE 4.8D

**FINDINGS**

- A. AP view of pelvis shows a multiloculated lytic lesion causing destruction about the symphysis pubis. There is no periosteal reaction in the adjacent pubic rami.
- B. Coronal T1-weighted MRI shows lobulated mass centered at the symphysis and isointense to muscle.
- C, D. This mass shows high signal in axial fat-saturated T2-weighted sequence (C) and heterogeneous enhancement with gadolinium on T1-weighted fat-saturated sequence (D).

**DIFFERENTIAL DIAGNOSIS** Chondrosarcoma, metastasis, plasmacytoma, infection

**DIAGNOSIS** Chondrosarcoma

**DISCUSSION** Chondrosarcomas are malignant, cartilage-containing tumors that arise *de novo* or from preexisting

cartilage-containing lesions such as osteochondromas. In the Mayo Clinic series, approximately 24% of chondrosarcomas were found in the pelvis, and of those, about 24% were found at the symphysis; it is unusual to find chondrosarcoma distal to the ankle or wrist [11]. Chondrosarcomas are the third most common primary malignant bone tumor [12]. Chondrosarcomas tend to present in patients between the ages of 30 and 60, but the age distribution is broad. Lesions in the axial skeleton tend to present in an older age group than lesions in the peripheral skeleton. Lack of reactive bone is ominous for an aggressive, malignant process. Without the characteristic calcification and lobular structure, the diagnosis of chondrosarcoma cannot be made prospectively, and a biopsy is required. Chondrosarcomas follow a slow clinical evolution. They tend to metastasize late in the clinical course, and although the lesions are often large, patients rarely present with metastatic disease [13].

**CLINICAL HISTORY** *A 36-year-old man with worsening pelvic pain.*

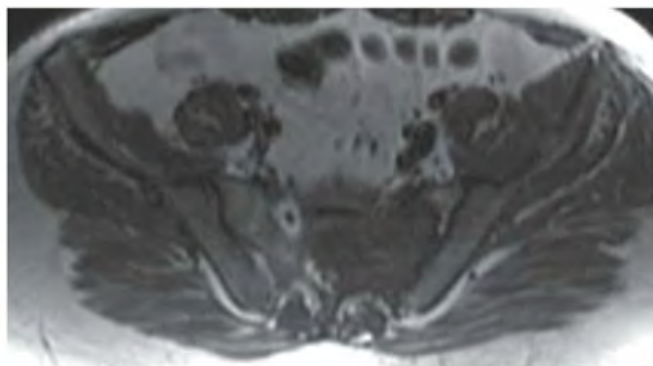


FIGURE 4.9A

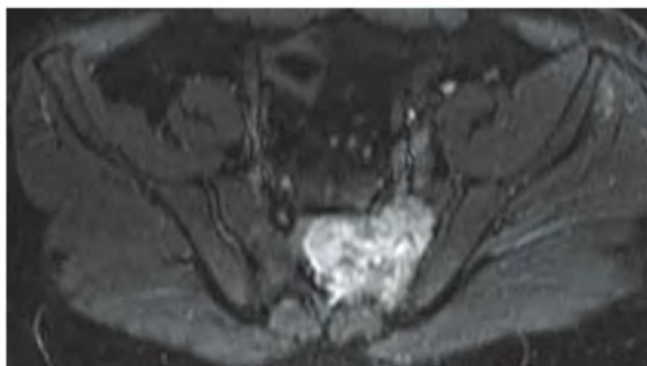


FIGURE 4.9B

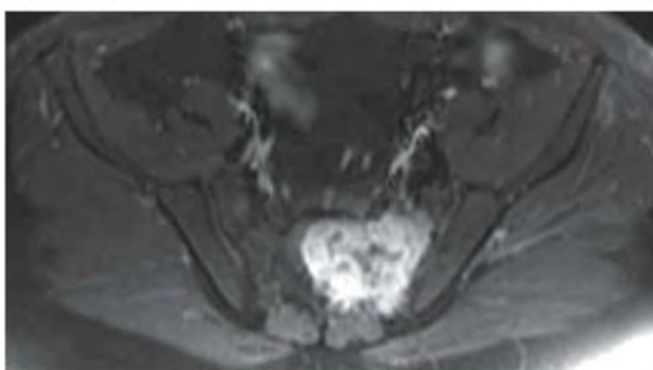


FIGURE 4.9C

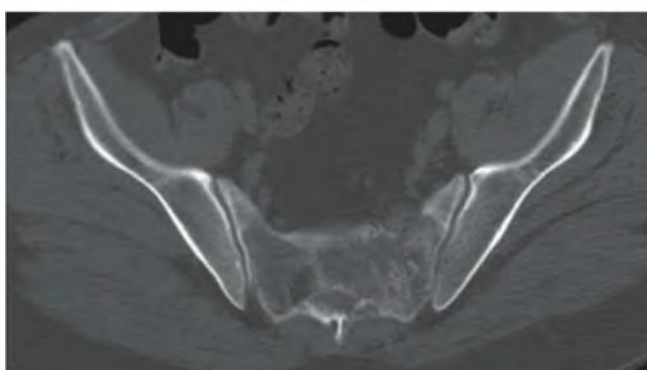


FIGURE 4.9D



FIGURE 4.9E



FIGURE 4.9F

## FINDINGS

- A. Axial T1-weighted MRI shows a lesion occupying the left sacrum, obliterating the left S2 neural foramen and extending across the midline.
- B. Axial short tau inversion recovery (STIR) MRI shows heterogeneous high signal within the lesion.
- C. Axial T1-weighted fat-suppressed MRI following gadolinium infusion shows intense enhancement of the lesion, with a few regions of nonenhancement.
- D. Axial CT scan shows a destructive lesion in the left sacrum with loss of the anterior sacral cortex. Focal regions of mineralization are present within the lesion.
- E. AP radiograph shows vague increase in density overlying the left sacrum, perhaps with speckled mineralization.
- F. Coronal image from positron emission tomography (PET) scan shows intense activity corresponding to the lesion (maximum standard uptake value (SUVmax) was 6.4).

**DIFFERENTIAL DIAGNOSIS** Osteosarcoma, chondrosarcoma, lymphoma, metastasis.

## DIAGNOSIS Osteosarcoma

**DISCUSSION** An aggressive, destructive lesion centered within bone that has internal mineralization raises the necessity for a tissue diagnosis. Of the other possibilities in the differential diagnosis, metastases tend to be multiple and smaller and frequently have a known primary site, chondrosarcomas tend to have a lobular morphology and rings-and-arcs calcifications, and lymphomas tend to be infiltrative. Although the peak incidence for onset of osteosarcoma is in the second decade of life (45% of the osteosarcomas in the Mayo Clinic series), more osteosarcomas actually occur in the third or later decades (50% in the Mayo Clinic series) [14]. Only about 2% of osteosarcomas are found in the sacrum. PET and PET/CT have become important modalities in the imaging evaluation of bone lesions [15]. However, an abnormal PET scan is nonspecific and does not obviate the need for a tissue diagnosis.



FIGURE 4.10A



FIGURE 4.10B

**FINDINGS**

- A. Radiograph of the pelvis shows shallow, minimally dysplastic acetabula. Both femoral heads are normally formed and located.
- B. Frog-leg lateral radiograph of left hip shows the shallow acetabulum and normally shaped femoral head.

**DIFFERENTIAL DIAGNOSIS** None.

**DIAGNOSIS** Acetabular dysplasia.

**DISCUSSION** Acetabular dysplasia is a common cause of early osteoarthritis in adults [18]. The normal acetabulum is nearly a full hemisphere, forming the socket for the femoral head. The dysplastic acetabulum is like a shallow bowl,

normally oriented but forming only a shallow socket for the femoral head. As a consequence, both the anterior and posterior articular surfaces are reduced in area, and a smaller proportion of the femoral head is covered by bone. On the radiograph, the roof of the acetabulum normally covers the top of the femoral head and inclines downward at its lateral margin. In acetabular dysplasia, the roof often fails to reach a horizontal orientation at its lateral margin, with much less incline downward. Patients are usually moderately symptomatic when they present at 30 or 40 years old, but will progress inevitably to end-stage osteoarthritis if untreated. An acetabular osteotomy provides more complete bony coverage of the femoral head and can prevent accelerated osteoarthritis [19].

**CLINICAL HISTORY** A 16-year-old male with recently healed left acetabular fracture with childhood history of “walking funny.”



FIGURE 4.11A

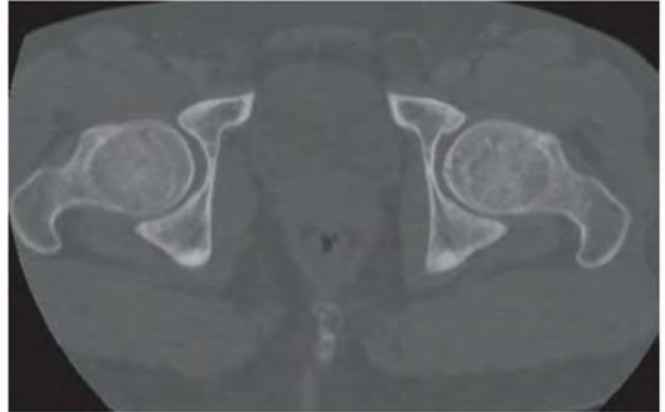


FIGURE 4.11B

### FINDINGS

- A. AP view of pelvis shows bilateral mild superior hip joint space narrowing, subchondral sclerosis, and subchondral cystic changes. Note is made of deformity of bilateral proximal femoral head and neck junctions with lateral extensions of epiphyseal scars, described as “pistol grip deformity.”
- B. Axial CT image through bilateral femoral head and neck junction shows an abnormal “bump” anteriorly with associated subchondral cysts.

**DIFFERENTIAL DIAGNOSIS** Prior traumatic osteoarthritis, femoroacetabular impingement (FAI), prior slipped capital femoral epiphysis (SCFE).

**DIAGNOSIS** Femoroacetabular impingement.

**DISCUSSION** In this case, the FAI was secondary to previous SCFE. FAI is early progressive osteoarthritis of the hip joint due to abnormal mechanical relation between proximal femur and acetabulum. Pincer type is due to abnormally shaped acetabulum, whereas cam type is due to abnormal femoral head-neck junction shape [20]. Abnormal femoral head-neck junction shape can be seen as a result of prior SCFE, Legg-Calve-Perthes disease, trauma, adult-onset avascular necrosis, or unknown (idiopathic) causes [21]. SCFE occurs most often in overweight boys during their pubescent years. There is posteromedial slip of the femoral epiphysis off the proximal femur.

**CLINICAL HISTORY** A 44-year-old woman with a “knot” in her right thigh for a few months.

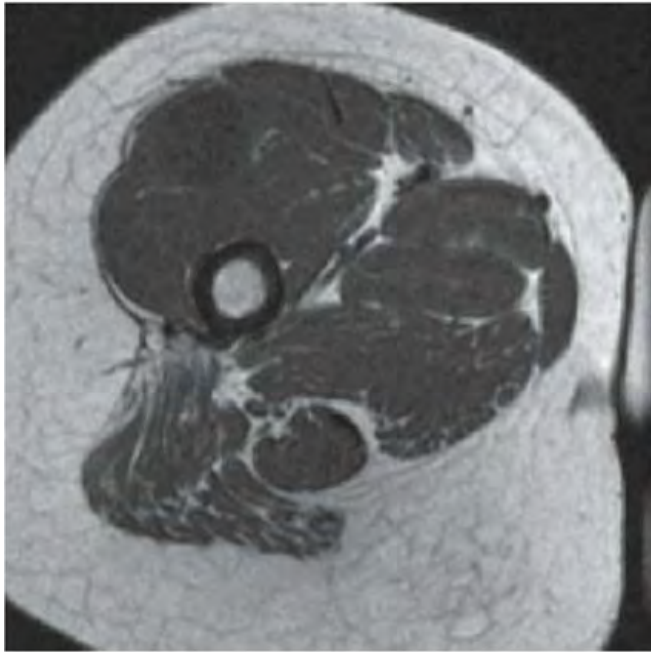


FIGURE 4.12A

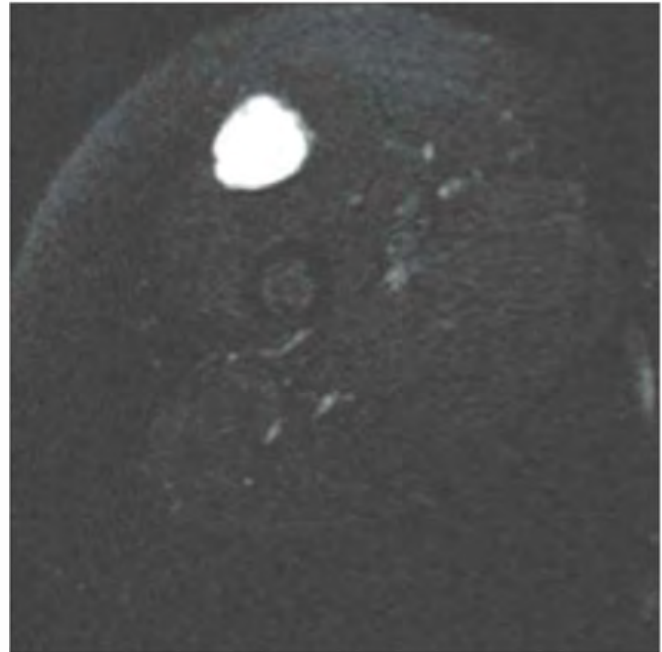


FIGURE 4.12B

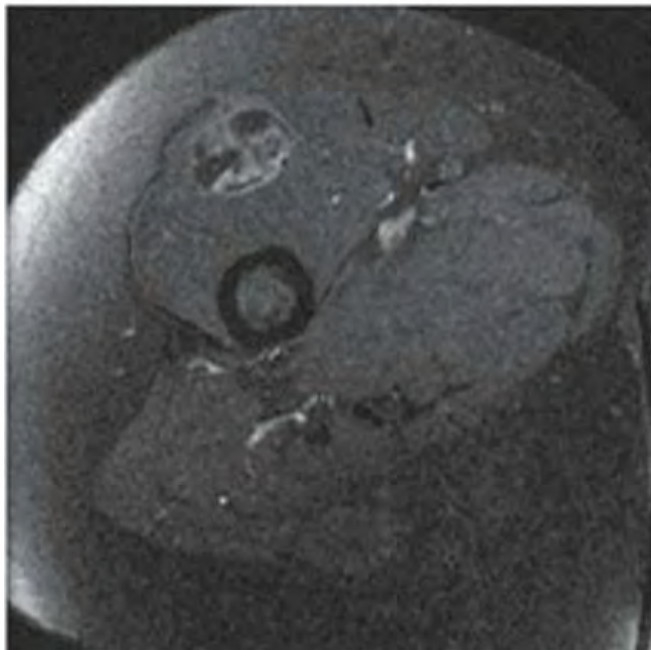


FIGURE 4.12C

### FINDINGS

- A. Axial T1-weight MRI shows a round well-circumscribed mass within the vastus lateralis muscle which is isointense to muscle.
- B. On T2-weighted fat-saturated MRI image, this mass is uniformly bright in signal.

- C. After intravenous gadolinium administration, this mass shows patchy enhancement on T1-weighted fat-saturated MRI sequence.

**DIFFERENTIAL DIAGNOSIS** Soft tissue sarcoma, intramuscular myxoma, nerve sheath tumor.

**DIAGNOSIS** Intramuscular myxoma.

**DISCUSSION** The location of the mass is within the vastus lateralis muscle. Intramuscular myxoma is a benign, soft tissue tumor that presents as a deep mass within skeletal muscle [22]. It is a hypocellular and hypovascular lesion with a gelatinous consistency. On CT, the lesion is spherical or ovoid and is sharply margined, but with no discernible capsule. Attenuation is typically 10 to 30 Hounsfield units, the lesions are homogeneous, and they do not exhibit enhancement. On MRI, the lesions have low signal intensity on T1-weighted images and high signal intensity on T2-weighted images. Typical size at presentation is 6 cm, and the most common location is in the thigh musculature. The possibility of soft tissue sarcoma, particularly sarcomas with myxoid components, can only be definitively excluded by biopsy. CT-guided biopsy may be nondiagnostic if only fine-needle aspiration is used; usually aspiration with a large-bore needle (larger than 20 gauge) is required to sample the gelatinous material. Surgical excision is virtually always curative. The lesion is more common in women (2:1) and is found in adults (mean age 52 years). Association of intramuscular myxomas with fibrous dysplasia of bone is called Mazabraud syndrome [23].

**CLINICAL HISTORY** A 17-year-old girl with progressive stiffness involving the hip and other joints.



FIGURE 4.13A

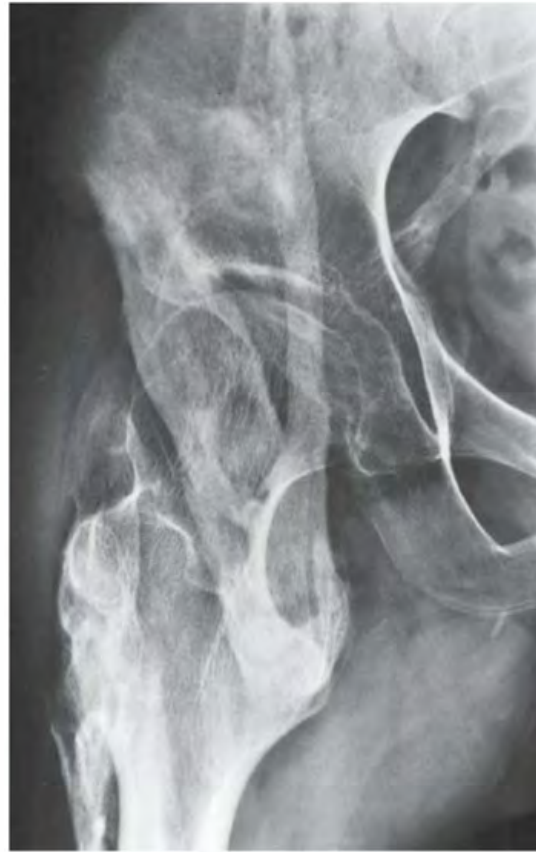


FIGURE 4.13B

### FINDINGS

- A. AP radiograph at presentation reveals a deformity of the femoral neck, with broadening and a small medial inferior protuberance.
- B. Two years later, AP radiograph shows ossification of the sacrotuberous ligament, as well as ossification of a small band from the medial femoral neck to the high iliac crest, and a larger band from the mid femoral neck to the supra-acetabular region.

**DIFFERENTIAL DIAGNOSIS** Burns, trauma, paralysis, diffuse idiopathic skeletal hyperostosis, fibrodysplasia ossificans progressiva (FOP).

**DIAGNOSIS** Fibrodysplasia ossificans progressiva.

**DISCUSSION** Ossification in the soft tissues can be recognized and distinguished from calcification by the presence of a cortical and trabecular structure. The most commonly seen soft tissue ossification is that occurring after trauma, not only in the form of myositis ossificans, but more frequently at sites of ligamentous sprains. Burns and paralysis may also be associated with focal or periarticular soft tissue ossification. Diffuse idiopathic skeletal hyperostosis is a condition of soft tissue ossification, but in this condition it is

always enthesal (at the attachment of ligaments, capsules, and tendons to bone).

FOP is a rare and catastrophic genetic disorder of progressive heterotopic ossification, with extensive and cumulative disabling extraskeletal ossification [24]. Individuals with FOP appear normal at birth except for great toe malformations that look like congenital bunions. Then starting first decade of life, patients undergo multiple “flare-ups” in response to minor traumas including vaccinations or minor bumps and bruises from sports events. During these “flare-ups,” there is transient inflammatory reaction that leads to new heterotopic ossifications. This rare condition occurs mostly as new mutations, but when inherited, it is transmitted in autosomal dominant fashion [25]. FOP has been recently linked to mutations in the bone morphogenetic protein type 1 receptor gene [26]. Severe disability results from progressive immobilization of the limbs, jaw, and chest wall. Life-threatening complications include restrictive chest wall disease [27,28] and falls [29]. Falls can be particularly catastrophic, and frequently they initiate a painful flare-up that leads to the permanent loss of movement. Intracranial injuries are common and may be severe, probably the result of deficiencies in coordinated gait and protective reflexes. Most patients die of thoracic insufficiency syndrome.

**CLINICAL HISTORY** A 50-year-old man in a high-speed motor vehicle crash.



FIGURE 4.14A



FIGURE 4.14B

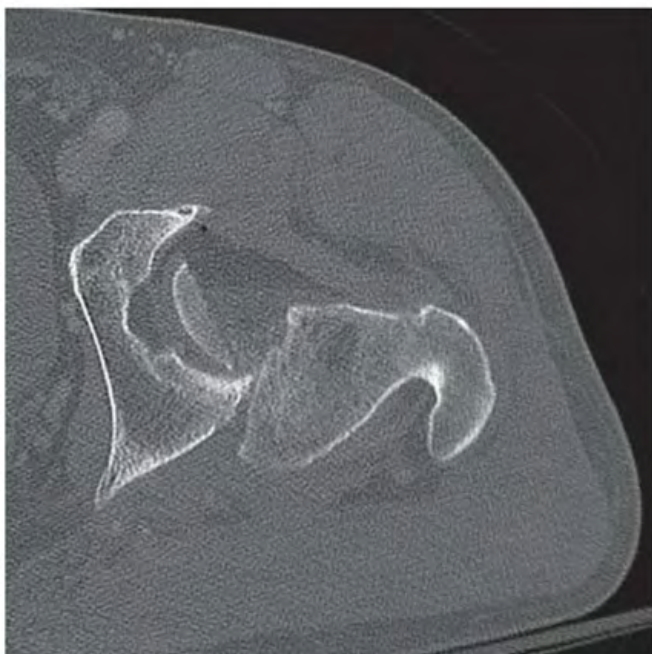


FIGURE 4.14C

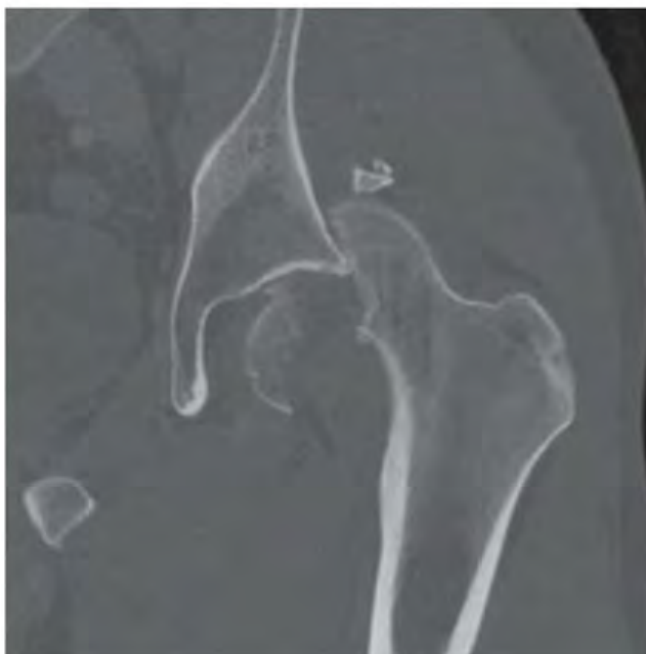


FIGURE 4.14D

**FINDINGS** (A) AP view of the pelvis and (B) AP view of left hip show superior and lateral displacement of the left femur. In addition, there is comminuted fracture of the left femoral head. Axial (C) and coronal (D) CT images of the left hip show posterior hip dislocation with impacted femoral head fracture, with the head coming to rest posterior to the iliac wing.

**DIFFERENTIAL DIAGNOSIS** Anterior hip dislocation, posterior hip dislocation.

**DIAGNOSIS** Posterior hip dislocation.

**DISCUSSION** Hip dislocations result from severe trauma such as motor vehicle accidents. Posterior dislocations, with or without acetabular fractures, account for 85% to 90% of traumatic hip dislocations. The mechanism of injury is a blow along the axis of the femoral shaft with the hip flexed (e.g., hitting the dashboard with the knee). The posterior wall or column of the acetabulum is often fractured, and the femoral shaft or knee may also be injured. Associated fractures of the femoral head occur occasionally, and intra-articular

fragments may be particularly problematic for reduction. The thigh is characteristically adducted after a posterior dislocation. CT can identify intra-articular fragments and confirm relocation of the hip after reduction. The presence of gas bubbles in the hip joint capsule after trauma, in the absence of penetrating injury, is a reliable indicator of recent hip dislocation [30]. Most bubbles are located anterior to the femoral neck, but bubbles may also be found posteriorly.

If hip dislocation is unsuspected because of spontaneous relocation or reduction at the scene, the presence of gas should alert the clinician to the possibility of complications. Complications of hip dislocation include avascular necrosis of the femoral head, transient or permanent sciatic nerve palsy, myositis ossificans, and posttraumatic degenerative arthrosis. A posteriorly dislocated hip stretches and twists the external iliac, common femoral, and circumflex arteries, resulting in changes in extraosseous blood flow. Although collateral circulation from gluteal vessels may preserve intraosseous blood flow, delayed relocation may produce a progressive and delayed form of arterial damage that leads to osteonecrosis [31].

**CLINICAL HISTORY** A 59-year-old man found unconscious after a ground-level fall.



FIGURE 4.15A

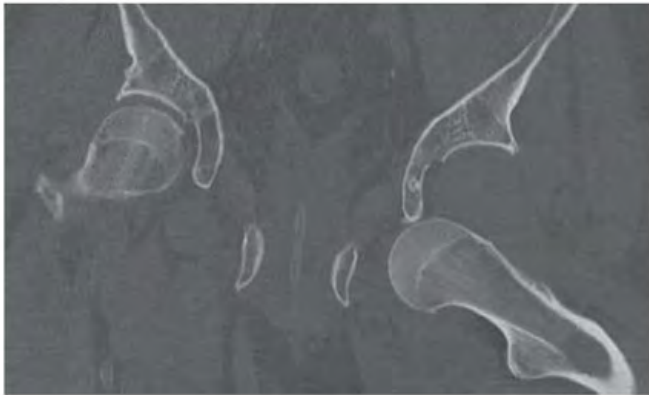


FIGURE 4.15B

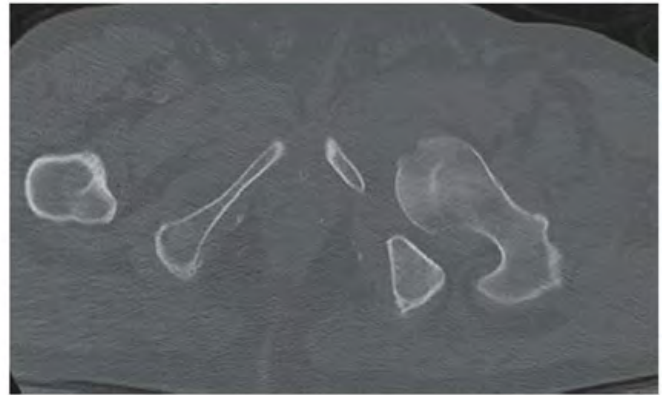


FIGURE 4.15C

**FINDINGS** (A) AP radiograph of the pelvis shows antero-inferior dislocation of left femoral head from the acetabulum. The femoral head overlies the obturator foramen and is inferior to the empty acetabulum. The femur is severely abducted. No fracture is seen. Coronal (B) and axial (C) CT images confirm these findings. There are no intra-articular fracture fragments.

**DIFFERENTIAL DIAGNOSIS** Anterior hip dislocation, posterior hip dislocation.

**DIAGNOSIS** Anterior hip dislocation.

**DISCUSSION** This case illustrates an obviously dislocated hip, but where has the femoral head come to rest? About 11% of traumatic hip dislocations are anterior [32], with the femoral head in most cases resting inferiorly over the obturator

foramen, as in this case. The mechanism of injury is forced abduction, external rotation, and flexion of the hip, causing the femoral head to slip anteriorly and medially through the hip capsule, but beneath the strong pubofemoral ligament. The pubofemoral ligament runs from the base of the superior pubic ramus to the lesser trochanter. In approximately 10% of anterior hip dislocations, forced abduction, external rotation, and extension of the hip cause the femoral head to rupture the anterior hip capsule above the pubofemoral ligament, with the femoral head resting superiorly, above the level of the anterior pubic ramus, over the anterior abdominal wall. The iliofemoral ligament may be torn or avulsed from its insertion at the anterior inferior iliac spine. Associated with anterior hip dislocations may be an impaction fracture of the superolateral aspect of the femoral head where it impinges on the anterior inferior rim of the acetabulum after it dislocates. Long-term sequelae include arthritis and osteonecrosis.

**CLINICAL HISTORY** A 43-year-old woman with bone pain and muscle weakness.



FIGURE 4.16

**FINDINGS** AP radiograph of the pelvis shows symmetrically dense bones, involving principally the cortices. The medullary space is present, and the trabecular pattern is normal. There are degenerative changes in the hips, sacroiliac joints, and lumbar spine.

**DIFFERENTIAL DIAGNOSIS** Osteopetrosis, fluorosis, hypervitaminosis A, renal osteodystrophy, sickle cell anemia, other causes of diffuse sclerosis.

**DIAGNOSIS** Fluorosis.

**DISCUSSION** Generalized osteosclerosis and hyperostosis can be seen in a variety of metabolic and systemic conditions. Fluorosis may be related to chronic ingestion of drinking water with endemic, excessive levels of fluoride (four parts or more per million), occupational exposure, or fluoride-containing medication. Endemic regions with large populations include parts of India and China [33,34]. In

some circumstances, endemic fluorosis has been described even when fluoride levels in drinking water are not excessive. Tea plants may concentrate the fluoride found in the water and soil. The fluoride content of leaves from these tea plants is related to the length of time they have been growing, resulting in high fluoride levels in tea that is brewed from old leaves and stems, but not in tea brewed from tender leaves and buds [35]. Among occupational exposures, aluminum workers are at particular risk of fluorosis.

The definitive diagnosis is from direct measurements of bone fluoride content. Bone fluoride content is related to exposure, and radiographic findings are found more frequently among those with higher bone fluoride content [36,37]. Radiographic findings include osteopenia, osteosclerosis and hyperostosis involving the axial skeleton, periostitis and enthesopathy in the appendicular skeleton, and dental abnormalities. Early degenerative arthropathy may also be seen. Clinically, there may be decreasing range of motion in the limbs that often progresses to rigidity.

**CLINICAL HISTORY** A 8-year-old girl with sacroiliac joint pain and chronic disease.



FIGURE 4.17A



FIGURE 4.17B

### FINDINGS

- A. AP radiograph of the pelvis shows symmetric sclerotic changes in the sacroiliac joints, greater on the iliac side, with irregular widening of the joint spaces. Symmetric sclerosis also involves the acetabula.
- B. AP radiograph of the right knee shows widened growth plates with fraying along the metaphyseal side, particularly at the medial aspects of the distal femur and proximal tibia. The bones are normally formed and the joint spaces are preserved.

**DIFFERENTIAL DIAGNOSIS** Rickets, juvenile idiopathic arthritis.

**DIAGNOSIS** Rickets.

**DISCUSSION** The history indicates chronic, systemic disease, and the changes in the growth plates at the knee are classic for rickets in an older child. Sacroiliac disease may also occur in childhood onsets of spondyloarthropathy, particularly ankylosing spondylitis. In this case, the patient has vitamin-D-resistant rickets. Rickets can manifest with a wide variety of symptoms, including symptoms that suggest sacroiliitis [38]. It has been suggested that secondary hyperparathyroidism with subchondral bone resorption may result in subchondral insufficiency fractures or microfractures at the sacroiliac joints, causing the symptoms. On MRI, the changes in the physal regions can be striking, with high T2-weighted signal in the broad region of unossified cartilage [39].

**CLINICAL HISTORY** A 75-year-old woman with progressive right buttock pain, now unable to walk.

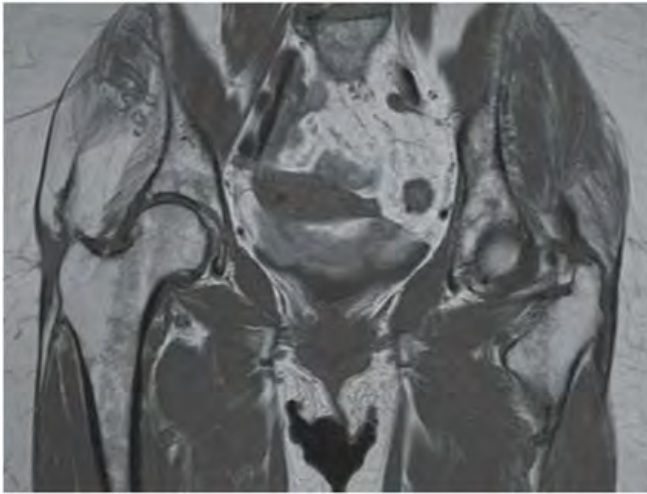


FIGURE 4.18A

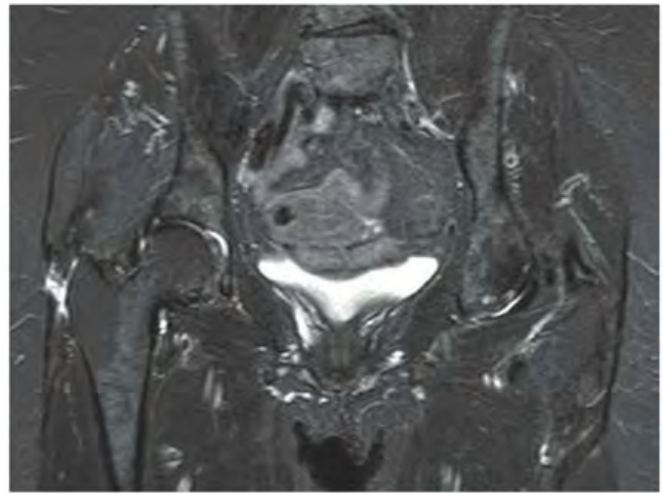


FIGURE 4.18B

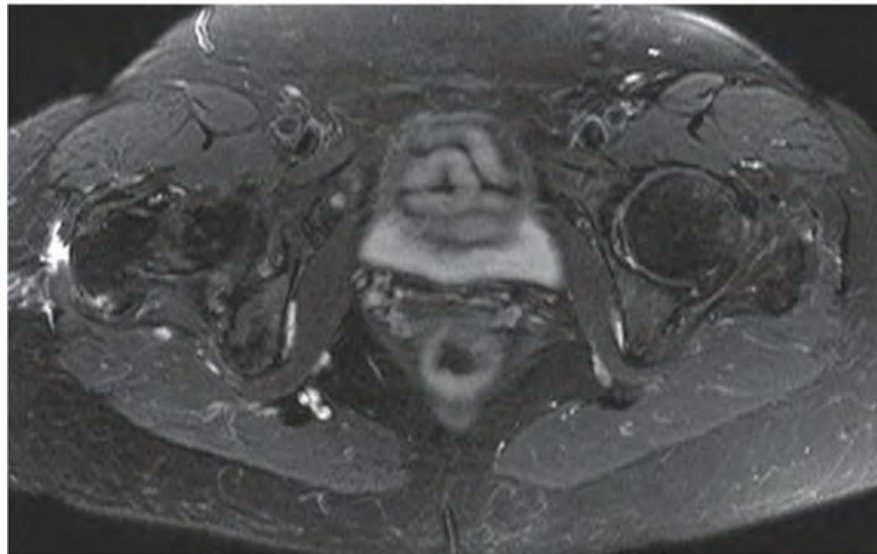


FIGURE 4.18C

**FINDINGS** (A) Coronal T1-weighted MRI shows asymmetric marked atrophy of right gluteus medius muscle. There is also mild right gluteus minimus muscle atrophy. Coronal (B) and axial (C) T2-weighted fat-saturated images show focal gap filled with fluid at the insertion of gluteus medius tendon at the right greater trochanter, representing a tear.

**DIFFERENTIAL DIAGNOSIS** None.

**DIAGNOSIS** Gluteus medius tendon tear.

**DISCUSSION** Like the rotator cuff muscles around the glenohumeral joint, there are several muscles that surround

the hip joint to strengthen the ball-and-socket joint. Their insertions around the greater trochanter of the proximal femur have been described. Gluteus minimus inserts on the anterior facet of greater trochanter while gluteus medius tendon inserts on the medial and posterior facets of the greater trochanter, best seen on the axial images. In this case, tear of the gluteus medius is accompanied by marked fatty atrophy of the muscle seen on the T1-weighted images, indicating chronic nature of injury. Gluteus medius tears, or tendinosis, are a common finding on MRI in older patients who present with buttock, hip, or groin pain [40,41].

**CLINICAL HISTORY** A 66-year-old woman with increasing left-sided back pain.



FIGURE 4.19A

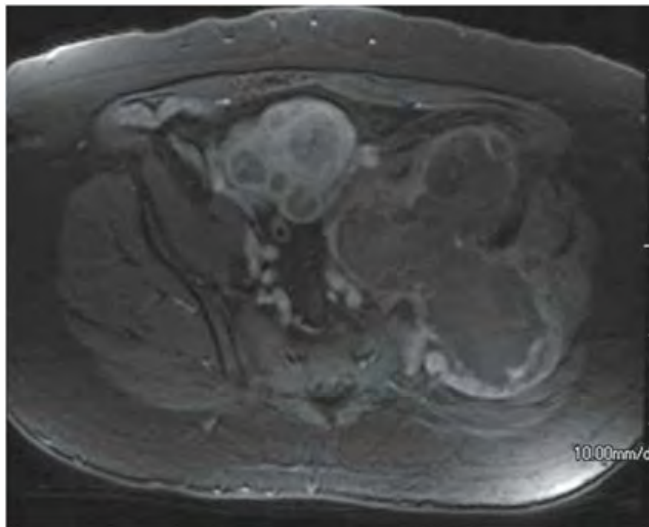


FIGURE 4.19B

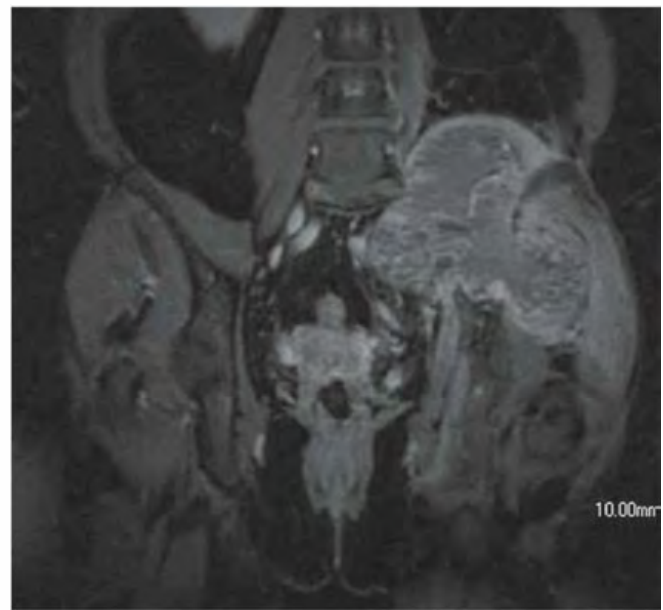


FIGURE 4.19C

**FINDINGS** (A) AP radiograph of the pelvis shows typical findings of Paget disease in the left hemipelvis and hip, including with asymmetric enlargement of the bone, thickening of the cortex, and coarsening of the trabecular pattern. In addition, there is a large lytic lesion in the left iliac wing. Axial (B) and coronal (C) postcontrast T1-weighted fat-saturated MRI images show a large heterogeneously enhancing mass centered in the left iliac wing with soft tissue mass extending anteriorly into the pelvis and superiorly into the left paraspinal region.

**DIFFERENTIAL DIAGNOSIS** Paget disease, sarcoma, metastasis.

**DIAGNOSIS** Sarcoma arising in Paget disease.

**DISCUSSION** Paget disease (osteitis deformans) is a bone disease seen in middle-aged and elderly individuals. It is characterized by excessive and abnormal remodeling of bone. Usually asymptomatic, Paget disease has a prevalence of 3% in the adult population older than 40 years. In most cases, involvement is polyostotic. Although any bone may be involved, the preponderance of cases involves the pelvis, spine, skull, femur, or tibia. The incidence of sarcoma arising in symptomatic Paget disease has been estimated at less than 1% [42,43], with the most common lesions being malignant fibrous histiocytoma and osteosarcoma. The prognosis for patients with sarcomas arising in Paget disease is poor. Involvement of pagetic bone by metastases is very unusual.

**CLINICAL HISTORY** A 21-year-old man with *Chlamydia-urethritis* and *uveitis*, now with back pain.

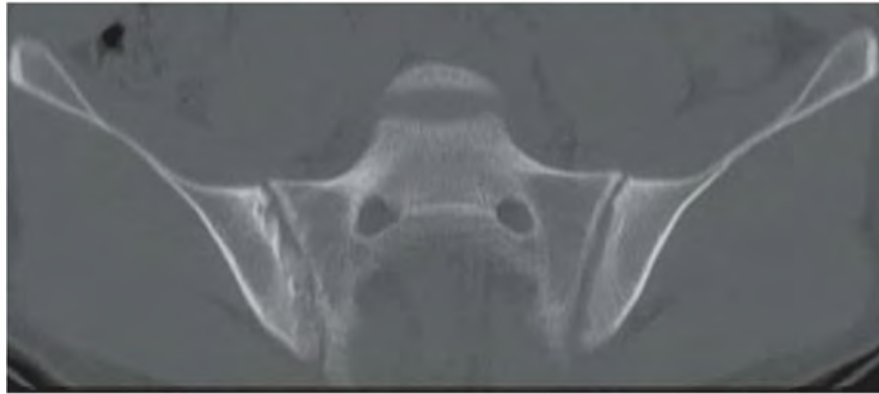


FIGURE 4.20A

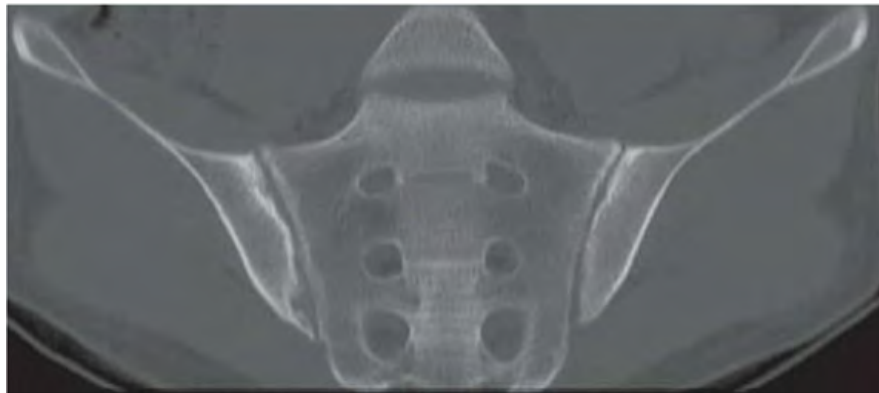


FIGURE 4.20B

**FINDINGS** Oblique coronal CT reformations through the sacrum (anterior, A, and posterior, B) show asymmetric subchondral sclerosis and erosions of the sacroiliac joints, greater on the right, and mostly on the iliac side of the joints.

**DIFFERENTIAL DIAGNOSIS** Ankylosing spondylitis, reactive arthritis, psoriatic arthropathy, enteropathic arthropathy, septic arthritis

**DIAGNOSIS** Reactive arthritis

**DISCUSSION** Combined with urethritis and uveitis, the asymmetry of sacroiliac involvement is the key to the diagnosis of reactive arthritis (also known as postinfectious arthritis, and previously known as Reiter's syndrome) [44,45]. Reactive arthritis can follow either dysentery or venereal disease and is much more common in males.

Normal sacroiliac joint contains true synovial joint only in the anteroinferior one-third of the joint. Because the normal sacral cartilage is thicker than the iliac cartilage [46], early erosive changes of sacroiliitis are seen first on the iliac side. In early stages of sacroiliitis, erosions and osteoporosis around the joint can lead to apparent joint space widening [47]. This stage is followed by subchondral sclerosis and eventual joint space narrowing and ankylosis. Many spondylonegative arthropathies involve the sacroiliac joints. Although both ankylosing spondylitis and enteropathic arthropathy can present asymmetrically, they are more often found to be symmetric. Psoriatic arthropathy and reactive arthritis should be considered in asymmetric cases. Lack of sacral involvement makes septic arthritis less likely; infection typically involves the subchondral bone on both sides of the joint.

**CLINICAL HISTORY** A 29-year-old man with history of intravenous drug abuse.



FIGURE 4.21A



FIGURE 4.21B

**FINDINGS** (A, B) Coronal and axial T2-weighted fat saturated MRI demonstrates fluid within the right sacroiliac joint, spreading anteriorly under the iliopsoas and posteriorly along the gluteal fascial plane.

**DIFFERENTIAL DIAGNOSIS** Ankylosing spondylitis, psoriatic arthritis, reactive arthritis, inflammatory bowel disease, rheumatoid arthritis, septic arthritis.

**DIAGNOSIS** Septic sacroiliitis.

**DISCUSSION** Increased signal intensity on T2-weighted MRI in the sacroiliac joint area, with fluid in the joint space, is characteristic of sacroiliitis. The inflammatory changes in the adjacent muscle are characteristic of acute infection, but not for the human leukocyte antigen (HLA-B27)

spondyloarthropathies [48,49]. The findings and history of intravenous drug abuse further support the diagnosis of septic sacroiliitis.

The sacroiliac joint may become infected through the hematogenous route, by direct extension from contiguous infection, and by direct implantation from surgery or trauma. Blood flow in the iliac subchondral bone is slow, and this is a favored site for hematogenous implantation; the sacroiliac joint becomes involved by contiguous extension. Gram-negative bacteria are frequently implicated in the population testing positive for HIV, whereas intravenous drug abuse itself is more commonly associated with staphylococcal infections. Pelvic abscesses and decubitus ulcers may extend to the sacroiliac joint, and infection may occur as a complication of trauma, surgery, or instrumentation, including injections and acupuncture [50].



FIGURE 4.22A



FIGURE 4.22B

**FINDINGS** (A) AP and (B) frog lateral radiographs show multiple small calcifications in the right hip, with secondary erosive changes of the femoral neck. The calcifications are dense and punctate and do not have a cortical or trabecular structure. The erosions are shallow and well margined, and degenerative arthritis is not evident. The morphology of the underlying bone is otherwise normal.

**DIFFERENTIAL DIAGNOSIS** Synovial osteochondromatosis, synovial hemangiomatosis, synovial sarcoma.

**DIAGNOSIS** Synovial osteochondromatosis.

**DISCUSSION** The presence of innumerable calcifications in the joint or synovium, with shallow, well-margined erosions, is virtually diagnostic of primary synovial osteochondromatosis. Synovial hemangiomatosis with multiple phleboliths would be an extremely rare mimic, as would be synovial sarcoma [51]. Pigmented villonodular synovitis (PVNS) causes erosions similar to synovial osteochondromatosis, but PVNS does not calcify. However, in one case

report, it has been described coexisting in the same joint as synovial osteochondromatosis [52].

Synovial osteochondromatosis is a condition in which there are multiple intracapsular cartilaginous nodules whose presence results in swelling, effusion, superficial erosions of bone, and degenerative arthritis. The nodules may be attached to the synovium or loose within the joint. Highly cellular nodules tend to be poorly calcified, whereas nodules with low cellularity tend to be heavily calcified. The pathogenesis of synovial osteochondromatosis is uncertain, but there is increasing evidence that the process is neoplastic rather than reactive [53]. The lesion occurs in adults, with the average age of presentation in the 50s. There is a male predominance of nearly 2:1. The most common sites are the knee (70%) and the hip (20%), and the condition is monoarticular. No relationship between the extent of calcification and ossification and the age of the patient has been shown. Well-established degenerative disease appears in only a few cases at presentation, and the malignant risk has been estimated at 5% [54]. Malignant lesions arising in synovial osteochondromatosis include chondrosarcoma [55].

**CLINICAL HISTORY** A 38-year-old man with history of back pain and ulcerative colitis. Radiographs are 5 years apart.



FIGURE 4.23A



FIGURE 4.23B



FIGURE 4.23C

**FINDINGS**

- A. AP radiograph from 10 years earlier demonstrates normal sacroiliac joints. Note laminectomy defect and surgical fusion at L4–5.
- B. AP radiograph from 5 years earlier demonstrates bilaterally symmetric erosions of both sacroiliac joints, with surrounding sclerosis.
- C. Current AP radiograph demonstrates complete ankylosis of both sacroiliac joints. Colectomy has been performed.

**DIFFERENTIAL DIAGNOSIS** Ankylosing spondylitis, psoriatic arthritis, reactive arthritis, rheumatoid arthritis, septic arthritis.

**DIAGNOSIS** Ankylosing spondylitis.

**DISCUSSION** Ankylosing spondylitis is a chronic inflammatory disease with predominant manifestations in the spine and sacroiliac joints. The etiology is unknown, but there is a genetic component; 90% to 95% of Caucasian patients with classic ankylosing spondylitis have HLA-B27 (compared with 9% of all Caucasians). Symptomatic disease affects about 1% of the general population; the prevalence of severe disease is about 0.1%. Therefore, the disease is much less common than rheumatoid arthritis.

Inflammatory bowel diseases associated with ankylosing spondylitis include ulcerative colitis, Crohn disease, and

Whipple disease. The causal relationship of the bowel disease and the ankylosing spondylitis has not been proven definitively, but it is thought that the diseases are incidentally coexistent in some patients (those with HLA-B27) and that the spondylitis may be secondary to the bowel disease in the others (those without HLA-B27). The disease activity in the bowel does not appear to be correlated with the disease activity in the sacroiliac joints or spine.

Ankylosing spondylitis typically begins in the lumbosacral region and ascends to the cervical spine [56,57]. Local pain and tenderness over the sacroiliac joints in the early phases of the disease are common, and may dominate the initial clinical presentation. Initial involvement of the sacroiliac joints may be asymmetric or unilateral, although ultimately, bilaterally symmetric involvement is virtually invariable. Inflammatory involvement of the synovial portion of the sacroiliac joints can manifest as patchy periarticular osteoporosis, erosions of the subchondral bone leading to fraying of the osseous surface and widening of the joint space, and sclerosis of the subchondral bone. These changes predominate on the iliac side of the joint, although in advanced disease both sides are involved. Calcification and ossification of the ligamentous portion of the sacroiliac joint will accompany changes in the synovial portion of the joint. The sacroiliac joints may ultimately become blurred, sclerotic, and fused.

**CLINICAL HISTORY** A 35-year-old woman with chronic right hip pain.



FIGURE 4.24A

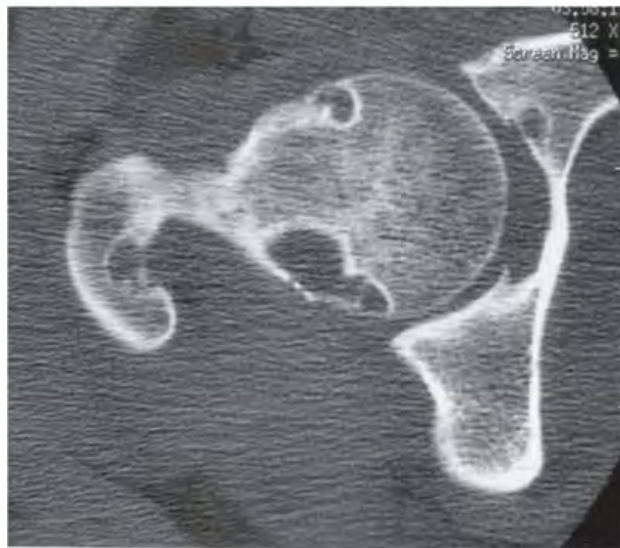


FIGURE 4.24B

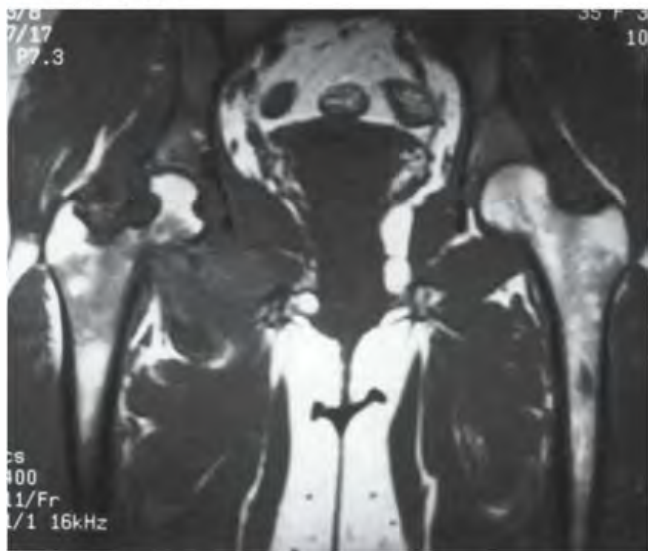


FIGURE 4.24C

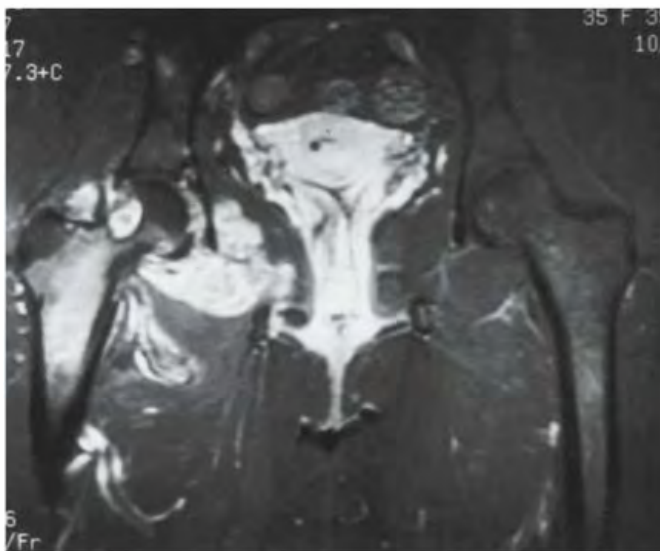


FIGURE 4.24D

**FINDINGS**

- A, B. CT scan of the right hip shows scalloped erosions of the femoral head, femoral neck, greater trochanter, and acetabulum. The erosions have well-defined sclerotic margins.
- C. Coronal T1-weighted MRI shows lobulated, low signal intensity, soft tissue masses about the right hip involving the proximal femur and pelvis. The masses have eroded the bones. Marrow changes are also present in the proximal femur.
- D. Coronal T1-weighted MRI with fat saturation after intravenous gadolinium administration shows marked enhancement of the soft tissue masses about the right hip.

**DIFFERENTIAL DIAGNOSIS** Pigmented villonodular synovitis (PVNS), tuberculosis, synovial chondromatosis, amyloid arthropathy, rheumatoid arthritis.

**DIAGNOSIS** Pigmented villonodular synovitis.

**DISCUSSION** Although tuberculosis of the hip and synovial cysts in rheumatoid arthritis may result in erosions and lobulated masses about the joint, the MRI findings

are not that of simple, fluid-filled structures. Synovial chondromatosis would typically demonstrate calcifications, which are not present in this case. PVNS is a benign neoplasm (rather than an inflammatory condition) of the synovium that usually presents in adults as recurrent non-articular hemorrhagic effusions. Common locations include the knee or hip, but any synovial tissue may be involved. Involvement of the synovium may be focal or diffuse. Chronic, erosive changes from thickened, nodular, synovial proliferation may be seen on radiographs. Localized osteoporosis is common. Arthritic changes such as joint space narrowing and osteophytes are generally absent. MRI shows effusion and multiple low signal intensity synovial masses on T1-weighted and T2-weighted images that typically enhance after gadolinium injection [58]. Amyloid deposition may have a similar pattern, but would generally involve multiple joints. The lesion in PVNS is pigmented on gross examination because of hemosiderin deposits from repeated bleeding. The presence of hemosiderin causes the lesion to have low signal intensity on all MRI pulse sequences. Treatment of PVNS is surgical. Although there is no metastatic potential, the lesion may recur locally if synovectomy is incomplete.

**CLINICAL HISTORY** A 50-year-old woman with progressive hip pain.



FIGURE 4.25A



FIGURE 4.25B



FIGURE 4.25C

## FINDINGS

- A. AP radiograph of the left hip shows minimal superior lateral cartilage space narrowing, with associated osteophyte formation and subchondral sclerosis.
- B, C. Six years later. AP and frog lateral radiographs of the left hip show the findings have progressed, including medial femoral osteophyte formation and further cartilage space narrowing.

**DIFFERENTIAL DIAGNOSIS** Osteoarthritis, inflammatory arthritis.

**DIAGNOSIS** Osteoarthritis.

**DISCUSSION** Osteoarthritis of the hip is one of the most common conditions in adults leading to the continuing use of medication, elective surgery, or both. In young adults, there is usually an underlying abnormality of the hip, such as previous trauma, previous hip disease, or acetabular dysplasia. In older adults, no underlying abnormality may be obvious, but a genetic basis for development of osteoarthritis

is becoming apparent [59]. Radiographic findings of osteoarthritis in the hip are those of osteoarthritis in other joints, including cartilage space narrowing, subchondral sclerosis, osteophyte formation, and preservation of bone mineralization. Erosions are notably absent, but subchondral cyst formation is common. Serial radiographs may document the progress of hip osteoarthritis. In a retrospective study of adult patients with osteoarthritis of the hip who ultimately received total hip replacements, the progression of cartilage space narrowing ranged from 0 to 2.6 mm per year, with a mean progression of 0.4 mm per year. Progression was slower in patients with hypertrophic bony changes [60].

Intra-articular injection of local anesthetic has been advocated as a diagnostic test to determine whether an osteoarthritic hip is the source of clinical symptoms, thus aiding in the clarification of the cause of pain. In one study, patients who had relief after administration of the intra-articular anesthetic were treated successfully by joint replacement, whereas those who did not obtain relief proved to be unsuitable candidates for joint replacement [61].

**CLINICAL HISTORY** A 39-year-old woman with chronic hip and hand pain.



FIGURE 4.26

**FINDINGS** AP radiograph of the pelvis shows bilateral protrusio acetabuli is noted with axial migration of both hips symmetrically. No osteophytes are noted. The sacroiliac joints are normal. Bone structure appears normal.

**DIFFERENTIAL DIAGNOSIS** Rheumatoid arthritis, osteoarthritis, spondyloarthropathy.

**DIAGNOSIS** Rheumatoid arthritis.

**DISCUSSION** Protrusio acetabuli is defined radiographically and is present when the medial acetabular wall protrudes medially by 3 mm or more in men or 6 mm or more in women [62]. It is a complication seen primarily in rheumatoid arthritis, but it may also be present in seronegative spondyloarthropathy, osteoarthritis, juvenile chronic arthritis, and other hip conditions. Its presence does not appear to be correlated with disease duration, clinical severity of hip involvement, or previous medication. In this case, the lack of sacroiliac

joint or spine abnormality and the lack of hypertrophic bone formation favor rheumatoid arthritis.

Any condition that causes weakening of the bone may cause protrusio, including entities such as Paget disease, osteomalacia, polyostotic fibrous dysplasia, therapeutic irradiation, and osteogenesis imperfecta. Prior fractures of the acetabulum, particularly with medial displacement from lateral compression, may produce this deformity. Protrusio may also occur on a familial or idiopathic basis. Protrusio acetabuli is a classic finding in rheumatoid arthritis of the hip and, as a rule, the changes are bilateral and symmetric. Subchondral cystic lesions, subchondral collapse of the acetabulum and femoral head, and osteoporosis may be associated findings. When sclerosis is present, it is a sign of reparative response and secondary osteoarthritis. Typical progression of the protrusion in rheumatoid arthritis is 2 to 3 mm per year, but a small subset may have rapid progression (7.5 mm over 6 weeks) occurring at the same time as a marked increase in symptoms and disability [63].



FIGURE 4.27

**FINDINGS** AP view of pelvis shows axial joint space narrowing in left greater than right hip joints. For the amount of joint space narrowing, there is relatively small amount of osteophytes and subchondral sclerosis. There is ankylosis of both sacroiliac joints.

**DIFFERENTIAL DIAGNOSIS** Ankylosing spondylitis, enteropathic spondylitis.

**DIAGNOSIS** Ankylosing spondylitis.

**DISCUSSION** In early and mid stages of osteoarthritis, there is asymmetric hip joint space narrowing, mostly in

the superolateral portion, according to the pattern of weight bearing. In contrast, inflammatory arthritis affects hip joints by causing diffuse joint space narrowing, otherwise known as “axial” joint space narrowing. Inflammatory arthritis includes both rheumatoid arthritis and seronegative spondyloarthropathies such as ankylosing spondylitis and psoriasis. In ankylosing spondylitis, hip disease is associated with more severe spine disease [57]. Often, there may be signs of secondary osteoarthritis, as in this case with small osteophytes.



FIGURE 4.28

**FINDINGS** AP radiograph of the pelvis shows both femoral heads are enlarged and flattened on top.

**DIFFERENTIAL DIAGNOSIS** Juvenile idiopathic arthritis, septic arthritis.

**DIAGNOSIS** Juvenile idiopathic arthritis.

**DISCUSSION** Childhood arthritis has been combined into a single classification of juvenile idiopathic arthritis [64,65]. Although ankylosis may occur after septic arthritis, the finding of bilaterally symmetric ankylosis of the hips

suggests juvenile idiopathic arthritis rather than infection. The dysplastic overgrowth of the femoral heads suggests chronic disease. Similar dysplastic changes may be seen in a variety of other conditions, including neuromuscular syndromes, hemophilia, and Legg-Calve-Perthes disease, but the presence of ankylosis excludes them. Of the various forms of juvenile idiopathic arthritis, Still disease would be the most likely because of the lack of sacroiliac joint involvement, although ankylosis of the hips occurs in juvenile-onset seronegative spondyloarthritis. Adult-form rheumatoid arthritis typically does not produce ankylosis of large synovial joints.

**CLINICAL HISTORY** A 42-year-old man with small fingernails.



FIGURE 4.29A

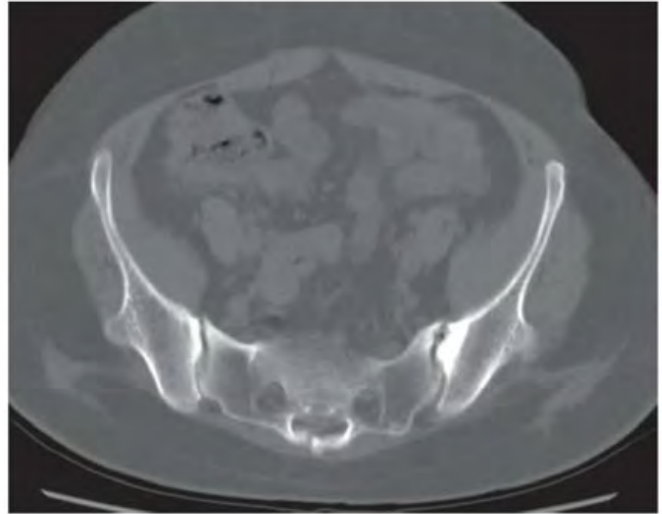


FIGURE 4.29B



FIGURE 4.29C



FIGURE 4.29D

### FINDINGS

- A. AP view of the pelvis shows small horns on each iliac body.
- B. CT scan through the pelvis shows small horns projecting posteriorly.
- C. Sagittal T1-weighted MRI of the knee shows a hypoplastic patella.
- D. AP view of the elbow shows hypoplasia of the proximal radius with absent radial head.

**DIFFERENTIAL DIAGNOSIS** None.

**DIAGNOSIS** Nail-patella syndrome (osteonychodysostosis, Fong's syndrome).

**DISCUSSION** Posteriorly located iliac horns are pathognomonic of nail-patella syndrome. These bony outgrowths are located at the origin of the gluteus medius muscles [66]. The iliac horns are present in 80% of patients with this syndrome, and may be unilateral. Eighty percent to ninety percent of patients have absent or hypoplastic finger nails and toenails. Other skeletal anomalies are often present, including hypoplastic patellae, hypoplastic capitella, and hypoplastic, dislocated radial heads. This disorder is autosomal dominant, but about 20% of cases are sporadic, with no family history. Nail-patella syndrome has multiple extraskeletal associations, the most common of which are renal disease (50%) and eye disorders, such as glaucoma and cataracts.

**CLINICAL HISTORY** A 57-year-old man with progressive anemia.

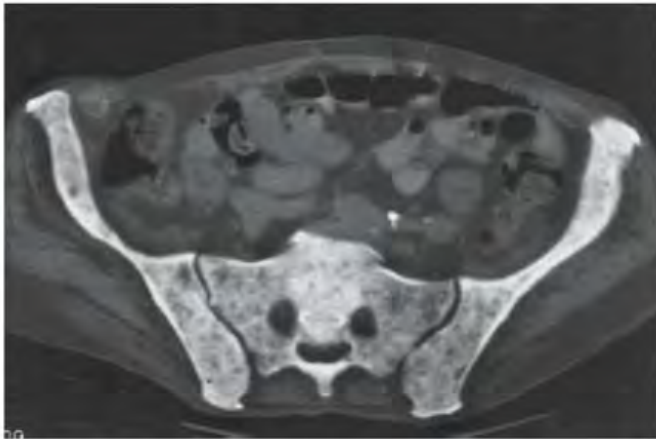


FIGURE 4.30A

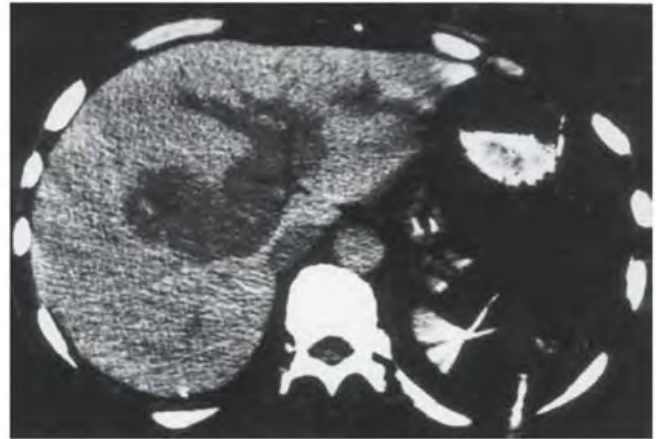


FIGURE 4.30B

### FINDINGS

- A. Axial CT scan of the pelvis shows mottled sclerosis of the sacrum and both iliac wings, without cortical destruction or bone expansion. The cortex itself is not thickened, and the trabecular bone pattern is obscured.
- B. Axial CT scan of the upper abdomen shows surgical clips from a prior splenectomy. A low-attenuation lesion in the center of the liver was proved by biopsy to represent extramedullary hematopoiesis.

**DIFFERENTIAL DIAGNOSIS** Paget disease, lymphoma, leukemia, metastases, myelofibrosis, mastofibrosis.

**DIAGNOSIS** Myelofibrosis.

**DISCUSSION** Paget disease would be the most common benign cause of sclerosis in the pelvis in an older adult, but the distinctive pattern of cortical thickening and trabecular coarsening is absent. Other differential considerations include mastocytosis, leukemia, and lymphoma. The degree of sclerosis is usually less marked in leukemia and lymphoma patients, and often there are lytic regions, cortical destruction, and soft tissue involvement. Metastases would typically have more asymmetric distribution, as well as cortical involvement. The absence of proliferative hyperostosis would argue against fluorosis or retinoid intoxication.

Myelofibrosis is a replacement of the bone marrow with fibrosis, necessitating extramedullary hematopoiesis [67].

It can be primary (idiopathic) or secondary to exposure to environmental toxins, such as benzene, or in association with a chronic blood dyscrasia, such as polycythemia vera, chronic myelocytic leukemia, and miscellaneous anemias. One hypothesis [67] regarding the etiology of the marrow fibrosis postulates exposure to an excessive quantity of platelet-derived growth factor from altered megakaryocytes. The population typically affected includes patients in their 60s and 70s.

The onset is commonly insidious and prognosis is variable. The fibrosis initially involves sites of active marrow production including the vertebrae, ribs, and pelvis. Intramedullary hematopoiesis then shifts to the proximal and distal ends of the femora, humeri, and tibiae. These are the secondary sites to undergo osteosclerosis, and then the marrow production will shift to tertiary osseous or extraosseous sites. The radiographic findings include sclerosis in 40% to 50% of cases, and cortical thickening (most marked on the endosteal surface rather than periosteal surface). Extramedullary hematopoiesis may be located in the paravertebral location or within the liver or spleen, as seen in this case. Polymyalgia and polyarthralgia may be related to an immunologic etiology, as seen in rheumatoid arthritis, or may result from secondary hyperuricemia or recurrent hemarthrosis from low platelet counts. MRI shows replacement of the normal fatty marrow with hypointense fibrosis on T1-weighted MRI. The apophyses are more resistant to reconversion than epiphyses.



FIGURE 4.31

**FINDINGS** AP radiograph of the pelvis. There are cystic changes with sclerotic borders involving the left pubis and ischium, right ilium adjacent to the sacroiliac joint, and right pubis. A lace-like pattern is noted in the right femoral neck and shaft, with a widening of the bone.

**DIFFERENTIAL DIAGNOSIS** Hemangiomatosis, metastases, lymphoma, eosinophilic granuloma, osteomyelitis, tuberculosis.

**DIAGNOSIS** Hemangiomatosis.

**DISCUSSION** The lesions are multifocal, and although they have both lucent and sclerotic components, the impression

should be more of a multifocally abnormal trabecular pattern, rather than multiple lesions with bone destruction and reactive bone formation. Hemangioma of bone is one of the few benign bone lesions with a female predominance (the others are giant cell tumor and aneurysmal bone cyst). The lesions consist of abnormal vascular spaces and fat, and they may enlarge slowly in a permeative fashion, allowing the trabecular bone to remodel. Common sites of involvement include the axial skeleton, femur, and pelvis, but any bone may be involved. Contiguous involvement of multiple bones is not uncommon. The lesions may occur in a synchronous or metachronous fashion. Lymphangiomatosis and cystic angiomatosis are related multifocal vascular lesions of bone with a virtually indistinguishable appearance [68].

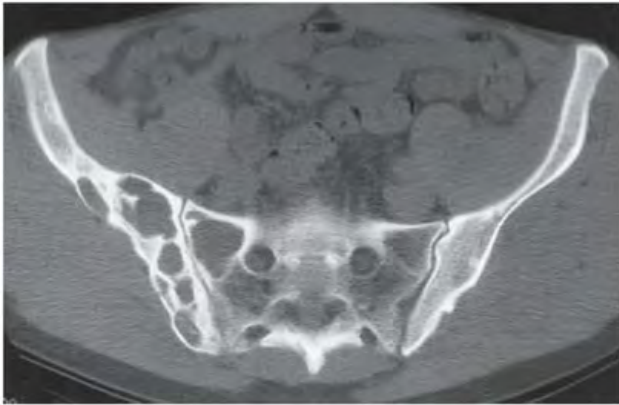


FIGURE 4.32A

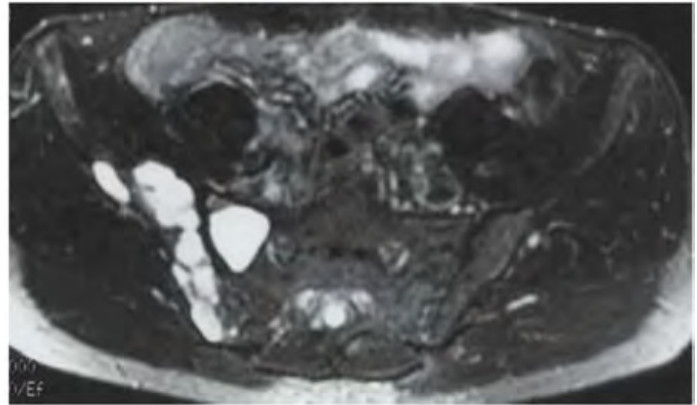


FIGURE 4.32B

**FINDINGS**

- A. Axial CT of the pelvis with soft tissue window shows multiple lytic lesions on both sides of the right sacroiliac joint. The lesions have soft tissue attenuation. The bone is moderately expanded. There is no cortical destruction or soft tissue component.
- B. Axial T2-weighted MRI with fat saturation through the pelvis demonstrates high signal intensity in the lytic lesions, with no soft tissue involvement.

**DIFFERENTIAL DIAGNOSIS** Metastases, lymphoma, multiple myeloma, angiomatosis, tuberculosis, fungal osteomyelitis.

**DIAGNOSIS** Cystic angiomatosis.

**DISCUSSION** The presence of multiple lucent lesions in contiguous bones of the pelvis, with remodeled, sclerotic margins, suggests an indolent process. The MRI is suggestive of fluid signal intensity, favoring some form of angiomatosis, including lymphangiomatosis or hemangiomatosis. Cystic angiomatosis shows multiple cystic areas in bone, with or without involvement of other organ systems. Occasionally, the lesions may be sclerotic [69]. Other multifocal vascular lesions, such as multifocal hemangioma, hemangioendothelioma, and angiosarcoma, may have a similar radiographic appearance. Indolent or atypical infections, such as caused by tuberculosis, atypical mycobacteria, or fungal pathogens, may have a similar appearance, but soft tissue extension, or at least edema, would be expected. The lack of cortical destruction makes metastases, lymphoma, and myeloma less likely.



FIGURE 4.33A



FIGURE 4.33B

**FINDINGS** (A) AP radiograph of the pelvis shows dysplastic changes of the pelvis including bilateral femurs (see close up of right hip in (B)). The cortex and trabecular bone pattern are preserved with normal bone density.

**DIFFERENTIAL DIAGNOSIS** None.

**DIAGNOSIS** Multiple hereditary exostoses (MHE) (osteochondromatosis).

**DISCUSSION** MHE (also known as, osteochondromatosis, multiple osteochondromas, diaphyseal aclasis) is one of the most common skeletal dysplasias. The condition is inherited with autosomal dominant transmission and incomplete penetrance. The expression is variable, with more severe manifestations in males. In one large series, 62% of cases were inherited, and 38% of cases were sporadic [70]. The skeleton is involved symmetrically, and the limbs are affected more than the spine. Forty percent are about the knee.

These lesions, like other cartilaginous tumors, form in bones that undergo enchondral ossification as opposed to intramembranous ossification. The number of exostoses varies. Deformities of the tubular bones are present and cause disproportionately short limbs, but the degree of shortness appears to be unrelated to the number of exostoses. Growth of the lesions slows as the skeleton matures, and new lesions do not appear in adulthood. The exostoses are radiologically and histologically indistinguishable from solitary ones. They may appear sessile or pedunculated, with the sessile variety showing a greater propensity for malignant transformation. Rate of malignant degeneration of osteochondroma is higher in MHE patients (3% to 5%) than those with a solitary osteochondroma (1%). Most commonly, chondrosarcoma can develop from the cartilage cap. More rarely, osteosarcomas can develop from the stalk [71]. Signs of malignant degeneration include cartilage cap thickening greater than 2 cm, continued growth or new pain after skeletal maturity, soft tissue mass, or calcification within the cartilage cap [72].

**CLINICAL HISTORY** A 39-year-old woman with acute onset of left pelvic pain.



FIGURE 4.34A

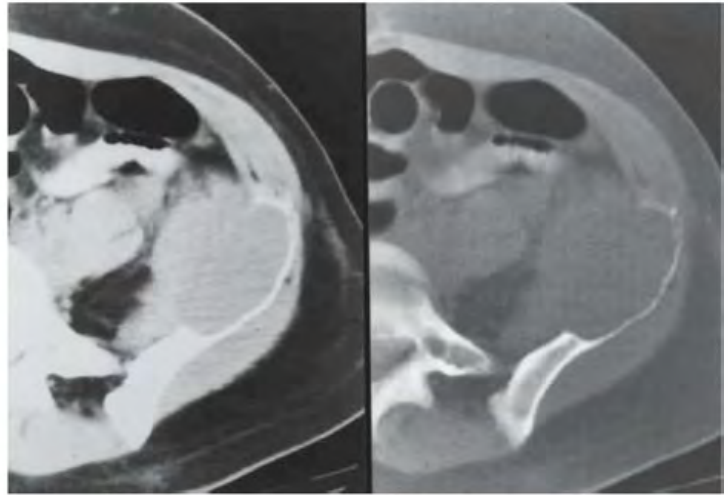


FIGURE 4.34B

### FINDINGS

- A. AP radiograph of the pelvis shows an expansile, lytic lesion in the left iliac wing. A pathologic fracture is present at the inferior margin of the lesion.
- B. Axial CT scan with soft tissue and bone windows shows destruction of the anterior cortex with soft tissue mass. There is no mineralization within the mass.

**DIFFERENTIAL DIAGNOSIS** Plasmacytoma, lymphoma, desmoplastic fibroma, bone cyst, metastasis, giant cell tumor.

**DIAGNOSIS** Plasmacytoma.

**DISCUSSION** The imaging features in this case are nonspecific but alarming, because of the cortical breakthrough. A biopsy is necessary for diagnosis.

Plasmacytoma (also called solitary myeloma) is a malignant neoplasm arising from a single clone of plasma cells that has a solitary focus in the marrow; when multiple foci of disease are present, the condition is called multiple myeloma. Serum protein electrophoresis may show a monoclonal spike of immunoglobulins, corresponding to the products of the neoplastic clone, but sometimes both the findings from serum protein electrophoresis and the findings from blind iliac crest bone marrow aspiration are negative in plasmacytoma. Regardless of whether the initial lesion is resected, virtually all patients with plasmacytoma ultimately develop multiple myeloma. However, 10 years or more may pass before the progression of disease becomes apparent. Plasmacytoma commonly presents as an expansile lesion in the spine, a rib, the pelvis, or the sacrum, with pathologic fracture.



FIGURE 4.35A

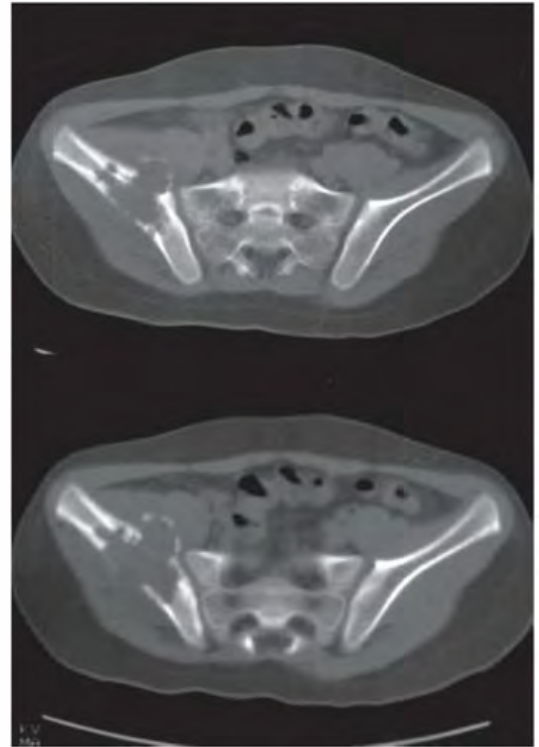


FIGURE 4.35B

**FINDINGS**

- A. AP radiograph of the pelvis shows a large, focal lytic lesion in the right iliac wing. The zone of transition appears to be relatively sharp, and there may be trabeculations within the lesion.
- B. Representative CT scan images show a lucent lesion centered in the cortex. The posterior cortex has been largely destroyed, and the anterior cortex has been expanded. No mineralization is present within the lesion. There are no fluid-fluid levels. Edema gives the adjacent soft tissues lower attenuation than the normal contralateral side.

**DIFFERENTIAL DIAGNOSIS** Ewing's sarcoma, osteosarcoma, eosinophilic granuloma, lymphoma, aneurysmal bone cyst, osteomyelitis.

**DIAGNOSIS** Eosinophilic granuloma.

**DISCUSSION** The lesion has aggressive features, particularly on the CT scan. Cortical destruction, expansion into the soft

tissues, and peritumoral edema represent a combination of features that is frequently seen in Ewing's sarcoma and lymphoma. The lack of mineralization makes osteosarcoma less likely, and the location is not typical; however, fibroblastic and telangiectatic variants of osteosarcoma may not have much visible mineralization. The expansile nature of the lesion fits well with aneurysmal bone cyst. MRI would be helpful to determine whether the lesion is cystic or solid. Rapidly growing aneurysmal bone cysts may expand the periosteum faster than it can make bone, sometimes making it appear as if it has been destroyed, even though it may still be present. Finally, infection can be considered. The paucity of reactive bone formation relative to the extent of the destruction makes this less likely. This lesion requires a tissue diagnosis, and biopsy should be recommended. A CT-guided approach parallel to the anterior aspect of the iliac wing would preserve most surgical options should the lesion prove malignant.

**CLINICAL HISTORY** A 78-year-old woman with progressive bilateral groin pain and inability to walk, and two companion cases.



FIGURE 4.36A

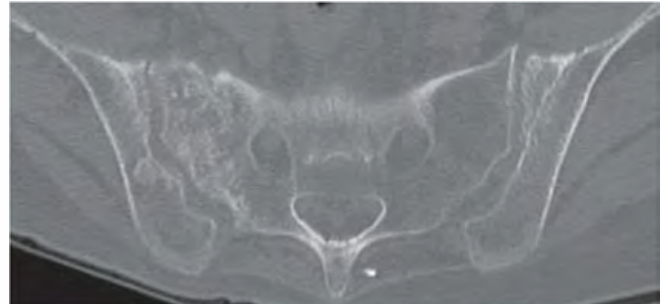


FIGURE 4.36B

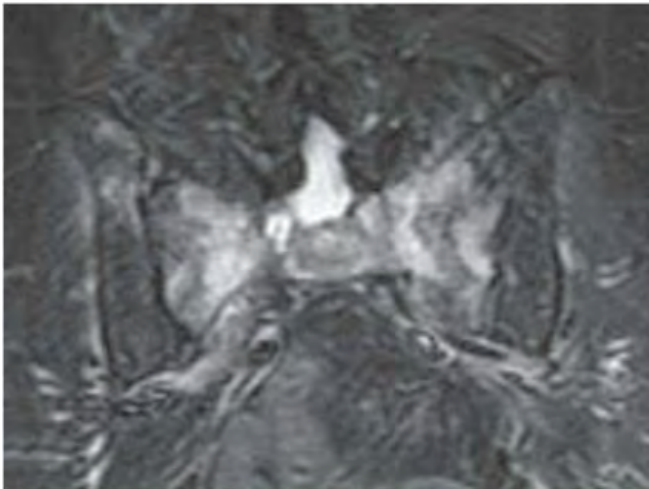


FIGURE 4.36C

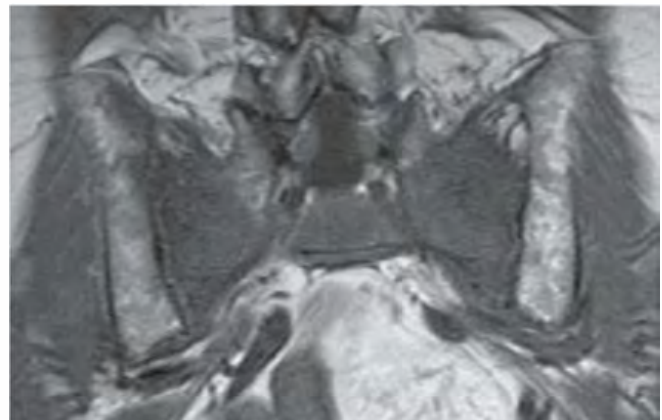


FIGURE 4.36D

## FINDINGS

- A. AP radiograph of the pelvis shows healing fractures of the inferior and superior pubic rami, bilaterally. The bones are osteopenic.
- B. Companion case 1: An 81-year-old woman with low back pain. Axial CT through sacrum demonstrating sclerosis of the right sacral ala.
- C, D. Companion case 2: A 72-year-old woman with low back pain. Coronal STIR and T1-weighted MRI showing marked edema in each side of the sacrum.

**DIFFERENTIAL DIAGNOSIS** None.

**DIAGNOSIS** Insufficiency fractures.

**DISCUSSION** Insufficiency fractures in elderly women may present with progressive inguinal or back pain, limping, and

inability to walk. Predisposing conditions include osteoporosis, osteomalacia, rheumatoid arthritis, pelvic irradiation, prolonged corticosteroid treatment, and mechanical changes following hip replacement surgery [73]. Initial radiographs at the time of presentation may not necessarily show the fracture, and radionuclide bone scan, CT, or MRI may be required for the diagnosis. MRI would appear to have the greatest sensitivity and specificity for occult fractures such as these in the elderly [74]. Most patients improve with nonsurgical treatment of the fracture and the underlying cause. Similar appearing stress fractures (as opposed to insufficiency fractures) in the inferior pubic rami have been described in young, healthy female military recruits, an injury that appears to result from increased stride length when marching during basic training in mixed-sex groups [75]. Sacral and pubic rami stress fractures have also been described in long-distance runners.

**CLINICAL HISTORY** A 57-year-old woman with bone pain and history of mastectomy for breast cancer 10 years earlier.



FIGURE 4.37

**FINDINGS** AP radiograph of the pelvis demonstrates a diffuse, mixed lytic and sclerotic process without distortion of the cortical surface or pathologic fracture. Radiographs of the thoracic and lumbar spine (not shown) are similar.

**DIFFERENTIAL DIAGNOSIS** Metastases, multiple myeloma, osteomalacia.

**DIAGNOSIS** Diffuse breast carcinoma metastases.

**DISCUSSION** The diffuse distribution of mixed osteolytic and osteoblastic changes is characteristic of disseminated cancer. The skeleton is the most common site of metastatic disease in the body, particularly from primary tumors arising in the prostate, breast, thyroid, lung, and kidney [76].

Metastatic breast carcinoma commonly spreads to bone without visceral involvement. Median survival in breast cancer patients with only bone metastases is approximately 2 to 3 years. Complications from bone metastases and their treatment are frequently the principle cause of morbidity and proximal cause of death in breast cancer patients. The most common symptom is bone pain from structural damage, periosteal irritation, and nerve involvement. Increased bone resorption leading to hypercalcemia may also cause bone pain, and this pain is often ameliorated by treatment with bisphosphonates. Pathologic fractures are a late complication. Intensive screening for metastatic disease in breast cancer patients without bone symptoms has been found to have no effect on the 5-year survival rate, even though more metastases can be detected earlier [77].

**CLINICAL HISTORY** A 29-year-old man with bone pain and right inguinal mass.



FIGURE 4.38A

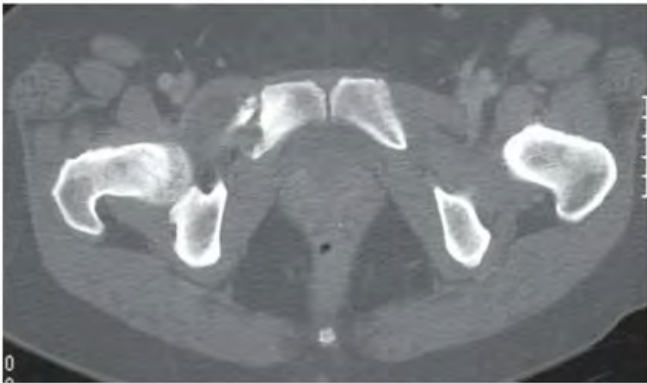


FIGURE 4.38B

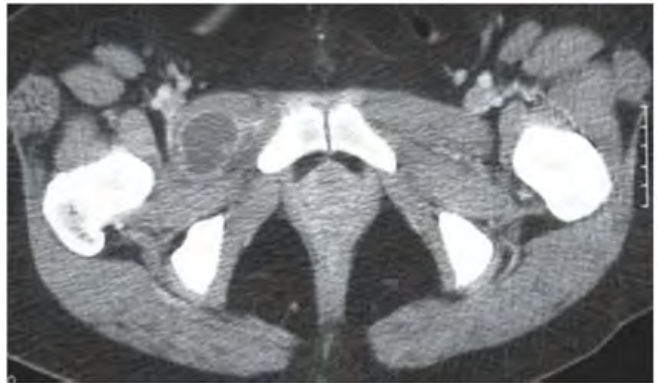


FIGURE 4.38C

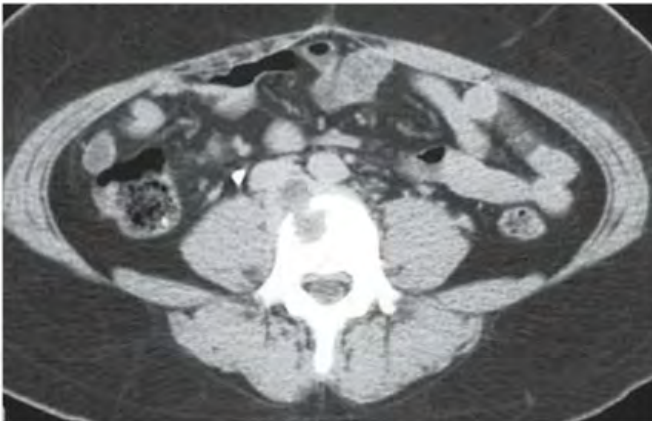


FIGURE 4.38D

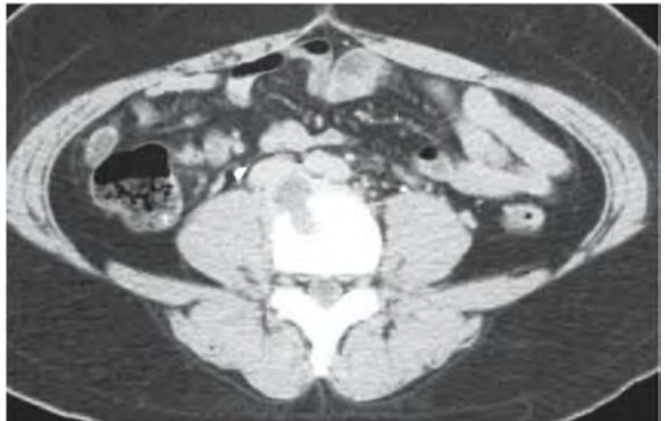


FIGURE 4.38E

**FINDINGS** (A) AP radiograph of the pelvis. A lytic process involves the right superior pubic ramus. Some reactive sclerosis is present. Contrast-enhanced axial CT scans at two levels through the superior pubic rami viewed with bone settings (B) and soft tissue settings (C) show bone destruction on the right, with reactive sclerosis and low-attenuation soft tissue mass. The soft tissue mass has an enhancing rim. (D, E) Contrast-enhanced axial CT scan at the L5 level shows a destructive bone lesion involving the anterior aspect of the vertebral body, with extension into the anterior soft tissues. The lesion has low attenuation and an enhancing rim.

**DIFFERENTIAL DIAGNOSIS** Metastases, multiple myeloma, tuberculosis, osteomyelitis, lymphoma, leukemia.

**DIAGNOSIS** Tuberculosis.

**DISCUSSION** Differential considerations include other fungal or pyogenic types of osteomyelitis, as well as metastatic or multifocal neoplasms. The presence of reactive bone formation is much more common in infections than in tumors. The morphology of the bone involvement and the large size of the soft tissue lesions relative to the bone lesions suggest a nonpyogenic infectious agent, beginning in bone but causing abscess formation. Factors that suggest the specific diagnosis

include a positive chest radiograph or tuberculin skin test, low frequency of neurologic symptoms in the presence of severe spine involvement, normal erythrocyte sedimentation rate, and indolent symptoms disproportionate to a destructive radiographic appearance.

The prevalence of tuberculosis has been rising in North America after notable successes from public health measures earlier in the 20th century. It is seen most commonly in immunocompromised patients and among immigrant populations [78]. Skeletal involvement is the result of hematogenous spread, typically from the lungs. Between 25% and 60% of cases concerning bone involve the spine. The body of L1 is the most commonly affected site in the spine, but involvement of multiple contiguous levels (classically three levels) is frequent. Involvement of the upper cervical levels, thoracolumbar junction, posterior elements, and sacroiliac joints is also known to occur. Paravertebral abscesses are common and may extend into the groin or thigh. MRI can be very helpful in differentiating pyogenic spondylitis from tuberculous spondylitis [79]. Tuberculosis may also spread to the joints [80], resulting in a granulomatous synovial infection that requires synovial biopsy or joint aspiration for diagnosis. In the typical situation, the process is monarticular, and there is osteomyelitis adjacent to the involved joint.

**CLINICAL HISTORY** A 32-year-old woman with pelvic pain.



FIGURE 4.39A

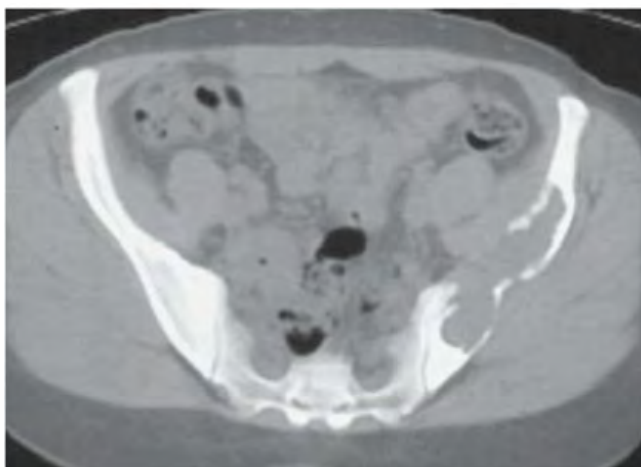


FIGURE 4.39B

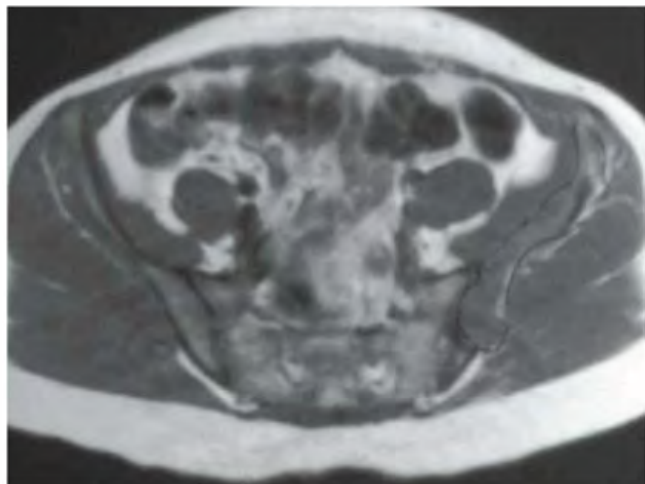


FIGURE 4.39C

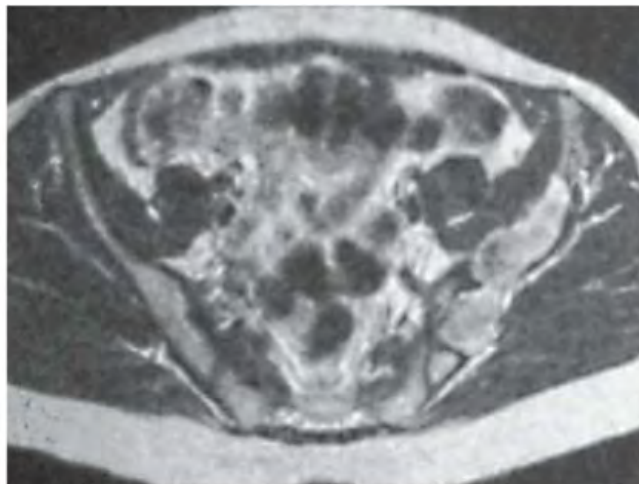


FIGURE 4.39D

## FINDINGS

- A. AP radiograph of the pelvis shows a large destructive lesion in the left iliac wing, with loss of the iliopectineal line. The lesion appears to have no internal matrix mineralization. Some surrounding reactive bone formation may be present.
- B. CT scan shows a lucent lesion in the ilium with thinning of the cortex. A break in the mineralized cortex is present anteriorly. The lesion is mildly expansile, with no evident soft tissue mass. There is no mineralization within the lesion.
- C. Axial proton-density MRI shows intermediate signal within the lesion, with apparently intact periosteum. No extension into the soft tissues is present.
- D. Axial T2-weighted MRI shows heterogeneous high signal within the lesion. There is no surrounding soft tissue or marrow edema.

**DIFFERENTIAL DIAGNOSIS** Plasmacytoma, lymphoma, chondrosarcoma, osteosarcoma, bone cyst, fibroma, giant cell tumor, fibrous dysplasia, metastasis.

**DIAGNOSIS** Desmoplastic fibroma.

**DISCUSSION** Desmoplastic fibroma is a rare, benign, primary bone tumor that is the osseous counterpart of the extra-abdominal desmoid tumor of soft tissues (fibromatosis). There is a male predominance, and most patients are 20 to 30 years old at presentation. The most frequently affected sites are the pelvis and femur. Although soft tissue extension may be present in desmoplastic fibroma, the radiographic features are typically those of nonaggressive lesions: geographic pattern of destruction, sharply defined margins, and reactive bone formation at the margins [81,82].

The imaging features in this case are not specific, but the lack of mineralization decreases the likelihood of fibrous dysplasia and the bone-forming or cartilage-forming tumors. The MRI appearance is variable, but foci of low to intermediate signal on T2-weighted images, which are not due to calcification, can aid diagnosis [83]. Plasmacytoma, lymphoma, and metastasis might be expected to have a more aggressive appearance, with cortical penetration, soft tissue mass, and soft tissue edema, but the appearance is not specific enough to obviate the need for biopsy. There is a high incidence of local recurrence after treatment of desmoplastic fibroma by intralesional curettage [84], but no metastatic potential has been documented.

**CLINICAL HISTORY** A 67-year-old woman with total hip replacement who is unable to walk.



FIGURE 4.40A



FIGURE 4.40B

### FINDINGS

- A. AP radiograph of the right hip shows a total hip replacement, with superior and lateral dislocation of the prosthetic femoral head.
- B. True lateral radiograph shows the anterior position of the prosthetic femoral head. The prosthesis has cemented acetabular and femoral components.

**DIFFERENTIAL DIAGNOSIS** None.

**DIAGNOSIS** Dislocated total hip replacement.

**DISCUSSION** Lateral hip dislocation is a common complication of total hip replacement, with an overall incidence of 2% to 3%. It is associated with significant cost and morbidity. An increased incidence of dislocation has been observed in women, in the elderly, in patients with cerebral dysfunction, with small femoral head components, and after revision procedures [85–87]. Approximately

one-third of dislocations will occur within a few weeks of surgery. Most cases can be treated successfully by closed reduction, but sometimes surgery is required, particularly in cases of recurrent dislocation.

The principal causes of recurrent dislocation are component malposition and separation, and nonunion of the greater trochanter [88]. Separation of the greater trochanter results in failure of the abductor mechanism, so that the unopposed adductor muscles tend to pull the hip out of its socket.

Total hip replacement and total knee replacement are the most common elective orthopedic operations in the United States. Osteoarthritis is the most common indication for total hip replacement. The cost effectiveness of total hip replacement compares favorably with nonsurgical treatments for advanced arthritis [89]. Even in elderly patients, dramatic improvements in pain and function can be achieved consistently with low complication rates and length of hospital stays comparable to younger patients [90].

**CLINICAL HISTORY** A 73-year-old man with painful total hip prosthesis. Radiographs at presentation and 3 months later.



FIGURE 4.41A



FIGURE 4.41B

### FINDINGS

- AP radiograph of the left hip shows a hybrid total hip prosthesis with a partially cemented femoral component. There is a lucent zone at the prosthesis-to-bone interface of the proximal medial and lateral portions of the femoral component.
- Three months later, AP radiograph shows that regions of lucency at the prosthesis-to-bone interface have enlarged, and new lucent zones have developed more distally at the femoral prosthesis-to-bone interface. The femoral stem has also detached from the bone cement along its lateral aspect.

**DIFFERENTIAL DIAGNOSIS** Total hip replacement failure caused by osteolysis or infection.

**DIAGNOSIS** Total hip replacement failure caused by osteolysis.

**DISCUSSION** Loss of bone at the interface with a prosthetic joint replacement may cause catastrophic failure from loosening of components. Radiographic findings [91] that suggest loosening of prosthetic components include widening

of the lucent zone at the prosthesis-to-bone interface or metal-to-bone interfaces to greater than 2 mm, migration of components from their original positions, development of a lucent gap between metal and cement, cement fracture, periosteal reactive bone, and osteolysis. Osteolysis in total joint replacements is usually caused by foreign body granulomatous reaction. The mechanical friction on polyethylene components abrades microscopic particles of the plastic, which then incite an osteolytic granulomatous foreign body reaction. Migration of polyethylene debris and its accompanying reaction along cement-to-bone or metal-to-bone interfaces, often in the form of a thin membrane, may eventually cause gross loosening. Massive localized osteolysis may also occur; these lesions are filled with the same polyethylene foreign body reaction that causes component loosening.

Polyethylene osteolysis usually progresses slowly over many years. Debris may pass through lymphatics to regional lymph nodes. Because the radiolucent polyethylene liners of total joint replacements are responsible for the joint space on radiographs, thinning or gross failure of the polyethylene is evident on radiographs as narrowing of the joint space. Many polyethylene components have embedded metal markers that indicate their position on radiographs.

**CLINICAL HISTORY** A 72-year-old woman with right groin pain referred from an outside institution for removal of a “tumor.” She is 5 years status post right total hip arthroplasty.

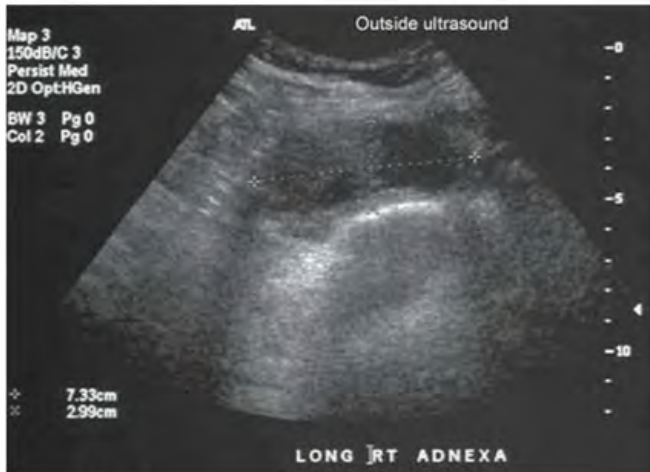


FIGURE 4.42A

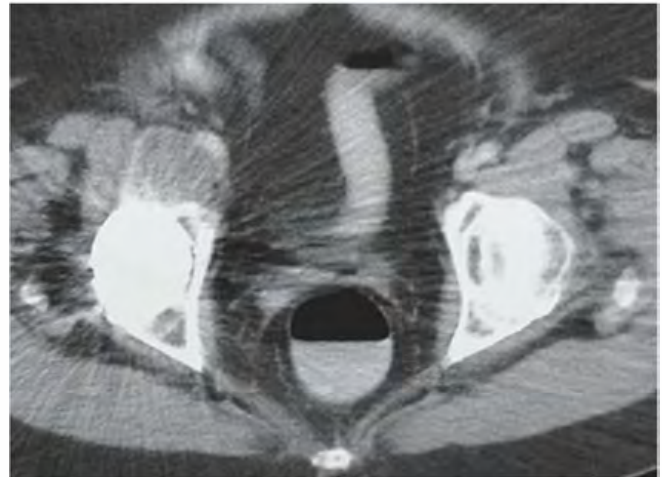


FIGURE 4.42B

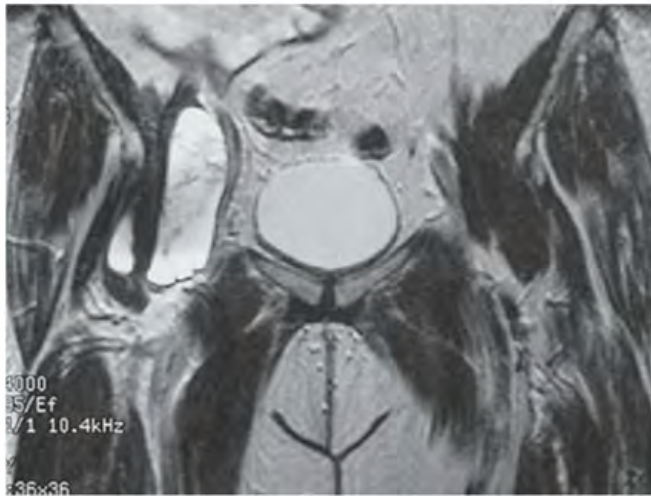


FIGURE 4.42C



FIGURE 4.42D

**FINDINGS**

- A. An ultrasound demonstrates a complex cystic mass, which was misinterpreted by an outside institution as being adnexal in location.
- B, C. On axial CT and coronal T2-weighted MRI, an elongated cystic structure extends along the anterior border of the iliopsoas muscle to the level of the hip arthroplasty distally. The mass displaces the right external iliac artery and vein medially.
- D. A conventional hip arthrogram demonstrates flow of contrast from the hip joint superiorly and medially into the cystic mass.

**DIFFERENTIAL DIAGNOSIS** Distended iliopsoas bursa, inguinal hernia, abscess, sarcoma.

**DIAGNOSIS** Iliopsoas bursitis.

**DISCUSSION** The iliopsoas bursa is the largest bursa in the body. This bursa communicates with the hip joint in 15% of normal adults. Bursal communication with the hip is more commonly seen after hip arthroplasty, possibly due to surgical disruption of the bursal wall or increased intra-articular pressure from excess joint fluid. The iliopsoas bursa may

become distended due to any condition that causes excess joint fluid or bursal synovial proliferation. Distended iliopsoas bursae have been associated with hip arthroplasties, arthritis (inflammatory and degenerative), trauma, overuse, osteomyelitis, and metastatic disease. A joint effusion is commonly, but not always, seen at presentation.

The diagnosis of a distended iliopsoas bursa can typically be made with standard CT or MRI, with attention to the anatomic location and communication with the hip joint [92–94]. On ultrasonography, the location and joint communication can be harder to assess [95]. However, ultrasound best evaluates for mass effect on adjacent structures [96]. In cases where an outside institution has labeled the mass as suspicious for a neoplasm, or when the bursal contents are complex in nature, it may be helpful to do an enhanced study to exclude a solid neoplasm. Alternatively, a conventional hip arthrogram can be performed to prove that the bursa communicates with the hip joint. Treatment is usually only necessary if the distended bursa is painful or is impinging adjacent structures. Therapeutic options include treatment of the underlying cause of excess joint fluid (loose prosthesis replacement, anti inflammatory medication), the use of sclerosing agents, and surgical bursectomy.

**CLINICAL HISTORY** A 56-year-old man with left hip pain. Other history withheld.



FIGURE 4.43A



FIGURE 4.43B

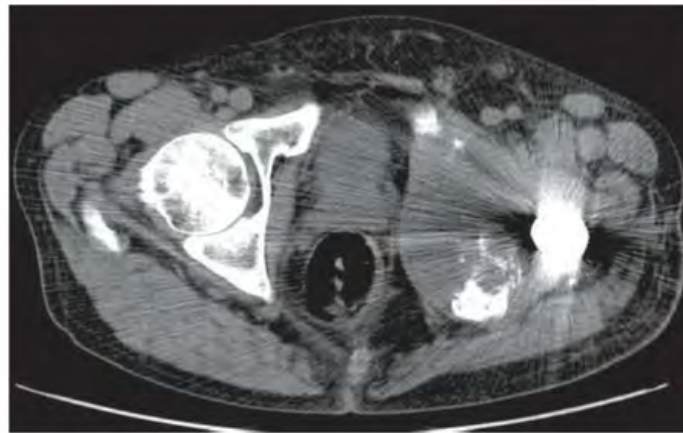


FIGURE 4.43C

**FINDINGS**

- A. AP radiograph of the pelvis shows a left modular bipolar femoral endoprosthesis. Compared with the contralateral side, the left periacetabular region is osteopenic. Loss of cortex at the lateral aspect of the left ischium suggests a destructive process.
- B. AP radiograph of the left hip obtained 4 months earlier shows no bone loss and intact cortex.
- C. CT scan of the pelvis obtained 2 months later shows advanced destructive changes around the acetabulum.

**DIFFERENTIAL DIAGNOSIS** Metastasis, infection, primary bone sarcoma, complex regional pain syndrome, osteolysis.

**DIAGNOSIS** Metastasis (from lung carcinoma).

**DISCUSSION** Comparison to previous imaging is a key strategy for the radiologist, particularly in the area of post-surgical imaging. Modular prosthetic hip components are used exclusively for reconstruction of large portions of the proximal femur. Bipolar and other hemiarthroplasties are

used exclusively for proximal femoral disease, as opposed to hip disease. These two factors suggest that this patient may have had previous resection of a proximal femur for malignant neoplasm. Indeed, this patient was known to have lung carcinoma with previous resection of a metastasis for palliation, following a pathologic fracture of the subtrochanteric portion of the femur. Infection and primary bone sarcoma could also result in destructive changes in the bone, but are much less likely in the clinical circumstance.

Complex regional pain syndrome has been well described following total knee arthroplasty [97], but may also occur following total hip arthroplasty [98]. One might then hypothesize that the bone loss was the result of regional osteoporosis. Osteolysis is a common event in total hip replacement, but is less of an issue in hemiarthroplasties. Although many hemiarthroplasties do not have polyethylene components, bipolar prosthesis have a polyethylene liner between the prosthetic head and neck that allows motion between these two components (hence the name bipolar). Motion may also occur between the prosthetic head and the native acetabulum, reducing the potential wear on the polyethylene.

**CLINICAL HISTORY** A 68-year old man with left hip pain and bilateral total hip replacements.



FIGURE 4.44A

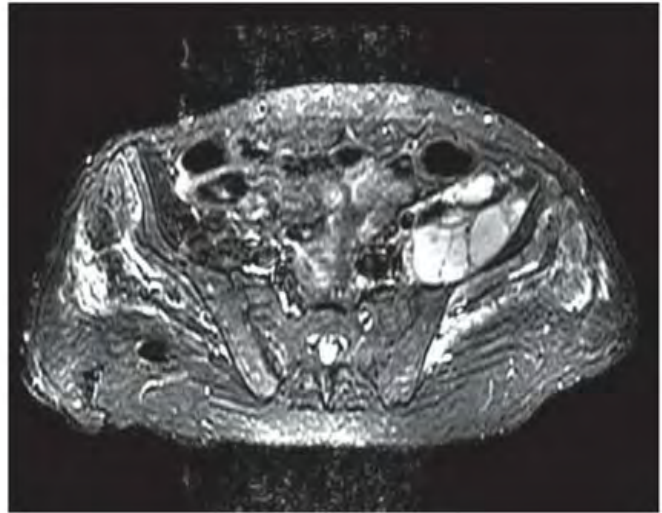


FIGURE 4.44B

### FINDINGS

- A. Coronal proton density MRI demonstrates low signal and artifact from the metallic hip prosthesis. A lobulated fluid collection is seen adjacent to the supra-acetabular region of the iliac bone on the left side, displacing the iliopsoas muscle superiorly.
- B. Axial STIR MRI above the level of the prostheses shows septations in the fluid collection. Abnormal high signal is also seen posterior to the left iliac wing.

**DIFFERENTIAL DIAGNOSIS** Abscess, synovial cyst, hematoma.

**DIAGNOSIS** Abscess from septic hip.

**DISCUSSION** Fluid collections surrounding a total hip replacement may indicate infection. In this case, percutaneous

needle aspiration of the collection produced pus. The use of cross-sectional imaging in the evaluation of complications of total hip replacement has been gaining popularity as techniques for reducing artifacts have improved. In one study, MRI was able to visualize the periprosthetic soft tissues around total hip replacements, including the prosthetic-bone interface, and provided substantially more diagnostic information about osteolysis than radiographs [99]. The prosthesis itself cannot be evaluated by MRI, and because a relatively large metallic object may result in spatial distortion, other means of imaging guidance should be used if percutaneous needle sampling is to be performed. CT also has a role in the assessment of osteolysis and other complications after total hip replacement [100].

**CLINICAL HISTORY** A 32-year old woman who crashed her bicycle 1 week prior to imaging.

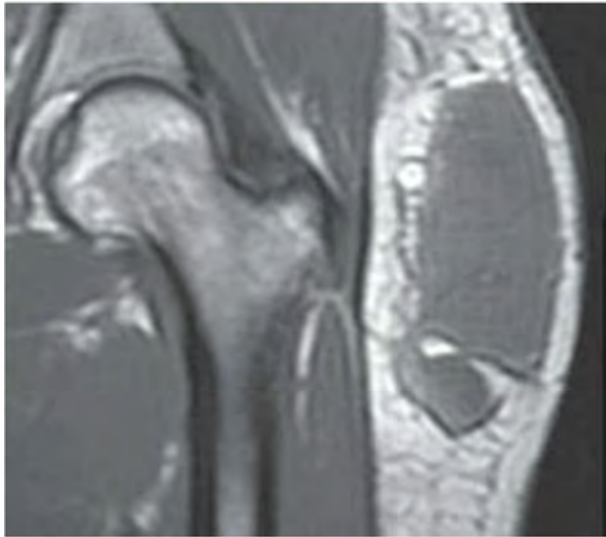


FIGURE 4.45A

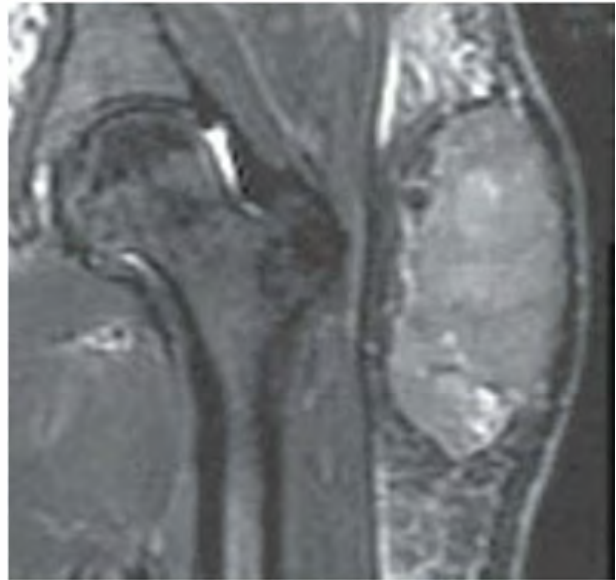


FIGURE 4.45B

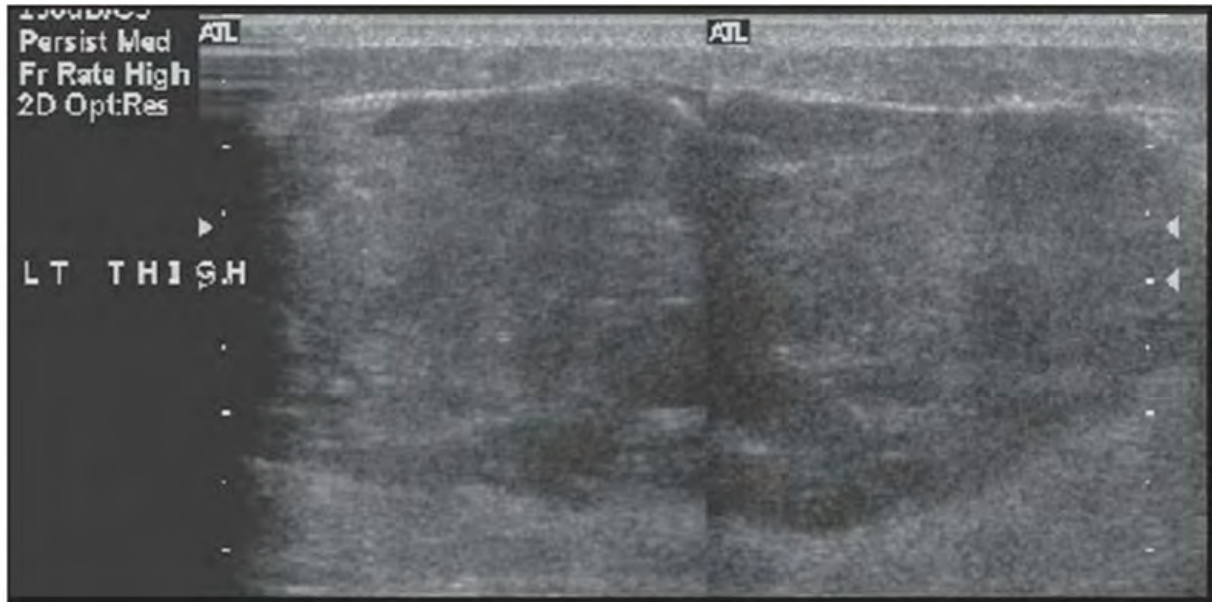


FIGURE 4.45C

### FINDINGS

- Coronal T1-weighted MRI demonstrates a subcutaneous mass of intermediate signal intensity.
- The coronal inversion recovery shows the mass to have heterogeneous increased signal intensity.
- An ultrasound shows mixed echogenicity.

**DIFFERENTIAL DIAGNOSIS** Hematoma, malignant fibrous histiocytoma, soft tissue neoplasm, abscess.

**DIAGNOSIS** Hematoma.

**DISCUSSION** In the clinical context of trauma in a young patient with a new mass, a hematoma would be the most likely diagnosis. However, from a purely imaging perspective, sarcomas and benign soft tissue neoplasms can have a similar appearance to this case, and can be first discovered after trauma. Features that would indicate malignancy include enhancement after contrast administration, internal blood flow on Doppler exam, and failure to decrease in size over time. An abscess would typically have an enhancing rim, complex internal fluid and debris, and surrounding inflammatory change in a patient with systemic symptoms. If the etiology of a mass is unclear, either short-term follow-up or needle biopsy should be performed.

**CLINICAL HISTORY** A 17-year-old girl with episodic bone and joint pain.



FIGURE 4.46

**FINDINGS** AP radiograph of the pelvis reveals patchy osteosclerosis of all visualized bones. Dense sclerosis of both femoral heads is noted, with subchondral collapse.

**DIFFERENTIAL DIAGNOSIS** Sickle cell disease, osteopetrosis, Gaucher disease, trauma, systemic lupus erythematosus, renal osteodystrophy, endogenous or exogenous corticosteroid excess.

**DIAGNOSIS** Sickle cell disease.

**DISCUSSION** Patchy osteosclerosis combined with bilateral osteonecrosis of the femoral heads suggests a systemic disease leading to diffuse bone infarcts. Sickle cell anemia is an autosomal dominant anemia characterized by sickle-shaped erythrocytes and accelerated hemolysis. A single amino acid substitution in the beta hemoglobin chain is responsible. Episodes of microvascular occlusion (“crises”) result in severe bone pain, bone infarcts, and other effects.

Bone infarcts manifest radiographically as regions of sclerosis, where new bone is apposed to infarcted bone when the site becomes revascularized. The process of creeping substitution may replace some infarcted bone, but if the repair is interrupted by repeated episodes of infarction, the bone simply becomes more and more dense. Osteonecrosis of the femoral head is a common complication of sickle cell disease. In one study, 10% of patients with sickle cell disease demonstrated radiographic evidence of unilateral or bilateral osteonecrosis of the femoral head [101]. Collapse of the necrotic femoral head may lead to degenerative arthritis. Treatment may be accomplished with conventional hip replacement arthroplasty [102]. Due to the increased risk of surgical complications, such as high-output congestive failure, intraoperative femoral fracture, infection, blood loss, transfusion reaction, and loosening of prosthesis, alternative methods of treatment have been performed with some success. These include core decompression and acrylic cement injection [103,104].

## SOURCES AND READINGS

1. Farsad K, Kattapuram SV, Sacchi R, Ono J, Nielsen GP. Sacral chordoma. *Radiographics*. 2009;29(5):1525–1530.
2. Diel J, Ortiz O, Losada RA, Price DB, Hayt MW, Katz DS. The sacrum: pathologic spectrum, multimodality imaging, and subspecialty approach. *Radiographics*. 2001;21(1):83–104.
3. Unni KK, Inwards CY. *Dahlin's Bone Tumors: General Aspects and Data on 10,165 Cases*. Philadelphia, PA: Lippincott Williams & Wilkins; 2010:248–261.
4. Unni KK, Inwards CY. *Dahlin's Bone Tumors: General Aspects and Data on 10,165 Cases*. Philadelphia, PA: Lippincott Williams & Wilkins; 2010:7.
5. Mitchell MJ, Logan PM. Radiation-induced changes in bone. *Radiographics*. 1998;18:1125–1136.
6. Kwon JW, Huh SJ, Yoon YC, et al. Pelvic bone complications after radiation therapy of uterine cervical cancer: evaluation with MRI. *AJR Am J Roentgenol*. 2008;191(4):987–994.
7. Harkin JC, Reed RJ. *Tumors of the Peripheral Nervous System*. Washington, DC: Armed Forces Institute of Pathology; 1969:51–97.
8. Siegel MJ. Magnetic resonance imaging of musculoskeletal soft tissue masses. *Radiol Clin North Am*. 2001;39(4):701–720.
9. Giles FJ, O'Brien SM, Keating MJ. Chronic lymphocytic leukemia in (Richter's) transformation. *Semin Oncol*. 1998;25:117–125.
10. Bessudo A, Kipps TJ. Origin of high-grade lymphomas in Richter syndrome. *Leuk Lymphoma*. 1995;18:367–372.
11. Unni KK, Inwards CY. *Dahlin's Bone Tumors: General Aspects and Data on 10,165 Cases*. Philadelphia, PA: Lippincott Williams & Wilkins; 2010:60–91.
12. Murphey MD, Walker EA, Wilson AJ, Kransdorf MJ, Temple HT, Gannon FH. From the archives of the AFIP: imaging of primary chondrosarcoma: radiologic-pathologic correlation. *Radiographics*. 2003;23(5):1245–1278.
13. Donati D, El Ghoneimy A, Bertoni F, Di Bella C, Mercuri M. Surgical treatment and outcome of conventional pelvic chondrosarcoma. *J Bone Joint Surg [Brit]*. 2005;87(11):1527–1530.
14. Unni KK, Inwards CY. *Dahlin's Bone Tumors: General Aspects and Data on 10,165 Cases*. Philadelphia, PA: Lippincott Williams & Wilkins; 2010:122–157.
15. Eftekhari F. Imaging assessment of osteosarcoma in childhood and adolescence: diagnosis, staging, and evaluating response to chemotherapy. *Cancer Treat Res*. 2009;152:33–62.
16. Roovers EA, Boere-Boonekamp MM, Geertsma TS, Zielhuis GA, Kerkhoff AH. Ultrasonographic screening for developmental dysplasia of the hip in infants. Reproducibility of assessments made by radiographers. *J Bone Joint Surg Br*. 2003;85(5):726–730.
17. Mandel DM, Loder RT, Hensinger RN. The predictive value of computed tomography in the treatment of developmental dysplasia of the hip. *J Pediatr Orthop*. 1998;18:794–798.
18. Murphy SB, Kijewski PK, Millis MB, Harless A. Acetabular dysplasia in the adolescent and young adult. *Clin Orthop*. 1990;261:214–223.
19. Yasunaga Y, Takahashi K, Ochi M, et al. Rotational acetabular osteotomy in patients forty-six years of age or older: comparison with younger patients. *J Bone Joint Surg Am*. 2003;85-A(2):266–272.
20. Ganz R, Parvizi J, Beck M, Leunig M, Nötzli H, Siebenrock KA. Femoroacetabular impingement: a cause for osteoarthritis of the hip. *Clin Orthop Relat Res*. 2003;417:112–120.
21. Dodds MK, McCormack D, Mulhall KJ. Femoroacetabular impingement after slipped capital femoral epiphysis: does slip severity predict clinical symptoms? *J Pediatr Orthop*. 2009;29(6):535–539.
22. Nielsen GP, O'Connell JX, Rosenberg AE. Intramuscular myxoma: a clinicopathologic study of 51 cases with emphasis on hypercellular and hypervascular variants. *Am J Surg Pathol*. 1998;22:1222–1227.
23. Iwasko N, Steinbach LS, Disler D, et al. Imaging findings in Mazabraud's syndrome: seven new cases. *Skeletal Radiol*. 2002;31(2):81–87.
24. Kaplan FS, Le Merrer M, Glaser DL, et al. Fibrodysplasia ossificans progressiva. *Best Pract Res Clin Rheumatol*. 2008;22(1):191–205.
25. Semonin O, Fontaine K, Daviaud C, Ayuso C, Lucotte G. Identification of three novel mutations of the noggin gene in patients with fibrodysplasia ossificans progressiva. *Am J Med Genet*. 2001;102(4):314–317.
26. Shore EM, Feldman GJ, Fenstermacher DA, et al. A recurrent mutation in the BMP type I receptor ACVR1 causes inherited and sporadic fibrodysplasia ossificans progressiva. *Nat Genet*. 2006;38(5):525–527.
27. Kocyigit H, Hizli N, Memis A, Sabah D, Memis A. A severely disabling disorder: fibrodysplasia ossificans progressiva. *Clin Rheumatol*. 2001;20(4):273–275.
28. Kussmaul WG, Esmail AN, Sgar Y, Ross J, Gregory S, Kaplan FS. Pulmonary and cardiac function in advanced fibrodysplasia ossificans progressiva. *Clin Orthop*. 1998;346:104–109.
29. Glaser DL, Rocke DM, Kaplan FS. Catastrophic falls in patients who have fibrodysplasia ossificans progressiva. *Clin Orthop*. 1998;356:110–116.
30. Fairbairn KJ, Mulligan ME, Murphey MD, Resnik CS. Gas bubbles in the hip joint on CT: an indication of recent dislocation. *AJR Am J Roentgenol*. 1995;164:931–934.
31. Yue JJ, Wilber JH, Lipuma JP, et al. Posterior hip dislocations: a cadaveric angiographic study. *J Orthop Trauma*. 1996;10:447–454.
32. Erb RE, Steele JR, Nance EP Jr, Edwards JR. Traumatic anterior dislocation of the hip: spectrum of plain film and CT findings. *AJR Am J Roentgenol*. 1995;165:1215–1219.
33. Mithal A, Trivedi N, Gupta SK, Kumar S, Gupta RK. Radiological spectrum of endemic fluorosis: relationship with calcium intake. *Skeletal Radiol*. 1993;22:257–261.
34. Lian ZC, Wu EH. Osteoporosis—an early radiographic sign of endemic fluorosis. *Skeletal Radiol*. 1986;15:350–353.
35. Cao J, Bai X, Zhao Y, et al. The relationship of fluorosis and brick tea drinking in Chinese Tibetans. *Environ Health Perspect*. 1996;104:1340–1343.
36. Boillat MA, Garcia J, Velebit L. Radiological criteria of industrial fluorosis. *Skeletal Radiol*. 1980;5:161–165.
37. Czerwinski E, Nowak J, Dabrowska D, Skolarczyk A, Kita B, Ksiezzyk M. Bone and joint pathology in fluoride-exposed workers. *Arch Environ Health*. 1988;43:340–343.
38. Onur O, Celiker R, Cetin A, Alikasifoglu A, Ugur O, Basgoze O. Hypophosphatemic rickets with sacroiliitis-like presentation in an adolescent. *Scand J Rheumatol*. 1997;26:332–335.
39. Ecklund K, Doria AS, Jaramillo D. Rickets on MR images. *Pediatr Radiol*. 1999;29(9):673–675.
40. Pfirrmann CW, Chung CB, Theumann NH, Trudell DJ, Resnick D. Greater trochanter of the hip: attachment of the abductor mechanism and a complex of three bursae—MR imaging and MR bursography in cadavers and MR imaging in asymptomatic volunteers. *Radiology*. 2001;221(2):469–477.
41. Kingzett-Taylor A, Tirman PF, Feller J, et al. Tendinosis and tears of gluteus medius and minimus muscles as a cause of hip pain: MR imaging findings. *Am J Roentgenol*. 1999;173(4):1123–1126.
42. Wick MR, Siegal GP, Unni KK, McLeod RA, Greditzer HC 3rd. Sarcomas of bone complicating osteitis deformans (Paget's disease): fifty years' experience. *Am J Surg Pathol*. 1981;5:47–59.
43. Lopez C, Thomas DV, Davies AM. Neoplastic transformation and tumour-like lesions in Paget's disease of bone: a pictorial review. *Eur Radiol*. 2003;13(suppl 4):L151–L163.
44. Carter JD. Reactive arthritis: defined etiologies, emerging pathophysiology, and unresolved treatment. *Infect Dis Clin North Am*. 2006;20(4):827–847.
45. Carter JD, Hudson AP. Reactive arthritis: clinical aspects and medical management. *Rheum Dis Clin North Am*. 2009;35(1):21–44.
46. McLauchlan GJ, Gardner DL. Sacral and iliac articular cartilage thickness and cellularity: relationship to subchondral bone end-plate thickness and cancellous bone density. *Rheumatology (Oxford)*. 2002;41(4):375–380.
47. Braun J, Sieper J, Bollow M. Imaging of sacroiliitis. *Clin Rheumatol*. 2000;19(1):51–57.

48. Sturzenbecher A, Braun J, Paris S, Biedermann T, Hamm B, Bollow M. MR imaging of septic sacroiliitis. *Skeletal Radiol.* 2000;29(8):439–446.
49. Lau SM, Chou CT, Huang CM. Unilateral sacroiliitis as an unusual complication of acupuncture. *Clin Rheumatol.* 1998;17(4):357–358.
50. Levine DS, Forbat SM, Saifuddin A. MRI of the axial skeletal manifestations of ankylosing spondylitis. *Clin Radiol.* 2004;59(5):400–413.
51. Ishida T, Iijima T, Moriyama S, Nakamura C, Katagawa T, Machinami R. Intra-articular calcifying synovial sarcoma mimicking synovial chondromatosis. *Skeletal Radiol.* 1996;25:766–769.
52. Ekman EF, Cory JW, Poehling GG. Pigmented villonodular synovitis and synovial chondromatosis arthroscopically diagnosed and treated in the same elbow. *Arthroscopy.* 1997;13:114–116.
53. Sciort R, Dal Cin P, Bellemans J, Samson I, Van den Berghe H, Van Damme B. Synovial chondromatosis: clonal chromosome changes provide further evidence for a neoplastic disorder. *Virchows Arch.* 1998;433:189–191.
54. Davis RI, Hamilton A, Biggart JD. Primary synovial chondromatosis: a clinicopathologic review and assessment of malignant potential. *Hum Pathol.* 1998;29:683–688.
55. Hermann G, Klein MJ, Abdelwahab IF, Kenan S. Synovial chondrosarcoma arising in synovial chondromatosis of the right hip. *Skeletal Radiol.* 1997;26:366–369.
56. Levine DS, Forbat SM, Saifuddin A. MRI of the axial skeletal manifestations of ankylosing spondylitis. *Clin Radiol.* 2004;59(5):400–413.
57. Jang JH, Ward MM, Rucker AN, et al. Ankylosing spondylitis: patterns of radiographic involvement – a re-examination of accepted principles in a cohort of 769 patients. *Radiology.* 2011;258(1):192–198.
58. Al-Nakshabandi NA, Ryan AG, Choudur H, et al. Pigmented villonodular synovitis. *Clin Radiol.* 2004;59(5):414–420.
59. Loughlin J, Dowling B, Chapman K, et al. Functional variants within the secreted frizzled-related protein 3 gene are associated with hip osteoarthritis in females. *Proc Natl Acad Sci USA.* 2004;101(26):9757–9762.
60. Conrozier T, Jousseau CA, Mathieu P, et al. Quantitative measurement of joint space narrowing progression in hip osteoarthritis: a longitudinal retrospective study of patients treated by total hip arthroplasty. *Br J Rheumatol.* 1998;37:961–968.
61. Crawford RW, Gie GA, Ling RS, Murray DW. Diagnostic value of intraarticular anaesthetic in primary osteoarthritis of the hip. *J Bone Joint Surg Br.* 1998;80:279–281.
62. Resnick D. Anatomy of individual joints. In: Resnick D, ed. *Diagnosis of Bone and Joint Disorders*. 4th ed. Philadelphia, PA: Saunders; 2002;708–792.
63. Damron TA, Heiner JP. Rapidly progressive protrusio acetabuli in patients with rheumatoid arthritis. *Clin Orthop.* 1993;289:186–194.
64. Johnson K, Gardner-Medwin J. Childhood arthritis: classification and radiology. *Clin Radiol.* 2002;57(1):47–58.
65. Cohen PA, Job-Deslandre CH, Lalande G, Adamsbaum C. Overview of the radiology of juvenile idiopathic arthritis (JIA). *Eur J Radiol.* 2000;33(2):94–101.
66. Goshen E, Schwartz A, Zilka LR, Zwas ST. Bilateral accessory iliac horns: pathognomonic findings in nail-patella syndrome. Scintigraphic evidence on bone scan. *Clin Nucl Med.* 2000;25(6):476–477.
67. Guerzazi A, de Kerviler E, Cazals-Hatem D, Zagdanski AM, Frija J. Imaging findings in patients with myelofibrosis. *Eur Radiol.* 1999;9(7):1366–1375.
68. Lomansey LM, Martinez S, Demos TC, Harrelson JM. Multifocal vascular lesions of bone: imaging characteristics. *Skeletal Radiol.* 1996;25:255–261.
69. Ishida T, Dorfman HD, Steiner GC, Norman A. Cystic angiomas of bone with sclerotic changes mimicking osteoblastic metastases. *Skeletal Radiol.* 1994;23:247–252.
70. Legeai-Mallet L, Munnich A, Maroteaux P, Le Merrer M. Incomplete penetrance and expressivity skewing in hereditary multiple exostoses. *Clin Genet.* 1997;52:12–16.
71. Wicklund CL, Pauli RM, Johnston D, Hecht JT. Natural history study of hereditary multiple exostoses. *Am J Med Genet.* 1995;55(1):43–46.
72. Bernard SA, Murphey MD, Flemming DJ, Kransdorf MJ. Improved differentiation of benign osteochondromas from secondary chondrosarcomas with standardized measurement of cartilage cap at CT and MR imaging. *Radiology.* 2010;255(3):857–865.
73. Schapira D, Militeanu D, Israel O, Scharf Y. Insufficiency fractures of the pubic ramus. *Semin Arthritis Rheum.* 1996;25:373–382.
74. Pandley R, McNally E, Ali A, Bulstrode C. The role of MRI in the diagnosis of acute hip fractures. *Injury.* 1998;29:61–63.
75. Hill PF, Chatterji S, Chambers D, Keeling JD. Stress fracture of the pubic ramus in female recruits. *J Bone Joint Surg Br.* 1996;78:383–386.
76. Roodman GD. Mechanisms of bone metastasis. *N Engl J Med.* 2004;350(16):1655–1664.
77. Roselli Del Turco M, Palli D, Cariddi A, Ciatto S, Pacini P, Distanti V. The efficacy of intensive follow-up testing in breast cancer cases. *Ann Oncol.* 1995;6(suppl 2):37–39.
78. Vohra R, Kang HS, Dogra S, Sagar RR, Sharma R. Tuberculous osteomyelitis. *J Bone Joint Surg Br.* 1997;79:562–566.
79. Jung NY, Jee WH, Ha KY, Park CK, Byun JY. Discrimination of tuberculous spondylitis from pyogenic spondylitis on MRI. *Am J Roentgenol.* 2004;182(6):1405–1410.
80. Sawlani V, Chandra T, Mishra RN, Aggarwal A, Jain UK, Gujral RB. MRI features of tuberculosis of peripheral joints. *Clin Radiol.* 2003;58(10):755–762.
81. Taconis WK, Schutte HE, van der Heul RO. Desmoplastic fibroma of bone: a report of 18 cases. *Skeletal Radiol.* 1994;23(4):283–288.
82. Bohm P, Krober S, Greschniok A, Laniado M, Kaiserling E. Desmoplastic fibroma of the bone. A report of two patients, review of the literature, and therapeutic implications. *Cancer.* 1996;78:1011–1123.
83. Vanhoenacker FM, Hauben E, De Beuckeleer LH, Willemens D, Van Marck E, De Schepper AM. Desmoplastic fibroma of bone: MRI features. *Skeletal Radiol.* 2000;29(3):171–175.
84. Inwards CY, Unni KK, Beabout JW, Sim FH. Desmoplastic fibroma of bone. *Cancer.* 1991;68:1978–1983.
85. Mahoney CR, Pellicci PM. Complications in primary total hip arthroplasty: avoidance and management of dislocations. *Instr Course Lect.* 2003;52:247–255.
86. Woolson ST, Rahimtoola ZO. Risk factors for dislocation during the first 3 months after primary total hip replacement. *J Arthroplasty.* 1999;14(6):662–668.
87. Yuan L, Shih C. Dislocation after total hip arthroplasty. *Arch Orthop Trauma Surg.* 1999;119(5–6):263–266.
88. Joshi A, Lee CM, Markovic L, Vlati G, Murphy JC. Prognosis of dislocation after total hip arthroplasty. *J Arthroplasty.* 1998;13:17–21.
89. Hirsch HS. Total joint replacement: a cost-effective procedure for the 1990s. *Med Health R I.* 1998;81:162–164.
90. Brander VA, Malhotra S, Jet J, Heinemann AW, Stulberg SD. Outcome of hip and knee arthroplasty in persons aged 80 years and older. *Clin Orthop.* 1997;345:67–78.
91. Weissman BN. Imaging of total hip replacement. *Radiology.* 1997;202:611–623.
92. Pritchard RS, Shah HR, Nelson CL, Fitz Randolph RL. MR and CT appearance of iliopsoas bursal distention secondary to diseased hips. *J Comput Assist Tomogr.* 1990;14(5):797–800.
93. Steinbach LS, Schneider R, Goldman AB, Kazam E, Ranawat CS, Ghelman B. Bursae and abscess cavities communicating with the hip. Diagnosis using arthrography and CT. *Radiology.* 1985;156(2):303–307.
94. Varma DG, Richli WR, Chamsangavej C, Samuels BI, Kim EE, Wallace S. MR appearance of the distended iliopsoas bursa. *Am J Roentgenol.* 1991;156(5):1025–1028.
95. Janus C, Hermann G. Enlargement of the iliopsoas bursa: unusual cause of cystic mass on pelvic sonogram. *J Clin Ultrasound.* 1982;10(3):133–135.
96. Bianchi S, Martinoli C, Keller A, Bianchi-Zamorani MP. Giant iliopsoas bursitis: sonographic findings with magnetic resonance correlations. *J Clin Ultrasound.* 2002;30(7):437–441.
97. Katz MM, Hungerford DS, Krackow KA, Lennox DW. Reflex sympathetic dystrophy as a cause of poor results after total knee arthroplasty. *J Arthroplasty.* 1986;1:117–124.

98. Robbins GM, Masri BA, Garbuz DS, Duncan CP. Evaluation of pain in patients with apparently solidly fixed total hip arthroplasty components. *J Am Acad Orthop Surg*. 2002;10:86–94.
99. Potter HG, Nestor BJ, Sofka CM, Ho ST, Peters LE, Salvati EA. Magnetic resonance imaging after total hip arthroplasty: evaluation of periprosthetic soft tissue. *J Bone Joint Surg Am*. 2004;86-A:1947–1954.
100. Puri L, Wixson RL, Stern SH, Kohli J, Hendrix RW, Stulberg SD. Use of helical computed tomography for the assessment of acetabular osteolysis after total hip arthroplasty. *J Bone Joint Surg Am*. 2002;84-A:609–614.
101. Milner PF, Kraus AP, Sebes JJ, et al. Sickle cell disease as a cause of osteonecrosis of the femoral head. *N Engl J Med*. 1991;325:1476–1481.
102. Al-Mousawi F, Mallik A, Al-Arabi A, Al-Bagali M, Al-Sadadi A, Booz MM. Total hip replacement in sickle cell disease. *Int Orthop*. 2002;26(3):157–161.
103. Styles LA, Vichinsky EP. Core decompression in avascular necrosis of the hip in sickle-cell disease. *Am J Hematol*. 1996;52:103–107.
104. Hernigou P, Bachir D, Galacteros F. Avascular necrosis of the femoral head in sickle cell disease. Treatment of collapse by injection of acrylic cement. *J Bone Joint Surg Br*. 1993;75:875–880.



CHAPTER

# 5

## **Femur and Thigh**

**CLINICAL HISTORY** 20-year-old man with pain in the left proximal thigh following a non-contact football injury.

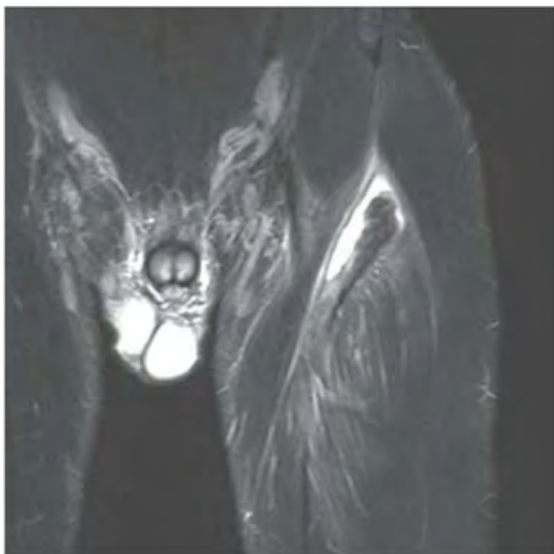


FIGURE 5.1A

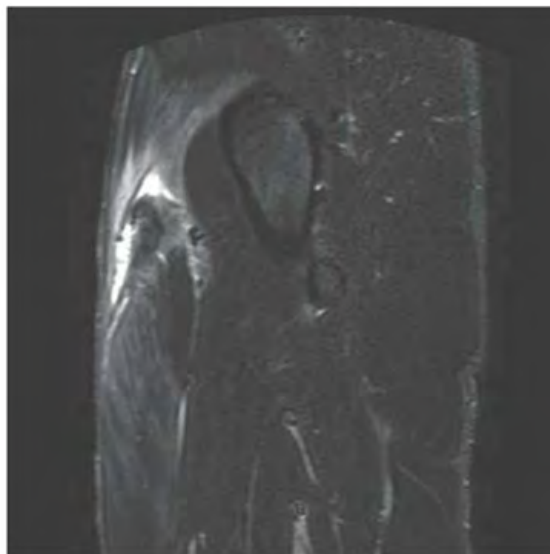


FIGURE 5.1B

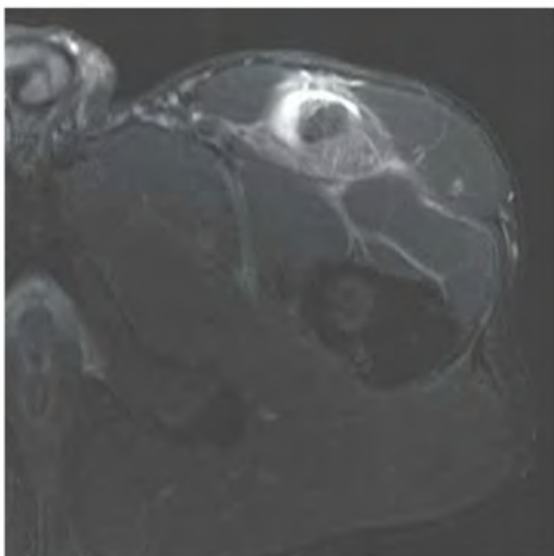


FIGURE 5.1C

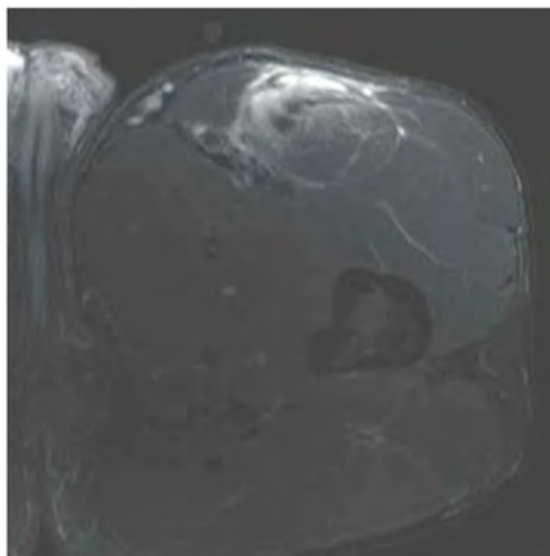


FIGURE 5.1D

## FINDINGS

- A, B. Coronal and sagittal T2-weighted MRI with fat suppression show discontinuity and distal retraction of the proximal rectus femoris tendon. The tendon is thickened and redundant, and is surrounded by fluid. Feathery edema is seen along the musculotendinous junction of the rectus femoris muscle belly.
- C. Axial T2-weighted MRI with fat suppression at the level of the femoral neck shows the thickened and retracted rectus femoris tendon, with surrounding fluid and edema.
- D. Axial T2-weighted MRI with fat suppression at the level of the lesser trochanter shows edema along the musculotendinous junction of the rectus femoris.

**DIFFERENTIAL DIAGNOSIS** none

**DIAGNOSIS** Rectus femoris strain, grade 3.

**DISCUSSION** Rectus femoris muscle has two origins; direct or straight head originating from the anterior inferior iliac spine, and the indirect or reflected head originating from the acetabular rim. Avulsion of the direct head is more common than the avulsion of the indirect head because the direct head is taut in the beginning of hip flexion [1]. In this case, both heads are torn from the origin, with inferior retraction of the muscle belly and associated hematoma. Unlike the other quadriceps muscles, the rectus femoris is both a hip flexor and a knee extensor; it is thus more vulnerable to injury under tension.

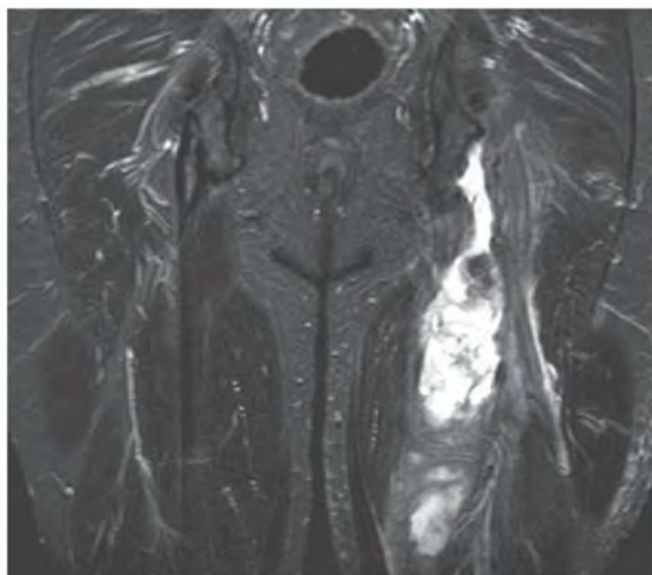


FIGURE 5.2A

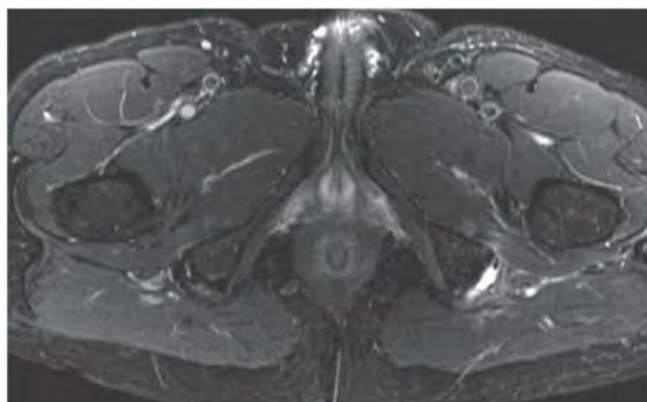


FIGURE 5.2B

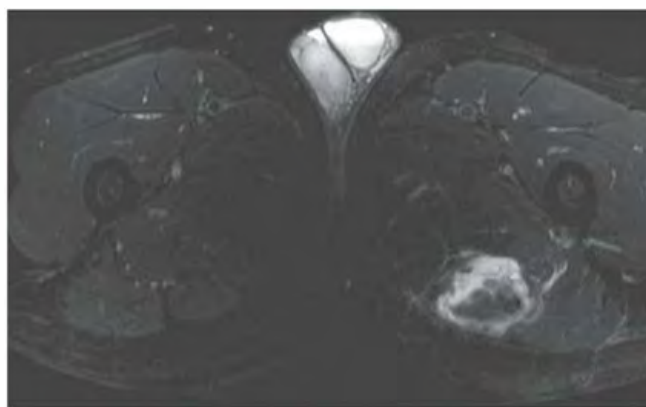


FIGURE 5.2C

**FINDINGS**

- Coronal fat-saturated T2-weighted MRI image shows a long fluid collection containing debris in left medial thigh, inferior to the ischial tuberosity. Normal right hamstrings tendon is seen.
- Axial STIR image at the level of hamstrings insertion at ischial tuberosities shows normal insertion on right, but no tendons at the left.
- Axial STIR image at midthigh level shows the hematoma and retracted left hamstrings muscle.

**DIFFERENTIAL DIAGNOSIS** None.

**DIAGNOSIS** Hamstrings tear with associated hematoma.

**DISCUSSION** The hamstring muscles, located in the posterior thigh, include the long head of biceps femoris, the

semimembranosus, and the semitendinosus. They are major knee flexors and also aid in hip extension. Semitendinosus and biceps femoris tendons insert together as a conjoint tendon whereas semimembranosus tendon inserts just lateral to the conjoint tendon on the ischial tuberosity. Various factors can injure the proximal portions of the hamstring muscles affecting the origin of the hamstrings, including the tendinous enthesis, the underlying ischial tuberosity, and the surrounding tissues [2,3]. Chronic attrition can result in insertional tendinosis and/or small partial tears. In young patients, apophysitis can occur from repeated traction injuries. Abrupt injury at the origin from hip hyperflexion and knee extension results in osseous avulsions of the apophysis in children and proximal tendon ruptures in adults.

**CLINICAL HISTORY** A 62-year-old man with chronic renal failure treated by long-term hemodialysis.



FIGURE 5.3A



FIGURE 5.3B

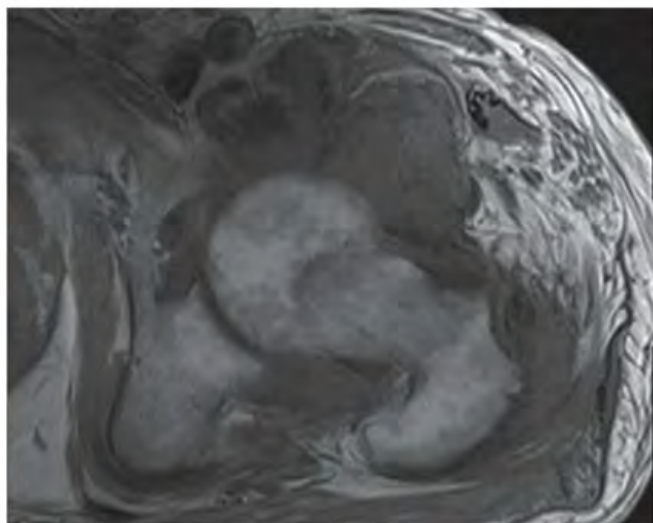


FIGURE 5.3C

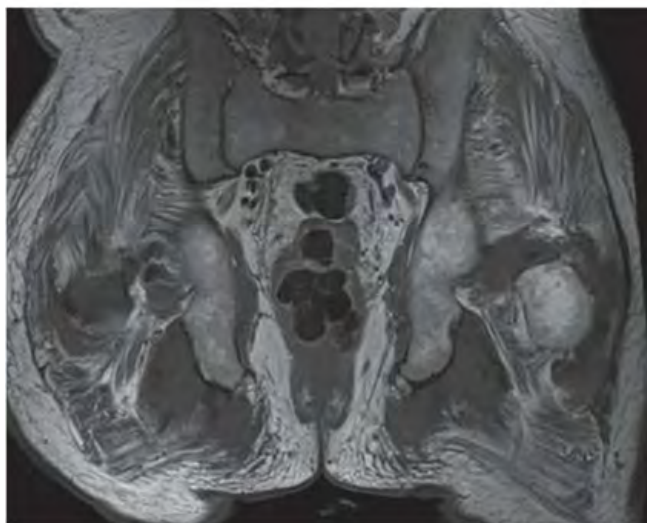


FIGURE 5.3D

**FINDINGS**

- A. Coronal T1-weighted MRI through both hips shows intermediate signal masses surrounding both femoral heads and necks. The underlying bones appear intact. Diffuse muscle atrophy is present.
- B. Coronal T2-weighted fat-suppressed MRI shows that the masses around the hips have low-to-intermediate signal. There is no bone marrow edema.
- C. Axial T1-weighted MRI of the left hip shows intermediate signal masses around the femoral head and neck, with particular prominence anteriorly. Similar masses involve the tendon insertions at the greater trochanter.
- D. Coronal T1-weighted MRI through the ischial tuberosities shows masses involving the bilateral hamstring origins.

**DIFFERENTIAL DIAGNOSIS** Amyloidosis.

**DIAGNOSIS** Dialysis-related amyloidosis.

**DISCUSSION** The differential diagnosis revolves around the distribution of abnormalities. The bilateral symmetry makes

infection and neoplasm very unlikely. The low-to-intermediate T2 signal of the masses suggests a noninflammatory process, and if gadolinium had been given intravenously (contraindicated in renal failure), one might have seen no enhancement; intense enhancement would be expected in a disease such as rheumatoid arthritis. These features and the involvement of joints and tendons suggest a form of chronic deposition disease. The prevalence of dialysis-related amyloidosis is related to the number of years of hemodialysis and is present in virtually all patients who have had 20 or more years of hemodialysis [4]. The underlying pathophysiology is accumulation of a protein in beta-pleated sheets or similar configurations. Unlike other forms of amyloidosis, dialysis-related amyloidosis primarily affects the musculoskeletal system and tends to spare the visceral organs until late in the course. Imaging features include periarticular masses of low-to-intermediate signal on T1- and T2-weighted MRI, pressure erosions of adjacent bone, and masses in tendon and muscle [5]. Other common manifestations include destructive spondyloarthropathy and carpal tunnel syndrome.



FIGURE 5.4

**FINDINGS** Anteroposterior (AP) radiograph of both hips. Both femoral heads are sclerotic and show subchondral fractures of the weight-bearing superior quadrants. Step-off at the lateral margins of both articular surfaces indicates the amount of collapse—a few millimeters in this case. There is relatively little acetabular disease.

**DIFFERENTIAL DIAGNOSIS** Osteonecrosis, osteoarthritis.

**DIAGNOSIS** Osteonecrosis.

**DISCUSSION** The principal differential diagnostic consideration is osteoarthritis. The severity of the femoral head involvement with the relative sparing of the acetabulum indicates that the primary process is in the femoral head rather than the hip joint. Secondary osteoarthritis develops soon after femoral head collapse in osteonecrosis, but that is not yet seen in this case. Some patients with osteonecrosis present with the abrupt onset of hip pain, but femoral neck fracture is generally not a consideration without a history of falling or trauma. Most bones have a dual blood supply through the rich network of vessels that supply the periosteum and the ramifications of the nutrient arteries that supply the endosteum. Portions of bone that are covered with articular cartilage, or that are enclosed within joint capsules, have no periosteum and therefore have only an endosteal blood supply, leaving them more vulnerable to ischemic

infarction. The femoral head is the most important clinical site of osteonecrosis because of its critical weight-bearing function.

Men are affected by osteonecrosis of the femoral head more often than women by a 4:1 ratio, and the usual age range of patients at presentation is 30 to 70 years. Known causes of osteonecrosis include sickle cell disease, Gaucher disease, corticosteroids, trauma, alcoholism, collagen vascular diseases, renal transplantation, and pancreatitis, but many cases are idiopathic [6]. The typical clinical complaint is abrupt onset of hip pain without trauma. In 50% of cases, bilateral involvement is present; bilateral disease is usually asymmetric. After the ischemic event, the infarcted, avascular region becomes revascularized from the periphery, and creeping substitution of devitalized bone occurs. When repair begins, plain films may show an increase in bony density around the periphery of the infarction. This increased peripheral density may slowly progress centrally as repair proceeds. Sometimes the dead bone is incompletely resorbed, and a sclerotic zone remains indefinitely. Because this repair process involves both resorption and replacement of bone, the mechanical strength may decrease transiently, and subchondral insufficiency fractures may result. Insufficiency fractures of the subchondral bone may be recognized by a crescentic lucent zone that separates the fragment. This late segmental collapse of the femoral head may rapidly lead to deformity and secondary osteoarthritis of the hip.



FIGURE 5.5

**FINDINGS** AP radiograph of the pelvis shows bilateral deficiency of the proximal femurs. On the right side, the femur is very short, with presence of only the distal portion. The acetabulum has not developed. On the left side, a small femoral head is present within a shallow acetabulum. The femoral neck and proximal shaft are absent, and the portion of shaft that is present is dysplastic.

**DIFFERENTIAL DIAGNOSIS** Developmental dysplasia of the hip, proximal focal femoral deficiency (PFFD), postsurgical state.

**DIAGNOSIS** Proximal focal femoral deficiency.

**DISCUSSION** Aplasia, present in this case on the right, is not an aspect of developmental dysplasia of the hip. There is no

normal development of the acetabulum or the portions of the femur present, suggesting the abnormality is not postsurgical or otherwise acquired.

PFFD designates a spectrum of developmental deficiencies of the proximal femur, ranging from shortening and varus deformity of the shaft to aplasia of the femoral head, neck, and proximal shaft. Dysplastic changes in the acetabulum correlate with the degree of femoral head deformity or hypoplasia, and they represent the secondary effects of growth in the absence of a normal femoral head and normal weight-bearing stresses. The superior femoral epiphysis is typically mobile within the acetabulum, but in some cases it may be fixed and fused as part of the anomaly [11]. Congenital but not heritable, the cause of PFFD is unknown. The condition is unilateral more frequently than bilateral. When bilateral, it is usually asymmetric.

**CLINICAL HISTORY** A 38-year-old woman with right hip pain. A, radiograph, B, bone scan, and C, MRI at presentation.



FIGURE 5.6A

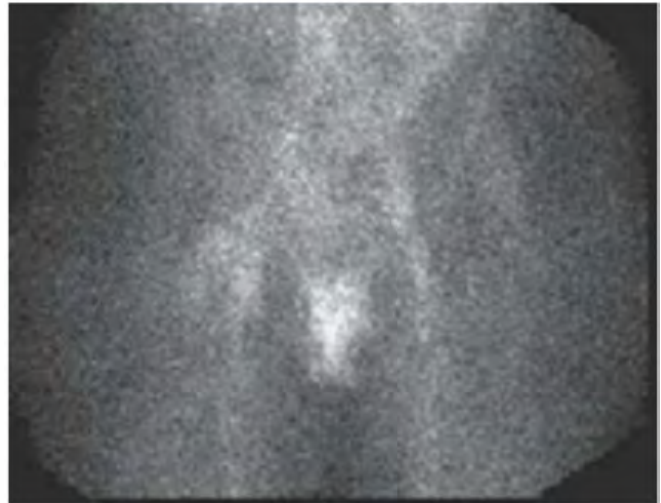


FIGURE 5.6B

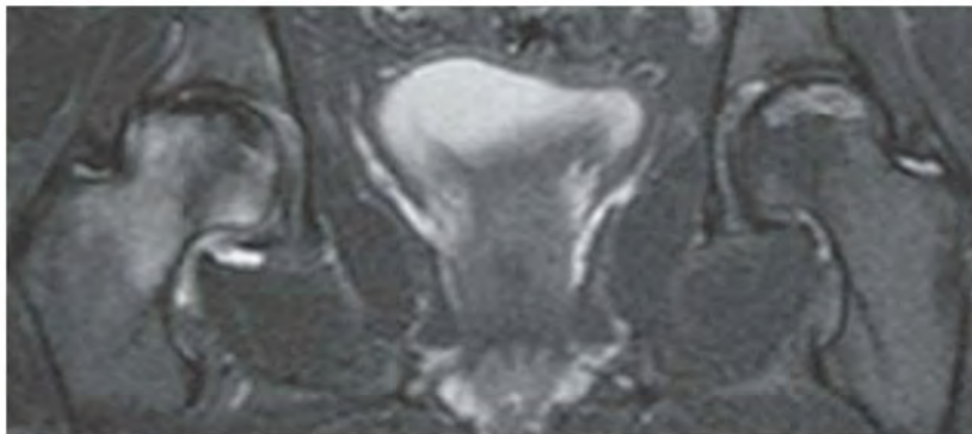


FIGURE 5.6C

## FINDINGS

- A. AP view of the right femoral head showing a crescentic subchondral lucency.
- B. Anterior nuclear medicine blood pool image demonstrating increased radiotracer uptake at the right hip.
- C. Coronal T2-weighted fat-suppressed MRI through both hips shows bilateral abnormalities. On the right side, the normally low-signal fatty marrow of the femoral head and neck shows extensive marrow edema. The very low signal crescentic line along the weight-bearing surface corresponds to the subchondral fracture seen on the radiograph. There is a small right hip effusion. On the left side, there is a serpiginous high-signal line along the weight-bearing portion of the femoral head, with normal low signal from the fatty marrow on both sides of the line.

**DIFFERENTIAL DIAGNOSIS** Osteonecrosis, fracture, septic joint, osteomyelitis, transient osteoporosis.

**DIAGNOSIS** Osteonecrosis.

**DISCUSSION** In this case, the left femoral head shows a region of previous osteonecrosis with repair. The right femoral head is acutely osteonecrotic, with extensive marrow edema. Osteonecrosis begins with interruption of the blood supply to the femoral head. The precise event that initiates the loss of circulation may be unknown, although a large number of clinical conditions appear to be associated with it. One possible event is an increase in intraosseous pressure within the femoral head; when this pressure exceeds the perfusion pressure, blood flow stops. Ischemic necrosis of the marrow and bone follows with the onset of pain, but radiographs

will be normal. Intramedullary pressure measurements of the proximal femur will be elevated. The typical distribution of infarction is a wedge-shaped region under the weight-bearing surface of the femoral head. The articular cartilage itself remains viable, because its nutrition is derived from the synovial fluid. MRI best demonstrates early osteonecrosis [6]. The region of infarction is evident as a loss of the normal bright marrow signal on T1-weighted images. The radionuclide bone scan may show changes of initial loss of radionuclide accumulation in the avascular stage, with subsequent variable

increases in accumulation in the reparative stage. The nuclear scan is less sensitive than MRI and gives poor anatomic detail. The frequent asymmetric bilaterality of osteonecrosis of the femoral head may complicate interpretation of the bone scan.

Initial treatment of osteonecrosis is controversial. The treatment of osteonecrosis of the femoral head focuses on preserving the normal articular surface, typically by core decompression of the neck and head, or placement of a vascularized fibular graft [7]. As one might expect, the earlier the stage at which osteonecrosis is treated, the better the long-term outcome [8].

**CLINICAL HISTORY** A 44-year-old woman with severe right hip pain. A, radiograph, B, bone scan, and C-D, MRI at presentation; E, MRI after 6 weeks.



FIGURE 5.7A



FIGURE 5.7B

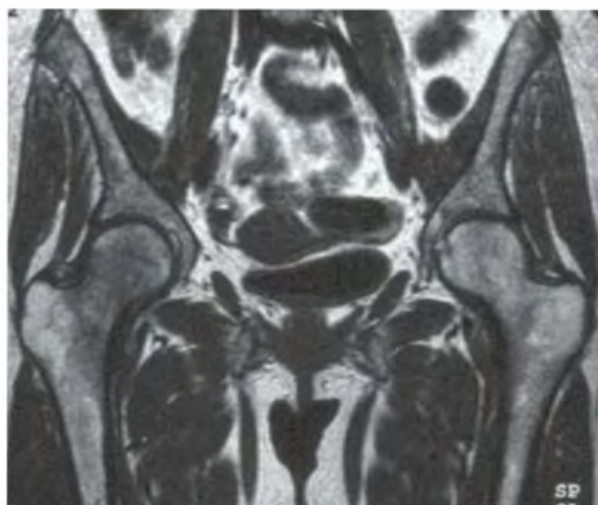


FIGURE 5.7C

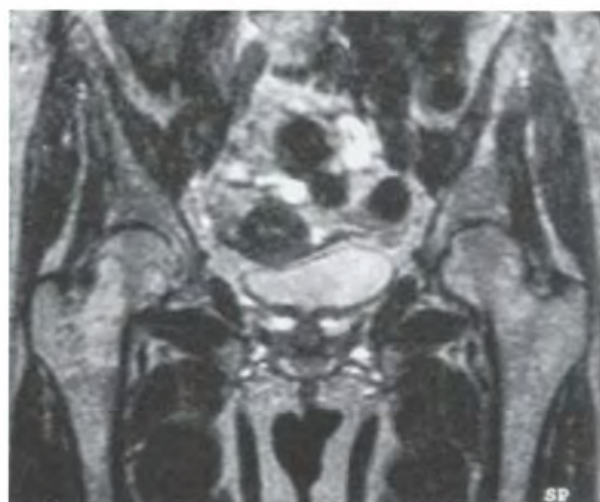


FIGURE 5.7D

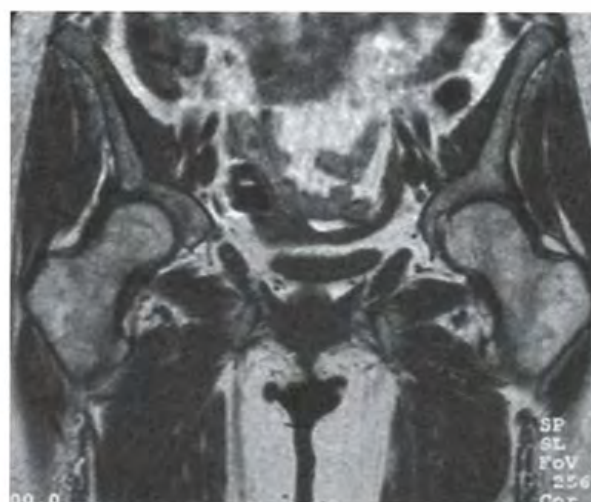


FIGURE 5.7E

## FINDINGS

- A. AP radiograph of the pelvis is normal.
- B. Bone scan shows increased radiotracer uptake in the right femoral head and neck.
- C. Coronal T1-weighted MRI of the hips shows loss of the normal bright marrow signal in the right proximal femur, including the entire head and neck.
- D. Coronal T2-weighted MRI shows edema in the marrow of the entire right proximal femur. There is no effusion in the right hip.
- E. Coronal T1-weighted MRI taken 6 weeks later demonstrates near-complete normalization of marrow signal, indicating resolution of the edema.

**DIFFERENTIAL DIAGNOSIS** Osteonecrosis, transient bone marrow edema, reflex sympathetic dystrophy, osteomyelitis, fracture.

**DIAGNOSIS** Transient bone marrow edema.

**DISCUSSION** In the absence of fracture, the key clinical and radiologic differential diagnosis is between osteonecrosis, which would typically require surgical intervention, and transient bone marrow edema or reflex sympathetic dystrophy, either of which would not. The distinction is clear from the MRI. Transient bone marrow edema is a condition

characterized by a rapidly developing bone marrow edema and osteoporosis, affecting periarticular bone that is self-limited, reversible, and has no clear-cut inciting event. It affects previously healthy middle-aged men and women in the third trimester of pregnancy. Its etiology is still unclear, but in view of similarities to regional migratory osteoporosis and reflex sympathetic dystrophy, vascular and neurologic disturbances have been proposed as the possible pathogenetic mechanisms.

Pain in the hip area and functional disability of the affected limb are the main clinical signs. Diagnosis is supported by local radiologic osteopenia whose gradual disappearance parallels the spontaneous recovery. Transient bone marrow edema usually presents with monoarticular joint pain [9]. It typically involves either hip in men or the left hip in women. Self-limited but aggravated by activity, the pain regresses in 2 to 6 months without permanent sequelae. Radiographs are often normal, but they may show a rapidly developing periarticular osteoporosis, particularly in the femoral head, which returns to normal after resolution of symptoms. MRI shows diffuse edema and hip effusion, but no infarction [10]. Bone scans demonstrate increased activity consistent with the bone marrow edema. The initial site of involvement in regional migratory osteoporosis may be the hip, in which case the initial presentation may have been called transient bone marrow edema (osteoporosis) of the hip.



FIGURE 5.8

**FINDINGS** AP radiograph of the pelvis shows bilaterally small femoral heads with a flattened morphology. Both hips are normally located, but the acetabula are shallow, steep, and dysplastic, to accommodate the abnormal shape of the femoral heads. The femoral necks assume a horizontal orientation but do not appear particularly abnormal in size or shape, given the deformity of the heads. The bones otherwise appear relatively normal.

**DIFFERENTIAL DIAGNOSIS** Multiple epiphyseal dysplasia, spondyloepiphyseal dysplasia, Legg-Calvé-Perthes disease, developmental dysplasia of the hip, slipped capital femoral epiphysis (SCFE), achondroplasia, juvenile chronic arthritis, mucopolysaccharidosis.

**DIAGNOSIS** Multiple epiphyseal dysplasia (dysplasia epiphysealis multiplex).

**DISCUSSION** Bilateral hip disease during childhood may encompass all of the entities in the differential diagnosis. Legg-Calvé-Perthes disease is associated with dysplastic enlargement and flattening of the femoral heads, and juvenile chronic arthritis is associated with epiphyseal overgrowth, cartilage loss, and ankylosis. The hips are normally located, eliminating developmental dysplasia of the hip from further

consideration, and although the patient's age would be typical for SCFE, the radiologic appearance is not. Skeletal changes in the mucopolysaccharidoses may include irregular epiphyses, but biochemical abnormalities will be present clinically, and there is frequent involvement of the thorax and skull, sites that are not affected in multiple epiphyseal dysplasia. The femoral heads in achondroplasia are typically small and dysplastic, with short and disproportionately broad necks, but the absence of bony abnormalities in the pelvis and lumbar spine excludes achondroplasia as a diagnosis in this case. Multiple epiphyseal dysplasia and spondyloepiphyseal dysplasia may be indistinguishable radiographically, except for the absence or presence of spinal column dysplasia. Radiographs of the spine are not included for this case because they were normal.

Multiple epiphyseal dysplasia is a term used to designate a heterogeneous group of disorders that appear to have an abnormality of the epiphyseal chondrocyte in common [12]. Chondrocytes in the growth plates appear to be defective in morphology and organization and deficient in number, with abnormal production of matrix, leading to delayed and disorderly growth and ossification of the ends of the bones. When the hips are involved, the profound loss of growth of the femoral heads results in a markedly decreased range of motion and a waddling gait.



FIGURE 5.9A



FIGURE 5.9B

**FINDINGS**

- A. AP radiograph of the left hip. There are expansile lesions in the ischium. There are dysplastic changes in the left proximal femur, with mild expansion and mineralization. The mineralization has a ground-glass appearance; some portions are curvilinear and densely sclerotic. There is a bowing deformity of the proximal femur.
- B. Follow-up AP radiograph of the left hip after treatment shows osteotomy of the proximal femoral shaft, with intramedullary rod fixation. The bowing deformity has been corrected.

**DIFFERENTIAL DIAGNOSIS** Fibrous dysplasia, Paget disease, osteogenesis imperfecta, osteomalacia.

**DIAGNOSIS** Fibrous dysplasia (with shepherd's crook deformity).

**DISCUSSION** Bowing deformities of the proximal femur in adults include the items in the differential diagnosis. Paget disease can be eliminated because of the young age of the patient, and the lack of cortical thickening and bony enlargement. Osteogenesis imperfecta would affect all bones and would include osteoporosis as a feature. Osteomalacia,

particularly in the setting of renal osteodystrophy, could result in bowing deformity, but other radiologic features should be present. Fibrous dysplasia, both monostotic and polyostotic, commonly involves the proximal femur, and the distinctive shepherd's crook bowing deformity of fibrous dysplasia is illustrated by this case.

Fibrous dysplasia is a benign fibro-osseous lesion that is neither familial nor hereditary, but appears to be a developmental abnormality involving the proliferation and maturation of fibroblasts [13]. Bowing deformities result from biomechanically insufficient bone, and from malunion of pathologic fractures. Orthopedic management is typically restricted to treatment of complications. The results of curettage, bone grafting, and mechanical realignment of proximal femoral lesions are much better in monostotic forms of the disease [14]. Long-term follow-up has shown that bone graft is resorbed and remodeled in fibrous dysplasia.

Malignant transformation has been documented, but it is rare and, in some cases, may have occurred due to previous radiation treatment. Its occurrence has been documented in both polyostotic and monostotic varieties of fibrous dysplasia [15]. These reported secondary sarcomas have been mostly osteosarcomas, but fibrosarcoma, chondrosarcoma, and giant cell sarcoma has also been reported.

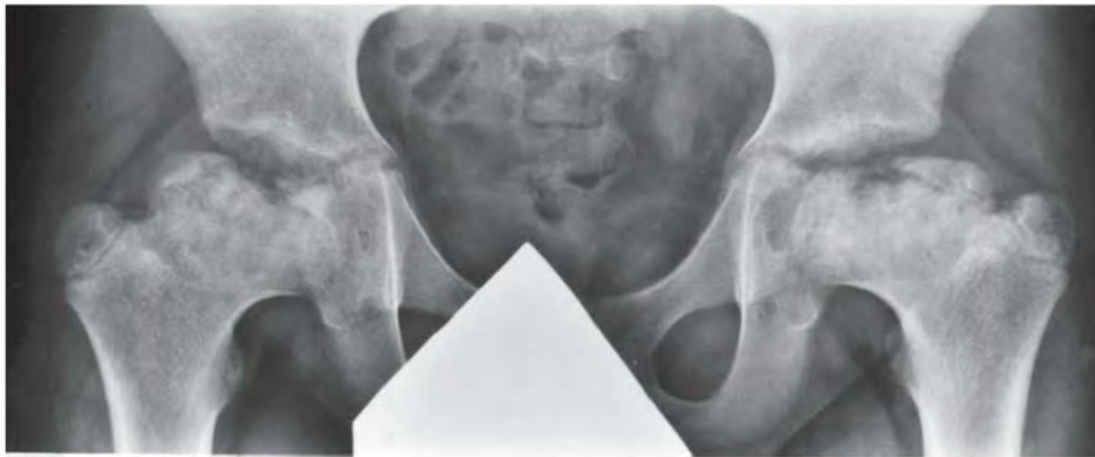


FIGURE 5.10

**FINDINGS** AP radiograph of both hips shows large femoral heads with short broad necks (coxa magna). The femoral heads are too large to fit fully into the acetabula. The capital femoral epiphyses are enlarged and ossifying from multiple centers.

**DIFFERENTIAL DIAGNOSIS** Developmental dysplasia of the hip, epiphyseal dysplasia, Legg-Calvé-Perthes disease, SCFE, juvenile idiopathic arthritis.

**DIAGNOSIS** Legg-Calvé-Perthes disease.

**DISCUSSION** The abnormalities are bilateral and nearly symmetric, and characterized by enlarged, deformed femoral heads. The relatively mild changes in the acetabula suggest the disease is primarily in the femoral heads. Overgrowth of the femoral heads may occur in juvenile idiopathic arthritis, but there is no apparent joint disease seen in this case. Developmental dysplasia of the hip usually presents in infancy, whereas SCFE usually presents in adolescence.

Legg-Calvé-Perthes disease is idiopathic osteonecrosis of the capital femoral epiphysis in a skeletally immature child. Boys are affected more often than girls by a 4:1 ratio. The mean age of onset is 7 years, and the range is 2 to 13 years.

In 20% of cases, the condition is bilateral. The bone age of affected children is usually 1 to 3 years behind their chronological age. Interruption of the blood supply to the femoral head leads to partial or total osteonecrosis. Enchondral ossification of the capital femoral epiphysis and activity at the growth plate both stop. The articular cartilage, nourished by synovial fluid, continues to grow. If the disease is detected at this stage, the ossific nucleus of the capital femoral epiphysis will be smaller than normal, and overgrowth of the articular cartilage will be apparent as joint space widening. The patient may be asymptomatic.

Revascularization of the femoral head leads to centripetal ossification, usually from multiple sites that are not contiguous with the original ossific nucleus, resulting in an appearance often described as fragmentation of ossification. Apposition of new bone to the dead bone may increase the radiographic density of the head. Resorption of subchondral bone may lead to subchondral fracture and the onset of clinical symptoms: hip pain and limp. The severity of the clinical findings is highly variable and does not necessarily correlate with the radiographic findings. The end result is a short, thick femoral neck and an enlarged femoral head (coxa magna). Premature closure of the growth plate accentuates the deformity. Secondary osteoarthritis is a complication in early adult life.

**CLINICAL HISTORY** A 65-year-old man with newly diagnosed prostate cancer.



FIGURE 5.11A



FIGURE 5.11B

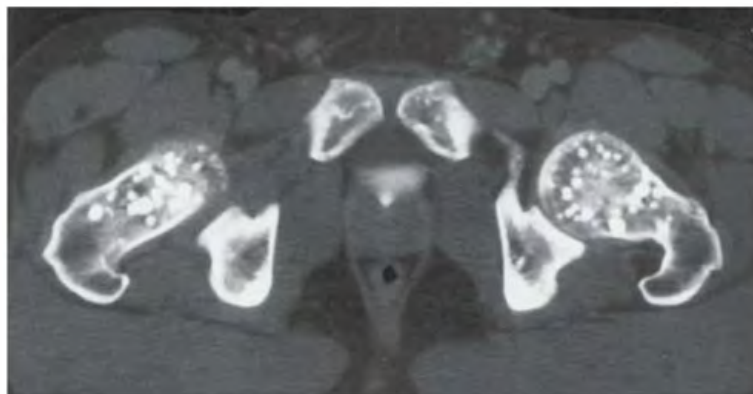


FIGURE 5.11C

### FINDINGS

- A, B. AP radiographs of the hips show multiple oval sclerotic foci present in the femoral head, neck, and intertrochanteric region. A few are noted in the acetabulum.
- C. Axial computed tomography (CT) (bone windows) obtained after intravenous contrast enhancement. There are multiple focal bone densities in the acetabula and proximal femurs on both sides.

**DIFFERENTIAL DIAGNOSIS** Osteopoikilosis, metastatic disease.

**DIAGNOSIS** Osteopoikilosis.

**DISCUSSION** Multiple sclerotic lesions may be seen with metastatic disease, mastocytosis, and occasionally lymphoma.

However, the symmetric periarticular distribution of the sclerotic lesions, their well-defined borders, their uniform size, their oval shape, and their orientation to the long axis of the bone supports the diagnosis of osteopoikilosis. Osteopoikilosis (spotted bones, osteopathia condensans disseminata) is an uncommon osteosclerotic dysplasia with sporadic and familial occurrence. The lesions may increase or decrease in size or number. Symptoms are generally absent or mild, and its discovery is frequently incidental. Histologically identical to bone islands, the lesions have no clinical significance beyond their confusion with osseous metastatic disease [16]. Osteopoikilosis can show increased activity on bone scan [17].

**CLINICAL HISTORY** A 15-year-old boy with right hip pain.



FIGURE 5.12A



FIGURE 5.12B

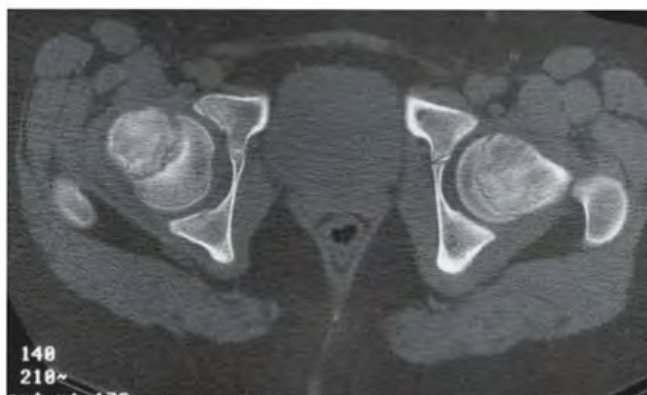


FIGURE 5.12C

## FINDINGS

- A. AP pelvis radiograph shows abnormal right proximal femur. The growth plate appears widened, with irregularity of the metaphyseal margin. The femoral neck appears slightly displaced laterally compared with the capital femoral epiphysis, and an imaginary line drawn along the superior cortex of the femoral neck would not intersect the femoral head (as it would on the normal left side).
- B. Frog lateral radiograph better shows the abnormal displacement and angulation of the femoral neck relative to the femoral head. An imaginary line drawn along the anterior cortex of the neck would completely miss the head, rather than intersect its margin.
- C. Axial CT shows the widened, abnormal growth plate and abnormal alignment of neck and shaft. The growth plate has a rounded contour.

**DIFFERENTIAL DIAGNOSIS** Slipped capital femoral epiphysis (SCFE), healing Salter type I fracture.

**DIAGNOSIS** Slipped capital femoral epiphysis.

**DISCUSSION** SCFE is displacement of the femoral head relative to the femoral neck through the open growth plate in an adolescent. The head remains in the acetabulum as the neck progressively displaces anteriorly and superiorly (the head

goes inferiorly and posteriorly). SCFE occurs in boys and girls of approximately the same skeletal age shortly before closure of the growth plate (chronologic age of about 11 years in girls and 14 years in boys). Boys are affected more often than girls by a ratio of 2.5:1. Many patients are overweight and have mildly delayed skeletal ages. Bilateral involvement is present in about half of the patients, and some cases are familial. The etiology is not known; the pathophysiology may be related to an endocrine process or a biomechanical problem.

The slippage between the femoral head and neck occurs between the proliferative and hypertrophic zones of the growth cartilage, and early abnormalities of the growth plate may be seen on MRI before changes on radiographs [18]. SCFE is different from a Salter type I fracture, which occurs between the hypertrophic and provisional calcification zones of the cartilage. SCFE may be a chronic, slow process that allows bony remodeling of both head and neck as the deformity progresses, or it may be a relatively acute process (usually lasting less than 3 weeks) whose presentation is not unlike that of a stress fracture. SCFE is treated by stabilization of the head without attempt at anatomic reduction. Pins may be used to fix the position of the head and promote closure of the growth plate. Dysplasia of the hip and early osteoarthritis may develop, and osteonecrosis is a devastating complication that is more common in acute slips.



FIGURE 5.13A

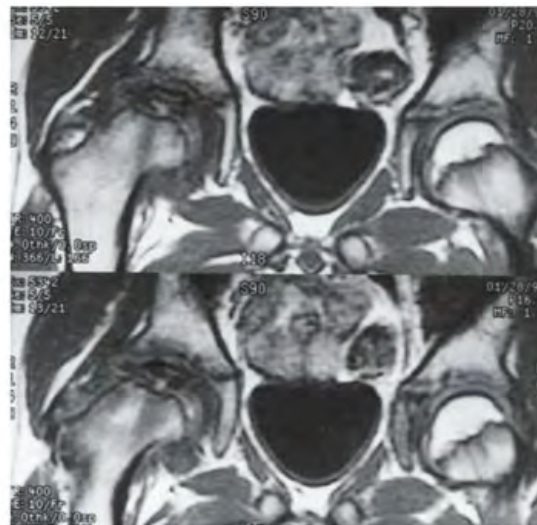


FIGURE 5.13B

**FINDINGS**

- A. AP radiograph of both hips. The right femoral head is sclerotic and diminutive. Periarticular osteoporosis is present.
- B. T1-weighted coronal MRI shows a low-signal-intensity, small, flattened head. Associated marrow edema (dark on T1-weighted MRI) extends into the femoral neck. The opposite hip is normal.

**DIFFERENTIAL DIAGNOSIS** Legg-Calvé-Perthes disease, other cause of femoral head osteonecrosis.

**DIAGNOSIS** Legg-Calvé-Perthes disease.

**DISCUSSION** The therapy goal for Legg-Calvé-Perthes disease is to prevent the development of femoral head deformity and subsequent osteoarthritis. Centering of the femoral head within the acetabulum during the revascularization and

ossification stages of healing presumably allows the acetabulum to act as a mold for the healing femoral head, averting the development of deformity. Acetabular coverage for the femoral head may be obtained by abduction of the femoral head relative to the acetabulum with a brace, varus osteotomy of the proximal femur, or osteotomy of the pelvis. MRI of the hip may be helpful for estimating the extent of epiphyseal necrosis and delineating the morphology of the uncovered, unossified portion of the femoral head for treatment planning [19,20]. The amount of ultimate deformity depends on the age at onset and the remaining growth potential of the femur. The degree of synovitis accompanying Legg-Calvé-Perthes disease appears to correlate with the extent of epiphyseal necrosis and the clinical outcome [21]. Osteonecrosis of the femoral head and other growing epiphyses may occur as a result of trauma, infection, sickle cell disease, or other conditions. The pathophysiology and the gamut of radiologic findings are similar to that of Legg-Calvé-Perthes disease.

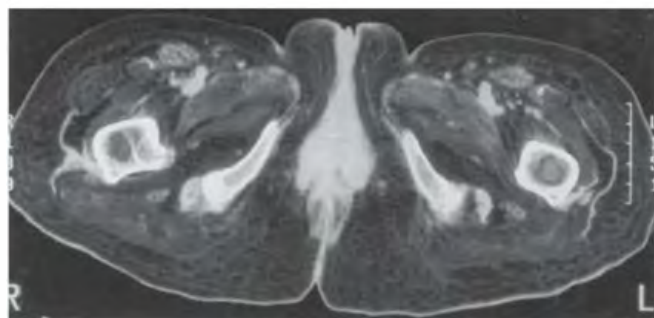


FIGURE 5.14A

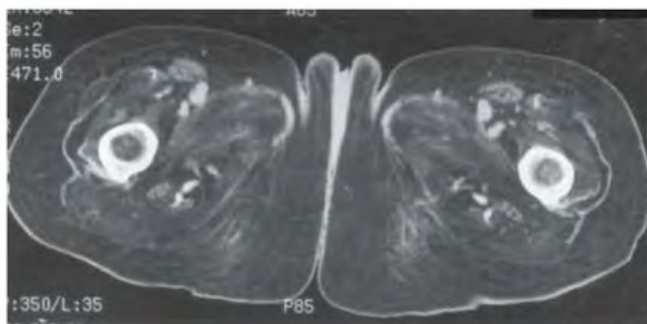


FIGURE 5.14B

**FINDINGS**

A, B. Axial CT through the proximal thigh demonstrates marked fatty replacement of all the visualized musculature. The bones are normal, with hematopoietic marrow in the proximal femurs.

**DIFFERENTIAL DIAGNOSIS** Polymyositis, paralysis, corticosteroid excess, arthrogryposis, muscular dystrophy.

**DIAGNOSIS** Polymyositis.

**DISCUSSION** Fatty replacement of the musculature may occur on a neuropathic basis or a myopathic basis. In this particular case, the diagnosis is polymyositis and there are no specific distinguishing features. There is a lack of the dysplastic bone and joint changes common in arthrogryposis and muscular dystrophy, suggesting a disease process acquired in adulthood. The presence of soft tissue calcification would strongly implicate dermatomyositis or polymyositis, but none is present on these images.

Clinically, patients with polymyositis demonstrate proximal muscle weakness and pain, which may be progressive

or self-limited. This entity may occur with a skin rash (dermatomyositis), Raynaud's phenomenon, other connective tissue diseases (overlap syndromes), and cancers. The latter association is noted more often in elderly men; however, in general, polymyositis is encountered more frequently in women.

Polymyositis is marked by muscle inflammation followed by atrophy and fibrosis. Soft tissue calcifications may occur in the subcutaneous and deep tissues and, when present, may help distinguish this entity from other causes of muscle atrophy. There is progressive atrophy with fatty replacement, as seen here, which may be demonstrated on CT or MRI [22,23]. The soft tissue changes are best assessed with MRI, which shows increased signal intensity on T2-weighted images within the muscle in the acute setting, and fatty replacement in the chronic setting. Although bony changes are not a feature, arthralgias, contractures, and juxta-articular osteoporosis may develop. When bony findings such as erosive changes occur, an overlap syndrome or other connective tissue disorders should be considered. Although the primary target of this entity is skeletal muscle, pulmonary fibrosis, pericarditis, dysphasia, and dysphagia may also be present.

**CLINICAL HISTORY** *Acute hip distress in an infant girl with fever. A, radiograph, and B-C, MRI at presentation; D, radiograph after 6 months.*

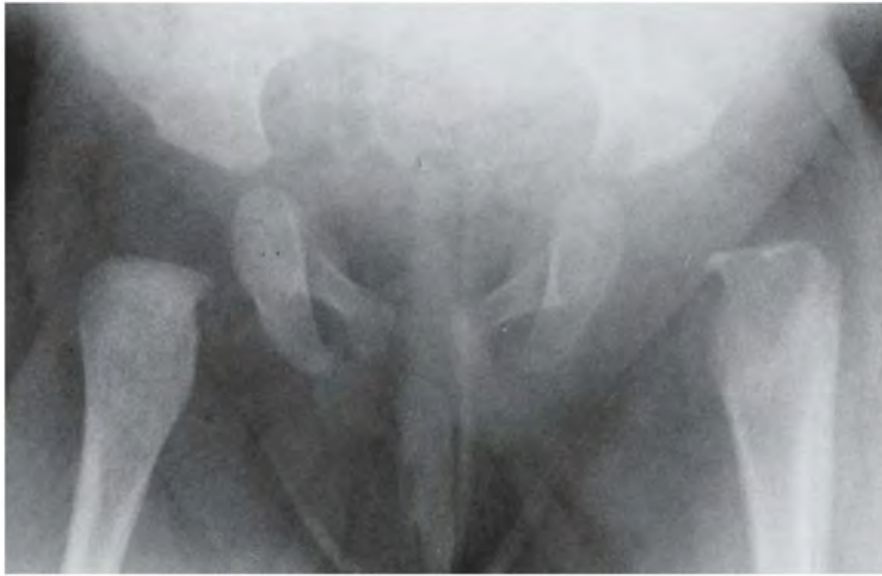


FIGURE 5.15A

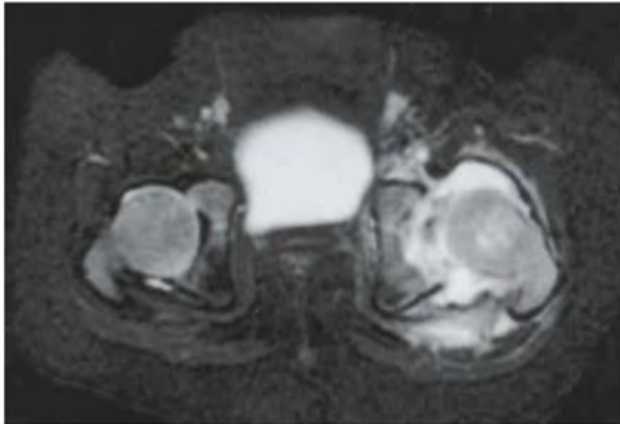


FIGURE 5.15B

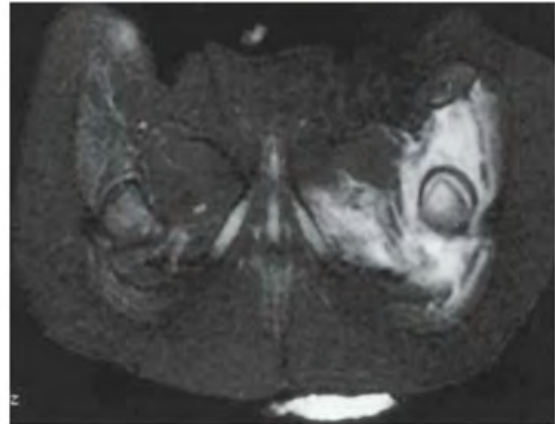


FIGURE 5.15C



FIGURE 5.15D

**FINDINGS**

- A. AP radiographs of the pelvis and femurs show lateral subluxation of left hip and periosteal reaction in the femur.
- B, C. Axial T2-weighted MRI demonstrates marked high-signal fluid in the left hip joint, mixed with low-signal debris. This is causing a secondary lateral subluxation of the left hip. Edema is seen in the musculature and soft tissues surrounding the hip.
- D. AP radiograph taken 6 months later shows delayed ossification of the capital femoral epiphysis, with associated underdeveloped concavity of the acetabulum and broadening of the femoral neck.

**DIFFERENTIAL DIAGNOSIS** Septic arthritis, developmental dysplasia of the hip, Legg-Calvé-Perthes disease.

**DIAGNOSIS** Septic arthritis, with secondary osteonecrosis of the capital femoral epiphysis.

**DISCUSSION** The historical facts in this case make the etiology clear. Lateral subluxation of the hip can be the result of mild developmental dysplasia of the hip, but the clinical presentation and the periosteal reaction along the proximal femur is indicative of infection. In the follow-up radiograph,

the left proximal femur shows the characteristic changes of osteonecrosis of the growing capital femoral epiphysis: delayed ossification (to be followed by ossification from multiple separate centers), dysplastic enlargement, and a short, broad neck. Sometimes distinction of this entity from Legg-Calvé-Perthes or juvenile idiopathic arthritis can be difficult, and additional imaging should be directed by each child's clinical presentation [24,25].

Septic arthritis in young children can result from seeding of the joint through hematogenous spread from a remote source, contiguous spread from osteomyelitis, or direct introduction by penetrating trauma. The knee and hip are the most commonly affected sites, and *Staphylococcus aureus* is the most common organism. The most common presenting sign is that of joint effusion. On sonography, the surrounding capsular structures can be edematous. Juxta-articular osteoporosis quickly ensues due to the aggressive hyperemia. The elicited pannus quickly erodes the cartilage and then bone, leading to joint space loss and associated erosions.

Complications of septic arthritis can include fibrous or osseous ankylosis, synovial cysts, cellulitis or abscesses of the surrounding tissues, osteomyelitis, avascular necrosis, and secondary degenerative joint disease. In this case, the avascular necrosis was presumably a result of an increase in capsular pressure combined with the septic capillary thrombosis.

**CLINICAL HISTORY** A 75-year-old man with left hip pain after a fall.



FIGURE 5.16A

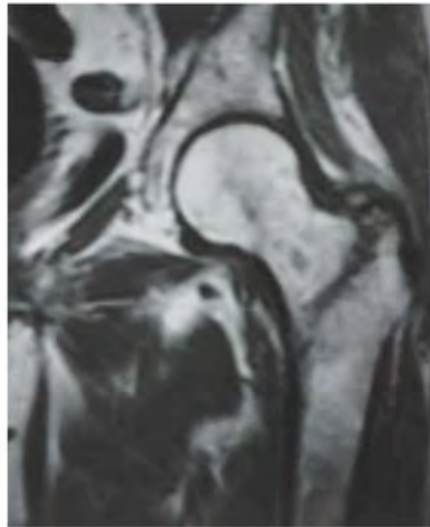


FIGURE 5.16B



FIGURE 5.16C

### FINDINGS

- AP radiograph of the left hip is well positioned (the hip is not externally rotated). The presence of a faint zone of sclerosis in the intertrochanteric region is equivocal and was not prospectively identified as a fracture.
- Coronal T1-weighted MRI shows a line of hypointensity extending in the sagittal plane between the greater and lesser trochanters.
- Coronal T2-weighted, fat-suppressed MRI shows a line of hyperintensity in the intertrochanteric region, thicker superiorly and not quite reaching the medial cortex.

**DIFFERENTIAL DIAGNOSIS** None.

**DIAGNOSIS** Intertrochanteric femur fracture.

**DISCUSSION** The major fracture line of intertrochanteric fractures extends diagonally from superolateral (greater trochanter) to inferomedial (lesser trochanter). Biomechanical analysis of the fracture suggests a bending movement with the lesser trochanter as the fulcrum, as might occur when stumbling off a curb or falling onto the knee. Most

intertrochanteric fractures are comminuted, with the greater and lesser trochanters sometimes present as separate fragments; the lesser trochanter fragment would be the equivalent of a butterfly fragment. Unlike intracapsular femoral neck fractures, these injuries tend to heal promptly and without complication. The incidence of avascular necrosis of the femoral head is about 1%.

Intertrochanteric fractures occur with almost equal frequency in males and females. They occur most frequently in elderly patients older than 75, although they can occur in any age group as a result of massive trauma, such as automobile accidents. Nondisplaced fractures, as seen in this case, are usually two-part in nature and may not be evident on radiographs; even true lateral or oblique views may not show the fracture. MRI is exquisitely sensitive and highly specific in identifying radiographically occult intertrochanteric fractures, and the risk of avascular necrosis as a complication may sometimes be estimated [26,27]. The radionuclide bone scan may not be positive for as many as 4 days [28,29] and is no longer considered an appropriate option in this clinical setting. Treatment consists of open reduction and internal fixation with a dynamic hip screw.



FIGURE 5.17

**FINDINGS** AP radiograph of the pelvis shows osteopenia. The femoral shafts have bowing deformities, and there are horizontal lines with periosteal reactive bone along the medial aspects.

**DIFFERENTIAL DIAGNOSIS** Osteomalacia, osteoporosis, insufficiency fractures.

**DIAGNOSIS** Osteomalacia, with Looser's zones.

**DISCUSSION** Osteomalacia is the adult manifestation of a systemic disease in which the calcification of osteoid is deficient; the childhood counterpart is rickets. The common final pathway in both conditions is the lack of available calcium or phosphorus (or both) for mineralization of osteoid. In rickets, the predominant effect is on the growth plates; in osteomalacia, the predominant effect is on remodeling of mature bone. Dietary deficiency of vitamin D, usually coupled with inadequate exposure to sunlight so that photochemical synthesis of vitamin D in the skin does not occur, results in reduced gastrointestinal calcium absorption, hypocalcemia, and secondary hyperparathyroidism to mobilize calcium from the skeleton.

Pure vitamin D deficiency–induced rickets and osteomalacia is relatively rare in the United States, except among immigrants, food faddists, the institutionalized elderly, and patients on total parenteral nutrition. Other causes include failure of enzymatic conversion of 25-hydroxyvitamin D to its physiologically more active metabolite 1,25-dihydroxyvitamin D, end-organ insensitivity to 1,25-dihydroxyvitamin D, genetic and acquired renal tubular reabsorptive defects, and gastrointestinal malabsorption of dietary calcium or phosphorus.

In the United States, gastrointestinal malabsorption from a variety of etiologies is the most common cause of osteomalacia. It may also be caused by chronic use of anticonvulsant medications or of aluminum-containing antacids. In osteomalacia, the radiologic findings are more subtle than in rickets, because the adult skeleton is less metabolically active. Osteopenia is the predominant appearance, and it may be indistinguishable from osteoporosis unless Looser's zones or bowing deformities are present. Occasionally, the bone texture may be recognized as subtly coarsened. As in osteoporosis, the risk of fractures from trauma escalates with deteriorating bone strength.

**CLINICAL HISTORY** *A young boy with right distal thigh pain for 2 weeks.*



FIGURE 5.18A



FIGURE 5.18B

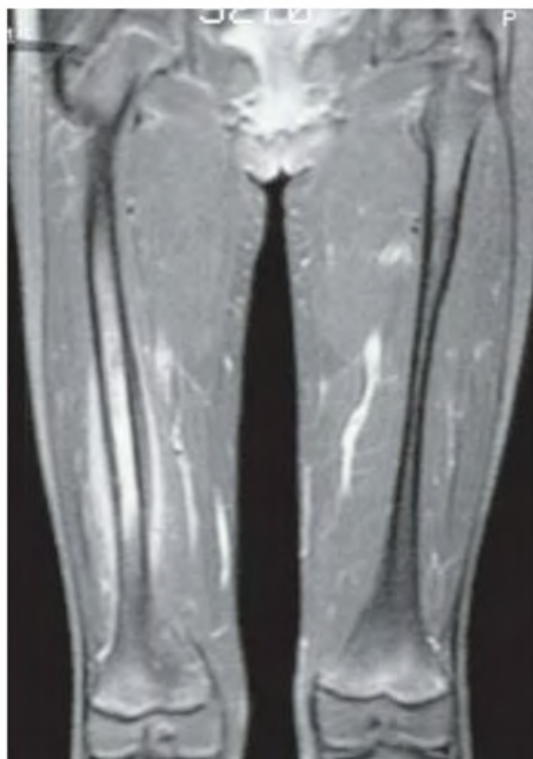


FIGURE 5.18C

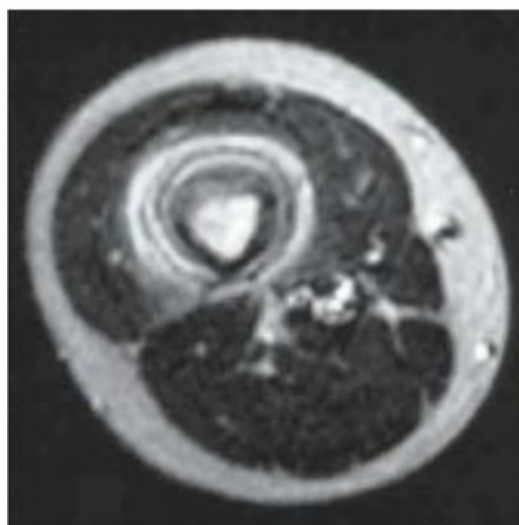


FIGURE 5.18D

## FINDINGS

- A, B. Lateral and AP radiographs of the right femur show a region of cortical thickening and sclerosis involving the middle third of the shaft. Smooth periosteal elevation is present in a single layer.
- C. Coronal inversion recovery MRI of both femurs shows a high-signal-intensity abnormality in the right femoral shaft and surrounding edema. The marrow abnormality has a diffuse margin, with the normal marrow in the proximal and distal shaft. The soft tissue abnormality has tapered margins proximally and distally. It appears symmetric and fusiform in morphology.
- D. Axial T2-weighted MRI through the middle of the lesion shows high signal intensity in the medullary space, in the anterior femoral cortex, and in the surrounding soft tissues. The femur is surrounded by a couple of layers of dark periosteal new bone.

**DIFFERENTIAL DIAGNOSIS** Ewing sarcoma, osteosarcoma, lymphoma, osteomyelitis, stress fracture.

**DIAGNOSIS** Stress fracture.

**DISCUSSION** The exquisite sensitivity of MRI to changes in the bone marrow and soft tissues may lead to an overestimation of the aggressiveness and extent of some benign bone lesions, particularly in children [30,31]. Such lesions include chondroblastoma, osteoid osteoma, eosinophilic granuloma (EG), and stress fractures. Commonly seen potentially misleading MRI features include prominent marrow edema, soft tissue edema, and apparent mass effect adjacent to the bone lesion. Features that these lesions have in common that may explain the MRI findings include associated inflammatory reactions caused by the lesions, and their occurrence in childhood, when the periosteum is attached more loosely.

**CLINICAL HISTORY** A 58-year-old man with recurrent episodes of thigh pain and drainage, separated by decades of good health after a fracture at age 22.



FIGURE 5.19A

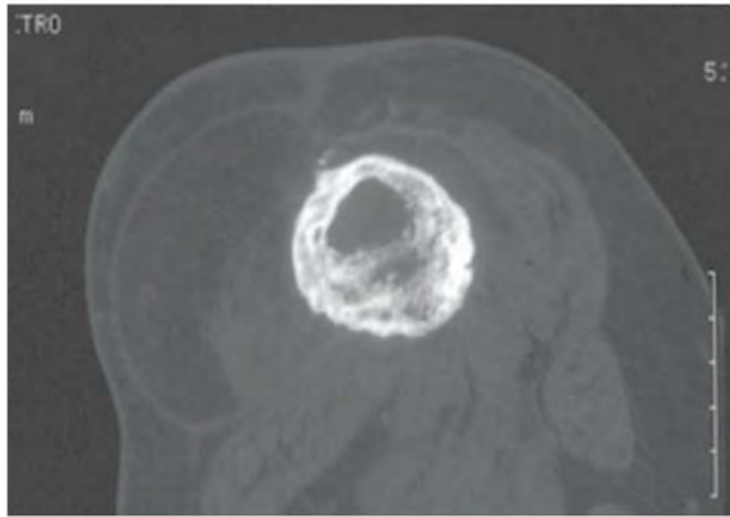


FIGURE 5.19B

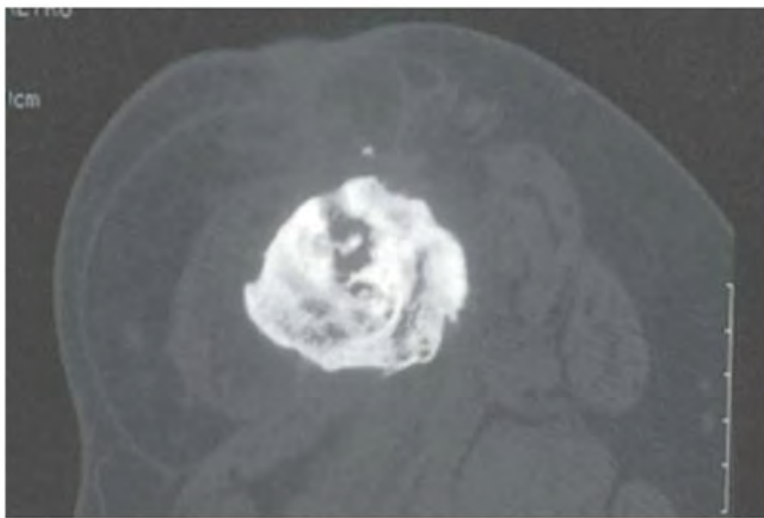


FIGURE 5.19C

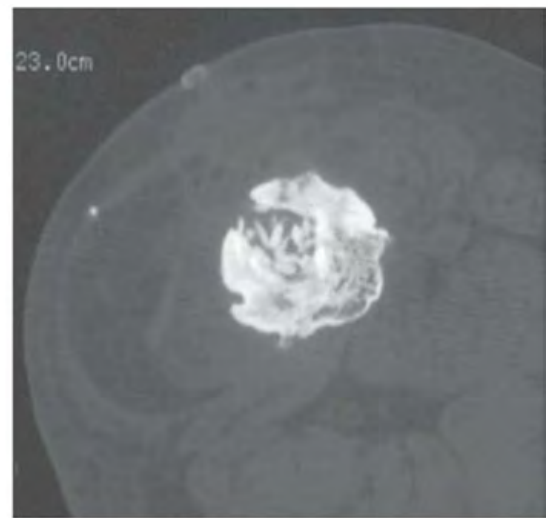


FIGURE 5.19D

**FINDINGS**

- A. Radionuclide bone scan shows intense radionuclide accumulation at the distal femoral shaft on the right.
- B. CT through the femur shows a healed fracture with a central remodeled medullary space that lacks the normal fatty marrow.
- C. Nearby CT slice shows a small opening in the femoral cortex with smooth, remodeled, corticated margins. A sinus tract leading to the skin surface extends from the opening in the cortex.
- D. CT after treatment shows debridement of the femoral cavity and packing with bone chips.

**DIFFERENTIAL DIAGNOSIS** Chronic osteomyelitis, squamous cell carcinoma.

**DIAGNOSIS** Chronic osteomyelitis.

**DISCUSSION**

Chronic osteomyelitis is exceedingly difficult to eradicate, and quiescent, minimally symptomatic periods of many years are not unusual between episodes of sinus tract formation and purulent drainage. Pathogens may persist indefinitely within the interstices of sequestra, inaccessible to systemically administered antibiotics, so the treatment of chronic osteomyelitis is surgical. The main implication of a chronic sinus tract is the potential complication of squamous cell carcinoma [32,33]. Epithelialization of the sinus tract lining may be the initial event, and malignant transformation of this process may lead ultimately to squamous cell carcinoma [34]. The lower extremity is a favored site for chronic osteomyelitis with sinus tract formation.

**CLINICAL HISTORY** A 44-year-old man recently immigrated from Southeast Asia with leg pain and swelling.



FIGURE 5.20A



FIGURE 5.20B

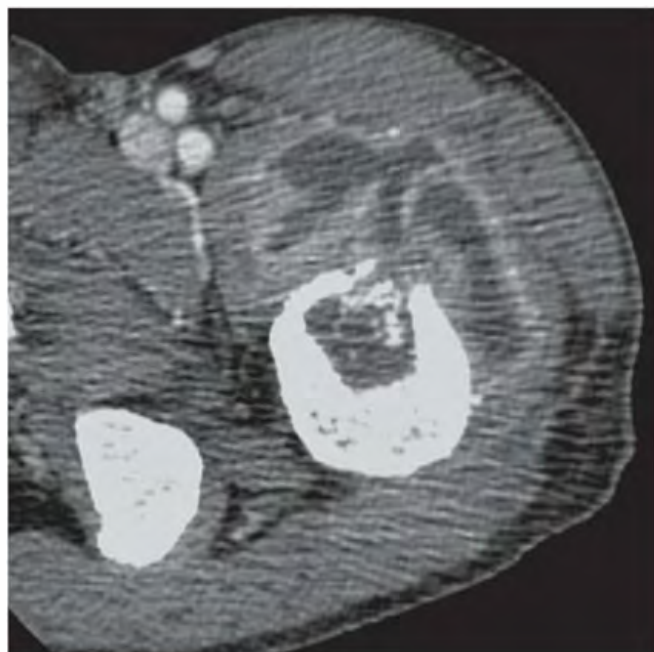


FIGURE 5.20C



FIGURE 5.20D

**FINDINGS** AP (A) and oblique (B) views of left proximal femur shows a geographic lytic lesion in the intertrochanteric region. There is prominent soft tissue swelling around the proximal femur. Axial (C) and sagittal (D) contrast-enhanced CT images show a large rim-enhancing fluid collection in anterior thigh communicating with the intramedullary cavity through the lytic lesion in proximal femur. Within the lytic lesion, there are small foci of ossifications, representing sequestrum.

**DIFFERENTIAL DIAGNOSIS** Chronic osteomyelitis, cystic soft tissue sarcoma.

**DIAGNOSIS** Chronic osteomyelitis (tubercle bacillus).

**DISCUSSION** In chronic osteomyelitis, sequestrum, necrotic bone surrounded by purulent and granulating material, can serve as continuous nidus of bacteria [35]. Cloaca is the

cortical and periosteal defect through which pus drains from the medullary cavity.

Skeletal tuberculosis is rare and usually seen in endemic countries, especially in children (50% of cases in kids between age 1 and 10 years). Although tuberculosis has a lower incidence in the United States and Europe, osteoarticular tuberculosis should always be considered in patients who are very young (less than 10 years) or very old (greater than 80 years) or the immunocompromised, especially in immigrant populations [36]. Ninety to ninety-five percent of cases involve one bone; multifocal cases are rare. It is most often seen with disseminated pulmonary infection [37]. Most common (50%) lesions are found in the spine; 30% in hip or knee and 10% sacroiliac joints.

This case of isolated femoral tuberculosis in an immunocompetent 44-year-old man without pulmonary or spine involvement was successfully treated with abscess drainage, femoral lesion curettage, and intramedullary rod fixation along with the standard TB pharmacotherapy.

**CLINICAL HISTORY** A 64-year-old woman with right thigh pain for several months. She has been taking bisphosphonate medication for several years.



FIGURE 5.21A

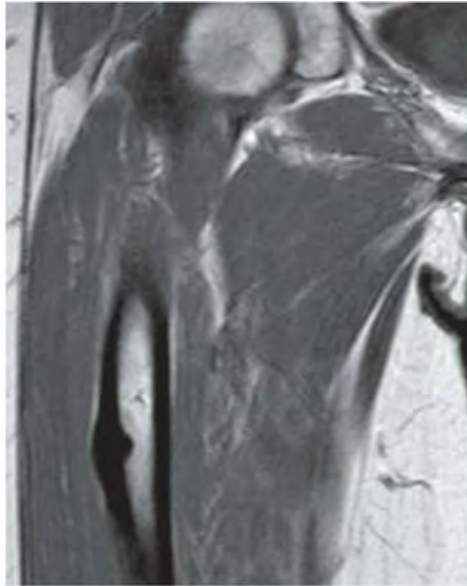


FIGURE 5.21B



FIGURE 5.21C

### FINDINGS

- A. AP radiograph of the right hip shows focal triangular-shaped cortical thickening in lateral femoral cortex in the subtrochanteric region.
- B. Coronal T1-weighted MRI shows abnormal cortical thickening in the lateral subtrochanteric femoral cortex that extends both periosteally and endosteally.
- C. Coronal fat-saturated T2-weighted MRI shows endosteal high signal adjacent to the cortical thickening.

**DIFFERENTIAL DIAGNOSIS** Stress fracture, bisphosphonate-related fracture.

**DIAGNOSIS** Bisphosphonate-related fracture.

**DISCUSSION** There have been an increasing number of reports of atypical subtrochanteric femur fractures in

women who have been undergoing bisphosphonate therapy, ironically for postmenopausal osteoporosis, for usually more than 3 years [38]. Bisphosphonates are known to inhibit osteoclastic activity and are thought to inhibit normal bone remodeling. It has been hypothesized that this lack of normal remodeling leads to a mound of abnormal cortical bone in lateral cortex of subtrochanteric femur [39]. With no or little trauma, these patients may develop transverse insufficiency fractures (abnormal bone fracturing under normal stress) at a location where stress fractures typically do not occur. Fifty to sixty percent of patients have bilateral disease. Sudden catastrophic completion of these fractures may occur with minimal provocation. Atypical insufficiency fractures have also been reported in patients receiving bisphosphonates for treatment of osteolytic metastases [40]. Some controversy has accompanied the reports of bisphosphonate-related fractures [41].

**CLINICAL HISTORY** A 54-year-old woman on chronic hemodialysis for renal failure. A, radiograph at presentation, B, radiograph after 2 weeks of treatment.



FIGURE 5.22A



FIGURE 5.22B

### FINDINGS

- A. AP hip radiograph shows an amorphous calcific mass overlying the greater trochanter.
- B. Follow-up radiograph taken after 2 weeks of treatment.

**DIFFERENTIAL DIAGNOSIS** Tumoral calcinosis, chondrosarcoma, synovial sarcoma, osteosarcoma, myositis ossificans, synovial osteochondromatosis.

**DIAGNOSIS** Periarticular calcinosis (tumoral calcinosis, metastatic calcification).

**DISCUSSION** If we consider only the initial radiograph and ignore the clinical history, the radiologic differential diagnosis is that of a densely mineralized soft tissue lesion

surrounding the proximal femur. The underlying bone is intact, and the morphology of the calcifications is not that of osteoid (which would be very dense and cloud-like), cartilage (rings and arcs), myositis ossificans (peripheral), or sarcoma (dystrophic). Rather, the calcifications in aggregate have a multilocular structure like a bunch of grapes, and the individual clumps have a cystic appearance, like milk of calcium. The clinical history and the rapid improvement with treatment (by modification of the dialysate) clinches the diagnosis. Metastatic soft tissue deposits of calcium found around joints in patients on dialysis for chronic renal failure is in the form of hydroxyapatite. Because the crystals are often aqueous suspensions (milk of calcium), CT and upright radiographs may demonstrate fluid-sediment levels [42].



FIGURE 5.23A



FIGURE 5.23B

**FINDINGS** AP (A) and lateral (B) femur radiographs show multiple lytic lesions of varying size.

**DIFFERENTIAL DIAGNOSIS** Multiple myeloma, metastases, lymphoma.

**DIAGNOSIS** Multiple myeloma.

**DISCUSSION** Multiple myeloma is a malignant neoplasm of plasmacytes, the cells of the bone marrow that make immunoglobulins. Myeloma arises in the bone marrow and involves it diffusely. Bony abnormalities usually occur at multiple sites, including the vertebrae in 66% of patients, the ribs in 45%, the skull in 40%, the shoulder girdle in 40%, the pelvis in 30%, and the long bones in 25% of patients. Myeloma lesions are sharply defined, purely lytic areas of bone destruction with no reactive bone formation. The pattern of destruction may be geographic, moth-eaten, or permeated; involvement may be so diffuse that the bones will be simply osteopenic or even normal in radiographic appearance. The lesions may be expansile, may penetrate the cortex, and may form large extraosseous soft tissue masses. Pathologic fractures are common. The plain film skeletal survey is a better method for disclosing sites of

bone destruction than the radionuclide bone scan, but MRI shows the replacement of the normal marrow by myeloma tissue in a diffuse or multifocal pattern, and is currently the most sensitive study for detection of multiple myeloma lesions in bone [43,44].

Several differential points may help distinguish between multiple myeloma and osseous metastases in a patient with multiple destructive bone lesions. Myeloma tissue produces a number of osteoclast-stimulating factors resulting in bone destruction that is cleanly margined and purely lytic. Although metastases also produce osteoclast-stimulating factors, they tend to provoke reactive bone, frequently resulting in a more ragged and irregular appearance. Myeloma may involve the intervertebral discs and the mandible, but metastases rarely do. Metastases often involve the vertebral pedicles, but myeloma rarely does. A large soft tissue mass is more likely to be present with myeloma than with metastases. The bone scan is usually positive in the presence of bone metastases and often negative in myeloma. Bisphosphonates have been advocated for reducing the incidence of pathologic fractures and skeletal pain in patients with multiple myeloma [45]. Bisphosphonates stabilize the hydroxyapatite crystalline structure of newly formed bone and interfere with osteoclastic resorption.



FIGURE 5.24A



FIGURE 5.24B

**FINDINGS**

- A. AP radiograph of the femur. The middle third of the femoral shaft is involved by a densely mineralized lesion that fills the medullary cavity. More proximally, there is a second, small, round intramedullary lesion in the subtrochanteric region. There is no evidence of cortical expansion or breakthrough, and no periosteal reaction.
- B. Detail of anterior whole-body radionuclide bone scan. There is markedly increased uptake of the radiotracer in these two areas, relative to normal cortex and medullary space.

**DIFFERENTIAL DIAGNOSIS** Osteosarcoma, Ewing sarcoma, lymphoma.

**DIAGNOSIS** Osteosarcoma with skip metastasis.

**DISCUSSION** Any blastic bone lesion in the femur of a child or adolescent should raise concern for osteosarcoma. Although osteosarcomas are relatively uncommon, they may have a range of different radiologic appearances that may be mistaken for a variety of benign lesions, and vice versa. The presence of a small, proximal satellite lesion in the same bone

raises the differential diagnosis of blastic lesions in children that may produce skip metastases. In addition to osteosarcoma, the differential diagnosis includes Ewing sarcoma and lymphoma. Both Ewing sarcoma and lymphoma tend to cause permeated bone destruction and raise successive layers of periosteum as they penetrate the cortex to form soft tissue masses, features that are absent in this case. In addition, the dense, blastic appearance of this lesion would be unusual for either Ewing sarcoma or lymphoma.

Osteosarcoma is the most common primary malignant bone-forming neoplasm. Metaphyseal sites about the knee are the most common location, but diaphyseal or epiphyseal involvement is seen in approximately 20% to 30% of cases, and diaphyseal or epiphyseal tumor without metaphyseal involvement may be seen in 10% to 20% of cases. This tumor demonstrates avid uptake of radionuclide on conventional bone scanning, even in metastatic foci outside of bone. Skip lesions are not considered metastatic per se, but represent intramedullary spread of tumor. The frequency of skip lesions has been reported from less than 2% to about 20% [48]. Skip metastases may also occur in Ewing sarcoma [49]. The extent of tumor involvement is best assessed with MRI [50].

**CLINICAL HISTORY** A 49-year-old woman with right leg pain.



FIGURE 5.25A



FIGURE 5.25B

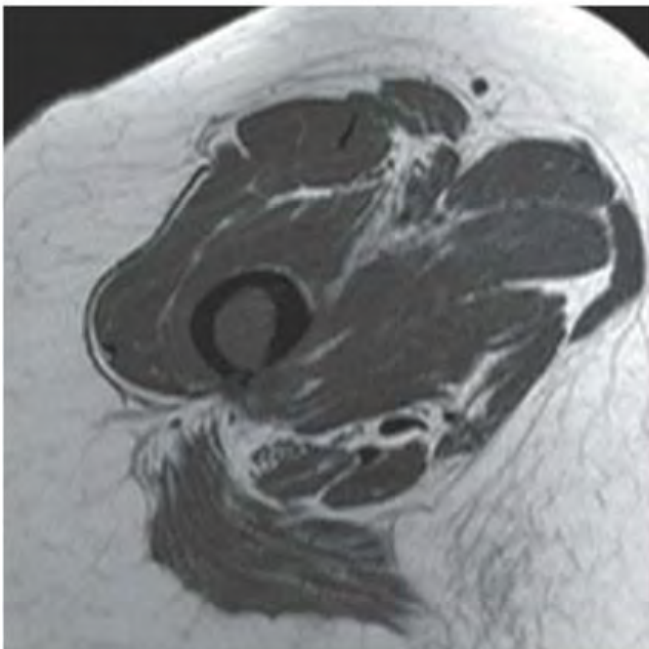


FIGURE 5.25C

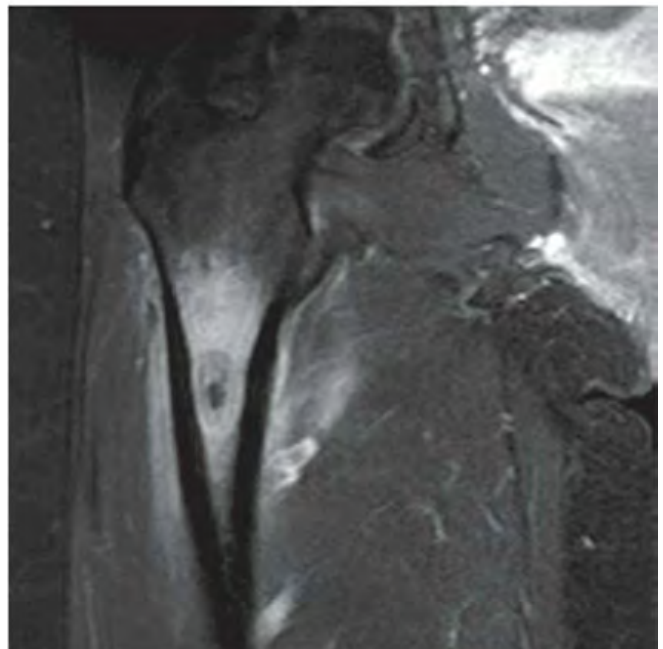


FIGURE 5.25D

**FINDINGS** AP (A) and frog lateral (B) views of the right hip show a geographic lytic lesion without sclerotic margin in proximal diaphysis of femur in the subtrochanteric region. There is focal cortical breakthrough on the posteromedial femur. On axial T1-weighted MR image (C), the lesion is isointense to muscle without associated soft tissue mass. (D) Coronal STIR image shows extensive bone marrow edema around this lesion. There is a small amount of adjacent soft tissue edema without a drainable fluid collection.

**DIFFERENTIAL DIAGNOSIS** Osteomyelitis, metastasis, multiple myeloma, lymphoma, eosinophilic granuloma (EG).

**DIAGNOSIS** Eosinophilic granuloma.

**DISCUSSION** Langerhans cell histiocytosis (LCH), previously called histiocytosis X, includes a spectrum of diseases that involve idiopathic abnormal proliferation of histiocytes. Most commonly, this disease presents as a focal lytic osseous

lesion, also called EG, constituting 1% of biopsied primary bone tumors [46]. EG occurs mostly in young patients (less than 30 years old) with slight male preference. Osseous EG lesions occur mostly in the flat bones such as skull, ribs, and pelvis. About 30% of EG lesions occur in long bones. Whereas in the long bones, EG can appear as well-defined geographic lytic lesions, EG lesions can be more permeative in appearance in the ribs, while skull lesions have the “beveled edge” appearance. In the long bone lesions, there may be associated lamellated periosteal reaction.

In general, LCH patients are categorized into those with single-site disease in single system, those with multifocal disease in single system (e.g., bone, lung), or those with multisystemic disease [47]. Systemic forms of LCH include Letterer-Siwe disease (acute disseminated form accounting for 10% of LCH cases) in infants with lymphadenopathy, splenomegaly, and rash and Hand-Schüller-Christian disease (chronic disseminated form accounting for 20%) in young kids (age 1 to 5 years) with exophthalmos and diabetes insipidus.



FIGURE 5.26A



FIGURE 5.26B

**FINDINGS**

- A. AP femur radiograph at presentation shows layered periosteal reaction and thickening of the femoral cortex. A soft tissue mass surrounds the femur.
- B. AP radiograph of the femur after treatment shows an intramedullary rod in place. A large fusiform bony mass surrounds the femur, with both layered and sunburst periosteal reaction.

**DIFFERENTIAL DIAGNOSIS** Ewing sarcoma, osteosarcoma, lymphoma, osteomyelitis, stress fracture.

**DIAGNOSIS** Ewing sarcoma.

**DISCUSSION** The aggressive appearance of this lesion suggests a malignant lesion such as round cell tumor, osteosarcoma, or lymphoma, or a benign lesion with aggressive features such as acute osteomyelitis. Stress fractures of the long bones in children heal with periosteal callus that may be mistaken for the periosteal reaction to tumor or infection. Hematogenous osteomyelitis spreads through bone in a fashion similar to Ewing sarcoma, leading to a superficially similar radiologic appearance, but the diaphyseal rather than metaphyseal location strongly favors tumor rather than

infection. Both may occur in the same age group and have similar clinical presentations.

Ewing sarcoma is a tumor consisting of small, round, undifferentiated cells, probably of neuroectodermal histogenesis. Although 75% of Ewing sarcomas occur in patients less than 20 years old, these lesions may develop at any age. They are the most common primary bone tumor in the first decade of life, and the second most common (behind osteosarcoma) in the second decade. Patients present with local pain and swelling, fever, anemia, and elevated erythrocyte sedimentation rate; the clinical impression is often that of osteomyelitis. Up to 30% of patients will have metastases at presentation. Ewing sarcoma may develop in practically any bone, although the majority of cases involve the sacrum, innominate bone, and long bones of the lower extremities. Only 3% of tumors affect the hands and feet. Most Ewing sarcomas are found in the metadiaphysis of long bones, mostly the femur, but they also occur in the diaphysis and metaphysis. In the long bones, the typical radiographic appearance is that of permeated intramedullary bone destruction with periosteal reactive bone. Treatment is typically radiotherapy, often combined with surgery and chemotherapy. After treatment, response to radiotherapy can be followed by enhanced MRI and positron emission tomography (PET) [51], although the role of PET is still under investigation [52].

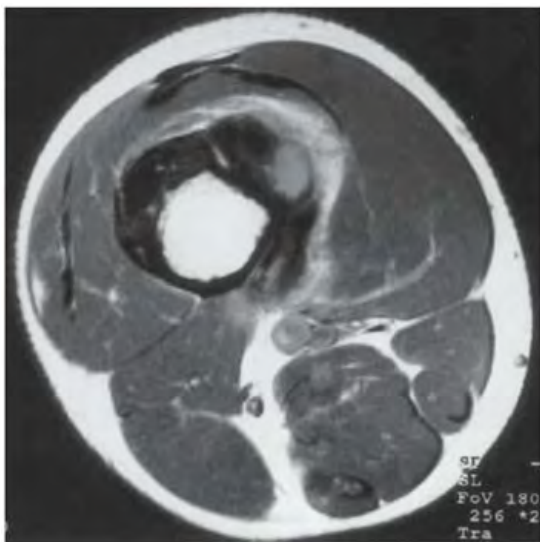


FIGURE 5.27A

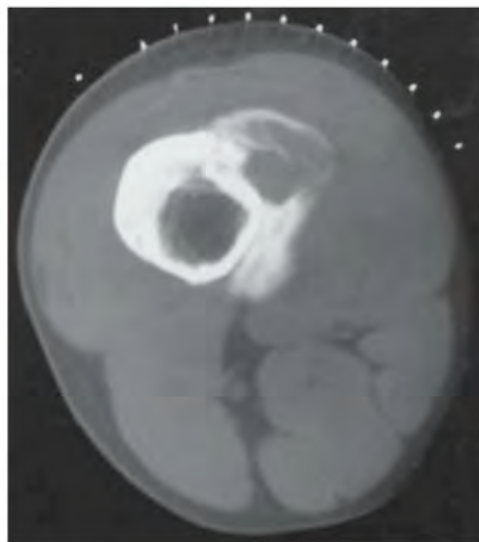


FIGURE 5.27B

**FINDINGS**

- A. Axial T1-weighted MRI shows a mass on the anteromedial surface of the femoral shaft. The mass has regions of signal void as well as regions of intermediate signal. The interface of the lesion with the surrounding tissue is irregular. The marrow space has not become involved.
- B. Axial CT shows a densely ossified mass on the surface of the bone with a broad pedicle. The mass has a cleavage plane posteriorly, but a significant nonmineralized region. There is no involvement of the medullary space.

**DIFFERENTIAL DIAGNOSIS** Aneurysmal bone cyst, periosteal chondroma, parosteal osteosarcoma or other surface variant, Ewing sarcoma, lymphoma, osteochondroma.

**DIAGNOSIS** High-grade surface osteosarcoma.

**DISCUSSION** The imaging shows a bone-forming lesion on the cortical surface, making the primary consideration a surface variant of osteosarcoma. The other items in the differential diagnosis, although they may occur on the

cortical surface, would not be expected to form bone. The amorphous mineralization wrapping partially around the cortex is distinguishable from periosteal reaction or cortical expansion. The lack of involvement of the medullary space indicates that this is not a lesion penetrating the cortex from the inside to form a soft tissue mass.

Several variants of osteosarcomas arising on the surface of bone have been recognized, with distinctive radiologic and pathologic features [53,54]. Parosteal osteosarcomas are densely ossified surface masses that may have unossified portions. Periosteal osteosarcomas are chondroblastic lesions, and high-grade surface osteosarcomas are like classic high-grade intramedullary osteosarcomas except that they arise on the surface. Histologically, parosteal osteosarcomas are usually low grade, whereas periosteal and high-grade surface osteosarcomas are generally high-grade tumors. The densely ossified mass wrapping partially around the cortex with a cleavage plane is characteristic of parosteal osteosarcoma, but the infiltrative margin and the significant unmineralized proportion should be considered aggressive features.

**CLINICAL HISTORY** A 41-year-old man with thigh mass.



FIGURE 5.28A



FIGURE 5.28B

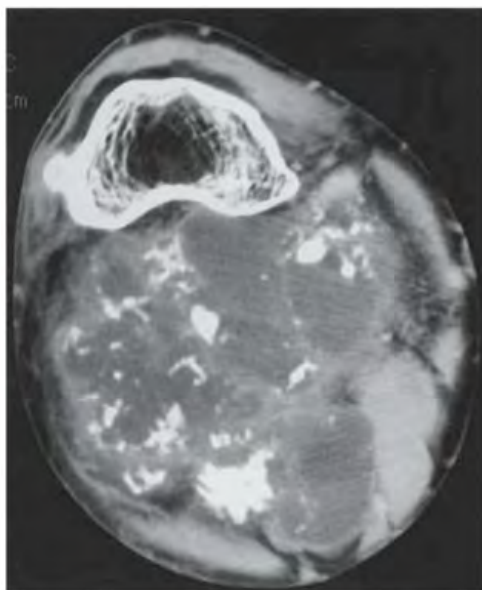


FIGURE 5.28C

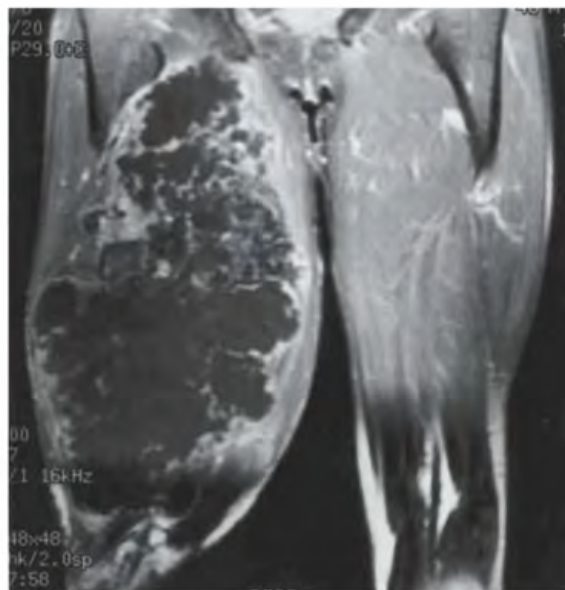


FIGURE 5.28D

## FINDINGS

- A, B. AP and lateral radiographs of the distal thigh show a mass along the posterior aspect of the distal femur, with mineralization in the form of rings and arcs.
- C. Coronal T1-weighted MRI with fat saturation after intravenous gadolinium injection shows lobular regions of the lesion with low-attenuation matrix and peripheral calcifications. These peripheral calcifications superimposed over the lobular structure result in the radiographic rings-and-arcs appearance. The lesion is exostotic.
- D. Coronal T1-weighted MRI with contrast shows a low-signal-intensity soft tissue mass with peripheral enhancement in a lobular configuration.

**DIFFERENTIAL DIAGNOSIS** Chondrosarcoma, osteochondroma.

**DIAGNOSIS** Chondrosarcoma.

**DISCUSSION** The morphology and specific features of this lesion leave no doubt that it represents an exostotic cartilage

lesion. The large size and relatively sparse calcification suggests that it is malignant and, in this circumstance, the lesion should be treated as a sarcoma until proven otherwise. Needle biopsy may be misleading because of sampling error in such a large lesion; in general, the biologic behavior of a sarcoma is that of its highest-grade part, regardless of how large or small that part is in relation to the remainder of the lesion.

Calcified rings and arcs, dense punctate calcifications, or flocculent calcifications (small, loosely aggregated masses) are patterns of mineralization of chondroid matrix, formed by benign and malignant cartilage-forming lesions. The rings-and-arcs configuration of mineralization corresponds to calcification and ossification around the periphery of cartilaginous lobules. Chondroid matrix that is not mineralized typically has attenuation on CT that is lower than muscle but greater than water. On MRI, chondroid matrix has low signal on T1-weighted images and high signal on T2-weighted MRI, similar to hyaline cartilage [55].

**CLINICAL HISTORY** *An 18-year-old man with sudden, severe left hip pain.*



FIGURE 5.29A

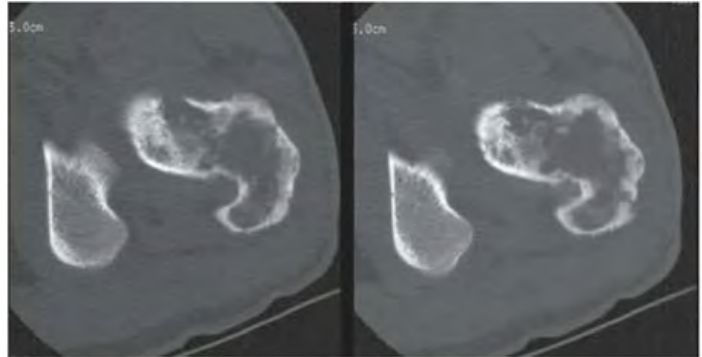


FIGURE 5.29B



FIGURE 5.29C

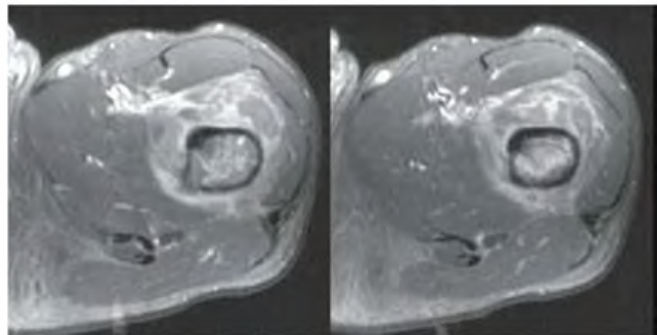


FIGURE 5.29D

**FINDINGS**

- A. AP radiograph of the left hip shows permeated destruction of bone involving the femoral neck and intertrochanteric region.
- B. Consecutive axial CT shows permeated bone destruction with pathologic fracture seen best in the lateral aspect of the lesser trochanter but extending laterally through the greater trochanter. Irregular mineralization within the intramedullary lesion may represent reactive bone or residual trabecular bone. There is no mineralization in the soft tissues.
- C, D. Coronal and axial T1-weighted MRI with fat saturation after intravenous gadolinium injection shows high signal in the soft tissues immediately surrounding the proximal femur, with circumferential mass effect and heterogeneous enhancement within the femoral lesion with interior portions that are nonenhancing.

**DIFFERENTIAL DIAGNOSIS** Osteosarcoma, lymphoma, Ewing sarcoma, osteomyelitis.

**DIAGNOSIS** Non-Hodgkin B-cell lymphoma, involving bone secondarily.

**DISCUSSION** Non-Hodgkin lymphoma involving the bone usually occurs in the setting of disseminated disease, typically presenting first in the abdomen. Non-Hodgkin lymphoma is more likely to involve bone than Hodgkin lymphoma, and the axial skeleton is the predominant site of occurrence. The undifferentiated and histiocytic forms more commonly involve bone, and large lesions frequently have necrotic portions. Involvement of the bone and bone marrow is frequently occult and is best demonstrated by MRI [56].

The mechanism of bone destruction in lymphoma is similar to that of multiple myeloma, with lymphoma cells producing osteoclast-activating factors that mediate the bone destruction [57]. The lesions are therefore lytic, and may have a moth-eaten or permeated appearance. A soft tissue component is not uncommon. Periosteal reaction and sclerosis are seen more commonly in Hodgkin lymphoma, but may also be a feature in non-Hodgkin lymphoma. Pathologic fracture is noted in as many as 25% of cases. It has been suggested that 18F-fluorodeoxyglucose-positron emission tomography (FDG-PET) may be more accurate than 67 Ga scanning in staging the extent of disease [58].



FIGURE 5.30A



FIGURE 5.30B

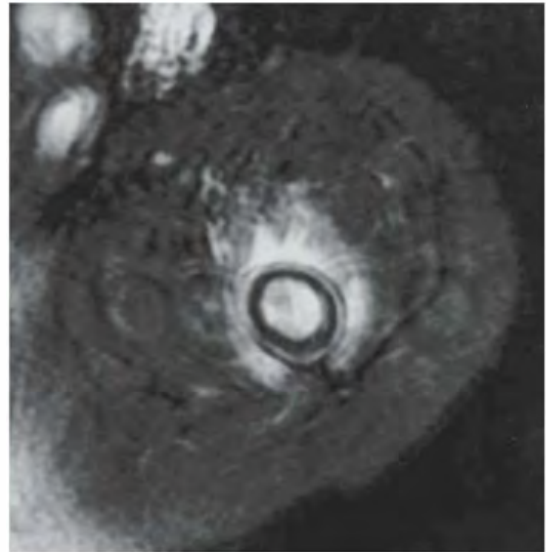


FIGURE 5.30C

### FINDINGS

- A. AP radiograph demonstrates a faint lucency in the distal femoral metadiaphysis, with a thin rim of smooth diaphyseal periosteal reaction.
- B. Coronal T1-weighted MRI of the proximal femur demonstrates replacement of the normal marrow hyperintensity with geographic areas of low signal intensity.
- C. Axial T2-weighted MRI shows high signal of the involved marrow. Associated edematous changes are noted in the adjacent soft tissues. The periosteal reaction is evident as a thin, well-defined, low-signal-intensity circle surrounding the bone.

**DIFFERENTIAL DIAGNOSIS** Osteomyelitis, lymphoma, leukemia, metastases, stress fracture, eosinophilic granuloma.

**DIAGNOSIS** Leukemia.

**DISCUSSION** The patchy involvement of the medullary space eliminates osteomyelitis and stress fracture as considerations, although either may cause subtle periosteal reaction. Leukemia is a neoplasm of leukocytes that may involve

bone secondarily, and it is the most common malignancy in children. Leukemic infiltration of many organs and tissues, including the marrow spaces, will be present and may have a diffuse or nodular character. Packing of the marrow spaces with leukemic cells causes pressure atrophy of cancellous trabeculae, and is seen radiographically as diffuse osteopenia. In children, lucent metaphyseal bands may occur, reflecting zones of trabeculae that are thinner and sparser than normal in areas of rapid bone growth. Nodular collections of leukemic cells cause focal areas of medullary, cortical, or subperiosteal bone destruction. Leukemic infiltration can extend through the cortex by way of the haversian systems, enlarging them by eroding the bone. This causes the cortex to appear fuzzy and osteopenic, often with lucent streaks. Infiltration of subperiosteal spaces lifts the periosteum and stimulates bone formation. Widespread marrow space involvement is the rule, and can be confirmed by MRI or bone marrow aspiration [59,60]. In patients who have been treated successfully for leukemia with chemotherapy, it may be difficult to distinguish fibrosis from residual lesions in the bone marrow by any imaging method other than biopsy [61].



FIGURE 5.31A



FIGURE 5.31B

**FINDINGS** AP radiographs of the right (A) and left (B) hips show extensive soft tissue calcification about the hips and thighs. The calcifications are mostly rounded, dense, and amorphous, but some of the calcifications in the medial thighs appear sheet-like. The bones appear relatively normal.

**DIFFERENTIAL DIAGNOSIS** Dermatomyositis, polymyositis, scleroderma, parasitic infestation, mixed connective tissue disease, fibrodysplasia ossificans progressiva, burns, calcific myonecrosis, hemangiomatosis, tumoral calcinosis.

**DIAGNOSIS** Mixed connective tissue disease (calcinosis universalis).

**DISCUSSION** The differential diagnosis is that of extensive soft tissue calcification. Many of these possibilities can be discarded on the basis of clinical history, and the morphology and distribution of the calcifications may be helpful [72]. Calcinosis universalis refers to a widespread distribution of soft tissue calcifications. It is a nonspecific, descriptive term, not a disease entity. In considering the morphology of soft tissue calcifications as a means of narrowing the differential diagnosis, some general patterns may be applicable.

- Central lucency would be typical of phleboliths.
- Osseous masses with cortex and medullary space would be typical of fibrodysplasia ossificans progressiva and burns.
- Peripheral calcifications around soft tissue masses would be typical of posttraumatic myositis ossificans.
- Calcifications of uniform size and shape would be typical of parasitic infestation.
- Cystic calcifications would be typical of tumoral calcinosis.
- Reticulated or linear soft tissue calcifications would be typical of dermatomyositis or collagen vascular disease.

Periarticular calcifications are associated with hypercalcemic states and collagen vascular disease. The bilateral distribution of the calcifications favors a systemic disease rather than a localized process. The clinical history may be used to eliminate additional diagnostic possibilities, particularly tumoral calcinosis (no history of hemodialysis for renal failure), calcific myonecrosis (no history of compartment syndrome), and myositis ossificans (no history of trauma). Mixed connective tissue disease refers to syndromes of rheumatic disease with features that overlap those of more well-defined disease, including rheumatoid arthritis, scleroderma, systemic lupus erythematosus, and dermatomyositis.

**CLINICAL HISTORY** 23-year-old laborer with aching left hip pain for approximately one year.



FIGURE 5.32A

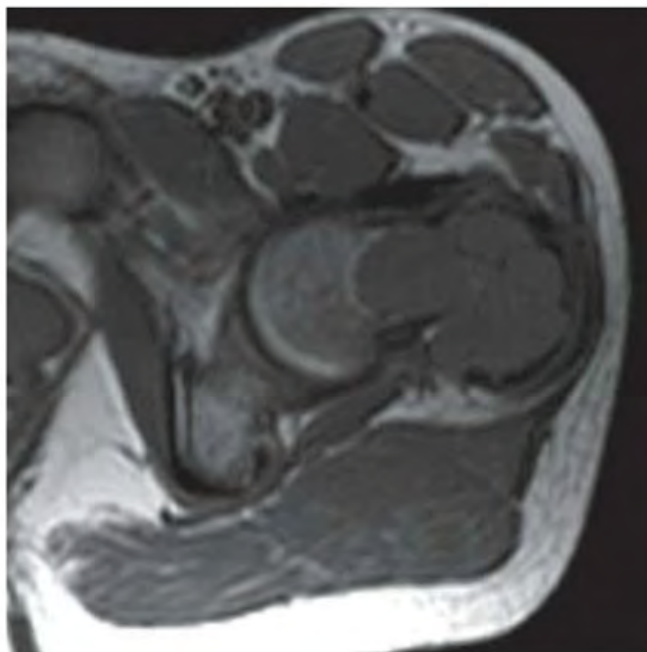


FIGURE 5.32B

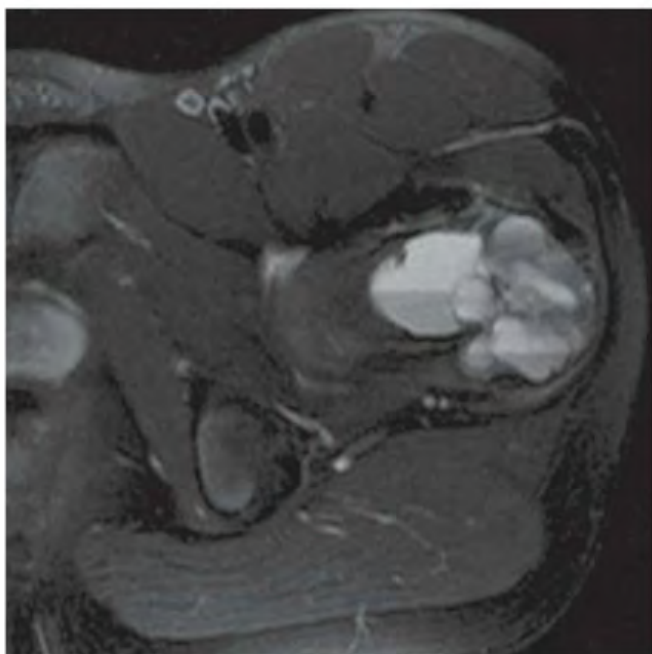


FIGURE 5.32C

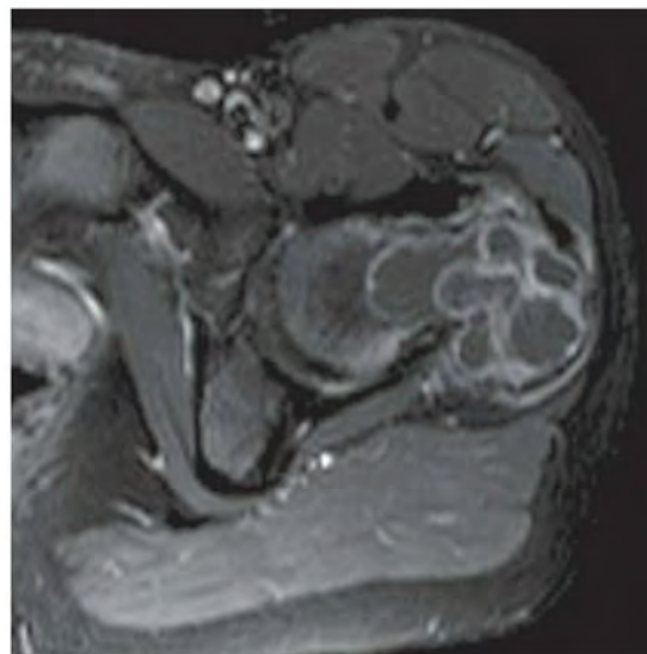


FIGURE 5.32D

**FINDINGS**

- A. AP radiograph of the left hip demonstrates an expansile, lucent lesion with thin septations in the greater trochanter of the proximal femur, extending into the neck and the intertrochanteric region.
- B. Axial T1-weighted MRI shows a lobulated lesion with intermediate signal intensity. There is cortical expansion but no soft tissue component or periosteal reaction.
- C. Axial T2-weighted MRI with fat suppression shows multiple fluid-fluid levels within the mostly T2-bright lesion.
- D. Axial T1-weighted MRI with fat suppression, following intravenous gadolinium injection, shows enhancing septations separating fluid compartments.

**DIFFERENTIAL DIAGNOSIS** Aneurysmal bone cyst, telangiectatic osteosarcoma, giant cell tumor, lymphoma, chondroblastoma.

**DIAGNOSIS** Aneurysmal bone cyst.

**DISCUSSION** Aneurysmal bone cysts (ABCs) are lytic, eccentric, expansile, blood-filled lesions with incomplete septations that allow for communicating compartments.

Their peak age of occurrence is in children and young adults. Choice locations are metaphyses of long bones and posterior elements of the spine. Primary ABCs are believed to form on the basis of trauma. One hypothesis postulates that arteriovenous fistulae form as a sequel to trauma and give rise to this nonneoplastic lesion [62]. ABCs may simulate aggressive malignant lesions by expanding rapidly and demonstrating cortical breakthrough of the soft tissue component. Secondary ABCs may comprise fully one-third of these lesions and occur in association with the following lesions: chondroblastoma, chondromyxoid fibroma, fibrous dysplasia, giant cell tumor, osteoblastoma, solitary bone cyst, brown tumor, angiosarcoma, nonossifying fibroma, giant cell reparative granuloma, malignant fibrous histiocytoma (MFH), and telangiectatic osteosarcoma [63,64]. Fluid levels, reflecting their hemorrhagic constituents, may be seen with CT or MRI, but they are not pathognomonic. Fluid levels may also be seen in giant cell tumor, solitary bone cyst, chondroblastoma, MFH, soft tissue hemangioma, synovial sarcoma, and telangiectatic osteosarcoma. Unlike giant cell tumor and chondroblastoma, ABCs rarely involve the end of the bone. Solid fibrous components may be seen on histologic examination.

**CLINICAL HISTORY** A 41-year-old man with hip pain.



FIGURE 5.33A

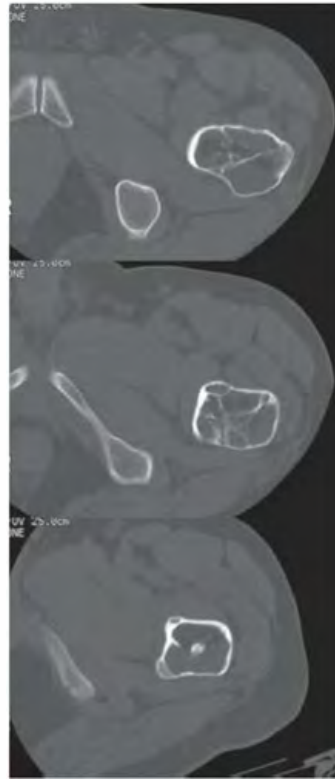


FIGURE 5.33B

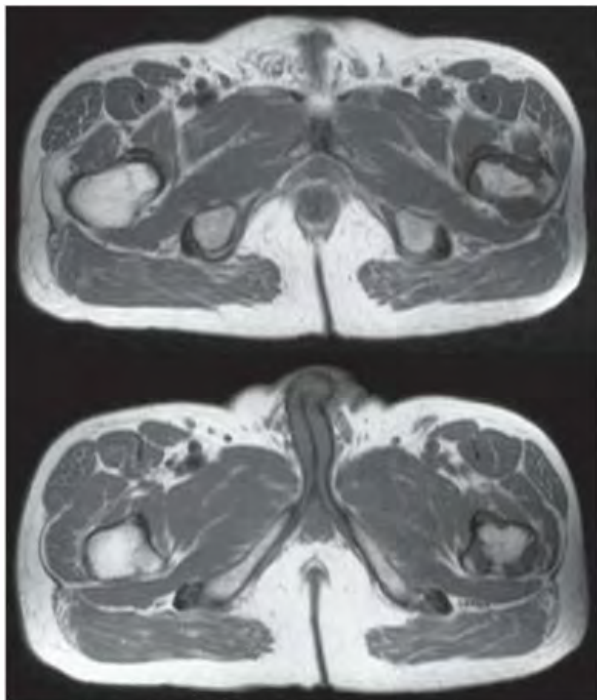


FIGURE 5.33C

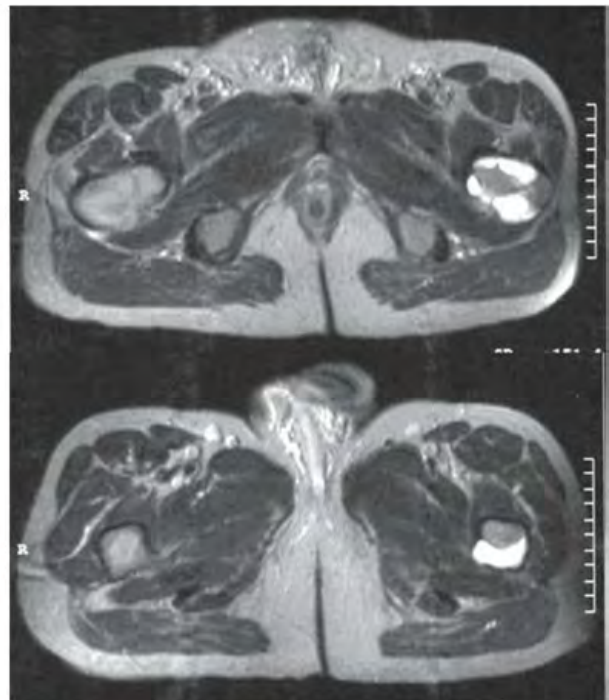


FIGURE 5.33D

## FINDINGS

- A. AP radiograph of the proximal femur shows thickened septa in a geographic lesion in the femoral neck, extending down to the proximal diaphysis. No periostitis is noted, but portions of the lesion appear sclerotic. There is no apparent cortical break or soft tissue mass.
- B. CT axial cut better defines the thickened septa. The loculations contain fluid density and are not expansile. Distribution is again noted in the femoral neck and proximal femoral diaphysis.
- C, D. Axial proton density and T2-weighted MRI demonstrates heterogenous regions of signal intensity within the lesion.

**DIFFERENTIAL DIAGNOSIS** Fibrous dysplasia, unicameral bone cyst, intraosseous lipoma, nonossifying fibroma, osteoblastoma, desmoplastic fibroma, posttraumatic deformity, bone infarct, Paget disease, liposclerosing myxofibrous tumor.

**DIAGNOSIS** Liposclerosing myxofibrous tumor of bone.

**DISCUSSION** The lesion has benign radiologic characteristics and, from a clinical management perspective, is straightforward. From an imaging perspective, the multiple different constituents of the lesion suggest a variety of possibilities,

none of which is completely satisfactory in explaining all of the features.

Atypical fibro-osseous lesions like this one, almost always in the proximal femur, are a common consultative diagnostic problem. The presence of a variety of patterns individually reminiscent of fibrous dysplasia, fibroxanthoma (nonossifying fibroma), myxofibroma, lipoma, cyst, bone infarct, Paget disease, and, occasionally, chondroma, indicates a benign process, but one that is difficult to label. The same variety of patterns is also evident on histologic examination, and the term liposclerosing myxofibrous tumor has been applied to these heterogenous lesions with consistent clinical, radiologic, and histologic features [65,66].

Discovered incidentally in most cases, liposclerosing myxofibrous tumors occur in a broad adult age range, but it is believed they represent hamartomas in childhood, rather than true neoplasms, and that gradual changes in their appearance as the body ages may account in part for their variability. In the majority of instances, asymptomatic discovery, lack of distortion of bone outline, and sclerotic borders are indications of stability over many years. There does not appear to be a particular predilection for pathologic fracture, and it is evident from imaging that bone has remodeled around these lesions to accommodate normal weight-bearing stresses. Malignant transformation has been reported to range from 10% to 16% [67], but this is likely an overestimation of the risk.

**CLINICAL HISTORY** A 15-year-old boy with thigh pain that is worse at night and is relieved by aspirin and nonsteroidal anti-inflammatory drugs.



FIGURE 5.34A

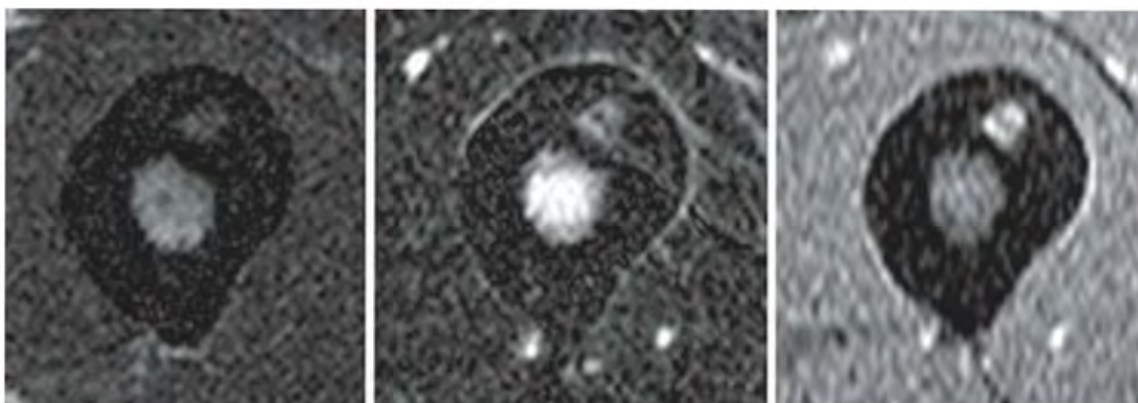


FIGURE 5.34B

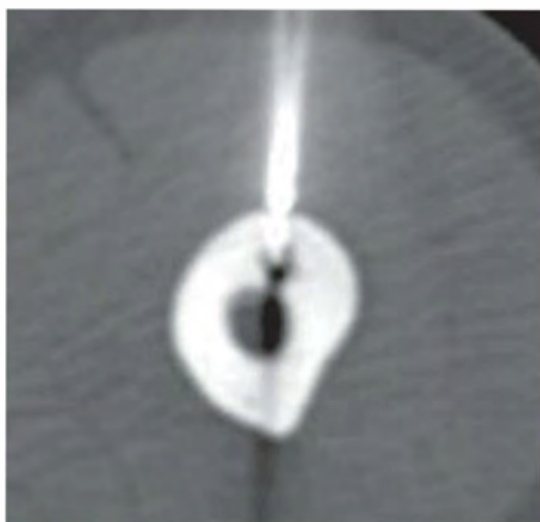


FIGURE 5.34C

**FINDINGS**

- A. Axial CT shows a round lesion in the femoral cortex surrounded by dense cortical bone. There is a dense, punctate, central calcification in the nidus.
- B. MRI (axial T1-weighted, T2-weighted fat-suppressed, and gadolinium-enhanced T1-weighted fat-suppressed sequences) demonstrates the nidus to have low T1 signal, high T2 signal, and intense arterial enhancement. Prominent marrow edema is also seen on the T2-weighted sequence.
- C. CT fluoroscopic image during radiofrequency ablation.

**DIFFERENTIAL DIAGNOSIS** Osteoid osteoma, stress fracture, osteosarcoma, Brodie abscess.

**DIAGNOSIS** Osteoid osteoma.

**DISCUSSION** Although any bone-forming lesion in the femur of an adolescent should trigger some consideration of osteosarcoma, however brief, the history and radiologic appearance of this lesion is virtually diagnostic of osteoid osteoma. Stress fractures may also occur at this particular location and

may be evident as cortical thickening, but there should not be a focal lesion at the center of the cortical reaction, and pain would be relieved at night but worse with activity during the daytime. Osteoid osteomas are relatively common bone-forming neoplasms that consist of a circumscribed nodule of woven bone and osteoid (called the nidus), and a surrounding reactive zone of thickened cortical or trabecular bone and loose fibrovascular tissue. Patients complain of a peculiar pain syndrome that is virtually unique among bone tumors: nocturnal pain that is relieved by aspirin and other prostaglandin inhibitors. Unlike other bone tumors, osteoid osteomas have abundant nerve fibers, particularly in the reactive zone, and this innervation appears to correlate with the pain syndrome [68]. The reactive zone results in a flare of bone and soft tissue edema on MRI, and there is typically an intense, reactive periosteal response that is disproportionate to the small size of the nidus (1 cm or less). Osteoid osteomas show intense arterial phase enhancement with washout on delayed phase MRI [69]. Treatment of osteoid osteoma is ablation, either percutaneously [70] or by surgery. Cost and morbidity are both lower using CT-guided percutaneous ablation rather than open surgery.

**CLINICAL HISTORY** A 63-year-old woman with an enlarging thigh mass.

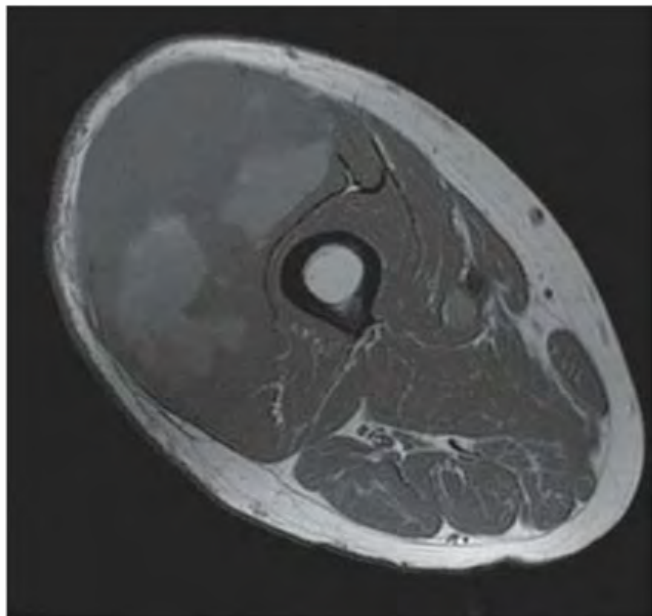


FIGURE 5.35A

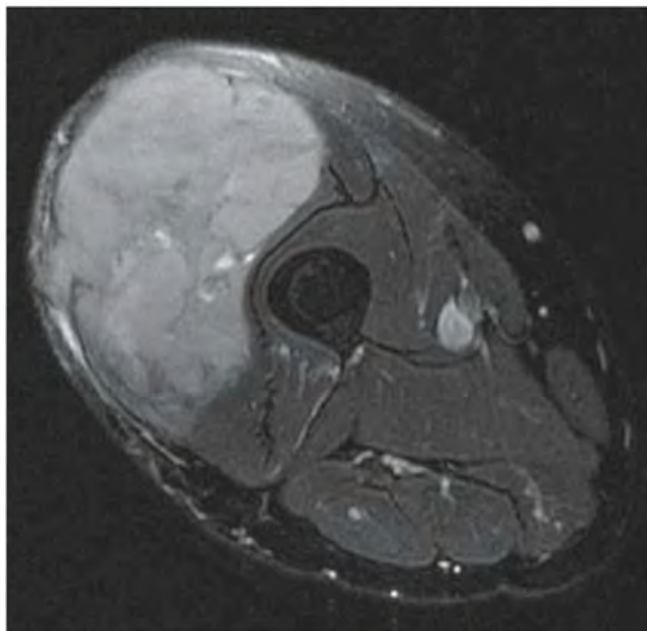


FIGURE 5.35B

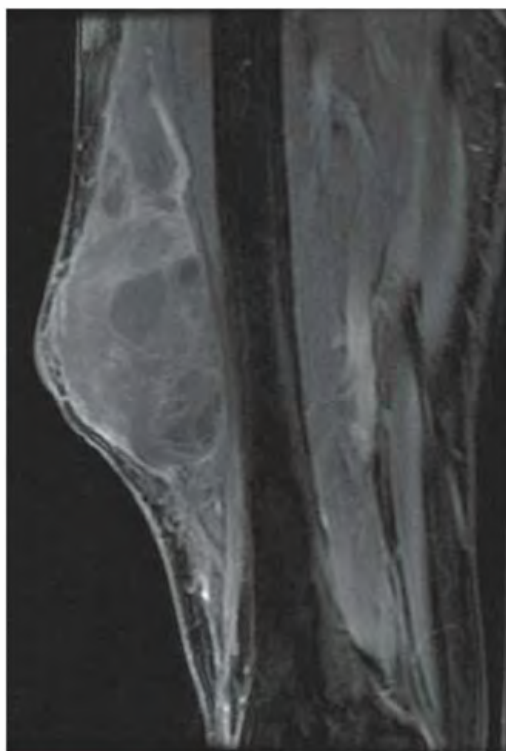


FIGURE 5.35C

## FINDINGS

- A, B. Axial T1-weighted and T2-weighted fat-suppressed MRI shows a large soft tissue mass in the anterolateral right thigh. The lesion has an ovoid shape with heterogeneous signal intensity. Regions of high T1-weighted signal intensity within the mass suggest hemorrhage.
- C. Coronal gadolinium-enhanced, T1-weighted, fat-suppressed MRI shows the lesion to have inhomogeneous enhancement.

**DIFFERENTIAL DIAGNOSIS** Soft tissue sarcoma, extraskeletal osteosarcoma, extraskeletal chondrosarcoma, myositis ossificans, lymphoma.

**DIAGNOSIS** Soft tissue sarcoma (malignant fibrous histiocytoma (MFH)).

**DISCUSSION** A large, necrotic mass in the deep soft tissues of an extremity, particularly the thigh, should be considered malignant until proven otherwise. The vast majority of soft tissue sarcomas present in adults. Patients typically complain of a slowly enlarging, palpable mass of long duration, and pain or tenderness of insidious onset. Patients may delay seeking medical attention, and this long chronicity may falsely suggest an indolent process. The patient shown above completed 6 months of acupuncture therapy before

having a physician evaluate the mass. Soft tissue sarcomas metastasize to lung, liver, or bone. They have nonspecific appearances on imaging, and there are no reliable criteria for distinguishing among them.

Once benign soft tissue masses with specific features, such as lipoma, myositis ossificans, aneurysm, bursitis, and hematoma, have been eliminated as possibilities, factors that suggest sarcoma include older age, location in the thigh, large size, round or ovoid shape, and involvement of adjacent bone. Malignant soft tissue masses usually have areas of inhomogeneity and lower density on CT or high signal intensity on T2-weighted MRI that correspond to regions of necrosis and hemorrhage. Sarcomas that calcify or ossify include synovial sarcoma, extraskeletal osteosarcoma, extraskeletal chondrosarcoma, rhabdomyosarcoma, MFH, and liposarcoma. Enhancement with intravenous contrast can be expected on both CT and MRI. The treatment of soft tissue sarcomas is surgical, sometimes with neoadjuvant and/or adjuvant radiation therapy and/or chemotherapy. Five-year survival rates of 25% to 60% have been reported. MFH is a pleomorphic sarcoma that arises most frequently in the deep soft tissues of the extremities, and less commonly in bone. MFH is the most common soft tissue sarcoma of late adult life. Cortical involvement by a primary soft tissue MFH is more common than with other sarcomas [71].

**CLINICAL HISTORY** A 22-year-old hockey player with posterior thigh mass and previous history of anterior thigh mass on the contralateral side.

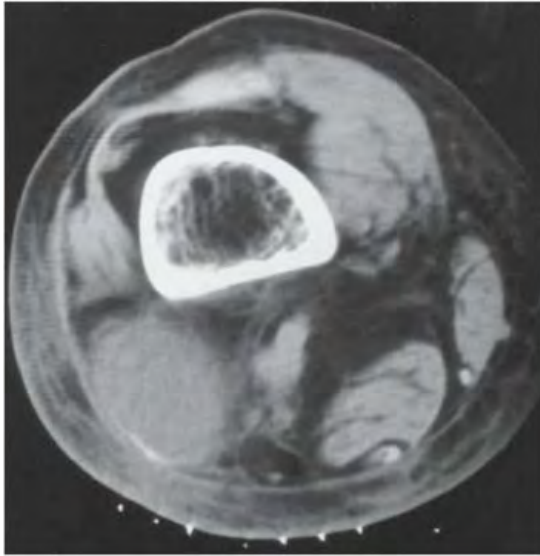


FIGURE 5.36A



FIGURE 5.36B

### FINDINGS

- A. Axial CT through the right distal thigh shows edema in the lateral subcutaneous tissues, with swelling of the biceps femoris and stranding of the adjacent fat. A thin rim of calcification lies along the posterolateral aspect of this muscle.
- B. Lateral radiograph of the left thigh shows an ossified mass in the anterior soft tissues that appears to be attached to bone. The soft tissue ossification appears mature, with a cortex and trabecular pattern. The underlying femur is intact.

**DIFFERENTIAL DIAGNOSIS** Myositis ossificans, soft tissue sarcoma, surface osteosarcoma, osteochondroma.

**DIAGNOSIS** Myositis ossificans.

**DISCUSSION** The radiologic appearance of the right side may raise soft tissue sarcoma as a possibility, and the most common soft tissue sarcoma in this age group tends to calcify (synovial sarcoma). However, the peripheral calcification (rather than central) and the clinical history (contusion in hockey player) provides the correct diagnosis. On the left side, a bony mass in the soft tissues adjacent to the femur

may initially raise the question of osteosarcoma. However, the lack of destruction and the well-formed cortex indicates a benign process. Osteochondromas would not typically be located in the diaphysis of a long bone.

Myositis ossificans commonly refers to posttraumatic heterotopic ossification in the muscles and other soft tissues after blunt trauma and hemorrhage. Most common in the quadriceps muscles or around the elbow, it progresses over a few weeks from hematoma to ill-defined calcification to well-organized cortical and trabecular bone. The process is similar to the formation and maturation of fracture callus, and may initially be confused with sarcoma. However, myositis ossificans evolves over a period of weeks into an organized, peripherally calcified mass that begins to ossify. The ectopic bone may ultimately blend with underlying bone, sometimes causing mechanical problems. Myositis ossificans may complicate acute or chronic bony or soft tissue trauma. It may occur in association with neurologic diseases of a wide variety, including paralysis and coma. A localized form that occurs without a history of significant trauma is called myositis ossificans circumscripta. Myositis ossificans may be mistaken for sarcoma on MRI [73], but the presence of an ossific rim on CT or radiography is diagnostic. The appearance on MRI depends on the stage of maturation [74].

**CLINICAL HISTORY** A 35-year-old woman with painless soft tissue mass in the medial thigh.

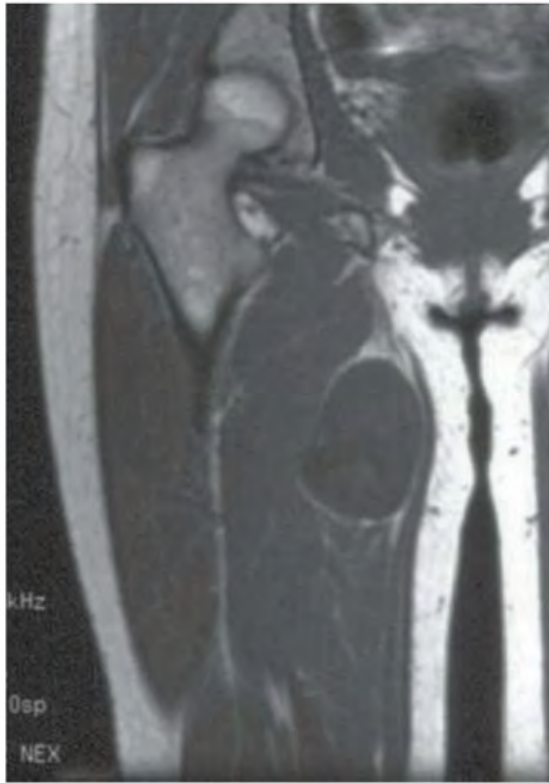


FIGURE 5.37A

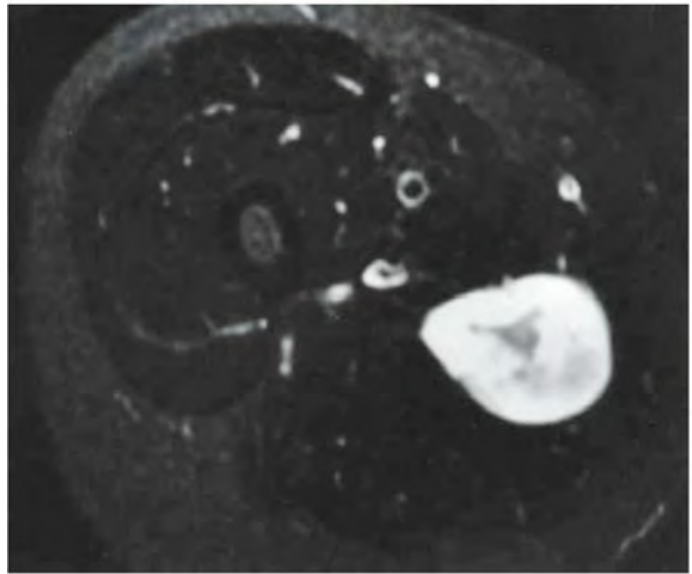


FIGURE 5.37B

## FINDINGS

- A. Coronal T1-weighted MRI shows a mass in the adductor muscle compartment with signal intensity similar to that of muscle. The adjacent muscles appear displaced around the lesion.
- B. Axial T2-weighted MRI with fat saturation demonstrates a well-defined, hyperintense soft tissue mass. The lesion has central regions of lower intensity signal.

**DIFFERENTIAL DIAGNOSIS** Soft tissue sarcoma, nerve sheath tumor (neurofibroma or schwannoma), myxoma.

**DIAGNOSIS** Neurofibroma.

**DISCUSSION** The imaging findings in this case are fairly nonspecific, and both benign and malignant soft tissue masses must be considered. Both malignant and benign soft tissue tumors tend to have a well-encapsulated appearance. Soft tissue sarcomas tend to be quite large at the time of

presentation, and when they are heterogeneous on MRI, the central portion tends to have high intensity (from liquefactive necrosis) rather than the periphery. The appearance on the T2-weighted MRI thus provides a clue to the diagnosis in this case.

Neurofibromas are seen most commonly around the spine, but they may occur in any peripheral nerve and favor the flexor compartments when present in the extremities. Radiographically, they may show erosion of the adjacent bone, but in this case, the lesion is not adjacent to bone. On MRI, a well-defined lesion is usually seen with increased signal intensity on T2-weighted images and often a decreased-signal-intensity center, or target appearance, which is somewhat specific for these lesions [75]. Enhancement with contrast is usually noted. When the presence of neurofibromatosis is already established, the diagnosis of these lesions is fairly straightforward, although the possibility of malignant degeneration of a neurofibroma to neurofibrosarcoma should always be considered.

**CLINICAL HISTORY** A 43-year-old man with painless soft tissue mass in the medial thigh.

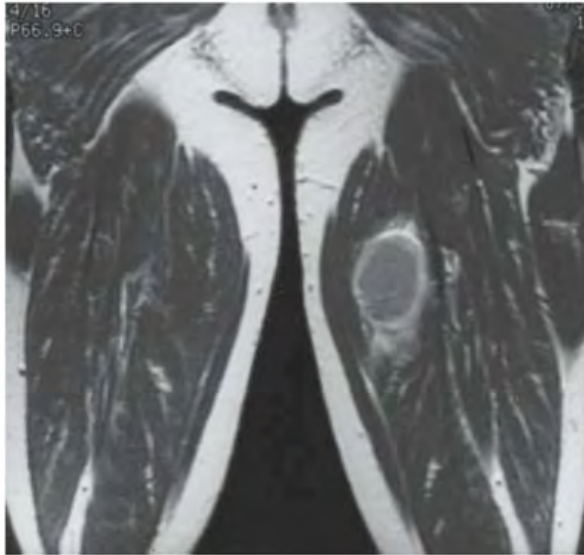


FIGURE 5.38A

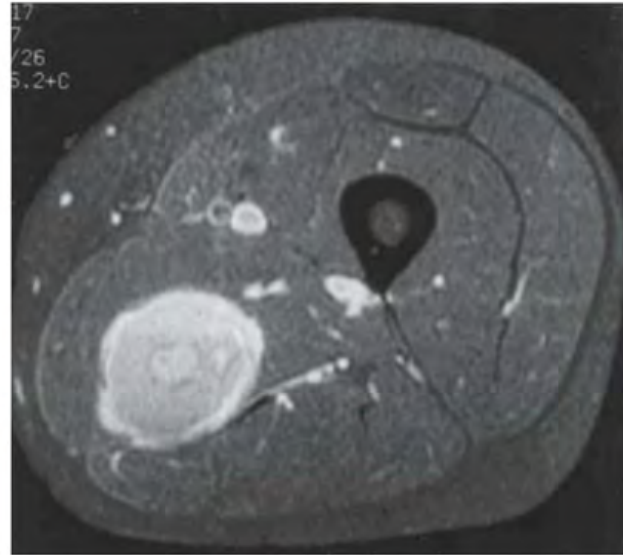


FIGURE 5.38B

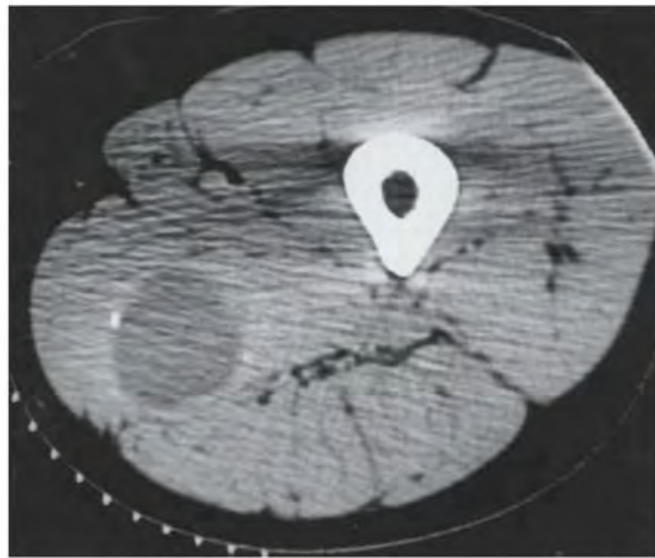


FIGURE 5.38C

### FINDINGS

- Coronal T1-weighted MRI after gadolinium injection shows an ovoid mass in the adductor magnus muscle with rim enhancement.
- Axial T1-weighted MRI with fat saturation after gadolinium injection shows enhancement and a target appearance.
- CT scan shows a well-defined mass with low attenuation coefficients and a fleck of dystrophic border calcification.

**DIFFERENTIAL DIAGNOSIS** Soft tissue sarcoma, benign mesenchymal tumor, nerve sheath tumor.

**DIAGNOSIS** Glomus tumor.

**DISCUSSION** The imaging features of this case are not specific, and a biopsy is mandatory. Glomus tumors are benign neoplasms whose cell of origin appears to be the neuromyoarterial glomus; they are considered to be a subtype of benign hemangiopericytoma. These lesions occur in males and females with equal incidence and principally involve the soft tissues. Bony involvement usually occurs as a result of infiltration from the adjacent soft tissues, with the most common location being the subungual aspect of the distal phalanges of the hands. Primary bone lesions are unusual [76]. Other soft tissue sites are the palms, wrist, chest wall, foot, and eyelid. Multiple lesions are more common in children than in adults. The treatment is surgical excision; there is no metastatic or malignant potential.

**CLINICAL HISTORY** A 33-year-old woman with bone pain and muscle weakness.



FIGURE 5.39A



FIGURE 5.39B

**FINDINGS** AP radiographs of the upper femurs (A) and knees (B) show marked cortical thickening is present along the distal femoral shafts and the proximal tibial and fibular shafts bilaterally. The thickening includes both periosteal and endosteal surfaces. There are no associated soft tissue or joint abnormalities.

**DIFFERENTIAL DIAGNOSIS** Healed fractures, stress fracture, chronic infection, melorheostosis, Paget disease, hypertrophic osteoarthropathy, osteopetrosis, Camurati-Engelmann disease.

**DIAGNOSIS** Camurati-Engelmann disease (progressive diaphyseal dysplasia).

**DISCUSSION** The absolute symmetry of the findings suggests a systemic disease, eliminating most of the items from the differential diagnosis, all of which could result in cortical thickening. Hypertrophic osteoarthropathy would not result in narrowing of the medullary cavity, and Paget

disease would begin at the ends of the bones rather than in the diaphyses. Osteopetrosis should involve all portions of all the bones.

Camurati-Engelmann disease is a dysplastic condition characterized radiographically by fusiform cortical thickening of the diaphyses of the long bones, resulting from endosteal and periosteal bone deposition. The medullary cavity is narrowed, and the hyperostosis is bilaterally symmetric. On histology, the thickened bone shows intense, simultaneous increases in both osteoblastic and osteoclastic activity. The increased bone turnover may be reflected in increased activity on radionuclide bone scan and in biochemical markers [81]. Although the causation and pathogenesis is uncertain, it has been proposed that the disease is the result of defective haversian bone formation or deficient cortical vascular supply. In the latter case, localized cortical hypoxia would be the stimulus for bone formation. The condition may occur sporadically or as an autosomal dominant heritable condition with variable expressivity [82].

**CLINICAL HISTORY** *An 18-year-old man with marked soft tissue swelling of the thigh.*



FIGURE 5.40A



FIGURE 5.40B

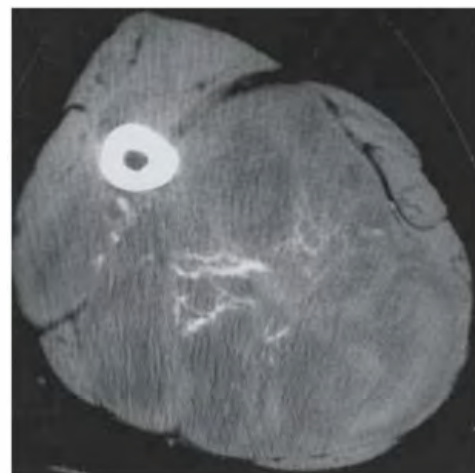


FIGURE 5.40C

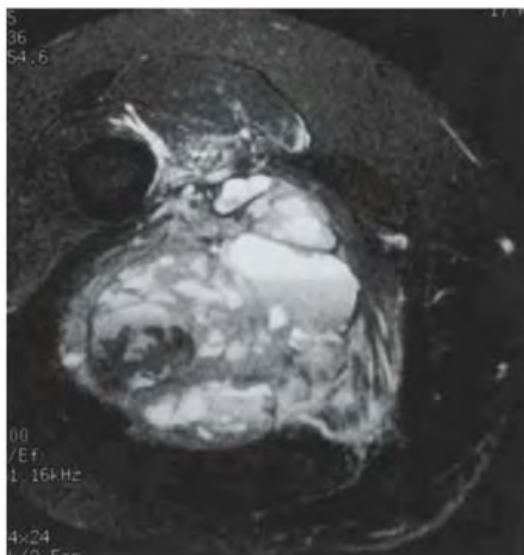


FIGURE 5.40D

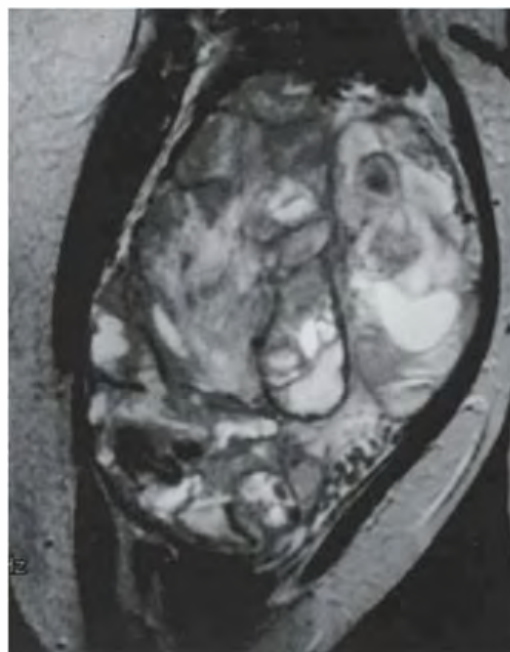


FIGURE 5.40E

**FINDINGS**

- A, B. Lateral and AP radiographs demonstrate ill-defined calcification in an enormous posterior thigh soft tissue mass. The underlying femur appears normal.
- C. CT without contrast injection shows that the posterior compartment mass is predominantly low attenuation, but it has calcified septations. It has replaced most of the muscles and may extend into the anterior and adductor compartments. The underlying femur appears intact.
- D, E. Axial and coronal T2-weighted MRI with fat saturation demonstrates marked heterogeneity with compartmentalized fluid-fluid levels suggesting a hemorrhagic component.

**DIFFERENTIAL DIAGNOSIS** Soft tissue sarcoma, myositis ossificans, extraskeletal osteosarcoma, tumoral calcinosis.

**DIAGNOSIS** Synovial sarcoma.

**DISCUSSION** This huge, heterogeneous soft tissue is very suspicious for malignancy and should be considered to be a

sarcoma unless proven otherwise. Biopsy is necessary. The most common primary malignancy of the musculoskeletal soft tissues is MFH, but in the young adult, synovial sarcoma is more common. Synovial sarcomas are more likely to be calcified than other types of mesenchymal sarcomas (synovial sarcomas have an approximately 30% incidence of radiographic calcification). Other malignant sarcomas that may calcify include extraskeletal chondrosarcoma and osteosarcoma, as well as the occasional soft tissue sarcoma. The MRI features of these lesions are protean and not specific [77], and calcification is difficult to recognize on MRI. Synovial sarcomas bear a superficial resemblance to synovial cells on light microscopy, but they are not actually thought to arise from the synovium. Although synovial sarcomas frequently arise within a few centimeters of joints, actual involvement of the synovium by a synovial sarcoma is rare. The age of peak incidence is 20 to 49 years. Synovial sarcomas are slow-growing lesions, but local recurrence and metastases may occur. Treatment is by wide resection.

**CLINICAL HISTORY** A 39-year-old man with painless posterior thigh mass.



FIGURE 5.41A



FIGURE 5.41B

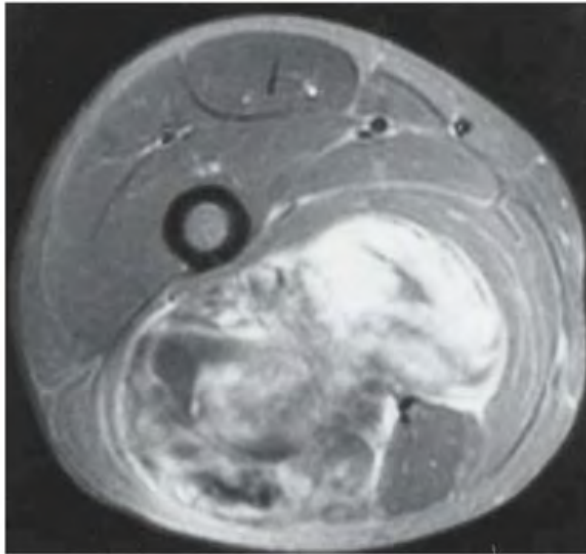


FIGURE 5.41C



FIGURE 5.41D

## FINDINGS

- A. Lateral radiograph of the thigh shows a large, fat-containing soft tissue lesion in the posterior thigh musculature.
- B. CT through the midportion of the lesion shows a heterogeneous lesion, with some regions of fat attenuation. The lesion occupies the posterior muscular compartment and does not involve the bone.
- C. Axial T2-weighted MRI with fat saturation shows that some portions of the image have high signal whereas other portions have low signal, which is consistent with fat.
- D. Sagittal T1-weighted MRI shows a heterogeneous lobular lesion containing fat.

**DIFFERENTIAL DIAGNOSIS** Soft tissue sarcoma, lipoma, nerve sheath tumor, myositis ossificans.

**DIAGNOSIS** Liposarcoma.

**DISCUSSION** A large mass in the deep soft tissues of the thigh is always worrisome. The specific imaging features of this lesion suggest a sarcoma containing fat, but biopsy is necessary. Benign lipomas would be bland and nearly homogeneously fat, reflecting a paucity of cellular components. Myositis ossificans would be expected to calcify around the periphery and should not contain fat. Nerve sheath tumors often contain lipid but would typically present at a much smaller size because of early nerve impingement.

Liposarcoma is the most common soft tissue sarcoma of the lower extremities in adults between the ages of 26 and 45; however, most liposarcomas are found in patients in their 50s and 60s [78]. Liposarcoma usually arises in the deep soft tissues, and patients present with a large, painless mass. Liposarcoma originates from a primitive mesenchymal cell (not from mature fat), and there are several morphologic subtypes, all with histologic evidence of fat differentiation. The well-differentiated and myxoid subtypes are low or intermediate grade. They typically have large amounts of gross fat or extracellular myxoid material, whereas the round cell, pleomorphic, and dedifferentiated subtypes are considered high grade and are typically very cellular, with little if any gross fat.

Radiographs usually show a nonspecific soft tissue mass, but on CT and MRI, the appearance of liposarcoma tends to reflect the degree of fat differentiation. The lower-grade lesions generally appear fat-like, with low attenuation on CT and signal characteristics similar to subcutaneous fat on MRI. The higher-grade lesions frequently have no radiologically evident fat [79]. Large size, lobular shape, circumscription, heterogeneity, enhancement, hemorrhage, and necrosis are common features of liposarcomas. Soft tissue sarcomas of other histologic types may also contain fat as the result of engulfment, especially in recurrent lesions. Liposarcomas are treated operatively with wide margins. Most patients are candidates for limb-sparing surgery [80].



FIGURE 5.42A

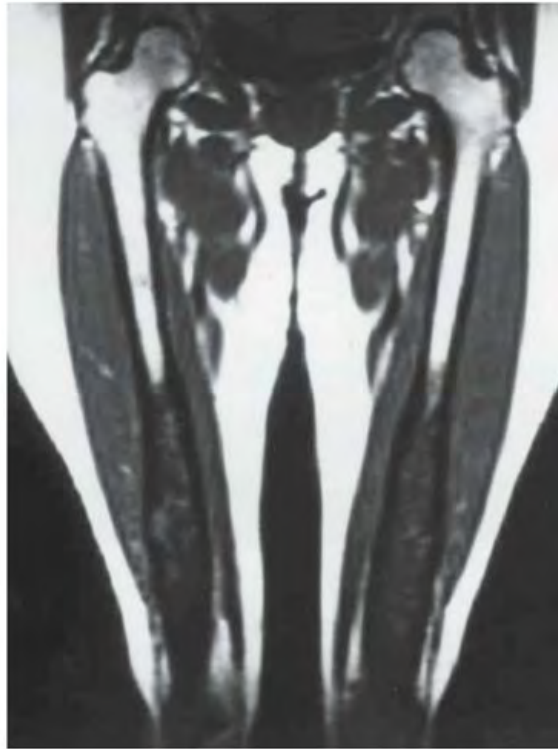


FIGURE 5.42B

### FINDINGS

- A. AP radiograph of the distal femur shows abnormality involving the distal half of the femur. The bone is mildly expanded, and the medullary space is irregularly sclerotic with some lucent lesions. There is no layered periosteal reaction or soft tissue mass. The morphology of the proximal femur appears normal.
- B. Coronal T1-weighted MRI of both femurs shows normal bone and marrow signal proximally. The distal halves of the femurs, including the condyles, show expanded but not thinned cortex, and low signal replacing the normal high fatty-marrow signal. The surrounding musculature appears normal. The lesions demonstrate heterogeneous high signal on T2-weighted images (not shown).

**DIFFERENTIAL DIAGNOSIS** Osteonecrosis, eosinophilic granuloma, metastatic disease, multifocal chronic osteomyelitis, enchondromatosis, Camurati-Engelmann disease, healed trauma, radiation change, Paget disease, Gaucher disease, Erdheim-Chester disease.

**DIAGNOSIS** Erdheim-Chester disease.

**DISCUSSION** Patchy areas of sclerosis with intramedullary component may be seen with infarcts, but the typical lacy pattern of calcification is not noted in this case, and the

cortical expansion would be unexplained. Paget disease may demonstrate sclerosis and bone enlargement, but usually in a cortical distribution. Radiation changes may show patchy areas of sclerosis, similar to bone infarcts, and the expansion of the cortex might be explained by whatever underlying process was treated by radiation, but we have no history of radiation, and the bilateral distribution would be puzzling. Gaucher disease may produce cortical expansion and infarcts, but not cortical thickening. Chronic osteomyelitis, metastatic disease, enchondromatosis, and EG could have some similar radiologic features, but the symmetric distribution would be unusual. Other systemic diseases that result in hyperostosis or multiple osteosclerotic lesions would tend to be more widely distributed.

Lipid granulomatosis, or Erdheim-Chester disease, is an exceedingly rare condition that demonstrates patchy areas of sclerosis with or without focal osteolytic regions [83,84]. Predominant changes occur at diaphyseal sites and involve corticomedullary sclerosis. There is increased uptake of radionuclide on bone scan and gallium scan. Cholesterol deposition in foam cells, fibrosis, lipid granulomas, and lymphocyte and plasma cell infiltration are histologic findings. A relationship to Langerhans histiocytosis has been suggested [85]. Extraskelletal manifestations may affect the cardiopulmonary system and kidneys.



FIGURE 5.43A



FIGURE 5.43B



FIGURE 5.43C

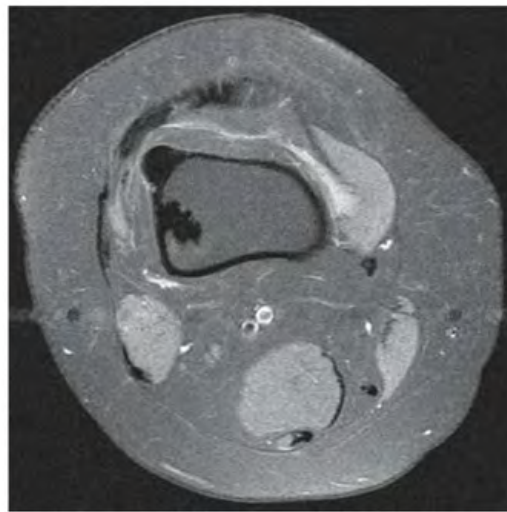


FIGURE 5.43D

### FINDINGS

- A, B. Lateral and AP radiographs of the right knee show several cortically based longitudinal sclerotic densities along distal right femur. The densities extend off the surface of the lateral aspect of the shaft and condyle.
- C. Sagittal proton density MRI with fat suppression shows low signal structures along the anterior femoral shaft cortex and within the medullary space of the metaphysis and epiphysis.
- D. Axial proton density MRI with fat suppression through the metaphysis shows the periosteal and endosteal components of the disease process.

**DIFFERENTIAL DIAGNOSIS** Prior trauma, sclerotic metastases, melorheostosis, multicentric osteosarcoma, osteopathia striata

### DIAGNOSIS Melorheostosis

**DISCUSSION** Melorheostosis is an uncommon non-hereditary, benign, mesodermal dysplasia that presents as cortical hyperostosis of tubular bones, often described as “dripping candle wax” in appearance and postulated to follow sclerotomal pattern. Melorheostosis usually occurs unilaterally in lower extremities. Most patients are asymptomatic, but presenting symptoms can include joint pain, contracture, or swelling [93]. Osteopathia striata is not a likely differential diagnosis since osteopathia striata is a more diffuse disease.

**CLINICAL HISTORY** A 50-year-old man with knee pain.



FIGURE 5.44A

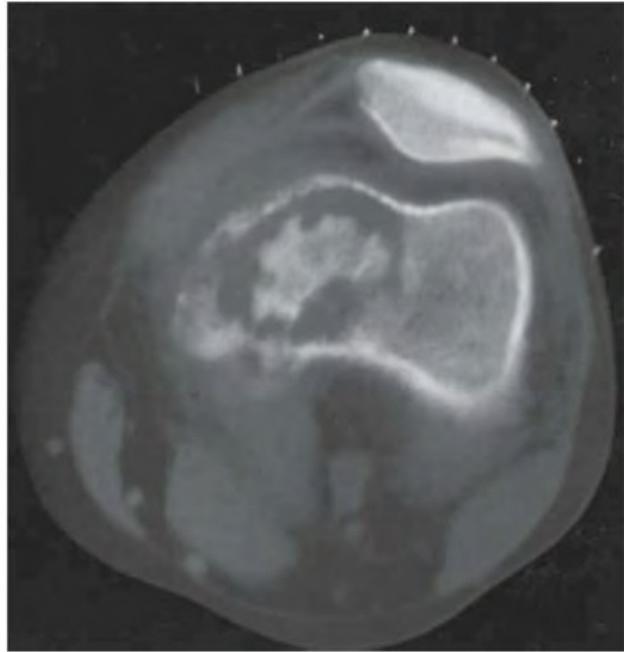


FIGURE 5.44B



FIGURE 5.44C

## FINDINGS

- A. AP radiograph of the distal femur shows permeated bone destruction without reactive bone formation or mineralization.
- B. Axial CT shows replacement of the medial femur with a lucent lesion. The cortex is violated in multiple areas, with associated extraosseous soft tissue extension and joint effusion. A giant sequestrum of medullary bone with irregular margins is present centrally.
- C. Coronal T1-weighted MRI shows a lesion of intermediate signal intensity in the medial femoral metadiaphysis with cortical penetration. Several irregularly shaped signal voids are present within the lesion. Marrow infarcts are present in the tibia.

**DIFFERENTIAL DIAGNOSIS** Osteosarcoma, malignant fibrous histiocytoma (MFH), osteomyelitis, metastases, lymphoma.

**DIAGNOSIS** MFH, arising in bone infarct.

**DISCUSSION** The cortical destruction here implies an aggressive process. The central sequestration may represent dystrophic or matrix calcification or a remnant from a preexisting process, such as malignant degeneration in a preexisting bone infarct with a bony sequestrum, now engulfed by tumor. The latter is most likely, due to the focal nature of the calcific component and its irregular shape. MFH may occur as primary lesions or secondary to dedifferentiation of chondrosarcoma or malignant degeneration in an infarct, radiation, or Paget disease. Fifteen percent of primary lesions may demonstrate dystrophic calcification or sequestration. Lesions arising from bone infarcts may show retained calcification in the underlying infarct. Typical radiographic features include bony lysis with a permeative pattern. Diaphyseal sites in long bones are favored locations. They tend to be sizable

lesions with a broad zone of transition. Periosteal reaction may or may not accompany these findings. These lesions have a higher incidence in males. The age range is broad, with a peak at approximately 50 years. These lesions carry a poor prognosis, with metastases occurring to lung, bone, and lymph nodes.

MFH of bone is a rare entity [86,87]. As in this case, it is typically seen in men between 40 and 60 years old. Approximately one-half of patients will present with a pathologic fracture. MFH may develop in a preexisting bone infarct, lipoma, Paget disease, or radiation therapy. The distribution is the metaphyses of long bones, usually in the lower extremity. The radiographic presentation is that of an aggressive lesion, usually osteolytic, with limited reactive periostitis and an associated soft tissue mass. The appearance is difficult to distinguish from a fibrosarcoma; MFH tends to have a more aggressive appearance, whereas fibrosarcoma is more likely to have a sequestrum. Other considerations include a nonexpansile osteolytic metastasis (such as lung or breast), multiple myeloma, lymphoma, and osteosarcoma. Infection should always be mentioned whenever a small cell tumor is included.

Pathologically, MFH is characterized by a storiform appearance that distinguishes it from the herringbone appearance seen in fibrosarcoma. The osseous form of this disease has local recurrences in up to 80% of patients in the early experience, but is comparable to primary osteosarcoma of bone at this time. Metastases occur hematogenously as well as to lymphatics. Sarcoma associated with bone infarct is rare, with most reported cases being MFH, fibrosarcoma, or osteosarcoma [88,89]. The pathogenesis of sarcoma arising in bone infarct is unknown, but the most common sites are the tibia, femur, and humerus. Most patients have multiple infarcts of unknown cause with large medullary components. The prognosis for patients with these sarcomas is poor [90].

**CLINICAL HISTORY** A 3-year-old girl with swollen left leg.

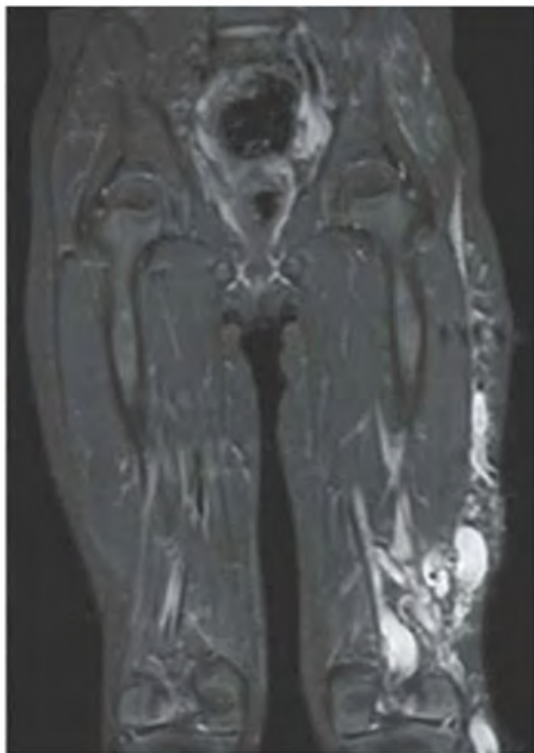


FIGURE 5.45A



FIGURE 5.45B

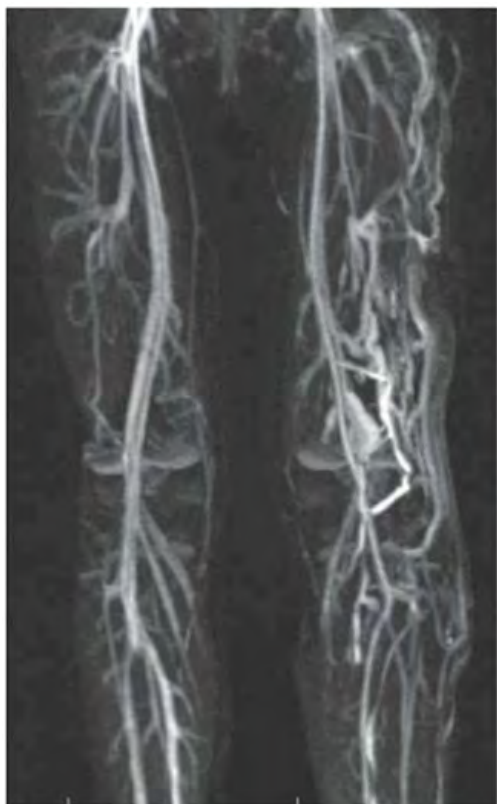


FIGURE 5.45C

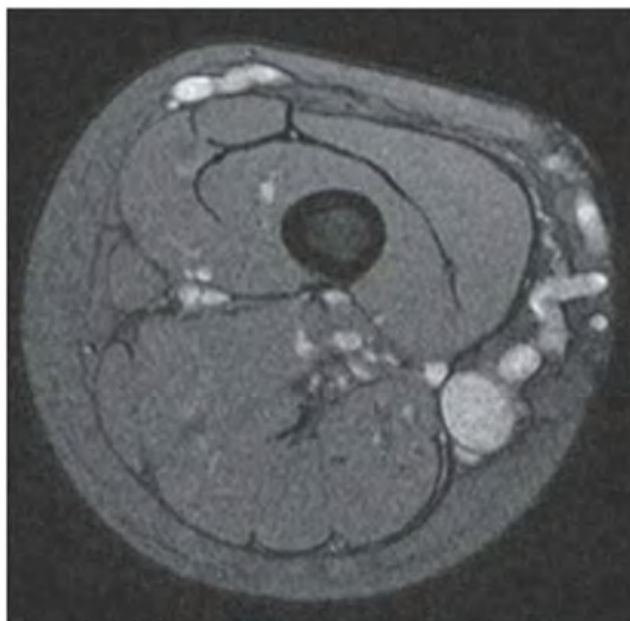


FIGURE 5.45D

**FINDINGS** (A, B) Coronal postcontrast fat-saturated T1-weighted MRI shows large tortuous tubular enhancing lesions along the entire length of left leg. On reformatted MR angiography image (C), these serpiginous structures communicate with internal vessels. On axial postcontrast T1-weighted fat-saturated sequence image (D), the serpiginous enhancing lesions are found in the subcutaneous tissue and represent large varices. There is presence of normal deep draining veins.

**DIFFERENTIAL DIAGNOSIS** Proteus syndrome, Maffucci syndrome, Klippel-Trenaunay syndrome.

**DIAGNOSIS** Klippel-Trenaunay syndrome.

**DISCUSSION** Klippel-Trenaunay syndrome is characterized by a triad of (1) port wine stain, (2) lymphovenous

malformations, and (3) soft tissue and bony hypertrophy of affected limb, first characterized by Klippel and Trenaunay in 1900 [91]. Of note, Parkes Weber described two patients with the triad of symptoms plus arteriovenous malformations in the affected limbs. There are some debates regarding combining the syndrome into one name (Klippel-Trenaunay-Weber syndrome). Both syndromes are seen equally in male and female patients in sporadic manner. This case shows extensive varicose veins in left leg, which is longer than the right leg, representing mild asymmetric hypertrophy. Before treatment of varicosities, presence of deep draining veins must be confirmed first, for some Klippel-Trenaunay patients rely solely on these superficial veins for their extremity venous drainage due to atresia or agenesis of deep veins [92]. Some cases are accompanied by lymphedema and pain.

**CLINICAL HISTORY** A 34-year-old male with history of mountain-biking accident.

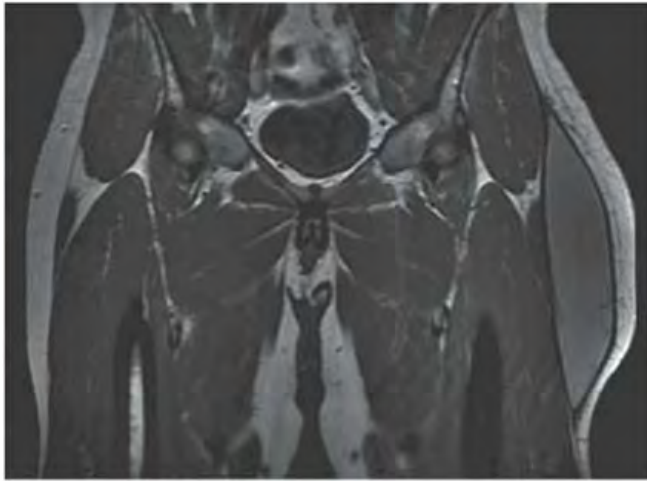


FIGURE 5.46A

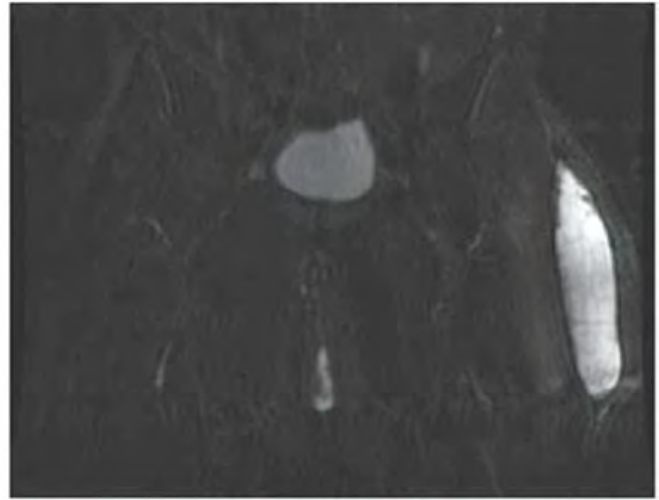


FIGURE 5.46B

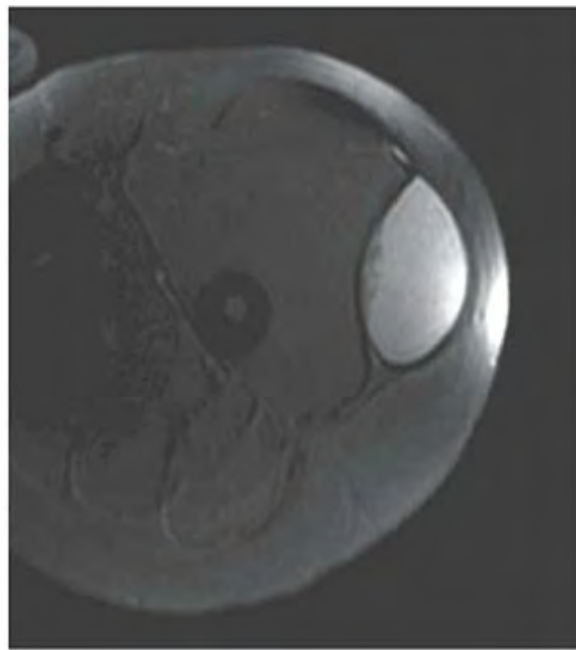


FIGURE 5.46C

## FINDINGS

- A. Coronal T1-weighted MRI through the pelvis shows an lentiform fluid collection over the left lateral hip.
- B, C. On coronal (B) and axial (C) STIR images, this collection shows mostly uniform high T2 signal with few peripheral foci of debris. Collection is between the subcutaneous fat and the underlying gluteal muscles. There is no edema in the overlying skin or underlying muscles.

**DIFFERENTIAL DIAGNOSIS** Hematoma, Morel-Lavallée lesion, cystic sarcoma.

## DIAGNOSIS

Morel-Lavallée lesion.

**DISCUSSION** Morel-Lavallée lesion is a sequela of internal degloving injury where the hypodermis gets separated away from the underlying fascia. In this space, there is an evolving collection containing blood, lymphatic fluid, and fat. Depending on timing of injury, this collection can show various MR signals due to degrading hemoglobins or presence of fat globules [94]. Over the time, Morel-Lavallée lesions tend to develop a thin epithelial wall and contain serous solution, as in this case. Treatment options include serial aspirations and, if necessary, sclerodesis [95]. Complications include secondary infections of these collections.

## SOURCES AND READINGS

- Ouellette H, Thomas BJ, Nelson E, Torriani M. MR imaging of rectus femoris origin injuries. *Skeletal Radiol*. 2006;35(9):665–672.
- Davis KW. Imaging of the hamstrings. *Semin Musculoskelet Radiol*. 2008;12(1):28–41.
- Lempainen L, Sarimo J, Heikkilä J, Mattila K, Orava S. Surgical treatment of partial tears of the proximal origin of the hamstring muscles. *Br J Sports Med*. 2006;40(8):688–691. Epub 2006 Jun 21.
- Nangaku M, Miyata T, Kurokawa K. Pathogenesis and management of dialysis-related amyloid bone disease. *Am J Med Sci*. 1999;317(6):410–415.
- Kiss E, Keusch G, Zanetti M, et al. Dialysis-related amyloidosis revisited. *AJR Am J Roentgenol*. 2005;185(6):1460–1467.
- Watson RM, Roach NA, Dalinka MK. Avascular necrosis and bone marrow edema syndrome. *Radiol Clin North Am*. 2004;42(1):207–219.
- Scully SP, Aaron RK, Urbaniak JR. Survival analysis of hips treated with core decompression or vascularized fibular grafting because of avascular necrosis. *J Bone Joint Surg Am*. 1998;80:1270–1275.
- Iorio R, Healy WL, Abramowitz AJ, Pfeifer BA. Clinical outcome and survivorship analysis of core decompression for early osteonecrosis of the femoral head. *J Arthroplasty*. 1998;13:34–41.
- Schapira D. Transient osteoporosis of the hip. *Semin Arthritis Rheum*. 1992;22:98–105.
- Froberg PK, Braunstein EM, Buckwalter KA. Osteonecrosis, transient osteoporosis, and transient bone marrow edema: current concepts. *Radiol Clin North Am*. 1996;34(2):273–291.
- Court C, Carlzioz H. Radiological study of severe proximal femoral focal deficiency. *J Pediatr Orthop*. 1997;17:520–524.
- Goldman AB. Heritable diseases of connective tissue, epiphyseal dysplasias, and related conditions. In: Resnick D, ed. *Diagnosis of Bone and Joint Disorders*. 4th ed. Philadelphia, PA: WB Saunders; 2002:4382–4448.
- Smith SE, Kransdorf MJ. Primary musculoskeletal tumors of fibrous origin. *Semin Musculoskelet Radiol*. 2000;4(1):73–88.
- Guille JT, Kumar SJ, MacEwen GD. Fibrous dysplasia of the proximal part of the femur. Long-term results of curettage and bone-grafting and mechanical realignment. *J Bone Joint Surg Am*. 1998;80:648–658.
- Kaushik S, Smoker WR, Frable WJ. Malignant transformation of fibrous dysplasia into chondroblastic osteosarcoma. *Skeletal Radiol*. 2002;31(2):103–106.
- Ghandur-Mnaymneh L, Broder LE, Mnaymneh W. Lobular carcinoma of the breast metastatic to bone with unusual clinical, radiologic, and pathologic features mimicking osteopoikilosis. *Cancer*. 1984;53:1801–1803.
- Mungovan JA, Tung GA, Lambiase RE, Noto RB, Davis RP. Tc-99m MDP uptake in osteopoikilosis. *Clin Nucl Med*. 1994;19(1):6–8.
- Umans H, Liebling MS, Moy L, Haramati N, Macy NJ, Pritzker HA. Slipped capital femoral epiphysis: a physeal lesion diagnosed by MRI, with radiographic and CT correlation. *Skeletal Radiol*. 1998;27:139–144.
- Lahdes-Vasama T, Lamminen A, Merikanto J, Martinen E. The value of MRI in early Perthes' disease: an MRI study with a 2-year follow-up. *Pediatr Radiol*. 1997;27:517–522.
- Lamer S, Dorgeret S, Khairouni A, et al. Femoral head vascularisation in Legg-Calvé-Perthes disease: comparison of dynamic gadolinium enhanced subtraction MRI with bone scintigraphy. *Pediatr Radiol*. 2002;32(8):580–585.
- Hochbergs P, Eckerwall G, Egund N, Jonsson K, Wingstrand H. Synovitis in Legg-Calvé-Perthes disease. Evaluation with MR imaging in 84 hips. *Acta Radiol*. 1998;39:532–537.
- Swash M, Brown MM, Thakkar C. CT muscle imaging and the clinical assessment of neuromuscular disease. *Muscle Nerve*. 1995;18:708–714.
- Vliet AM, Thijssen HO, Joosten E, Merx JL. CT in neuromuscular disorders: a comparison of CT and histology. *Neuroradiology*. 1988;30:421–425.
- Buchmann RF, Jaramillo D. Imaging of articular disorders in children. *Radiol Clin North Am*. 2004;42(1):151–168.
- Gash A, Walker CR, Carty H. Case report: complete photopenia of the femoral head on radionuclide bone scanning in septic arthritis of the hip. *Br J Radiol*. 1994;67:816–818.
- Oka M, Monu JU. Prevalence and patterns of occult hip fractures and mimics revealed by MRI. *AJR Am J Roentgenol*. 2004;182(2):283–288.
- Hirata T, Konishiike T, Kawai A, Sato T, Inoue H. Dynamic magnetic resonance imaging of femoral head perfusion in femoral neck fracture. *Clin Orthop*. 2001;(393):294–301.
- Scott SM, Manaster BJ, Alazraki N, Wooten WW, Murphy K. Technetium 99m imaging of bone trauma: reduced sensitivity caused by hydrocortisone in rabbits. *AJR Am J Roentgenol*. 1987;148:1175–1178.
- Hetsroni I, Shabat S, Mann G. A false negative technetium 99m bone scan in a 53-year-old man with a fractured tibia and fractured clavicles conducted 88 h after the accident. *Injury*. 2004;35(2):199–202.
- Tuite MJ, De Smet AA, Gaynon PS. Tibial stress fracture mimicking neuroblastoma metastasis in two young children. *Skeletal Radiol*. 1995;24:287–290.
- Hayes CW, Conway WF, Sundaram M. Misleading aggressive MR imaging appearance of some benign musculoskeletal lesions. *Radiographics*. 1992;12:1119–1134.
- Sankaran-Kutty M, Corea JR, Ali MS, Kutty MK. Squamous cell carcinoma in chronic osteomyelitis. Report of a case and review of the literature. *Clin Orthop Relat Res*. 1985;198:264–267.
- McGrory JE, Pritchard DJ, Unni KK, Ilstrup D, Rowland CM. Malignant lesions arising in chronic osteomyelitis. *Clin Orthop*. 1999;(362):181–189.
- Wuk K. Squamous cell carcinoma arising from chronic osteomyelitis of the ankle region. *J Foot Ankle Surg*. 1990;29:608–612.
- Jennin F, Bousson V, Parlier C, Jomaah N, Khanine V, Laredo JD. Bony sequestrum: a radiologic review. *Skeletal Radiol*. 2011;40:963–975.
- Gelal F, Sabah D, Dogan R, Avci A. Multifocal skeletal tuberculosis involving the lumbar spine and a sacroiliac joint: MR imaging findings. *Diagn Interv Radiol*. 2006;12:139–141.
- Capuani C, Accadbled F, Delisle M-B, Gomez-Bouchet A. Multifocal skeletal tuberculosis in 2 immunocompetent children. *J Rheumatol*. 2010;37(11):2441–2442.
- Porrino JA Jr, Kohl CA, Taljanovic M, Rogers LF. Diagnosis of proximal femoral insufficiency fractures in patients receiving bisphosphonate therapy. *AJR Am J Roentgenol*. 2010;194(4):1061–1064.
- Bush LA, Chew FS. Subtrochanteric femoral insufficiency fracture in woman on bisphosphonate therapy for glucocorticoid-induced osteoporosis. *Radiol Case Rep*. 2009;4:261 [Online].
- Bush LA, Chew FS. Subtrochanteric femoral insufficiency fracture following bisphosphonate therapy for osseous metastases. *Radiol Case Rep*. 2008;3:232 [Online].
- Rogers LF, Taljanovic M. FDA statement on relationship between bisphosphonate use and atypical subtrochanteric and femoral shaft fractures: a considered opinion. *AJR Am J Roentgenol*. 2010;195:563–566.
- Olsen KM, Chew FS. Tumoral calcinosis: pearls, polemics, and alternative possibilities. *Radiographics*. 2006;26:871–885.
- Daffner RH, Lupetin AR, Dash N, Deeb ZL, Sefczek RJ, Schapiro RL. MRI in the detection of malignant infiltration of bone marrow. *AJR Am J Roentgenol*. 1986;146:353–358.
- Uetani M, Hashmi R, Hayashi K. Malignant and benign compression fractures: differentiation and diagnostic pitfalls on MRI. *Clin Radiol*. 2004;59(2):124–131.
- Terpos E, Rahemtulla A. Bisphosphonate treatment for multiple myeloma. *Drugs Today (Barc)*. 2004;40(1):29–40.
- Stull MA, Kransdorf MJ, Devaney KO. Langerhans cell histiocytosis of bone. *Radiographics*. 1992;12:801–823.
- Abbott GF, Rosado-de-Christenson ML, Franks TJ, Frazier AA, Galvin JR. Pulmonary langerhans cell histiocytosis. *Radiographics*. 2004;24:821–841.
- Enneking WF, Kagan A. Skip metastases in osteosarcoma. *Cancer*. 1975;36:2192–2205.

49. Davies AM, Makwana NK, Grimer RJ, Carter SR. Skip metastases in Ewing's sarcoma: a report of three cases. *Skeletal Radiol*. 1997;26:379-384.
50. Saifuddin A. The accuracy of imaging in the local staging of appendicular osteosarcoma. *Skeletal Radiol*. 2002;31(4):191-201.
51. Bredella MA, Caputo GR, Steinbach LS. Value of FDG positron emission tomography in conjunction with MR imaging for evaluating therapy response in patients with musculoskeletal sarcomas. *AJR Am J Roentgenol*. 2002;179:1145-1150.
52. Bastiaannet E, Groen H, Jager PL, et al. The value of FDG-PET in the detection, grading and response to therapy of soft tissue and bone sarcomas: a systematic review and meta-analysis. *Cancer Treat Rev*. 2004;30:83-101.
53. Levine E, De Smet AA, Huntrakoon M. Juxtacortical osteosarcoma: a radiologic and histologic spectrum. *Skeletal Radiol*. 1985;14:38-46.
54. Murphey MD, Robbin MR, McRae GA, Flemming DJ, Temple HT, Kransdorf MJ. The many faces of osteosarcoma. *Radiographics*. 1997;17:1205-1231.
55. Cohen EK, Kressel HY, Frank TS, et al. Hyaline cartilage origin of bone and soft tissue neoplasms: MR appearance and histologic correlation. *Radiology*. 1988;167:477-481.
56. Rahmouni A, Montazel JL, Divine M, et al. Bone marrow with diffuse tumor infiltration in patients with lymphoproliferative diseases: dynamic gadolinium-enhanced MR imaging. *Radiology*. 2003;229(3):710-717.
57. Roodman GD. Mechanisms of bone lesions in multiple myeloma and lymphoma. *Cancer*. 1997;80(suppl 8):1557-1563.
58. Hong SP, Hahn JS, Lee JD, Bae SW, Youn MJ. 18F-fluorodeoxyglucose-positron emission tomography in the staging of malignant lymphoma compared with CT and 67Ga scan. *Yonsei Med J*. 2003;44(5):779-786.
59. States LJ. Imaging of metabolic bone disease and marrow disorders in children. *Radiol Clin North Am*. 2001;39(4):749-772.
60. Deely DM, Schweitzer ME. MR imaging of bone marrow disorders. *Radiol Clin North Am*. 1997;35:193-212.
61. Tardivon AA, Vanel D, Munck JN, Bosq J. Magnetic resonance imaging of the bone marrow in lymphomas and leukemias. *Leuk Lymphoma*. 1998;25:55-68.
62. Biesecker JL, Marcove RC, Huvos AG, Mike V. Aneurysmal bone cysts. A clinicopathologic study of 66 cases. *Cancer*. 1970;26:615-625.
63. Hudson TM. *Radiologic-Pathologic Correlation of Musculoskeletal Lesions*. Baltimore, MD: Williams & Wilkins; 1987;261-285.
64. Kransdorf MJ, Sweet DE. Aneurysmal bone cyst: concept, controversy, clinical presentation, and imaging. *AJR Am J Roentgenol*. 1995;164:573-580.
65. Ragsdale BD. Polymorphic fibro-osseous lesions of bone: an almost site-specific diagnostic problem of the proximal femur. *Hum Pathol*. 1993;24:505-512.
66. Gilkey FW. Liposclerosing myxofibrous tumor of bone. *Hum Pathol*. 1993;24:1264.
67. Kransdorf MJ, Murphey MD, Sweet DE. Liposclerosing myxofibrous tumor: a radiologic-pathologic-distinct fibro-osseous lesion of bone with a marked predilection for the intertrochanteric region of the femur. *Radiology*. 1999;212(3):693-698.
68. O'Connell JX, Nanthakumar SS, Nielsen GP, Rosenberg AE. Osteoid osteoma: the uniquely innervated bone tumor. *Mod Pathol*. 1998;11:175-180.
69. Liu PT, Chivers FS, Roberts CC, Schultz CJ, Beauchamp CP. Imaging of osteoid osteoma with dynamic gadolinium-enhanced MR imaging. *Radiology*. 2003;227(3):691-700.
70. Rosenthal DI, Hornicek FJ, Torriani M, Gebhardt MC, Manin HJ. Osteoid osteoma: percutaneous treatment with radiofrequency energy. *Radiology*. 2003;229(1):171-175.
71. Murphey MD, Gross TM, Rosenthal HG. Musculoskeletal malignant fibrous histiocytoma: radiologic-pathologic correlation. *Radiographics*. 1994;14:807-826.
72. Banks KP, Bui-Mansfield LT, Chew FS, Collinson F. A compartmental approach to the radiographic evaluation of soft-tissue calcifications. *Semin Roentgenol*. 2005;40(4):391-407.
73. Jelinek J, Kransdorf MJ. MR imaging of soft-tissue masses. Mass-like lesions that simulate neoplasms. *Magn Reson Imaging Clin N Am*. 1995;3:727-741.
74. Parikh J, Hyare H, Saifuddin A. The imaging features of post-traumatic myositis ossificans, with emphasis on MRI. *Clin Radiol*. 2002;57(12):1058-1066.
75. Varma DG, Mouloupoulos A, Sara AS, et al. MR imaging of extracranial nerve sheath tumors. *J Comput Assist Tomogr*. 1992;16:448-453.
76. Wold LE, Sweet RG, Sim FH. Vascular lesions of bone. *Pathol Ann*. 1985;20:101-137.
77. Jones BC, Sundaram M, Kransdorf MJ. Synovial sarcoma: MR imaging findings in 34 patients. *AJR Am J Roentgenol*. 1993;161:827-830.
78. Kransdorf M, Murphey MD. *Imaging of Soft Tissue Tumors*. Philadelphia, PA: WB Saunders; 1997:79-94.
79. Jelinek JS, Kransdorf MJ, Shmookler BM, Aboulafia AJ, Malewer MM. Liposarcoma of the extremities: MR and CT findings in the histologic subtypes. *Radiology*. 1993;186:455-459.
80. Peterson JJ, Kransdorf MJ, Bancroft LW, O'Connor MI. Malignant fatty tumors: classification, clinical course, imaging appearance and treatment. *Skeletal Radiol*. 2003;32(9):493-503.
81. Hernandez MV, Peris P, Guanabens N, et al. Biochemical markers of bone turnover in Camurati-Engelmann disease: a report on four cases in one family. *Calcif Tissue Int*. 1997;61:48-51.
82. Saraiva JM. Progressive diaphyseal dysplasia: a three-generation family with markedly variable expressivity. *Am J Med Genet*. 1997;71:348-352.
83. Veyssier-Belot C, Cacoub P, Caparros-Lefebvre D, et al. Erdheim-Chester disease. Clinical and radiologic characteristics of 59 cases. *Medicine (Baltimore)*. 1996;75(3):157-169.
84. Evans S, Williams F. Case report: Erdheim-Chester disease: polyostotic sclerosing histiocytosis. *Clin Radiol*. 1986;37(1):93-96.
85. Brower AC, Worsham GF, Dudley AH. Erdheim-Chester disease: a distinct lipoidosis or part of the spectrum of histiocytosis? *Radiology*. 1984;151(1):35-38.
86. Hoekstra HJ, Ham SJ, van der Graaf WT, Kamps WA, Molenaar WM, Schraffordt Koops H. Malignant fibrous histiocytoma of bone: a clinicopathologic study of 81 patients. *Cancer*. 1998;82:993-994.
87. Picci P, Bacci G, Ferrari S, Mercuri M. Neoadjuvant chemotherapy in malignant fibrous histiocytoma of bone and in osteosarcoma located in the extremities: analogies and differences between the two tumors. *Ann Oncol*. 1997;8:1107-1115.
88. Galli SJ, Weintraub HP, Proppe KH. Malignant fibrous histiocytoma and pleomorphic sarcoma in association with medullary bone infarcts. *Cancer*. 1978;41:607-609.
89. Desai P, Perino G, Present D, Steiner GC. Sarcoma in association with bone infarcts. Report of five cases. *Arch Pathol Lab Med*. 1996;120:482-489.
90. Gaucher AA, Regent DM, Gillet PM, Pere PG, Aymard BM, Clement V. Case report 656: malignant fibrous histiocytoma in a previous bone infarct. *Skeletal Radiol*. 1991;20(2):137-140.
91. Servedo M. Klippel and Trenaunay's syndrome. 768 operated cases. *Ann Surg*. Mar 1985;201(3):365-373.
92. Samuel LM, Spitz L. Klippel-Trenaunay syndrome: clinical features, complications and management in children. *Br J Surg*. 1995;82(6):757-761.
93. Brown RR, Steiner GC, Lehman WB. Melorheostosis: case report with radiologic-pathologic correlation. *Skeletal Radiol*. 2000;29(9):548-552.
94. Mellado JM, Bencardino JT. Morel-Lavallée lesion: review with emphasis on MR imaging. *Magn Reson Imaging Clin N Am*. 2005;13(4):775-782.
95. Tejwani SG, Cohen SB, Bradley JP. Management of Morel-Lavallée lesion of the knee: twenty-seven cases in the national football league. *Am J Sports Med*. 2007;35(7):1162-1167.

CHAPTER

# 6

## Knee

**CLINICAL HISTORY** A 3-year-old boy with swelling of the left knee. A, asymptomatic right knee radiograph; B-C, left knee radiograph; D-F, sagittal left knee MRI.

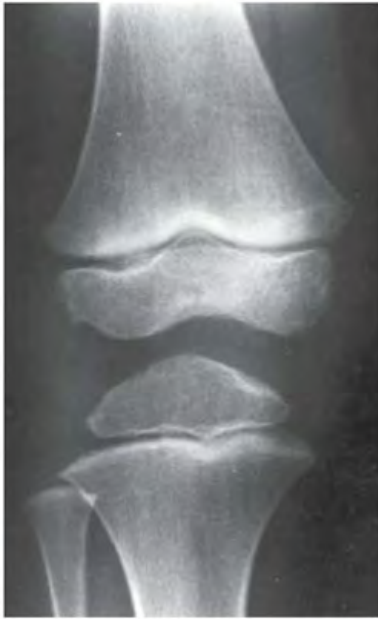


FIGURE 6.1A



FIGURE 6.1B



FIGURE 6.1C

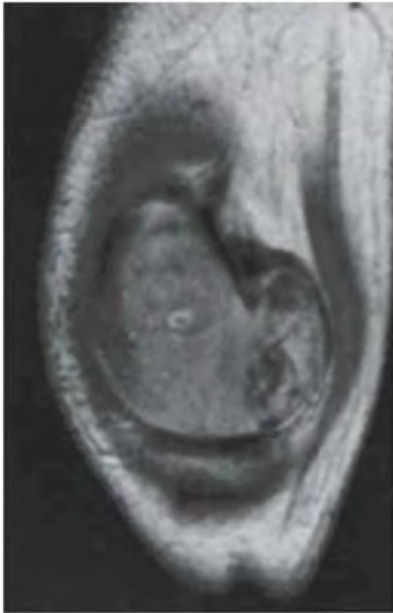


FIGURE 6.1D



FIGURE 6.1E



FIGURE 6.1F

**FINDINGS**

- A. Anteroposterior (AP) radiograph of the right knee is normal.
- B, C. AP and lateral radiographs of the left knee demonstrate small, multifocal ossifications seen medial and posterior to the normal epiphysis.
- D–F. Sagittal magnetic resonance imaging (MRI) through the medial femoral condyle using T1 weighting, proton density, and T1 weighting after intravenous gadolinium demonstrates cartilaginous overgrowth of the posterior aspect of the femoral epiphysis, with a secondary center of ossification. There is no mass lesion separate from this epiphyseal overgrowth.

**DIFFERENTIAL DIAGNOSIS** Articular chondroma, loose body, osteochondritis dissecans.

**DIAGNOSIS** Articular chondroma (dysplasia epiphysealis hemimelica).

**DISCUSSION** Articular chondroma, also called dysplasia epiphysealis hemimelica or Trevor disease [1], histologically consists of hyaline cartilage. It may be considered an epiphyseal form of osteochondroma. It is unilateral and typically affects only one-half of the epiphysis of a long bone (usually the medial portion), as seen here. The most common location is in the lower extremity, particularly about the ankle, which explains the alternate term of tarsal aklasis. It may or may not be associated with multiple exostoses. It is usually manifested in childhood. Complications include impaired growth and joint abnormalities, particularly deformities of alignment from the asymmetric growth. MRI is the most helpful imaging study in evaluating these lesions [2].



FIGURE 6.2A



FIGURE 6.2B



FIGURE 6.2C



FIGURE 6.2D

## FINDINGS

- A, B. AP and lateral radiographs of the knee. There is a lucent lesion in the lateral femoral condyle. There is very little reactive bone, if any. The posterior cortex may be violated on the lateral view.
- C, D. Coronal T2-weighted and sagittal T1-weighted MRI demonstrates T1 hypointensity and T2 isointensity to muscle, with multiple round areas of T2 hyperintensity at the margins.

**DIFFERENTIAL DIAGNOSIS** Giant cell tumor, chondroblastoma, clear cell chondrosarcoma.

**DIAGNOSIS** Giant cell tumor.

**DISCUSSION** The diagnostic possibilities for a large, solitary epiphyseal lesion in an adult include giant cell tumor, chondroblastoma, and clear cell chondrosarcoma. Chondroblastomas usually have sclerotic borders. Calcification is seen in 50% of patients, and periosteal reaction is seen in 50% of patients. Clear cell chondrosarcoma typically occurs in the proximal femur or proximal humerus. Therefore, the most likely diagnosis is giant cell tumor.

Giant cell tumor of bone (osteoclastoma) is an uncommon lesion thought to arise from osteoclasts. The presence of giant cells is only one histologic component of the tumor, and other types of tumors may have giant cells. Giant cell tumors can occur at any age, but the typical patient is a young adult. The location is almost invariably in the epiphysis, with extension to the subchondral cortex and into the metaphysis. Less than 2% of these tumors occur adjacent to open growth plates. Giant cell tumors probably arise in the cutback zone

of the metaphysis, where osteoclasts are plentiful and active. About 50% of tumors are found about the knee, but other long bones and the sacrum are also commonly involved.

The typical radiographic appearance is a geographic, lytic tumor near the end of a long bone, extending to or very close to the subarticular cortex. Lytic regions correspond to nonmineralized tumor tissue, destroying and replacing cancellous bone. A lobular pattern of growth may leave ridges or trabeculations in surrounding bone. Giant cell tumors are often expansile and may have cystic blood-filled regions similar to aneurysmal bone cysts. The zone of transition from tumor to normal bone is usually sharp and abrupt, but without a sclerotic margin (growth rate I-B). Some lesions erode from the epiphysis into the joint cavity and provoke synovitis. Approximately 10% of patients present with pathologic fracture. Computed tomography (CT) or MRI may be required to show the extent of tumor and the relationship to the adjacent joint. Giant cell tumors appear as areas of intense isotope uptake on bone scan and sometimes have a doughnut appearance, with greater activity at the margins.

The typical treatment of giant cell tumor is curettage; adjuvant treatment of the surgical bed with a high-speed burr, phenol, or cryotherapy; and packing with methylmethacrylate. The reported overall rate of recurrence is about 25%. There are case reports of pulmonary and skin metastases from giant cell tumors [3,4]. Older literature suggests the existence of malignant giant cell tumors, but these may have represented primary malignant lesions such as osteosarcoma or malignant fibrous histiocytoma (MFH) that have prominent giant cells at histology. Spontaneous malignant transformation of a conventional giant cell tumor is rare [5].



FIGURE 6.3A



FIGURE 6.3B

**FINDINGS** Lateral (A) and AP (B) radiographs of the knee. There is a large, destructive lesion involving the medial aspect of the distal femoral metaphysis, with cortical destruction and large soft tissue mass. The lesion extends to the growth plate but does not appear to cross into the epiphysis. Laminated, interrupted periosteal reaction is seen at the superior margin of the tumor. The margins of the lesion are poorly defined. Dense, amorphous regions of mineralization are present within the lesion.

**DIFFERENTIAL DIAGNOSIS** Osteosarcoma, Ewing sarcoma, lymphoma, metastasis.

**DIAGNOSIS** Osteosarcoma, high-grade intramedullary type.

**DISCUSSION** This destructive lesion should be unmistakable for a bone tumor. The lesion is moderately mineralized, and the mineralization has the dense, amorphous, cloud-like pattern characteristic of osteoid matrix. The location of the

lesion and age of the patient is typical for the diagnosis. The age distribution of osteosarcoma has a sharp peak (46% of cases) between the ages of 10 and 20, but it has been described in very young children and in elderly adults. Osteosarcomas have been described in virtually every part of the skeleton, but the least common sites are probably the hands and feet.

In the Mayo Clinic series of bone tumors [6], the most common anatomic sites of osteosarcomas were distal femur (31%), proximal tibia (15%), proximal humerus (8%), pelvis (7%), proximal femur (5%), and femoral shaft (4%). Of osteosarcomas that occur in the long bones, only about 10% are found in the diaphysis alone, without extension to the metaphysis or epiphysis. The majority of osteosarcomas have no known cause, but in this series, more than 5% were found in irradiated bone, and more than 3% were found in regions of Paget disease. Patients older than 60 are much more likely to have a preexisting condition (38%).

**CLINICAL HISTORY** A young adult woman with headache, dizziness, prolonged bleeding time, and hypertension.

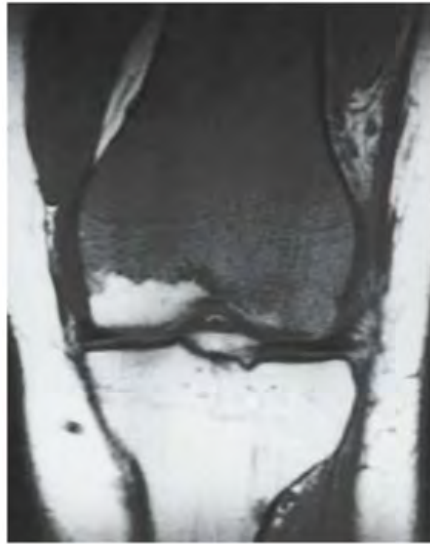


FIGURE 6.4A



FIGURE 6.4B



FIGURE 6.4C

**FINDINGS** (A, B) Coronal and (C) sagittal T1-weighted MRI demonstrate replacement of the normal fatty high-signal-intensity marrow with conglomerate deposits of low-signal-intensity material in both the femur and tibia. The visualized articular surfaces are normal.

**DIFFERENTIAL DIAGNOSIS** Polycythemia vera, multiple myeloma, lymphoma, leukemia, hemoglobinopathies.

**DIAGNOSIS** Polycythemia vera.

**DISCUSSION** Polycythemia vera is an idiopathic monoclonal marrow-proliferating process. Hyperplasia is most pronounced in the red blood cell constituents of the bone

marrow. The main complications are thrombosis and bleeding diathesis. Multiple focal lytic lesions are characteristic. On MRI, replacement of the normal fatty marrow is reflected by decreased signal intensity on T1-weighted imaging, as seen here, showing an intermediate signal intensity on T2-weighted MRI between muscle and fat [7]. Later in the disease, marrow may be replaced by fibrosis and produce a clinical and radiologic appearance of myelofibrosis with extramedullary hematopoiesis. In this phase, there is decreased signal intensity in the bone marrow on both T1-weighted and T2-weighted MRI [8,9]. Secondary forms of polycythemia may occur and give rise to similar features. Gout, due to hyperuricemia, may complicate the radiographic findings. Definitive diagnosis is by bone marrow biopsy.

**CLINICAL HISTORY** A 20-year-old woman with knee pain and swelling for 3 months.



FIGURE 6.5A

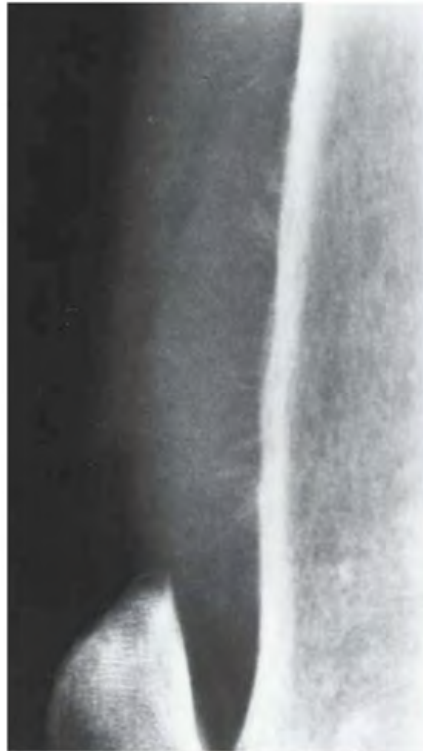


FIGURE 6.5B

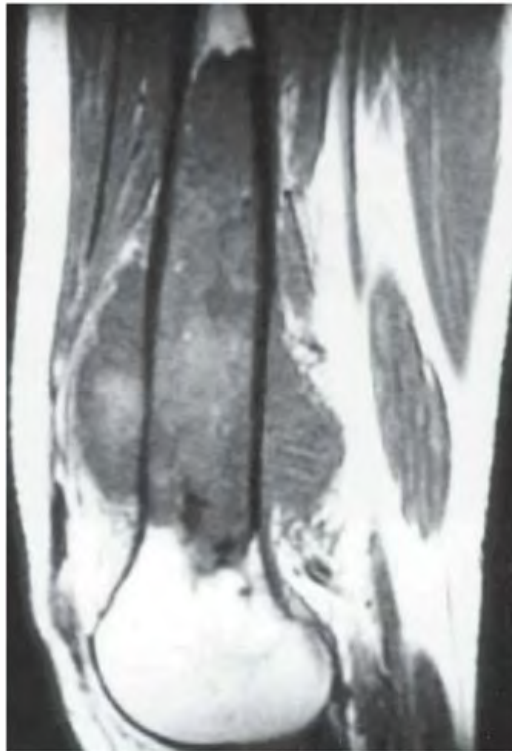


FIGURE 6.5C



FIGURE 6.5D

**FINDINGS**

- A. AP radiograph of the distal femur. There is a mildly expansile lesion in the distal femur causing slight irregularity of the texture of the cortical bone, with a few localized areas of amorphous mineralization distally. There is subtle periosteal elevation medially and laterally at the distal shaft. The proximal and distal intramedullary extent of the lesion is imperceptible.
- B. Lateral radiograph of the distal femur, photographic detail. There is permeation of tumor through the anterior femoral cortex into the soft tissues, with sunburst periosteal reaction and soft tissue mass. The destruction of the cortex is evident as unsharpness of its margins and vague lucency; the overall structure of the cortex remains intact.
- C. Sagittal T1-weighted MRI shows an extensive intramedullary lesion with heterogeneous signal. The lesion penetrates the cortex anteriorly and posteriorly to form large soft tissue masses. Small regions of very low signal at the inferior extent of the tumor correspond to the mineralized matrix seen on the AP radiograph.
- D. Radionuclide bone scan. Anterior whole-body scan (photographic detail) shows intense activity in the distal femur, corresponding to the tumor. There is also a modest regional increase in activity in the proximal femur and proximal tibia.

**DIFFERENTIAL DIAGNOSIS** Osteosarcoma, Ewing sarcoma, lymphoma, metastasis.

**DIAGNOSIS** Osteosarcoma, high-grade intramedullary type.

**DISCUSSION** This case illustrates a high-grade intramedullary osteosarcoma whose radiographic features are more subtle but nonetheless highly aggressive. The true extent of the lesion is shown dramatically by the MRI. The radionuclide bone scan shows a pattern of falsely extended uptake that corresponds to hyperemia and osteoporosis in the otherwise normal adjacent bone [10]. In contrast to the preceding cases, the lesion in this case is only slightly ossified.

**CLINICAL HISTORY** *A 24-year-old woman with mass behind her left knee.*



FIGURE 6.6A



FIGURE 6.6B



FIGURE 6.6C

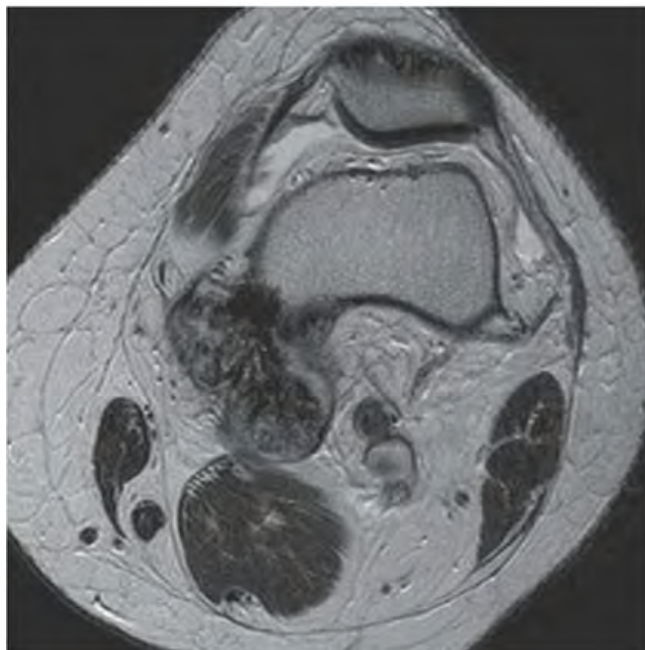


FIGURE 6.6D



FIGURE 6.6E

## FINDINGS

- A, B. AP and lateral radiographs of the left knee show ill-defined dense osteoid densities centered about the posteromedial cortex of distal femoral metadiaphysis.
- C, D. Coronal fat-saturated T2-weighted and axial T2-weighted MR images show a T2-dark cortically based mass without intramedullary extension.
- E. Axial CT (bone windows) shows a dense lesion arising from the posterior cortex of the left knee. The lesion has destroyed the cortex at the posterior medial margin of the femoral shaft, but there is no apparent tumor extending into the medullary space. The bulk of the tumor appears to be densely mineralized.

**DIFFERENTIAL DIAGNOSIS** Parosteal osteosarcoma, osteochondroma, periosteal osteosarcoma, high-grade surface osteosarcoma, myositis ossificans.

**DIAGNOSIS** Parosteal osteosarcoma (juxtacortical osteosarcoma).

**DISCUSSION** Parosteal osteosarcomas represent approximately 5% of osteosarcomas. They differ from the conventional high-grade intramedullary osteosarcoma in several significant ways. Parosteal osteosarcoma arises on the cortical surface rather than within the medullary space, and virtually all are found in the metaphysis of a long bone, especially the posterior surface of the distal femoral metaphysis (66% of cases). The peak age at diagnosis is in the third decade, with more than 80% of patients older than 20. The presentation is nonspecific—often dull aching pain or mechanical difficulties caused by the mass itself. The lesions are commonly diagnosed and

treated incorrectly for years as atypical osteochondromas that somehow recur locally. Even with late diagnosis, the prognosis is often better than for conventional osteosarcoma because they are, by definition, of low histologic grade (a higher-grade osteosarcoma arising on the surface of bone would be classified by the pathologist as either a periosteal osteosarcoma or a high-grade surface osteosarcoma).

The radiographic appearance is a lobulated, juxtacortical mass with densely ossified tumor tissue attached to the cortex, often by a stalk. Variable amounts of lucent, nonossified tissue are usually present, making the lesion larger than apparent on plain radiographs. The peripheral portions of the lesion tend to have the least ossification. A cleavage plane between tumor and underlying bone may be visible at the edge of the stalk in approximately two-thirds of cases, and it is characteristic of the slow, lobular growth of the tumor as it becomes larger than its attachment to the bone. Tumor invasion of the medullary cavity may occur by direct extension through the stalk. Such invasion is found in the minority of cases and can often be documented by CT or MRI [11]. Localized regions of histopathologic dedifferentiation to high-grade spindle cell sarcoma is not uncommon (28%), either at presentation or at local recurrence [12]. The presence of a poorly defined soft tissue component distinct from the mineralized matrix is suggestive of a high-grade focus [13]. Parosteal osteosarcoma is the only malignant primary bone tumor that is more common in females than males (by a ratio of nearly 2:1 in the Mayo Clinic series) [12]. The treatment of parosteal osteosarcoma is surgical. Recurrences with simple curettage are common, but wide excision with clear surgical margins may be curative. Long-term survival rates of 80% to 90% may be expected for patients without regions of dedifferentiation.

**CLINICAL HISTORY** A 35-year-old man with chronic, aching knee pain.



FIGURE 6.7A

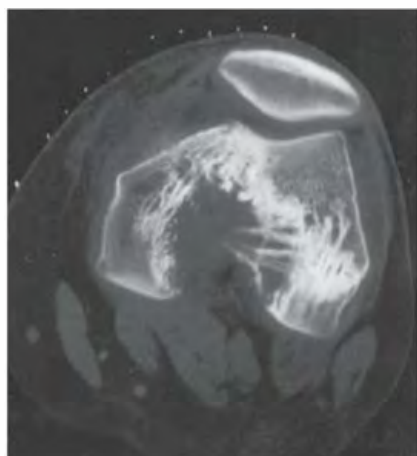


FIGURE 6.7B

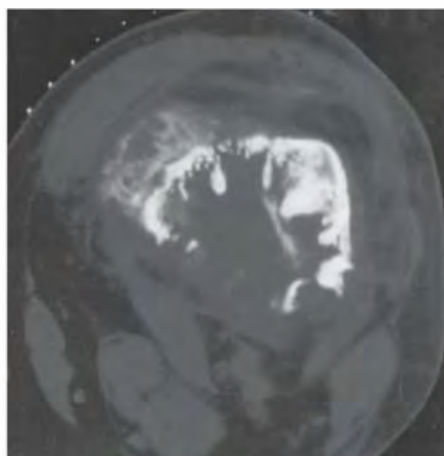


FIGURE 6.7C

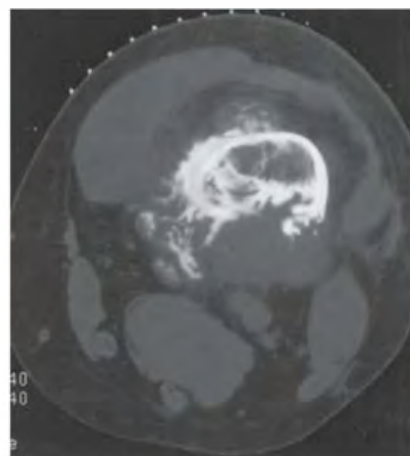


FIGURE 6.7D

## FINDINGS

- A. AP radiograph of the knee. Bone loss is present at the intercondylar portion of the distal femur, probably extending to the medial cortex, with prominent reinforcement of the remaining trabeculae. Amorphous sclerosis is seen at the medial edge of the femur and along the more superior portion of the cortex adjacent to the intercondylar bone defect.
- B. Axial noncontrast CT at the level of the femoral condyles shows a central destructive lesion with surrounding, sclerotic, reinforced trabecular bone. At the anteromedial cortex is a small, faintly mineralized soft tissue mass.
- C. CT at the distal shaft shows extensive cortical bone destruction with prominent reinforced trabecular bone. Dense amorphous mineralization is seen on the endosteal surface of the anterior cortex. A mineralized soft tissue mass is present.
- D. CT more proximally along the femoral shaft shows a large, partially mineralized soft tissue mass.

**DIFFERENTIAL DIAGNOSIS** Osteosarcoma, chondrosarcoma, lymphoma, metastasis, desmoplastic fibroma.

**DIAGNOSIS** Osteosarcoma, low-grade intramedullary type.

**DISCUSSION** This case has features of an aggressive lesion as well as an indolent lesion. The presence of cortical destruction, cortical penetration, and formation of soft tissue mass suggests an aggressive process. The presence of reinforced trabeculae compensating structurally for the regions of cortical destruction suggests a lesion that has been present for some time. The mineralization of the soft tissue portion of the lesion suggests a bone-forming tumor.

Low-grade osteosarcomas are well-differentiated bone-forming malignancies whose radiologic and histopathologic appearances are challenging to the diagnostician [12,14]. Rare lesions, they occur in adults and are typically found around the knee. The prognosis for long-term survival is excellent, but local recurrences may be accompanied by dedifferentiation to high-grade tumor and metastatic spread.

**CLINICAL HISTORY** *A 47-year-old man with knee pain.*



FIGURE 6.8A



FIGURE 6.8B

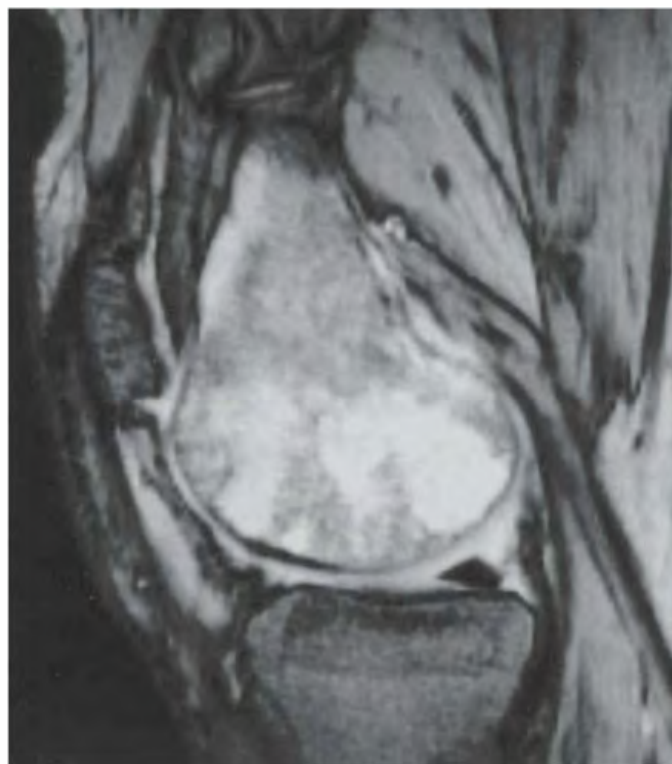


FIGURE 6.8C

**FINDINGS**

- A, B. AP and lateral radiographs show a lytic lesion in the medial femoral condyle with ill-defined borders, but extending to the articular surface. An associated soft tissue mass is not noted, and there is no associated periostitis.
- C. Sagittal T2-weighted MRI demonstrates high signal intensity in this lesion, without definite cortical violation.

**DIFFERENTIAL DIAGNOSIS** Malignant fibrous histiocytoma (MFH) of bone, metastasis, osteosarcoma, fibrosarcoma, chondrosarcoma, lymphoma.

**DIAGNOSIS** MFH of bone.

**DISCUSSION** MFH is a lesion that may occur in soft tissue or bone. MFH is considered to be of histiocytic origin. Histologically, the lesions show fibrogenic differentiation, and multinucleated malignant giant cells may be a prominent feature. MFH arising in bone is relatively rare, comprising only 1% of primary malignant bone tumors [12]. MFH more frequently arises in the soft tissues. The age range of

patients is wide, but most patients are adults. Although most lesions occur around the knee, lesions have been reported in the extremities, spine, and skull. In long bones, the lesions are usually metaphyseal. As with other types of bone tumors, the typical clinical presentation is pain and swelling. Approximately 25% of MFH in bone is secondary to a preexisting pathologic process, most commonly previous radiation therapy, Paget disease, or bone infarction. Joint implants or their alloys have also been named as an inciting factor for MFH of bone [15].

The radiographic appearance is usually one of aggressive bone destruction with a moth-eaten or permeative pattern, as seen here. Reactive bone tends to be scant, and there will be no mineralized tumor matrix. The differential diagnosis includes metastasis, osteosarcoma, fibrosarcoma, chondrosarcoma, and lymphoma. The pathologic distinction between MFH and other bone sarcomas may be difficult. The presence of even microscopic foci of neoplastic osteoid or chondroid would cause the lesion to be classified as an osteosarcoma or chondrosarcoma, respectively. The distinction between MFH and fibrosarcoma is considered by some to be arbitrary, and they are radiologically indistinguishable.

**CLINICAL HISTORY** A 52-year-old woman with knee pain for several weeks, without a precipitating episode of trauma.



FIGURE 6.9A



FIGURE 6.9B

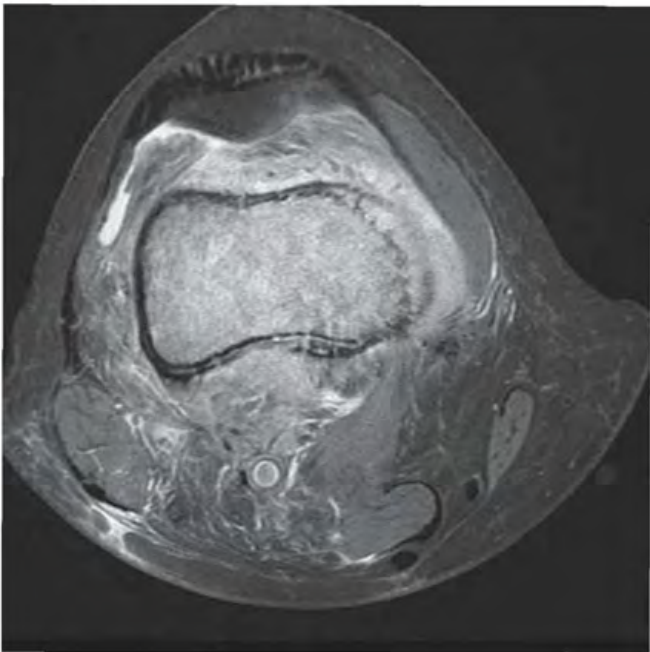


FIGURE 6.9C



FIGURE 6.9D

## FINDINGS

- A. AP radiograph of the knee shows very subtle permeated destruction along the medial cortex of the femoral metaphysis.
- B. Coronal T1-weighted MRI shows a large lesion replacing the normal fatty marrow, extending from the femoral shaft into the medial condyle. The periosteum is lifted by the lesion, and there is soft tissue extension.
- C. Axial T2-weighted MRI with fat suppression shows high signal in the lesion, medial and posterior cortical destruction, soft tissue extension, and surrounding edema.
- D. Sagittal proton density MRI with fat suppression shows anterior and posterior soft tissue involvement and an enlarged popliteal lymph node.

**DIFFERENTIAL DIAGNOSIS** Lymphoma, metastases, plasmacytoma, osteosarcoma, infection.

**DIAGNOSIS** Primary lymphoma of bone.

**DISCUSSION** Primary lymphoma of bone can have a near-normal appearance on radiographs [16]. MRI, as seen here, can show a large abnormality. In this case, the diagnosis was made by CT-guided needle biopsy. Sclerotic lymphoma of bone is one circumstance in which the percutaneously

guided needle biopsy can be falsely negative. The infiltrative nature of the disease and the fragility of the cells may result in such severe crush artifacts that evidence of malignancy may be destroyed during the process of obtaining the specimen.

Patients with lymphoma involving bone may present with symptoms related to a bone lesion, or bone lesions may be discovered during staging after the diagnosis has been made from an extraskkeletal site. Patients presenting with lymphoma of bone are considered to have primary lymphoma of bone if they have no evidence of the disease elsewhere. Primary lymphoma of bone constituted 3.9% of the cases of malignant bone lesions in the Mayo Clinic series [17]. There is a broad age range at time of diagnosis, and most lymphomas involve the portion of the skeleton containing red marrow. Bone destruction is the primary radiographic feature of primary lymphoma, and generally results in a permeated destruction of cortical and trabecular bone. A mottled and patchy appearance is typical. Approximately 50% of cases may have evidence of reactive bone or thickening of the cortex, but this reactive bone is typically sparse, and periosteal bone formation as might be seen in Ewing's sarcoma is notably unusual. Soft tissue extension may be obvious, large, and asymmetric. Pathologic fracture is common. In a minority of cases, irregular sclerosis is present at the affected site, rather than a mixture of lysis and sclerosis.

**CLINICAL HISTORY** A female college varsity soccer player with persistent pain after injury. The team doctor ordered an MRI.



FIGURE 6.10A



FIGURE 6.10B



FIGURE 6.10C

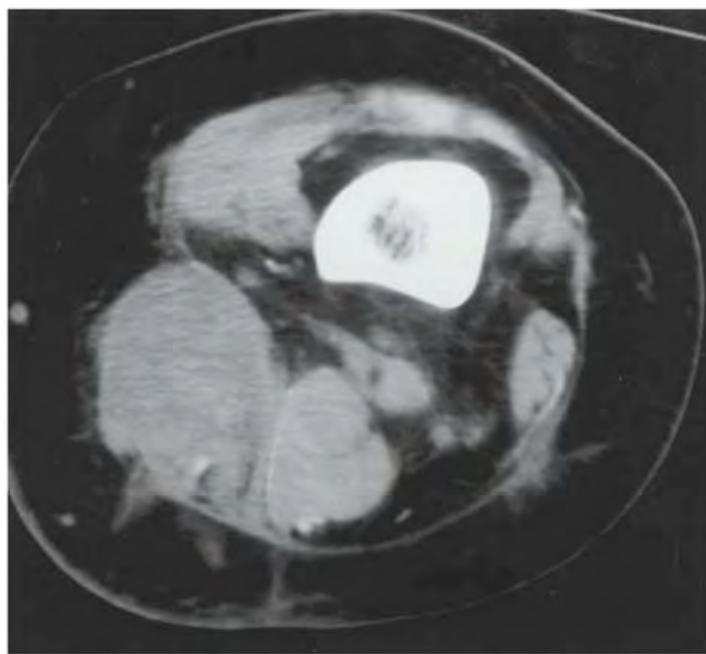


FIGURE 6.10D

**FINDINGS**

- A. Coronal T1-weighted MRI shows enlargement of the sartorius muscle. The margins of the muscle are slightly irregular, and subcutaneous edema is present.
- B. Coronal T2-weighted MRI shows high signal intensity in the sartorius muscle.
- C. Axial T2-weighted MRI shows the enlargement of the sartorius, with high signal intensity and surrounding edema.
- D. Axial CT at the time of needle biopsy shows enlargement of the sartorius.

**DIFFERENTIAL DIAGNOSIS** Non-Hodgkin lymphoma, intramuscular metastasis, soft tissue sarcoma, inflammatory disease, intramuscular tear and/or hemorrhage.

**DIAGNOSIS** Non-Hodgkin lymphoma.

**DISCUSSION** Factors that favor malignancy in a soft tissue mass are large size, deep location (e.g., intramuscular), and surrounding edema. The abnormality of the sartorius in this case has an aggressive appearance because of the diffuse nature of the enlargement and the markedly irregular margins around the muscle belly. The differential diagnosis includes inflammatory disease, intramuscular tear and/or hemorrhage, intramuscular metastasis, and soft tissue sarcoma. Lymphoma, presenting as an intramuscular mass without evidence of disease elsewhere, is a distinctly rare entity. Primary intramuscular non-Hodgkin lymphoma has a good prognosis, and because the treatment is not surgical, percutaneous needle biopsy is the key diagnostic procedure in this circumstance [18].

## 6.11

**CLINICAL HISTORY** A 9-year-old boy with swollen and painful knee.  
A-B, radiographs at presentation; C-D, radiographs one year later.



FIGURE 6.11A



FIGURE 6.11B



FIGURE 6.11C



FIGURE 6.11D

## FINDINGS

- A. Lateral radiograph of the knee shows marked synovial hypertrophy and effusion, with epiphyseal overgrowth.
- B. AP radiograph shows squaring of the condyles and degenerative changes.
- C, D. One year later. Lateral and AP radiographs demonstrate the progression of the findings, with the additional feature of erosions of the articular surface.

**DIFFERENTIAL DIAGNOSIS** Hemophilia, juvenile idiopathic arthritis, postinfectious arthropathy.

**DIAGNOSIS** Hemophilic knee.

**DISCUSSION** The early findings in this case may be attributable to juvenile idiopathic arthritis or hemophilia. Juvenile idiopathic arthritis is more common in females and generally shows osteoporosis as an early finding. Erosive changes are frequent in juvenile idiopathic arthritis and are not noted in the initial film, although joint destruction is already evident.

Hemophilia A is a clotting disorder related to factor VIII deficiency. It is transmitted as an X-linked disorder and therefore occurs almost exclusively in males. Although other varieties of hemophilia exist, this is the most common type. The primary radiographic feature of this disorder is hemarthrosis, as seen on the lateral views in this instance, with joint destruction after repeated episodes [19]. Some cardinal features include squaring of the inferior pole of the patella and widening of the intercondylar notch. These findings, however, can also be observed in juvenile idiopathic arthritis [20]. Differentiating features include subperiosteal hemorrhage and intraosseous cystic lesions that are not subarticular. The latter finding is related to intraosseous hemorrhage and, when substantial in size, is referred to as a pseudotumor. These are seen most often in the ilium and calcaneus. Extremity overgrowth or undergrowth may occur, depending on whether hyperemia or early fusion of the growth plate is the predominant effect of the disorder. Avascular necrosis of the epiphysis can occur secondary to elevated intra-articular pressures from hemarthrosis [21]. Avascular necrosis may occur in juvenile idiopathic arthritis as a result of steroid treatment.

## 6.12

**CLINICAL HISTORY** A 7-year-old girl with joint swelling. A, radiograph at presentation; B, radiograph 7 months later.



FIGURE 6.12A



FIGURE 6.12B

## FINDINGS

- A. Lateral knee radiograph taken at presentation. There is widening and fraying of the distal femur, proximal fibula, and tibia physes.
- B. Lateral knee radiograph taken 7 months later. There is interval sclerosis and filling in of the physeal widening.

**DIFFERENTIAL DIAGNOSIS** Rickets, metaphyseal dysplasia.

**DIAGNOSIS** Rickets.

**DISCUSSION** Rickets and osteomalacia are childhood and adult manifestations, respectively, of a systemic disease in which the calcification of osteoid is deficient. The common final pathway in both conditions is the lack of available calcium or phosphorus (or both) for mineralization of osteoid. In rickets, the predominant effect is on the growth plates; in osteomalacia, the predominant effect is on remodeling of mature bone. When rickets or osteomalacia occurs in conjunction with chronic renal failure, the condition is called renal osteodystrophy.

Dietary deficiency of vitamin D, usually coupled with inadequate exposure to sunlight so that photochemical synthesis of vitamin D in the skin does not occur, results in reduced gastrointestinal calcium absorption, hypocalcemia, and secondary hyperparathyroidism to mobilize calcium from the skeleton. Pure vitamin D deficiency-induced rickets and osteomalacia is relatively rare in the United States, except among immigrants, food faddists, the institutionalized elderly, and patients on total parenteral nutrition. Other causes include failure of enzymatic conversion of 25-hydroxyvitamin D to its physiologically more active metabolite 1,25-dihydroxyvitamin D, end-organ insensitivity to 1,25-dihydroxyvitamin D, genetic and acquired renal tubular reabsorption defects, and gastrointestinal malabsorption

of dietary calcium or phosphorus. In the United States, gastrointestinal malabsorption from a variety of etiologies is the most common cause of rickets and osteomalacia. Rickets and osteomalacia may occur in association with polyostotic fibrous dysplasia and neurofibromatosis, and may be caused by chronic use of anticonvulsant medications or aluminum-containing antacids.

In rickets, there is widening of the growth plate because of continued cartilage growth in the absence of normal mineralization and ossification. Radiographic findings are most apparent in the most active regions of growth, and the uncalcified cartilage may become quite bulky. Frequent sites of radiographic abnormalities include the costochondral junctions of ribs, the distal femur, both ends of the tibia, the proximal humerus, the distal radius, and the ulna. Irregular, disorganized mineralization of the zone of provisional calcification creates a frayed appearance. Mechanical stress on the thickened growth plate may lead to widening, cupping, and bowing deformities. Bone texture (trabecular pattern) appears coarsened, and there is a delayed appearance of ossification centers. Rachitic bone is less resistant to bending and shearing loads, and stress fractures and bowing deformities are common. Transverse zones of lucency on the concave side of long bones, called Milkman pseudofractures or Looser zones, are focal collections of nonmineralized osteoid; they probably do not represent insufficiency injuries. After the initiation of successful treatment of rickets, the uncalcified osteoid calcifies, so that the zone of provisional calcification appears as a wide band that narrows the growth plate to its normal thickness. Ossification of nonmineralized subperiosteal osteoid is apparent as new periosteal bone.

Metaphyseal dysplasia is a rare disorder caused by an inborn error in enchondral ossification that results in widened, irregular-appearing growth plates. Laboratory values are normal, however.

## 6.13

**CLINICAL HISTORY** A 3-year-old boy with anemia and a companion case. A, radiograph at age 3; B, radiograph at age 12; C, companion case.



FIGURE 6.13A



FIGURE 6.13B

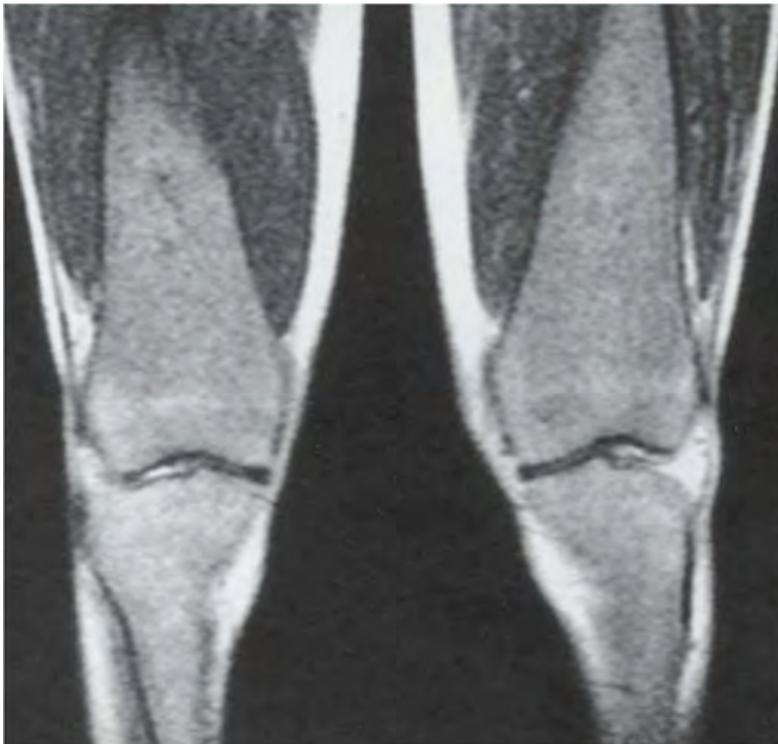


FIGURE 6.13C

## FINDINGS

- A. AP radiograph of a knee taken at age 3 shows Erlenmeyer flask deformities of the femur and tibia.
- B. AP radiograph of the knee taken at age 12 shows a progressive Erlenmeyer flask deformity.
- C. Companion case. Coronal T1-weighted MRI of a young adult shows diffuse replacement of the fatty marrow, with intermediate signal and Erlenmeyer flask deformities.

**DIFFERENTIAL DIAGNOSIS** Gaucher disease, chronic anemias, Pyle disease, Niemann-Pick disease.

**DIAGNOSIS** Gaucher disease.

**DISCUSSION** Anemias, Pyle disease, Niemann-Pick disease, and Gaucher disease can produce Erlenmeyer flask deformities. The bone marrow is one of the largest organs of the body. Confined to the intramedullary space of bone, it consists of a meshwork of trabecular bone with fat cells, myeloid cells, reticulum cells, and supporting structures. At birth, the marrow cavities of the tubular bones, the flat bones, and the vertebrae have a predominance of hematopoietic cells. With advancing age, the hematopoietic marrow regresses and is replaced by fatty marrow, beginning distally in the extremities and progressing to incompletely encompass the pelvis, spine, and cranium. The process may reverse (called marrow reconversion) when there is an increased demand for hematopoiesis, as might occur in anemia or replacement of normal hematopoietic marrow by a pathologic process. Radiographic findings of marrow disorders are indirect and nonspecific.

When chronic marrow space expansion occurs in the growing skeleton, adaptive bone changes may occur during the development of the bone. Actual enlargement of the marrow space will alter the normal bony contours; such changes do not occur acutely, nor do they occur in the adult. MRI is the best method for direct imaging of the bone marrow. Because marrow is a conglomeration of different tissues, the appearance on MRI may vary, both with the composition of the marrow and the particular technical parameters. In general, fatty marrow has the predominant signal characteristics of fat, and hematopoietic marrow has signal characteristics more similar to muscle. Nuclear scans with technetium Tc-99m sulfur colloid or technetium Tc 99mTc methylene diphosphonate can provide physiologic assessments of the reticuloendothelial marrow elements and the surrounding bone, respectively.

The prototype for the lipid storage diseases is Gaucher disease (glucocerebroside lipidosis). In this autosomal recessive condition, deficiency of glucocerebrosidase results in the progressive accumulation of histiocytes laden with glucocerebroside lipids in the bone marrow and other organs and tissues. Secondary changes in bone are observed [22]. The classic radiographic finding is the Erlenmeyer flask deformity, which is undermodeling of the metaphysis due to marrow space packing. Cortical thinning by endosteal erosion and osteopenia are additional radiographic abnormalities that may be evident. Osteonecrosis of the femoral head is a common association, and is usually bilateral. After prolonged enzyme replacement therapy with macrophage-targeted glucocerebrosidase (glucosylceramidase), marrow composition, bone mass, and bone morphology revert toward normal.



FIGURE 6.14A

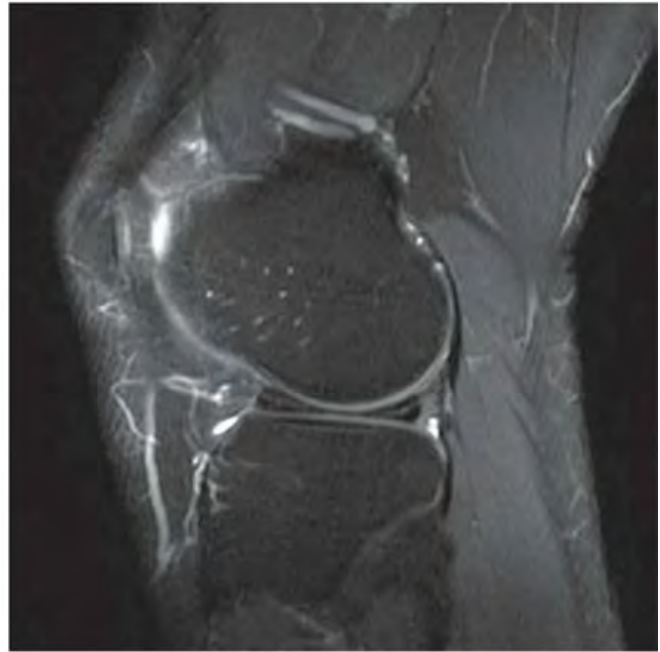


FIGURE 6.14B

**FINDINGS** (A, B) Coronal inversion recovery, and sagittal proton density, fat-suppressed MRI demonstrates a large lateral meniscus with diffusely abnormal signal.

**DIFFERENTIAL DIAGNOSIS** Discoid meniscus, complex meniscal tear.

**DIAGNOSIS** Discoid meniscus with complex tear.

**DISCUSSION** A discoid meniscus is a developmental anomaly that predisposes the patient to meniscal tears. Instead of the

meniscus being C shaped, it is shaped like a disc. With meniscal tissue now present in the joint space, it is more likely to degenerate and tear. The majority of adolescent patients with a meniscal tear have this anomaly. A discoid meniscus appears abnormally large on MRI. It will measure at least 12 mm wide on coronal images and have three or more sagittal images (4 mm thickness each) with a bow-tie appearance. The discoid meniscus is typically lateral in location and does not predispose the patient to tears of the nondiscoid medial meniscus [23]. Treatment of symptomatic patients includes repair of a tear, if present, and saucerization of the excess meniscal tissue [24].

**CLINICAL HISTORY** An 8-year-old boy with knee pain; radiographs are 5 months apart. A, radiograph at presentation; B, radiograph 5 months after presentation; C, radiograph 10 months after presentation.



FIGURE 6.15A

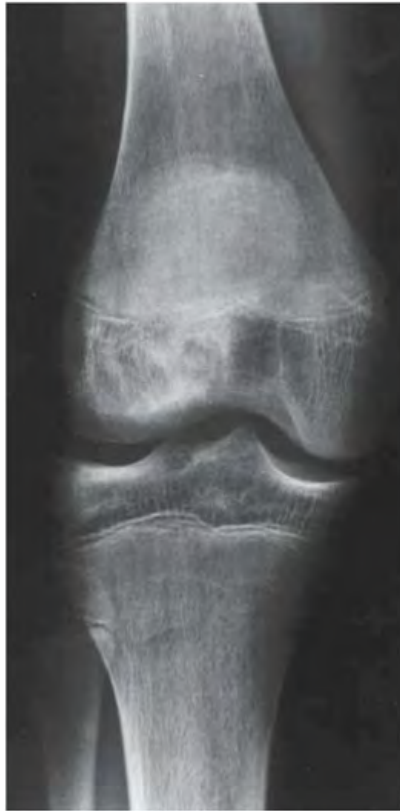


FIGURE 6.15B



FIGURE 6.15C

### FINDINGS

- A. AP film of the right knee demonstrates normal articular surfaces, but medial femoral condyle overgrowth.
- B. AP radiograph of the right knee taken 5 months later demonstrates increased density to the lateral femoral condyle, with a smooth subarticular band.
- C. AP radiograph of the right knee taken 10 months later demonstrates a more defined, solid band of sclerosis within the femoral condyle.

**DIFFERENTIAL DIAGNOSIS** Bone infarct due to hemoglobinopathy, Gaucher disease, steroid medication, trauma, pancreatitis.

**DIAGNOSIS** Sickle cell anemia.

**DISCUSSION** Sickle cell anemia occurs when valine is substituted for glutamate in the beta chain of hemoglobin. The result is an abnormal form of hemoglobin that is less effective at carrying oxygen and predisposed to causing thromboses. The skeletal manifestations of this process include widening of the marrow space, bone infarcts, and an overall dense appearance of the bones. H-shaped vertebra and a snow-capped appearance of the humeral heads is classic. Osteomyelitis is not uncommon, and the diaphysis represents a common site for its occurrence in this condition. Salmonella is a more frequent pathogen in these cases. The main complication is infarctions due to the abnormal configuration of the hemoglobin, as seen here.

**CLINICAL HISTORY** A 38-year-old woman treated with corticosteroids for inflammatory arthritis.



FIGURE 6.16A



FIGURE 6.16B



FIGURE 6.16C

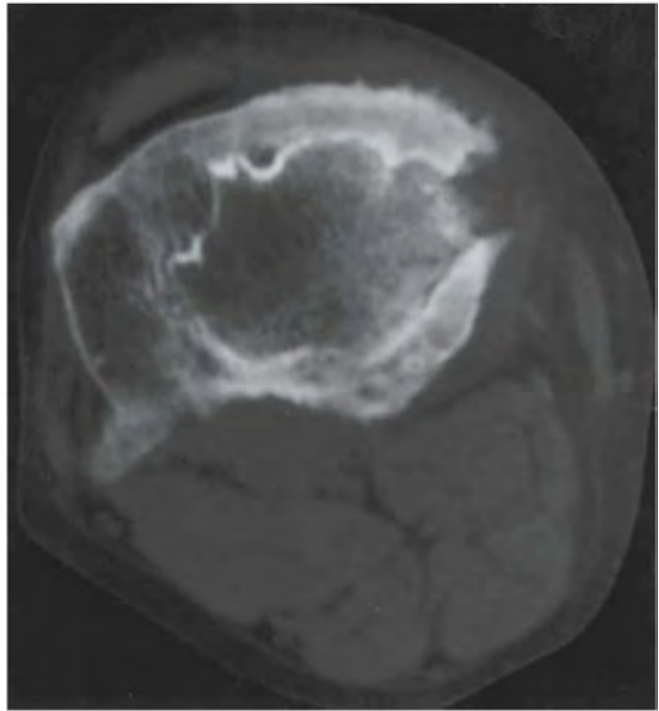


FIGURE 6.16D

**FINDINGS**

- A, B. Lateral and AP radiographs of knee. There are extensive regions of irregular calcification in the distal femur and proximal tibia. There is no mass effect or bone destruction.
- C. Coronal T1-weighted MRI shows the lesions with low-signal-intensity borders and fatty centers.
- D. Axial CT through the tibial epiphysis shows a calcified central lesion with well-defined, serpentine, sclerotic borders and more irregular sclerosis in the surrounding bone.

**DIFFERENTIAL DIAGNOSIS** None.

**DIAGNOSIS** Calcified medullary infarcts with subchondral collapse of the tibial articular surface.

**DISCUSSION** Ossification around the margins of medullary infarcts occurs after revascularization and repair. Bone repair occurs as a process of creeping substitution, and the sclerotic margin represents the portion being repaired. New bone is layered on the infarcted trabeculae, which are then removed very slowly and replaced by living bone. This process is generally too slow to observe progression on serial radiographs. Complications related to bone infarction include subchondral collapse, secondary osteoarthritis and related sequelae, and the rare development of sarcomas such as osteosarcoma or MFH [25].



FIGURE 6.17A

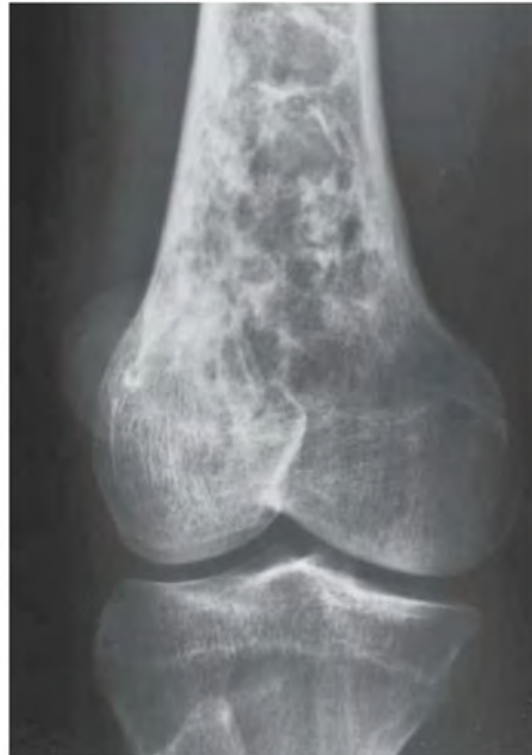


FIGURE 6.17B

**FINDINGS** A, B. Lateral (A) and AP (B) radiographs of the knee. There are sclerotic and cystic-appearing changes in distal femoral metaphysis. The trabecular pattern appears coarsened. There is no cortical destruction, periosteal reactive bone, or soft tissue involvement.

**DIFFERENTIAL DIAGNOSIS** Radiation changes, marrow infarcts, Paget disease, metastases, osteosarcoma, lymphoma, infection.

**DIAGNOSIS** Radiation changes.

**DISCUSSION** A mixed lytic and sclerotic pattern may be seen in Paget disease, metastases, certain primary bone tumors, infection, and radiation. There is no cortical thickening, however, making Paget disease less likely. There is no cortical destruction to suggest tumor or infection.

Therapeutic irradiation is a common treatment for osseous metastases. Sites of bone pain confirmed as abnormal by radiographs or bone scan in patients with known metastases are often radiated as palliative treatment. Irradiated osseous lesions heal by sclerosis and filling in of lytic areas. Radiation effects are independent of the source of the radiation. In the immature skeleton, radiation in total doses of 2,000 cGy or more impairs bone growth. The epiphysis is particularly sensitive, since radiation causes direct cellular injury to chondrocytes, and possibly vascular damage to fine physeal blood vessels. The greater the growth potential at

the time of irradiation, the more profound the effect. If an entire growing bone is irradiated, loss of bone growth in the whole bone results in a small bone. Focal doses affect the irradiated portion; for example, angular deformities could result from an asymmetrically irradiated growth plate. Radiotherapy also increases the risk for epiphyseal plate trauma, including the occurrence of slipped capital femoral epiphysis and avascular necrosis. Scoliosis may follow irradiation of the spine.

In the mature skeleton, the primary complication is radiation osteonecrosis. This is a dose-related effect and occurs due to effects on osteoblasts. The mandible is a common site of involvement, and radiation osteonecrosis occurs more frequently after treatment for oral cancers as opposed to other head and neck tumors [26]. Treatment of radiation-induced osteonecrosis with hyperbaric oxygen may be of benefit [27]. Radiographs and CT will show irregular sclerosis in the irradiated bone. Radiation osteitis shows predominantly sclerosis and periostitis, and predisposes the patient to ischemic necrosis, infection, and fracture.

On bone scan, irradiated bone may initially show increased radionuclide accumulation from hyperemia and new bone formation. After several weeks or months, the bone scan will show decreased radionuclide accumulation due to decreased bone formation and decreased vascularity. On MRI, irradiated bone has the signal characteristics of fatty marrow. The anatomic location and extent of these changes conforms to the size and shape of the radiation portal.

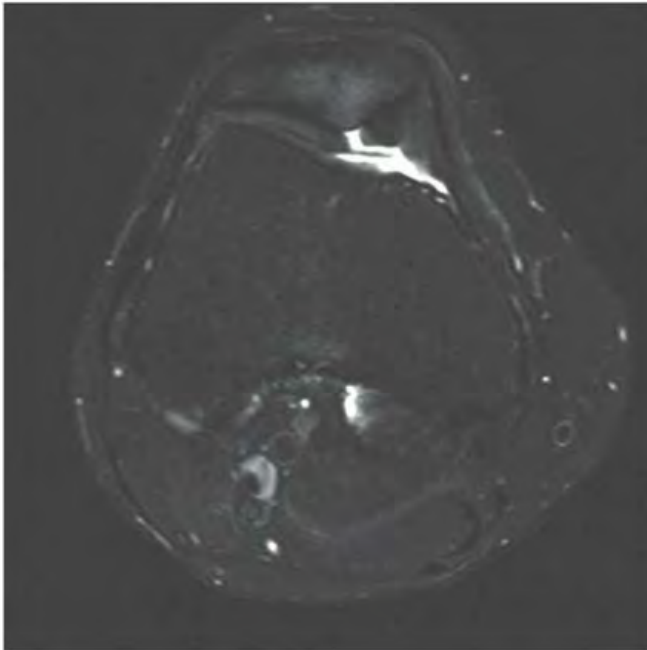


FIGURE 6.18A



FIGURE 6.18B

**FINDINGS** (A, B) Axial and sagittal proton density, fat-saturated MRI demonstrates a fissure and full-thickness loss of the articular cartilage along the patellar ridge associated with subchondral edema.

**DIFFERENTIAL DIAGNOSIS** None.

**DIAGNOSIS** Chondromalacia patellae.

**DISCUSSION** Chondromalacia patellae refers to patellar cartilage damage causing pain. Many different staging methods have been proposed. A method described by Outerbridge [28] is commonly used.

Stage 1: Softening or swelling of the cartilage, seen as signal intensity changes on MRI.

Stage 2: Fragmentation or fissuring of the cartilage measuring half an inch or less.

Stage 3: Fragmentation or fissuring of the cartilage measuring greater than half an inch.

Stage 4: Full-thickness cartilage loss.

Changes in the subchondral bone may be seen. MRI and arthroscopy correlation is better with higher stages [29]. The medial facet, as seen this case, is a common location [30]. Causes include patellar tracking disorders and trauma.



FIGURE 6.19

**FINDINGS** AP standing radiograph of both knees. The bones are osteoporotic. Uniform joint space loss is present with minimal proliferative bone changes. Some secondary osteoarthritic changes are present in the lateral compartment of the left knee, but these are rather modest compared to the amount of joint space loss.

**DIFFERENTIAL DIAGNOSIS** Rheumatoid arthritis, osteoarthritis, pyrophosphate arthropathy.

**DIAGNOSIS** Rheumatoid arthritis.

**DISCUSSION** This case shows features of systemic inflammatory arthritis, with uniform cartilage space loss and osteoporosis. The presence of subchondral sclerosis and modest osteophyte formation is indicative of secondary degenerative changes, a common feature in rheumatoid arthritis that involves the hips and knees.

Rheumatoid arthritis is a systemic autoimmune disease manifested in the musculoskeletal system by inflammatory polyarthritis of the small synovial joints. The pathogenesis is not understood and no causative agent has been proven. Genetic factors affect the susceptibility to, and expression of, the disease. Rheumatoid arthritis is generally distinguished

from other arthritides by the presence of rheumatoid factor (RF) in the serum. Rheumatoid arthritis has a prevalence of 1% in the general population, with women affected more often than men by a ratio of 3:1. High RF titers often correlate with more severe disease.

The typical age of presentation is 25 to 55 years old. In 70% of cases the onset is insidious and occurs over weeks to months, in 20% of cases the onset occurs over days to weeks, and in 10% of cases the onset is acute and occurs over hours to days. The acute onset mimics the onset of septic arthritis. The clinical course of rheumatoid arthritis is progressive in 70% of cases, leading to disabling, destructive disease. The clinical progression may be rapid or slow. In 20% of cases the disease is intermittent, with remissions generally lasting longer than exacerbations, but in 10% of cases the remissions last several years. The clinical diagnosis is based on criteria that include morning stiffness; symmetric swelling of the proximal interphalangeal, metacarpophalangeal, or wrist joints; rheumatoid nodules; serum RF; and specific radiographic findings. In the knee, the typical inflammatory changes are commonly superimposed on secondary degenerative changes, but the proliferative bone response tends to be disproportionately modest in comparison to the loss of joint space.

**CLINICAL HISTORY** A 56-year-old man with recurrent episodes of knee pain, and a companion case.



FIGURE 6.20A



FIGURE 6.20B

## FINDINGS

- A. Knee radiograph shows chondrocalcinosis of the medial and lateral menisci. Chondrocalcinosis of the articular cartilage is also evident, particularly in the femur. Medial joint space narrowing and osteophyte formation are present.
- B. Companion case. AP radiograph of the shoulder shows chondrocalcinosis of the articular cartilage of the humerus.

**DIFFERENTIAL DIAGNOSIS** None.

**DIAGNOSIS** Calcium pyrophosphate dihydrate (CPPD) crystal deposition disease.

**DISCUSSION** CPPD crystal deposition disease is a polyarticular arthritis with deposition of CPPD crystals in articular tissues. Its initial presentation may be monoarticular. The definitive clinical diagnosis requires the identification of CPPD crystals from joint fluid, but the radiologic findings can be diagnostic. CPPD deposition disease has been associated with hyperparathyroidism, hemochromatosis, aging, and osteoarthritis. It has been weakly associated with hypothyroidism, ochronosis, Paget disease, Wilson's

disease, acromegaly, diabetes, and gout. CPPD crystal deposition disease has three manifestations: chondrocalcinosis, crystal-induced synovitis, and pyrophosphate arthropathy.

CPPD crystals are generated locally in the articular tissues, where asymptomatic deposits may accumulate in cartilage, joint capsules, intervertebral discs, tendons, and ligaments. In cartilage, these deposits may be evident radiographically as chondrocalcinosis. Chondrocalcinosis is most common in the knees, wrists, elbows, and hips. It is found in both fibrocartilage and hyaline cartilage.

Shedding of crystals into the joint space after rupture of a deposit causes an acute, self-limited, crystal-induced synovitis. This acute synovitis is clinically similar to acute gouty arthritis and has been known as pseudogout. As with gouty arthritis, acute episodes of inflammatory synovitis may recur intermittently. During an acute episode, CPPD crystals can be recovered by joint aspiration and identified by polarized light microscopy or more definitive physical means. Uncommonly, these episodes can run together into a subacute or chronic crystal synovitis that resembles rheumatoid arthritis, except the large joints of the limbs tend to be involved, rather than the small joints of the hands and feet.

**CLINICAL HISTORY** A 23-year-old woman with knee pain for 2 months.

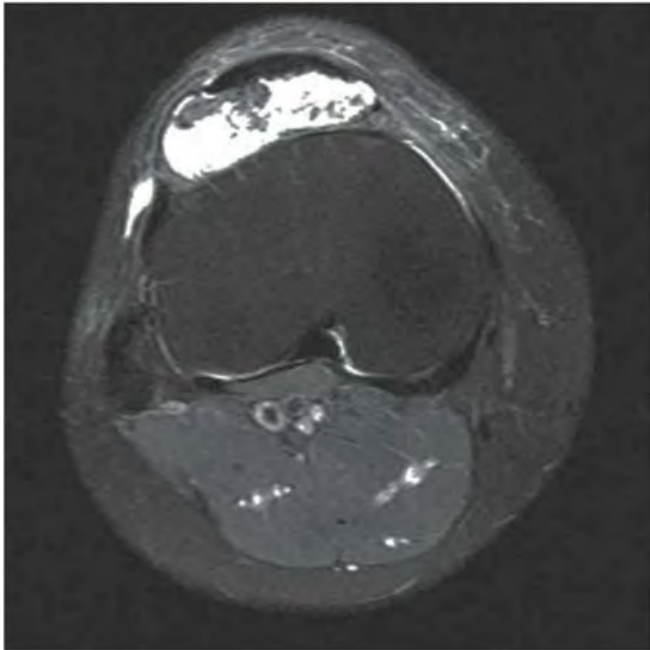


FIGURE 6.21A

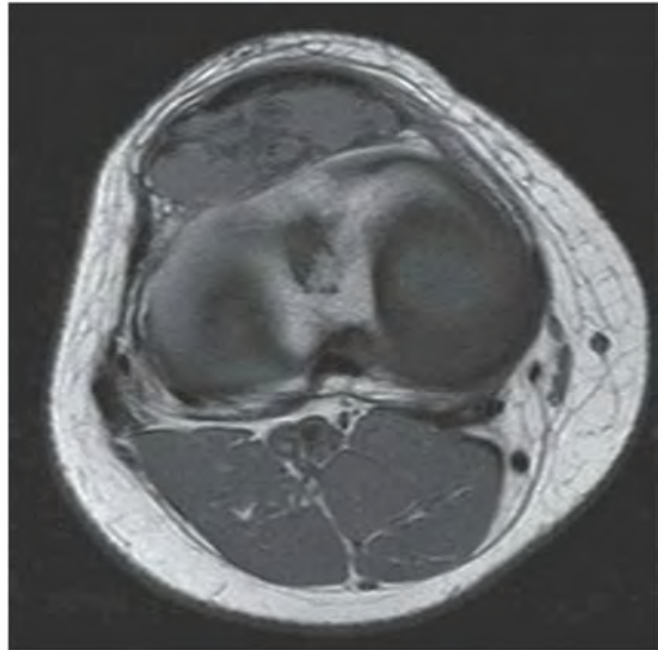


FIGURE 6.21B

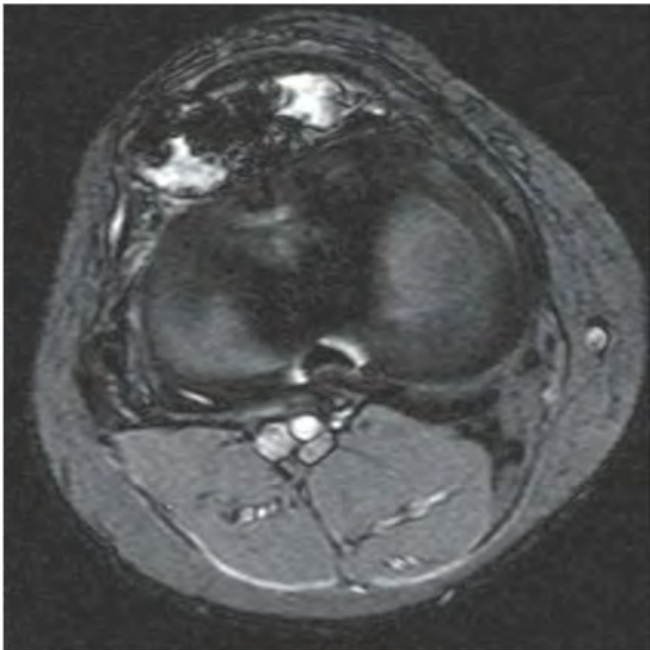


FIGURE 6.21C

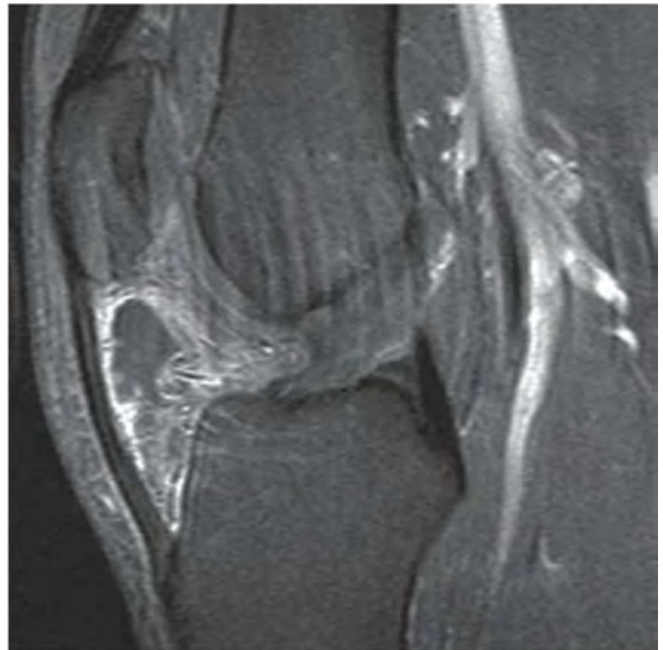


FIGURE 6.21D

## FINDINGS

- A. Axial T2-weighted, fat-suppressed MRI shows a large effusion and a low signal intensity nodular intraarticular, extrasynovial lesion abutting the posterior aspect of the patellar tendon in the infrapatellar fat pad.
- B. Axial T1-weighted MRI shows iso signal intensity of the nodular lesion.
- C. Axial T2\*-weighted gradient-recalled echo MRI shows low-signal blooming of portions of the lesion.
- D. Sagittal T1-weighted, fat-suppressed, postgadolinium MRI shows synovial enhancement.

**DIFFERENTIAL DIAGNOSIS** Pigmented villonodular synovitis (PVNS), hemophilia, synovial hemangiomatosis.

**DIAGNOSIS** PVNS, diffuse form.

**DISCUSSION** The knee is the most common location for PVNS. It may present in diffuse or localized (nodular) forms. The differential diagnosis includes other causes of synovial hemosiderin deposition, but these can be easily dismissed in this case. Hemophilia causes a degenerative arthropathy that should be advanced by adulthood, which is not seen here. The slow-flowing, blood-filled venous spaces of synovial

hemangiomatosis should be evident, but are absent here as well [31]. A degenerative arthropathy that resembles hemophilia has also been described in synovial hemangiomatosis [32]. PVNS does not generally cause bony erosions in the knee because it has a loose joint capsule, unlike most other joints where erosions are common. MR imaging reveals characteristic features of a heterogeneous, synovially based, plaque-like thickening that often is associated with nodularity. The signal intensity of the synovial thickening is intermediate to low on T1-weighted images and low on T2-weighted MR images. Preferential shortening of T2 relaxation time caused by hemosiderin is particularly pronounced on gradient-echo images, which demonstrate an enlargement of the low-signal-intensity areas (“blooming”) that is caused by magnetic susceptibility artifact. The blooming effect, which specifically signifies the presence of hemosiderin as the cause of low signal intensity, is nearly pathognomonic of PVNS at MR imaging. Although synovial hemangioma and hemophilic arthropathy may show similar MR imaging findings (caused by repetitive intra-articular hemorrhage and synovial hemosiderin deposition), diffuse intra-articular PVNS can be distinguished from these conditions because it is not associated with either serpentine vascular channels (hemangioma) or a clinical history of hemophilia [33].

## 6.22

**CLINICAL HISTORY** An 8-year-old boy with swollen knee (his other joints feel fine), and a companion case. A, Lateral radiograph; B, AP radiograph; C, both knees, companion case.



FIGURE 6.22A



FIGURE 6.22B

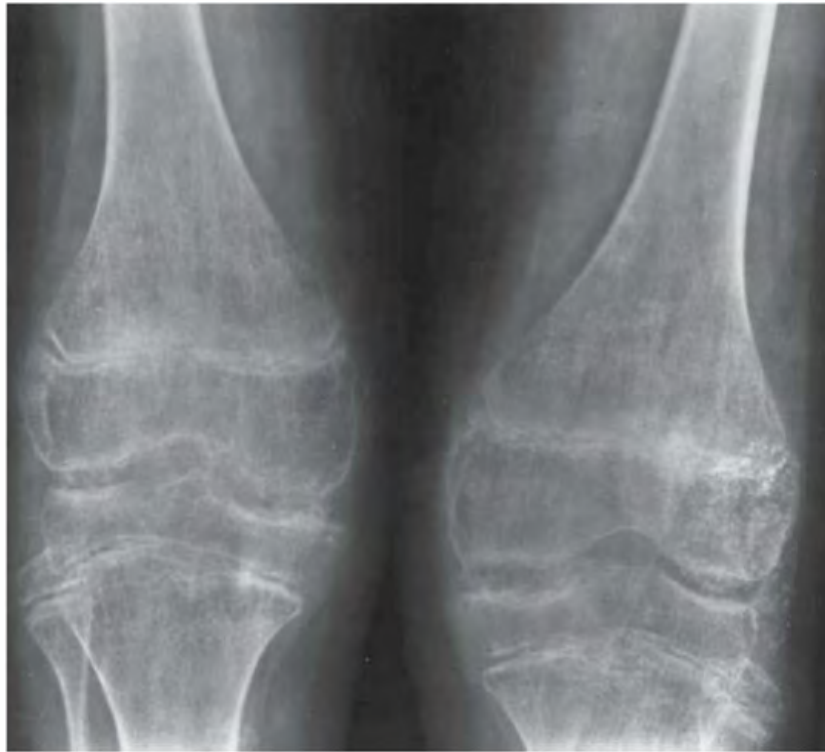


FIGURE 6.22C

**FINDINGS**

- A, B. Lateral and AP radiographs of the knee show effusion only.
- C. Companion case: boy with the same disease for 2 years. AP radiograph of both knees shows profound osteopenia. The epiphyses are symmetrically overgrown, and irregularity of the subchondral bone is present.

**DIFFERENTIAL DIAGNOSIS** Juvenile idiopathic arthritis, hemophilia, trauma, infection.

**DIAGNOSIS** Juvenile idiopathic arthritis.

**DISCUSSION** The findings in this case, a monoarticular arthritis of a large joint manifested by effusion in a child, represent the initial presentation of juvenile idiopathic arthritis and are entirely nonspecific. The differential diagnosis would include trauma and infection, as well as systemic disease such as juvenile idiopathic arthritis and hemophilia. The

companion case shows the same disease process at a more advanced stage, where the systemic nature of the condition is evident in the bilateral symmetric involvement of both knees. Also evident is the superimposition of inflammatory arthritis on growing joints.

Juvenile idiopathic arthritis has formerly been referred to as juvenile chronic arthritis and juvenile rheumatoid arthritis [34,35]. Unlike adult rheumatoid arthritis, juvenile idiopathic arthritis has a predilection for large joints. Because the disease has its onset in the skeletally immature child, growth disturbances are typically present, as either overgrowth or undergrowth. If hyperemia is the predominant effect, as is typically the case in the knees, overgrowth of the femoral condyles and proximal tibia occurs and is recognized radiographically by disproportionate enlargement of the ends of the bones at the knee as compared with the widths of the femoral and tibial shafts. If erosion of cartilage by inflammatory pannus and consequent epiphyseal destruction is the predominant effect, undergrowth occurs. A common location for undergrowth is the distal ulna, resulting in ulnar minus variance.

## 6.23

**CLINICAL HISTORY** *An 18-year-old man with chronic disease and short stature, and a companion case.*



FIGURE 6.23A



FIGURE 6.23B



FIGURE 6.23C

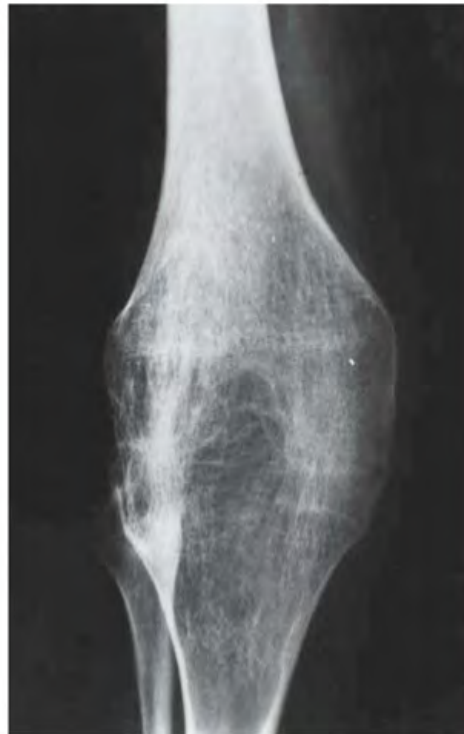


FIGURE 6.23D

## FINDINGS

- A, B. Lateral and AP radiographs of the knee. There is marked overgrowth of the femoral epiphysis, tibial epiphysis, fibular epiphysis, and patella. There is osteoporosis. The cartilage spaces are narrowed diffusely, and there is subchondral sclerosis and irregularity of all the articular surfaces. The musculature is atrophic, and there is a small effusion.
- C, D. Companion case. Lateral and AP radiographs of the knee. There is ankylosis of the joint, with remodeled trabecular bone flowing continuously across the site of the joint. Diffuse osteoporosis is present.

**DIFFERENTIAL DIAGNOSIS** Juvenile idiopathic arthritis, hemophilia, septic arthritis.

**DIAGNOSIS** Juvenile idiopathic arthritis.

**DISCUSSION** In this case, the stigmata of inflammatory joint disease in the growing skeleton—marked overgrowth

from prolonged hyperemia—are present. Diffuse cartilage loss is a result of the inflammatory joint disease itself, and early secondary degenerative change follows. Osteoporosis and muscular atrophy may result from hyperemia, chronic disease, and disuse, but they may also result from the systemic corticosteroids used to treat the disease. Other skeletal complications of treatment include osteonecrosis and insufficiency fractures.

The companion case shows one of the end-stage sequelae of juvenile idiopathic arthritis: bony ankylosis. Bony ankylosis is a common characteristic of end-stage juvenile idiopathic arthritis, but it is very unusual in adult-onset rheumatoid arthritis. Other findings, similar to conventional adult-onset rheumatoid arthritis, are not uncommon, including bursal cyst formation, subchondral cysts, muscle and ligamentous atrophy, cortical erosions at capsular attachment sites, protrusio acetabuli, and soft tissue swelling.

**CLINICAL HISTORY** An 81-year-old woman with swollen, painful knees. A, right and left AP radiographs; B, right lateral radiograph; C, left lateral radiograph.

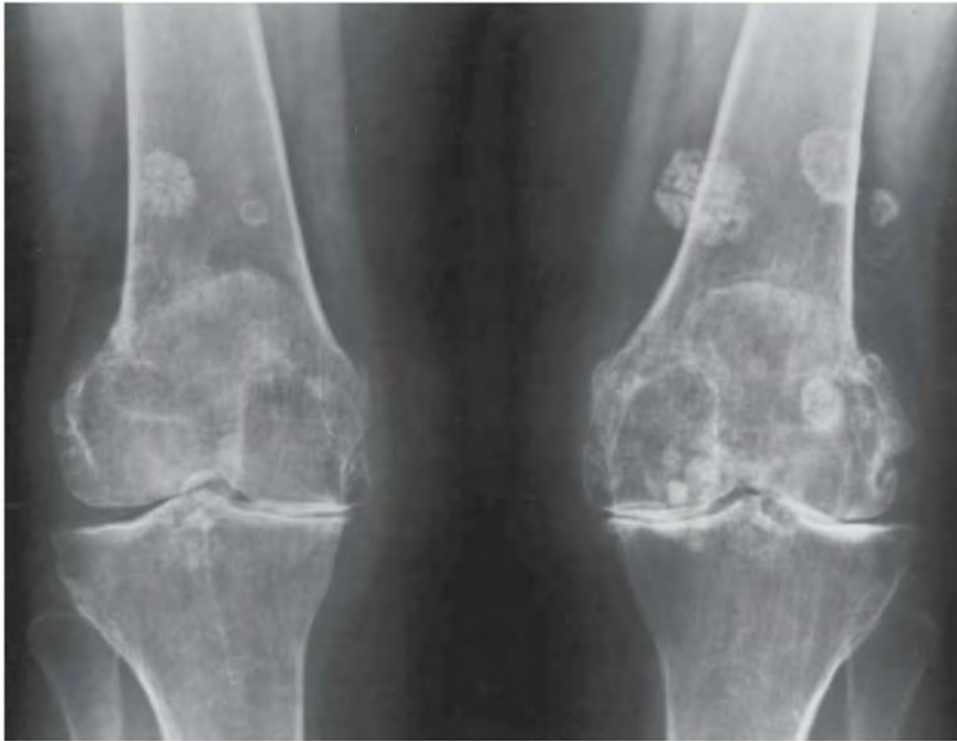


FIGURE 6.24A



FIGURE 6.24B



FIGURE 6.24C

**FINDINGS** (A) AP and (B, C) lateral radiographs of both knees. There are multiple round, dense, loose bodies within the joint, with a lamellated appearance. Both knees show degenerative changes, with asymmetric joint space narrowing, subchondral sclerosis, and osteophyte formation.

**DIFFERENTIAL DIAGNOSIS** Primary or secondary synovial osteochondromatosis, trauma.

**DIAGNOSIS** Secondary synovial osteochondromatosis.

**DISCUSSION** The presence of bilateral calcified loose bodies in the setting of osteoarthritis suggests secondary synovial osteochondromatosis. In this circumstance, fragments of bone and cartilage from the margins of the articular surfaces where osteophyte formation occurs become detached. Loose in the joint capsule, the cartilaginous portions may continue to grow. Other preexisting articular derangements that may be associated with secondary osteochondromatosis include avascular necrosis, osteochondritis dissecans, neuropathic arthropathy, trauma, and rheumatoid arthritis [36]. Bursal synovial osteochondromatosis has been reported to develop secondary to underlying osteochondromas [37]. In

the secondary form, loose bodies tend to be highly variable in size and relatively few in number, as in this case.

Primary synovial osteochondromatosis occurs by synovial metaplasia that gives rise to cartilaginous bodies that frequently calcify. The loose bodies tend to be more or less uniform in size and are typically present in large numbers. The process evolves in stages, from synovial metaplasia to synovial metaplasia with intra-articular bodies. In the inactive stage, bodies are present without synovial metaplasia [38]. The knees and hips are sites of predilection, and typically only one joint is involved. Although it is principally an intra-articular process, bursal and tenosynovial forms have been documented [39,40].

Plain films fail to show calcification in 5% to 30% of cases [41]. Adjacent bone erosions may occur, and CT may demonstrate these latter findings to better advantage. Early on, the joint space may be enlarged. Later, secondary degenerative changes may predominate, causing joint space narrowing. Clinical symptoms include limitation of motion and pain. After resection, recurrences may occur, and rare instances of malignant transformation to chondrosarcoma have been described [42]. With the intra-articular form, men are affected twice as often as women, whereas the extra-articular variety displays no sex predilection.

**CLINICAL HISTORY** A 43-year-old woman with recurrent episodes of knee pain.



FIGURE 6.25A



FIGURE 6.25B

**FINDINGS** Lateral (A) and AP (B) radiographs of the knee show a large joint effusion. There is uniform loss of the cartilage space in both medial and lateral compartments, subchondral sclerosis, osteophyte formation, and subchondral cyst formation. The overall mineralization of the bones is normal. Involvement of the medial, lateral, and patellofemoral compartments is more or less symmetric.

**DIFFERENTIAL DIAGNOSIS** Primary or secondary osteoarthritis, pyrophosphate arthropathy, rheumatoid arthritis.

**DIAGNOSIS** Pyrophosphate arthropathy.

**DISCUSSION** Pyrophosphate arthropathy refers to the pattern of degenerative joint disease resulting from CPPD crystal deposition disease [43]. Deposition of CPPD

crystals in the cartilage (chondrocalcinosis) and recurrent episodes of crystal-induced inflammatory arthritis leads to degenerative joint disease. Unlike primary osteoarthritis, pyrophosphate arthropathy of the knee typically involves medial, lateral, and patellofemoral joint compartments uniformly. Hypertrophic bone changes tend to be florid, with extensive subchondral sclerosis, prominent osteophyte formation, and subchondral cyst formation. Fragmentation resembling neuropathic arthropathy may occur. Involvement is often not bilaterally symmetric. Because chondrocalcinosis will not be present in advanced pyrophosphate arthropathy (cartilage will have been destroyed), the radiographic differential diagnosis of three-compartment degenerative change at the knee is primary osteoarthritis, or secondary osteoarthritis after inflammatory arthritis such as infection.

**CLINICAL HISTORY** A 43-year-old woman with left knee pain and stiffness.



FIGURE 6.26A



FIGURE 6.26B

**FINDINGS** Lateral (A) and AP (B) radiographs of the left knee demonstrate soft tissue calcification along the thigh and lower leg, and mild soft tissue atrophy.

**DIFFERENTIAL DIAGNOSIS** Dermatomyositis, polymyositis, scleroderma, burns.

**DIAGNOSIS** Dermatomyositis.

**DISCUSSION** Dermatomyositis and polymyositis are diseases of unknown etiology, thought to occur on an autoimmune basis, affecting striated muscle by diffuse, nonsuppurative inflammation and degeneration. The pathogenesis involves an autoimmune mechanism. There may be some overlap with other collagen vascular disorders, which is considered as a specific subtype of polymyositis and is most notable in Sjögren's syndrome. In dermatomyositis, the skin is also involved. Multiple clinical classifications are based on various features, particularly progressive muscle weakness and rash. There is an associated risk of malignancy in patients with dermatomyositis who are older

than 40, particularly men. The diagnosis is made by serum enzyme studies, electromyography, and muscle biopsy. MRI may be more sensitive, although less specific, than biopsy [44,45].

Early on, manifestations include deep and superficial soft tissue edema. The process may be halted with treatment or may progress to further changes. This will show increased signal intensity on T2-weighted images, and short-tau inversion recovery pulse sequences with MRI. Later stages are characterized by muscle atrophy and fibrosis. Although not common, articular abnormalities may also be seen. The characteristic radiographic abnormality is widespread soft tissue calcification, particularly of intermuscular fascial planes between large proximal limb muscles. There may be subcutaneous calcifications similar to those in scleroderma. Bone scanning may detect uptake of radionuclide.

Location and distribution may help differentiate this entity from other forms of autoimmune myopathies. Changes in dermatomyositis are typically symmetric in a proximal distribution, with particular predilection for the vasti, glutei, adductors, and hamstrings [46,47].



FIGURE 6.27A



FIGURE 6.27B

**FINDINGS** Lateral (A) and AP (B) radiographs of the right knee demonstrate osteopenia with atrophy of the soft tissues. The diaphyses are gracile. No articular erosions or joint space narrowing is identified.

**DIFFERENTIAL DIAGNOSIS** Poliomyelitis, paralysis (from any cause), osteogenesis imperfecta.

**DIAGNOSIS** Poliomyelitis.

**DISCUSSION** Poliomyelitis is a viral infection that causes acute flaccid paralysis. Once a common childhood epidemic disease of worldwide proportions, endemic polio

has been eliminated from the Western Hemisphere since 1991. Global eradication is considered feasible, but the disease remains endemic in Afghanistan and Pakistan [48]. Many patients who have recovered from poliomyelitis will continue to present with musculoskeletal sequelae. Poliomyelitis classically demonstrates unilateral hypoplasia of the lower extremity. There is atrophy of the surrounding muscles with fatty infiltration. Other skeletal manifestations are clubfoot, hip dislocations, and scoliosis. Postpoliomyelitis syndrome is a weakness described in patients who have been recovered from their initial paralysis for 10 to 15 years; the knee is a particularly symptomatic joint in this condition [49].



FIGURE 6.28

**FINDINGS** Coronal T1-weighted MRI demonstrates widening of the medial growth plate of the distal femur with low-density material, and continuation with linear extension into the medial femoral metaphysis.

**DIFFERENTIAL DIAGNOSIS** None.

**DIAGNOSIS** Salter type II fracture.

**DISCUSSION** Growth plate injuries have been categorized into five basic types in the Salter-Harris system.

1. Type I Salter injuries are noted radiographically by widening of the growth plate and soft tissue swelling. The injury is usually by a shearing mechanism through the zone of hypertrophy. These typically occur in children less than 5 years old.
2. Type II Salter injuries are the most common type, typically occurring at the end of long bones. Avulsion of the

growth plate occurs with the line of fracture then extending through the metaphysis, as seen here. The prognosis for these injuries is good.

3. Type III Salter injuries involve a vertical component through the epiphysis and growth plate, and separation of the growth plate with sparing of the adjacent metaphysis.
4. Type IV Salter injuries are similar to type III, but also disrupt the underlying metaphysis.
5. Type V Salter injuries constitute isolated compression of the growth plate. As a result of these injuries to the growth plate, physeal bars may form and interfere with subsequent growth in that location. This complication is generally more common with higher level Salter injuries.

MRI may demonstrate a different Salter-Harris class of injury than radiography in up to 50% of cases of physeal trauma [54].

**CLINICAL HISTORY** *An 89-year-old man with knee pain.*

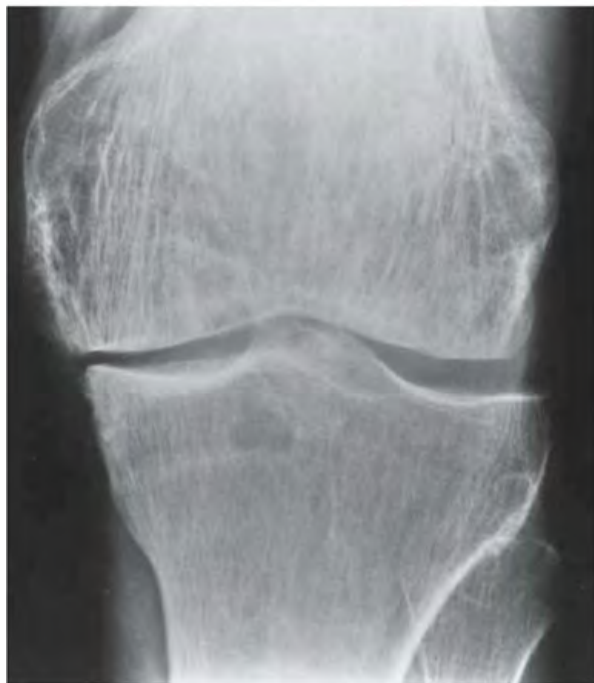


FIGURE 6.29A



FIGURE 6.29B

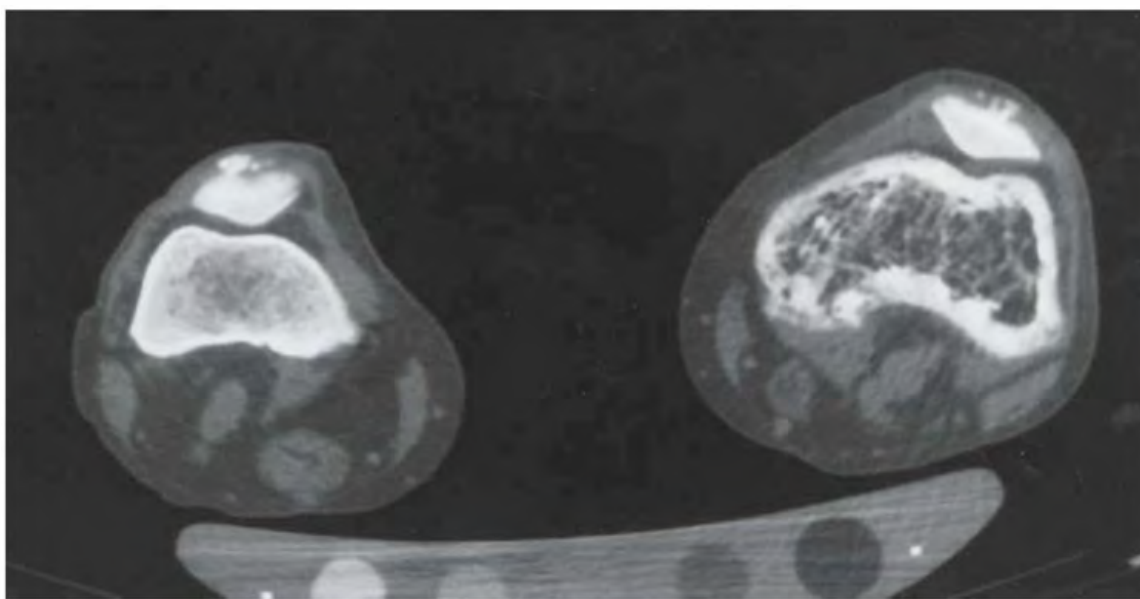


FIGURE 6.29C

## FINDINGS

- A. AP radiograph of the knee demonstrates coarsening of the vertical trabecular pattern, with obliteration of the intercondylar notch.
- B. Coronal T1-weighted MRI of the knee shows enlargement of the entire distal femur. The trabecular bone pattern is prominent and outlined by the bright signal of the fatty marrow. Degenerative changes are present in the medial compartment of the knee.
- C. Axial CT shows enlargement of the involved distal femur compared to the opposite side. The cortical thickening is quite striking.

**DIFFERENTIAL DIAGNOSIS** None.

**DIAGNOSIS** Paget disease of the femur, with secondary osteoarthritis.

**DISCUSSION** Paget disease (osteitis deformans) is a bone disease seen in middle-aged and elderly individuals. It is characterized by excessive and abnormal remodeling of bone. Usually asymptomatic, Paget disease has a prevalence of 3% in the adult population older than 40. In most cases, involvement is polyostotic. Although any bone may be involved, the majority of cases involve the pelvis, spine, skull, femur, or tibia.

Current evidence suggests that Paget disease is a slowly developing viral infection of osteoclasts. The disease has active and quiescent (inactive) phases. The active phase begins with a focus of excessive osteoclastic activity,

resulting in a localized area of osteolysis where bone is replaced by nonossified fibrovascular tissue. The demarcation between normal uninvolved bone and the area of osteolysis is typically quite sharp. Subsequently, the areas of osteolysis are filled in with pagetic bone, even as the osteoclastic activity continues. Pagetic bone consists of layers of disorganized woven bone separated by resorption cavities and nonossified fibrovascular tissue. Bone is formed both endosteally and periosteally. The combination of osteoclastic and osteoblastic activity results in rapid remodeling and turnover of bone. Eventually, for unknown reasons, the osteoclastic activity moderates and, after the osteolytic areas have filled with bone, the rate of bone turnover decreases. With the decrease in turnover, the bone enters the quiescent phase of Paget disease. Focal areas of pagetic bone may be replaced by islands of lamellar bone, but haversian systems and remodeling along lines of stress do not occur. Slow endosteal and periosteal apposition of bone may continue to thicken the cortex and enlarge the bone, sometimes obliterating the marrow space.

Paget disease involving subchondral bone is thought to result in accelerated osteoarthritis in the adjacent joint [50], although the magnitude of the association is uncertain [51]. Biomechanical modification of the articular surface is thought to be the pathogenesis of the early joint degeneration. Insufficiency microfractures of the subchondral bone may also contribute, as pagetic bone does not remodel along lines of stress and is weaker than normal bone.

**CLINICAL HISTORY** A 27-year-old man who twisted a knee during soccer.

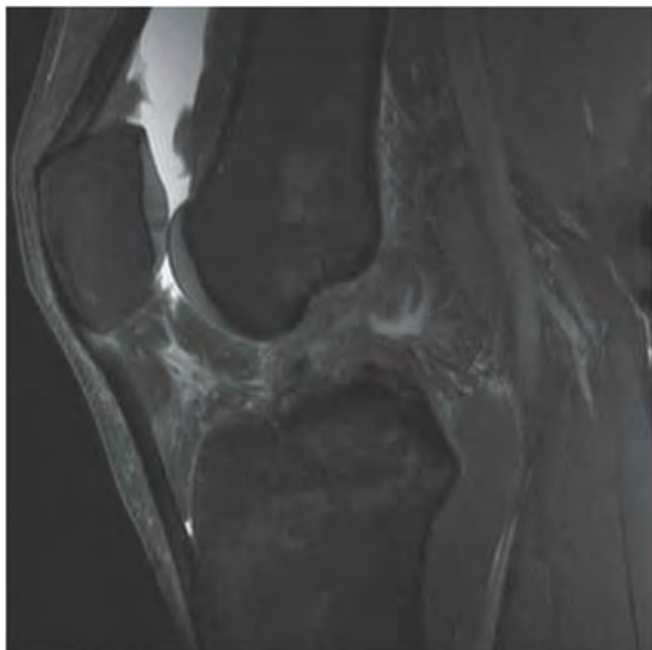


FIGURE 6.30A



FIGURE 6.30B



FIGURE 6.30C

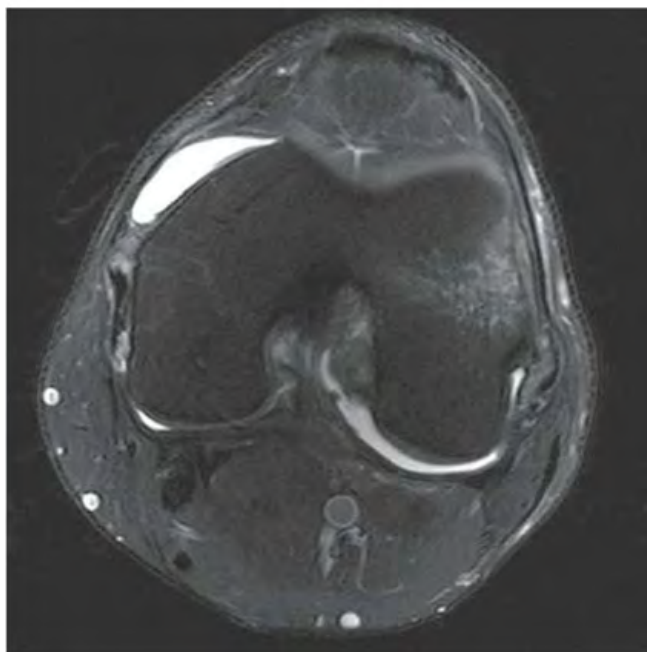


FIGURE 6.30D

**FINDINGS** Sagittal (A, B), coronal (C), and axial (D) proton density, fat-suppressed MRI of the knee shows intermediate-intensity material within the intercondylar notch. The sagittal images show no normal anterior cruciate ligament (ACL) fibers within the intercondylar notch (A) and pivot shift pattern bone marrow edema in the lateral femoral condyle and the lateral tibial plateau (B). Coronal image demonstrates an avulsion fragment of the lateral joint capsule at the lateral tibial plateau (*arrow* in C). This is known as a Segond fracture. Axial image shows a normal posterior cruciate ligament (PCL) with no normal ACL fibers visualized (D).

**DIFFERENTIAL DIAGNOSIS** None.

**DIAGNOSIS** ACL sprain, grade 3.

**DISCUSSION** The ACL is a straight, predominantly low-signal ligament that fans distally as it attaches to the anterior tibial plateau. Usually when there is a complete tear of the ACL, it is simply not visualized. ACL tears are mechanically caused from a valgus force with a rotatory motion resulting in anteromedial rotary instability. Most commonly, ACL tears occur at its proximal femoral attachment; however, they may also occur at its midportion, and rarely at its distal tibial attachment. Characteristic bone bruise pattern includes marrow edema at the posterolateral tibial plateau and the midportion of the lateral femoral condyle [52]. An important associated condition is the Segond fracture [53]. This fracture is an avulsion fracture of the lateral tibial plateau at the insertion of the meniscotibial portion of the lateral capsular ligament.

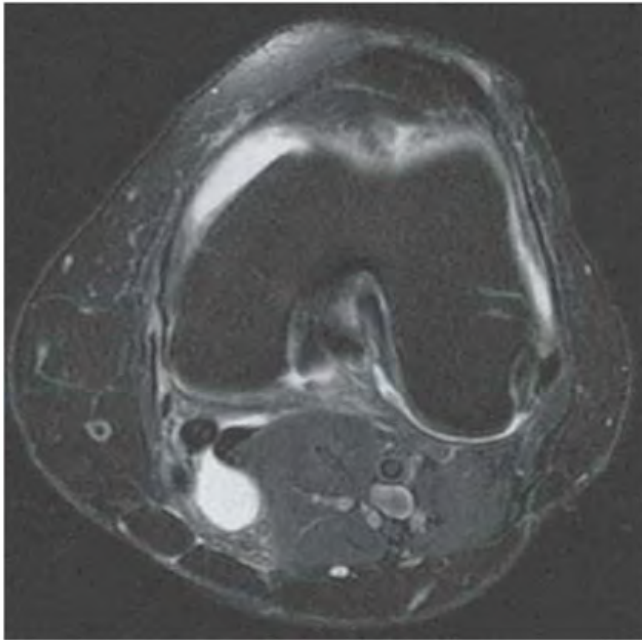


FIGURE 6.31A

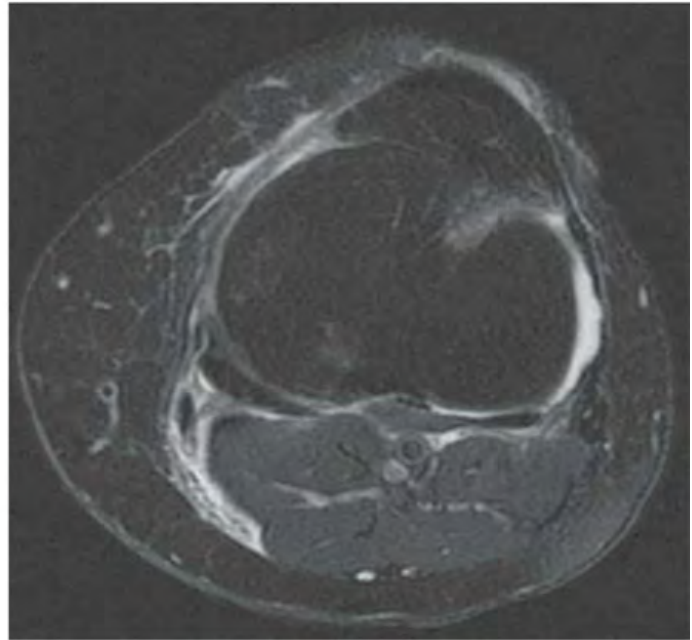


FIGURE 6.31B

**FINDINGS** Axial T2-weighted MRI (A, B) demonstrates a small joint effusion, with fluid tracking between the semimembranosus and medial head of the gastrocnemius. The second image demonstrates fluid tracking in the medial fascial plane, distal to this collection.

**DIFFERENTIAL DIAGNOSIS** Ruptured Baker cyst, thrombophlebitis, cellulitis, fasciitis, myositis.

**DIAGNOSIS** Ruptured Baker cyst.

**DISCUSSION** An outpouching of synovial lining into a bursa causes a Baker cyst. The most common location for its occurrence is in the semimembranosus-gastrocnemius bursa. It is classically situated, as seen here, between the semimembranosus tendon and the medial head of the gastrocnemius muscle group. The neck of the cyst can frequently be seen on MRI, confirming communication with the joint space. Popliteal cysts can be readily detected with ultrasound or MRI, showing a smooth, thin-walled collection of fluid that may contain septations, synovial tissues, or loose bodies.

The point of communication may become constricted or obliterated, and a clear communication with the joint may not be demonstrated. Inflammatory conditions such as rheumatoid arthritis and osteoarthritis are common predisposing factors. Ligamentous and meniscal tears, chronic effusions, and increased age are other associations.

Sometimes, as in this case, the cyst may rupture and a well-defined collection may not be appreciated. Fluid in these cases may be detected in the bursa and adjacent interstitial tissues. Fluid can track extensively along the fascial planes, usually coursing inferiorly due to the effects of gravity. The primary differential diagnosis for an unruptured popliteal cyst is ganglion cyst. These are usually related to the cruciate ligaments, more often the PCL than the ACL [55]. The main distinguishing feature for a popliteal cyst is its predilection for the semimembranosus-gastrocnemius bursa. A ruptured cyst shows edema in the medial soft tissues, which can be seen with trauma; however, the preponderance of fluid coupled with the absence of bone bruises or muscle/ligamentous injury suggests that this process originated in the bursa and favors the diagnosis of Baker cyst.

**CLINICAL HISTORY** A 28-year-old woman with severe knee pain and swelling after a fall.

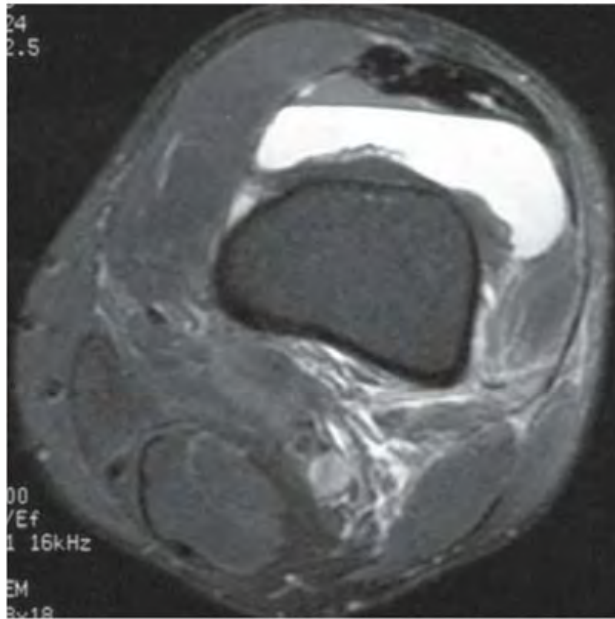


FIGURE 6.32A

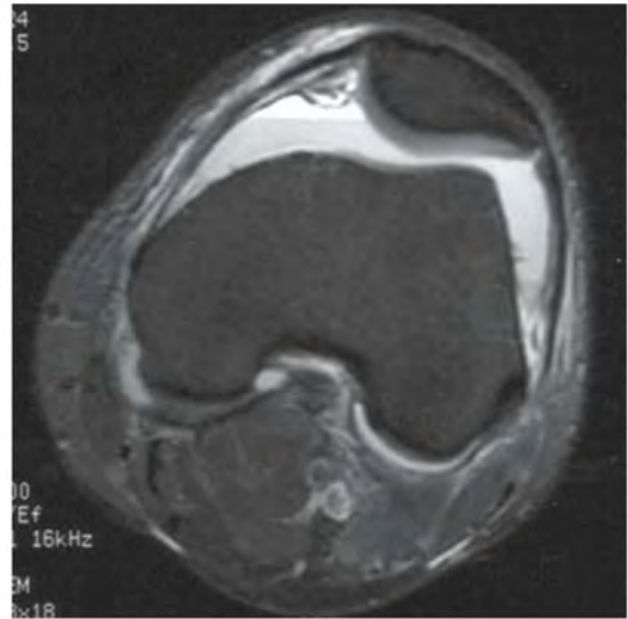


FIGURE 6.32B



FIGURE 6.32C

## FINDINGS

- Axial T2-weighted MRI of the knee at the level of the suprapatellar recess shows a large effusion distending the suprapatellar recess. Fluid-fluid levels are present extending horizontally across the recess, with fluid of suppressed signal intensity layered on fluid of very high signal intensity.
- Axial T2-weighted MRI of the knee at the level of the patella shows a large effusion with a horizontal serum-sediment level.
- Coronal T1-weighted MRI shows a depressed lateral tibial plateau fracture.

**DIFFERENTIAL DIAGNOSIS** None.

**DIAGNOSIS** Lateral tibial plateau fracture.

**DISCUSSION** Tibial plateau fractures are the result of compressive loading of the tibia. Approximately 76% of cases involve the lateral tibial plateau alone, 11% involve the medial condyle alone, 10% involve both condyles, and 3% of cases involve the posterior margin. Lipohemarthrosis is a manifestation of an intra-articular fracture and, at the knee, most commonly occurs with fractures of the tibial plateau. Traumatic disruption of the cortex allows liquid marrow to extrude into the joint, where it layers on top of blood because of its lesser density. A second fluid-fluid level may be seen as the cellular elements of blood sediment dependently and separate from the serum, but this is not evident in this case.

A linear demarcation between fat and blood may be seen on the radiograph if the exposure was made with a horizontal beam. Because the suprapatellar recess is the most anterior part of a distended knee joint capsule when the knee is extended, the fat will collect in that specific location. On MRI, a similar demarcation is seen as a fluid-fluid level, with the fatty component occupying the nondependent portion of the joint capsule. The fatty layer should follow the signal characteristics of marrow fat or subcutaneous fat on various imaging parameters. Chemical shift artifact, seen here as a dark line between the fat and the blood, may enhance the separation. The distinction is made most easily on sagittal or axial images. Only one-third of intra-articular fractures of the knee will be associated with a lipohemarthrosis.

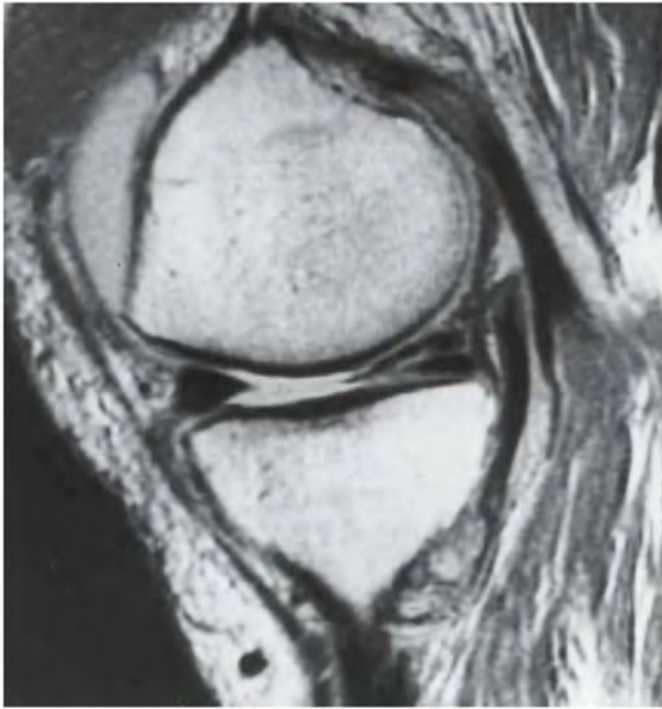


FIGURE 6.33A



FIGURE 6.33B

**FINDINGS** Sagittal proton density MRI (A, B) of the knee through the medial compartment. The posterior horn of the medial meniscus has a band of high signal extending horizontally and obliquely to the inferior articular surface. The anterior horn is normal. There is a large effusion.

**DIFFERENTIAL DIAGNOSIS** Meniscal tear, meniscal degeneration.

**DIAGNOSIS** Medial meniscal tear.

**DISCUSSION** On MRI, the normal menisci and ligaments are visualized as low-signal structures. Meniscal tears are evident as high-signal regions on T1-weighted or proton density MRI that involves an articular margin. Gross distortions of meniscal shape or intrameniscal fluid collections indicate meniscal tears with displaced fragments. Torn meniscal fragments can interfere with motion, causing locking, and may erode the articular cartilage, leading to early degenerative arthritis. Acute traumatic meniscal tears generally occur in young people when the meniscus is compressed between the femoral condyle and tibial plateau during crush and twisting

injuries. In older individuals, degenerative meniscal tears are thought to result from multiple subacute traumatic episodes that lead to chondrocyte death, increased mucinous ground substance (myxoid degeneration), and loss of mechanical integrity.

The appearance of increased intrameniscal signal intensity on MRI has been divided into three grades, with histologic correlation [56]. The normal meniscus has uniformly low signal intensity.

1. In MRI grade 1, globular increased-signal-intensity region is present within the meniscus and corresponds histologically to early mucinous degeneration.
2. In MRI grade 2, a horizontal, linear increased-signal-intensity region is present, without involvement of an articular surface, and corresponds to more advanced meniscal degeneration.
3. In MRI grade 3, the increased-signal-intensity region communicates with at least one articular surface and corresponds to a tear; in 5% to 6% of these, the tears are considered intrasubstance cleavage tears and may not be visible on arthroscopy.

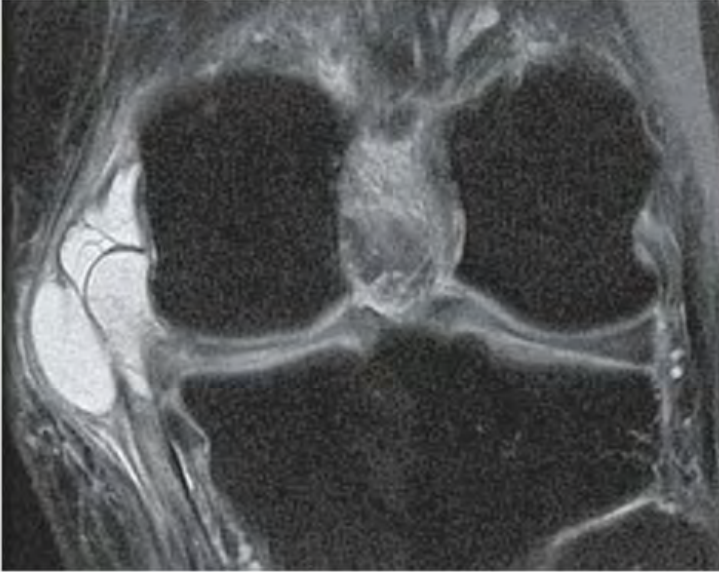


FIGURE 6.34A



FIGURE 6.34B

**FINDINGS** Coronal and sagittal (A, B) proton density, fat-suppressed MRI of the knee show a multilobulated cystic structure adjacent to the medial meniscus. This structure displaces the MCL. There is high signal in the posterior horn of the medial meniscus.

**DIFFERENTIAL DIAGNOSIS** None.

**DIAGNOSIS** Complex medial meniscal tear with parameniscal cyst.

**DISCUSSION** The normal meniscus remains low signal on all pulse sequences. High signal on T2-weighted images within the meniscus must reach an articular surface to fulfill the criteria for a meniscal tear. Areas of high signal on

T2-weighted imaging within the substance of the meniscus that does not reach an articular surface are usually classified as mucoid degeneration.

A complication of a meniscal tear is a parameniscal cyst. The communication between the cyst and the tear allows joint fluid to enter using a ball-valve mechanism; therefore, the cyst continues to grow and may become symptomatic. The posterior horn of the medial meniscus and anterior horn of the lateral meniscus are common locations for the development of a parameniscal cyst. Parameniscal cysts that are medially located tend to be more symptomatic due to the close proximity to the MCL. Medial parameniscal cysts are twice as common as lateral parameniscal cysts [57]. Parameniscal cysts may be asymptomatic [58].

**CLINICAL HISTORY** A 35-year-old man with knee trauma, locking, and effusion.



FIGURE 6.35A



FIGURE 6.35B

### FINDINGS

- A. Sagittal T1-weighted MRI demonstrates double PCL sign.
- B. Coronal T1-weighted MRI demonstrates an extra density inferior to the ACL origin.

**DIFFERENTIAL DIAGNOSIS** Tear of the ACL, bucket-handle tear of the meniscus.

**DIAGNOSIS** Bucket-handle tear, medial meniscus.

**DISCUSSION** The differential diagnosis for the double PCL sign includes tear of the ACL and bucket-handle tear of the meniscus. The ACL in this case is intact.

Bucket-handle tears consist of vertical tears of the meniscus with translocation of the medial fragment. This is an unstable injury. The meniscal fragment generally demonstrates low signal intensity on all pulse sequences. When the medial fragment lies in the intercondylar region, it may parallel the course of the PCL, as seen here. Additional signs

of a bucket-handle tear include an anteriorly flipped meniscal fragment, a fragment flipped into the intercondylar notch, and an absent bow tie on sagittal images [59].

Traumatic acute meniscal tears occur in younger patients, basically by a compressive mechanism at the femorotibial articulation. Acute traumatic meniscal tears generally occur in young people when the meniscus is compressed between the femoral condyles and tibial plateaus during crush and twisting injuries. In older individuals, degenerative meniscal tears are thought to result from multiple sub-acute traumatic episodes that lead to chondrocyte death, increased mucinous ground substance, and loss of mechanical integrity. MRI and arthroscopy dominate the workup for internal derangement of the knee. On MRI, the normal menisci and ligaments are visualized as low-signal structures. Meniscal tears are evident as high-signal regions on T1 or proton density sequences that involve an articular margin. Gross distortions of meniscal shape or intrameniscal fluid collections indicate meniscal tears with displaced fragments.

**CLINICAL HISTORY** A 24-year-old woman with twisting knee injury.



FIGURE 6.36A



FIGURE 6.36B

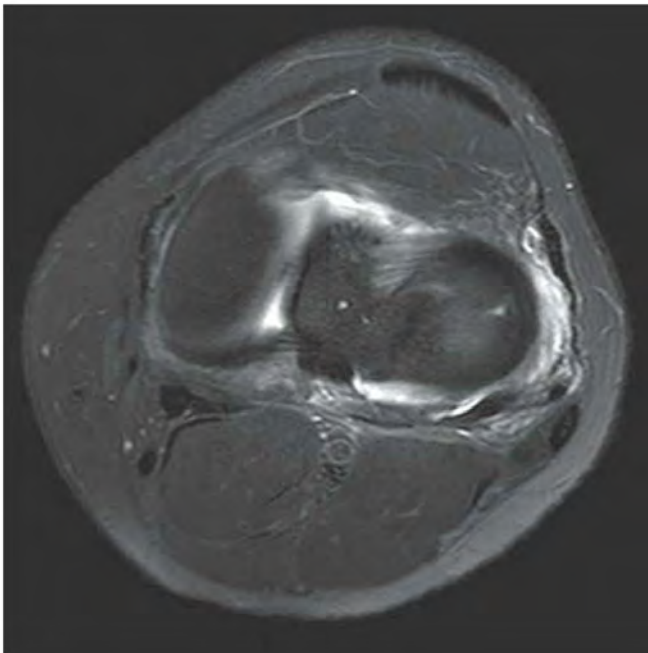


FIGURE 6.36C

**FINDINGS** (A) Sagittal proton density, fat-suppressed coronal, and (B, C) axial T2-weighted, fat-suppressed MRI shows small vertical areas of high signal within the body of

the lateral meniscus. The middle third of the lateral meniscus is irregular in shape and does not resemble a normal bow tie configuration. The axial image demonstrates an oblique irregular area of high signal extending perpendicular to the horizontal axis of the meniscus.

**DIFFERENTIAL DIAGNOSIS** None.

**DIAGNOSIS** Radial tear of the lateral meniscus.

**DISCUSSION** A radial tear is defined as a tear perpendicular to the free edge of the meniscus. When a tear has both a radial and a longitudinal component, it is referred to as a flap tear. On sagittal sequences, a radial tear may be manifested by a few vertical striations of high signal on peripheral sections. When a radial tear occurs in the medial meniscus, the posterior horn is usually involved. This usually presents in older patients. However, the most common location of a radial tear is the middle third of the meniscus, most likely due to the large curvature in this region. Radial tears are more common in patients who have undergone a prior partial meniscectomy [60]. ACL tears may be associated with radial tears occurring at the posterior horn of the lateral meniscus.

**CLINICAL HISTORY** A 21-year-old woman with knee injury, and a companion case (D).



FIGURE 6.37A

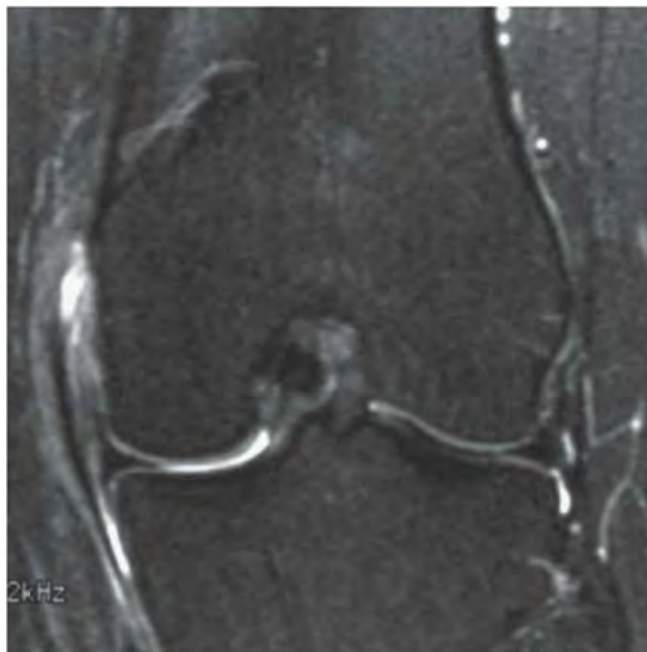


FIGURE 6.37B



FIGURE 6.37C



FIGURE 6.37D

## FINDINGS

- A, B. Coronal T1-weighted and T2-weighted MRI shows hemorrhage in the medial collateral ligament (MCL), with tear through the proximal origin. Abnormal signal is present at the expected location of the ACL.
- C. Axial T2-weighted MRI shows edema and hemorrhage at the medial aspect of the distal femur where the MCL should originate.
- D. Companion case. Detail of AP radiograph of the knee demonstrates calcification of the proximal portion of the MCL.

**DIFFERENTIAL DIAGNOSIS** None.

**DIAGNOSIS** Acute MCL sprain. An ACL sprain is present. Not shown but also present was a tear of the posterior horn of the medial meniscus. The companion case is an old MCL sprain with heterotopic ossification (Pellegrini-Stieda disease).

**DISCUSSION** Injury of the collateral ligaments may be imaged directly with MRI, which has been demonstrated to have 87% accuracy in identifying these injuries [61]. Partial tears are thickened and edematous, and they may

contain hemorrhage, whereas complete tears are discontinuous. The MCL is comprised of superficial and deep fibers, with the latter tenaciously fixed to the capsule and medial meniscus. This imparts a degree of rigidity to this structure, which renders it more susceptible to tears with associated injuries than its lateral counterpart. Valgus stress in flexion is a common mechanism for precipitating injury to the MCL. O'Donoghue's unhappy triad, present in this particular case, is a common set of associated injuries that consists of medial meniscal tear, ACL tear, and MCL disruption [62].

Conservative treatment is advocated for isolated tear of the MCL, whereas surgical treatment is recommended when associated injuries are present. The MCL may calcify as a sequela of trauma, which is radiographically detectable as a curvilinear density. Maturation with trabecular bone formation and frank ossification may occur, resulting in an appearance called Pellegrini-Stieda disease. Bone spurs at tendinous and ligamentous insertion sites, or enthesopathies, should be distinguished from this entity. Enthesophytes typically do not run the entire course of the ligament, and frequently occur at symmetric multiple sites in conjunction with an underlying condition such as spondyloarthropathy or diffuse idiopathic skeletal hyperostosis.

**CLINICAL HISTORY** A 25-year-old woman who twisted a knee while playing soccer.



FIGURE 6.38A

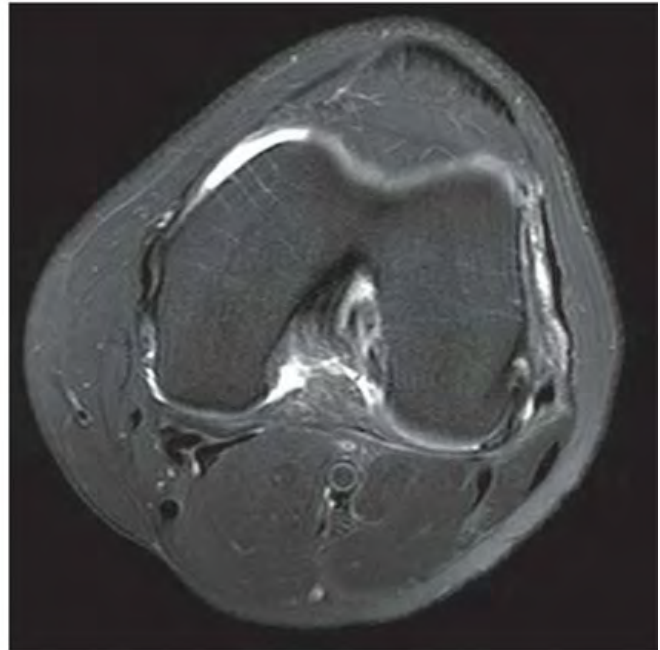


FIGURE 6.38B

**FINDINGS** Sagittal proton density fat-suppressed (A), and axial T2-weighted, fat-suppressed (B) MR images show abnormal increased signal in the ACL with partial disruption. There is a small knee effusion.

**DIFFERENTIAL DIAGNOSIS** None.

**DIAGNOSIS** ACL sprain, grade 2.

**DISCUSSION** Because the ACL is active throughout the knee's range of motion, it can be injured by a variety of non-contact, deceleration, hyperextension, twisting, and pivoting mechanisms. The ACL is the most frequently injured knee ligament, and is commonly associated with medial meniscal

tears, capsular tears, and transchondral impaction fractures. O'Donoghue's triad, a frequent association of injuries, consists of ACL tear, MCL tear, and medial meniscal tear [63,64]. Occasionally, loading of the ACL will result in an avulsion fracture of its insertion at the medial tibial spine. An avulsion fracture at the margin of the lateral tibial plateau where the knee capsule attaches (Segond fracture) is indicative of severe internal derangement, including ACL tear. PCL sprains are less common than ACL sprains by at least one-tenth. Trabecular microfractures (also called bone bruises) are seen on MRI as regions of localized edema, with intact overlying articular cartilage and subcortical bone. They occur from impaction trauma and are commonly associated with meniscal tears and ACL sprains.

**CLINICAL HISTORY** A 38-year-old woman with positive posterior drawer test after her knee hit the dashboard in a recent motor vehicle accident.



FIGURE 6.39

**FINDINGS** Sagittal T2-weighted MRI demonstrates focal discontinuity of the midportion of the PCL. A moderate joint effusion is present.

**DIFFERENTIAL DIAGNOSIS** None.

**DIAGNOSIS** PCL sprain, grade 3.

**DISCUSSION** Acute PCL tear is characterized by increased signal intensity and disruption of the fibers of the PCL. The PCL is disrupted in its midsubstance in this instance, the most common location for its occurrence [65]. These

tears are generally precipitated by hyperextension or a posterior impact during flexion. The posterior drawer sign in PCL tears refers to the posterior translation of the tibia relative to the femur seen with PCL disruption. The PCL is a much sturdier and thicker ligament than the ACL; therefore, PCL tears are often accompanied by other ligamentous and meniscal injuries, including ACL tears. As many as 50% of PCL sprains are isolated and are sustained in a dashboard injury or a fall directly on to a flexed knee. The remaining PCL sprains have complex mechanisms of injury and are associated with injuries of the ACL, MCL, medial meniscus, or other structures.

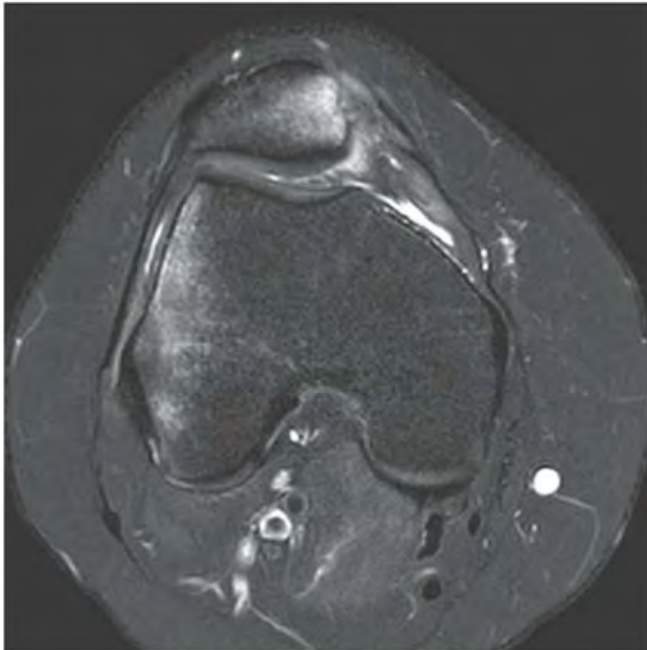


FIGURE 6.40A

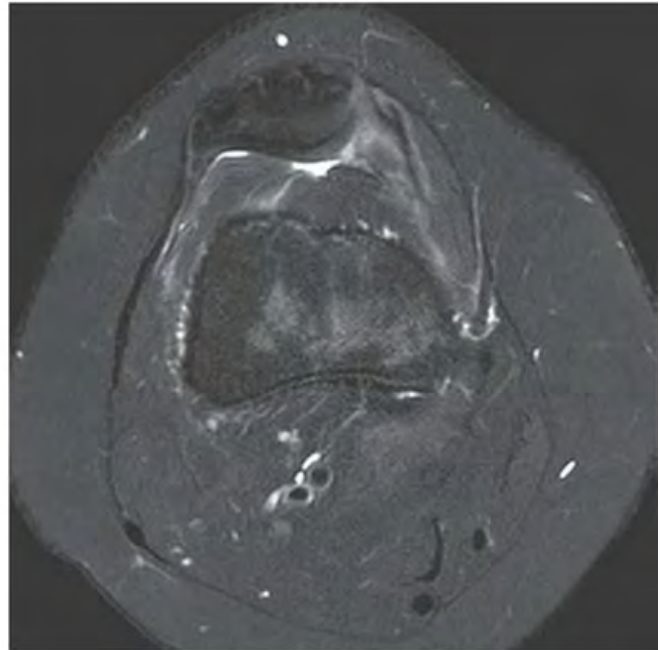


FIGURE 6.40B

**FINDINGS** Axial T2-weighted, fat-suppressed MRI (A) shows bone marrow edema in the medial patella and antero-lateral aspect of the lateral femoral condyle. There is an osteochondral injury in the medial patella and a tear of the medial patellar retinaculum. A more proximal image (B) demonstrates torn wavy medial patellofemoral ligament (MPFL).

**DIFFERENTIAL DIAGNOSIS** None.

**DIAGNOSIS** Transient lateral patellar dislocation.

**DISCUSSION** Transient lateral dislocation of the patella typically occurs in young adults involved in athletic activities and results from a twisting motion of the knee. The femur rotates internally on a fixed tibia while the knee is flexed, and contraction of the quadriceps occurs, resulting in lateral dislocation of the patella out of the trochlear groove. The classic bone contusion pattern seen after lateral patellar dislocation

includes involvement of the anterolateral aspect of the lateral femoral condyle and the inferomedial aspect of the patella. Associated soft tissue injuries include sprain or disruption of the medial soft tissue restraints. These restraints include the medial retinaculum, the MPFL, and the medial patello-tibial ligament. The MPFL has been shown to be the most important stabilizing structure of the patella preventing lateral subluxation. It is located just deep to the vastus medialis obliquus muscle as a low-signal-intensity band extending from the superior pole of the patella to the adductor tubercle. The medial retinaculum arises from the midpole of the patella and is located just distal to the MPFL. At the level of the medial retinaculum, the vastus medialis obliquus muscle should no longer be visualized [66]. The treatment of osteochondral fractures of the patella or lateral femoral condyle remains controversial. Currently, it is recommended to repair osteochondral fragments that are greater than 1.5 cm in size, have a sufficient osseous surface, and are part of the weight-bearing area of the patellofemoral articulation [67].

**CLINICAL HISTORY** A 77-year-old man with chronic knee pain.



FIGURE 6.41A

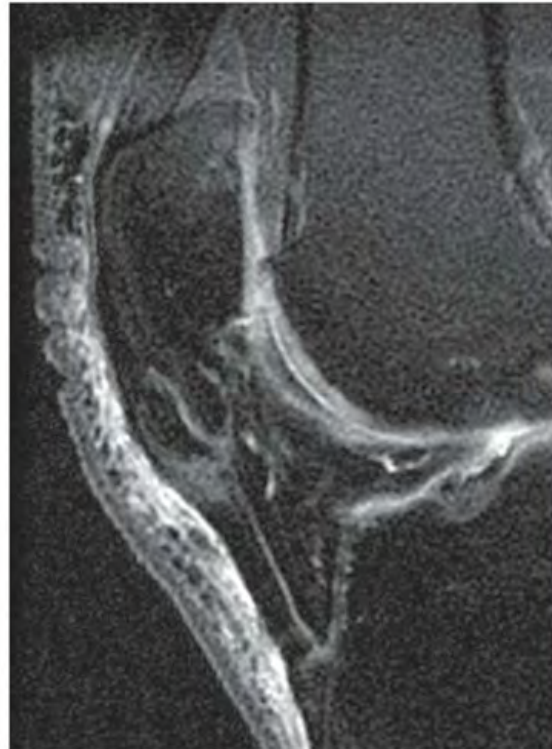


FIGURE 6.41B

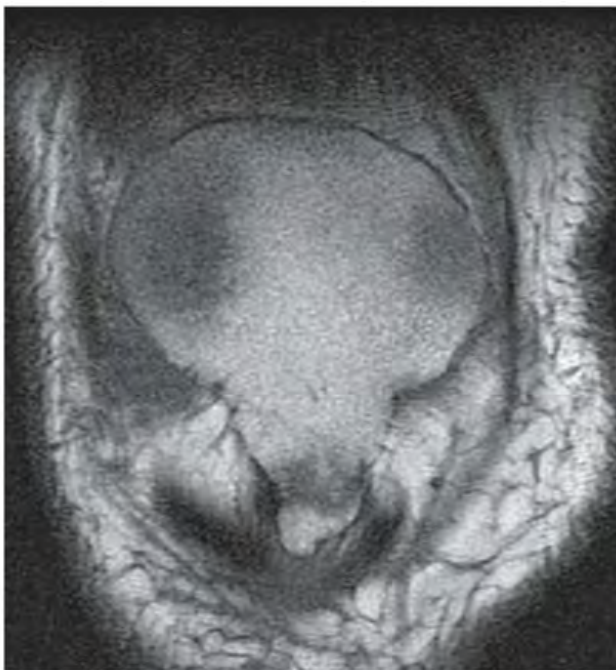


FIGURE 6.41C

## FINDINGS

- A. Lateral radiograph of the anterior knee shows elongation and fragmentation of the patellar distal pole.

B. Sagittal proton density, fat-suppressed MRI demonstrates the low-signal deformity of the patella. Increased signal in the proximal patellar tendon is likely due to magic angle artifact.

C. Coronal T1-weighted MRI shows the elongated distal patellar pole.

**DIFFERENTIAL DIAGNOSIS** Chronic Sinding-Larsen-Johansson (SLJ) disease, old patellar fracture.

**DIAGNOSIS** SLJ disease.

**DISCUSSION** SLJ disease is an osteochondrosis of the distal patellar pole. This occurs as a result of repetitive traction microtrauma from the patellar tendon. SLJ is sometimes referred to as jumper's knee. Osgood-Schlatter disease is a similar entity located at the tibial tubercle. SLJ disease appears radiographically as fragmentation of the ossification center, with subsequent formation of separate bony fragments and elongation of the distal patellar pole. On MRI and ultrasound, soft tissue swelling, patellar tendon edema, and bursitis can be seen, in addition to the fragmented ossification center [68]. This is a self-limited process that requires no treatment [69].

**CLINICAL HISTORY** A 19-year-old adolescent girl with knee pain following injury.



FIGURE 6.42A



FIGURE 6.42B



FIGURE 6.42C

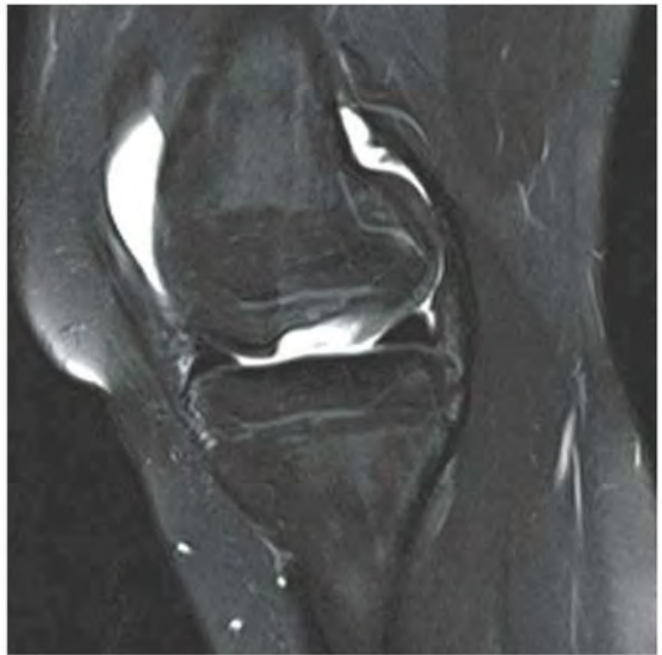


FIGURE 6.42D

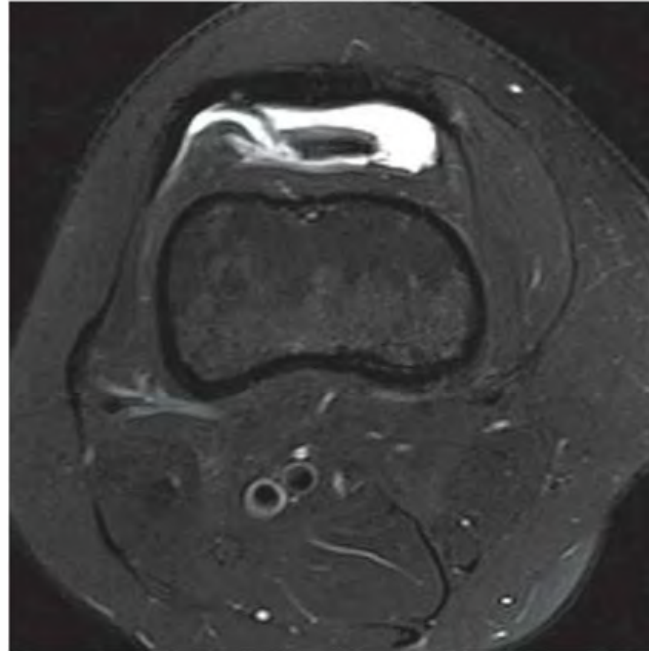


FIGURE 6.42E

**FINDINGS** (A, B) Radiographs of the knee show a focal sclerotic lesion in the articular surface of the lateral aspect of the medial femoral condyle. A faint intra-articular body is present in the suprapatellar bursa. Coronal T1-weighted (C), and sagittal T2-weighted, fat-suppressed (D) MRI through the femoral condyles shows an osteochondral lesion in the medial femoral condyle. (E) Axial T2-weighted, fat-suppressed MRI through the suprapatellar bursa shows the detached fragment.

**DIFFERENTIAL DIAGNOSIS** None.

**DIAGNOSIS** Osteochondral fracture (osteochondritis dissecans).

**DISCUSSION** The lateral aspect of the medial femoral condyle is a prime location for osteochondritis dissecans. The irregularity of the articular surface in this location is classic for this entity. Although subchondral insufficiency fracture of the knee (SIFK) may produce similar findings, it tends to involve the weight-bearing portion of the medial femoral condyle and occurs in an older population.

Osteochondritis dissecans is subsumed under the more general category of osteochondral injuries. The primary

etiology for its occurrence is trauma. It is observed more frequently in males, has a peak incidence in the second decade, and can be bilateral in 25% of cases. The histologic appearance may be confusing; therefore, radiologic findings may be more reliable. Irregularity and fragmentation of the articular surface of the medial femoral condyle on its lateral aspect is classic [70]. The lateral femoral condyle and patella are other favored locations. On occasion, a curvilinear subchondral lucency or fracture may be detected. When the injury is strictly chondral, radiographs will appear normal. Conversely, a subchondral injury may occur without damage to the overlying cartilage.

The fragment may be in situ or detached. Secondary signs include soft tissue swelling and effusion. On MRI, when fluid is seen surrounding an in situ fragment, it is felt to be unstable. Detached fragments may become resorbed or may persist as intra-articular bodies. In the latter instance, the fragment may grow by apposition of cartilage and bone. Treatment is determined by manifested symptoms. Pain and instability may warrant surgery. The size of the lesion may predict instability—lesions larger than 8 by 8 mm are associated with instability [71]. Long-term complications include osteoarthritis [72].



FIGURE 6.43A



FIGURE 6.43B

**FINDINGS** Lateral (A) and AP (B) radiographs of the knee show that the patella has assumed a horizontal orientation within the joint. No fracture is identified.

**DIFFERENTIAL DIAGNOSIS** None.

**DIAGNOSIS** Horizontal intercondylar dislocation of the patella.

**DISCUSSION** Patellar dislocations are usually the result of a direct blow to the patella. The common patellar dislocation is to the lateral side, with the patella retaining its normal orientation relative to the knee. Unusual forms of patellar dislocation exist, including horizontal dislocation [73], vertical axis rotation, and superior dislocation. Horizontal intercondylar dislocation of the patella occurs when the patella is rotated 90 degrees along its horizontal axis, so that the articular surface faces inferiorly (as in most reported cases) or superiorly (extremely rare).

The mechanism of injury is thought to be a direct blow to the superior pole of the patella in the flexed knee, of

sufficient force to displace the upper bony margin of the patella into the intercondylar notch of the femur. When the knee is subsequently extended, the femur acts like a bottle opener to avulse the patella from its attachment to the quadriceps mechanism. The detached patella is thereby dislocated between the femur and the tibia into the intercondylar notch, with the articular surface facing inferiorly and the superior pole pointing posteriorly. The patella is generally detached incompletely from the quadriceps mechanism, forcing it to retain its abnormal orientation. Male adolescents are the most prone to this type of injury.

In vertical axis dislocation, a direct blow to the patella while the knee is extended rotates the patella along its long (vertical) axis, so that the medial edge becomes lodged in the patellofemoral groove [74–76]. In vertical patellar dislocation, a direct blow to the inferior pole of the patella while the knee is extended may displace the patella superior to the patellofemoral groove. If degenerative change is preexisting, interlocking osteophytes may prevent the patella from returning to the normal position [77].

**CLINICAL HISTORY** A 6-month-old girl with failure to thrive. A, right knee radiograph; B, left knee radiograph.



FIGURE 6.44A



FIGURE 6.44B

### FINDINGS

- A. AP radiograph of the right knee. There is a small bony excrescence extending medially from the distal femoral metaphysis.
- B. AP radiograph of the left knee. There is a triangular fragment of bone adjacent to the medial aspect of the distal metaphysis of the femur. The fragment is slightly displaced and has unsharp margins.

**DIFFERENTIAL DIAGNOSIS** None.

**DIAGNOSIS** Battered child.

**DISCUSSION** Corner fractures in a very young child are virtually pathognomonic for child abuse. However, the most common fractures seen in child abuse [85] are spiral fractures of the long bones of the lower limb in toddlers, fractures of the clavicle, and simple linear fractures of the skull outside the occiput. These fractures are not specific to child abuse and may occur with accidental trauma. Child abuse is likely when injuries are discovered that are more extensive or more severe than the history given for the trauma; when the injuries are of different ages, indicating prior episodes of trauma; or when there is fracture without adequate explanation.

Corner fractures are caused by indirect torsional, acceleration, and deceleration forces generated when an infant is shaken violently. Massive forces develop as the head and extremities flail about. In the long bones of the extremities, radiologic-pathologic studies have shown the fundamental

lesion to be a series of microfractures occurring in a plane through the immature metaphyseal primary spongiosa, which is the zone of growing bone where delicate trabeculae are first apposed to central calcified cores. The fracture fragment consists of a thin plate of bone, calcified cartilage, the growth plate, and the attached epiphysis. This fracture is recognized as a transverse subepiphyseal lucency with an adjacent linear density abutting the growth plate. If the fragment is tipped or viewed obliquely, it will have a bucket-handle appearance. If the periphery is thicker than the central portion, it will have a corner fracture appearance. These metaphyseal lesions are injuries highly specific for intentional injury and differ from the usual Salter types of growth plate fractures, in which the fracture plane is between the calcified and uncalcified zones of cartilage. Shaking may separate a long bone from its periosteal envelope, leading to subperiosteal hemorrhage and periosteal elevation. Once the periosteum begins to make new reactive bone, its displaced position will become evident.

It may become critical to establish the age of a fracture by radiologic appearance in relation to the historical timing of the trauma. Dating fractures by roentgenography is imprecise. In general, a fracture with definite but slight periosteal new bone may be as recent as 4 to 7 days old; unless immobilized or internally fixed, a fracture 20 days old will almost always have well-defined periosteal new bone and soft callus. A fracture with a large amount of periosteal new bone or callus is more than 14 days old. Long bone fractures in infants heal with widespread periosteal new bone formation.

**CLINICAL HISTORY** A 40-year-old man with large knee effusion and pain for several years.



FIGURE 6.45A

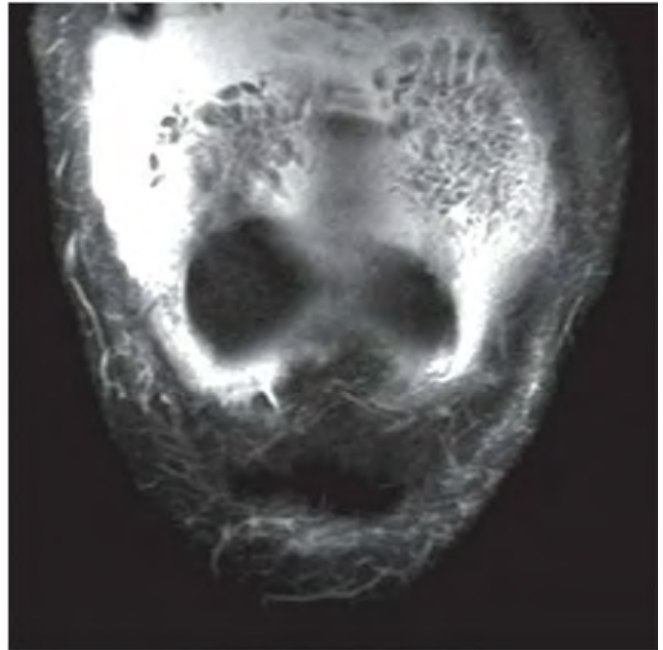


FIGURE 6.45B

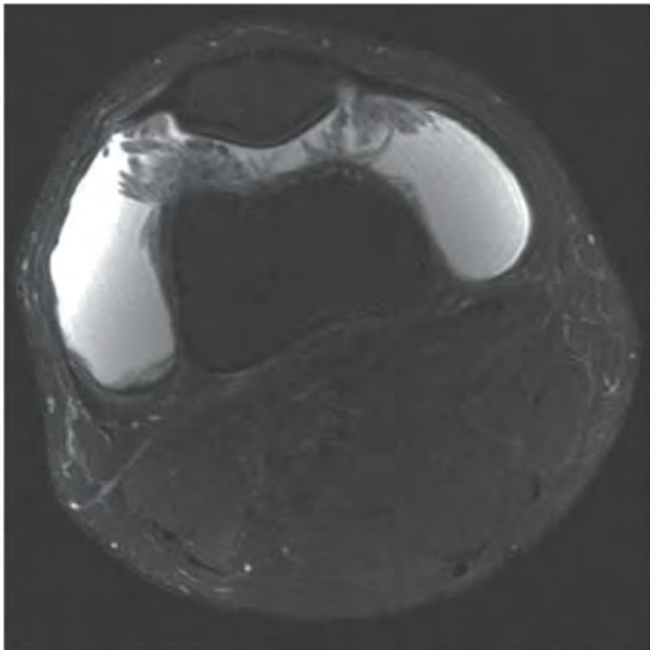


FIGURE 6.45C

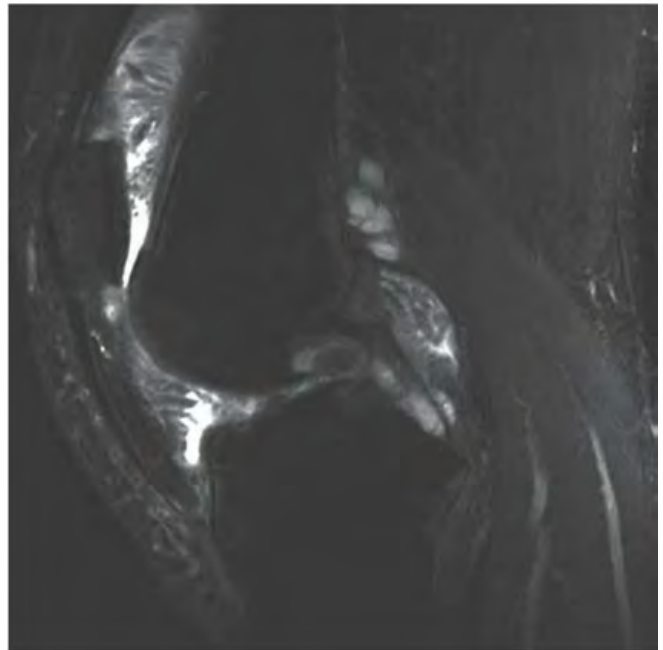


FIGURE 6.45D

## FINDINGS

- A. Coronal T1-weighted MRI through the patellofemoral groove of the distal femur shows arborizing, villous, fatty proliferation of the synovium.
- B. Coronal proton density, fat-suppressed MRI shows the effusion outlining the fatty synovial proliferation. The signal within the proliferation has been suppressed similar to the subcutaneous fat.
- C, D. Axial (C) and sagittal (D) T2-weighted, fat-suppressed MRI again shows arborizing fatty proliferation of the synovium with a large effusion.

**DIFFERENTIAL DIAGNOSIS** Lipoma arborescens, pigmented villonodular synovitis, synovial chondromatosis, rheumatoid arthritis, synovial hemangiomatosis, amyloid arthropathy.

**DIAGNOSIS** Lipoma arborescens.

**DISCUSSION** Although the differential diagnosis for synovial masses includes several possibilities, the fatty composition of the lesion provides the correct diagnosis. Lipoma arborescens (lipomatosis of the synovium) is characterized

by multiple, swollen, synovial villous projections of fatty tissue, with a tree-like branching pattern that gives it its name. Diffuse replacement of subsynovial tissue by mature fat cells produces a villous transformation of the synovium. It may begin de novo, but has also been associated with degenerative joint disease, rheumatoid arthritis, and posttraumatic conditions [78]. Although the etiology is unknown, it is thought to be a nonneoplastic reactive process. The condition is typically monoarticular and involves the knee, but involvement of multiple joints and involvement of the wrist, shoulder, and hip have been described.

Patients present with long-standing, slowly progressive joint swelling and pain. Radiographs typically show effusion and any associated articular disease. MRI always shows effusions and lipomatous proliferation with a villous morphology; the signal intensity is similar to that of fat on T1-weighted and T2-weighted images [79–82]. The proliferation may have broad-based polypoid morphology or a thin papillary one. Mass-like subsynovial fat deposition, erosive bone changes at articular margins, synovial cysts, and degenerative changes may be found in a minority of cases. The treatment is local excision of the lesion.

**CLINICAL HISTORY** A 37-year-old man with knee pain and swelling.



FIGURE 6.46A

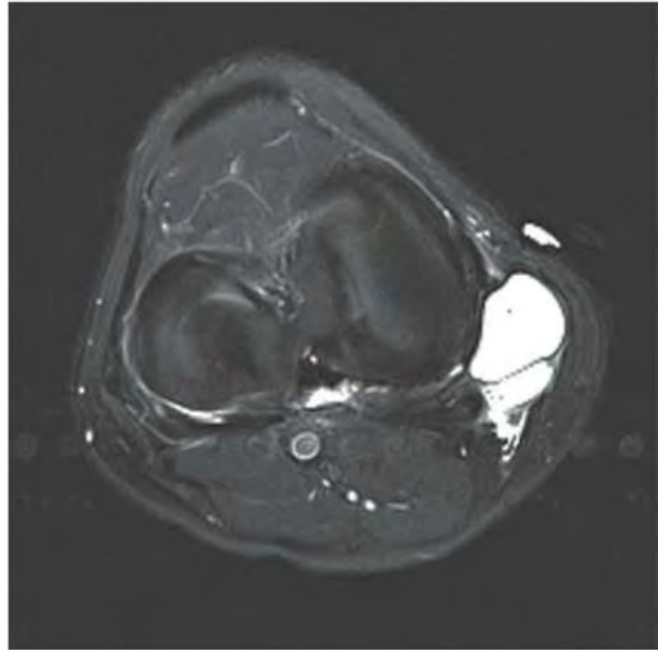


FIGURE 6.46B

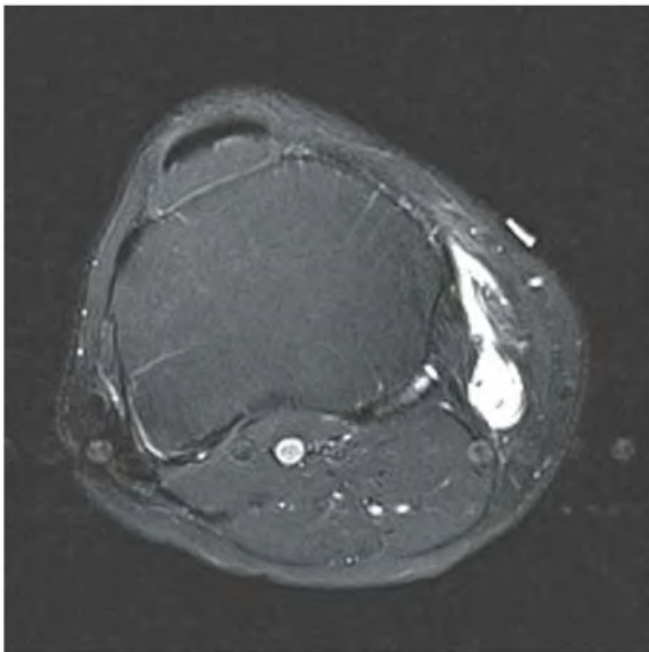


FIGURE 6.46C



FIGURE 6.46D

**FINDINGS** AP radiograph of the knee shows focal soft tissue mass density at the medial aspect (A). Axial T2-weighted, fat-suppressed (B, C), and coronal proton density, fat-suppressed (D) MRI shows a multilobulated cystic structure adjacent to the medial femoral condyle and medial tibial plateau. This structure is superficial to the MCL and displaces pes anserinus tendons.

**DIFFERENTIAL DIAGNOSIS** Pes anserinus bursitis, MCL bursitis, parameniscal cyst.

**DIAGNOSIS** Pes anserinus bursitis.

**DISCUSSION** The pes anserinus bursa lies deep to the pes anserinus, superficial to the tibial insertion of the MCL and the medial tibial condyle, and slightly distal to the

insertion of the semimembranosus tendon. The pes anserinus is formed by the conjoined tendons of the sartorius, gracilis, and semitendinosus muscles and inserts along the anteromedial surface of the tibia. Pes anserinus bursitis is believed to result from overuse friction to the bursa due to excessive valgus or rotatory stresses to the knee or by direct contusion [83].

Patients may present with classic symptoms of tenderness and swelling along the proximal medial tibia or may complain of vague medial knee pain, which may mimic medial meniscal or MCL injury. The MCL bursa is located along the middle third of the medial aspect of the knee between the superficial and deep layers of the MCL. The diagnosis of a parameniscal cyst is more likely if MR imaging demonstrates a direct communication of the meniscal tear with the cyst, and the cyst is centred more focally over the tear [84].

**CLINICAL HISTORY** A 65-year-old woman with severe knee pain.

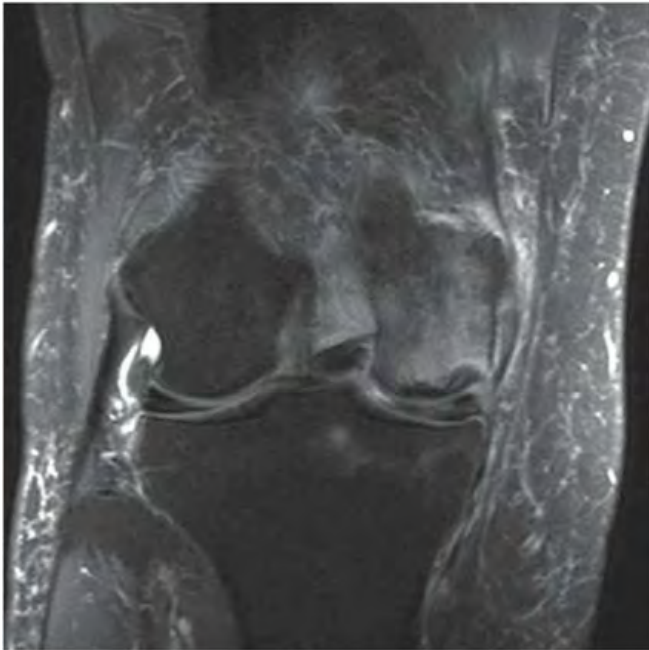


FIGURE 6.47A



FIGURE 6.47B



FIGURE 6.47C

**FINDINGS** Coronal fat-suppressed, proton density (A), coronal T1-weighted (B), and sagittal fat-suppressed proton density (C) MRI shows abnormal signal in the weight-bearing surface of the medial femoral condyle. A serpiginous low-signal region is surrounded by edema. There is no collapse of the articular surface.

**DIFFERENTIAL DIAGNOSIS** Subchondral insufficiency fracture, osteonecrosis, osteochondritis dissecans, osteoarthritis, contusion, transient bone marrow edema.

**DIAGNOSIS** Subchondral insufficiency fracture of the knee (SIFK).

**DISCUSSION** SIFK was originally thought to be the result of vascular insufficiency with venous occlusion leading to venous hypertension and finally hypoxia. The entity has more recently been shown to represent a subchondral insufficiency fracture with the localized osteonecrosis being the result of the fracture [86]. The pathogenesis of SIFK remains controversial. Several theories have been proposed as causes, including meniscal tears and/or chondromalacia associated with osteoarthritis, prior arthroscopic surgery, and insufficiency fractures associated with osteoporosis [87]. It is typically seen in elderly women with acute knee pain. It can be seen along the weight-bearing surface of either femoral condyle. Osteochondritis dissecans would typically be in a younger patient, with a similar-appearing lesion along the lateral aspect of the medial femoral condyle. Collapse of the subchondral bone can lead to accelerated osteoarthritis. Approximately 20% of cases resolve spontaneously [88].

**CLINICAL HISTORY** A 67-year-old woman with total knee replacement. A, postoperative radiograph; B, radiograph 2 years later.

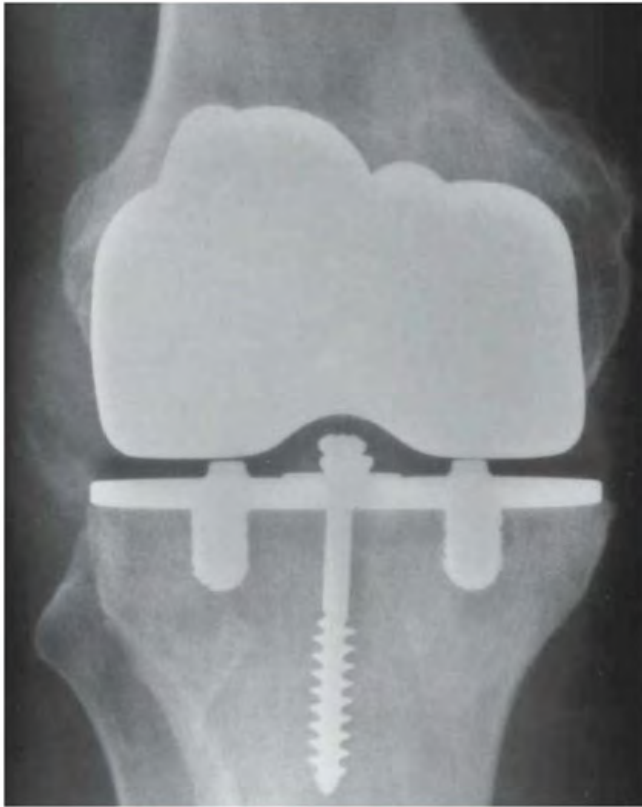


FIGURE 6.48A

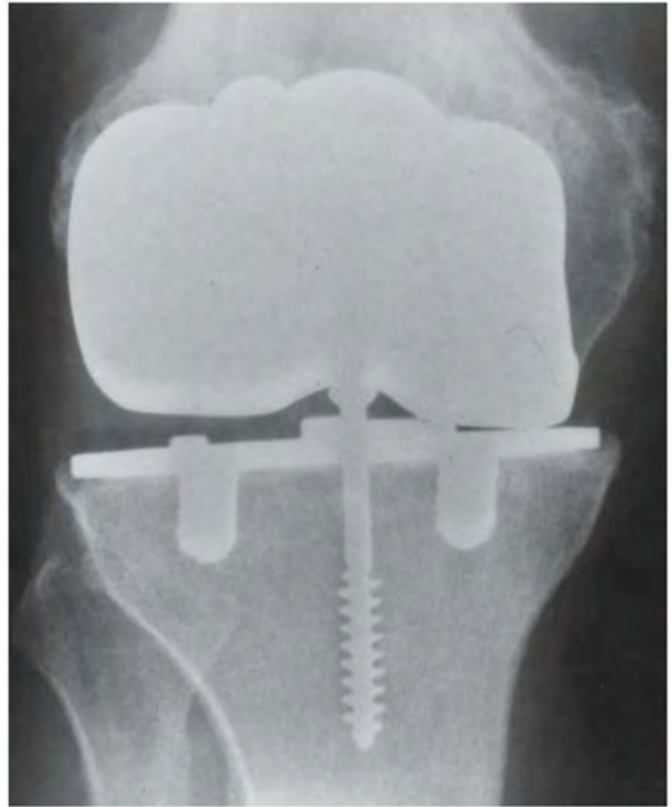


FIGURE 6.48B

### FINDINGS

- A. AP radiograph of weight-bearing knee shortly after initial surgery for total knee replacement shows normal position and alignment of the components.
- B. AP radiograph of weight-bearing knee 2 years later shows marked narrowing of the medial joint space, with metal articulating with metal. A varus deformity results.

**DIFFERENTIAL DIAGNOSIS** None.

**DIAGNOSIS** Total knee replacement with failure of tibial polyethylene.

**DISCUSSION** The radiographic joint space in a total knee replacement is the space between the metal components that is normally occupied by a polyethylene liner. Polyethylene, like other plastics, is radiolucent on radiographs and can generally be distinguished from joint fluid. Narrowing of the joint space in a total knee replacement is indicative of failure of the polyethylene, due to excessive wear from the surface, fragmentation, or even dislocation. Loss of polyethylene from the patellar component may be difficult to demonstrate on radiographs. Other complications involving total knee replacement include infection, osteolysis and component loosening, instability, and metallosis.

**CLINICAL HISTORY** A 73-year-old woman 10 years after total knee replacement.



FIGURE 6.49A

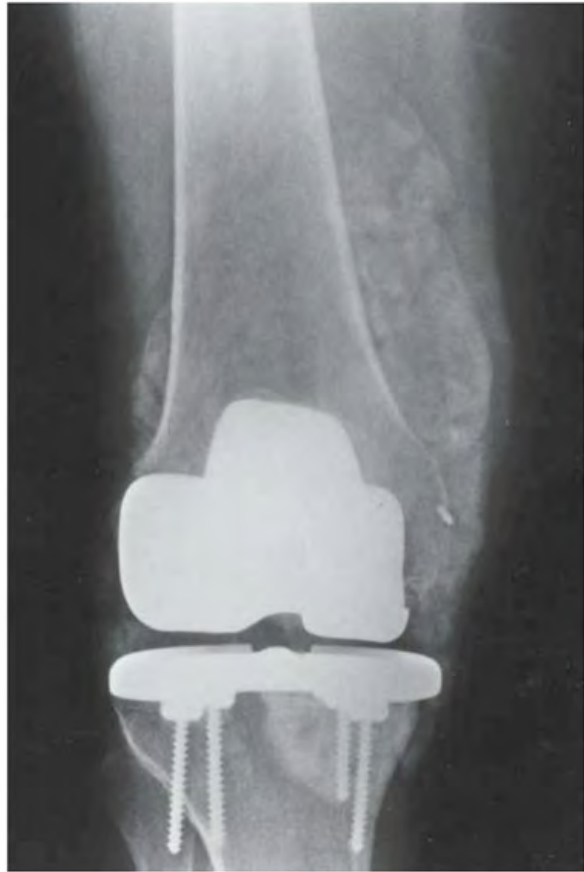


FIGURE 6.49B

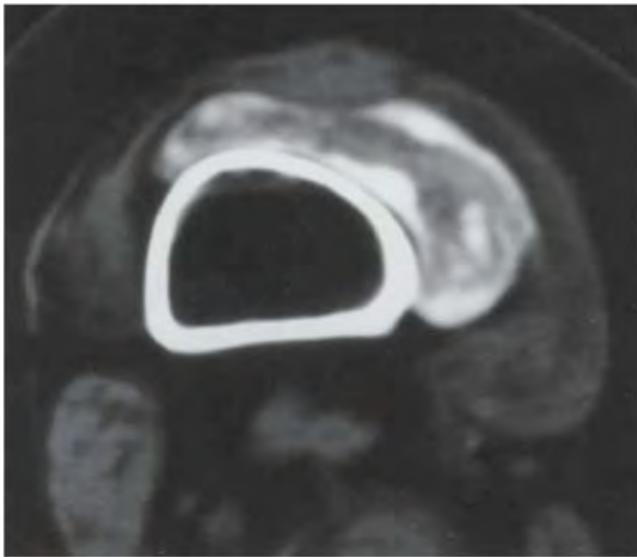


FIGURE 6.49C

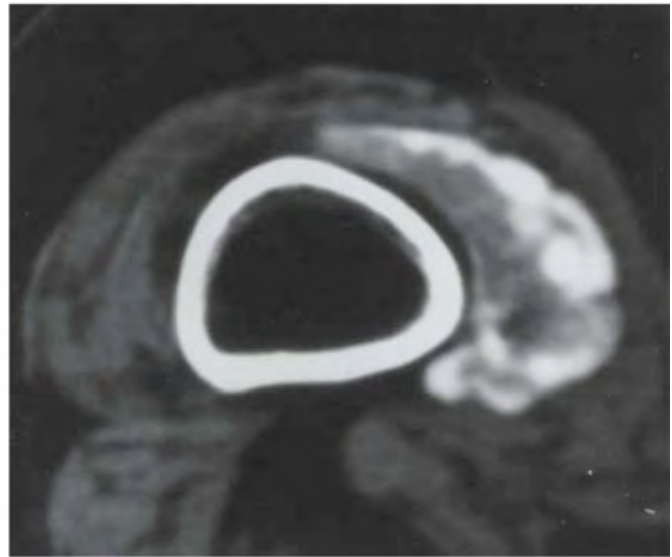


FIGURE 6.49D

**FINDINGS**

- A, B. Lateral and AP radiographs show a total knee prosthesis. Radiodense material outlines a distended joint capsule.
- C, D. Axial CT without the use of contrast material demonstrates that the radiodense material seen on the radiographs is metallic.

**DIFFERENTIAL DIAGNOSIS** None.

**DIAGNOSIS** Metallosis.

**DISCUSSION** The initial thought on encountering metallic density in a joint capsule is that radiographic contrast has been injected or secreted into the joint. Once it has been established that this is not the case, the obvious source of the metallic density is the metal that is already present within the joint, namely, the components of the knee prosthesis.

Metallosis is a complication of total joint replacements caused by abrasion of metal components, typically after failure of interposed polyethylene-bearing surfaces. In one

series, metallosis was present in 7 of 30 patients with total knee replacements using metal-backed patellar components [89]. Microscopic particles abraded from polyethylene surfaces are known to provoke a giant cell foreign body reaction that results in osteolysis and implant loosening, but a major role for metal debris-containing histiocytes in this process has also been suggested [90]. Metal and polyethylene particles may be carried away from joint replacements by lymphatics [91], but with uncertain systemic effects.

The characteristic radiographic finding of metallosis after total knee replacement is a radiodensity outlining the suprapatellar recess of the joint capsule caused by the presence of embedded metal particles [92]. Arthrocentesis produces a thick, dark gray or black fluid. At surgery, the joint capsule is typically filled with dark fluid and metallic debris, with a grossly blackened and hypertrophic synovium. Metallosis is treated by synovectomy and revision of the prosthesis. Although the metal-backed patellar component is no longer in use, patients with this implant are still common, and metallosis may follow failure of tibial polyethylene components.

**CLINICAL HISTORY** A 34-year-old woman with left knee pain resembling intermittent claudication. A-C, left knee MRI; D-E, bilateral knee CT.

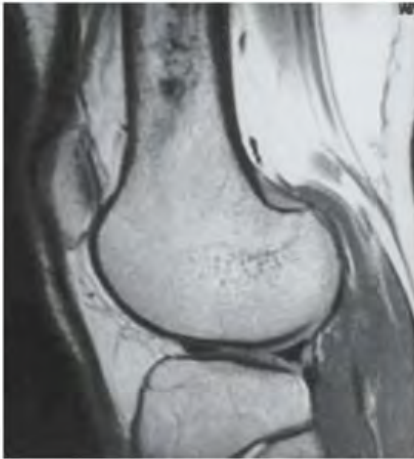


FIGURE 6.50A

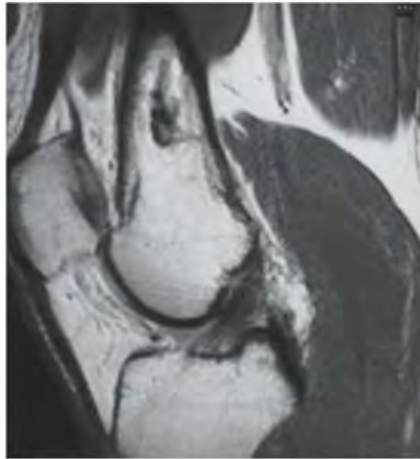


FIGURE 6.50B

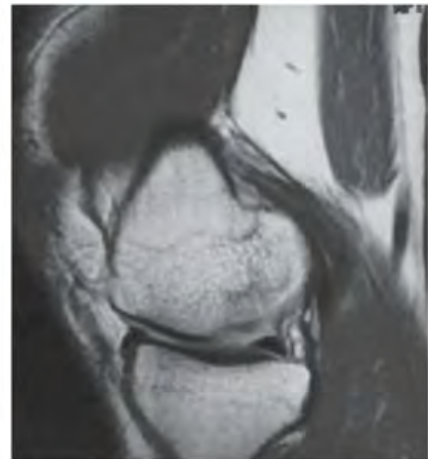


FIGURE 6.50C

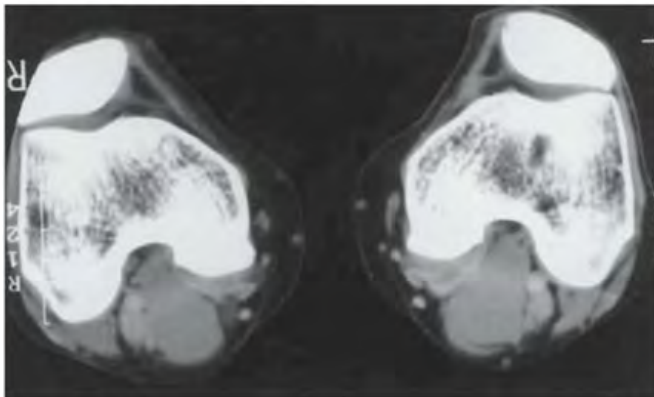


FIGURE 6.50D

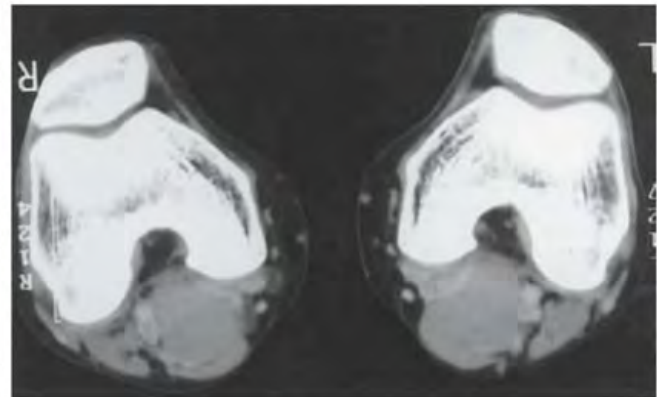


FIGURE 6.50E

## FINDINGS

- A–C. Sagittal proton density MRI of the left knee through the lateral femoral condyle, intercondylar notch, and medial condyle shows diminutive heads of the lateral and medial gastrocnemius muscle, with a large, anomalous muscle arising from the posterior aspect of the distal femoral shaft. An incidental enchondroma is present in the more proximal femoral shaft.
- D, E. Axial CT, after intravenous contrast medium injection of both knees at the level of the popliteal fossa, shows on each side an anomalous muscle occupying the popliteal fossa, displacing the popliteal vessels laterally.

**DIFFERENTIAL DIAGNOSIS** None.

**DIAGNOSIS** Popliteal artery entrapment syndrome.

**DISCUSSION** Various anomalies of the origin of the medial head of the gastrocnemius may result in aberrant location of the muscle belly [96–98]. In some circumstances, this aberrant location may result in compression of the popliteal vessels between the aberrant medial and lateral heads of the gastrocnemius muscle. Functional segmental occlusion of the popliteal artery with flexion may cause ischemic symptoms in the lower extremities. In the most common anomaly, a portion of the medial head of the gastrocnemius originates along the posterior aspect of the distal femoral shaft, proximal and lateral to its normal origin on the posterior face of the medial femoral condyle. This muscle then courses inferiorly

in the popliteal fossa to join the remaining fibers of the gastrocnemius in the calf. The medial and lateral heads may be smaller than normal, so that the overall bulk of the muscle is normal. The symptoms of claudication may be atypical, with symptoms related more to the degree of knee flexion than actual exertion.

Thrombotic and embolic complications may occur in the distal arteries. Popliteal artery entrapment may result when the artery has an atypical course, either with or without an

aberrant gastrocnemius origin. Patients are typically adults, men more commonly than women, who are physically active. Symptoms usually begin when the patients are in their early 30s, with the diagnosis not made until their late 30s. Radiographs are normal, but cross-sectional imaging will show the anomaly. Angiograms may be normal if they are done with the patient at rest with the knee in extension. The treatment is surgical.

**CLINICAL HISTORY** A 16-year-old girl with knee pain and limited extension. She had her ACL reconstruction surgery about 3 years ago.

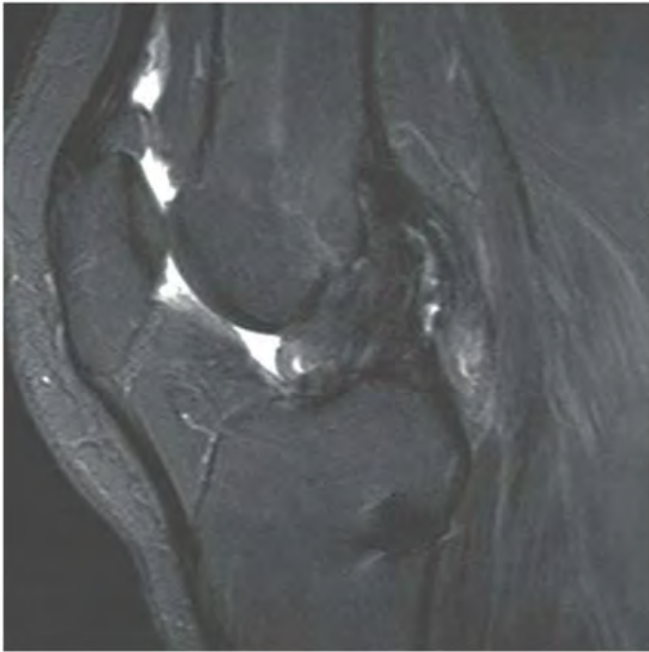


FIGURE 6.51A

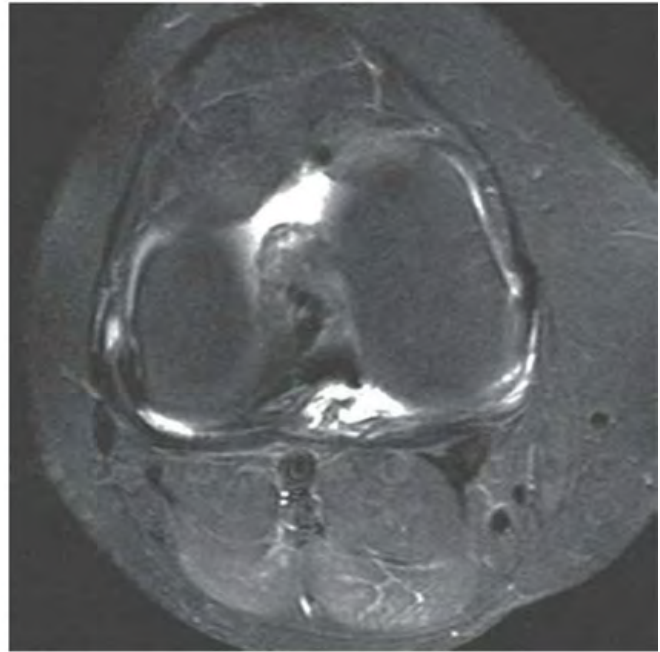


FIGURE 6.51B

**FINDINGS** Sagittal proton density, fat-suppressed (A), and axial T2-weighted, fat-suppressed (B) MRI shows intermediate-signal-intensity soft tissue lesion anterior to the intact ACL graft.

**DIFFERENTIAL DIAGNOSIS** None.

**DIAGNOSIS** Arthrofibrosis.

**DISCUSSION** The cyclops lesion was first described in 1990, and consists of a focal nodule of fibrous tissue in the intercondylar notch anterior to the ACL graft [93]. This nodule was dubbed the cyclops lesion because of its head-like appearance and its characteristic focal reddish-blue areas of discoloration due to venous channels, which resemble an

eye at arthroscopy. Characteristic clinical findings include a rubbery end point to full extension with or without a palpable pop, initial full range of motion that is later lost, and a rebound after manipulation into full extension. The origin of cyclops lesions is uncertain. Tissues that may contribute to the formation of cyclops lesions include fibrous tissue, fibrocartilage, bone, synovium, and fat from the infrapatellar fat pad [94]. On T1-weighted MR images, it appears as a focal nodular lesion of low signal intensity that is anterior to the graft in the intercondylar notch. On T2-weighted images, the nodule is heterogeneous but predominantly of low signal intensity and is well differentiated from high-signal-intensity joint fluid [95]. Patients with extension loss caused by cyclops lesions typically require second arthroscopy to resect the fibrous nodular-shaped tissue.

## SOURCES AND READINGS

1. Trevor D. Tarso-epiphyseal aclerosis: a congenital error of epiphyseal development. *J Bone Joint Surg Br.* 1950;32-B:204–213.
2. Schoenberg NY, Lehman WB. Magnetic resonance imaging of pediatric disorders of the ankle and foot. *Magn Reson Imaging Clin N Am.* 1994;2:109–122.
3. Tyler W, Barrett T, Frassica F, McCarthy E. Skin metastasis from conventional giant cell tumor of bone: conceptual significance. *Skeletal Radiol.* 2002;31:166–170.
4. Kitano K, Shiraishi T, Okabayashi K, Iwasaki A, Kawahara K, Shirakusa T. A lung metastasis from giant cell tumor of bone at eight years after primary resection. *Jpn J Thorac Cardiovasc Surg.* 1999;47:617–620.
5. Grote HJ, Braun M, Kalinski T, et al. Spontaneous malignant transformation of conventional giant cell tumor. *Skeletal Radiol.* 2004;33:169–175.
6. Unni KK, Inwards CY. *Dahlin's Bone Tumors: General Aspects and Data on 10,165 Cases.* 6th ed. Philadelphia, PA: Lippincott Williams & Wilkins; 2010:122–157.
7. Kaplan PA, Asleson RJ, Klassen CW, Duggan MJ. Bone marrow patterns in aplastic anemia: observations with 1.5 T MRI. *Radiology.* 1987;164:441–444.
8. Steiner RM, Mitchell DG, Reno VM, et al. MRI of bone marrow: diagnostic value in diffuse hematologic disorders. *Magn Res Q.* 1990;6:17–34.
9. Jensen KE, Nielssen A, Thomsen C. In vivo measurements of T1 relaxation processes in the bone marrow in patients with myelodysplastic syndrome. *Acta Radiol.* 1989;30:365–368.
10. Chew FS, Hudson TM. Radionuclide bone scanning of osteosarcoma: falsely extended uptake patterns. *AJR Am J Roentgenol.* 1982;139:49–54.
11. Yarmish G, Klein MJ, Landa J, Lefkowitz RA, Hwang S. Imaging characteristics of primary osteosarcoma: nonconventional subtypes. *Radiographics.* 2010; 30:1653–1672.
12. Unni KK, Inwards CY. *Dahlin's Bone Tumors: General Aspects and Data on 10,165 Cases.* 6th ed. Philadelphia, PA: Lippincott-Williams & Wilkins; 2010.
13. Jelinek JS, Murphey MD, Kransdorf MJ, Shmookler BM, Malawer MM, Hur RC. Parosteal osteosarcoma: value of MR imaging and CT in the prediction of histologic grade. *Radiology.* 1996;201:837–842.
14. Murphey MD, Robbin MR, McRae GA, Flemming DJ, Temple HT, Kransdorf MJ. The many faces of osteosarcoma. *Radiographics.* 1997;17:1205–1231.
15. Schuh A, Zeiler G, Holzwarth U, Aigner T. Malignant fibrous histiocytoma at the site of a total hip arthroplasty. *Clin Orthop.* 2004;425:218–222.
16. Krishnan A, Shirkhoda A, Tehranzadeh J, Armin AR, Irwin R, Les K. Primary bone lymphoma: radiographic-MR imaging correlation. *Radiographics.* 2003;23:1371–1383.
17. Unni KK, Inwards CY. *Dahlin's Bone Tumors: General Aspects and Data on 10,165 Cases.* 6th ed. Philadelphia, PA: Lippincott-Williams & Wilkins; 2010:201–209.
18. Hill S, Dunn A, Thomas JM. Lymphoma presenting as an intramuscular mass. *Br J Surg.* 1997;84:1741–1743.
19. Kerr R. Imaging of musculoskeletal complications of hemophilia. *Semin Musculoskelet Radiol.* 2003;7:127–136.
20. Boldero JL, Kemp HS. The early bone and joint changes in hemophilia and similar blood dyscrasias. *Br J Radiol.* 1966;39:172–180.
21. Paton RW, Evans DK. Silent AVN of the femoral head in hemophilia. *J Bone Joint Surg.* 1988;70B:737–739.
22. McHugh K, Olsen ØE, Vellodi A. Gaucher disease in children: radiology of non-central nervous system manifestations. *Clin Radiol.* 2004;59:117–123.
23. Rohren EM, Kosarek FJ, Helms CA. Discoid lateral meniscus and the frequency of meniscal tears. *Skeletal Radiol.* 2001;30:316–320.
24. Youm T, Chen AL. Discoid lateral meniscus: evaluation and treatment. *Am J Orthop.* 2004;33:234–238.
25. Duong S, Sallis JG, Zee SY. Malignant fibrous histiocytoma arising within a bone infarct in a patient with sickle cell trait. *Int J Surg Pathol.* 2004;12:67–73.
26. Curi MM, Dib LL. Osteoradionecrosis of the jaws: a retrospective study of the background factors and treatment in 104 cases. *Maxillofac Surg.* 1997;55:540–546.
27. Wood GA, Liggins SJ. Does hyperbaric oxygen have a role in the management of osteoradionecrosis? *Br J Oral Maxillofac Surg.* 1996;34:424–427.
28. Outerbridge R. The aetiology of chondromalacia patellae. *J Bone Joint Surg Br.* 1961;43:752–757.
29. van Leersum M, Schweitzer ME, Gannon F, Finkel G, Vinitzki S, Mitchell DG. Chondromalacia patellae: an in vitro study. Comparison of MR criteria with histologic and macroscopic findings. *Skeletal Radiol.* 1996;25:727–732.
30. Elias DA, White LM. Imaging of patellofemoral disorders. *Clin Radiol.* 2004;59:543–557.
31. Greenspan A, Azouz EM, Matthews J II, Decarie JC. Synovial hemangioma: imaging features in eight histologically proven cases, review of the literature, and differential diagnosis. *Skeletal Radiol.* 1995;24:583–590.
32. Price NJ, Cundy PJ. Synovial hemangioma of the knee. *J Pediatr Orthop.* 1997;17:74–77.
33. Murphey MD, Rhee JH, Lewis RB, Fanburg-Smith JC, Flemming DJ, Walker EA. Pigmented villonodular synovitis: radiologic-pathologic correlation. *Radiographics.* 2008;28:1493–1518.
34. Olson JC. Juvenile idiopathic arthritis: an update. *WMJ.* 2003;102:45–50.
35. Johnson K, Gardner-Medwin J. Childhood arthritis: classification and radiology. *Clin Radiol.* 2002;57:47–58.
36. Murphy FP, Dahlin DC, Sullivan CR. Articular synovial chondromatosis. *J Bone Joint Surg Am.* 1962;44:77–86.
37. Peh WC, Shek TW, Davies AM, Wong JW, Chien EP. Osteochondroma and secondary synovial osteochondromatosis. *Skeletal Radiol.* 1999;28:169–174.
38. Milgram JW, Dunn EJ. Periarticular chondromas and osteochondromas: a report of three cases. *Clin Orthop.* 1989;148:147–151.
39. DeBenedetti MJ, Schwinn CP. Tenosynovial chondromatosis in the hand. *J Bone Joint Surg Am.* 1979;61:898–903.
40. Lynn MD, Lee J. Periarticular tenosynovial chondrometaplasia: report of a case at the wrist. *J Bone Joint Surg Am.* 1972;54:450–452.
41. Manco LG, DeLuca DM. CT diagnosis of synovial chondromatosis of the TMJ. *AJR Am J Roentgenol.* 1987;148:574–576.
42. Kenan S, Abdelwahab IF, Klein MJ, Lewis MM. Case report 817: synovial chondrosarcoma secondary to synovial chondromatosis. *Skeletal Radiol.* 1993;22:623–626.
43. Bencardino JT, Hassankhani A. Calcium pyrophosphate dihydrate crystal deposition disease. *Semin Musculoskelet Radiol.* 2003;7:175–185.
44. Adams EM, Chow CK, Premkumar A, Plotz PH. The idiopathic inflammatory myopathies: spectrum of MR imaging findings. *Radiographics.* 1995;15:563–574.
45. Fraser DD, Frank JA, Dalakas M, et al. MRI in the inflammatory myopathies. *J Rheumatol.* 1991;18:1693–1700.
46. Hernandez RJ, Keim DR, Sullivan DB, et al. MRI appearance of the muscles in childhood dermatomyositis. *J Pediatr.* 1990;117:546–550.
47. Christopher-Stine L, Plotz PH. Adult inflammatory myopathies. *Best Pract Res Clin Rheumatol.* 2004;18:331–344.
48. Centers for Disease Control and Prevention (CDC). Progress toward poliomyelitis eradication—Afghanistan and Pakistan, January 2003–May 2004. *MMWR Morb Mortal Wkly Rep.* 2004;53:634–637.
49. Grant AD, Atar D, Lehman WB. Postpoliomyelitis syndrome problems of knee function: a review. *Bull Hosp Joint Dis.* 1993;53:27–29.
50. Altman RD. Articular complications of Paget's disease of bone. *Semin Arthritis Rheum.* 1994;23:248–249.
51. Helliwell PS. Osteoarthritis and Paget's disease. *Br J Rheumatol.* 1995;34:1061–1063.

52. Zeiss J, Paley K, Murray K, Saddemi SR. Comparison of bone contusion seen by MRI in partial and complete tears of the anterior cruciate ligament. *J Comput Assist Tomogr*. 1995;19:773-776.
53. Goldman AB, Pavlov H, Rubenstein D. The Second fracture of the proximal tibia: a small avulsion that reflects major ligamentous damage. *AJR Am J Roentgenol*. 1988;151:1163-1167.
54. Jaramillo D, Hoffer FA, Shapiro F, Rand F. MRI of fractures of the growth plate. *AJR Am J Roentgenol*. 1990;155:1261-1265.
55. Recht MP, Applegate G, Kaplan P, et al. The MR appearance of cruciate ganglion cysts: a report of 16 cases. *Skeletal Radiol*. 1994;23:597-600.
56. Stoller DW, Cannon WD Jr, Anderson LJ. The knee. In: Stoller DW, ed. *Magnetic Resonance Imaging in Orthopaedics and Sports Medicine*. Philadelphia, PA: Lippincott-Raven Publishers; 1993:177-178.
57. Campbell SE, Sanders TG, Morrison WB. MR imaging of meniscal cysts: incidence, location, and clinical significance. *AJR Am J Roentgenol*. 2001;177:409-413.
58. Tschirch FT, Schmid MR, Pfirrmann CW, Romero J, Hodler J, Zanetti M. Prevalence and size of meniscal cysts, ganglionic cysts, synovial cysts of the popliteal space, fluid-filled bursae, and other fluid collections in asymptomatic knees on MR imaging. *AJR Am J Roentgenol*. 2003;180:1431-1436.
59. Dorsay TA, Helms CA. Bucket-handle meniscal tears of the knee: sensitivity and specificity of MRI signs. *Skeletal Radiol*. 2003;32:266-272.
60. Magee T, Shapiro M, Williams D. Prevalence of meniscal radial tears of the knee revealed by MRI after surgery. *AJR Am J Roentgenol*. 2004;182:931-936.
61. Yao L, Dungan D, Seegar LL. MRI of tibial collateral ligament injury: comparison with clinical examination. *Skeletal Radiol*. 1994;23:521-524.
62. Staron RB, Haramati N, Feldman F, et al. O'Donoghue's triad: MRI evidence. *Skeletal Radiol*. 1994;23:633-636.
63. O'Donoghue DH. Surgical treatment of fresh injuries to the major ligaments of the knee. *J Bone Joint Surg Am*. 1950;32:721-731.
64. Kaplan PA, Dussault RG. MRI of the knee: menisci, ligaments, tendons. *Topics Magn Reson Imaging*. 1993;5:228-248.
65. Sonin AH, Fitzgerald SW, Friedman H, et al. PCL injury: MRI diagnosis and patterns of injury. *Radiology*. 1994;190:455-458.
66. Sanders TG, Medynski MA, Feller JF, Lawhorn KW. Bone contusion patterns of the knee at MR imaging: footprint of the mechanism of injury. *Radiographics* 2000;20 Spec No:S135-S151.
67. Arendt EA, Fithian DC, Cohen E. Current concepts of lateral patella dislocation. *Clin Sports Med*. 2002;21:499-519.
68. De Flaviis L, Nessi R, Scaglione P, et al. Ultrasonic diagnosis of Osgood-Schlatter and Sinding-Larsen-Johansson diseases of the knee. *Skeletal Radiol*. 1989;18:193-197.
69. Medlar RC, Lyne ED. Sinding-Larsen-Johansson disease. Its etiology and natural history. *J Bone Joint Surg Am*. 1978;60:1113-1116.
70. Aichroth P. Osteochondritis dissecans of the knee: a clinical study. *J Bone Joint Surg Br*. 1971;53:440-447.
71. Mesgarzadeh M, Schneek CD, Bonakdarpour A. MRI of the knee and correlation with normal anatomy. *Radiographics*. 1988;8:707-733.
72. Linden B. Osteochondritis dissecans of the femoral condyles. A long-term follow up study. *J Bone Joint Surg Am*. 1977;59:769-776.
73. Brady TA, Russell D. Interarticular horizontal dislocation of the patella. *J Bone Joint Surg Am*. 1965;47:1393-1396.
74. Corso SJ, Thal R, Forman D. Locked patellar dislocation with vertical axis rotation. A case report. *Clin Orthop*. 1992;279:190-193.
75. Rao R, Bains RS, Lum G. Acute traumatic vertical axis rotational dislocation of the patella. *Orthopedics*. 1997;20:713-715.
76. Corfield AR, Stevenson J. Vertical patellar dislocation: a case report. *Eur J Emerg Med*. 2004;11:170-171.
77. Hanspal RS. Superior dislocation of the patella. *Injury*. 1985;16:487-488.
78. Resnik D. Tumors and tumor-like lesions in or about joints. In: Resnick D, ed. *Diagnosis of Bone and Joint Disorders*. 4th ed. Philadelphia, PA: WB Saunders; 2002:4160-4161.
79. Martin S, Hernandez L, Romero J, et al. Diagnostic imaging of lipoma arborescens. *Skeletal Radiol*. 1998;27:325-329.
80. Soler T, Rodriguez E, Bargiela A, Da Riba M. Lipoma arborescens of the knee: MR characteristics in 13 joints. *J Comput Assist Tomogr*. 1998;22:605-609.
81. Kloen P, Keel SB, Chandler HP, Geiger RH, Zarins B, Rosenberg AE. Lipoma arborescens of the knee. *J Bone Joint Surg Br*. 1998;80:298-301.
82. Vilanova JC, Barcelo J, Villalon M, Aldoma J, Delgado E, Zapater I. MR imaging of lipoma arborescens and the associated lesions. *Skeletal Radiol*. 2003;32:504-509.
83. Rennie WJ, Saifuddin A. Pes anserine bursitis: incidence in symptomatic knees and clinical presentation. *Skeletal Radiol*. 2005;34:395-398.
84. McCarthy CL, McNally EG. The MRI appearance of cystic lesions around the knee. *Skeletal Radiol*. 2004;33:187-209.
85. Kleinman PK. *Diagnostic Imaging of Child Abuse*. Baltimore, MD: Williams & Wilkins; 1987:5-28.
86. Yamamoto T, Bullough PG. Spontaneous osteonecrosis of the knee: the result of subchondral insufficiency fracture. *J Bone Joint Surg Am*. 2000;82:858-866.
87. Gil HC, Levine SM, Zoga AC. MRI findings in the subchondral bone marrow: a discussion of conditions including transient osteoporosis, transient bone marrow edema syndrome, SONK, and shifting bone marrow edema of the knee. *Semin Musculoskelet Radiol*. 2006;10:177-186.
88. Soucacos PN, Johnson EO, Soultanis K, Vekris MD, Theodorou SJ, Beris AE. Diagnosis and management of the osteonecrotic triad of the knee. *Orthop Clin North Am*. 2004;35:371-381.
89. Rader CP, Lohr H, Whittmann R, Eulert J. Results of total knee arthroplasty with a metal-backed patellar component: a 6-year follow-up study. *J Arthroplasty*. 1996;11:923-930.
90. Al Saffar N, Revel PA. Interleukin-1 production by activated macrophages surrounding loosened orthopaedic implants: a potential role in osteolysis. *Br J Rheumatol*. 1994;33:309-316.
91. Shinto Y, Uchida A, Yoshikawa H, et al. Inguinal lymphadenopathy due to metal release from a prosthesis: a case report. *J Bone Joint Surg Br*. 1993;75-B:266-269.
92. Weissman BN, Scott RD, Brick GW, Corson JM. Radiographic detection of metal-induced synovitis as a complication of arthroplasty of the knee. *J Bone Joint Surg Am*. 1991;73-A:1002-1007.
93. Jackson DW, Schaefer RK. Cyclops syndrome: loss of extension following intra-articular anterior cruciate ligament reconstruction. *Arthroscopy*. 1990;6:171-178.
94. Bradley DM, Bergman AG, Dillingham MF. MR imaging of cyclops lesions. *AJR Am J Roentgenol*. 2000;174:719-726.
95. Recht MP, Piraino DW, Cohen MA, Parker RD, Bergfeld JA. Localized anterior arthrofibrosis (cyclops lesion) after reconstruction of the anterior cruciate ligament: MR imaging findings. *AJR Am J Roentgenol*. 1995;165:383-385.
96. Atila S, Akpek ET, Yucel C, Tali EK, Isik S. MR imaging and MR angiography in popliteal artery entrapment syndrome. *Eur Radiol*. 1998;8:1025-1029.
97. Hoelting T, Schuermann G, Allenberg JR. Entrapment of the popliteal artery and its surgical management in a 20-year period. *Br J Surg*. 1997;84:338-341.
98. Murray A, Halliday M, Croft RJ. Popliteal artery entrapment syndrome. *Br J Surg*. 1991;78:1414-1419.

CHAPTER

7

# Lower Leg

**CLINICAL HISTORY** *Progressive bowing of lower extremities. A-B, radiographs at age 3; C, radiograph at age 7.*



FIGURE 7.1A



FIGURE 7.1B



FIGURE 7.1C

### FINDINGS

- A, B. Anteroposterior (AP) and lateral radiographs of the left knee at age 3 years demonstrate a varus deformity of the tibia with a prominent medial metaphyseal beak.
- C. AP radiograph of the knee at age 7 years shows progression of the varus deformity, slanting of the medial tibial plateau, with persistent metaphyseal beak.

**DIFFERENTIAL DIAGNOSIS** Blount disease, posttraumatic deformity, rickets, physiologic bowing.

**DIAGNOSIS** Blount disease (tibia vara).

**DISCUSSION** The diagnosis in this case is made by recognizing the abnormally small, beaked appearance of the medial portion of the tibial metaphysis, with genu varus. These findings, in conjunction with a normal appearance

of the lateral portion of the tibial metaphysis and normal femoral metaphysis, lead to the correct diagnosis.

Blount disease of the tibia is an entity subsumed within the larger group of disorders known as osteochondroses, recognized individually by the specific site of involvement within the skeleton. Other examples of osteochondroses include such entities as Legg-Calvé-Perthes disease of the capital femoral epiphysis and Kienböck disease of the lunate. Blount disease specifically affects the medial portion of the proximal tibial metaphysis. The etiology of the abnormal development of the medial portion of the metaphysis is unknown. Abnormal development of the medial metaphysis results in the characteristic metaphyseal beak and genu varus deformity. Magnetic resonance imaging (MRI) is helpful to evaluate the growth plate in patients who are already affected and in patients who are at risk, such as toddlers with delayed resolution of physiologic tibial bowing [1,2].

**CLINICAL HISTORY** (A) A 3-year-old boy with progressive tibial bowing deformity. (B) Companion case.



FIGURE 7.2A



FIGURE 7.2B

### FINDINGS

- A. AP radiograph of the lower leg. There is anterolateral bowing of the tibia, with increased sclerosis of the medullary cavity. A nonunion of the fibula is noted distal to the angular deformity.
- B. AP radiograph of the lower leg shows anterolateral bowing of the shafts of the tibia and fibula.

**DIFFERENTIAL DIAGNOSIS** Neurofibromatosis (NF), osteogenesis imperfecta, fibrous dysplasia, posttraumatic deformity.

**DIAGNOSIS** Neurofibromatosis (Type 1).

**DISCUSSION** NF is an autosomal dominant disorder affecting neural crest cells. Cases may be classified according

to the genetic defect as Type 1 (NF-1), Type 2 (NF-2), or schwannomatosis. Among other manifestations, NF-1 is associated with cutaneous and peripheral neurofibromas, skeletal deformities, and café au lait spots. Scoliosis and kyphosis are the most common skeletal abnormalities. Tibial bowing may occur in approximately 3% of NF-1 cases. The bowing is anterolateral, usually involves both tibia and fibula, and is associated with medullary sclerosis. These abnormal bones are prone to fractures and development of a pseudoarthrosis; orthopedic intervention may become frustrating as fractures and osteotomies fail to heal [3]. NF-1 is the most common form of NF; patients with NF-2 develop bilateral acoustic neuromas and do not have musculoskeletal manifestations.



FIGURE 7.3A



FIGURE 7.3B

**FINDINGS**

- A. AP radiograph of the legs. The bones are osteoporotic. There are multiple healed femoral shaft fractures and severe posterior bowing deformities of the lower legs. The epiphyses at the knees are enlarged and have a popcorn appearance.
- B. Frog lateral radiograph of both lower extremities shows osteoporosis, bowing deformities of the femurs, tibias, and fibulas, and multiple healed fractures.

**DIFFERENTIAL DIAGNOSIS** Osteogenesis imperfecta, fibrous dysplasia.

**DIAGNOSIS** Osteogenesis imperfecta.

**DISCUSSION** Osteogenesis imperfecta is a group of inborn connective tissue disorders characterized by radiographically decreased bone density. The underlying problem is one of abnormal collagen synthesis, in which a variety of different

molecular defects in collagen produce a continuous spectrum of phenotypes. In the skeleton, the bone matrix is deficient, resulting in thin, osteoporotic, and fragile bones that are subject to repeated insufficiency fractures and consequent deformity. The condition is heritable, but cases are often sporadic. In general, there are autosomal recessive severe forms that present at birth and autosomal dominant forms that present later and have a mild course. The condition ranges from severe, congenital involvement with multiple fractures in utero and perinatal death to mild, late manifestations in adulthood. The severe forms account for 10% of cases, and the less severe forms account for 90% of cases. The incidence of osteogenesis imperfecta is 1 per 20,000 to 60,000 live births. Associated clinical features, with variable expression, include blue sclerae (90%); thin, translucent skin; hypermobile, lax peripheral joints; abnormal teeth (dentinogenesis imperfecta); and deafness (fragile otic bones). Bisphosphonate treatment has been helpful for patients with moderate to severe disease [4].



FIGURE 7.4A



FIGURE 7.4B

**FINDINGS**

- A. AP radiograph of the lower extremities shows diffusely sclerotic bones without development of the medullary space. The metaphyses are undertubulated and club shaped.
- B. Radiograph of an upper extremity of the same patient shows similar findings.

**DIFFERENTIAL DIAGNOSIS** Osteopetrosis, pyknodysostosis.

**DIAGNOSIS** Osteopetrosis, precocious form.

**DISCUSSION** All of the bones in this very young child show a generalized chalk-white density. The medullary cavity seems obliterated by the uniform density. The bone has a shape similar to a juggling club, with a narrow middle

portion and a wider distal portion of uniform diameter. This shape is the result of longitudinal growth at the physis without bone resorption and remodeling in the cutback zone of the metaphysis, leaving the new bone the same diameter as the physis.

Osteopetrosis is a disorder due to abnormal function of the osteoclasts. There are autosomal recessive and dominant types. The autosomal dominant, or delayed form, is the most common. The precocious form (shown in this case) is inherited as an autosomal recessive trait and is usually lethal due to obliteration of the marrow. The osteoclasts fail to normally remodel bone. The unopposed osteoblastic activity leads to the generalized increase in bone density. The autosomal dominant form, of which there are two distinct genetic entities, was formerly known as marble bone disease or Albers-Schonberg disease [9].

**CLINICAL HISTORY** An 18-year-old man with short stature. A, Postoperative radiograph; B, 5-month radiograph; C, 7-month radiograph.



FIGURE 7.5A

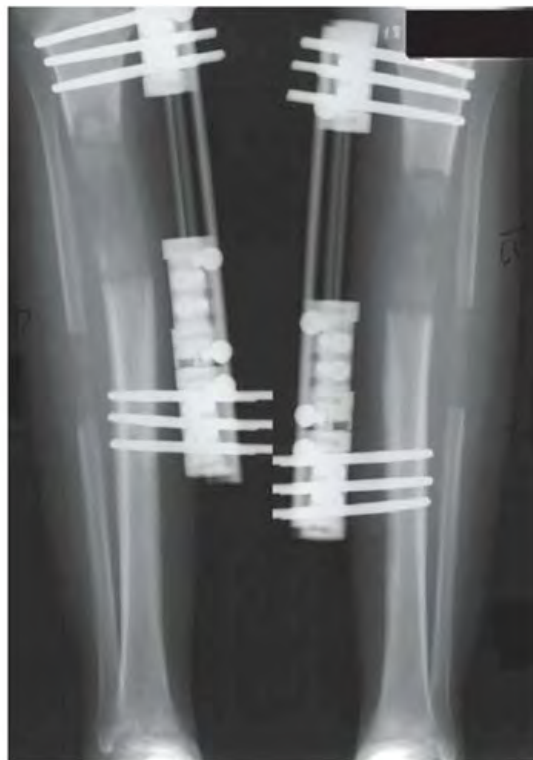


FIGURE 7.5B



FIGURE 7.5C

**FINDINGS**

AP radiographs of the lower legs.

- A. Pin-rod external fixators are present bilaterally, and osteotomies have just been performed through the proximal tibial and fibular shafts.
- B. After 5 months of treatment, there has been a 6-cm gain in length.
- C. After 7 months of treatment, the distracted fragments are bridged by remodeling bone.

**DIFFERENTIAL DIAGNOSIS** Limb lengthening for short stature (from any cause).

**DIAGNOSIS** Congenital adrenocortical hyperplasia with limb lengthening.

**DISCUSSION** Congenital adrenal hyperplasia is an autosomal recessive defect, involving the enzyme 21-hydroxylase, that results in failure to synthesize cortisol. There is a secondary overproduction of androgenic hormones that cause precocious

puberty. The effect on the growing skeleton is rapid growth but premature closure of the epiphyses, so that a tall child becomes a short adult. The incidence of congenital adrenal hyperplasia is approximately 1 in 16,000, with a salt-wasting form from adrenal insufficiency and a simply virilizing form from excess androgens [5]. Conventional treatment is steroid replacement with exogenous corticosteroids. Surgical limb lengthening using the callus distraction (callotaxis) has been applied to patients with developmentally short stature, such as those with achondroplasia [6–8]. In this technique, the cortex of the bone is partially cut, leaving the medullary contents intact. After 2 weeks, as soft callus forms, the two bone segments are slowly distracted by means of an external fixator, stretching out the callus as the gap between the fragments is increased 1 mm or so per day to lengthen the bone. Several centimeters of length can be gained, and the complication rate is relatively low. Once the desired length has been attained, healing and remodeling ultimately results in cortical bone formation. In this case, pin-rod external fixators have been used, and both tibias have been lengthened symmetrically.



FIGURE 7.6

**FINDINGS** AP radiograph of both lower extremities demonstrates a mild tibia vara without beaking of the proximal medial metaphyses or widening of the physes.

**DIFFERENTIAL DIAGNOSIS** Physiologic bowing, Blount disease, rickets.

**DIAGNOSIS** Physiologic bowing.

**DISCUSSION** The diagnosis in this case is made by recognizing that this is a young child with slight bowing of

femurs and tibias centered at the knee, without any intrinsic abnormality. In particular, there is no medial tibial metaphyseal fragmentation. Mild enlargement of the medial tibial metaphyses can be present [10].

Physiologic bowing is thought to be related to the fetal position within the close confines of the uterus. It is self-limited. Parents usually bring these children in for evaluation between 1 and 2 years of age because of their bowed legs. Once the toddler begins to stand and walk, normal weight-bearing stresses correct the slight bowing.

**CLINICAL HISTORY** A 4-year-old girl with short stature.



FIGURE 7.7A



FIGURE 7.7B



FIGURE 7.7C

### FINDINGS

- Standing AP radiograph of the lower limbs. The long bones are short and thick with flared metaphyses.
- Posteroanterior radiograph of the forearm and hand shows short but thick bones in the hand and forearm. The fingers have a stubby appearance.
- AP radiograph of the upper arm shows a disproportionately short humerus. Note that with all the bones, there is a normal cortical and trabecular structure, and the bones have normal density.

**DIFFERENTIAL DIAGNOSIS** None.

**DIAGNOSIS** Achondroplasia.

**DISCUSSION** Achondroplasia is a genetic disorder of abnormal enchondral ossification [11]. The long bones are abnormally short with metaphyseal flaring. Bone shortening is most prominent in the proximal aspect of the extremity (rhizomelic micromelia). The hand bones are short and broad, producing what is sometimes called a trident appearance. The acetabula are flat and the iliac bones are squared. Additional findings in achondroplasia (not shown) include a large cranium compared with the face, a small foramen magnum, a narrowed interpediculate distance in the lower lumbar spine, and concavity of the posterior vertebral bodies. The limb shortness in achondroplasia is being treated with increasing frequency by surgical limb lengthening (callotaxis).

**CLINICAL HISTORY**

*A 42-year-old man with 1-month history of right anterior leg pain.*



FIGURE 7.8A



FIGURE 7.8B

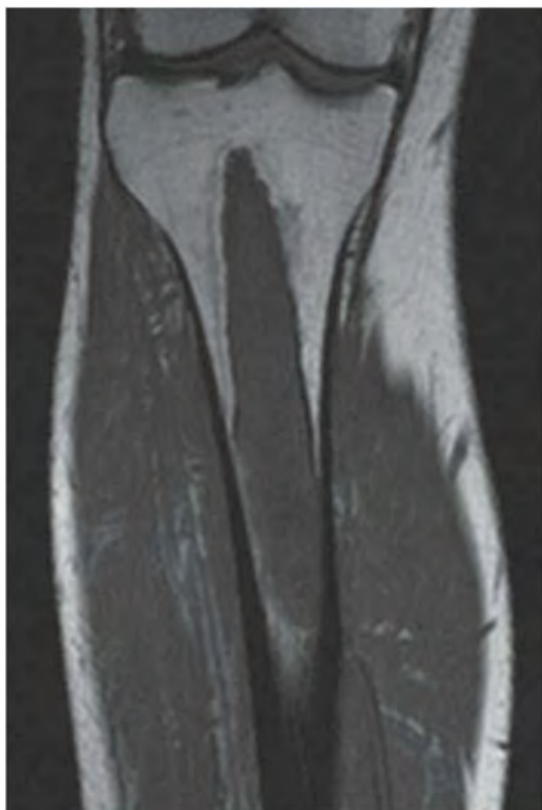


FIGURE 7.8C

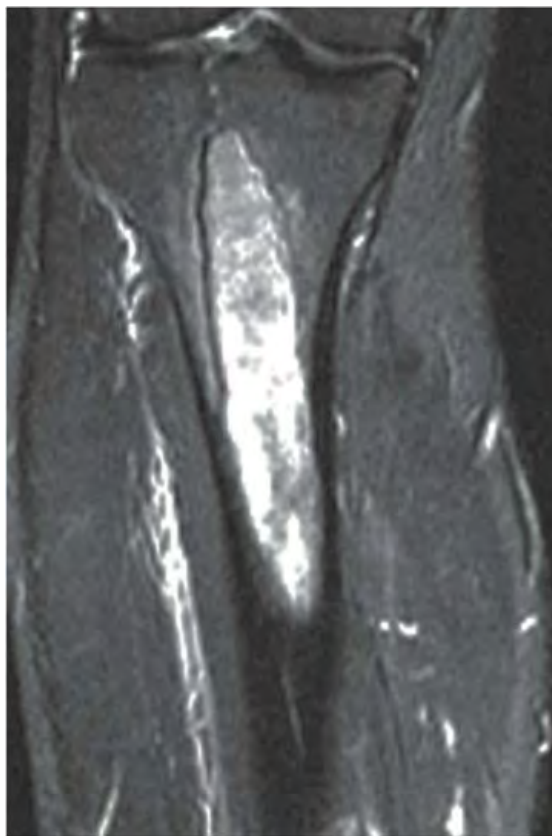


FIGURE 7.8D



FIGURE 7.8E

**FINDINGS** An AP radiograph (A), and coronal reconstructed computed tomography (CT) (B) of the proximal tibial diaphysis shows a focal lesion with ground-glass mineralization. The lesion has a faint sclerotic margin and is oriented along the long axis of the bone. (C) Coronal T1-weighted MRI shows an intramedullary lesion with low signal intensity. (D) Coronal T2-weighted, fat-suppressed MRI shows a heterogeneous intermediate and high-signal-intensity lesion with a low-signal-intensity margin. Increased radiotracer uptake is seen in the lesion on bone scan (E).

**DIFFERENTIAL DIAGNOSIS** None.

**DIAGNOSIS** Fibrous dysplasia.

**DISCUSSION** Fibrous dysplasia is a benign fibro-osseous lesion that is neither familial nor hereditary. Fibrous dysplasia appears to be a developmental abnormality involving the proliferation and maturation of fibroblasts, in which benign fibrous tissue, with abnormally arranged, dysplastic

trabeculae of immature woven bone, replaces normal bone. The dysplastic trabeculae are no thicker than 0.1 mm, so they are not individually visible on clinical radiographs. If present in sufficient preponderance, however, they give the lesions a ground-glass density; if not, the lesions are radiolucent.

The lesions are medullary, but may replace both cancellous and cortical bone. The abnormal area may be sharply circumscribed and margined by a thick layer of reactive bone, or it may blend gradually with the adjacent normal bone. The cortex may be either thickened or thinned, but frequently the outer size and shape of the affected bone is unchanged.

Bowing deformities result from biomechanically insufficient bone and from malunion of pathologic fractures. Lesions in the long bones are often discovered because of fracture or deformity. Therapy is restricted to orthopedic management of complications. The monostotic form is not associated with other abnormalities or disease. In this case, the patient underwent lesion curettage and bone grafting due to the risk of pathologic fracture.

**CLINICAL HISTORY** A 75-year-old woman with thigh mass.



FIGURE 7.9A

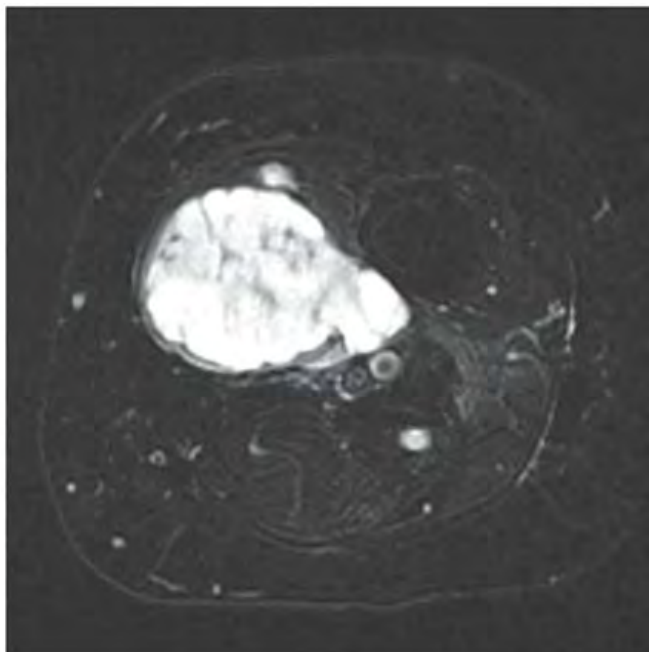


FIGURE 7.9B

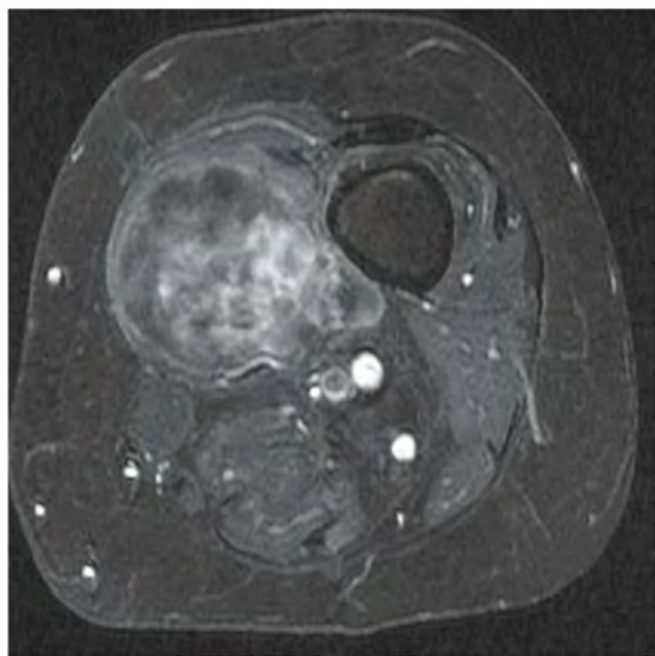


FIGURE 7.9C

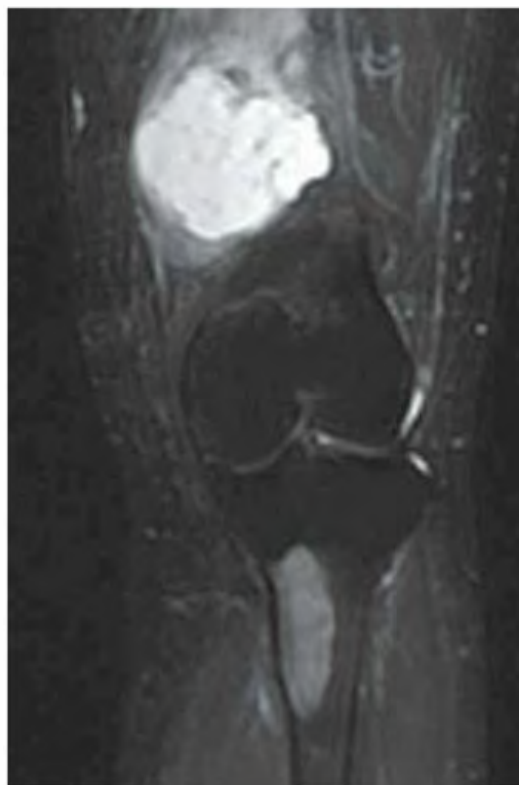


FIGURE 7.9D



FIGURE 7.9E



FIGURE 7.9F



FIGURE 7.9G

**FINDINGS** (A–C) Axial T1-weighted, T2-weighted, fat-suppressed, and postgadolinium T1-weighted, fat-suppressed MRI shows a lobulated mass in the distal vastus medialis. The mass shows high signal intensity on T2-weighted image and some internal contrast enhancement. Coronal inversion recovery MRI (D) shows the distal thigh mass and a well-defined intramedullary bony lesion in the proximal tibia that shows high signal intensity. Radiographs of the proximal tibia (E, F) demonstrate an ovoid lesion with ground-glass opacity and a thin sclerotic rim. (G) Bone scan (detailed view) shows increased uptake in the proximal tibia.

**DIFFERENTIAL DIAGNOSIS** Fibrous dysplasia with intramuscular myxoma, metastatic lesions involving bone and soft tissue.

**DIAGNOSIS** Mazabraud syndrome.

**DISCUSSION** Monostotic or polyostotic fibrous dysplasia associated with a single or multiple intramuscular myxomas is referred to as Mazabraud syndrome. Mazabraud syndrome is rare and does not appear to be hereditary. There is a high incidence of myxoma in close proximity to a focus of fibrous dysplasia. Of all the reported cases of Mazabraud syndrome, approximately 70% occurred in women, and 81% were polyostotic fibrous dysplasia [12]. The MR signal intensity of lesions in fibrous dysplasia is quite variable. On T2-weighted images, lesions are homogeneous to mildly heterogeneous, with about 60% of cases showing a signal intensity greater than that of fat. The remaining lesions will show either intermediate or low signal intensity on T2-weighted images. All lesions demonstrate decreased signal intensity on T1-weighted images. The diagnosis of fibrous dysplasia is readily confirmed on the corresponding radiograph [13]. Intramuscular myxoma shows low signal intensity relative to adjacent skeletal muscle on T1-weighted images and high signal intensity on T2-weighted images. After administration of contrast material, heterogeneous enhancement is apparent with irregular rim enhancement. The degree of enhancement depends on the presence of solid myxoid and bridging fibrous septa at histologic examination. These features are unique and help differentiate myxoma from sarcoma [14].

**CLINICAL HISTORY** A 24-year-old woman with a painless soft tissue mass in the calf.

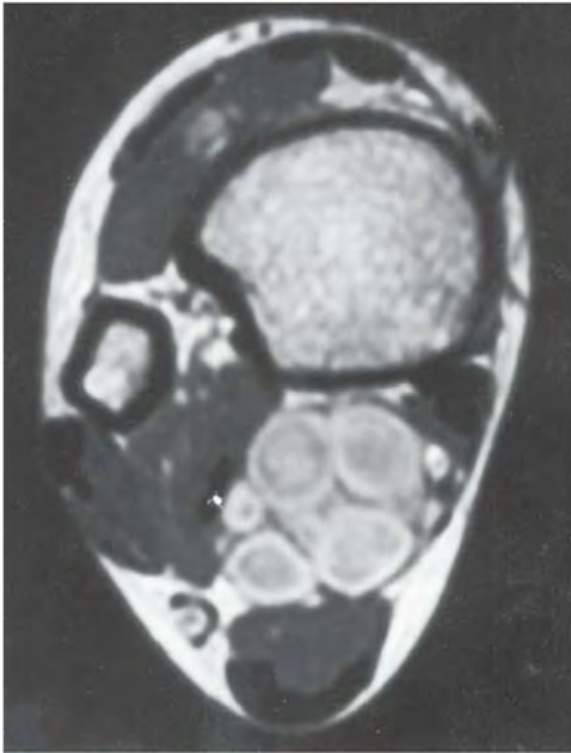


FIGURE 7.10A

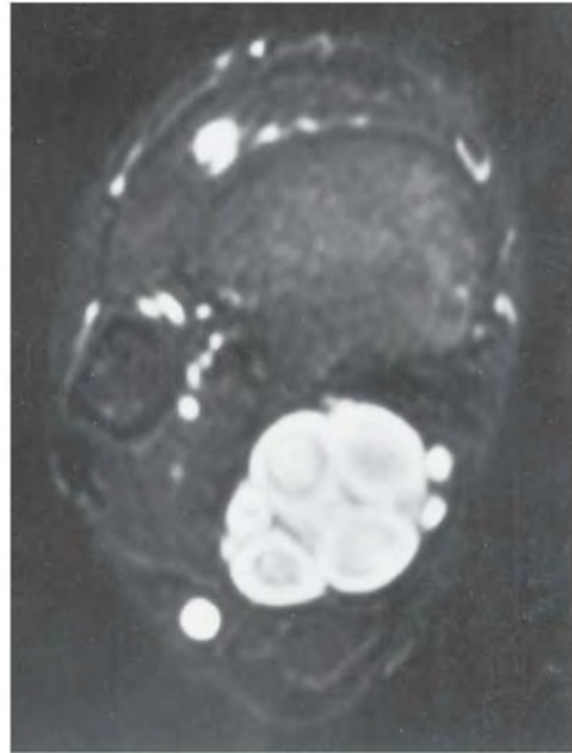


FIGURE 7.10B

**FINDINGS** Axial T1-weighted (A) and T2-weighted (B) MRI shows a cluster of well-defined structures, demonstrating central relative hypointensity on T1 and T2 with rings of hyperintensity. Serial images establish the cylindrical nature of these structures.

**DIFFERENTIAL DIAGNOSIS** Neurofibroma or schwannoma.

**DIAGNOSIS** Neurofibroma.

**DISCUSSION** The ring-like morphology and central foci of hypointensity seen in this case are typical of peripheral nerve sheath tumors. In conjunction with the cylindrical nature of the lesion on long axis images, the diagnosis is likely to

be neurofibroma. Most neurofibromas (90%) are solitary, slow-growing lesions found in young adults. The lesions may be superficial or deep and are usually painless. Because they are intimately associated with the underlying nerve, the patient may have dysesthesias. Because the lesion cannot be separated from the nerve, the nerve must be sacrificed at the time of surgical removal. MRI findings are often characteristic. The target appearance with a hyperintense rim and inner area of low signal intensity on T2 is typical of benign peripheral nerve tumors. It may be seen with either neurofibroma or schwannoma. Small foci of brighter signal intensity within the target area are said to represent thickened nerve bundles. This speckled appearance within a target lesion is characteristic of a peripheral nerve sheath tumor.



FIGURE 7.11A



FIGURE 7.11B

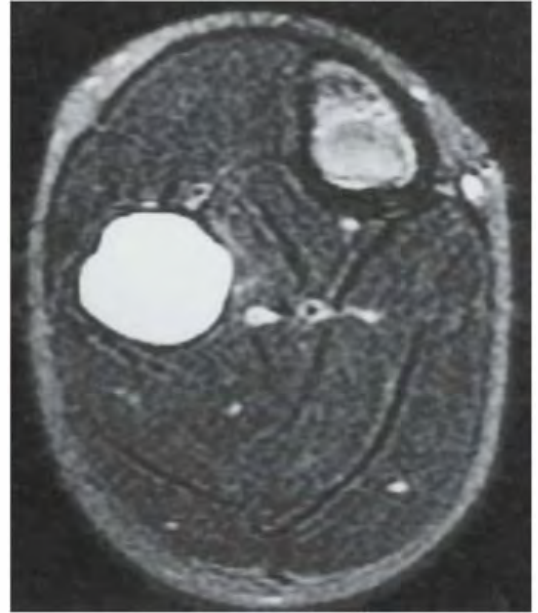


FIGURE 7.11C

**FINDINGS**

- A, B. Coronal T1-weighted MRI without and with gadolinium demonstrates T1 hypointensity and rim enhancement in a geographic, mildly expansile process of the proximal fibula diaphysis.
- C. The T2 hyperintensity is homogeneous on the axial image. The lesion is central in transverse location.

**DIFFERENTIAL DIAGNOSIS** Simple bone cyst, aneurysmal bone cyst, fibrous dysplasia.

**DIAGNOSIS** Simple bone cyst.

**DISCUSSION** The diagnosis is made in conjunction with a plain radiograph (not shown). The expansile lesion in the metaphysis or diaphysis is homogenous, with fluid signal characteristics and no aggressive features. There is no solid component and no septations within the lesion. The lesion has no mineralization within.

**CLINICAL HISTORY** A 37-year-old woman with swelling, and a companion case.



FIGURE 7.12A



FIGURE 7.12B

### FINDINGS

- A. AP radiograph of the lower leg. There is an exostotic bony lesion arising from the medial tibial metaphysis. The cortex and marrow space of the lesion is contiguous with that of the underlying bone. Broadening of the proximal fibula represents another en plaque lesion.
- B. Companion case. Lateral radiograph of the knee shows a pedunculated lesion arising from the posterior aspect of the proximal tibial cortex. The cortex and medullary space of the stalk are contiguous with the cortex and medullary space of the tibia.

**DIFFERENTIAL DIAGNOSIS** None.

### DIAGNOSIS

Osteochondroma.

**DISCUSSION** The diagnosis in this case is made by recognizing that the lesion is composed of mature bone, with cortex and medullary space that is contiguous with the underlying bone. This osteochondroma has a coat-hook morphology, whereas the companion case has a more pedunculated cauliflower morphology. Osteochondromas (also called benign exostoses) are outgrowths of histologically normal bone that arise in the vicinity of a growth plate.

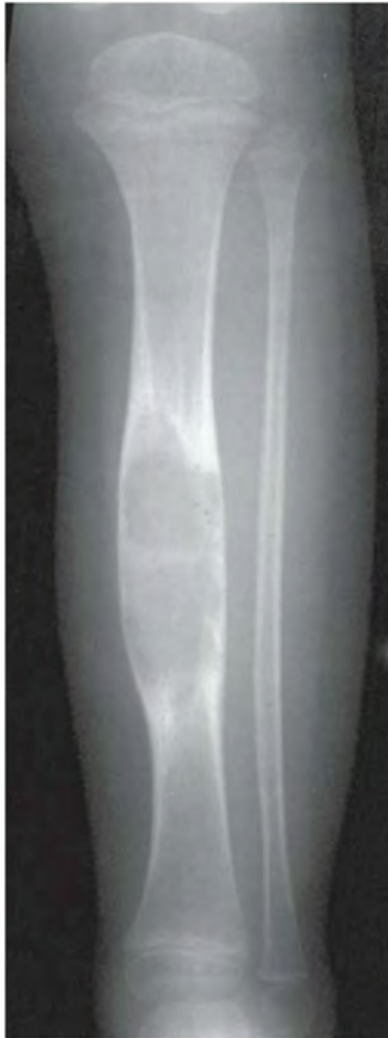


FIGURE 7.13A



FIGURE 7.13B

**FINDINGS** AP (A) and lateral (B) radiographs of the lower leg. There is an expansile lesion involving a long segment of the tibial diaphysis. The lesion has a hazy appearance and well-formed surrounding sclerosis. The lesion is somewhat asymmetric. There is no cortical penetration, periosteal reaction, or soft tissue mass.

**DIFFERENTIAL DIAGNOSIS** Fibrous dysplasia, osteoblastoma, adamantinoma, osteofibrous dysplasia.

**DIAGNOSIS** Osteoblastoma.

**DISCUSSION** A specific diagnosis is not possible in this case, but an expansile lesion with hazy mineralization in

the tibial midshaft of a child brings up the differential of fibrous dysplasia and osteoblastoma. Other midshaft tibial lesions in children include adamantinoma and osteofibrous dysplasia (ossifying fibroma), both of which should have a more bubbly or multilocular appearance and are typically found in the cortex rather than the medullary space. Although osteoblastomas have a distinct predilection for the spine, of the approximately 30% that involve the long bones, the vast majority of these involve the lower extremities and are centered in the diaphysis. Most osteoblastomas are radiographically lucent, but mottled, stippled, or hazy ground-glass mineralization may be present. Osteoblastoma is unusual in children less than 5 years old, and there is a male predilection.

**CLINICAL HISTORY** A 26-year-old intoxicated woman who fell down the stairs.



FIGURE 7.14A



FIGURE 7.14B

### FINDINGS

- A. Oblique radiograph of the ankle shows lateral dislocation of the talus and foot with disruption of the tibiofibular syndesmosis, and gross separation of the distal fibula from the tibia. A bone fragment representing the posterior malleolus is seen en face between the tibia and the fibula. The relationship of the talus to the lateral malleolus has been maintained. The displacement of the talus indicates that the deltoid ligament must be disrupted.
- B. Oblique radiograph of the proximal leg shows a fracture of the proximal fibular shaft.

**DIFFERENTIAL DIAGNOSIS** None.

**DIAGNOSIS** Maisonneuve fracture.

**DISCUSSION** A Maisonneuve fracture refers to an oblique fracture of the proximal fibular shaft that accompanies an

injury at the ankle. The mechanism appears to be one of severe external rotation in which the talus and distal fibula are separated from the tibia, often accompanied by avulsion of the posterior malleolus by the strong posterior ankle ligaments, tear of the interosseous membrane, and either fracture of the medial malleolus or tear of the deltoid ligament [15]. In this case, the talus has dislocated laterally and become impacted against the lateral aspect of the tibia, but in the typical case, the talus relocates into the mortise on the rebound, reducing the posterior malleolar fragment. The Maisonneuve fracture may also be found in less severe external rotation injuries in which the lateral side of the ankle mortise is disrupted anteriorly but the posterior structures and the interosseous membrane remain intact [16].



FIGURE 7.15A



FIGURE 7.15B

**FINDINGS** AP (A) and lateral (B) radiographs of the knee show a well-defined, multiloculated, lucent lesion with sclerotic borders in the metadiaphysis. It is cortically based and eccentric, with extension into the medullary space. There is minimal expansion of the cortical surface.

**DIFFERENTIAL DIAGNOSIS** None.

**DIAGNOSIS** Nonossifying fibroma (fibrous cortical defect).

**DISCUSSION** Nonossifying fibromas are histologically identical to fibrous cortical defects. Both are nonneoplastic proliferations of fibrous tissue and histiocytes that are self-limited and have no potential for growth or spread. Common radiologic usage of these terms refers to small, shallow, cortical lesions as fibrous cortical defects, and larger, multiloculated lesions as nonossifying fibromas. These lesions regress spontaneously, filling in with bone from the periphery and disappearing. The lesions are present at some time in perhaps one-third of all children. Fibrous cortical defects are

seen mostly in children between 4 to 8 years old. Located on the cortical surface of the metaphysis at the attachment of a tendon or ligament, mostly around the knee, they produce a 1- to 4-cm scalloped defect in the underlying bone. They are round or oval, lucent, and sharply margined by a sclerotic rim. Some have a bubbly appearance. Pathologic fractures may occur, but fibrous cortical defects are usually clinically silent. The distal femur, distal tibia, proximal tibia, and fibula are the reported locations for 90% of these lesions.

The lesion in this case has very indolent characteristics. The best way to estimate the rate of growth of a focal bone lesion is to evaluate the interface between the lesion and the host bone. The presence of a well-defined, thin, sclerotic rim of bone completely surrounding a lesion is indicative of a lesion whose rate of growth is slow enough to allow reactive osteoblastic activity. This rim of bone distributes biomechanical stress around the lesion and is typically better developed in weight-bearing bones. Lesions located in the diaphysis often do not have sclerotic margins, regardless of the growth rate.

**CLINICAL HISTORY** A 49-year-old woman with right tibial pain.



FIGURE 7.16A



FIGURE 7.16B

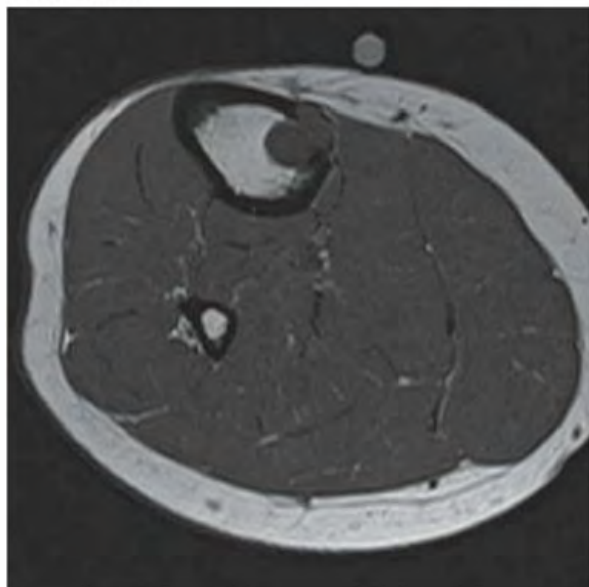


FIGURE 7.16C

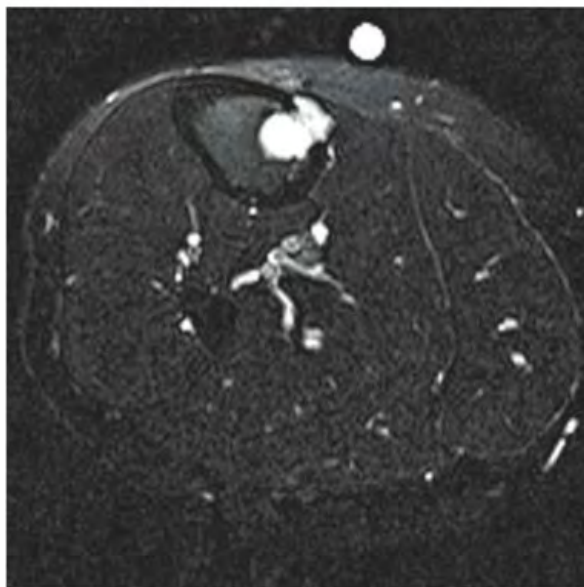


FIGURE 7.16D

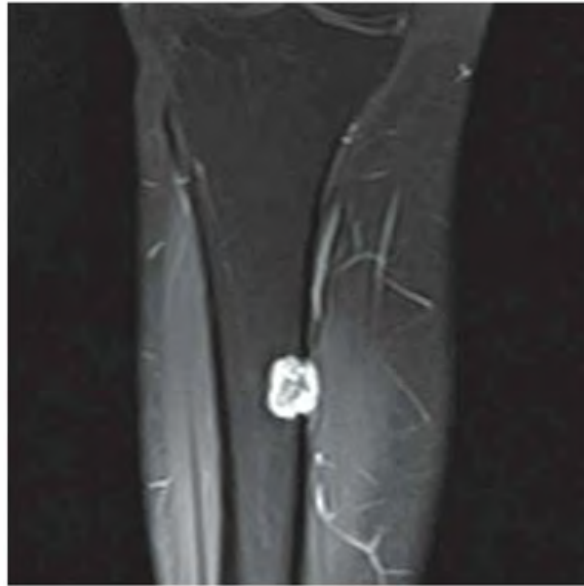


FIGURE 7.16E

## FINDINGS

- A, B. AP (A) and lateral (B) radiographs of the knee demonstrate a geographic, eccentric lesion in the tibial diaphysis. There is a small area of cortical perforation medially.
- C. Axial T1-weighted MRI shows lobulated low-signal-intensity lesion extending through the medial cortex of the tibia into the soft tissue.
- D. Axial T2-weighted, fat-suppressed MRI shows diffuse high signal intensity of the lesion.
- E. Coronal T1-weighted, fat-suppressed MRI after intravenous gadolinium injection shows intense but peripheral contrast enhancement.

**DIFFERENTIAL DIAGNOSIS** Metastasis, chondromyxoid fibroma.

**DIAGNOSIS** Chondromyxoid fibroma.

**DISCUSSION** The diagnosis in this case is not easily made. Chondromyxoid fibroma is the rarest of all the cartilage tumors, and the imaging findings are nonspecific, so one should always expect to be wrong when proposing the

diagnosis. The most common location for chondromyxoid fibroma is the proximal metaphysis of the tibia. The lesions are eccentric and often have a lobulated, well-defined margin. They have a sclerotic rim. Not infrequently, it also appears to erode through the cortex. A hemispherical defect appearing as a “bite” out of the bone has been described by some authors [17]. Cartilaginous matrix mineralization is not usually seen. Periosteal reaction is not a prominent feature. Internal characteristics of chondromyxoid fibroma on advanced imaging reflect the high water content of the lesion seen pathologically, with low attenuation on CT and low signal intensity on T1-weighted and very high signal intensity on T2-weighted MR images. Faint areas of calcification are unusual but are best appreciated by CT [18].

As the name indicates, histologically chondromyxoid fibroma is composed of a mixture of cartilaginous, myxoid, and fibrous elements. The lesion most commonly affects long bones, especially the tibia. In the Mayo Clinic series [19], chondromyxoid fibroma was the least common of the benign cartilage tumors, comprising only 3%, compared with 9% for chondroblastoma, 24% for chondroma (including enchondroma and periosteal chondroma), and 64% for osteochondroma.

**CLINICAL HISTORY** A 44-year-old woman who is an avid runner with left tibial pain with running.



FIGURE 7.17A



FIGURE 7.17B

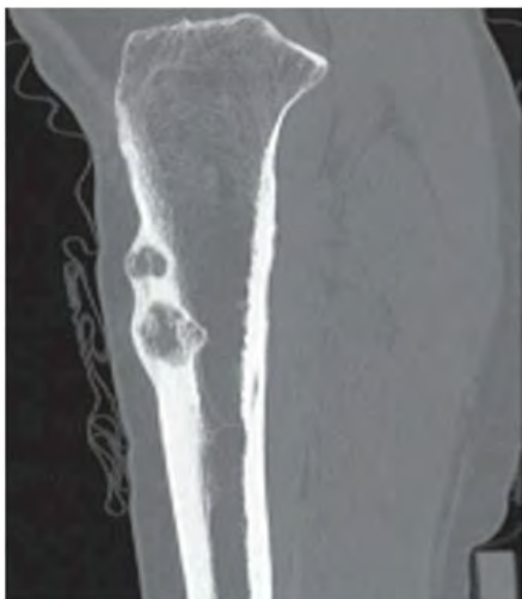


FIGURE 7.17C

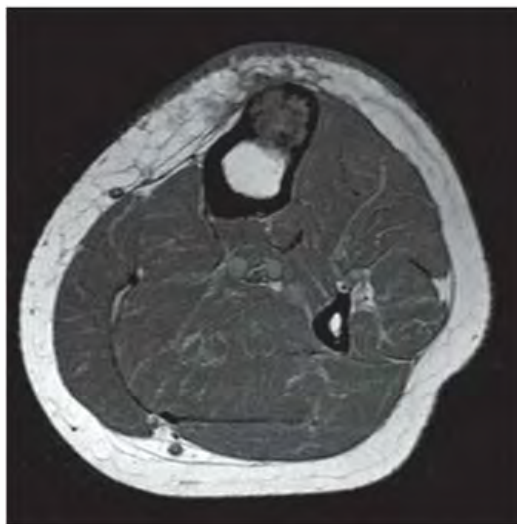


FIGURE 7.17D

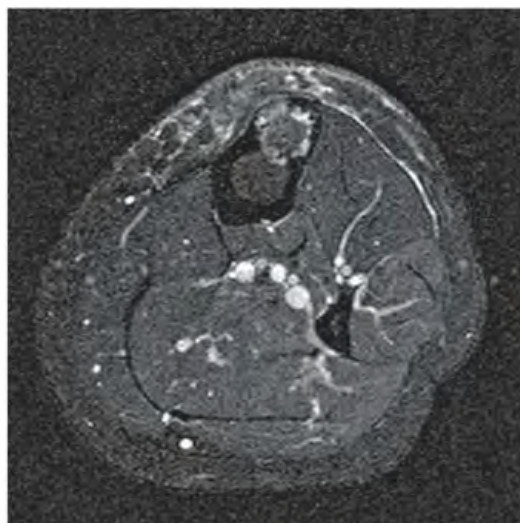


FIGURE 7.17E

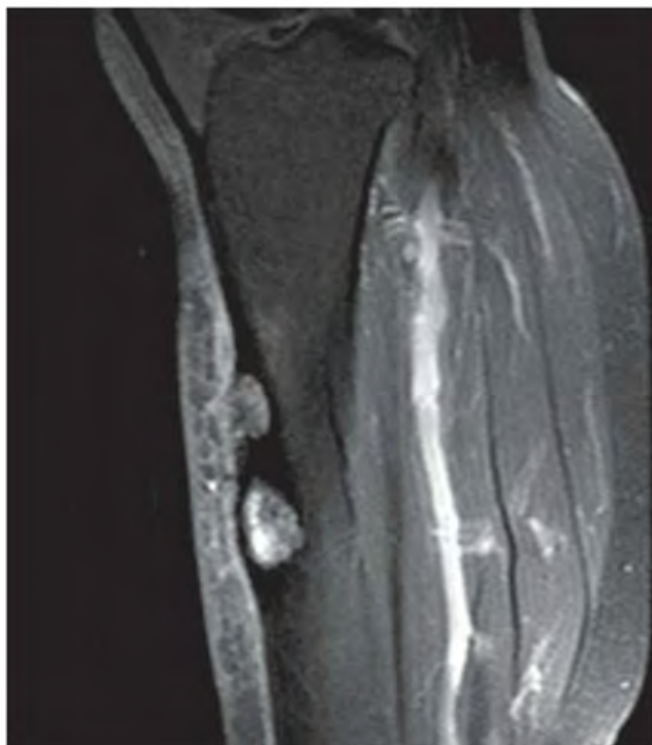


FIGURE 7.17F



FIGURE 7.17G

**FINDINGS** Lateral and AP radiographs (A, B) and sagittal reconstructed CT (C) of left tibia show an anterior cortex lesion with two lucent regions and surrounding sclerosis.

There is some coarse internal trabeculation without internal matrix mineralization on CT. Axial T1-weighted (D), short tau inversion recovery (STIR) (E), and sagittal postcontrast T1-weighted, fat-suppressed (F) MRI demonstrate low signal intensity on T1-weighted image and slightly heterogeneous iso-to-high signal intensity on STIR image. There is intense enhancement. The lesions are largely intracortical, but the inferior lesion does penetrate the medullary cavity, and the anterior cortex is also breached with subcutaneous edema. Intense radiotracer uptake is seen in the lesions on bone scan (G).

**DIFFERENTIAL DIAGNOSIS** Adamantinoma, ossifying fibroma, fibrous dysplasia.

**DIAGNOSIS** Adamantinoma.

**DISCUSSION** The radiologic diagnosis may be suggested by the particular location of the lesion in the anterior cortex of

the tibia at the mid diaphysis. Adamantinomas are malignant tumors thought to be of angioblastic or epithelioid origin. There is a wide age spectrum, but it is most prevalent in the 2nd and 3rd decades and may have a slightly higher incidence in males. A striking feature of this neoplasm is its predilection for involvement of the midshaft of the tibia, which accounts for about 80% to 85% of all cases. Multifocal lesions may rarely develop in a single bone or in two or more bones [20,21]. The clinical course tends to be long, and most patients present with pain or swelling. The most common radiographic appearance is multiple, sharply circumscribed, lucent lesions of different sizes with surrounding sclerosis. Involvement of the bone is typically asymmetric, with the anterior tibial cortex virtually always the epicenter of the lesion. A relationship with ossifying fibroma has been postulated, because some regions of the tumors may have a histologic and radiologic resemblance. Whether ossifying fibroma represents a precursor to adamantinoma or whether it represents a reparative response is unknown; both possibilities have been suggested. The treatment of adamantinoma is surgical, but local recurrence, lymphatic metastases, and hematogenous metastases may occur.

## 7.18

**CLINICAL HISTORY** A 35-year-old man with intermittent swelling of the posterior calf.



FIGURE 7.18A

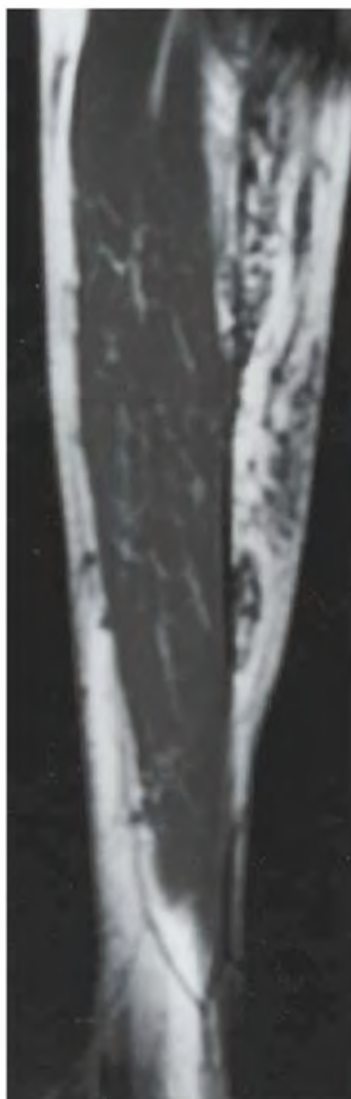


FIGURE 7.18B

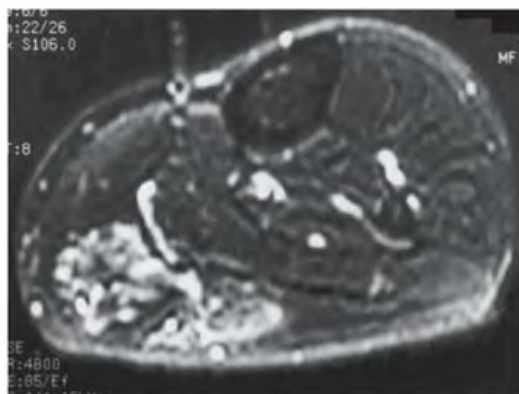


FIGURE 7.18C

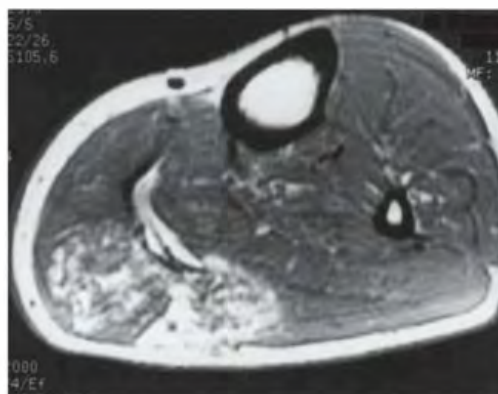


FIGURE 7.18D

**FINDINGS**

- A. Lateral radiograph demonstrates soft tissue swelling with a few phleboliths. The region of abnormality shows mottled densities within fat and loss of the normal sharp demarcation between the subcutaneous fat and the superficial fascia.
- B. Sagittal T1-weighted MRI demonstrates tubular structures with low signal intensity in a base of high signal intensity (fat).
- C. Axial T2-weighted MRI shows tubular structures of high-intensity signal posteriorly.
- D. Axial T1-weighted MRI after intravenous gadolinium injection shows enhancement of the lesion.

**DIFFERENTIAL DIAGNOSIS** Hemangioma, cellulitis.

**DIAGNOSIS** Hemangioma, soft tissue.

**DISCUSSION** Phleboliths within the soft tissue mass in the calf are suggestive of a vascular malformation. The MRI findings confirm the diagnosis. On T1-weighted MRI, hemangiomas characteristically have heterogenous signal intensity with some areas of fat-signal intensity. Low-intensity tubular structures of various sizes are usually evident. T2-weighted MRI shows fluid signal within the tubular structures, corresponding to sluggish blood flow. Hemangiomas may be classified histologically based on the predominant type of vascular channel [22]. The three main types are capillary, cavernous, and arteriovenous. The capillary type is most often found in the dermis or subcutaneous tissues, and typically does not undergo diagnostic imaging. The arteriovenous or venous types are rare. It is the cavernous type that often presents as a soft tissue mass requiring diagnostic imaging. Together, the classic radiographs and MRI findings are virtually diagnostic of cavernous hemangioma.

**CLINICAL HISTORY** A 15-year-old cross-country runner with lower leg pain.



FIGURE 7.19A



FIGURE 7.19B

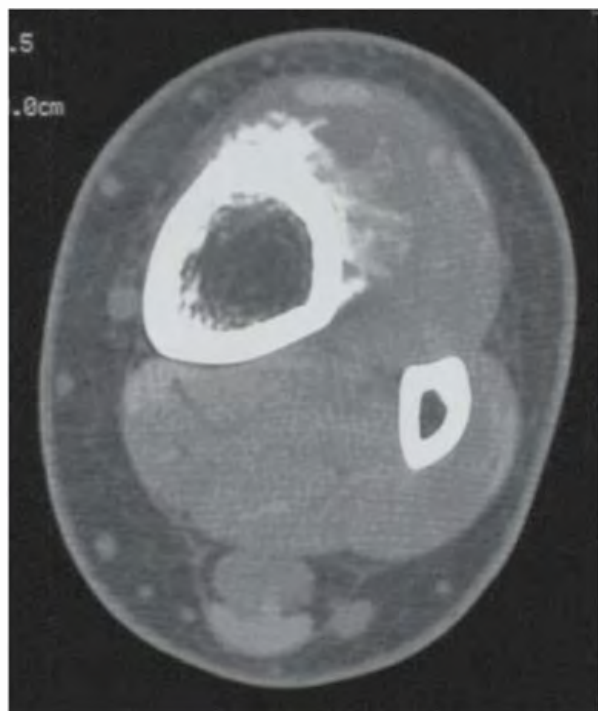


FIGURE 7.19C

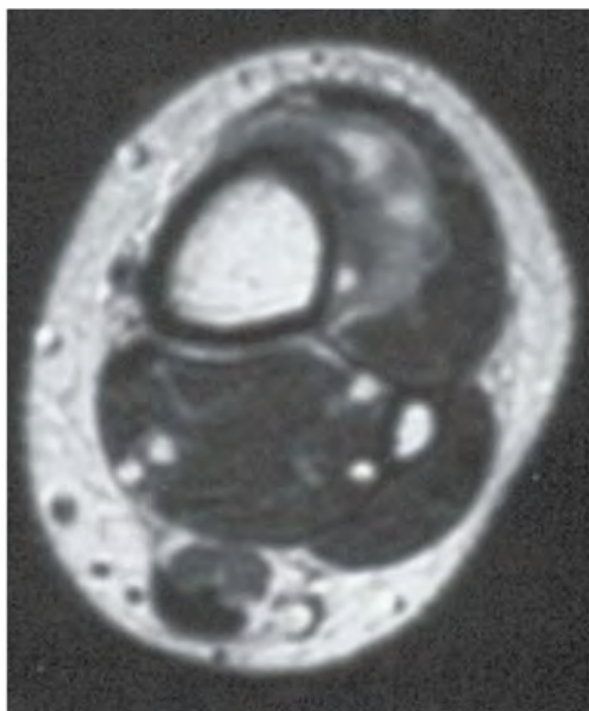


FIGURE 7.19D

## FINDINGS

- A, B. Lateral and AP detail views of the lower tibia demonstrate a mass on the cortical surface of the distal tibia. There are lucent and sclerotic regions, with spicules of bone projecting away from the cortex into the soft tissues.
- C. Axial CT with contrast enhancement shows the tumor mass extending from the cortical surface.
- D. Axial T1-weighted MRI after gadolinium injection shows an enhancing mass apposed to an intact cortex, with low-signal regions within.

**DIFFERENTIAL DIAGNOSIS** Parosteal osteosarcoma, periosteal osteosarcoma, high-grade surface osteosarcoma, lymphoma, juxtacortical chondroma.

**DIAGNOSIS** Periosteal osteosarcoma.

**DISCUSSION** Osteosarcoma is an uncommon, malignant, bone-forming tumor with three commonly recognized but rare variants that arise on the cortical surface: parosteal osteosarcoma, periosteal osteosarcoma, and high-grade surface osteosarcoma [23]. Periosteal osteosarcomas comprise about 1.5% of all osteosarcomas. Usually found in the diaphysis of the femur or tibia, the peak age of discovery is about 20 years, and most patients present after a few weeks or

months of pain, swelling, tenderness, or mass [24]. Periosteal osteosarcomas are moderately differentiated and chondroblastic, unlike the more common parosteal osteosarcomas, which are well differentiated and fibroblastic. The presence of any high-grade histologic features would cause the lesion to be classified as a high-grade surface osteosarcoma [25].

It is uncertain whether these surface osteosarcomas arise in the periosteum or in the outer layers of the cortex. On imaging, periosteal osteosarcomas appear as elongated, partially mineralized masses on the cortical surface of a long bone in the diaphyseal region, with thickened underlying cortex and solid periosteal reaction at the margins. Lucent regions within the tumor correspond to nonmineralized tumor cartilage, and brush-like spicules of bone extending from the underlying cortex into the tumor correspond mostly to trabeculae of reactive bone. Blotchy, punctate, and circular densities in the tumor represent mineralization of chondroid tumor matrix and reactive bone. The periphery of the lesion will have less mineralization. Periosteal osteosarcomas are much less dense radiographically than parosteal osteosarcomas, reflecting the difference in their histologic differentiation. Minimal involvement of the marrow space can be seen on CT or MRI [26]. Periosteal osteosarcomas are treated with wide excision. Their prognosis is better than that of high-grade intramedullary or high-grade surface osteosarcomas, but worse than parosteal osteosarcomas.

**CLINICAL HISTORY** An 8-year-old boy with *painless swelling of the lower leg.*



FIGURE 7.20A



FIGURE 7.20B

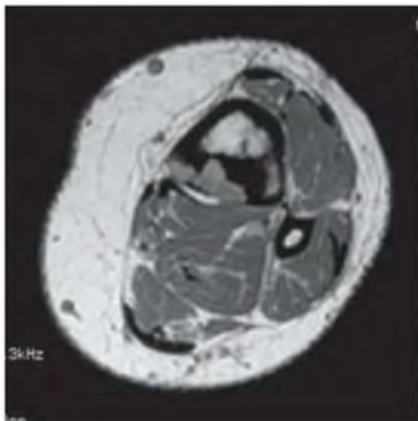


FIGURE 7.20C

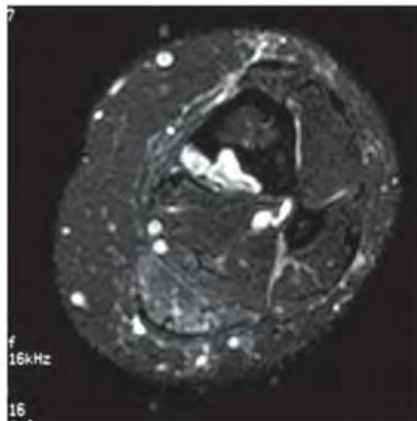


FIGURE 7.20D

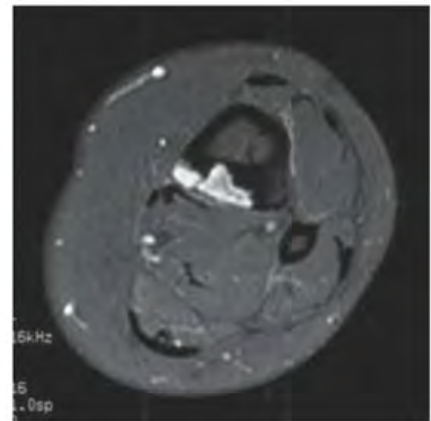


FIGURE 7.20E

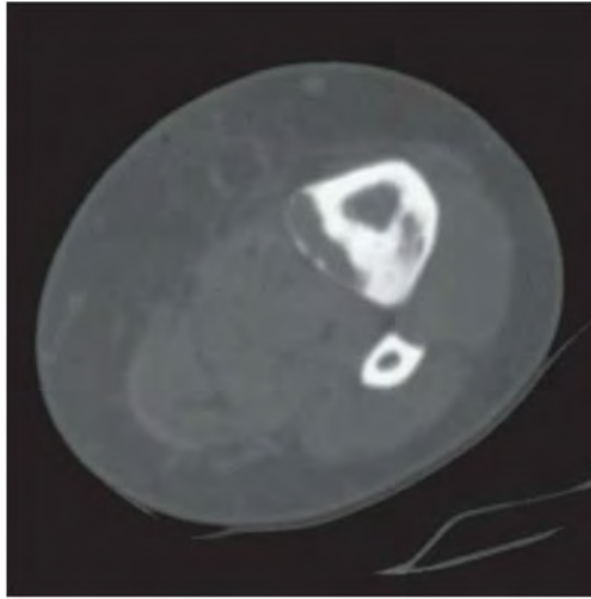


FIGURE 7.20F

## FINDINGS

- A, B. Lateral and AP radiographs of the lower leg show an expansile cortical lesion of the distal tibial shaft. Mature periosteal bone is heaped up around the lesion.
- C–E. Axial proton density (C), T2-weighted (D), and T1-weighted gadolinium-enhanced (E) MRI of the lower leg shows a heterogeneous cortical lesion with solid surrounding periosteal reaction and intense enhancement. There are no extraosseous or intramedullary components.
- F. Axial CT shows a thin rim of intact bone surrounding the superficial aspect of the lesion. The lateral portion of the lesion shows ground-glass mineralization.

**DIFFERENTIAL DIAGNOSIS** Adamantinoma, ossifying fibroma, NF, fibrous dysplasia.

**DIAGNOSIS** Ossifying fibroma (osteofibrous dysplasia).

**DISCUSSION** Ossifying fibroma is considered a benign fibro-osseous disorder that resembles fibrous dysplasia pathologically and radiologically except for its intracortical location. Campanacci rendered the first comprehensive description of this entity [27]. The lesions are slightly more common in males and generally occur when the patient is less than 10 years old. Involvement is virtually isolated to the tibia, usually in the mid diaphysis, although

rarely, fibular involvement may be seen. The lesions may resolve spontaneously or show some degree of progression. Although it appears to be a distinct entity, a relationship to adamantinoma and fibrous dysplasia has been suggested. Osteofibrous dysplasia may be a precursor to malignant adamantinoma, and simultaneous occurrence of both lesions has been documented [28–30]. Bony resorption with subsequent fibrous repair may be responsible for these lesions, or they may represent a particular type of fibrous dysplasia.

Certain trisomies may be associated with osteofibrous dysplasia [31]. Pathologically, osteoblastic rimming and lamellar trabeculae are histologically distinguishing features from conventional fibrous dysplasia [32]. These lesions may have a radiographic appearance similar to that of adamantinoma; however, discriminating features include ground-glass texture of the bone, anterior bowing, and absence of destructive or periosteal changes. In addition, fibrous dysplasia generally occurs in a younger population. These features enabled proper identification of fibrous or osteofibrous dysplasia in 87% of cases and adamantinoma in 95% of cases in one study [33]. MRI is nonspecific and not particularly useful in the evaluation of these lesions [34], except perhaps for anatomic extent. Conservative treatment is advocated, since there is a high postsurgical recurrence rate [35]. Prevalent complications include pathologic fracture and pseudoarthrosis. In a series of 11 patients, four had pathologic fracture, complicated by pseudoarthrosis in two of these instances.

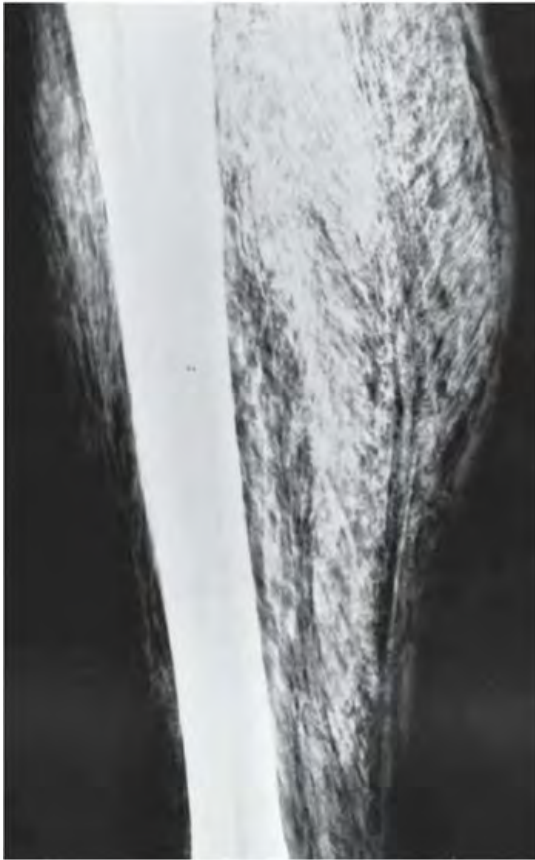


FIGURE 7.21A



FIGURE 7.21B

**FINDINGS** Lateral radiographs of the leg (A) and thigh (B) on the same side. Gas has dissected into the deep soft tissues outlining the muscle bundles and fascial planes.

**DIFFERENTIAL DIAGNOSIS** Infection, penetrating trauma, ulceration.

**DIAGNOSIS** Clostridial myonecrosis (gas gangrene).

**DISCUSSION** Clostridial myonecrosis usually results from trauma. Clostridial contamination of traumatic wounds may produce extensive tissue damage and gas formation in devitalized tissues (gas gangrene). The most common causative agent, *Clostridium perfringens*, is widely distributed in nature. Clostridial myositis has a classic radiographic appearance of extensive linear collections of gas that are dispersed widely throughout the affected muscles.

Spontaneous, non-trauma-related clostridial myonecrosis has been associated with colorectal carcinoma, leukemia, diabetes mellitus, and drug-related immunosuppression

[36,37]. The main underlying conditions in spontaneous clostridial myonecrosis consist of hematologic or gastrointestinal malignancy, and the most commonly implicated organisms are *C. perfringens* and *C. septicum* [38]. The mortality from spontaneous clostridial myonecrosis is higher than that occurring in the setting of trauma, with a survival rate of only 19% [39].

Symptoms consist of pain, edema, hemorrhagic bullae, and crepitus, frequently accompanied by shock. Gram-positive rods retrieved from the infected area help establish the diagnosis. *Clostridia* are gas-producing organisms, and the presence of gas, which may be suggested by crepitus in the infected area clinically and confirmed radiographically, should suggest the diagnosis.

Treatment is by debridement and antibiotic therapy. Hyperbaric oxygen therapy may be beneficial and has demonstrated a synergistic effect in decreasing morbidity and mortality in animal models. Retrospective human studies suggest this therapy may decrease mortality by a factor of two [40].



FIGURE 7.22A



FIGURE 7.22B



FIGURE 7.22C

## FINDINGS

- A. Whole-body radionuclide bone scan shows intense activity in the tibia, extending from the knee almost to the ankle. There is a bowing deformity. Additional areas of abnormality are seen in the lumbar spine and right shoulder.
- B, C. Companion case: A 78-year-old woman. AP and lateral radiographs of the tibia show marked cortical and trabecular thickening, beginning at the proximal end of the tibia and extending to the distal metadiaphysis. At the distal interface between abnormal and normal bone is a flame-shaped region of osteolysis.

**DIFFERENTIAL DIAGNOSIS** None.

**DIAGNOSIS** Paget disease.

**DISCUSSION** The intense activity on bone scan involving a long bone from one end toward the other is diagnostic of Paget disease. On the radiographs, the cortical thickening, coarse trabecular pattern, and the flame-shaped osteolysis are typical for Paget disease.

Paget disease commonly begins at the end of a long bone as a zone of osteolysis that is eventually replaced with

cortical and trabecular thickening [41,42]. The new bone is weak bone—a highly vascular mosaic of woven and lamellar bone—and a characteristic lateral bowing of the femur or anterior bowing of the tibia ensues. At sites of tuberosities, primary involvement can begin in the diaphysis, as in this case. This is classically described in the tibial tuberosity, but is also present at the femoral trochanters or humeral tuberosities. This form of Paget disease is most common in younger patients with monostotic disease who tend to have a normal alkaline phosphatase.

Differential considerations for unilateral anterior tibial bowing include the saber shin abnormality seen in syphilis, neurofibromatosis type 1 (in which case cortical thinning is more common), and amniotic band syndrome (obvious from birth). Treatment is usually supportive and directed at the complications of the disease; however, it is not clear who is at risk of complications or if the medication to decrease bone turnover is effective in decreasing the progression of the disease.

It is interesting to note that the initial site of Paget disease is at the end of a long bone, an area with extensive vascularity but little hematopoietic marrow. Therefore, the primary inciting event seems to depend on vascularity, but propagation of the disease is dependent on the osteoclastic activity of the hematopoietic marrow.



FIGURE 7.23A



FIGURE 7.23B



FIGURE 7.23C

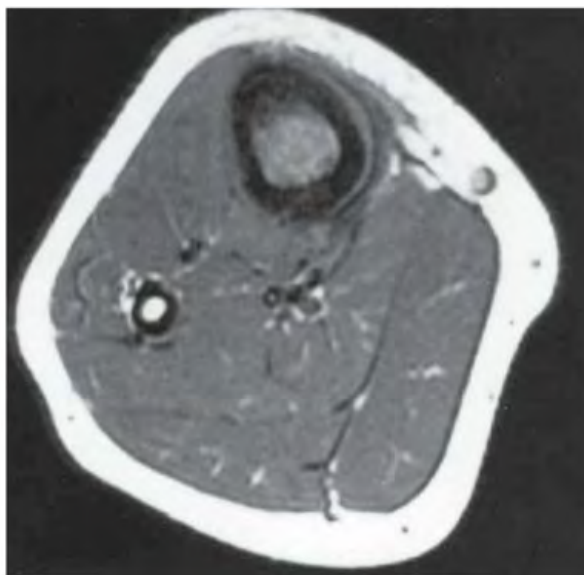


FIGURE 7.23D

**FINDINGS**

- A, B. Lateral and AP radiographs of the lower leg show a vague region of sclerosis in the proximal tibia and subtle periosteal reaction along the proximal shaft, seen posteriorly on the lateral radiograph and laterally on the AP radiograph.
- C. Coronal T1-weighted MRI shows replacement of the fatty marrow in the proximal tibia. Periosteal reactive bone is present along both sides of the shaft, with a pathologic buckle fracture of the lateral cortex of the metaphysis.
- D. Axial proton density MRI shows the intramedullary process permeating through the cortex into the surrounding soft tissues. Tiny focal regions of intermediate signal give the normally homogeneous low-signal cortical bone a mottled, blurred appearance. A layer of periosteal bone partially surrounds the tibia.

**DIFFERENTIAL DIAGNOSIS** Osteosarcoma, Ewing sarcoma, and lymphoma.

**DIAGNOSIS** Ewing sarcoma.

**DISCUSSION** The radiographs are exceedingly subtle and could easily be passed as normal. The MRI shows an extensive intramedullary lesion with a permeative growth pattern, characteristic of a rapidly enlarging process. The differential diagnosis is that of an aggressive intramedullary lesion, and includes neoplasm as well as infection. The location is common for osteosarcoma, Ewing sarcoma, and lymphoma, which are the most common bone tumors in the pediatric age group. Hematogenous osteomyelitis begins at the metaphyseal side of the growth plate and is unlikely for that reason. The lack of tumor ossification favors Ewing sarcoma and lymphoma, but no CT was obtained, and small regions could easily be missed on radiographs or MRI. Clearly, the definitive diagnosis must be made by biopsy.

**CLINICAL HISTORY** A 13-year-old girl with knee pain, and a companion case.



FIGURE 7.24A



FIGURE 7.24B



FIGURE 7.24C



FIGURE 7.24D

## FINDINGS

- A, B. AP and lateral radiographs of the knee. A lucent lesion in the proximal tibial metaphysis abutting the growth plate is present, with a somewhat lobular contour and surrounding sclerosis. The sclerosis merges imperceptibly with the surrounding bone. Soft tissue swelling is present, and a single layer of solid periosteal reactive bone is present posteriorly. There is no knee joint effusion.
- C, D. Companion case: a young man with knee pain. T2 coronal MRI demonstrates a geographic area of high signal intensity, with a low-signal-intensity rim in the metadiaphysis of the tibia and extension to the cortical surface. Extensive surrounding marrow edema is present.

**DIFFERENTIAL DIAGNOSIS** Eosinophilic granuloma, infection, lymphoma, metastasis.

**DIAGNOSIS** Brodie abscess.

**DISCUSSION** Brodie abscess is a local, subacute bone abscess that may present as a solitary bone lesion. Symptoms of recurrent pain and local tenderness with swelling and erythema may be present for months or years. Most cases occur in adolescents and young adults, but the reported age range is 6 to 61 years. Males are affected more often than

females by a 2:1 ratio. The typical location is the metaphysis or diaphysis of the femur or tibia. Brodie abscess may begin *de novo*, it may develop in the same site as the preceding episode of acute osteomyelitis, or it may follow an acute episode of osteomyelitis at another site. Only 25% of patients have a history of antecedent infection or show systemic signs of infection. *Staphylococcus aureus* is the most common offending organism.

Radiographically, Brodie abscess appears as a well-defined lucent area in cancellous bone, with smooth, round, geographic margins and a thick sclerotic rind that may merge imperceptibly with the surrounding bone. The lesion may appear lobulated, with lucent serpentine tracts extending along the bone, sometimes leading to a draining sinus on the skin. CT is valuable for defining the reactive sclerosis, and it can permit identification of tracts in the bone. The corresponding pathology is an avascular cavity, typically 1 to 4 cm in size, lined with granulation tissue and filled with fluid but usually not frank pus. Thickening of trabeculae adjacent to the lesion by reactive endosteal bone formation may form a sclerotic rind about the cavity.

Although Brodie abscesses have a characteristic appearance, they may be confused with other focal bone lesions, including tumors. The key radiologic feature of Brodie abscess is the extensive reactive bone formation that has a sharp interface with the lesion but merges gradually with surrounding normal bone.

**CLINICAL HISTORY** A 47-year-old man with knee pain for several weeks.



FIGURE 7.25A



FIGURE 7.25B



FIGURE 7.25C

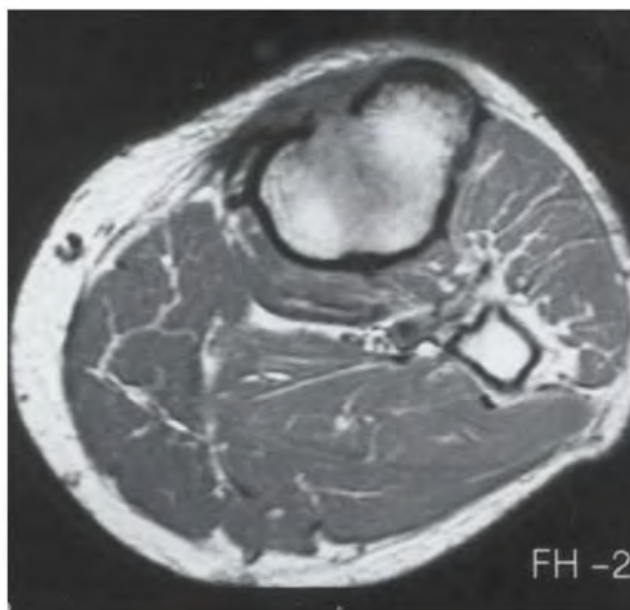


FIGURE 7.25D



FIGURE 7.25E

## FINDINGS

- A, B. Lateral and AP radiographs of the knee show a destructive process in the proximal tibia, with a larger, rounded proximal lesion and a smaller distal lesion. There may be vague rarefaction connecting these lesions, and there are some areas of surrounding sclerosis. The sclerosis does not completely surround the areas of destruction. No periosteal bone formation is present. There is no knee effusion.
- C. Coronal T1-weighted MRI shows the proximal lesion extending to the tibial articular surface, with a partial rim of low-signal reactive bone.
- D. Axial T1-weighted MRI through the more distal portion of the lesion shows a defect in the anterior tibial cortex, with well-localized soft tissue extension.
- E. Coronal T2-weighted, fat-suppressed MRI shows bright signal within the proximal tibia. There is no involvement of the knee joint.

**DIFFERENTIAL DIAGNOSIS** Infection, metastasis, lymphoma, adamantinoma, malignant transformation in Paget disease, radiation, or osteonecrosis.

**DIAGNOSIS** Tuberculous osteomyelitis.

**DISCUSSION** Extensive bone destruction is present with minimal reactive bone formation. The appearance is more suggestive of infection than neoplasm because of the morphology of the destruction, but the lack of reactive bone formation would be unexpected for a pyogenic pathogen.

Tuberculous osteomyelitis not involving a joint is uncommon. On radiographs, advanced lesions such as this may mimic chronic pyogenic osteomyelitis, Brodie abscess, tumor, or granulomatous lesions [43]. There are no particular imaging features that allow a conclusive radiologic diagnosis. Biopsy is mandatory to confirm the diagnosis. In one study, the prevalence of peripheral osteoarticular involvements in patients with known tuberculosis was 0.05%, with most of these cases involving the joint and the adjacent epiphyses [44]. Cases involving joints presented as destructive arthritis, whereas cases involving only bone had the appearance of lytic tumor.

Tuberculosis has undergone resurgence in recent years. Sites of predilection include the spine, hip, and knee. The mode of spread of mycobacterial infection to bone is hematogenous. Once settled in tissue, the host elicits an antigenic response, consisting of multinucleated giant cell and lymphocyte reaction. Caseating necrosis ensues, resulting in bony destruction and host reaction similar to pyogenic osteomyelitis. Marrow changes, as seen in the MRI, are similar to pyogenic infection, but the changes in tuberculosis often progress at a slower pace. Bursitis, as seen here, and tendinitis may be present. Phemister's triad in tuberculosis consists of juxta-articular osteoporosis, peripheral erosions, and conspicuous lack of joint space alteration until late in the clinical course. When joint space obliteration does occur, it usually does so by fibrosis rather than bony ankylosis. Note the relative sparing of the cartilage space in this case. On radiographs, advanced tuberculous osteomyelitis may mimic chronic pyogenic osteomyelitis, Brodie abscess, tumors, or other granulomatous lesions.



FIGURE 7.26A



FIGURE 7.26B

**FINDINGS**

- A. AP radiograph of the right leg shows a comminuted segmental fracture of the tibia, and a midshaft fracture of the fibula.
- B. Lateral radiograph shows gas in the anterior soft tissues as well as the fractures.

**DIFFERENTIAL DIAGNOSIS** None.

**DIAGNOSIS** Open segmental fracture.

**DISCUSSION** This patient was struck from the right side by a car, causing the tibia to bend around the bumper. The result is a pair of transverse fractures with butterfly fragments,

isolating a segment of the tibial shaft. Fractures caused by indirect loading result in injuries at a distance from the site of loading. They have fracture lines with predictable morphology, depending on the mode of loading. Bending results in tensile forces on the convex side of the bend, and compressive forces on the concave side of the bend. The tensile forces cause a transverse fracture, whereas the compressive forces cause symmetric oblique fractures and the butterfly fragment. Fractures of this morphology always result from loading under bending, and the butterfly fragment will be on the concave side of the bend. Sometimes bending will result in a single oblique fracture on the concave side that connects with the transverse fracture, leaving a fracture line that resembles a hockey stick.

**CLINICAL HISTORY** A 2-year-old boy whose mother says he fell down while she was not watching.



FIGURE 7.27A



FIGURE 7.27B

**FINDINGS** A, B. AP radiograph of the tibia (full (A) and detail (B)) shows a nondisplaced curved fracture of the distal tibial shaft.

**DIFFERENTIAL DIAGNOSIS** Accidental fracture, inflicted trauma.

**DIAGNOSIS** Toddler's fracture.

**DISCUSSION** There is a nondisplaced spiral-type fracture of the distal tibial metaphysis in this 2-year-old child. The age of the child and location of this fracture are typical of this stress-type injury. The repeated twisting falls of these young children as they are learning to walk result in this characteristic fracture.

Isolated spiral or oblique fractures of the tibial shaft are common injuries in ambulatory preschoolers (toddler's fracture). The fibula is usually intact. These injuries result from falls with torsion of the foot, and the traumatic episode is often innocuous or not witnessed. These fractures may be exceedingly subtle on radiographs because the low energy that produces the fracture is insufficient to displace it. The clinical presentation is often failure to bear weight, limping, or simply the appearance of pain when bearing weight. Follow-up examinations will show periosteal new bone, indicative of healing. Fractures from a similar mechanism may occur less frequently in the femur or metatarsals. Toddler's fractures must be distinguished from inflicted trauma in the battered child.

**CLINICAL HISTORY** A 19-year-old runner with anterior medial leg pain. A, Radiograph at presentation, and B, 8 weeks later; C-D, MRI at presentation.



FIGURE 7.28A



FIGURE 7.28B



FIGURE 7.28C



FIGURE 7.28D

**FINDINGS**

- A. Initial AP radiograph of the proximal tibia is normal.
- B. Eight weeks later, AP radiograph shows focal periosteal reaction along the lateral aspect of the proximal tibial shaft.
- C, D. Coronal T1-weighted (C) and STIR (D) MRI demonstrates a horizontally oriented linear band of low signal intensity in the proximal tibial metaphysis with adjacent marrow and periosteal edema.

**DIFFERENTIAL DIAGNOSIS** None.

**DIAGNOSIS** Stress fracture.

**DISCUSSION** The linear band of decreased signal intensity within the tibial metaphysis is oriented perpendicular to the long axis, abuts the cortex, and is surrounded by an ill-defined area of decreased signal intensity that represents marrow edema. This constellation of findings is characteristic of a stress fracture. The clinical history and follow-up radiograph showing the sclerotic changes of healing confirms the diagnosis.

Stress fractures occur after repetitive, prolonged muscular activity that places more stress on an area of bone than usual. Bone responds by remodeling and strengthening itself to accommodate the additional stress, but there is a vulnerable period in which the bone is weakened by intracortical bone resorption in preparation for the formation of new bone.

The term stress fracture encompasses both fatigue fractures and insufficiency fractures. Fatigue fractures, the type seen in athletes, are due to abnormal repetitive stresses exerted on normal bone (as in this case). Insufficiency fractures are due to normal stresses exerted on abnormal or insufficiently strong bone. For example, compression fractures of the spine in patients with senile osteoporosis are insufficiency fractures. The osteoporotic bone is no longer strong enough to withstand the normal compressive stress of the body weight.

The imaging features of stress fractures are usually straightforward: a linear band of increased density on radiography, linear decreased signal on T1-weighted or proton density MRI, or a linear focus of radiotracer uptake. Characteristically, these linear abnormalities are oriented perpendicular to the long axis of the involved bone. Pathophysiologically, the findings are due to callus formation around trabecular microfractures. Earlier changes of stress reaction can be much more difficult to detect. Plain radiographs may be normal when the patient is first seen, or may show only very subtle resorptive changes within the cortex [45]. MRI and radionuclide examinations may show only amorphous areas of abnormality, although they often suggest the diagnosis long before it can be made by plain radiographs.

Fatigue fracture locations vary according to the specific type of physical activity. Runners are prone to develop them in the tibia. Military recruits are prone to develop them in the metatarsals and calcanei.



FIGURE 7.29A



FIGURE 7.29B

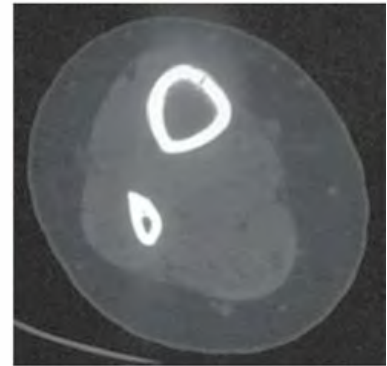


FIGURE 7.29C

## FINDINGS

- A. Case 1. Radionuclide bone scan. Anterior camera view of both lower legs shows intense activity at the midshaft of both tibiae, with a broad region of less focal and less intense activity along the proximal shafts.
- B. Case 2. Lateral lower leg radiograph (detail). The anterior cortex of the tibia is markedly thickened. There is a transverse lucency extending from the periosteal surface partially through the cortex, with a poorly defined region of lucency around the deep margin of the lucency.
- C. Case 3. Axial CT through the middle third of the tibial shaft shows a longitudinal lucent line through the anteromedial tibial cortex, with slight periosteal and endosteal reactive bone.

**DIFFERENTIAL DIAGNOSIS** Stress fractures at different stages.

**DIAGNOSIS** Case 1: bilateral tibial stress fractures and stress remodeling. Case 2: anterior tibial stress fracture with nonunion. Case 3: longitudinal anterior tibial stress fracture.

**DISCUSSION** The radionuclide bone scan in Case 1 shows increased activity along both tibial shafts, which is consistent with stress remodeling. The more focal areas of activity correspond to stress fractures. The lateral radiograph of the lower leg in Case 2 shows the anterior tibial cortical thickening of stress remodeling as well as the stress fracture. The lucency

around the deep margin of the fracture line is indicative of nonunion. The CT in Case 3 shows a longitudinal fracture of the anteromedial tibial cortex involving the middle third of the shaft.

Stress fractures of the tibia are usually seen in athletic or military populations. It is estimated to occur in 20% of recruits and a favored location is the posterior, medial cortex of the proximal tibial diaphysis. The most contributory factor to this injury is related to tibial bending strength in the anterior to posterior direction [46]. Fractures involving the middle third of the tibia are much less common and pose problems with diagnosis as well as treatment. Usually these fractures are transverse, though on occasion they may be vertical, as in companion Case 3 [47]. Very often, the initial radiographs show only thickening of the anterior cortex. Shin splints represent a milder condition in the same spectrum. An Aircast pneumatic brace may procure a quicker recovery and enable the patient to engage in athletic activities earlier [48].

Nonunion represents an uncommon complication, although anterior cortical midshaft tibial stress fractures are very prone to demonstrate this complication. In one series of athletes with these fractures, the overall time from initial symptoms to return to competition was 12.5 months [49]. If conservative therapy fails after a few months, then surgical treatment with resection of the fracture is advocated [50]. Intramedullary nailing may benefit patients with recurrent stress fractures, which are often seen in athletes and army recruits [51].

**CLINICAL HISTORY** A 43-year-old woman with 2-week history of lower leg pain and swelling.

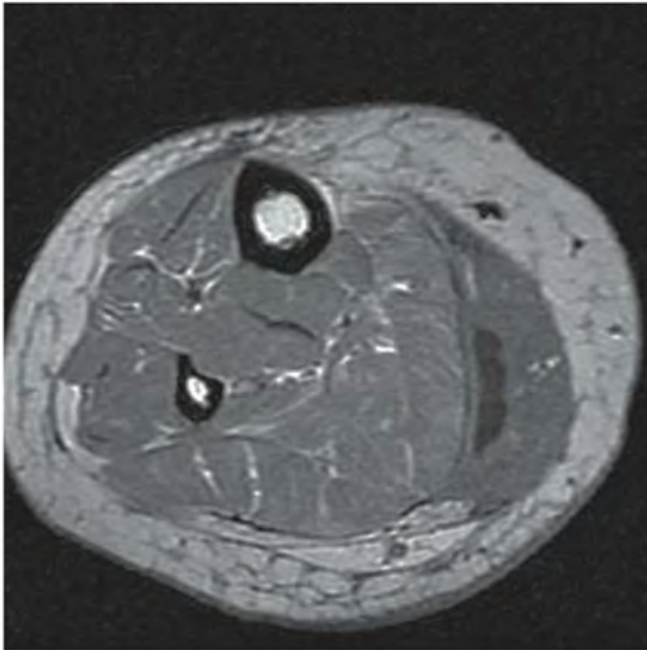


FIGURE 7.30A

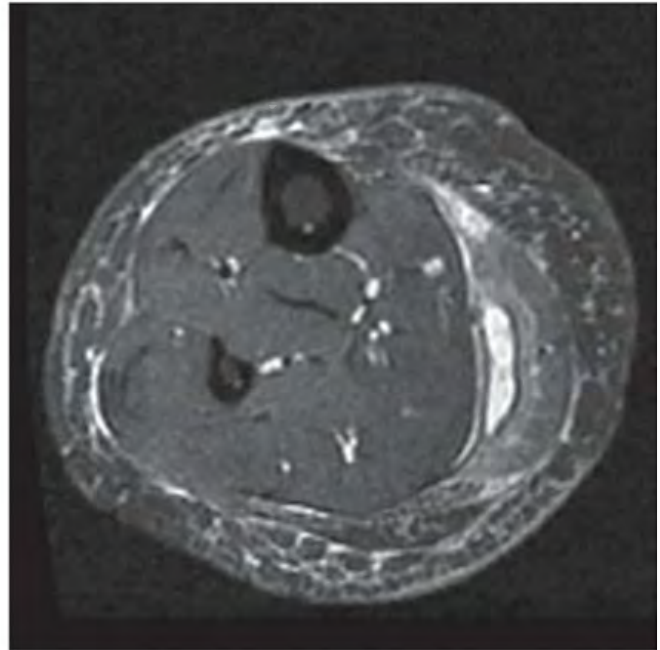


FIGURE 7.30B

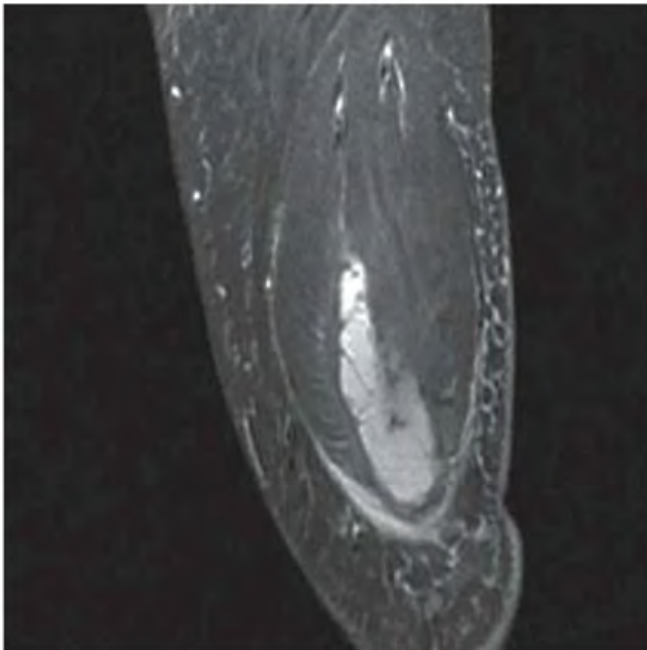


FIGURE 7.30C

**FINDINGS** Axial T1-weighted (A), STIR (B), and sagittal STIR (C) MRI shows a hematoma between the soleus and gastrocnemius muscles in the region of the torn plantaris tendon. The gastrocnemius shows edema representing muscle strain.

**DIFFERENTIAL DIAGNOSIS** None.

**DIAGNOSIS** Rupture of the plantaris tendon with adjacent gastrocnemius strain.

**DISCUSSION** The plantaris is often thought of as a vestigial, accessory muscle because it may be absent in 7% to 10% of the population. It originates from the distal aspect of the lateral supracondylar line of the femur, and the myotendinous junction occurs at the level of the origin of the soleus muscle from the tibia. The muscle lies between the medial head of the gastrocnemius muscle and the soleus muscle in the midportion of the leg. It courses along the medial aspect of the Achilles tendon, and inserts on the calcaneus [52]. The tendon of the plantaris can rupture when violently contracted and at clinical examination can simulate a rupture or partial tear of the medial head of the gastrocnemius muscle [53]. Rupture of either the plantaris or medial gastrocnemius muscles has been referred to as “tennis leg” due to its common association with that sport. A large, painful hematoma often accompanies a ruptured plantaris or a gastrocnemius muscle, and at clinical examination differentiation can be difficult. A torn gastrocnemius takes longer to heal and is often treated with casting to immobilize the injury, whereas a torn plantaris is clinically considered less severe and is generally treated conservatively [54]. When it is ruptured, MR imaging at the level of the myotendinous junction and the plantaris tendon in the midproximal portion of the lower leg may reveal an intermuscular hematoma between the soleus muscle and the medial head of the gastrocnemius muscle. An associated partial tear of the medial head of the gastrocnemius muscle may also be observed [54].



FIGURE 7.31

**FINDINGS** AP radiograph shows a vertical lucency originating in the notch region and extending to the metadiaphysis medial surface.

**DIFFERENTIAL DIAGNOSIS** None.

**DIAGNOSIS** Salter type IV fracture.

**DISCUSSION** Fractures involving the growth plate (physis) of a long or short tubular bone are classified with the Salter-Harris system as type I, II, III, IV, or V.

Type I fracture extends transversely through the plane of the physis.

Type II fractures are the most common; they have a metaphyseal fracture fragment in addition to a physeal fracture.

Type III fractures extend from the physis into the epiphysis.

Type IV fractures have metaphyseal and epiphyseal involvement (as in this case).

Type V fractures are due to axial loading; with an impaction crush injury of the physis.

The classification is important because it has prognostic significance. As one progresses from type I to type V there is a higher incidence of bad fracture outcome, with increased potential for growth disturbance or angular deformity. This is particularly true with lower extremity growth plate fractures.

**CLINICAL HISTORY** A 40-year-old man with calf pain. He has factor V Leiden deficiency and is on chronic warfarin for lower leg deep vein thrombosis.

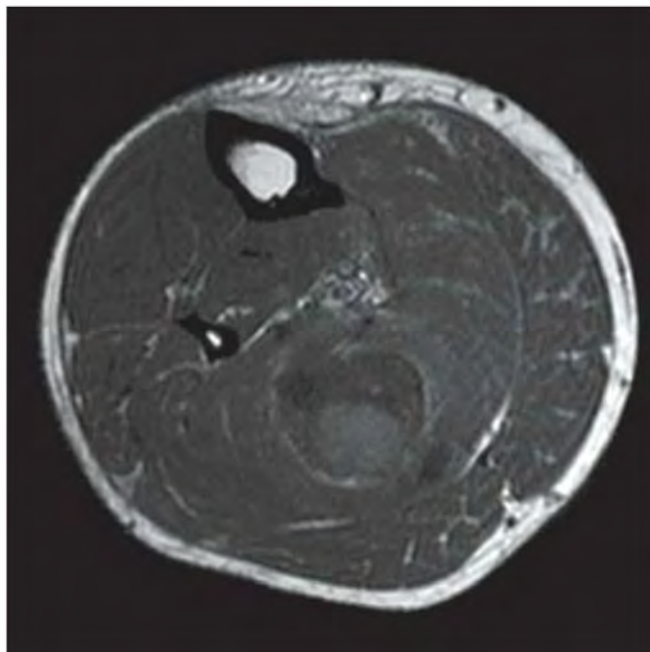


FIGURE 7.32A

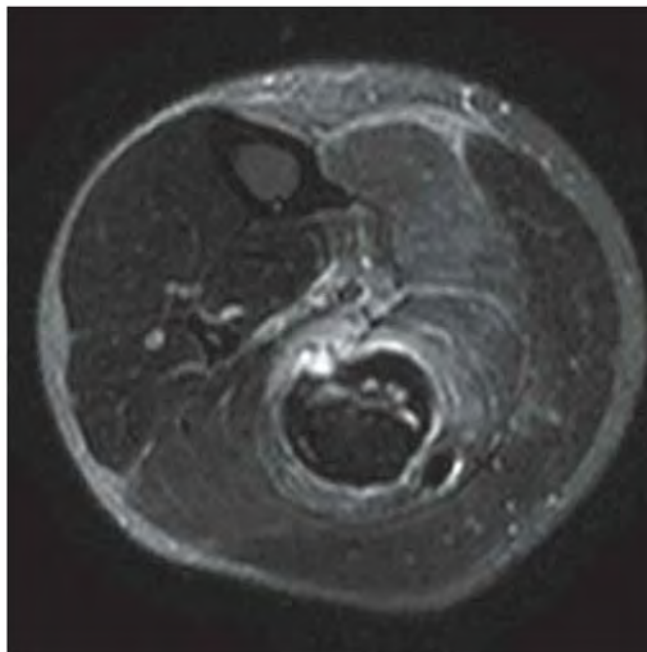


FIGURE 7.32B

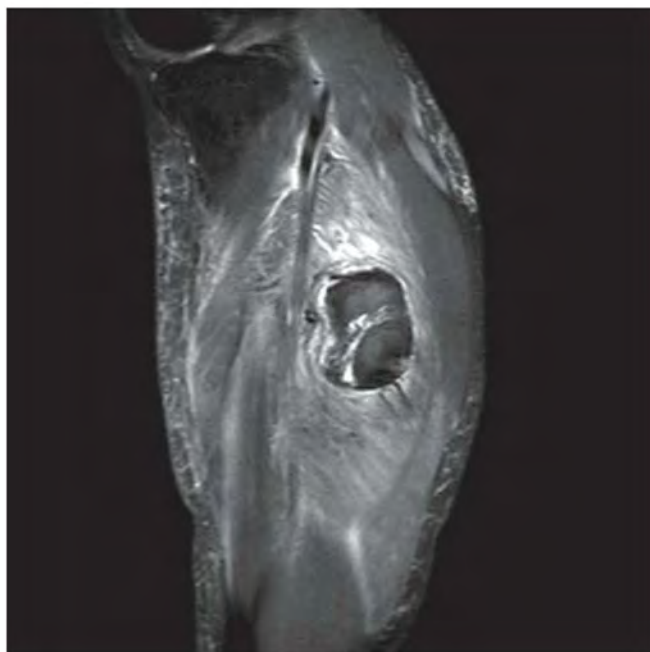


FIGURE 7.32C

**FINDINGS** A–C. Axial T1-weighted (A), fat-suppressed T2-weighted (B), and sagittal inversion recovery (C) MRI shows a round mass-like lesion in the soleus muscle of the lower leg. The lesion has a portion of high signal intensity on T1-weighted image with signal drop-off on fat-suppressed T2-weighted image. Areas of low-signal-intensity lesion are present in all sequences. There is surrounding muscle edema.

**DIFFERENTIAL DIAGNOSIS** Hematoma, hemorrhagic tumor, abscess, myonecrosis.

**DIAGNOSIS** Subacute intramuscular hematoma in soleus.

**DISCUSSION** Injury to the soleus is considered uncommon and is only rarely reported. It has been postulated, however, that injury to this muscle may occur more frequently than reported as soleus tears may be erroneously diagnosed as tears of the gastrocnemius. Hematomas are common after a myotendinous injury, and may be predominantly intramuscular or intermuscular in location. An intramuscular hematoma may mimic an intramuscular abscess or myonecrosis on MR images, since all of these lesions may contain a fluid-fluid level and demonstrate surrounding muscle edema and enhancement. The presence of blood breakdown products resulting in increased signal intensity on T1-weighted images (methemoglobin) or a low-signal-intensity rim with all sequences (hemosiderin) may suggest the diagnosis of intramuscular hematoma [58]. Differentiation between a simple hematoma and a hemorrhagic neoplasm may be difficult. Administration of contrast material aids in excluding a neoplasm when the lesion in question shows no enhancement. Conversely, the presence of an enhancing nodule in a muscle lesion may suggest the diagnosis of a neoplasm rather than a hematoma. When the diagnosis of a probably benign hematoma is in doubt, clinical correlation and a follow-up MR imaging examination may be indicated to establish appropriate evolution of the abnormality [59].

**CLINICAL HISTORY** An adult man with proximal leg mass and weakness of great toe dorsiflexion. Lately, the mass has been diminishing but dorsiflexion of the great toe has become painful.

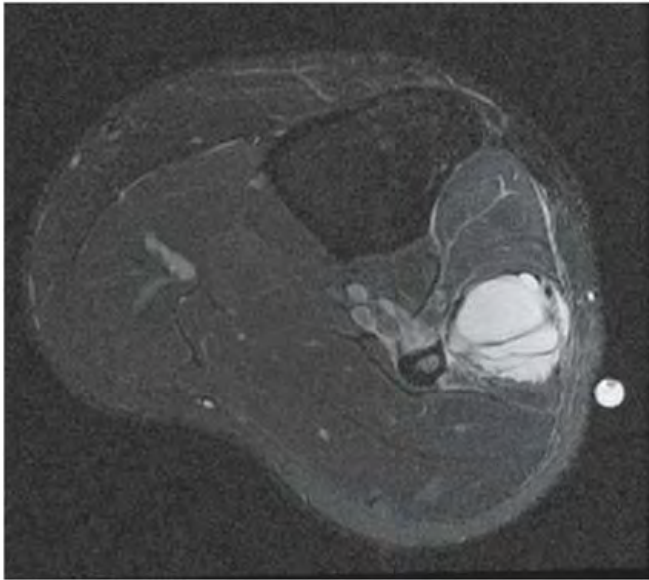


FIGURE 7.33A

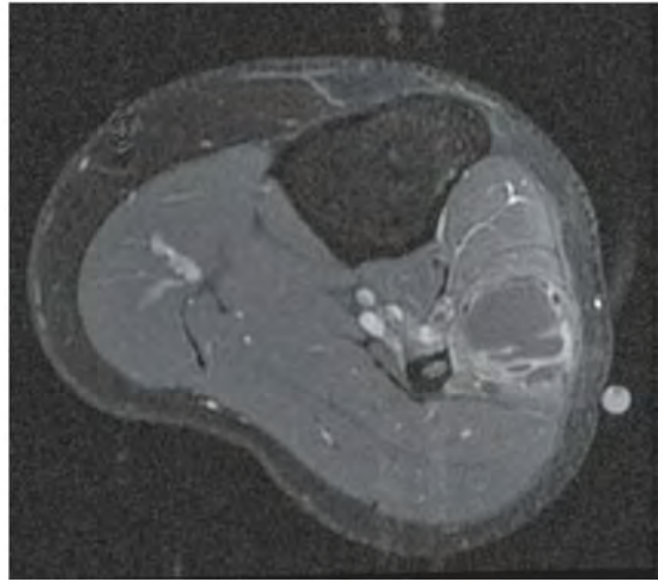


FIGURE 7.33B

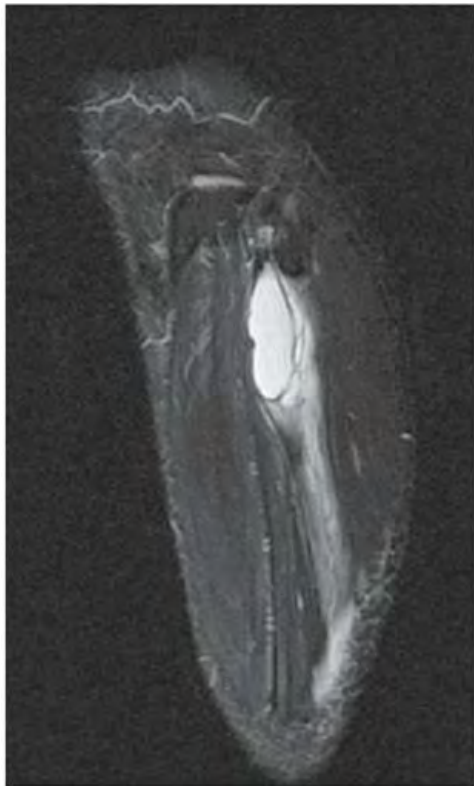


FIGURE 7.33C



FIGURE 7.33D

**FINDINGS**

- A. Axial T2-weighted fat-suppressed MRI shows a multiloculated cyst within the extensor digitorum longus muscle. The mass is separate from the bone.
- B. Axial T1 fat-suppressed MRI after intravenous gadolinium shows enhancement of the cyst walls but not of the cyst contents or the surrounding tissues.
- C. Sagittal T2-weighted fat-suppressed MRI shows a multiloculated cyst with fluid tracking distally from the lesion along fascial planes.
- D. Sagittal T1-weighted fat-suppressed MRI following intravenous gadolinium shows enhancement of the cyst walls but not of the cyst contents or the surrounding tissues. The fluid tracking distally along the fascial planes does not enhance.

**DIFFERENTIAL DIAGNOSIS** Peroneal nerve ganglion cyst, schwannoma, neurofibroma.

**DIAGNOSIS** Peroneal nerve ganglion cyst, with rupture.

**DISCUSSION** The clinical history of mass and weakness of great toe dorsiflexion suggests a mass lesion causing a deep

peroneal nerve palsy. The findings on MRI are those of a cystic lesion. Peroneal nerve ganglion cysts probably arise from the synovial capsule of the proximal tibiofibular joint and dissect along the sheath of the recurrent superior tibiofibular articular branch of the common peroneal nerve as they enlarge [55]. The lesions eventually reach the common peroneal nerve itself and lose their communication with the tibiofibular joint. Continued enlargement and cystic degeneration of the lesion results in signs and symptoms referable to mass effect on the common peroneal nerve or its branches. MRI is the most useful technique for demonstrating these lesions [56]. The differential diagnosis would include a nerve sheath tumor such as schwannoma or neurofibroma, but the absence of enhancement suggests a cystic lesion is far more likely. If imaging after gadolinium injection is delayed, the lesions may enhance because of gadolinium passage into the extracellular space. Rupture of the cyst may cause pain along the path of drainage even as the symptoms caused by the mass effect regress with decompression of the cyst [57].



FIGURE 7.34A



FIGURE 7.34B

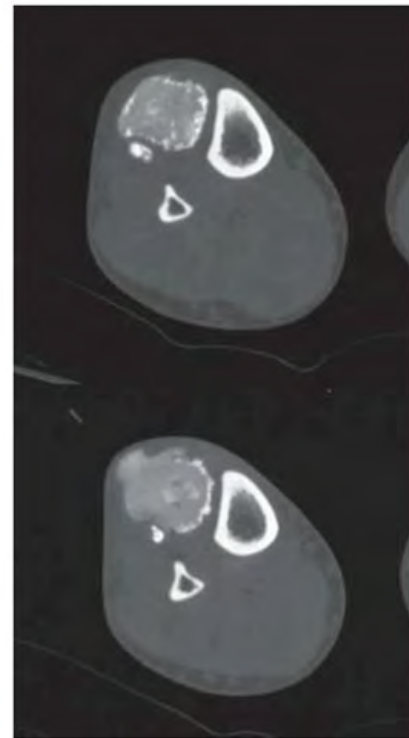


FIGURE 7.34C

**FINDINGS**

- A, B. AP and lateral plain radiographs show well-defined, dense sheets of calcification along the anterolateral calf.
- C. Axial CT shows the calcification is located in the anterior compartment of the leg. There is one main deposit of calcification and a few satellite lesions, all of which have well-defined sclerotic borders. The calcification is denser around the periphery of the lesion. There is no mass effect because the calcified lesion has replaced the musculature.

**DIFFERENTIAL DIAGNOSIS** Calcific myonecrosis, myositis ossificans, tumoral calcinosis.

**DIAGNOSIS** Calcific myonecrosis.

**DISCUSSION** Peripheral calcifications in a lesion may be seen in myositis ossificans; however, these lesions

demonstrate mature trabecular calcification as they evolve with sequential calcification from the periphery of the lesion to its center, and they typically do not demonstrate a fluid-filled central component. The changes illustrated in this case are more compatible with a diagnosis of calcific myonecrosis. Although dermatomyositis and polymyositis may demonstrate calcifications that are linear in nature, the calcifications typically are not isolated to a single muscle group.

Calcific myonecrosis is a posttraumatic lesion consisting of hematoma or cyst formation. Frequently there is a significant time lag between the insult and the presentation [60]. These lesions may demonstrate growth as well as other features simulating malignancy, and they may be confused for neoplastic processes such as soft tissue sarcomas. The radiologic manifestations consist of components of central liquefaction and calcification in a predominantly linear, peripheral distribution. It is this latter feature that facilitates its identification as a benign posttraumatic lesion in a similar spectrum to myositis ossificans, which also shows peripheral

calcification. Adjacent bony erosion may be noted. On MRI, a heterogeneous intramuscular lesion may be demonstrated with only peripheral enhancement [61]. Imaging features help distinguish this from compartment syndrome, although an association may exist in some instances where calcific myonecrosis occurs as a result of the latter. Ischemia is another etiology for its occurrence [62].

Peripheral nerve damage may represent a common final pathway, since injury to the common peroneal nerve has been implicated in some instances. The superficial location of this

nerve makes it more susceptible to injury, and it is the most commonly injured nerve in the lower extremity, with most documented cases of calcific myonecrosis occurring in a muscle innervated by this nerve [63]. Pathologically, these lesions consist of hypocellular fibrous tissue with hemosiderin-laden macrophages and cysts comprised of necrotic muscle tissue and hemorrhagic debris [64]. Recurrent hemorrhage within the lesion is probably responsible for its expansile nature. Surgical treatment carries a significant rate of complications, specifically from recalcitrant sinus tract formation and infection [65].



FIGURE 7.35A



FIGURE 7.35B

**FINDINGS**

- A. Detail of AP radiograph of the lower leg shows confluent lobulated radiolucencies extending along the tibial and fibular shafts, with endosteal scalloping. There is no apparent cortical penetration or periosteal reactive bone.
- B. AP radiograph of the humerus and shoulder shows similar radiolucent lesions in the shaft and head, clavicle, scapula, and ribs.

**DIFFERENTIAL DIAGNOSIS** Cystic angiomatosis, metastases, lymphoma.

**DIAGNOSIS** Cystic lymphangiomatosis (cystic angiomatosis).

**DISCUSSION** Cystic lymphangiomatosis represents a proliferation of cystic spaces filled with lymphatic fluid. The lesions

of cystic lymphangiomatosis do not differ histologically from cavernous or capillary hemangiomas, or from lymphangiomas, so these lesions are often referred to simply as cystic angiomatosis. Pathologically, cystic angiomatosis consists of numerous, dilated, cavernous, thin-walled vascular channels filling and sometimes eroding trabecular spaces. The radiologic appearance is solitary or multiple zones of rarefaction in the skeleton, typically involving more than one bone, not necessarily in a contiguous manner. Involvement of individual bones may include the epiphysis, metaphysis, or diaphysis. The margins tend to be well demarcated, without reactive bone formation and without mass effect. The differential diagnosis includes other solitary or multifocal bone lesions.

**CLINICAL HISTORY** *An 18-year-old man with recurrent bone pain.*



FIGURE 7.36A



FIGURE 7.36B



FIGURE 7.36C

### FINDINGS

- A, B. Radiographs of the tibia show dense sclerosis obliterating the trabecular bone pattern and medullary space. The area of involvement includes the proximal end of the tibia, extending nearly to the midshaft as well as the medial femoral condyle. The cortex is intact, without destruction, expansion, or periostitis. A bone biopsy tract is present in the metaphysis. Similarly dense sclerosis is present in the medial femoral condyle.
- C. Whole-body radionuclide bone scan shows increased activity in the left distal radius and thumb, left distal femur, left proximal tibia, left distal tibia, right proximal tibia, and right foot.

**DIFFERENTIAL DIAGNOSIS** Infection, radiation changes, lymphoma, osteosarcoma.

**DIAGNOSIS** Chronic recurrent multifocal osteomyelitis.

**DISCUSSION** The differential diagnosis of multiple dense bones includes congenital, neoplastic, inflammatory, and metabolic conditions. In this case, the distribution of the process is the major clue to the diagnosis. Chronic recurrent multifocal osteomyelitis [66,67] is a distinct clinical entity in which recurrent episodes of clinical inflammatory bone disease involve different bones at different times. Cultures are negative by definition; if positive, the condition would be subacute osteomyelitis. Biopsy specimens are sterile but show chronic inflammatory changes, with a predominance of lymphocytes in the inflammatory infiltrates. Although the condition does not respond specifically to antibiotics, because it has a benign, self-limited course, patients nonetheless improve when given antibiotics. The recommended treatment is nonsteroidal anti-inflammatory drugs [68].

**CLINICAL HISTORY** A 35-year-old woman with proximal muscle weakness.

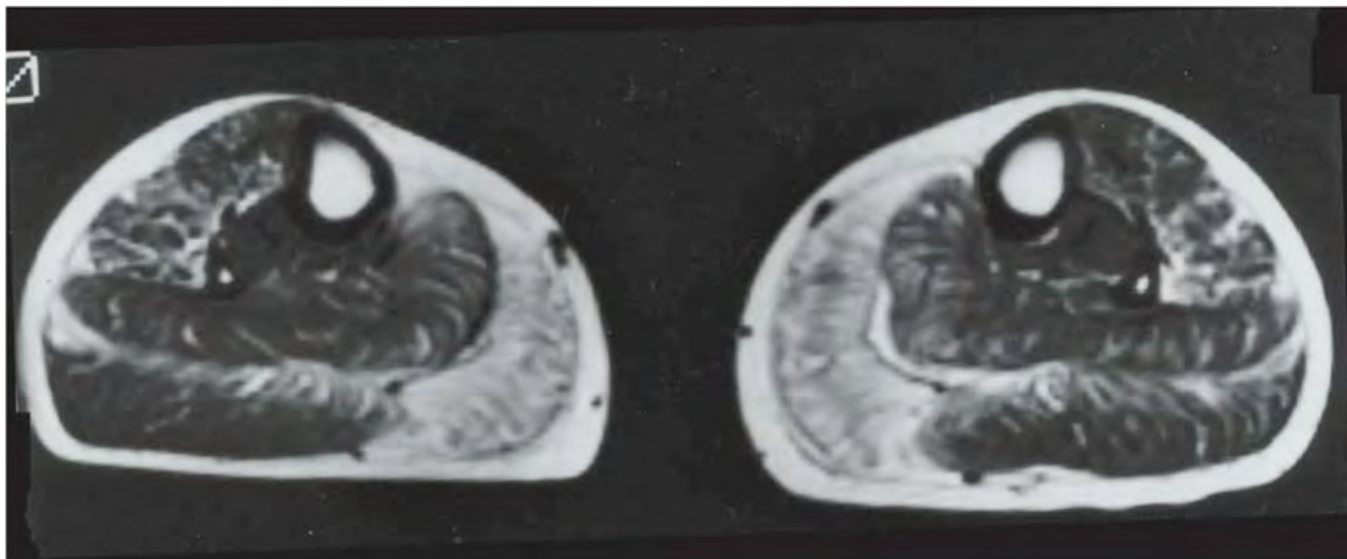


FIGURE 7.37A

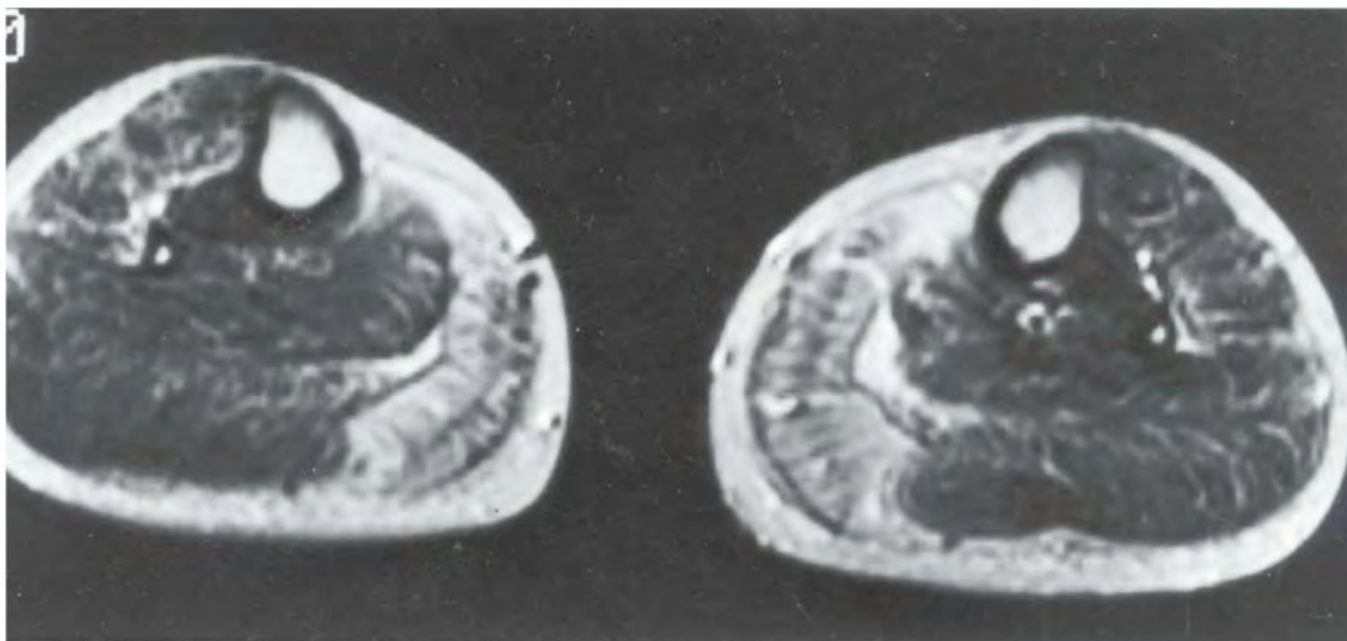


FIGURE 7.37B

## FINDINGS

- A. Axial T1-weighted MRI shows bilaterally symmetric, abnormally high signal intensity in the gastrocnemius muscles. There is no mass effect or bony involvement.
- B. Axial T2-weighted MRI also shows bilaterally symmetric, abnormally high signal intensity in the gastrocnemius muscles. Again, there is no mass effect.

**DIFFERENTIAL DIAGNOSIS** Polymyositis, dermatomyositis, denervation or disuse atrophy, compartment syndrome, viral myositis, pyomyositis, rhabdomyolysis, lymphoma.

**DIAGNOSIS** Polymyositis.

**DISCUSSION** The symmetric involvement suggests a systemic disease, and the lack of mass effect would make lymphoma and pyomyositis much less likely than the other possibilities, but the diagnosis cannot be made without consideration of the clinical setting. Polymyositis and dermatomyositis are diseases of striated muscle characterized by diffuse, nonsuppurative inflammation and degeneration. Dermatomyositis has specific skin changes that are absent in polymyositis.

Polymyositis typically affects women between the ages of 20 and 40. It may begin with a flu-like illness and then progresses to increasing symmetric muscle weakness, initially

prominent in the thighs. Skin changes (40% to 60%) and arthralgias or arthritis (20% to 50%) are variable. The disease may have many systemic manifestations, including cardiac, pulmonary, renal, ocular, neurologic, and gastroenteric symptoms. There is an association between polymyositis and the development of malignancy, but it is not as strong as the association between dermatomyositis and malignancy.

The first radiographic manifestation is that of subcutaneous fat and muscle edema [69,70]. This may resolve or progress to fibrosis or fatty replacement, with or without soft tissue calcification. The calcification classically outlines the fascial planes of muscles, but it may also be located in the subcutaneous tissue. CT may initially show muscle edema, and subsequently fatty replacement and calcification. On MRI, two types of muscle changes have been described. The earliest manifestation is inflammation of the muscle, which shows increased signal intensity on T2-weighted images and isointensity on T1-weighted images. Subsequently, fatty replacement may occur, and this manifestation shows increased signal intensity on both T1-weighted and T2-weighted MRI, as in this case. The hyperintensity of the muscle seen on T2-weighted or inversion recovery sequences appears to correlate with the clinical symptoms, and it may be more specific than laboratory parameters. Additionally, MRI has been shown to be cost-effective in determining the site for diagnostic biopsy [71].

**CLINICAL HISTORY** A 59-year-old diabetic man with right lower extremity cellulitis and worsening sepsis, and companion case.

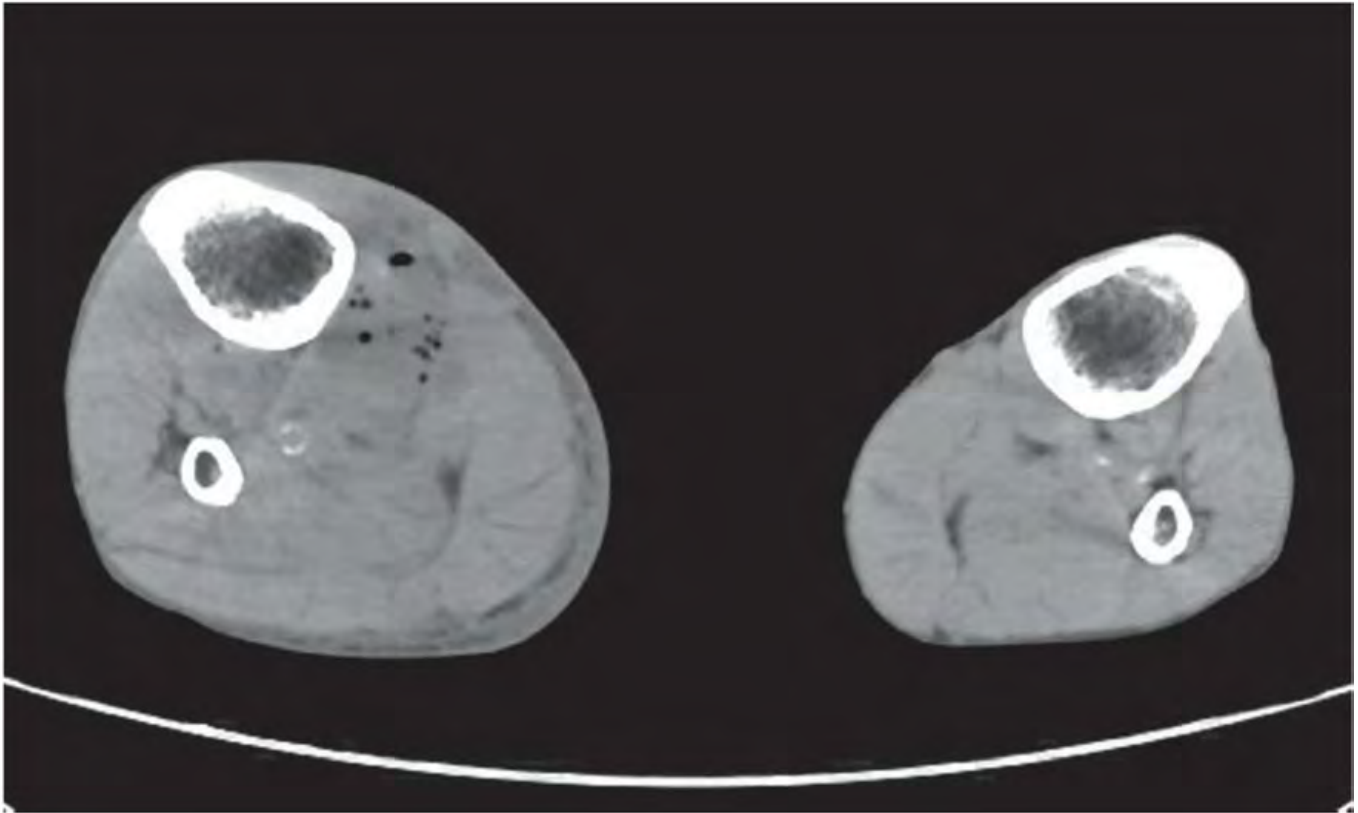


FIGURE 7.38A

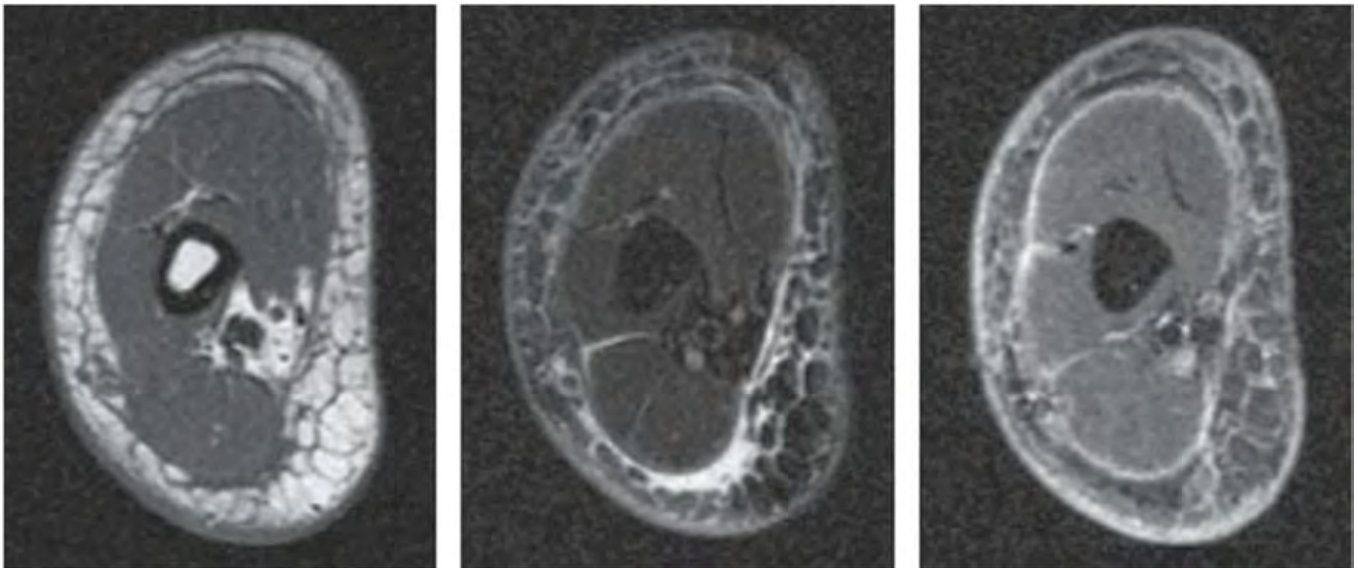


FIGURE 7.38B

## FINDINGS

- A. CT through both lower legs shows marked swelling on the right side. A collection of gas bubbles and a region of low attenuation involves the flexor digitorum longus, tibialis posterior, and soleus muscles. The subcutaneous tissues are edematous. The bones appear uninvolved. Atherosclerosis is present.
- B. Companion case. Axial T1-weighted, T2-weighted fat-suppressed, and enhanced T1-weighted fat-suppressed sequences through the upper arm in another patient with the same disease show thickened, enhancing fascial planes.

**DIFFERENTIAL DIAGNOSIS** Cellulitis, pyomyositis, necrotizing fasciitis, clostridial myonecrosis.

**DIAGNOSIS** Necrotizing fasciitis with abscess formation and cellulitis. The companion case is also necrotizing fasciitis and cellulitis, but without abscess formation.

**DISCUSSION** Necrotizing fasciitis is a severe infection involving deep fascial planes that often does not have a known causative factor or portal of entry for bacteria. Most patients have underlying conditions such as diabetes, alcoholism, or remote site of infection. These infections may progress rapidly, so rapid diagnosis and treatment is important for patient survival. The lower extremity is most commonly involved, but the process may also begin in the perineum, body wall, spine, or upper extremity. CT characteristics of necrotizing fasciitis include asymmetric fascial thickening and fat stranding, gas tracking along fascial planes, and abscesses [72]. MRI findings include thickening, high signal on T2-weighted or STIR sequences, and enhancement of the deep fascia [73]. Fluid collections, abscesses, and gas may also be present. However, findings on CT or MRI may not be present in all cases. Because the results of imaging may be nonspecific or inconclusive, correlation with clinical factors is crucial. Treatment of necrotizing fasciitis generally includes surgical debridement, and the morbidity and mortality may be significant.

**CLINICAL HISTORY** A 62-year-old immunosuppressed man with painful calf swelling.

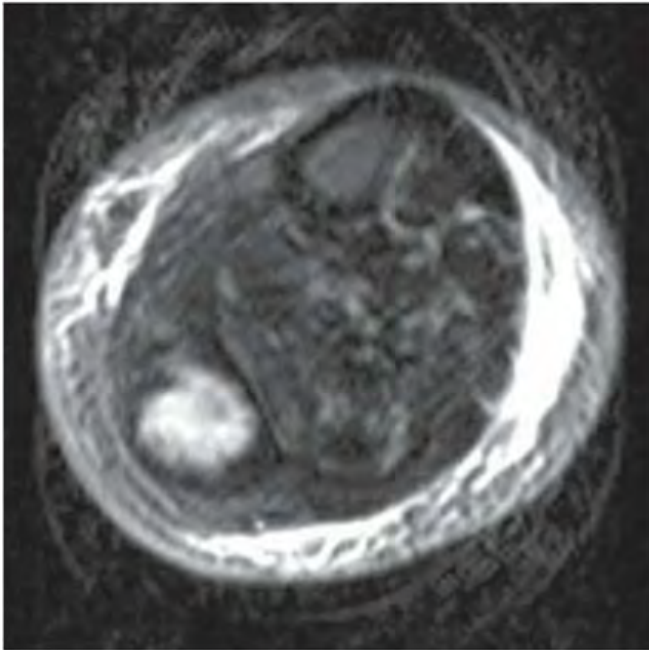


FIGURE 7.39A

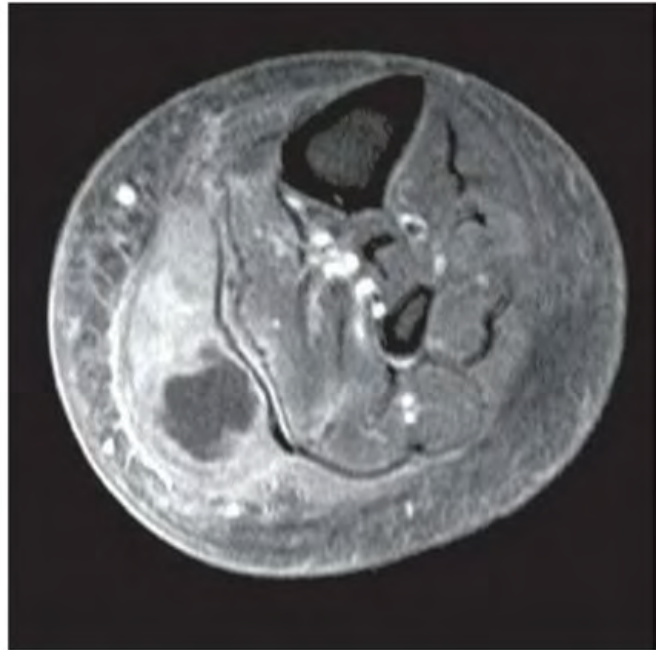


FIGURE 7.39B

### FINDINGS

- A. Axial T2-weighted, fat-suppressed MRI shows heterogeneous high signal within a focal mass in the soleus muscle. Extensive subcutaneous edema is present. The bones are not involved.
- B. Axial T1-weighted, fat-suppressed, postgadolinium MRI shows enhancement in the soleus muscle and its surrounding fascia. The high-signal collection demonstrated on T2-weighted MRI does not enhance, nor does the anterior subcutaneous edema.

**DIFFERENTIAL DIAGNOSIS** Pyomyositis with abscess, soft tissue sarcoma with necrosis or hemorrhage, muscle tear with hematoma.

**DIAGNOSIS** Pyomyositis with abscess.

**DISCUSSION** The inflammatory changes in the subcutaneous tissue and fascia would be very unusual features for a neoplasm or muscle tear. Pyomyositis, or pyogenic infection, is unusual outside of the tropics except in the setting of immunosuppression, either by drugs or the acquired immunodeficiency virus. In this case, cultures grew *Streptococci*.

Deep musculoskeletal infections are uncommon because muscle and bone are typically not exposed to pathogens in the environment, unlike the lung or gastrointestinal tract. Spontaneous infections typically follow an episode of mild trauma; presumably, there is a focus of hematoma or localized tissue necrosis that then becomes seeded hematogenously from another site. Entire muscles or muscle groups may become involved because they do not contain physical barriers to longitudinal spread of infection. Treatment is by surgical debridement and systemic antibiotics.

**CLINICAL HISTORY** A 45-year-old man with lower leg pain. A, right lower leg radiograph; B, left lower leg radiograph.



FIGURE 7.40A



FIGURE 7.40B

**FINDINGS** A, B. AP radiographs of the right (A) and left (B) lower legs demonstrate thick, solid, undulating periosteal reaction along the tibial and fibular shafts.

**DIFFERENTIAL DIAGNOSIS** Hypertrophic osteoarthropathy (HOA), venous stasis, thyroid acropachy.

**DIAGNOSIS** Hypertrophic osteoarthropathy.

**DISCUSSION** HOA classically consists of the triad of periostitis, clubbing, and arthritis. The primary (idiopathic) form of HOA (pachydermoperiostosis) is principally an autosomal dominant genetic disease. The secondary form of HOA has been observed to be associated with a wide variety of medical conditions [74]. The pathogenesis is uncertain. It is usually associated with malignant or inflammatory intrathoracic disease. Radiographically it typically produces

periosteal reaction that is symmetric and widely distributed, and involves the diaphyses of tubular bones, sparing the ends. On bone scan, it shows diffuse, symmetrically increased uptake along the cortical margins of the diaphyses of the long, tubular bones, sometimes referred to as the “parallel tract” or “double stripe” sign [75].

Thyroid acropachy is a rare complication of autoimmune thyroid disease. It can develop after thyroidectomy or radioactive iodine treatment of primary hyperthyroidism. It produces generalized and symmetric spiculated periosteal reaction that primarily involves the midportions of the diaphyses of tubular bones of the hands and feet [76]. Venous stasis, especially in the lower extremities, can result in generalized solid undulating periosteal reaction that initially can be separate from the cortex. Although not always present, clues to this diagnosis include widespread subcutaneous edema and phleboliths in varicose veins [76].

**CLINICAL HISTORY** A 12-year-old boy with ankle swelling and tenderness.



FIGURE 7.41A

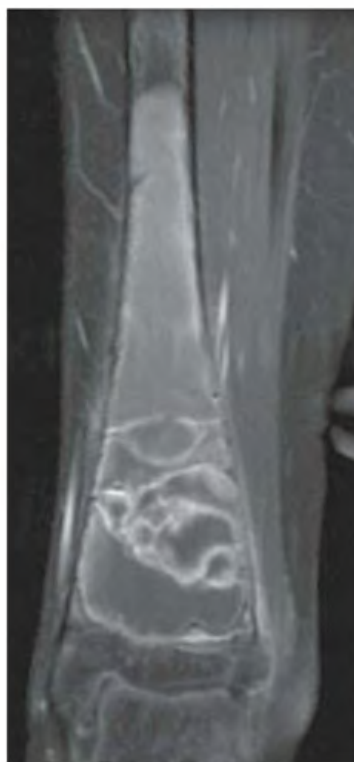


FIGURE 7.41B

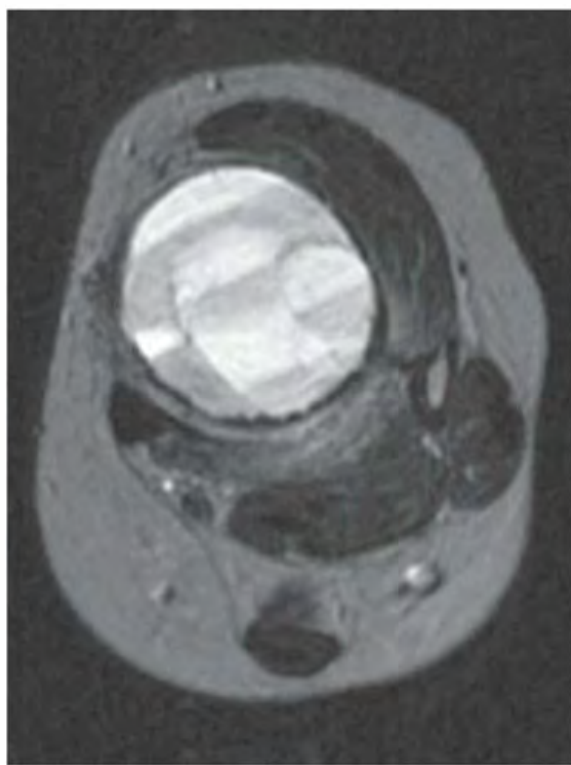


FIGURE 7.41C

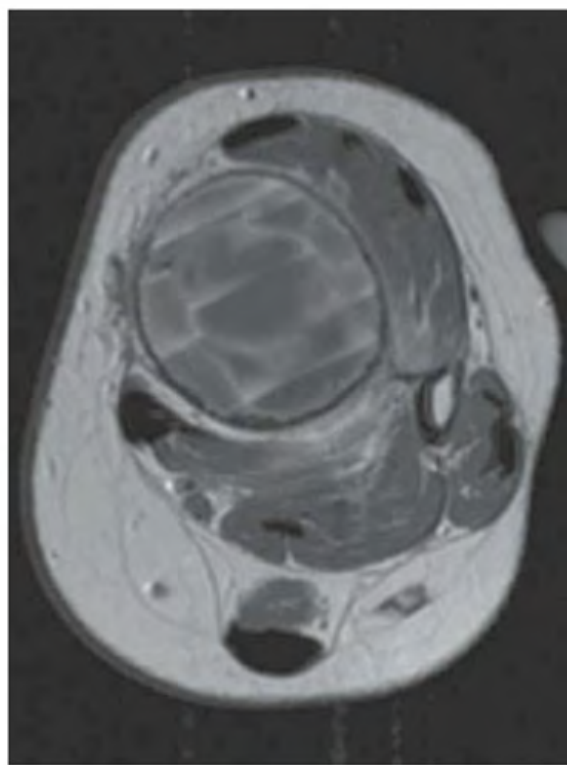


FIGURE 7.41D

**FINDINGS**

- A. Coronal T1-weighted MRI shows a long lesion in the distal tibia with mild expansion and heterogeneous internal signal.
- B. Coronal T1-weighted, fat-suppressed, postgadolinium MRI shows enhancement of the periphery of the lesion as well as complex curvilinear enhancement within its central portion.
- C. Axial T2-weighted MRI shows multiple fluid-fluid levels within the lesion, corresponding to separate compartments.
- D. Axial T1-weighted, fat-suppressed, postgadolinium MRI shows enhancement of the septations between compartments.

**DIFFERENTIAL DIAGNOSIS** Aneurysmal bone cyst, simple bone cyst.

**DIAGNOSIS** Aneurysmal bone cyst.

**DISCUSSION** Aneurysmal bone cysts are expansile, cystic lesions of bone. They probably result from a vascular disturbance caused by trauma [77] or underlying tumor. In one-third or more of cases, the pathologist can recognize an adjacent primary benign or malignant bone lesion. In this case, trauma as the antecedent event is well documented. Most cysts occur

in patients between 10 to 20 years old, and patients typically present with pain and/or swelling of less than 6-months' duration. More than 50% of aneurysmal bone cysts are found in long bones, usually metaphyseal. Twelve to thirty percent are found in the spine, often the posterior elements, and the remainder are found in the pelvis or other flat bones.

Aneurysmal bone cysts are eccentric, lucent lesions that expand the host bone and give it a blown-out or ballooned appearance (hence the term aneurysmal). Sometimes the expanded cortical shell is interrupted when periosteal bone growth is outpaced by expansion of the lesion, but the periosteum remains intact, although radiographically invisible. The walls may have trabeculations, but true bony septations are rare. Aneurysmal bone cysts may also be located centrally within a long bone, as in this case. The lesion consists of sponge-like, fibrovascular tissue, with cystic spaces or cavities filled with blood or serosanguineous fluid. The growth plate may be invaded. CT or MRI may demonstrate fluid-fluid levels, often in multiple compartments, and the periphery of the lesion and septations will enhance following contrast injection. Aneurysmal bone cysts are treated in a manner similar to giant cell tumors, unless an underlying lesion is found that should be treated more aggressively. The clinical course may vary from indolent and self-healing to rapid, relentless growth. Aneurysmal bone cysts have no metastatic potential.

**CLINICAL HISTORY** A 52-year-old woman with an incidentally identified lesion in her distal tibia.



FIGURE 7.42A



FIGURE 7.42B

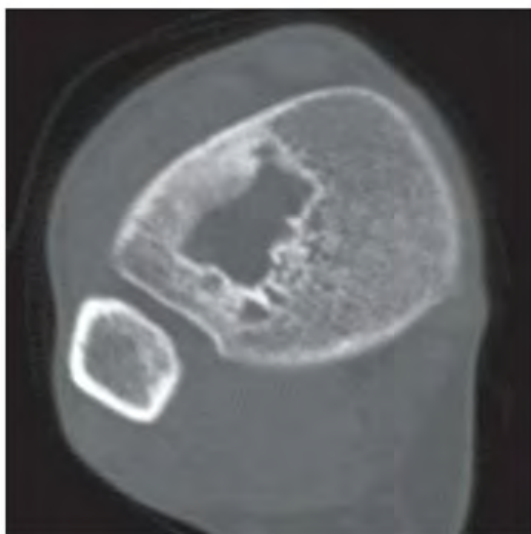


FIGURE 7.42C



FIGURE 7.42D



FIGURE 7.42E

**FINDINGS** Lateral (A) and AP (B) radiographs and axial CT (C) of the distal tibia show a well-defined lytic lesion in the distal tibial metaphysis with a thin sclerotic margin. Sagittal proton density (D) and fat-suppressed (E) MRI shows a lobulated intramedullary lesion with near-uniform suppression of signal on the fat-suppressed image, although a small focus of increased signal (cyst formation) is present anteriorly (*arrow* in E). The lesion shows a low-signal-intensity line that corresponds to the sclerotic rim on the plain radiograph.

**DIFFERENTIAL DIAGNOSIS** Bone infarct, simple bone cyst, fibrous dysplasia, intraosseous lipoma.

**DIAGNOSIS** Intraosseous lipoma.

**DISCUSSION** Intraosseous lipoma is one of the rarest primary bone tumors. It is composed of mature fat cells with

variable small quantities of fibrous and vascular tissue. Lipomas may undergo varying degrees of involution, with areas of fat necrosis, cyst formation, and dystrophic calcification [78]. Intraosseous lipomas demonstrated as geographic, radiolucent lesions with sclerotic margin and areas of calcification or trabeculation on plain radiographs. MRI and CT can be diagnostic with the identification of intralesional fat whereas radiographs can be ambiguous, especially if there is necrosis within the lesion. On radiographs, these lesions may mimic fibrous dysplasia, aneurysmal bone cysts, simple cysts, bone infarcts, and chondroid tumors [79]. Most lipomas can be managed conservatively. The main indications for surgical intervention are suspicion or evidence of malignancy although this is very rare. Other indications include cosmetic deformity or pain. Surgical treatment usually consist of curettage and packing with bone chips [80].

**CLINICAL HISTORY** A 22-year-old amateur rugby player with right ankle injury 3 weeks ago. A-B, Right achilles longitudinal and transverse sonogram; C-D, left achilles longitudinal and transverse sonogram.

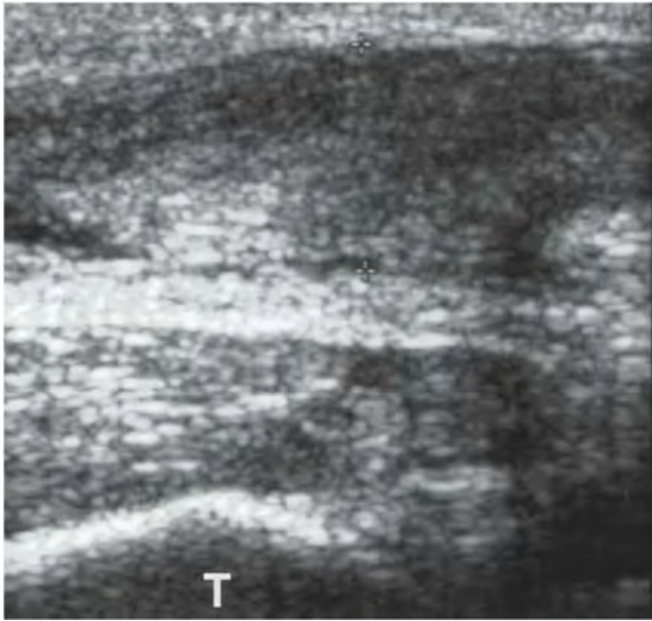


FIGURE 7.43A

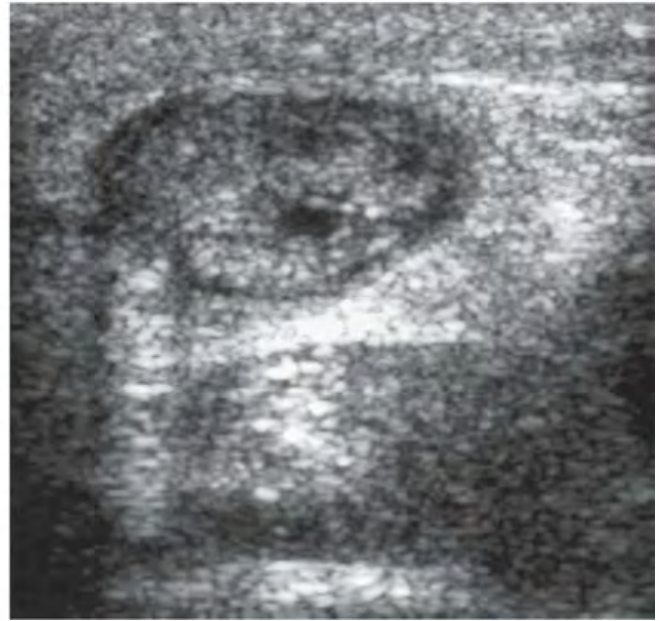


FIGURE 7.43B

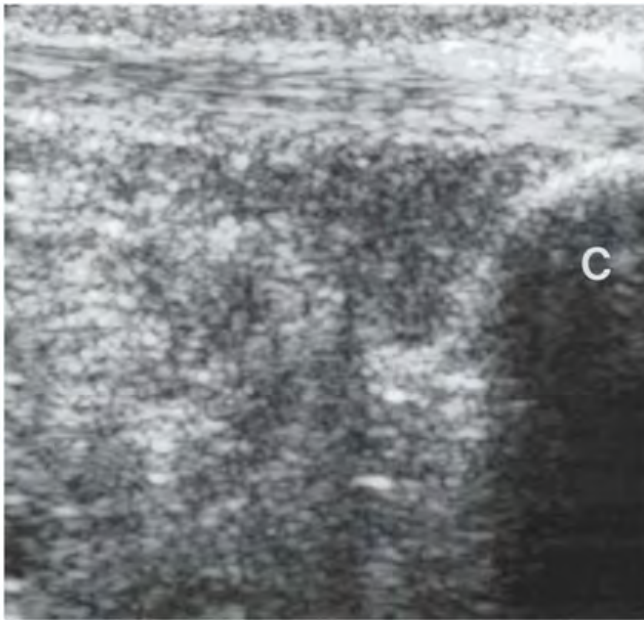


FIGURE 7.43C

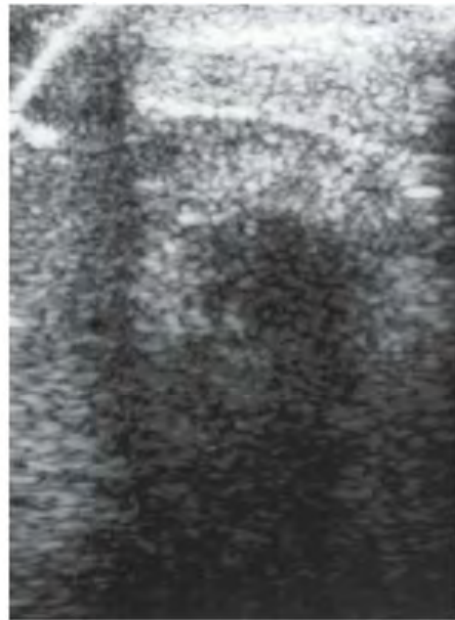


FIGURE 7.43D

**FINDINGS**

- A. Right Achilles tendon. Sonography of the Achilles tendon in the longitudinal plane, with the transducer placed on the posterior aspect of the heel cord, shows marked echogenic thickening of the entire tendon. The thickness of the tendon in the AP direction is 13 mm. No focal discontinuity of the tendon is demonstrated (T = tibia).
- B. Sonography in the transverse plane shows the enlarged, ovoid cross-section of the Achilles tendon. A discrete hypoechoic region is present within the substance of the tendon.
- C, D. Left Achilles tendon. Sonography of the uninjured contralateral Achilles tendon shows normal-thickness tendon in the longitudinal plane with slightly hypoechoic, organized, fibrillar texture. In the transverse plane, the tendon has a c-shaped cross section (C = calcaneus).

**DIFFERENTIAL DIAGNOSIS** Rupture of the Achilles tendon (partial or complete), tendinosis, hypercholesterolemia, post-surgical scar.

**DIAGNOSIS** Achilles tendinosis with partial intrasubstance tear.

**DISCUSSION** The Achilles tendon is particularly amenable to diagnostic sonography because of its superficial location, large size, and simple anatomy. The normal Achilles tendon is a flat structure with an organized, slightly hypointense fibrillar structure. Thickness of the normal Achilles tendon increases with age and height [84]. Tendinosis is indicated by thickening of the tendon, with increased sagittal diameter and sometimes focal hypoechoic regions [85,86].

Tendon rupture is diagnosed when the fibers of an enlarged tendon are interrupted by fluid, fat, or hemorrhage that fills the gap between the ends of the tear. Real-time imaging while plantar and dorsiflexing the foot can be a valuable tool in distinguishing an incomplete from a complete tear. Complete tears typically occur 3 cm proximal to the insertion on the calcaneus. Treatment options include casting or operative repair. Most surgeons favor open repair in individuals interested in continuing athletic endeavors, as the retear rate is lower in this population. One study found a correlation between recovery time and the Achilles tendon's appearance on sonography in a population of patients with achillodynia, and suggested its use as a prognostic tool [87]. Common postsurgical findings after Achilles tendon repair include hypoechoic areas within the tendon, inhomogeneous echogenicity, and loss of the fibrillar structure. These morphologic changes were not correlated with the clinical outcome of the repair [88].

**CLINICAL HISTORY** A 35-year-old man who felt pop and sharp pain while playing basketball.



FIGURE 7.44A

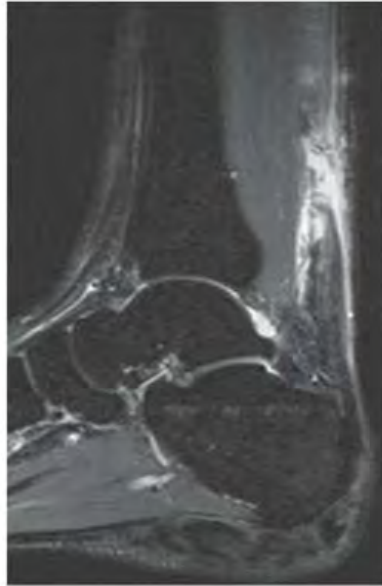


FIGURE 7.44B

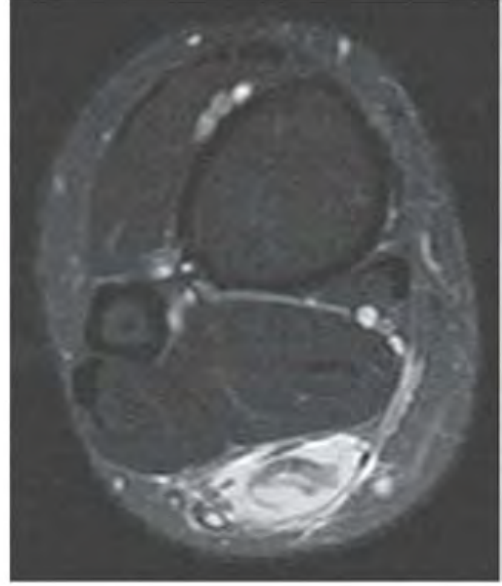


FIGURE 7.44C

## FINDINGS

- A. Sagittal T1-weighted MRI shows loss of the normally black signal intensity of the Achilles tendon between the soleus muscle belly and the calcaneal insertion.
- B, C. Sagittal inversion recovery and axial T2-weighted, fat-suppressed MRI shows discontinuity of the Achilles tendon approximately 5 cm proximal to the calcaneal attachment. The retracted margins of the tendon at the tear are thickened. Fluid (T2-weighted hyperintensity) is present through and around the tear.

**DIFFERENTIAL DIAGNOSIS** Achilles tendinosis, Achilles tendon rupture.

**DIAGNOSIS** Achilles tendon rupture.

**DISCUSSION** The Achilles tendon is formed by the merging of the superficial and deep fasciae of the gastrocnemius and soleus muscles; it inserts onto the posterior aspect of the calcaneus. The tendon itself consists of dense bundles of fibers separated by connective tissue septations (endotenon) that are continuous with the outer connective sheath (penitenon). Vessels run along the endotenon, but the blood supply is poor. The portion of the tendon with the most tenuous

blood supply is approximately 3 or 4 cm proximal to the calcaneal insertion. Spontaneous or activity-related Achilles tendon tears occur in the setting of underlying pathology. Tendon rupture may be considered to be the end point of tendinosis, a spectrum of disorders ranging from inflammation of the paratenon to partial tear and finally to complete rupture. Patients with underlying conditions, such as hyperparathyroidism, rheumatoid arthritis, renal failure, pseudohypoparathyroidism, pseudopseudohypoparathyroidism, and corticosteroid treatment, are predisposed to Achilles tendinosis and rupture, but the majority of patients who present with ruptures of the tendon have developed tendinosis while participating in sports-related activities [81]. Patients tend to be adults who participate in strenuous exercises on a limited, intermittent basis. Men are affected more than women by a ratio of approximately 3:1, and the mean age at injury in one large series was 41 years old [82]. On MRI, the normal Achilles tendon is hypointense on all imaging sequences and flattened in morphology. Partial tears appear as high-signal intratendinous collections within a thickened tendon. Complete acute ruptures appear as a discontinuity that is typically filled with fluid or granulation tissue. Chronic tendinosis appears as diffuse thickening without the increase in signal intensity [83].

## SOURCES AND READINGS

- Synder M, Vera J, Harcke HT, Bowen JR. Magnetic resonance imaging of the growth plate in late-onset tibia vara. *Int Orthop*. 2003;27:217–222.
- Iwasawa T, Inaba Y, Nishimura G, Aida N, Kameshita K, Matsubara S. MR findings of bowlegs in toddlers. *Pediatr Radiol*. 1999;29:826–834.
- Crawford AH. Neurofibromatosis. eMedicine (Jan 15, 2009). <http://emedicine.medscape.com/article/1260124-overview>.
- Rauch F, Glorieux FH. Osteogenesis imperfecta. *Lancet*. 2004;363:1377–1385.
- Therrell BL Jr, Berenbaum SA, Manter-Kapanke V, et al. Results of screening 1.9 million Texas newborns for 21-hydroxylase-deficient congenital adrenal hyperplasia. *Pediatrics*. 1998;101:583–590.
- Cattaneo R, Villa A, Catagni M, Tentori L. Limb lengthening in achondroplasia by Ilizarov's method. *Int Orthop*. 1988;12:172–179.
- De Bastiani G, Aldegheri R, Renzi-Brivio L, Trivella G. Limb lengthening by callus distraction (callotaxis). *J Pediatr Orthop*. 1987;7:129–134.
- Aldegheri R, Renzi-Brivio L, Agostini S. The callotaxis method of limb lengthening. *Clin Orthop*. 1989;241:137–145.
- Stoker DJ. Osteopetrosis. *Semin Musculoskelet Radiol*. 2002;6:299–305.
- Cheema JI, Grissom LE, Harcke HT. Radiographic characteristics of lower-extremity bowing in children. *Radiographics*. 2003;23:871–880.
- Lemyre E, Azouz EM, Teebi AS, Glanc P, Chen MF. Bone dysplasia series. Achondroplasia, hypochondroplasia and thanatophoric dysplasia: review and update. *Can Assoc Radiol J*. 1999;50:185–197.
- Case DB, Chapman CN Jr, Freeman JK, Polga JP. Best cases from the AFIP: atypical presentation of polyostotic fibrous dysplasia with myxoma (Mazabraud syndrome). *Radiographics*. 2010;30(3):827–832.
- Kransdorf MJ, Murphey MD. Diagnosis please. Case 12: Mazabraud syndrome. *Radiology*. 1999;212(1):129–132.
- McLaughlin A, Stalley P, Magee M, Soper J, Van der Wall H. Correlative imaging in an atypical case of Mazabraud syndrome. *AJR Am J Roentgenol*. 2007;189(6):W353–W356.
- Mulligan MM. Imaging in ankle fractures. eMedicine (Feb 20, 2009). <http://emedicine.medscape.com/article/398578-overview>.
- Merrill KD. The Maisonneuve fracture of the fibula. *Clin Orthop Rel Res*. 1993;(287):218–224.
- Wilson AJ, Kyriakos M, Ackerman LV. Chondromyxoid fibroma: radiographic appearance in 38 cases and in a review of the literature. *Radiology*. 1991;179:513–518.
- Robbin MR, Murphey MD. Benign chondroid neoplasms of bone. *Semin Musculoskelet Radiol*. 2000;4:45–58.
- Unni KK, Inwards CY. *Dahlin's Bone Tumors: General Aspects and Data on 10,165 Cases*. 6th ed. Philadelphia, PA: Lippincott Williams & Wilkins; 2010:286–294.
- Huvos AG, Marcove RC. Adamantinoma of long bones. A clinicopathological study of fourteen cases with vascular origin suggested. *J Bone Joint Surg Am*. 1975;57:148–154.
- Unni KK, Dahlin DC, Beabout JW, Ivins JC. Adamantinomas of long bones. *Cancer*. 1974;34:1796–1805.
- Murphey MD, Fairbairn KJ, Parman LM, Baxter KG, Parsa MB, Smith WS. Musculoskeletal angiomatous lesions: radiologic-pathologic correlation. *Radiographics*. 1995;15:893–917.
- Hudson TM. *Radiologic-Pathologic Correlation of Musculoskeletal Lesions*. Baltimore, MD: Williams & Wilkins; 1987:79–85.
- Unni KK, Inwards CY. *Dahlin's Bone Tumors: General Aspects and Data on 10,165 Cases*. 6th ed. Philadelphia, PA: Lippincott Williams & Wilkins; 2010:145–151.
- Schajowicz F, McGuire MH, Santini Araujo E, Muscolo DL, Gitelis S. Osteosarcomas arising on the surfaces of long bones. *J Bone Joint Surg Am*. 1988;70-A:555–564.
- Vanel D, Picci P, De Paolis M, Mercuri M. Radiological study of 12 high-grade surface osteosarcomas. *Skeletal Radiol*. 2001;30:667–671.
- Campanacci M. Osteofibrous dysplasia of long bones: a new clinical entity. *Ital J Orthop Trauma*. 1976;2:221–237.
- Alguacil-Garcia A, Alonso A, Pettigrew NM. Osteofibrous dysplasia of the tibia and fibula and adamantinoma. A case report. *Am J Clin Pathol*. 1984;82:420–424.
- Hazelbag HM, Van den Broeck LJ, Fleuren GJ, et al. Distribution of extracellular matrix components in adamantinoma of the long bones suggesting fibrous-to-epithelial transformation. *Hum Pathol*. 1997;28:183–188.
- Hazelbag HM, Werrels JW, Mollenomgers P, et al. Cytogenetic analysis of adamantinoma of long bones: further indications for a common histogenesis with osteofibrous dysplasia. *Cancer Genet Cytogenet*. 1997;97:5–11.
- Bridge JA, Dembrinski A, De Boer J, et al. Clonal chromosomal disorders in osteofibrous dysplasia. Implications for histopathogenesis and its relationship with adamantinoma. *Cancer*. 1994;73:1746–1752.
- Blackwell JB, McCarthy SW, Xipell JM, et al. Osteofibrous dysplasia of the tibia and fibula. *Pathology*. 1988;20:227–233.
- Bloem JL, van der Heul RO, Schuttevaer HM, et al. Fibrous dysplasia versus adamantinoma of the tibia: differentiation based on discriminant analysis of clinical and plain film findings. *AJR Am J Roentgenol*. 1991;156:1017–1023.
- Dominguez R, Saucedo J, Fenstermacher M. MRI findings in osteofibrous dysplasia. *Magn Reson Imaging*. 1989;7:567–570.
- Nakashima Y, Yamamuro T, Fujiwara Y, et al. Osteofibrous dysplasia. A study of 12 cases. *Cancer*. 1983;52:909–914.
- Ray D, Cohle SD, Lamb P. Spontaneous clostridial myonecrosis. *J Forensic Sci*. 1992;37:1428–1432.
- Migueluez M, Aguado JM. Recurrent episodes of spontaneous clostridial myonecrosis related to colorectal carcinoma. *Clin Infect Dis*. 1996;22:582–583.
- De Bastiani G, Aldegheri R, Renzi-Brivio L, Trivella G. Limb lengthening by callus distraction (callotaxis). *J Pediatr Orthop*. 1987;7:129–134.
- Nordkild P, Crone P. Spontaneous clostridial myonecrosis. A collective review and report of a case. *Ann Chirurg Gynaecol*. 1986;75:274–279.
- Stephen MB. Gas gangrene: potential for hyperbaric oxygen therapy. *Postgrad Med*. 1996;99:217–224.
- Tiegs RD. Paget's disease of bone: indications for treatment and goals of therapy. *Clin Ther*. 1997;19:1309–1329.
- Renier JC, Leroy E, Audran M. The initial site of bone lesions in Paget's disease. A review of two hundred cases. *Rev Rhum Engl Ed*. 1996;63:823–829.
- Vohra R, Kang HS, Dogra S, Saggarr RR, Sharma R. Tuberculous osteomyelitis. *J Bone Joint Surg Br*. 1997;79:562–566.
- Hugosson C, Nyman RS, Brismar J, Larsson SG, Lindahl S, Lundstet C. Imaging of tuberculosis. V. Peripheral osteoarticular and soft-tissue tuberculosis. *Acta Radiol*. 1996;37:512–516.
- Mulligan ME. The “gray cortex”: an early sign of stress fracture. *Skeletal Radiol*. 1995;24:201–203.
- Milgrom C, Giladi M, Simkin A, et al. An analysis of biomechanical mechanism of tibial stress fractures among Israeli infantry recruits. A prospective study. *Clin Orthop*. 1998;231:216–221.
- Jeske JM, Lomasney LM, Demos TC, Vade A, Bielski RJ. Longitudinal tibial stress fracture. *Orthopedics*. 1996;19:263–270.
- Swensen EJ Jr, DeHaven KE, Sebastianelli WJ, et al. The effect of pneumatic leg brace on return to play in athletes with tibial stress fractures. *Am J Sports Med*. 1997;25:322–328.
- Rettig AC, Shelbourne KD, McCarroll JR, Bisesi M, Watts J. The natural history and treatment of delayed union stress fractures of the anterior cortex of the tibia. *Am J Sports Med*. 1988;16:250–255.
- Mabit C, Pecout C. Non-union of a midshaft anterior tibial stress fracture: a frequent complication. *Knee Surg Sports Traumatol Arthrosc*. 1994;2:60–61.
- Chang PS, Harris RM. Intramedullary nailing for chronic tibial stress fractures. A review of 5 cases. *Am J Sports Med*. 1996;24:688–692.
- Bencardino JT, Rosenberg ZS, Brown RR, Hassankhani A, Lustrin ES, Beltran J. Traumatic musculotendinous injuries of the knee: diagnosis with MR imaging. *Radiographics*. 2000;20 Spec No:S103–S120.
- Menz MJ, Lucas GL. Magnetic resonance imaging of a rupture of the medial head of the gastrocnemius muscle. A case report. *J Bone Joint Surg Am*. 1991;73:1260–1262.
- Helms CA, Fritz RC, Garvin GJ. Plantaris muscle injury: evaluation with MR imaging. *Radiology*. 1995;195:201–203.

55. Stack RE, Bianco AJ, MacCarty CS. Compression of the common peroneal nerve by ganglion cysts. *J Bone Joint Surg Am.* 1965;47-A:773-778.
56. Coakley FV, Finlay DB, Harper WM, Allen MJ. Direct and indirect MRI findings in ganglion cysts of the common peroneal nerve. *Clin Radiol.* 1995;50:168-169.
57. Wang EC, Chew FS. Ruptured Peroneal Ganglion Cyst: MRI with Surgical Correlation. *Radiology Case Reports.* [Online] 2007;2:35.
58. May DA, Disler DG, Jones EA, Ballissoon AA, Manaster BJ. Abnormal signal intensity in skeletal muscle at MR imaging: patterns, pearls, and pitfalls. *Radiographics.* 2000;20 Spec No:S295-S315.
59. Boutin RD, Fritz RC, Steinbach LS. Imaging of sports-related muscle injuries. *Radiol Clin North Am.* 2002;40:333-362, vii.
60. Mentzel T, Goodlad JR, Smith MA, et al. Ancient hematoma: a unifying concept for a post-traumatic lesion mimicking an aggressive soft tissue neoplasm. *Mod Pathol.* 1997;10:334-340.
61. Ryre KN, Bae DK, Park YK, et al. Calcific tenosynovitis associated with calcific myonecrosis of the leg: imaging features. *Skeletal Radiol.* 1996;25:273-275.
62. Broder MS, Worrell RV, Shafi NQ. Cystic degeneration and calcification following ischemic paralysis of the leg. *Clin Orthop.* 1977;122:193-195.
63. Janzen DL, Connell DG, Vaisler BJ. Calcific myonecrosis of the calf manifesting as an enlarging soft tissue mass: imaging features. *AJR Am J Roentgenol.* 1993;160:1072-1074.
64. O'Keefe RJ, O'Connell JX, Temple HT, et al. Calcific myonecrosis. A late sequela to compartment syndrome of the leg. *Clin Orthop.* 1995;318:205-213.
65. Malisano LP, Hunter GA. Liquefaction and calcification of a chronic compartment syndrome of the lower limb. *J Orthop Trauma.* 1992;6:245-247.
66. Bjorksten B, Boquist L. Histopathological aspects of recurrent multifocal osteomyelitis. *J Bone Joint Surg Br.* 1980;62-B:376-380.
67. Gamble JG, Rinsky LA. Chronic recurrent multifocal osteomyelitis: a distinct clinical entity. *J Pediatr Orthop.* 1986;6:579-584.
68. Chun CS. Chronic recurrent multifocal osteomyelitis of the spine and mandible: case report and review of the literature. *Pediatrics.* 2004;113:380-384.
69. Fujitake J, Ishikawa Y, Fujii H, Nishimura K, Hayakawa K, Tatsuoka Y. Magnetic resonance imaging of skeletal muscles in the polymyositis. *Muscle Nerve.* 1997;20:1463-1466.
70. Schweitzer ME, Fort J. Cost-effectiveness of MR imaging in evaluating polymyositis. *AJR Am J Roentgenol.* 1995;165:1469-1471.
71. Schweitzer ME, Fort J. Cost-effectiveness of MR imaging in evaluating polymyositis. *AJR Am J Roentgenol.* 1995;165:1469-1471.
72. Wysocki MG, Santora TA, Shah RM, Friedman AC. Necrotizing fasciitis: CT characteristics. *Radiology.* 1997;203:859-863.
73. Schmid MR, Kossman T, Duewell S. Differentiation of necrotizing fasciitis and cellulitis using MR imaging. *AJR Am J Roentgenol.* 1988;170:615-620.
74. Yao Q, Altman RD, Brahn E. Periostitis and hypertrophic pulmonary osteoarthropathy: report of 2 cases and review of the literature. *Semin Arthritis Rheum.* 2009;38:458-466.
75. Ali A, Tetalman MR, Fordham EW, et al. Distribution of hypertrophic pulmonary osteoarthropathy. *AJR Am J Roentgenol.* 1980;134:771-780.
76. Rana RS, Wu JS, Eisenberg RL. Periosteal reaction. *AJR Am J Roentgenol.* 2009;193:W259-W272.
77. Moore TE, King AR, Travis RC, Allen BC. Post-traumatic cysts and cyst-like lesions of bone. *Skeletal Radiol.* 1989;18:93-97.
78. Milgram JW. Intraosseous lipomas. A clinicopathologic study of 66 cases. *Clin Orthop Relat Res.* 1988:277-302.
79. Propeck T, Bullard MA, Lin J, Doi K, Martel W. Radiologic-pathologic correlation of intraosseous lipomas. *AJR Am J Roentgenol.* 2000;175:673-678.
80. Campbell RS, Grainger AJ, Mangham DC, Beggs I, Teh J, Davies AM. Intraosseous lipoma: report of 35 new cases and a review of the literature. *Skeletal Radiol.* 2003;32:209-222.
81. Newnham DM, Douglas JG, Legge JS, Friend JA. Achilles tendon rupture: an underrated complication of corticosteroid treatment. *Thorax.* 1991;46:853-854.
82. Levi N. The incidence of Achilles tendon rupture in Copenhagen. *Injury.* 1997;28:311-313.
83. Tuite MJ. MR imaging of the tendons of the foot and ankle. *Semin Musculoskelet Radiol.* 2002;6:119-131.
84. Koivunen-Niemela T, Parkkola K. Anatomy of the Achilles tendon (tendo calcaneus) with respect to tendon thickness measurements. *Surg Radiol Anat.* 1995;17:263-268.
85. Kainberger FM, Engel A, Barton P, Huebsch P, Neuhold A, Salomonowitz E. Injury of the Achilles tendon: diagnosis with sonography. *AJR Am J Roentgenol.* 1990;155:1031-1036.
86. Astrom M, Gentz CF, Nilsson P, Rausing A, Sjoberg S, Westlin N. Imaging in chronic Achilles tendinopathy: a comparison of ultrasonography, magnetic resonance imaging and surgical findings in 27 histologically verified cases. *Skeletal Radiol.* 1996;25:615-620.
87. Archambault JM, Wiley JP, Bray RC, Verhoef M, Wiseman DA, Elliott PD. Can sonography predict the outcome in patients with achilodynia? *J Clin Ultrasound.* 1998;26:335-339.
88. Rupp S, Templehof S, Fritsch E. Ultrasound of the Achilles tendon after surgical repair: morphology and function. *Br J Radiol.* 1995;68:454-458.

CHAPTER

# 8

## **Ankle and Foot**

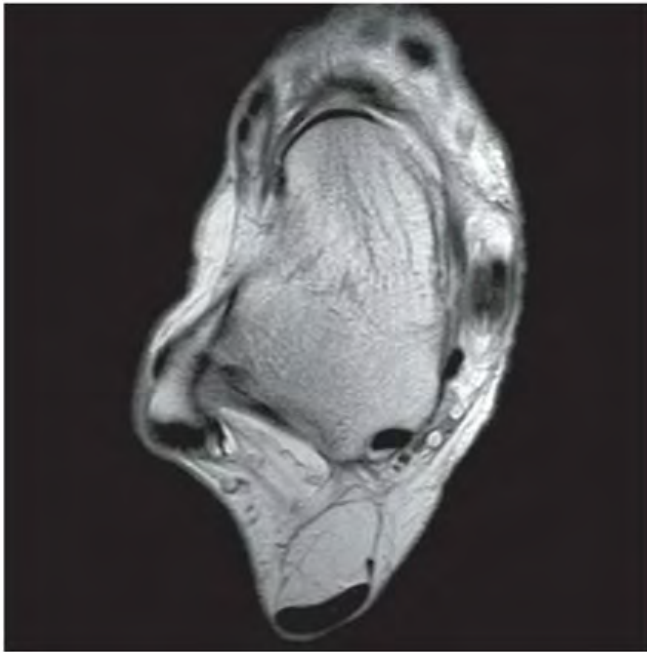


FIGURE 8.1A

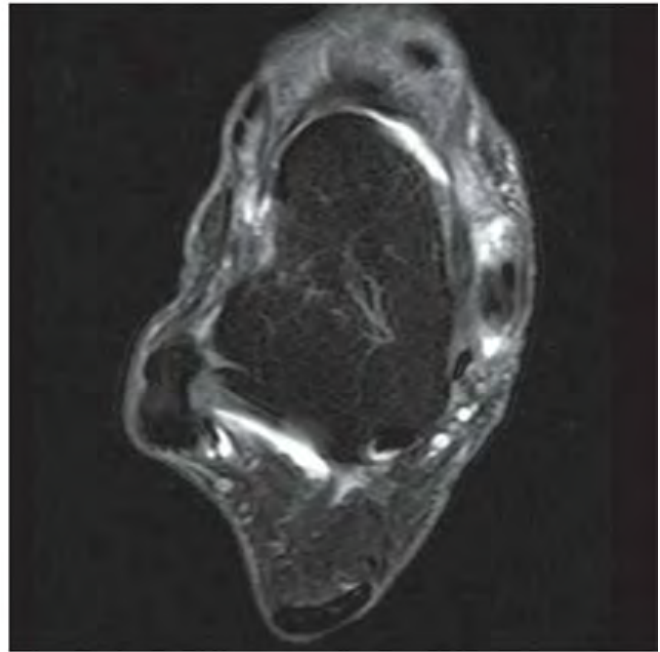


FIGURE 8.1B

**FINDINGS** (A) Axial proton density and (B) T2-weighted, fat-suppressed magnetic resonance images (MRI) of the ankle show a thickened and split posterior tibial tendon (PTT). There is increased T2-weighted signal within the tendon with surrounding fluid in the sheath.

**DIFFERENTIAL DIAGNOSIS** None.

**DIAGNOSIS** PTT longitudinal split tear.

**DISCUSSION** The PTT is the largest and thickest of the three medial flexor tendons. The tendon courses under the medial malleolus and attaches to the medial navicular bone, the three cuneiforms, and the bases of the first to fourth metatarsals. Most PTT tears occur at the level of the medial malleolus. This tendon is one of the primary arch supporters for the foot. Tears of this tendon can cause flatfoot deformity and significant chronic pain and osteoarthritis [1]. Sinus tarsi syndrome has been described in association with PTT tear [2].



FIGURE 8.2

**FINDINGS** Anteroposterior (AP) ankle radiograph shows an intra-articular fracture plane extending vertically through the medial aspect of the tibia, passing through the epiphysis, growth plate, and metaphysis, and separating the medial malleolus from the remainder of the tibia.

**DIFFERENTIAL DIAGNOSIS** None.

**DIAGNOSIS** Salter type IV fracture, medial malleolus.

**DISCUSSION** Salter type IV fractures pass through the metaphysis, growth plate, and epiphysis. In this case, a vertical

fracture in the sagittal plane can be seen passing through these three structures. These fractures require accurate open reduction and internal fixation (ORIF), because misalignment of the principal fragments would allow a bone bridge to form across the growth plate [3]. Such a bone bridge would tether the growth plate on one side and result in a progressive varus deformity as the open, lateral portion of the growth plate continued to lengthen the bone. The potential for deformity is greater in young children, who have a longer remaining growth period. The risk of complications is high if the fracture has more than 2 mm of displacement. A Salter type I or type II fracture of the fibula may be associated with this injury.

**CLINICAL HISTORY** *A 14-year-old boy with lacrosse injury.*



FIGURE 8.3A



FIGURE 8.3B



FIGURE 8.3C



FIGURE 8.3D



FIGURE 8.3E

**FINDINGS** (A, B) AP, lateral radiographs, (C) sagittal, (D) coronal reformatted, and (E) three-dimensional volume rendering computed tomography (CT) of the right ankle demonstrate a vertical fracture through the epiphysis that runs from anterior to posterior, and an oblique fracture through the posterior distal tibial metaphysis. The medial malleolus is intact, as is the lateral metaphysis. The central part of the distal tibial growth plate is closed, the most medial portion of the growth plate is open, and the lateral portion is abnormally widened.

**DIFFERENTIAL DIAGNOSIS** Salter type II fracture, Salter type III fracture, Salter type IV fracture, juvenile Tillaux fracture, triplane fracture.

**DIAGNOSIS** Triplane fracture.

**DISCUSSION** The radiographs and CT show fractures of the distal tibia that appear to involve the growth plate. One fracture component extends through the metaphysis in the oblique coronal plane, and one fracture extends through the epiphysis in the sagittal plane. Because the fracture through the growth plate that connects the metaphyseal and epiphyseal fractures is in the axial plane, the components of this fracture occur in three different planes, defining the diagnosis of a triplane fracture. The triplane fracture has elements of Salter type II and type III fractures, and because it crosses the epiphysis, growth plate, and metaphysis, it can also be considered a Salter type IV fracture. The juvenile

Tillaux fracture, in comparison, is a fracture in which the anterolateral aspect of the tibia epiphysis is avulsed by tension from the anterior tibiofibular ligaments during external rotation of the foot; the juvenile Tillaux fracture can be classified as a Salter type III fracture.

Triplane fractures only occur when physeal closure of the distal tibia is incomplete [4,5]. The distal tibial growth plate begins to close centrally, then medially, and finally laterally. Plantar flexion and external rotation are believed to be the mechanisms of injury in the triplane fracture, in which the lateral fragment of tibia that includes a portion of the epiphysis and metaphysis is avulsed by tension on the tibiofibular ligaments. Fracture of the fibula may accompany these injuries. When the separated epiphysis has two fragments, one of which has a portion of posterior tibial metaphysis attached to it and the other comprises a fragment of the medial epiphysis, a three-part triplane fracture is produced. Three-part fractures are usually more severe than two-part fractures, since there is greater displacement of the epiphyseal fragments. ORIF is used more frequently for three-part injuries.

The mean age at the time of fracture is about 15 years in boys and 13 years in girls, with a range from about 12 to 17 years in boys and 10 to 15 years in girls. Triplane fractures comprise 15% and 7% of ankle fractures in boys and girls under the age of 18 years, respectively, but the proportion would be much higher in the age range in which these fractures occur. If an epiphyseal gap of 3 mm or greater remains after ORIF, there is a greater risk of premature physeal closure [6].

**CLINICAL HISTORY** A 4-year-old boy who refuses to walk. A-B, 2 weeks after presentation; C-F, 6 weeks after presentation.



FIGURE 8.4A



FIGURE 8.4B



FIGURE 8.4C



FIGURE 8.4D



FIGURE 8.4E



FIGURE 8.4F

## FINDINGS

- A, B. Lateral and AP radiographs taken 2 weeks after initial presentation demonstrate a faint oval lucency of the distal tibial metaphyses with surrounding sclerosis. Soft tissue swelling is noted. Initial radiographs taken 2 weeks earlier were normal (not shown).
- C, D. Radiographs taken 6 weeks after presentation show that the lucency has grown larger and more defined. Periosteal reaction extends up the shafts of the tibia and fibula. The soft tissue swelling is marked.
- E, F. T2-weighted MRI taken 6 weeks after presentation demonstrates a focal area of increased signal in the distal tibial metaphysis, adjacent to but not crossing the growth plate, corresponding to the lucency noted on plain film. An ankle effusion and soft tissue edema is evident.

**DIFFERENTIAL DIAGNOSIS** Growth plate fracture; osteomyelitis caused by pyogenic, granulomatous, or fungal organism; malignant tumor such as osteosarcoma, lymphoma, or Ewing sarcoma.

**DIAGNOSIS** Atypical mycobacterium osteomyelitis.

**DISCUSSION** A growth plate fracture of the tibia in an otherwise healthy child should be healed at 6 weeks, although at 2-week follow-up, Salter type I fracture might show widening

of the growth plate and sclerosis on the metaphyseal side. The asymmetry of the widening and sclerosis would be unusual for trauma. The enlarging lucency in the metaphysis suggests a destructive process such as osteomyelitis or tumor. The location at the distal metaphysis is appropriate for hematogenous osteomyelitis, but the modesty of the reactive bone and the lack of involvement of the physis and epiphysis at the end of 6 weeks would be uncharacteristic of pyogenic osteomyelitis. The small size of the lesion would be distinctly unusual for a primary malignant bone tumor such as osteosarcoma, lymphoma, or Ewing sarcoma, although the metaphyseal sclerosis could represent neoplastic bone. The diagnosis in this case was confirmed at open biopsy. The lucency consisted of a fluid-filled cystic space, and cultures of the fluid were positive.

Nontuberculous mycobacterial musculoskeletal infections may take the form of tenosynovitis, synovitis, or osteomyelitis [7]. The spectrum of pathologic findings includes virtually no inflammation, mild-to-severe nonspecific chronic infection, granulomas without necrosis, and caseating epithelioid granulomas indistinguishable from tuberculosis. These pathologic changes explain the blandness of the imaging features in this case. Multiple lesions in the metaphyses and diaphyses, sinus tracts, and osteoporosis are other features of atypical mycobacterial infections. Joint space narrowing, as in tuberculosis, is a late finding. Delays in the diagnosis of atypical mycobacterial osteomyelitis are common, and the disease may be multifocal. These infections occur in both immunocompromised as well as immunocompetent individuals [8].



FIGURE 8.5A

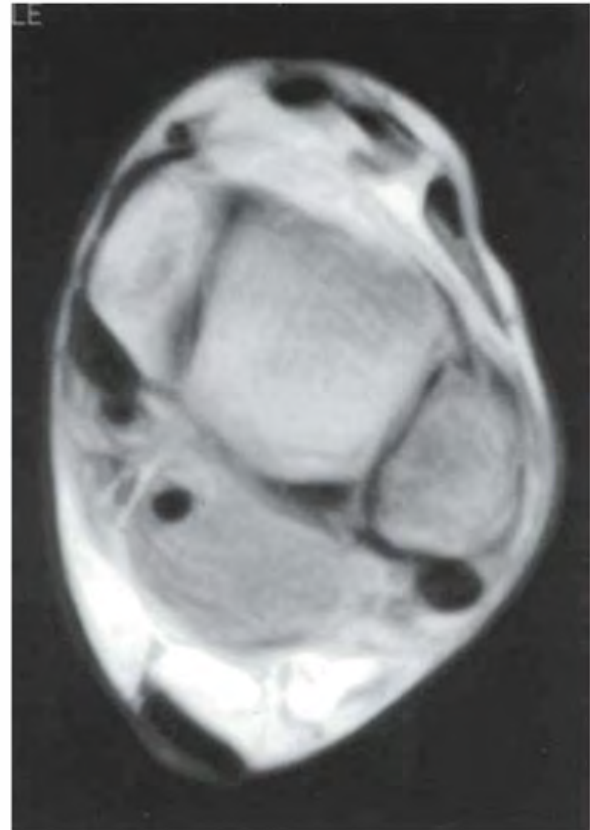


FIGURE 8.5B

### FINDINGS

- A. Sagittal T1-weighted MRI shows a mass in the distal soleus muscle, extending inferiorly along the deep aspect of the Achilles tendon and abutting the posterior aspect of the tibia and ankle. The mass has a lobular contour and heterogeneous intermediate signal intensity.
- B. Axial T1-weighted MRI at the level of the ankle joint shows the lesion in the posterior soft tissues, adjacent to the joint and surrounding the tendon of the flexor hallucis longus. The underlying bone is normal.

**DIFFERENTIAL DIAGNOSIS** Soft tissue sarcoma, extraskeletal Ewing sarcoma, lymphoma, benign soft tissue tumor, myotendinous injury, myositis ossificans, hematoma.

**DIAGNOSIS** Extraskeletal primitive neuroectodermal tumor (PNET).

**DISCUSSION** The finding of a large, lobulated, soft tissue mass in the deep tissues of the extremity of an adult is always cause for concern. There are no specific features on imaging that lead to the diagnosis in this case, but myotendinous injury, hematoma, and myositis ossificans are possibilities that should have a suggestive history (lacking in this case).

The age of the patient is less than the peak incidence for a mesenchymal soft tissue sarcoma. A biopsy is necessary for diagnosis.

PNET is a sarcoma of neuroectodermal origin. It appears closely related to Ewing sarcoma in histogenesis [9], with an appearance on light microscopy that may be indistinguishable (small, round, blue cells). Although both Ewing sarcoma and PNET may be primary to bone or soft tissue, Ewing sarcoma is much more likely to occur in bone, whereas PNET has an equal incidence in bone and soft tissue. Most patients with PNET are between 10 and 30 years old, with the most common soft tissue sites being the paravertebral region, the chest wall (called in this circumstance an Askin tumor), the retroperitoneum, and the lower extremities. Soft tissue PNETs present as rapidly enlarging soft tissue masses. Findings on imaging are nonspecific, and PNET is indistinguishable from Ewing sarcoma on imaging [10]. The margins of the tumor may be well defined, as in this case, and sometimes encapsulated, or they may appear infiltrative. Areas of hemorrhage may be present, and contrast enhancement on MRI is typically intense. The treatment of PNET is chemotherapy and surgical resection, sometimes with radiation therapy as well. The prognosis for patients with PNET is less favorable than for patients with Ewing sarcoma [11].



FIGURE 8.6A

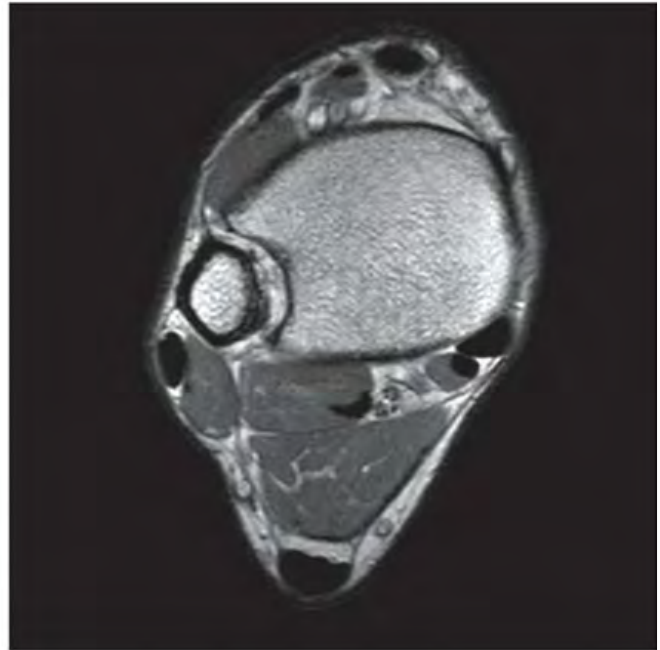


FIGURE 8.6B



FIGURE 8.6C

### FINDINGS

- A. Lateral radiograph of the ankle demonstrates soft tissue mass partially occupying the Kager's fat pad, posterior to the flexor hallucis longus.
- B, C. Axial and sagittal T1-weighted MRI shows accessory muscle anterior to the Achilles tendon.

**DIFFERENTIAL DIAGNOSIS** None.

**DIAGNOSIS** Accessory soleus muscle.

**DISCUSSION** According to cadaveric studies, an accessory soleus has a prevalence of 0.7% to 5.5%, with the muscle most commonly seen as a unilateral finding [12]. It arises from the deep surface of the soleus or from the fibula and the tibia. From its origin, the muscle descends anterior or anteromedial to the Achilles tendon. The accessory soleus is generally enveloped within its own fascia and derives its blood supply from the posterior tibial artery. The posterior tibial nerve supplies both the soleus proper and the accessory soleus muscle [13].

An accessory soleus may manifest clinically as a soft tissue mass in the ankle. Clinically evident accessory soleus muscles have a male predilection and commonly manifest in the 2nd and 3rd decades of life. On cross-sectional imaging the accessory muscle is demonstrated anterior to the Achilles tendon and superficial to the flexor retinaculum, typically extending medially to the area between the medial edge of the Achilles tendon and the medial malleolus. Treatment usually depends on the presence or severity of the symptoms. For symptomatic patients, conservative treatment or surgical approaches including fasciotomy or excision of the muscle can be performed [14].

**CLINICAL HISTORY** A 28-year-old woman with ankle sprain.

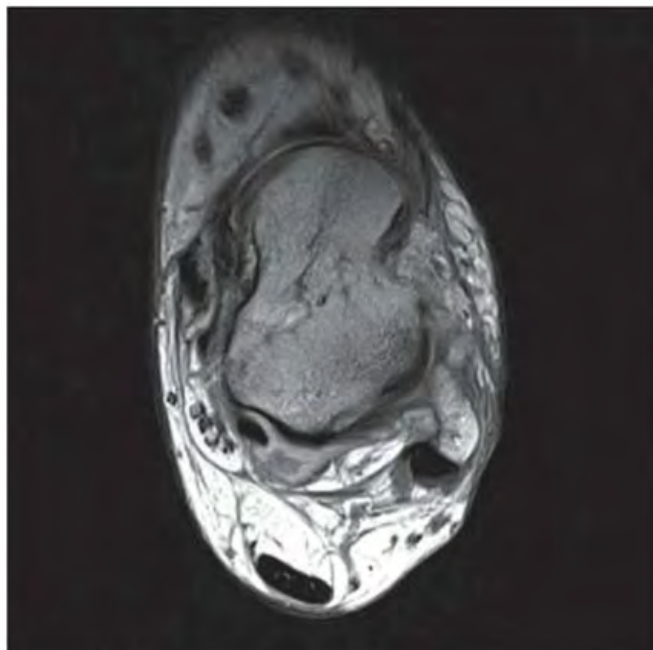


FIGURE 8.7A



FIGURE 8.7B

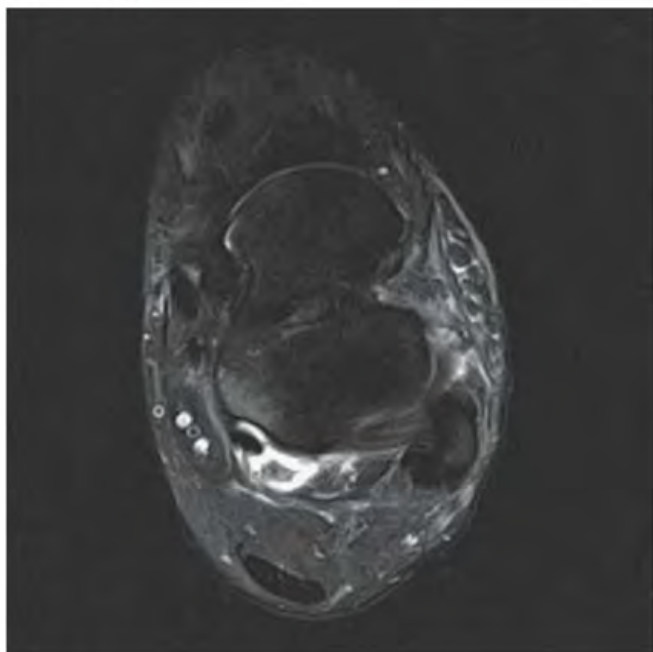


FIGURE 8.7C

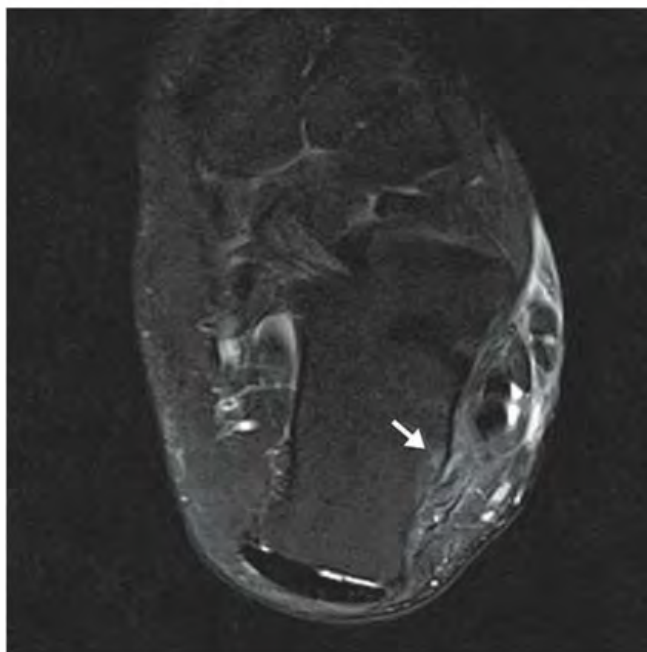


FIGURE 8.7D

**FINDINGS** (A, B) Axial proton density and (C, D) T2-weighted fat-suppressed MRI demonstrates complete tear of anterior talofibular (ATF) ligament surrounded by fluid signal. The calcaneofibular (CF) ligament is also torn underneath the peroneus tendon sheath. The posterior talofibular (PTF) ligament shows increased signal intensity with preserved fibers consistent with sprain. Also, noted is bone marrow edema in the posterior talus and peroneal tubercle of calcaneus.

**DIFFERENTIAL DIAGNOSIS** None.

**DIAGNOSIS** Lateral ankle ligament tear.

**DISCUSSION** The lateral collateral ligament complex is made up of three ligaments: the ATF, CF, and PTF ligaments. Injuries to this complex are very common, especially

in the young, active population. Of these ligaments, the ATF ligament is the weakest and most easily torn. As inversion stress increases, the CF ligament becomes torn. PTF ligament injury is uncommon, and is almost always associated with injury to both the ATF and CF ligaments. Acute grade I and II tears, stretching and partial tears, are often treated conservatively. The treatment of grade III tears, complete rupture of a ligament, is more controversial. Regardless of the treatment, the prognosis of most ankle sprains is quite good. Unfortunately, 10% to 20% of patients develop chronic instability [15]. MR arthrography of the ankle has been shown to be a highly sensitive modality for detecting and accurately staging lateral ankle ligament tears. MR arthrography allows the evaluation of the torn free ends of the ligaments to assess the feasibility of primary repair and the evaluation of adjacent structures, which may potentially be used in surgical reconstruction [16].



FIGURE 8.8A



FIGURE 8.8B

**FINDINGS**

- A. Oblique and AP radiographs of the foot demonstrate wavy, dense sclerosis beginning in the calcaneus, involving the cuboid, and extending through the third and fourth metatarsals and toes.
- B. Long-axis CT shows the sclerosis involving the cortex and medullary canal. There is no soft tissue mass or bone destruction.

**DIFFERENTIAL DIAGNOSIS** Melorheostosis, trauma, chronic osteomyelitis, osteosarcomatosis.

**DIAGNOSIS** Melorheostosis.

**DISCUSSION** Melorheostosis is a disorder of unknown cause that can present at any age. The most common appearance is cortical hyperostosis that can be likened to dripping candle wax. Involvement is usually limited to a single extremity and is often along a sclerotomal distribution [17], in this case L5. When the soft tissues are involved, muscle and tendon contractures can lead to skeletal deformities such as scoliosis and growth disturbances. Most patients are asymptomatic, but this condition can be painful [18]. Diseases associated with melorheostosis include osteopoikilosis, osteopathia striata, neurofibromatosis, and tuberous sclerosis. Treatment is most often surgical, to correct deformities and remove soft tissue masses [19].



FIGURE 8.9A



FIGURE 8.9B

### FINDINGS

- A. AP radiograph of the ankle shows epiphyseal overgrowth, flattening of the talar dome, sclerosis, and cystic changes. A 1-cm lucency with sclerotic borders is noted in the medullary space of the talus.
- B. CT of both ankles demonstrates a well-defined ovoid lucent lesion in the right talus with surrounding sclerosis. The lesion has soft tissue attenuation within. Articular irregularity is present at the dome of the talus, and the talus appears mildly contracted in size compared with the contralateral asymptomatic side. Soft tissue density within the ankle joint may represent fluid or synovial hypertrophy.

**DIFFERENTIAL DIAGNOSIS** Hemophilia, juvenile idiopathic arthritis, septic arthritis, sickle cell disease.

**DIAGNOSIS** Hemophilic pseudotumor.

**DISCUSSION** Abnormality of the articular surface of bone associated with synovial hypertrophy in a pediatric patient can be seen in juvenile idiopathic arthritis, hemophilia, and the rheumatoid-negative spondyloarthropathies. The cystic lesion is remote from the subarticular bone, which would be unusual for a subchondral cyst in the arthritic conditions mentioned, but could represent a pseudotumor from intraosseous hemorrhage in hemophilia.

Intraosseous bleeding and the subsequent inflammatory reaction that clears the hemorrhage may create radiolucent

defects in bone, called pseudotumors. Repeated bleeding into a pseudotumor may cause it to recur and enlarge, simulating malignancy. Osteonecrosis or osteomyelitis in the setting of sickle cell disease involving the talus may have a similar appearance to this case. Septic arthritis may also result in osteomyelitis and osteonecrosis. Radiographic manifestations in hemophilia may be strikingly similar to certain arthritic conditions, particularly juvenile idiopathic arthritis. Because the pathomechanical basis for these findings differs (intra-articular hemorrhage with secondary inflammation versus chronic inflammation without hemorrhage), features specific for hemorrhage should be sought when attempting to distinguish between these diagnoses. The obvious differential point is the presence of a hemorrhagic effusion, which can be ascertained on MRI, but other differentiating features include localized periosteal reaction due to subperiosteal hemorrhage and pseudotumor due to intraosseous hemorrhage.

Soft tissue hemorrhage may result in a soft tissue pseudotumor, which can cause pressure erosions and scalloping on the adjacent bone with or without exuberant periosteal reaction, again simulating neoplasm. Most pseudotumors arise near the large bones of the proximal skeleton in adults, but in younger patients, before skeletal maturity, they tend to occur distal to the wrist or ankle. Distal pseudotumors usually respond well to conservative management, whereas resection is often the treatment of choice for proximal pseudotumors [20]. Large proximal pseudotumors may lead to life-threatening hemorrhage. Emergent surgical treatment carries a significant intraoperative mortality.



FIGURE 8.10A



FIGURE 8.10B

**FINDINGS** (A, B) Lateral and mortise radiographs of the ankle show disordered mineralization in the distal tibial epiphysis. The epiphysis is ossifying from multiple centers. There is a dense horizontal line of sclerosis across the distal tibial metaphysis. The ossification patterns in the medial and lateral malleoli are also disordered.

**DIFFERENTIAL DIAGNOSIS** Osteonecrosis, epiphyseal dysplasia, trauma, osteomyelitis.

**DIAGNOSIS** Osteonecrosis in sickle cell disease.

**DISCUSSION** The appearance of the epiphysis with multiple centers of ossification is that of revascularized osteonecrosis. In this case, the patient was known to have sickle cell disease, and the clinical question was the cause of his ankle pain. Sickle cell disease is caused by an inherited structural defect in hemoglobin that leads to red cell dysfunction. The radiologic features of sickle cell disease in bone are the result of bone marrow hyperplasia, vascular occlusion, and osteomyelitis [21]. Hyperplasia of the bone marrow expands the marrow space. Vascular occlusion results in osteonecrosis. Any portion of any bone may be infarcted; frequent sites include

the medullary space of long bones, growing epiphyses, and the hands. Involvement of growing epiphyses leads to growth disturbances. If the femoral head is involved, the pathophysiologic events and sequelae are indistinguishable from those of Legg-Calvé-Perthes disease. A growth disturbance in the vertebral body leads to development of H-shaped vertebrae. Localized infarctions of bone with repair or dystrophic calcification result in focal areas of bony sclerosis scattered about the skeleton.

Patients with sickle cell disease have a high incidence of osteomyelitis. Unlike hematogenous osteomyelitis in other situations, the infection in sickle cell disease is most frequent at the diaphysis of the long bones, where the oxygen tension is lowest. In approximately 50% of cases, *Salmonella* species or mixed flora are the causative organisms (their presence is exceedingly unusual under any other circumstance); the remaining cases are usually caused by *Staphylococcus* species. Chronicity and recurrence are common. Osteomyelitis may be difficult to differentiate from infarction on both clinical and radiologic grounds [22,23]; either one can be a complication of the other. The radiographic signs of osteomyelitis would superimpose on whatever preexisting bone changes existed from the sickle cell disease.

**CLINICAL HISTORY** A 63-year-old man with newly diagnosed prostate cancer.



FIGURE 8.11A



FIGURE 8.11B



FIGURE 8.11C

## FINDINGS

- A. Whole-body radionuclide bone scan demonstrates increased uptake in several locations, with particular involvement of the ends of the bones (bilaterally in the tibiae, distal femurs, right proximal humerus, tali, and left distal femoral shaft). The sites of involvement are relatively large. The axial skeleton appears spared.
- B, C. Two radiographic views of the distal right tibia demonstrate a lesion with a lacy calcified matrix and a sclerotic serpiginous rind. There is no cortical expansion or penetration.

**DIFFERENTIAL DIAGNOSIS** Metastases, enchondroma, marrow infarction (osteonecrosis).

**DIAGNOSIS** Marrow infarction.

**DISCUSSION** Metastases typically involve the axial skeleton more than the appendicular skeleton. Lesions in the ankle and feet are unusual. Metastases also tend to be focal and discrete. Enchondroma and marrow infarcts can demonstrate radionuclide accumulation on bone scans. Accumulation in enchondromas is a reflection of reactive bone formation and

enchondral ossification. Accumulation in infarcts is a reflection of repair and remodeling after revascularization. During the ischemic phase of marrow infarction, the bone scan may be cold or normal. Enchondroma and marrow infarction may have a similar radiographic appearance. The serpiginous rind of calcification and the location at the end of the bone is more suggestive of marrow infarction than enchondroma, and the multifocal involvement is more common in marrow infarction than in enchondroma.

There are multiple potential causes for marrow infarction, including exogenous steroids, alcoholism, sickle cell disease, trauma, Gaucher disease, and pancreatitis. Abnormal fat metabolism in alcoholism and pancreatitis is believed to cause osteonecrosis by fat embolism. On MRI, medullary infarcts are usually multiple and have a diagnostic appearance. They have an irregular, serpiginous, sharply defined, low-signal border on T1-weighted and proton-density images, which often has high signal on T2-weighted images. This appearance corresponds to the margin of revascularization and remodeling. Contemporaneous radiographs are often normal, but the infarcted marrow may eventually calcify. This dystrophic calcification in infarcts may resemble the mineralized matrix of an endosteal cartilage tumor.

**CLINICAL HISTORY** A 32-year-old woman with chronic swelling and ankle pain.



FIGURE 8.12A



FIGURE 8.12B



FIGURE 8.12C



FIGURE 8.12D



FIGURE 8.12E



FIGURE 8.12F

## FINDINGS

- A, B. AP and mortise radiographs of the ankle demonstrate erosive changes in the tibia and fibula. The erosions are shallow and have sclerotic margins. The cartilage space is preserved. The distribution of abnormality suggests a primary synovial process rather than a multifocal bone process.
- C. Lateral radiograph shows erosive changes of the talus along the anterior superior aspect as well as the posterior aspect, indicating a diffuse process.
- D–F. Coronal fat-saturated T2-weighted MRI, sagittal fat-saturated T2-weighted MRI, and sagittal T1-weighted MRI demonstrates profuse synovial hypertrophy and associated lesions in the subcortical bone, some of which appear to be communicating with the joint. There are low-signal-intensity foci within the hypertrophied synovium and within the intraosseous lesions.

**DIFFERENTIAL DIAGNOSIS** Pigmented villonodular synovitis (PVNS), synovial osteochondromatosis, amyloid arthropathy, tuberculosis, synovial hemangiomatosis.

**DIAGNOSIS** Pigmented villonodular synovitis (PVNS).

**DISCUSSION** All of the entities in the differential diagnosis can demonstrate synovial hypertrophy and bony erosions. The lack of calcifications on the radiographs makes synovial osteochondromatosis much less likely. The

low-MR-signal-intensity foci within the synovium and bone on T2-weighted images may be seen with PVNS or amyloidosis, but the monoarticular nature of the process favors PVNS over amyloidosis. These low-signal foci would not be expected with tuberculosis or hemangiomatosis.

PVNS is believed to be a benign neoplasm of the synovium. It is typically a monoarticular process that has a predilection for the large joints of the lower extremity, especially the knee [24]; however, any synovial joint may be involved. Radiographic findings include joint effusion, juxta-articular erosions, and relative sparing of the cartilage space. In later stages, secondary osteoarthritis may be seen. Ankylosis is not a feature. The synovial masses generally do not calcify or ossify in PVNS, an important point of differentiation from synovial osteochondromatosis [25]. On MRI, PVNS demonstrates foci of low signal intensity on all pulse sequences due to widespread hemosiderin deposits from repeated episodes of intra-articular hemorrhage. These hemosiderin deposits also give the synovium a pigmented appearance at gross inspection. Amyloidosis may show a similar pattern of low-signal foci on MRI, but amyloidosis is most often a systemic, multiarticular process that is related to long-term hemodialysis [26].

PVNS is treated by synovectomy, but because complete surgical removal is difficult, recurrence rates may be as high as 50%. Development of malignancy in the setting of PVNS is an extremely rare event. Cases of malignant PVNS have been reported in patients with previously documented and treated benign PVNS, as well as in patients with PVNS and malignancy at initial presentation [27,28].



FIGURE 8.13

**FINDINGS** Oblique ankle radiograph. There is amorphous dense soft tissue calcification, distributed in vertical sheets. No underlying osseous abnormality is identified. No joint disease is present.

**DIFFERENTIAL DIAGNOSIS** Dermatomyositis, systemic lupus erythematosus (SLE), scleroderma, hypervitaminosis D, hyperparathyroidism, pseudohypoparathyroidism, pseudopseudohypoparathyroidism, parasitic infection.

**DIAGNOSIS** Dermatomyositis.

**DISCUSSION** Extensive soft tissue calcification is present, some of which is subcutaneous, but some appears to be intramuscular and possibly intratendinous. The calcifications are amorphous in character, without defined internal structure. Numerous disorders can be associated with soft tissue calcifications, including dermatomyositis, SLE, scleroderma, hypervitaminosis D, hyperparathyroidism, pseudohypoparathyroidism, pseudopseudohypoparathyroidism, and parasitic infection.

Dermatomyositis is an idiopathic disorder with non-infectious inflammation of the skin and skeletal muscle. Polymyositis involves muscle alone. Multiple types of the disease have been described based on the clinical presentation, and a clinical form associated with underlying malignancy has been described. Regardless of subtype, nearly all patients experience muscle weakness, usually proximal. Skin rashes

and arthralgias are common clinical findings and may be the presenting symptoms. Involvement of cardiac, pulmonary, renal, neurologic, and gastrointestinal tissues will alter the presentation. Laboratory tests reveal elevation of creatine kinase during active inflammation, and electromyographic alterations can be detected. Soft tissue findings tend to be more common and severe in children than adults. Soft tissue swelling may be appreciated by dedicated soft tissue films in areas of complaint, but soft tissue calcifications represent the most dramatic radiographic finding. Distinct patterns of soft tissue calcification have been described, the most common of which are linear, sheet-like calcification in the interfascial planes. Reticular and rounded calcifications may be seen in the subcutaneous tissues, and deep rounded calcifications are common. In childhood disease, spontaneous remission of soft tissue calcifications has been reported with the onset of puberty. Joint changes on radiographs are rare and usually limited to soft tissue swelling. Distal tuft resorption may be seen in association with soft tissue calcification, which may be confused with scleroderma.

MRI is a useful method for evaluating the extent and activity of disease. Actively involved muscle tends to demonstrate increased signal on T2-weighted images; inversion recovery or fat-suppressed, T2-weighted images are the most sensitive method for displaying these changes [29]. Antimyosin scintigraphy may be even more sensitive than MRI for detecting active disease [30]. Identification of active disease is useful for directing biopsy.

**CLINICAL HISTORY** A 73-year-old woman with persistent lateral foot pain after twisting her ankle.

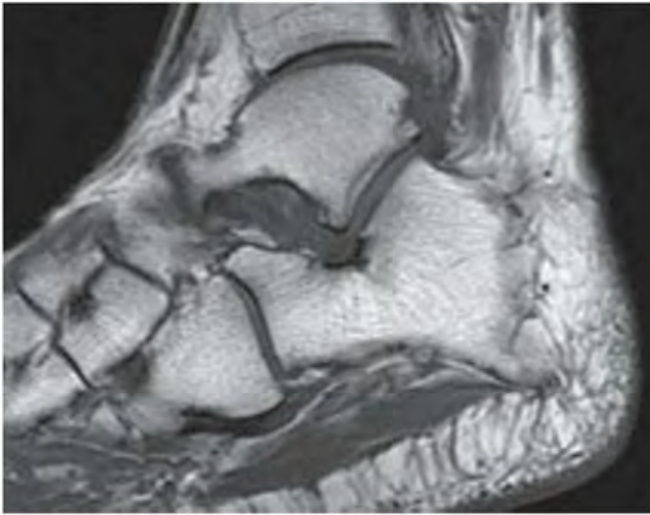


FIGURE 8.14A

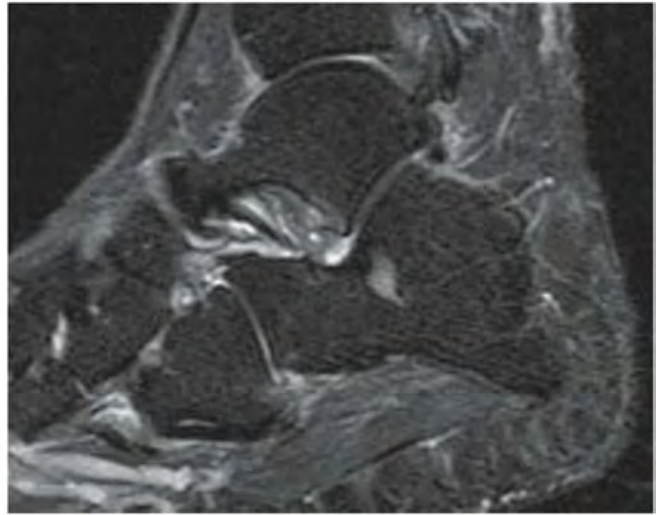


FIGURE 8.14B

**FINDINGS** (A, B) Sagittal T1-weighted and inversion recovery MRI of the hindfoot shows edema and resultant loss of the normal fat signal within the sinus tarsi region.

**DIFFERENTIAL DIAGNOSIS** None.

**DIAGNOSIS** Sinus tarsi syndrome.

**DISCUSSION** The sinus tarsi is the space between the talar neck and distal calcaneus. This space contains ligaments, neurovascular structures, and fat. In a severe ankle

inversion injury, inflammation or hemorrhage in this region may produce chronic pain. The ligaments within the sinus tarsi may also be torn, producing a sensation of instability. MRI can demonstrate ligamentous tears within the sinus tarsi—usually the cervical ligament or interosseous talocalcaneal ligament [32,33]—as well as edema or fibrosis within the surrounding fat. Sinus tarsi syndrome may also occur due to flatfoot deformities and inflammatory arthropathies [34]. Treatment is usually conservative. An arthroscopic subtalar joint synovectomy is an effective treatment when conservative measures fail [35].

## 8.15

**CLINICAL HISTORY** A 20-year-old man with foot pain.



FIGURE 8.15A



FIGURE 8.15B



FIGURE 8.15C

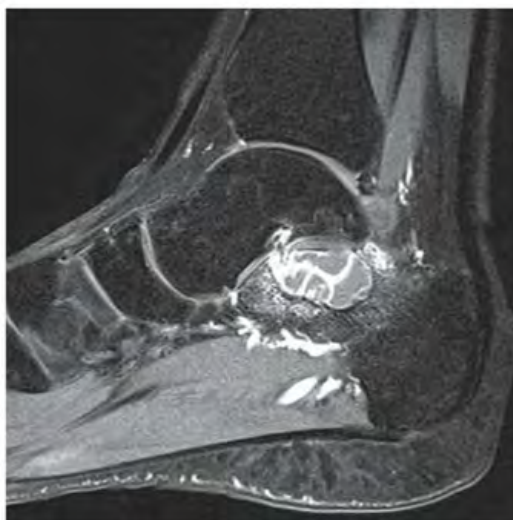


FIGURE 8.15D

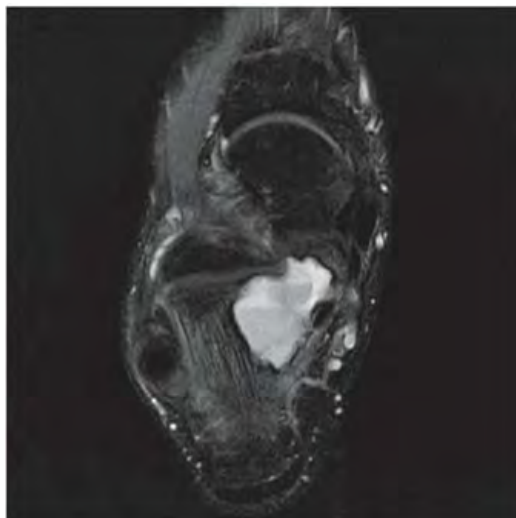


FIGURE 8.15E

**FINDINGS**

- A. Lateral radiograph of the ankle (detailed view) shows a lucent lesion in the calcaneus.
- B. Sagittal CT reformation shows lytic lesion in the posterior calcaneus with cortical thinning adjacent to the posterior subtalar joint. There is no sclerotic margin. No matrix mineralization is seen.
- C, D. Sagittal T1-weighted and postcontrast fat-suppressed T1-weighted MRI shows a mass in the calcaneus with peripheral rim and internal nodular enhancement. There are internal thick septa with contrast enhancement, also.
- E. Axial T2-weighted fat-suppressed MRI shows cystic lesion with fluid-fluid level and surrounding prominent marrow edema.

**DIFFERENTIAL DIAGNOSIS** Chondroblastoma, giant cell tumor, aneurysmal bone cyst.

**DIAGNOSIS** Chondroblastoma with secondary aneurysmal bone cyst.

**DISCUSSION** Chondroblastomas are rare tumors that occur predominantly in patients less than 20 years old. They occur

almost exclusively in the epiphyses, but may extend into the diaphyses of long bones. Two-thirds arise in the lower extremities, and half around the knee. When chondroblastomas occur outside the usual age group, they arise in unusual locations.

The radiographic appearance is an ovoid or rounded lucent epiphyseal lesion that is eccentrically or centrally located. The margins are geographic, usually with a thin, reactive bony rim. Scattered mottled calcifications, like those of other cartilage tumors, may be present. They can be secondarily involved by an aneurysmal bone cyst in 10% to 15% of cases. Common preexisting tumors of secondary aneurysmal bone cyst are giant cell tumors, osteoblastomas, and angiomas. Less common underlying processes include fibrous dysplasia, chondroblastoma, chondromyxoid fibroma, unicameral bone cyst, fibrous histiocytoma, eosinophilic granuloma, osteosarcoma, and fibrosarcoma. Secondary involvement of a chondroblastoma by an aneurysmal bone cyst is more likely in patients older than 20 years [31]. Intralesional fluid-fluid levels are common to both chondroblastomas and aneurysmal bone cysts and are therefore not generally helpful for distinguishing the two entities.

**CLINICAL HISTORY** A 47-year-old alcoholic with chronic ankle pain but no history of trauma.



FIGURE 8.16A



FIGURE 8.16B



FIGURE 8.16C

**FINDINGS** (A–C) Lateral, AP, and mortise radiographs of the right ankle show subchondral lucency, subchondral sclerosis, and flattening of the talar dome.

**DIFFERENTIAL DIAGNOSIS** Osteochondral fracture, osteonecrosis, osteoarthritis, neuropathic osteoarthropathy.

**DIAGNOSIS** Osteonecrosis.

**DISCUSSION** The radiographic findings of linear subchondral lucency, subchondral sclerosis, and collapse of the articular surface are diagnostic of osteonecrosis (avascular necrosis) involving an articular surface. Note the preservation of joint space and normal appearance of the tibial plafond, indicating that the disease process is primary to the talus rather than the joint itself. The opposing joint surface is typically normal in osteonecrosis until late in the disease, when manifestations of secondary degenerative joint disease may be seen. Once revascularization of the necrotic bone has become reestablished, attempts at repair by creeping substitution result in sclerosis as new viable bone is apposed to necrotic bone. Sclerosis represents the earliest radiographic

manifestation of osteonecrosis. Resorption of bone may result in a loss of mechanical strength, sometimes leading to subchondral fracture. Subchondral fracture may be evident as linear subchondral lucency—the crescent sign—and it is a highly specific sign of osteonecrosis. The subchondral fracture may even contain nitrogen gas formed in the joint during traction. Continued application of forces across the joint with associated attempts at repair leads to collapse of the articular surface, as in this case. The joint surface may then fragment, and resulting joint incongruity eventually leads to the development of osteoarthritis.

Atraumatic osteonecrosis of the talar dome has numerous causes, including alcoholism, SLE, sickle cell disease, excessive corticosteroids (endogenous or exogenous), pancreatitis, dysbarism, and marrow packing disorders such as Gaucher disease. Some cases have no apparent cause, but the majority of patients with atraumatic osteonecrosis of the talus have osteonecrosis elsewhere, especially the femoral head, and approximately half have bilateral involvement of the tali [36]. Atraumatic osteonecrosis is relatively uncommon, with most cases of osteonecrosis being related to fractures of the talar neck [37].



FIGURE 8.17A



FIGURE 8.17B



FIGURE 8.17C

**FINDINGS** (A) Lateral radiograph of the foot. The talus remains within the ankle mortise, but the relationship of the posterior facets of the talus and calcaneus is abnormally widened and oriented. Easy to overlook, the head of the talus overlaps the navicular, rather than articulating with it. Oblique (B) and AP (C) radiographs of the ankle and foot. The entire midfoot has dislocated medially and inferiorly. Most obvious are the naked articular surfaces of the distal aspect of the talus and the proximal aspect of the navicular.

**DIFFERENTIAL DIAGNOSIS** None.

**DIAGNOSIS** Subtalar dislocation.

**DISCUSSION** Simultaneous dislocation of the talocalcaneal and talonavicular joints is referred to as subtalar dislocation.

Of the ligamentous supports about the talus, the talonavicular and talocalcaneal ligaments and capsules are weaker than the calcaneonavicular ligaments and capsule and the ankle ligaments, so the entire midfoot and calcaneus may dislocate as a single unit [38]. Most of these injuries represent high-energy trauma, such as that sustained in motorcycle accidents or falls from a height, but relatively minor stumbling trauma may also cause this injury. Approximately 90% of subtalar dislocations are closed. In approximately 80% of cases, the foot dislocates medial to the talus. Severe open subtalar dislocations occur in major trauma [39], typically motorcycle accidents. Associated injuries include injuries of the tibial nerve, ruptures of the PTT, lacerations of the posterior tibial artery, and articular fractures of the subtalar joint, talonavicular joint, and talar dome. The outcome is often poor, and the risk of osteonecrosis of the talus is significant.

**CLINICAL HISTORY** A 18-year-old adolescent boy with painful flatfoot deformity.



FIGURE 8.18A



FIGURE 8.18B



FIGURE 8.18C

### FINDINGS

- Lateral radiograph of the foot shows talocalcaneal coalition, “absent middle facet” sign, and C-sign. The posterior facet of the subtalar joint can be seen.
- Coronal CT shows a bony coalition between the talus and calcaneus at the sustentaculum tali; the posterior facet is visible and not bridged.
- Axial CT shows the bony coalition between the calcaneus and the talus.

**DIFFERENTIAL DIAGNOSIS** Tarsal coalition, surgical fusion.

**DIAGNOSIS** Tarsal coalition.

**DISCUSSION** A tarsal coalition is an abnormal bony or fibrous articulation between two tarsal bones. The condition is congenital and appears to result from lack of segmentation rather than fusion of a fully developed joint [40]. Tarsal coalitions are found most commonly as isolated deformities, but they may occur in association with other ipsilateral limb deformities as well as generalized syndromes. Heritable cases of apparently autosomal dominance have been described. Most symptomatic cases are either coalitions between the calcaneus and the navicular (calcaneonavicular), or between the calcaneus and the talus (talocalcaneal). These coalitions may be bilateral in approximately 50% of cases.

A talocalcaneal coalition prevents the rotational and gliding motions at the subtalar joint that normally occur during walking, resulting in a painful flatfoot deformity. The coalition may be fibrous, cartilaginous, or osseous. Typically, the coalition is cartilaginous but becomes ossified as the skeleton matures; with ossification comes rigidity and the onset of symptoms. With calcaneonavicular coalitions, the loss of subtalar motion is partial, and the pain is generally confined to the region of the coalition itself.

Special views and conventional or CT may be necessary to identify the presence and the precise site of coalition. An indirect sign of a coalition between the calcaneus and the talus is talar beaking. A talar beak is a bony spur from the anterior superior aspect of the talus consequent to limited subtalar motion, hypoplasia of the head of the talus, and dorsal subluxation of the navicular bone. A talar beak may occur in any condition that causes abnormal talonavicular motion. The C-sign may be evident on lateral views when a middle facet coalition is present. The dome of the talus forms the top of the C, the coalition forms the middle, and the sustentaculum forms the bottom. The middle facet of the subtalar joint should be visible in normal patients. Thus, when the middle facet is absent, a coalition should be suspected [41]. Coalitions between other adjacent tarsal bones are rare and generally asymptomatic.



FIGURE 8.19A



FIGURE 8.19B

**FINDINGS**

- A. Lateral radiograph of the foot shows that the long axes of the talus and calcaneus are nearly parallel. The longitudinal arch is abnormally high.
- B. AP radiograph of the foot shows an abnormally narrow talocalcaneal angle, with severe adduction and supination of the forefoot.

**DIFFERENTIAL DIAGNOSIS** Clubfoot, vertical talus, metatarsus adductus, skewfoot.

**DIAGNOSIS** Classic clubfoot (talipes equinovarus).

**DISCUSSION** Radiographic criteria for the diagnosis of certain congenital foot deformities in infancy are based on lateral and AP views obtained while weight bearing or with dorsiflexion stress simulating weight bearing. In the normal foot, until the age of about 2 years, the long axis of the talus and the long axis of the calcaneus form an angle (talocalcaneal angle) that is about 40 degrees on both lateral and AP radiographs. If one considers the talus to be fixed in the ankle mortise, then abnormal varus (medial) alignment of the calcaneus relative

to the talus will reduce the talocalcaneal angle in the AP projection, and abnormal valgus (lateral) alignment will increase it. Because of the geometric and ligamentous linkage between the talus and the calcaneus, the changes in the talocalcaneal angles will be approximately equal on both AP and lateral radiographs. Thus, on AP and lateral radiographs, a small talocalcaneal angle (close to parallel, perhaps 10 degrees or less) is called hindfoot varus, and a large talocalcaneal angle (perhaps 70 degrees or more) is called hindfoot valgus.

Talipes equinovarus, or classic clubfoot, is a common congenital abnormality with an incidence of 1 per 1,000 live births. The condition is bilateral in about half the cases and is three times more common in boys than in girls. When unilateral, it is usually the left foot that is abnormal. The deformity is believed to be caused by a combination of intrauterine and genetic factors. Clubfoot may also occur in association with arthrogryposis, meningomyelocele, and other neuromuscular and genetic syndromes. The key radiologic finding is hindfoot varus (decreased talocalcaneal angle) combined with forefoot plantar flexion and supination. Depending on the severity and rigidity of the deformity, clubfoot may be treated by serial manipulation and casting, or surgical release of the soft tissues and realignment of the foot.



FIGURE 8.20A



FIGURE 8.20B

**FINDINGS**

- A. Lateral radiograph of the foot shows an increased angle between the long axes of the talus and calcaneus (talocalcaneal angle).
- B. AP radiograph of the foot shows an increased talocalcaneal angle. The forefoot is pronated.

**DIFFERENTIAL DIAGNOSIS** Clubfoot, vertical talus, metatarsus adductus, skewfoot.

**DIAGNOSIS** Congenital vertical talus.

**DISCUSSION** Congenital vertical talus is an unusual deformity characterized by hindfoot valgus (increased talocalcaneal

angle) and dorsal dislocation of the navicular on the talus [42]. The navicular adapts to its abnormal position by becoming wedge shaped, and the forefoot is pronated as a consequence. The plantar arch will be flattened and, in severe cases, a rocker-bottom deformity (convex plantar surface of the foot) may result. The anterior and middle facets of the subtalar joint may be absent or replaced by fibrous tissue. Approximately half of the cases of congenital vertical talus occur in isolation; the remainder occurs in association with neurofibromatosis, arthrogryposis, meningomyelocele, or other central nervous system or genetic syndromes. Acquired vertical talus may occur in association with conditions such as cerebral palsy, poliomyelitis, and spinal muscular atrophy. Overcorrection of a classic clubfoot may create a vertical talus.



FIGURE 8.21A



FIGURE 8.21B

**FINDINGS** (A, B) AP and lateral radiographs demonstrate that the forefoot is adducted in varus, more pronounced on the left. There is an overall convex lateral border of the foot soft tissues, and a concave medial border. The hindfoot and midfoot are normal.

**DIFFERENTIAL DIAGNOSIS** Talipes equinovarus, skewfoot, metatarsus adductus.

**DIAGNOSIS** Metatarsus adductus.

**DISCUSSION** Metatarsus adductus is a congenital deformity characterized by medial deviation of the forefoot, without abnormality of the hindfoot [43]. It is the most common congenital foot deformity, with an incidence 10 times greater than that of classic clubfoot. The condition is bilateral in most cases, and it is thought to result from intrauterine

positioning. Two-thirds of these deformities are detected at birth, and the remainder becomes noticeable during the 1st year of life. The cause of the deformity has not been elucidated, but there is a hereditary component, as 25% of affected infants have a first-degree relative with similar findings. In the majority of cases, the deformity is flexible and resolves without treatment.

Metatarsus adductus can be recognized on radiographs by the marked medial deviation of the metatarsals with a normally aligned hindfoot. On weight-bearing radiographs or simulated weight-bearing radiographs in infants, a line drawn along the longitudinal axis of the calcaneus (calcaneal axial line) should extend through the base of the fourth metatarsal on an AP projection. If the forefoot is angulated medial to this line, it is adducted. An adducted forefoot occurring in combination with hindfoot valgus is called skewfoot, a different and unusual deformity that frequently requires surgical correction.

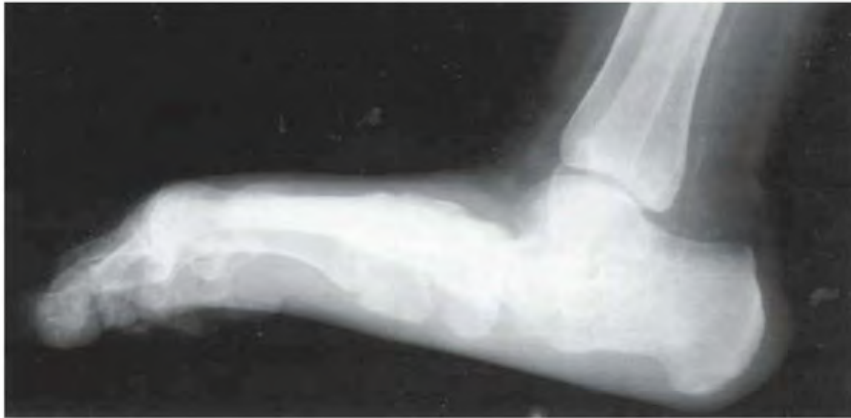


FIGURE 8.22A



FIGURE 8.22B

### FINDINGS

- A. Lateral radiograph of the foot shows an extreme flatfoot deformity. There are no hypertrophic bony changes, bone fragments, or dislocation. Extensive vascular calcification is present.
- B. AP radiograph of the foot shows the flatfoot deformity with pronation of the forefoot and valgus deviation of the toes. The bones are osteopenic, but erosive changes are absent.

**DIFFERENTIAL DIAGNOSIS** Heritable connective tissue dysplasia (such as Ehlers-Danlos syndrome, Marfan syndrome), SLE, arthrogryposis, congenital vertical talus, diabetic neuropathy, rheumatoid arthritis, stroke.

**DIAGNOSIS** Systemic lupus erythematosus (SLE).

**DISCUSSION** A severe flatfoot deformity in association with extensive vascular calcification is a common association in diabetic neuropathy, but the bony changes of neuropathic arthropathy are absent from this case. Congenital vertical talus also results in a severe flatfoot deformity but, in older patients, degenerative arthritis dominates the clinical picture. Ehlers-Danlos syndrome and arthrogryposis are conditions

in which infants present with joint laxity, whereas adults present with contractures. The absence of erosive changes eliminates rheumatoid arthritis as a consideration, although the osteoporosis and alignment deformities would otherwise be suggestive. The presence of severe vascular disease in combination with atrophy suggests stroke as a possibility.

Abnormalities of the hand can be found in about half of the patients with SLE, but abnormalities of the foot are found in about two-thirds [44]. The severity of the changes is related to the duration of disease. Nearly all patients with nonerosive deforming arthropathy of the hands (Jaccoud's type of arthropathy) will also have passively correctable joint deformities of the foot [45]. Such deformities include hallux valgus, subluxation of the lesser metatarsophalangeal (MTP) joints, and widening of the forefoot. Erosive or cystic changes of bone and cartilage are typically not seen in SLE, and neither are hypertrophic changes such as subchondral sclerosis, osteophyte formation, or asymmetric joint space narrowing. Vascular disease in SLE generally involves the microvascular circulation, but macrovascular occlusive disease occurs occasionally and is presumably related to immune complex-mediated endothelial damage [46]. Extensive vascular disease below the inguinal ligament in SLE has a poor prognosis, often resulting in treatment by amputation.



FIGURE 8.23

**FINDINGS** Lateral radiograph of the foot demonstrates fusion of the ankle, hindfoot, midfoot, and MTP joints. Diffuse osteopenia is noted.

**DIFFERENTIAL DIAGNOSIS** Juvenile idiopathic arthritis, sequelae of trauma or infection, corrected clubfoot.

**DIAGNOSIS** Juvenile idiopathic arthritis.

**DISCUSSION** The ankylosis of nearly the entire ankle and foot with osteopenia and remodeled bone suggests juvenile idiopathic arthritis as the underlying cause. Trauma, infection, and surgery are other situations where fusion of the foot may occur. Juvenile idiopathic arthritis [49], formerly known as juvenile chronic arthritis or juvenile rheumatoid arthritis, is a designation that includes seronegative juvenile-onset

rheumatoid arthritis (Still disease), juvenile onset of seropositive adult-type rheumatoid arthritis, and the seronegative spondyloarthropathies. The radiologic findings in juvenile idiopathic arthritis reflect the effect of a chronic inflammatory arthritis on a growing skeleton, and are generally not specific for a particular clinical entity. The radiographic findings include soft tissue swelling, osteoporosis, periostitis, erosions, ankylosis, and growth disturbances. The earlier the age of onset, the more severe the findings. Not all findings are likely to be present together, but combinations of these findings should point to the diagnosis. The disease may remit in adulthood, but permanent muscle wasting, growth deformities, loss of function from ankylosis, and secondary osteoarthritis are common sequelae. MRI and ultrasound are becoming more important in the evaluation and monitoring of patients with this disease [50].



FIGURE 8.24A

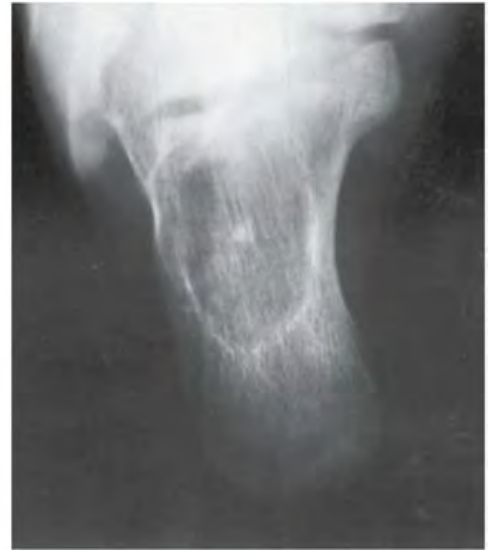


FIGURE 8.24B

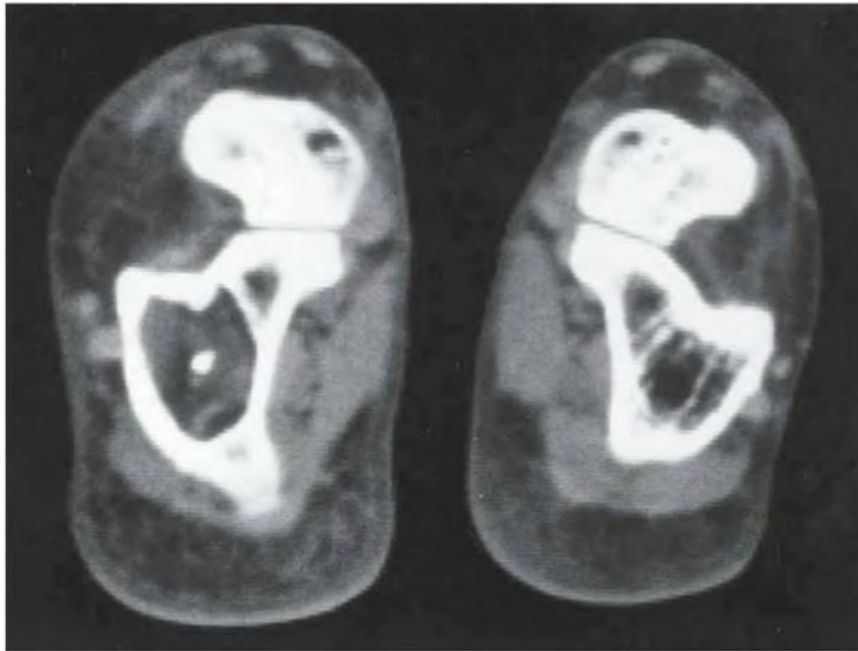


FIGURE 8.24C

**FINDINGS**

- A, B. Lateral and Harris view radiographs of the calcaneus demonstrate a geographic medullary lesion with sclerotic borders and lucent center. Dystrophic calcification is contained centrally.
- C. Coronal CT demonstrates that part of the lesion has low attenuation coefficients consistent with fat.

**DIFFERENTIAL DIAGNOSIS** Cyst, lipoma, giant cell tumor, eosinophilic granuloma.

**DIAGNOSIS** Intraosseous lipoma.

**DISCUSSION** Unicameral bone cyst, aneurysmal bone cyst, giant cell tumor, lipoma, and eosinophilic granuloma may

produce a lucent, well-defined lesion in the calcaneus. The anterior calcaneus is a particularly good site for unicameral bone cyst and intraosseous lipoma. A few foci of calcifications are typical for the intraosseous lipoma and correspond to areas of dystrophic calcification. Fat attenuation on the CT further supports this diagnosis. The other diagnostic possibilities would not be fat containing. Soft tissue lipomas are more common than their osseous counterparts. Most cases of intraosseous lipomas are found in the long bones, and 15% are seen in the calcaneus [47]. They classically have a lucent appearance, with a thin sclerotic border and nonaggressive features. Central dystrophic calcification is a cardinal feature of lipoma in the calcaneus, and a fatty constituent may be identified on MRI or CT. The histologic picture is mature adipose tissue mixed with a few degenerated bone trabeculae.

**CLINICAL HISTORY** A 55-year-old woman unable to continue a new, aggressive exercise program because of heel pain.

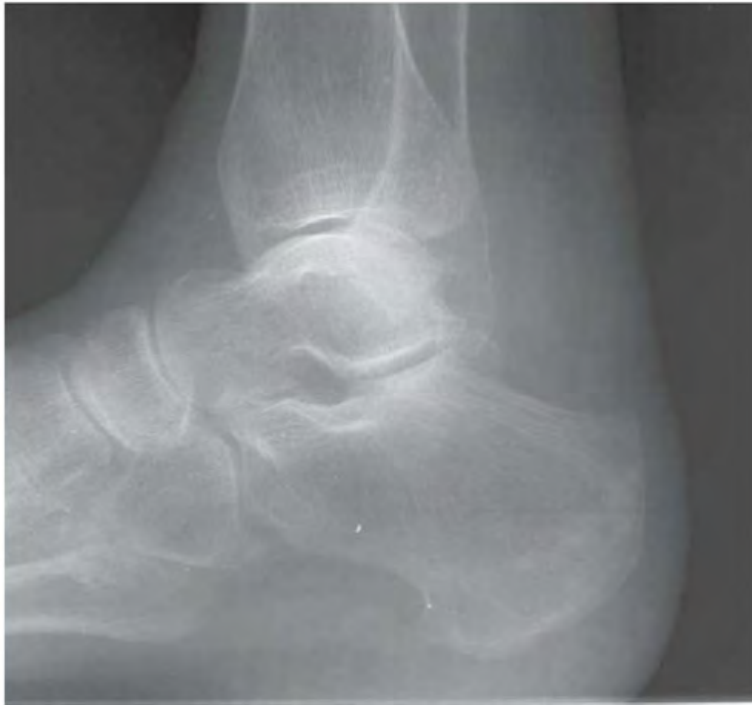


FIGURE 8.25A

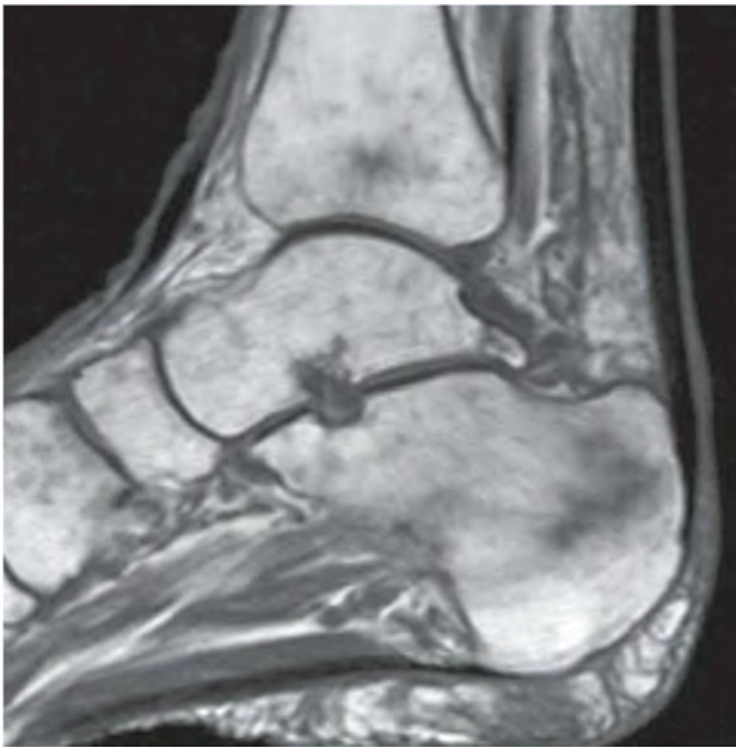


FIGURE 8.25B



FIGURE 8.25C

**FINDINGS**

- A. Lateral radiograph of the calcaneus shows an irregular band of sclerosis in the tuberosity, oriented perpendicular to the major weight-bearing trabeculae. The margins of the sclerosis are somewhat fluffy.
- B. Sagittal T1-weighted MRI shows a region of dark, curvilinear signal in the posterior calcaneus.
- C. Axial T2-weighted, fat-suppressed MRI shows the dark linear signal surrounded by edema.

**DIFFERENTIAL DIAGNOSIS** Traumatic fractures, fatigue fractures, pathologic fractures.

**DIAGNOSIS** Calcaneal fatigue fracture.

**DISCUSSION** The linear morphology and fluffy character of the sclerosis is characteristic of healing fatigue fracture. The history suggests that the lesion is related to locomotor

activity. The lack of mass or bone destruction eliminates possibilities such as blastic metastases or lymphoma.

Stress fractures may be divided into fatigue fractures, where normal bone fractures in response to abnormal loads, and insufficiency fractures, where abnormal bone fractures in response to normal loads. Fractures through focal lesions such as tumors are called pathologic fractures. Stress fractures through trabecular bone are similar to stress fractures through tubular bones, except that the individual weight-bearing trabeculae produce calcified endosteal callus. In aggregate, these form the fluffy densities visible on radiographs. Unlike traumatic fractures, the cortex is typically intact. As these fractures heal, the sclerosis remodels and ultimately disappears. The appearance and evolution of stress fractures is not related to the site or the character of the inciting stress. Although the tibia was the bone most commonly affected by stress fractures in one study of military recruits, the posterior calcaneal tuberosity was the most commonly affected site [48].

**CLINICAL HISTORY** A 45-year-old man with heel pain, and a companion case.

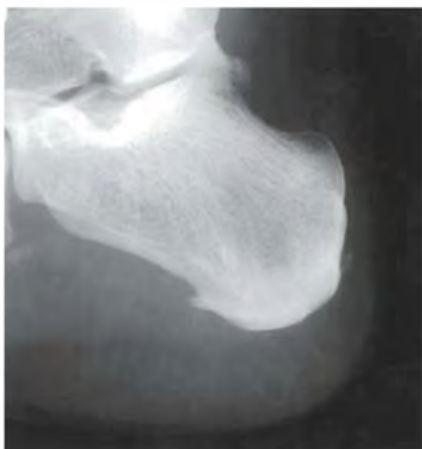


FIGURE 8.26A

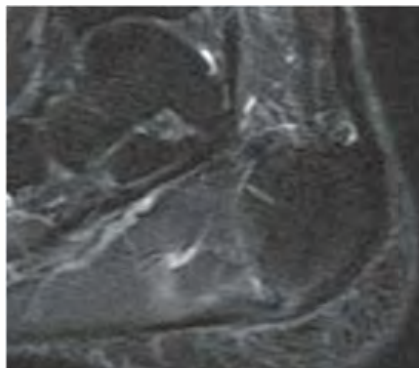


FIGURE 8.26B



FIGURE 8.26C



FIGURE 8.26D

## FINDINGS

- A. Lateral radiograph shows loss of the normal sharp tissue-fat plane at the plantar aspect of the attachment of the plantar aponeurosis to the calcaneus.
- B, C. Companion case. Sagittal inversion recovery and axial T2-weighted, fat-suppressed MRI shows thickening and increased signal of the attachment of the plantar aponeurosis. There is mild edema in the adjacent subcutaneous fat and calcaneal bone marrow.
- D. Lateral camera image of blood pool portion of three-phase radionuclide bone scan shows increased activity at the calcaneal attachment of the plantar aponeurosis.

**DIFFERENTIAL DIAGNOSIS** Plantar fasciitis, plantar fibromatosis, rupture of the plantar fascia, subcalcaneal bursitis, calcaneal stress fracture, spondyloarthropathy, rheumatoid arthritis.

**DIAGNOSIS** Plantar fasciitis.

**DISCUSSION** The plantar aponeurosis is a strong band of connective tissue that originates at the calcaneus and extends distally to coalesce with the ligaments that attach to the toes. Plantar fasciitis is an inflammatory process involving the plantar aponeurosis, typically at its origin. Plantar fasciitis can occur with repetitive microtrauma and is a somewhat common cause of heel pain in runners [51]. Approximately 7% of injuries in distance runners are related to plantar fasciitis. The plantar fascia stretches during the first half of the stance phase of walking or running, storing potential energy. Approximately 90% of this energy is returned as it recoils like a spring during the push-off. Peak stress as high as three times body weight occurs at the time of midstance, when most of the weight-bearing forces have been transferred from the hindfoot to the ball of the foot.

The most common presenting symptom of plantar fasciitis is pain, especially on rising in the morning. Tenderness may be found along the course of the plantar fascia or at its origin on the medial aspect of the calcaneal tuberosity. Radiographs may be normal or may show swelling and loss of fat-tissue planes along the plantar aponeurosis. Radionuclide studies most often show increased activity along the plantar fascia on early images, with focal accumulation of radiotracer at the inferior aspect of the calcaneus on delayed static images [52]. MRI shows signal-intensity changes at the proximal aspect of the calcaneus [53]. Plantar fasciitis may also be a feature of rheumatoid arthritis and the seronegative spondyloarthropathies [54].



FIGURE 8.27

**FINDINGS** Lateral radiograph of calcaneus shows soft tissue calcification posterior to the calcaneus but anterior to the Achilles tendon, in the location of the retrocalcaneal bursa. No erosions of the underlying bone are present.

**DIFFERENTIAL DIAGNOSIS** Hydroxyapatite deposition disease, gouty arthritis, pyrophosphate arthropathy, spondyloarthropathy, synovial osteochondromatosis.

**DIAGNOSIS** Hydroxyapatite deposition disease (calcific retrocalcaneal bursitis).

**DISCUSSION** Hydroxyapatite deposition disease is a heterogeneous group of conditions that have in common the abnormal presence of amorphous hydroxyapatite (basic calcium phosphate) crystals in the soft tissues. Ion contaminants such as carbonate, magnesium, fluoride, and chloride will be present within the crystals. Probably the result of multiple causes, there may be multiple mechanisms of deposition. The radiologic manifestations of hydroxyapatite deposition disease are similar to those of other crystal-associated conditions [60]: asymptomatic deposits, acute crystal-induced synovitis, and chronic destructive arthropathy.

Hydroxyapatite deposition disease typically involves the periarticular soft tissues, tendons, ligaments, bursae, and

joint capsules rather than the articular cartilage and subchondral bone. Deposits of hydroxyapatite in the soft tissues appear on radiographs as dense, homogeneous, sharply margined, and amorphous calcifications. They may have linear, angular, or round shapes and, unlike chondrocalcinosis, the calcifications do not conform to hyaline or fibrocartilage structures.

Recurrent episodes of calcific tendinitis or calcific bursitis are commonly associated with hydroxyapatite deposits. Most patients are adults in their 50s or 60s and present with acute pain, swelling, and tenderness. Symptoms respond rapidly to nonsteroidal anti-inflammatory agents. When the retrocalcaneal bursa is involved, the Achilles tendon is usually the site of hydroxyapatite deposits. Tendons may go on to atrophy and rupture, but it is unclear whether the deposits initially caused the local tissue damage, or whether preexisting tissue damage allowed the deposits to accumulate. The process is usually monoarticular, but multiple joints may be involved at the same time or successively. Other common sites of involvement include the supraspinatus tendon, the long head of the biceps tendon, the extensor tendons of the wrist, the myotendinous attachments along the linea aspera (thigh adductors) and at the medial border of the proximal tibia (pes anserinus), the olecranon bursa, the trochanteric bursa, and the ischial bursa.

**CLINICAL HISTORY** A 41-year-old woman with painful mass on plantar aspect of foot.

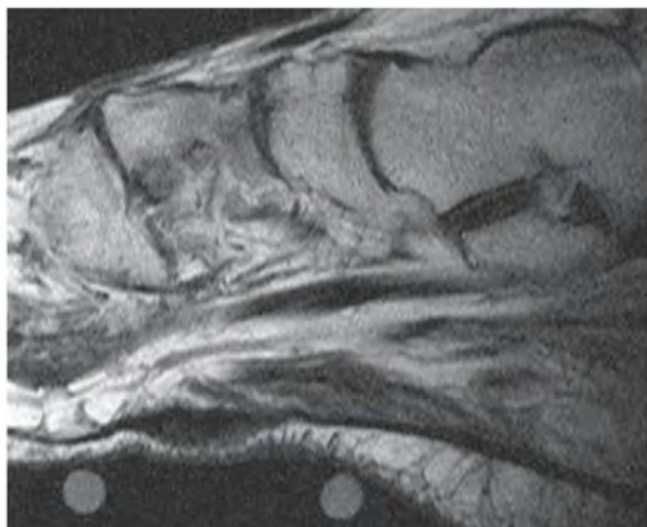


FIGURE 8.28A

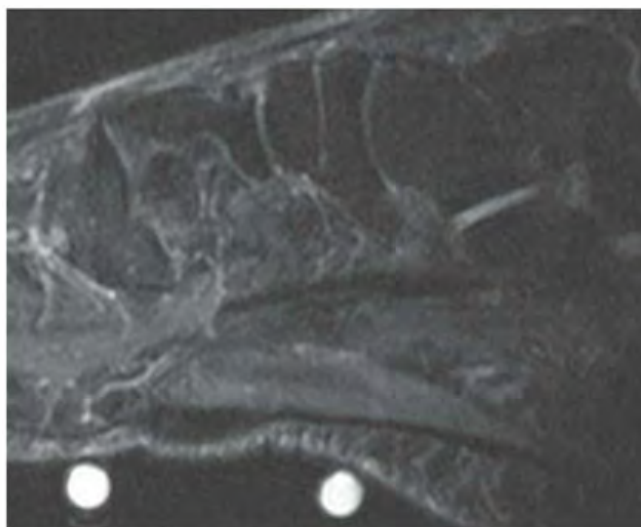


FIGURE 8.28B

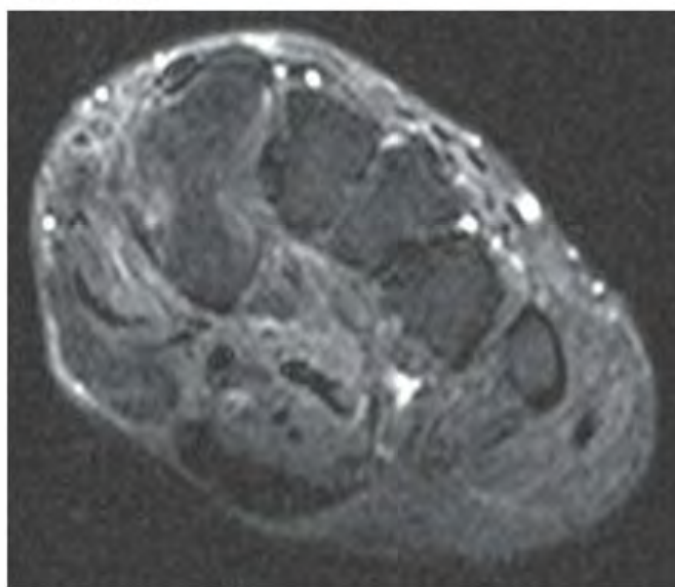


FIGURE 8.28C

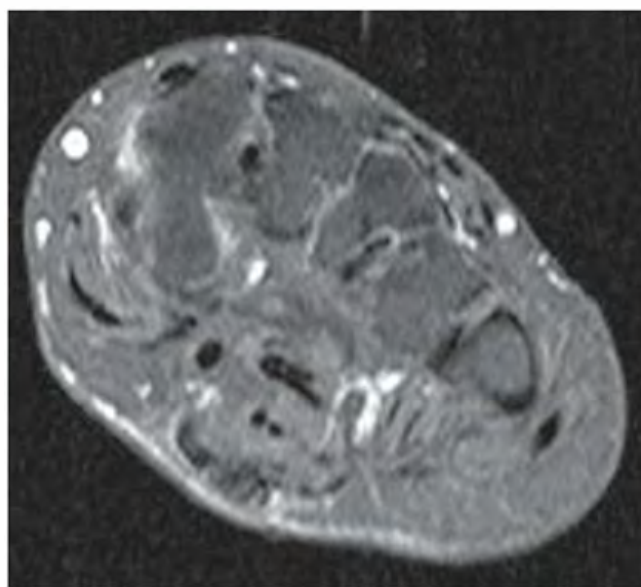


FIGURE 8.28D

## FINDINGS

- A–C. Sagittal T1-weighted and sagittal inversion recovery, and coronal T2-weighted, fat-suppressed MRI shows a low-signal, lobulated mass in the subcutaneous tissues of the foot under the longitudinal arch. The mass involves the plantar aponeurosis and abuts the underlying musculature.
- D. T1-weighted, gadolinium-enhanced, fat-suppressed MRI shows heterogeneous enhancement.

**DIFFERENTIAL DIAGNOSIS** Soft tissue sarcoma, foreign body granuloma, fibromatosis, metastasis, giant cell tumor of tendon sheath, abscess.

**DIAGNOSIS** Plantar fibromatosis.

**DISCUSSION** The fibromatoses encompass a group of lesions that demonstrate fibrous proliferation and may be locally aggressive but do not possess metastatic potential. Broad subdivisions include superficial and deep fibromatoses. The superficial variety has a predilection for the lower extremity. Common varieties of this class of lesions include palmar fibromatosis, plantar fibromatosis, and nodular fasciitis. They differ from keloids and cicatricial fibromatosis in that

they possess a greater cellular constituent in their matrix, specifically myofibroblasts [55]. On MRI, these lesions classically demonstrate decreased signal intensity on all pulse sequences, although a relatively more cellular lesion (with a higher cell-to-collagen ratio than typically present) may confer a higher signal intensity on T2-weighted pulse sequences [56,57]. Variability in the MRI appearance of these lesions on T1-weighted, T2-weighted, and proton-density-weighted pulse sequences may be related to the relative preponderance of the various constituents seen in the lesion, which include collagen, spindle cells, and mucopolysaccharides.

Plantar fibromatosis is a slow-growing, unencapsulated, nodular lesion that most frequently occurs in the plantar aponeurosis. Patients are typically adults who present with one or more firm, fixed, painless subcutaneous nodules in the plantar aspect of the foot. The MRI features commonly noted in plantar fibromatoses include an infiltrative margin, isointensity to muscle on T1-weighted MRI, and hyperintensity to muscle on T2-weighted images [58]. The lesions are well defined superficially against the normal adjacent subcutaneous fat, but may be inseparable from the underlying muscle. Enhancement patterns are variable, but profuse enhancement after contrast was seen in 60% of cases of plantar fibromatosis in one study on MRI [59].



FIGURE 8.29

**FINDINGS** Lateral radiograph of the calcaneus shows effusion in the retrocalcaneal bursa. Fluffy periostitis is present at the origin of the plantar aponeurosis on the plantar aspect of the calcaneus.

**DIFFERENTIAL DIAGNOSIS** Reactive arthritis, psoriatic arthritis, ankylosing spondylitis, rheumatoid arthritis, plantar fasciitis.

**DIAGNOSIS** Reactive arthritis.

**DISCUSSION** The calcaneus is a characteristic site of radiographic abnormalities in reactive arthritis. The prevalence of radiographic abnormalities involving the calcaneus among patients with reactive arthritis is 25% to 50%. The calcaneus may be the only site or the predominant site of findings, and correlative symptoms are frequently present. Bilateral

changes are common. At the posterior aspect of the calcaneus, retrocalcaneal bursitis and Achilles tendinitis results in thickening of the soft tissues and poorly defined erosions of the adjacent calcaneus. Unlike psoriatic arthritis or ankylosing spondylitis, enthesophytes at the Achilles tendon insertion are rare in reactive arthritis. On the plantar surface of the calcaneus, erosions, hyperostosis, and enthesophytes may be present. Initially, the enthesophytes are poorly defined and fuzzy in outline, but they often become better defined as they mature, and may become indistinguishable from the common plantar calcaneal spurs seen in normal patients. The presence or absence of radiologic evidence of enthesopathy correlates poorly with the presence or absence of clinical symptoms [61]. Although both osteoporosis and erosions may be seen in reactive arthritis, the associated bony proliferative changes help to distinguish it from rheumatoid arthritis.



FIGURE 8.30A



FIGURE 8.30B

**FINDINGS**

- A. AP radiograph of the left foot shows large erosions around the first interphalangeal (IP) and TMT joints. The erosions have sclerotic margins and overhanging edges. The great toe is swollen.
- B. AP radiograph of the right foot shows large erosions around the first IP, MTP, and TMT joints, and of the second distal IP (DIP) and proximal IP (PIP) joints. The erosions have sclerotic margins and overhanging edges. The first and second toes are swollen, and there is a medial soft tissue mass adjacent to the first MTP joint with increased density. The joint spaces appear preserved.

**DIFFERENTIAL DIAGNOSIS** Tophaceous gout, psoriatic arthritis, rheumatoid arthritis,

**DIAGNOSIS** Tophaceous gout.

**DISCUSSION** The well-defined nature of the erosions indicates the process is indolent. The lack of fusiform soft tissue swelling, uniform joint space loss, or juxta-articular osteoporosis allows exclusion of an inflammatory arthropathy. These findings, particularly in this distribution, represent gouty arthropathy. Gout represents deposition of urate crystals into soft tissues, and patients are typically hyperuricemic. Hyperuricemia can be due to excessive production of uric acid, decreased renal clearance of uric acid, or a combination of the two. The majority of cases of gout are

idiopathic, without known secondary disease to account for elevated levels of serum uric acid. Males are more frequently affected than females (20:1), and patients tend to be 40 to 50 years old at the onset of disease.

The disease most frequently manifests in the lower extremities, with 75% to 90% of patients having involvement of the first MTP joint. The first IP, TMT, ankle, and knee joints are frequently involved. Upper extremity involvement is common, particularly in the hands and elbows. In the past, 50% to 60% of patients would subsequently develop arthropathy, but this percentage has been decreased by pharmaceutical intervention. Patients typically do not have radiographically apparent arthropathy accompanying the initial onset of disease, and intermittent symptoms are usually present for years before findings become apparent. Lumpy, bumpy, soft tissue swelling may be seen due to tophaceous deposits, which are typically over extensor surfaces. Mineralization is usually preserved. Erosions tend to occur at the margins of joints or in a para-articular distribution. The erosions of gout are typically well margined and may demonstrate sclerotic borders. Despite erosive changes that may be extensive, the joint space is preserved until late in the disease, and lack of joint space narrowing is one of the most helpful clues to distinguish this erosive arthropathy from other erosive disorders. Tophaceous deposits may extend under the periosteum and produce overhanging edges at the margins of erosions, which is a helpful differentiating feature.

**CLINICAL HISTORY** A 50-year-old diabetic male with foot pain.



FIGURE 8.31A



FIGURE 8.31B



FIGURE 8.31C

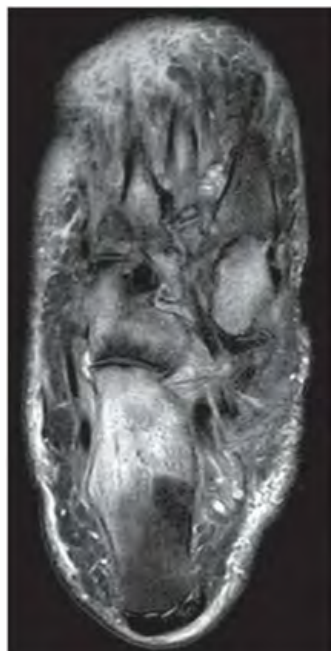


FIGURE 8.31D

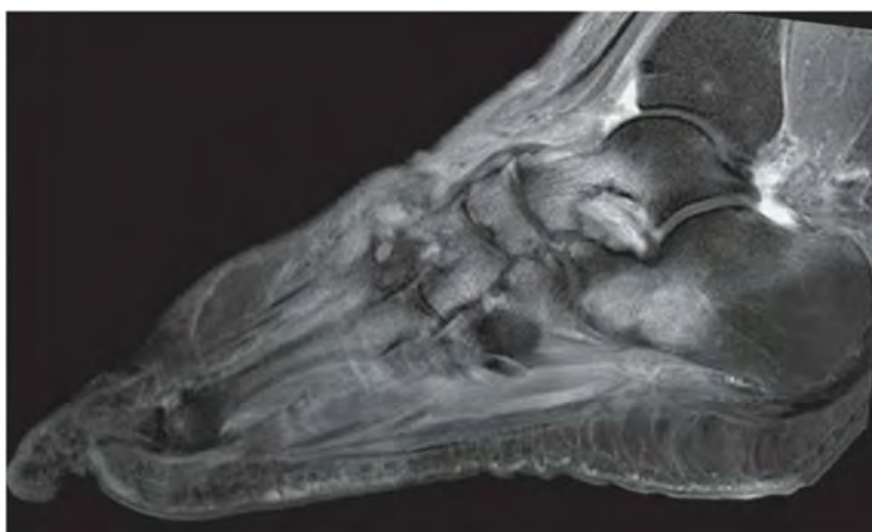


FIGURE 8.31E

## FINDINGS

- A, B. Lateral and AP radiographs of the foot show bony erosion, loose bodies, and heterotopic bone formation along the Lisfranc (tarsometatarsal) joints. Additionally, there is a fracture at the second metatarsal base. There are destructive changes at the navicular-cuneiform joint.
- C, D. Axial T1-weighted, and fat-suppressed T2-weighted MRI shows destruction, and fragmentation of the tarsometatarsal joints and marrow edema involving hindfoot, midfoot, and proximal phalanges at the tarsometatarsal joints.
- E. Sagittal postcontrast, T1-weighted, fat-suppressed MRI demonstrates enhancing bone marrow, bony erosions, and soft tissue enhancement. There is no synovial or soft tissue fluid collection.

**DIFFERENTIAL DIAGNOSIS** Neuropathic osteoarthropathy, infection, trauma.

**DIAGNOSIS** Neuropathic osteoarthropathy.

**DISCUSSION** Neuropathic joints (also called Charcot joints) have lost proprioception and deep pain sensation. With continued use of the joint, relaxation and hypotonia of the supporting structures lead to malalignment and recurrent injury. Rapidly progressive erosion of the articular cartilage, reactive subchondral sclerosis, fractures, and fragmentation of the subchondral bone result in a disorganized joint. The presence of joint debris induces synovitis and chronic effusion. The damage and derangement may occur over a period of days to weeks, with relatively little symptomatology. Both

lower motor neuron (peripheral) and upper motor neuron (central) lesions may result in neuropathic osteoarthropathy.

Diabetic neuropathy is the most common lower motor neuron lesion causing neuropathic osteoarthropathy. Other causes include alcoholism, tuberculosis, amyloidosis, leprosy, peripheral nerve trauma, steroids, and congenital indifference to pain. Syringomyelia is the most common upper motor neuron lesion. Other causes include meningomyelocele, trauma, multiple sclerosis, tabes dorsalis (syphilis), and cord compression. Neuropathic osteoarthropathy occurs in 0.1% of all diabetics and in 5% of those with diabetic neuropathy. Diabetic peripheral neuropathy causes loss of pain sensation and proprioception, leading to exceptional wear and tear without patient awareness of injury. The most frequent site of involvement is the foot (80%), especially the tarsometatarsal, intertarsal, and MTP joints; involvement may be unilateral or bilateral. Tarsometatarsal fracture dislocation (Lisfranc fracture dislocation) may occur spontaneously or with minimal trauma. Extensive sclerosis, osteophytosis, fractures, bony fragmentation, subluxation, dislocation, bony debris, effusion, and subchondral cysts are common findings. Chronic osteomyelitis is also relatively common in the diabetic foot, and the possible combination of neuropathic osteoarthropathy with infection can pose a diagnostic dilemma. MRI with gadolinium enhancement may be helpful in this circumstance. There are MRI features that help differentiate osteomyelitis from neuropathic osteoarthropathy. In osteomyelitis, the marrow edema pattern tends to affect single bone with diffuse involvement; edema distribution is focal rather than several joints or bones; typical locations are the weight-bearing regions such as toes, metatarsal heads, and calcaneus; and soft tissue changes are prominent with overlying ulcer, abscess, or sinus tract [62].

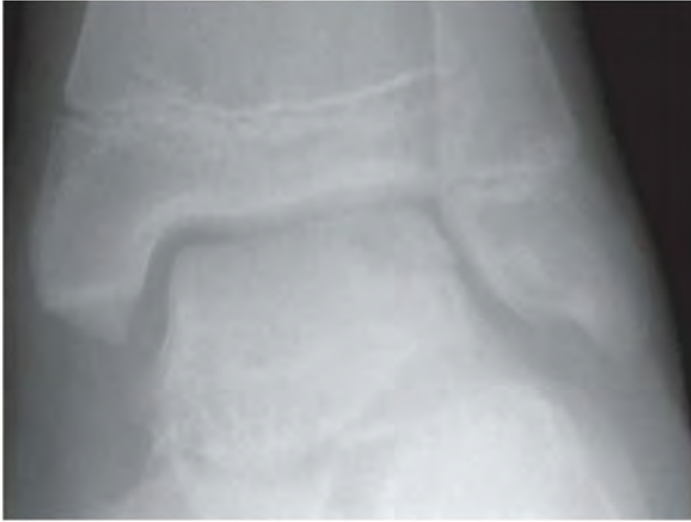


FIGURE 8.32A



FIGURE 8.32B

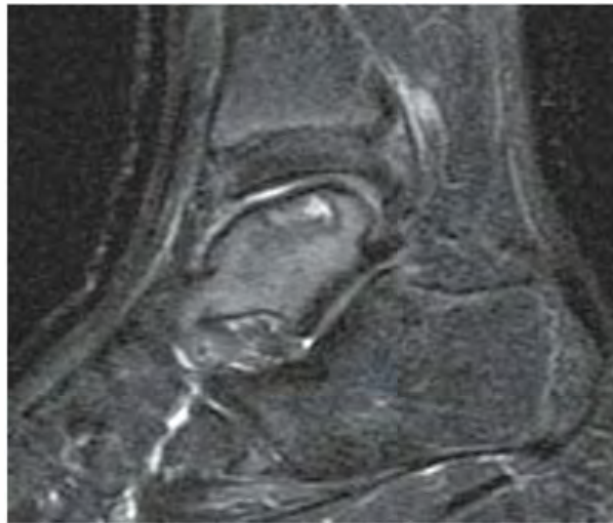


FIGURE 8.32C

**FINDINGS**

- A. Oblique radiograph demonstrates a crescentic lucency at the lateral aspect of the talar dome.
- B, C. Coronal T2-weighted, fat-suppressed and sagittal inversion recovery MRI shows an osteochondral injury to the lateral talar dome with fluid tracking beneath the fragment.

**DIFFERENTIAL DIAGNOSIS** Osteochondral lesion, arthritis, fracture.

**DIAGNOSIS** Osteochondral lesion of the talus.

**DISCUSSION** Osteochondral lesions of the talar dome, formerly referred to as osteochondritis dissecans, are focal

injuries to the cartilage and subchondral bone that typically occur secondary to trauma. It is controversial whether the osteochondral injury occurs at the time of the traumatic event, or whether it is the consequence of resultant instability [63]. In some cases, there is no history of trauma. On radiographs, there is a focal lucency in the anterolateral or posteromedial talar dome. MRI best demonstrates injury to the overlying cartilage and can identify fluid beneath the bone fragment, suggesting fragment instability. Treatment is initially conservative, with immobilization and then physical therapy. Surgical intervention consists of arthroscopic loose body removal, debridement, and drilling of the osteochondral lesion [64].



FIGURE 8.33A



FIGURE 8.33B



FIGURE 8.33C

**FINDINGS** (A–C) AP, oblique, and lateral radiographs of the left foot demonstrate medial and dorsal protrusion of portions of the navicular bone with increased density, and a comma-shaped deformity due to collapse of the lateral portion of the bone.

**DIFFERENTIAL DIAGNOSIS** Mueller-Weiss syndrome (spontaneous osteonecrosis of the tarsal navicular bone), Kohler disease.

**DIAGNOSIS** Mueller-Weiss syndrome.

**DISCUSSION** Kohler disease, osteochondrosis of the navicular in children, is a well-known disorder. Adult-onset spontaneous osteonecrosis of the navicular (Mueller-Weiss syndrome) is a distinct entity and should not be confused with Kohler disease. Kohler disease affects children between the ages of 3 and 7 years and is usually associated with minor

signs and symptoms or without clinical pathology. Mueller-Weiss syndrome has a characteristically painful clinical course with progressive deformity.

Kohler disease is unilateral in 75% to 80% and has a male preponderance. Mueller-Weiss syndrome is usually bilateral and seen predominately in women [65]. The etiology of Mueller-Weiss syndrome is still unclear. The radiographic abnormalities of Mueller-Weiss syndrome are characteristic. It is usually bilateral, although unilateral changes may be evident in younger individuals. Initial alterations include loss of volume in the lateral aspect of the tarsal navicular accompanied by an increase in radiodensity of this portion of the bone. The tarsal navicular assumes a comma-like shape because of lateral compression. Subsequently, dorsal protrusion and fragmentation of the bone may become evident [66]. Conservative therapy including custom-molded orthoses and anti-inflammatory medication may often fail. Surgical management may then be indicated.



FIGURE 8.34A



FIGURE 8.34B



FIGURE 8.34C



FIGURE 8.34D



FIGURE 8.34E

## FINDINGS

- A. Lateral radiograph demonstrates multiple ossific fragments projecting over the cuboid.
- B, C. Coronal CT demonstrates secondary osseous erosion and well-defined, corticated ossific fragments. One is interposed between the medial malleolus and talus.
- D, E. Sagittal T1-weighted MRI demonstrates osseous erosion of the talonavicular articulation and cuneiforms by the masses that are heterogeneous on all pulse sequences, but some focal hyperintense signal on T1 is seen, which suggests mature ossification with contained fatty elements.

**DIFFERENTIAL DIAGNOSIS** Pigmented villonodular synovitis (PVNS), synovial chondromatosis, hemangiomatosis.

**DIAGNOSIS** Synovial osteochondromatosis.

**DISCUSSION** The complex anatomy of the foot makes diagnosis from the conventional radiograph difficult, since it is impossible to characterize the calcification and its relationship to underlying bone. CT was very helpful in this case, revealing multiple rounded osteochondral fragments within the talocalcaneal navicular joints. Erosive changes are not associated with joint space narrowing, osteoporosis, or dissolution of the joint. The MRI examination with low signal on both T1-weighted and T2-weighted images puts PVNS in the differential, but the osteocartilaginous loose bodies shown on CT are very unusual in PVNS. Hemangiomatosis in the soft tissues with phleboliths could account for the calcifications and erosions, but the cross-sectional images are inconsistent. Synovial chondromatosis is the best diagnosis, given the radiologic findings.

Synovial chondromatosis is a self-limiting metaplasia of the synovium that presents as a monoarticular arthropathy or, in unusual cases, within a tendon sheath of the hand or foot. This disease is two to four times more common in men and tends to present in middle-aged patients who have complaints of swelling, stiffness, and pain. The knee is the most commonly involved joint, followed by the elbow, hip, and shoulder; however, any joint may be involved.

Not all cases of synovial chondromatosis (33%) have radiographically identifiable osteocartilaginous loose bodies. The loose bodies of this disease tend to be small, numerous, and uniform in size, as opposed to the large, scattered, osteocartilaginous densities that may accompany osteoarthritis or osteochondritis dissecans. Although degenerative changes may be a late manifestation of synovial chondromatosis, the loose bodies in extent and number are more prominent than the osteoarthritic changes, and there is relative preservation of the joint space, since the patients tend to present early in the course of the disease. Erosions are appreciated more commonly in tight joints than capacious articulations such as the knee.

CT is very helpful in complex areas of anatomy, such as the temporomandibular and intervertebral joints, in characterizing the extent of erosions and confirming the extraosseous nature of densities seen on conventional radiography. MRI is also very helpful in determining the extent of disease, and the multiplanar capabilities of this technique are particularly helpful in this regard. The most common appearance on MRI is that of an intra-articular process that is intermediate on T1-weighted images and bright on T2-weighted images, with focal areas of low signal on both sequences from ossification. Areas of increased signal on T1-weighted images within ossific loose bodies corresponding to fat may be appreciated [67].

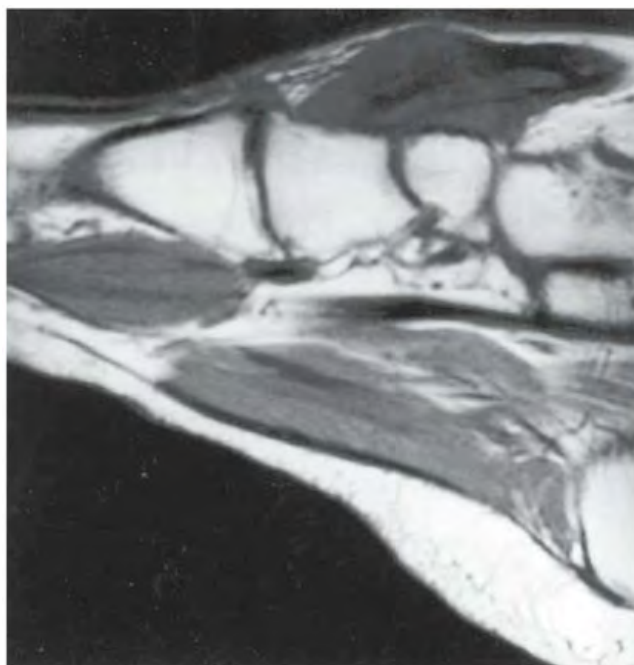


FIGURE 8.35A



FIGURE 8.35B



FIGURE 8.35C

## FINDINGS

- A. Sagittal T1-weighted MRI demonstrates a low-signal-intensity, well-defined mass medial and dorsal to the foot. The extensor hallucis longus tendon is incorporated into the mass.
- B, C. Axial T1-weighted images, without and with contrast, demonstrate minimal enhancement of the well-defined mass.

**DIFFERENTIAL DIAGNOSIS** Giant cell tumor of tendon sheath, synovial sarcoma, synovial chondromatosis, unusual infection such as *Mycobacterium marianum*.

**DIAGNOSIS** Giant cell tumor of the tendon sheath.

**DISCUSSION** Soft tissue masses around the ankle joint are uncommon. The neurovascular bundle is not involved, making the diagnosis of peripheral nerve sheath tumor unlikely. The lack of direct tendon involvement makes the diagnosis of clear cell sarcoma unlikely. The diagnosis of synovial sarcoma must be considered with a soft tissue mass around the ankle. However, the mass appears to arise in the flexor hallucis tendon sheath, and the most likely diagnoses include processes that might arise from the tenosynovial sheath, such as giant cell tumor of the tendon sheath, synovial chondromatosis, and an unusual infection such as *M. marianum*. The lack of inflammatory changes in the surrounding soft tissues

makes tuberculosis unlikely, and the lack of calcifications within the mass lowers the likelihood but does not exclude the diagnosis of tenosynovial chondromatosis.

The most likely diagnosis, given the radiologic findings, is giant cell tumor of the tendon sheath, which is a benign synovial proliferative disorder, histologically indistinguishable from PVNS. Giant cell tumor of the tendon sheath occurs most commonly in patients in their 30s through 50s, and presents more frequently in females than males with an approximate 2:1 ratio. This lesion most frequently presents in the hand, with only 5% to 15% of cases occurring in the foot, most typically in the first and second rays. In approximately 15% to 21% of cases, pressure erosion of adjacent bone can be seen, and bone may even be invaded, though rarely. Intralesional calcifications may be seen in 6% of cases, which may make radiologic distinction between giant cell tumor of tendon sheath and tenosynovial chondromatosis difficult. The mass appearance is typically nonspecific on T1-weighted images, and usually demonstrates intermediate signal. The diagnosis is usually considered based on T2-weighted images, which often reveal regions of intermediate to low signal. The relatively low signal on T2-weighted images is likely due to hemosiderin seen pathologically within these lesions. The MRI appearance varies, likely due to varying degrees of hemosiderin deposition. Moderate-to-intense enhancement is seen after contrast administration [68]. On ultrasound, these lesions are homogeneously hypoechoic and have detectable internal blood flow [69].

**CLINICAL HISTORY** A 47-year-old man with trauma from motor vehicle crash.



FIGURE 8.36A



FIGURE 8.36B

**FINDINGS** A, B. AP and lateral radiographs of the foot show fracture dislocations of the tarsometatarsal joints. The first metatarsal has been separated from the metatarsals of the lesser toes and is displaced dorsally and medially relative to the first cuneiform. The first cuneiform has been dislocated medially. The metatarsals of the lesser toes have dislocated dorsally and laterally as a group

**DIFFERENTIAL DIAGNOSIS** None.

**DIAGNOSIS** Lisfranc fracture dislocation, divergent type.

**DISCUSSION** Lisfranc fracture dislocation refers to any fracture dislocation involving multiple tarsometatarsal articulations. Abduction forces cause a lateral shift of the forefoot relative to the midfoot, frequently accompanied

by fracture at the base of the second metatarsal and cuboid. Misalignment of the second metatarsal relative to the second cuneiform is a prerequisite for the diagnosis. The bases of the second through fifth metatarsals are connected by ligaments. Although there is a ligament connecting the second metatarsal to the medial cuneiform, and a ligament connecting the medial cuneiform to the first metatarsal, there is no ligament joining the first and second metatarsals at their bases. When all of the metatarsals are dislocated laterally together, the injury may be called homolateral. When the first metatarsal is separated from the metatarsals of the lesser toes, the injury may be called divergent. Although the findings in this case are gross, if the metatarsals spontaneously relocate after the injury the findings may be very subtle and shown only by CT [70] or MRI. Stress views may be helpful in equivocal cases.

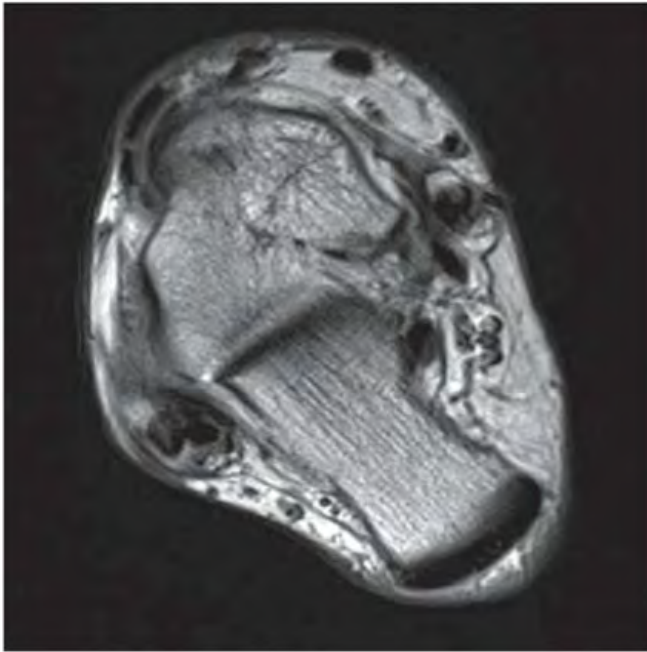


FIGURE 8.37A

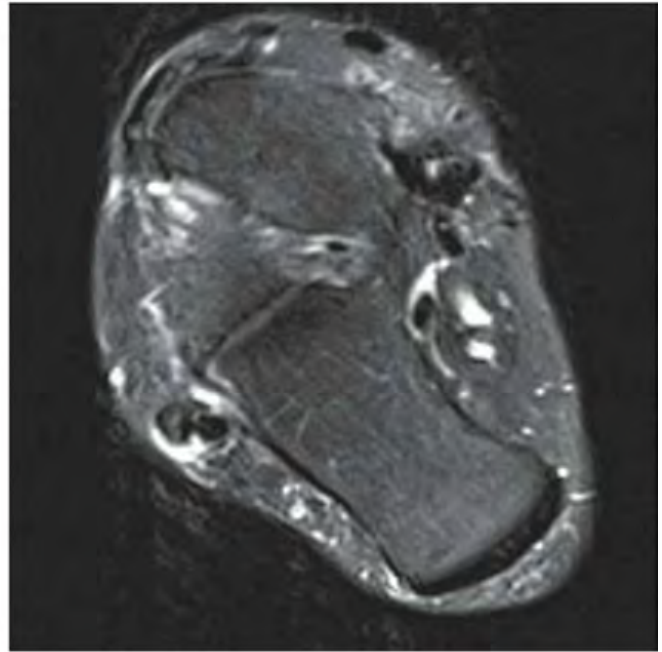


FIGURE 8.37B

**FINDINGS** Axial proton-density (A) and T2-weighted, fat-suppressed (B) MRI through the ankle and foot demonstrates three tendons located lateral to the calcaneus. A small amount of fluid is present in the tendon sheath.

**DIFFERENTIAL DIAGNOSIS** None.

**DIAGNOSIS** Peroneus brevis tendon split tear.

**DISCUSSION** The peroneus longus and brevis tendons are located on the posterior lateral aspect of the ankle and are major everters of the foot, with the peroneus brevis being

more effective [71]. The brevis attaches to the base of the fifth metatarsal. The longus has a broad-based insertion on the plantar surface of the base of the first metatarsal and medial cuneiform. Complete and partial tears can be seen in both of these tendons. Longitudinal split tears occur within the peroneus brevis during dorsiflexion when the brevis tendon is wedged between the lateral malleolus and peroneus longus tendon. When the peroneus brevis tendon splits, the peroneus longus tendon is partially surrounded by the two main peroneus brevis bundles [72]. Longitudinal peroneus brevis split tears are a clinically underappreciated cause of lateral ankle pain [73].



FIGURE 8.38

**FINDINGS** AP radiograph of foot. The marrow spaces are enlarged, causing the bones to have thin, scalloped cortices without much medullary structure. The shape of the long bones lacks the normal constriction of the diaphyses and gentle flaring of the metaphyses. Osteopenia is present.

**DIFFERENTIAL DIAGNOSIS** Hemoglobinopathy, Gaucher disease, leukemia, Pyle disease, fibrous dysplasia.

**DIAGNOSIS** Thalassemia.

**DISCUSSION** Thalassemia comprises a group of disorders caused by inherited abnormalities of globin production that lead to ineffective hematopoiesis and anemia. The defect is in the synthesis of one of the globin chains. There are many types of thalassemia distinguished on the basis of the specific globin chain affected and the particular defect present. Limb deformities and metaphyseal abnormalities are common skeletal manifestations of thalassemia. Marrow expansion of the metaphysis and limb deformities occur more frequently in females and more often with earlier institution of desferrioxamine therapy [74]. Other skeletal manifestations may include widening of the diploic space, a hair-on-end pattern

in the skull, and diminished pneumatization of the paranasal sinuses. Osteoporosis may predominate in adulthood, and this may occur predominantly on the basis of marrow hyperplasia [75]. Ischemic necrosis and infection of bone and soft tissue, in addition to growth disturbances, are potential complications of hemoglobinopathies in general [76]. Undertubulation is nonspecific and may be seen in multiple conditions. Widening of the marrow spaces with osteopenia is a hallmark feature of marrow replacement processes. In the younger patient, this raises the possibility of hemoglobinopathies.

In thalassemia,  $\beta$ -chain synthesis is defective and  $\alpha$ -chain synthesis predominates. The extraneous  $\alpha$ -globin chain production causes intracellular precipitation of this compound, which in turn causes hemolysis, derangement of erythropoiesis, and enlargement of the marrow spaces. Treatment, such as hypertransfusion, may diminish hyperactive erythropoiesis and thereby decrease the degree of marrow expansion. Complications of this are best appreciated on MRI and include iron overload. Iron deposition in several organs may be seen, and this may impart low signal intensity to the bone marrow [77]. Additional chelation therapy may limit the degree of iron deposition, which may appear less prominent in the peripheral skeleton [78].



FIGURE 8.39A



FIGURE 8.39B

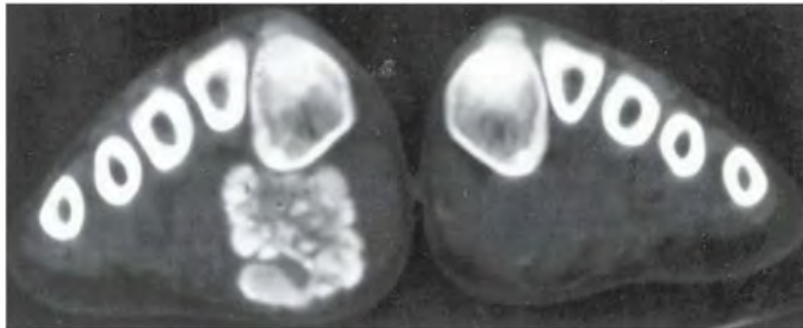


FIGURE 8.39C

**FINDINGS**

- A, B. Lateral and oblique radiographs of the foot show amorphous calcification in the plantar soft tissues. No changes in the bone are present.
- C. Axial CT (bone windows) shows calcifications with occasional fluid levels in the plantar soft tissues.

**DIFFERENTIAL DIAGNOSIS** Tumoral calcinosis, synovial osteochondromatosis, hydroxyapatite deposition disease, foreign body granulomas, osteosarcoma.

**DIAGNOSIS** Idiopathic tumoral calcinosis.

**DISCUSSION** Idiopathic tumoral calcinosis is an uncommon disorder characterized by accumulations of calcium

hydroxyapatite crystals in the periarticular soft tissues with granulomatous reaction [79]. An inborn error in phosphorus metabolism is thought to be the cause of these nonneoplastic lesions. About one-third of reported cases are familial. The masses tend to grow slowly over many years to large size; symptoms may be caused by their physical bulk. Most are discovered in the first or second decade of life. These accumulations are composed of multiple globules of calcification separated by radiolucent bands. Fluid levels are usually present but may not be evident, except on CT. The lesions are frequently found in the normal location of bursae. Fibrous septa may create a chicken-wire pattern of lucencies between the calcific densities. Smooth erosions of the bone surfaces adjacent to the lesions may be found. The treatment is surgical, but local recurrences are not uncommon.

**CLINICAL HISTORY** A 45-year-old man who is an amateur runner with foot pain.



FIGURE 8.40A

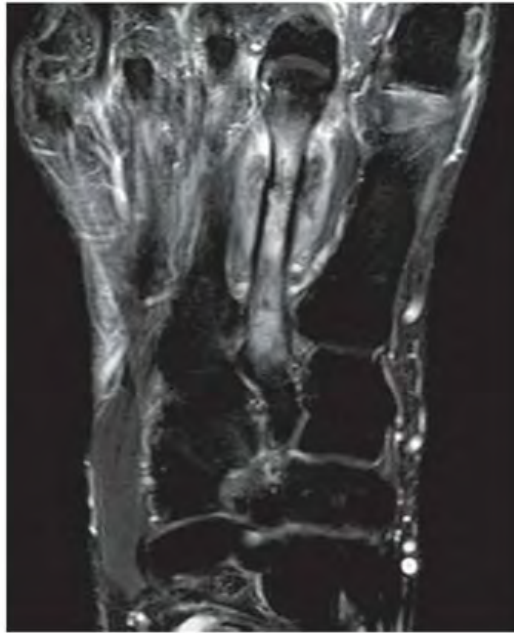


FIGURE 8.40B



FIGURE 8.40C

### FINDINGS

- A. Radiograph of the foot (detailed view) shows fluffy, fusiform periosteal callus surrounding the distal shaft of the second metatarsal fracture.
- B, C. Coronal T1-weighted and STIR MRI demonstrate a fracture of the distal second metatarsal shaft. There is prominent surrounding fracture callus, with hypointense regions corresponding to the calcification visible on the radiograph.

**DIFFERENTIAL DIAGNOSIS** None.

**DIAGNOSIS** Metatarsal stress fracture.

**DISCUSSION** On radiographs, stress fractures of long bones are evident as thin radiolucent lines that involve only a portion of the cortex, and are therefore incomplete fractures. By the time most cortical stress fractures are visible on plain film,

callus is usually present. Sometimes the callus is visible, but the fracture line itself cannot be demonstrated. A lucent line that is completely surrounded by sclerotic bone represents a stress fracture with nonunion. On radionuclide bone scan, the accelerated remodeling may be apparent as a diffuse but patchy increase in tracer accumulation. Stress fractures are focal hot spots. On MRI, stress fractures may show extensive endosteal and periosteal edema and evidence of bone healing. An actual fracture line is frequently not seen. The bone scan and MRI are far more sensitive than plain films for detecting stress reaction and stress fractures. Periosteal new bone formation and endosteal thickening in the absence of a demonstrable fracture line usually represents stress reaction, which is a healing process that occurs in the presence of microfractures. This process may be demonstrable by radionuclide bone scan if plain films are unrevealing. The condition is also called traumatic periostitis. The most common fatigue fractures in the forefoot occur at the shaft or neck of the second or third metatarsals [80].



FIGURE 8.41A

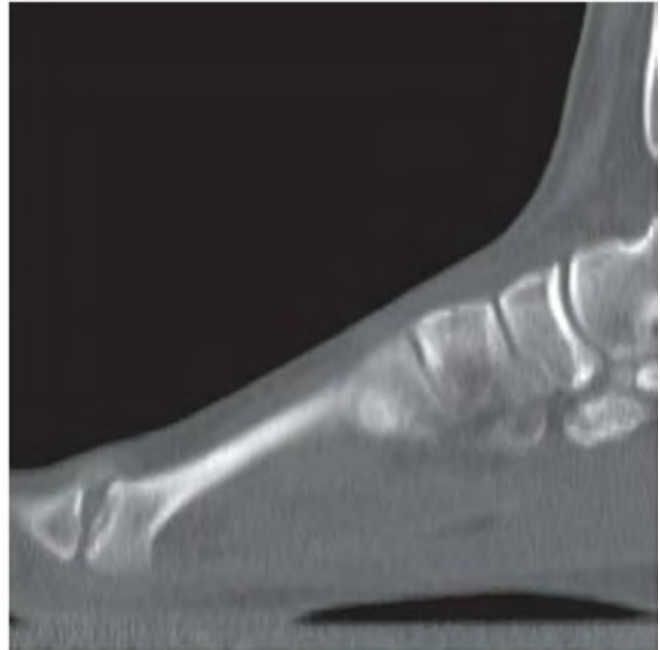


FIGURE 8.41B

**FINDINGS** (A) AP radiograph of the foot (detail of toes), and (B) sagittal reformatted CT of the left foot. The head of the second metatarsal is broad, flat, and dense. There is a subchondral low density at the head of the second metatarsal on CT. A corresponding adaptive change has occurred in the proximal end of the proximal phalanx.

**DIFFERENTIAL DIAGNOSIS** Posttraumatic osteoarthritis, postinflammatory osteoarthritis, Freiberg infraction.

**DIAGNOSIS** Freiberg infraction.

**DISCUSSION** The bones of the second MTP joint are dysplastic, suggesting a pathologic process involving the joint that occurred during skeletal growth. Both trauma and infection could involve a metatarsal joint and cause enough

damage to result in secondary osteoarthritis. The dysplastic changes suggest an abnormality of growth rather than direct injury, and the relative preservation of the cartilage space would be inconsistent with arthritis as the primary disease. Freiberg infraction is an osteochondrosis of the second metatarsal head that occurs in the 2nd decade while the epiphysis is still present. Of unknown etiology, it is believed to represent osteonecrosis, revascularization, subchondral collapse, and remodeling of the second metatarsal head. Chronic repetitive trauma leading to osteochondral injury and osteonecrosis has been suggested as the underlying cause [81]. Secondary degenerative arthritis occurs in early adulthood. The initial presentation is pain and tenderness over the metatarsal head, which typically resolves within a year or two. Chronic pain suggests the onset of secondary degenerative change. The condition is much more common in females.



FIGURE 8.42A

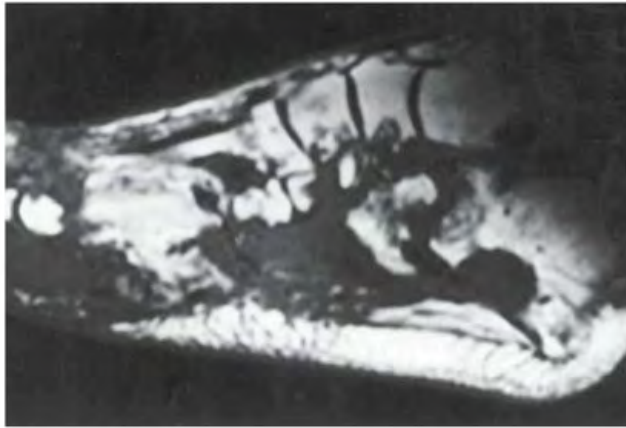


FIGURE 8.42B

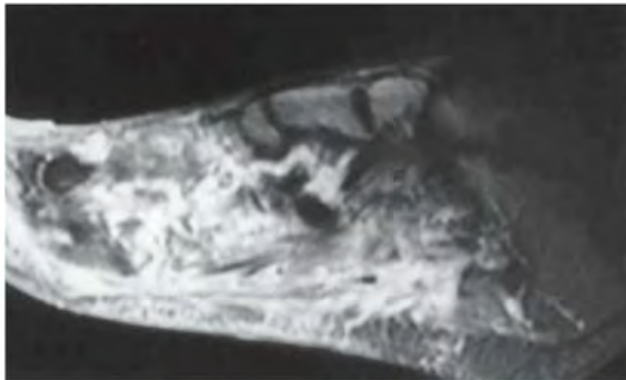


FIGURE 8.42C



FIGURE 8.42D

## FINDINGS

- A. Lateral radiograph. Multiple soft tissue calcifications are noted, most of which are round or linear. There is an erosion of the undersurface of the calcaneus and subtalar joint as well as the cuneiforms at their articulations with the metatarsals, with reinforcement of the existing trabecular pattern.
- B, C. Sagittal T1-weighted MRI without and with contrast demonstrates predominantly T1 hypointensity, with an area of T1 hyperintensity at the metatarsal bases and marked enhancement of the soft tissue mass.
- D. AP radiograph of the knee demonstrates additional soft tissue calcifications. A distal femoral central lucent lesion with scalloped borders and chondroid calcification is noted.

**DIFFERENTIAL DIAGNOSIS** Ollier disease, Maffucci syndrome, idiopathic tumoral calcinosis, synovial osteochondromatosis.

**DIAGNOSIS** Maffucci syndrome.

**DISCUSSION** The differential diagnosis of the foot includes entities that have soft tissue calcification. When the calcifications are recognized as phleboliths and the femoral lesion is recognized as an enchondroma, the diagnosis of Maffucci syndrome should be considered. MRI confirms the presence of hemangiomas in the foot and, if necessary, could confirm the presence of the enchondroma in the femur.

Maffucci syndrome is a mesodermal dysplasia consisting of multiple enchondromas and soft tissue hemangiomas. Maffucci syndrome is much less common than multiple enchondromatosis (Ollier disease), which itself is rather uncommon. The hemangiomatosis may be localized or extensive, and may occur anywhere in the skin or subcutaneous tissues. Malignant transformation of the bone lesions to chondrosarcoma has been recognized to occur in 20% of cases, based on retrospective reviews of the literature [82], but the lifetime risk of chondrosarcoma in these patients is probably much higher. The soft tissue hemangiomas are frequently found in close proximity to the bony lesions, and they may undergo malignant transformation, although with much less frequency [83].



FIGURE 8.43

**FINDINGS** AP radiograph of the forefoot. There is diffuse osteopenia. Severe hallux valgus and metatarsus primus varus is present, and there are large erosions at the first metatarsal head. Marginal erosions are seen along the medial aspect of the IP joint of the great toe, at the MTP joints of the lesser toes, and at the lateral sesamoid. The erosions appear to have a thin sclerotic border. A cock-up toe deformity with overriding is present at the third toe. The cartilage spaces of the MTP joints of the lesser toes are difficult to see because of the alignment abnormalities, but diffuse narrowing is evident at the second toe. There is a relative lack of hypertrophic bone.

**DIFFERENTIAL DIAGNOSIS** Rheumatoid arthritis, tophaceous gout, psoriatic arthritis, osteoarthritis.

**DIAGNOSIS** Rheumatoid arthritis.

**DISCUSSION** The symptoms of rheumatoid arthritis in the hand may also be found in the forefoot, including juxta-articular and chronic osteoporosis, marginal erosions, subchondral cysts,

and diffuse joint space narrowing. The MTP joints tend to be the site of greatest involvement. The relative lack of hypertrophic bone formation, such as osteophytes and subchondral sclerosis, eliminates osteoarthritis and neuropathic osteoarthropathy as possibilities. The erosions are marginal, involving the bare area of the bone that is not covered by cartilage, and is therefore directly exposed to the inflammatory pannus. Inflammatory erosions tend to have poorly defined margins, and the sclerotic rim seen in this case is indicative of healing and lack of acute disease activity. The presence of this sclerotic rim raises the question of tophaceous gout, but the distribution of disease would be unusual for gout. Furthermore, the erosions in gout represent a combination of bone loss and bone reaction, and the overhanging edges characteristic of this process are absent. Erosions in rheumatoid arthritis represent pure bone loss. Psoriatic arthritis may have an appearance that overlaps with the appearance of rheumatoid arthritis, but severe erosions in psoriatic arthritis are often more central and intra-articular rather than marginal. Periostitis would also be a distinguishing feature that is frequently present in psoriatic arthritis, but usually absent from rheumatoid arthritis.



FIGURE 8.44

**FINDINGS** AP radiograph of the foot shows multiple lesions deforming the foot. Many of the larger lesions are expansile, with thinned but intact overlying cortex. Some lesions have mineralized matrix with punctate calcifications. The second metatarsal has remodeled around the adjacent large lesion in the first metatarsal.

**DIFFERENTIAL DIAGNOSIS** None.

**DIAGNOSIS** Multiple enchondromatosis (Ollier disease).

**DISCUSSION** Multiple enchondromatosis (Ollier disease) is a nonfamilial, nonheritable, diffuse growth abnormality

in which the tubular bones may be bowed and shortened to a variable extent and filled with multiple enchondromas. The severity of involvement may range from a few lesions with mild deformities to countless ones with severe deformities. The lesions often become stable at puberty, but their growth may continue throughout the patient's lifetime. The individual lesions are radiologically and histologically identical to solitary enchondromas, but patients with multiple enchondromatosis may have as high as a 30% to 50% risk of developing chondrosarcoma in their lifetime. A lesion that becomes painful in the absence of pathologic fracture should trigger consideration of possible malignancy.

**CLINICAL HISTORY** A 37-year-old man with enlarging foot mass. There was no history of fracture.



FIGURE 8.45A

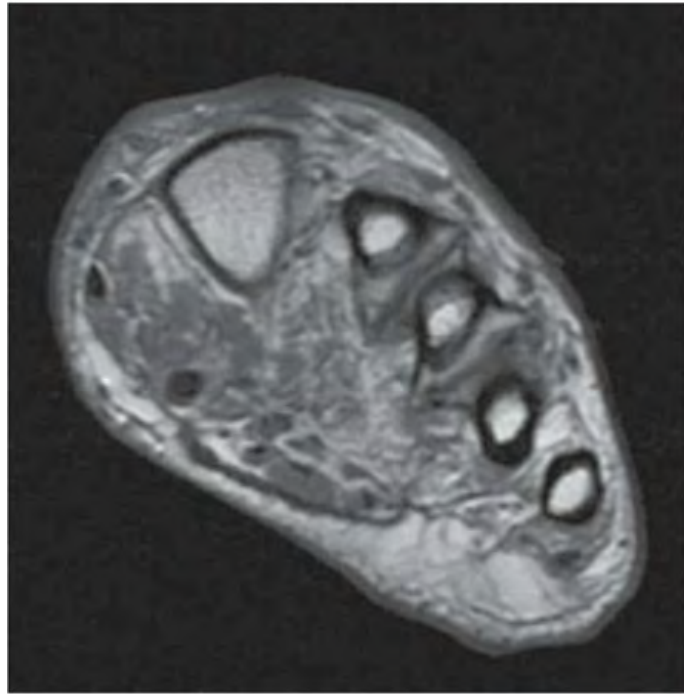


FIGURE 8.45B

## FINDINGS

- A. AP view of the foot shows an ossific lesion involving the shafts of the second, third, and fourth metatarsals. Incidental degenerative changes are seen at the great toe.
- B. MRI through the short axis of the foot shows that the ossific lesion arises from the cortex of the second, third, and fourth metatarsal shafts, and has the form of mature, reactive periosteal bone formation. There are broad pseudoarticulations. The original cortices and marrow spaces of the involved metatarsals are still delineated.

**DIFFERENTIAL DIAGNOSIS** Fracture, florid reactive periostitis, bizarre parosteal osteochondromatous proliferation (BPOP), acquired osteochondroma (Turret exostosis).

**DIAGNOSIS** BPOP (Nora's lesion).

**DISCUSSION** The conventional radiograph shows a lesion comprised of mature bone overlying the metatarsal shafts, which appear otherwise intact. The maturity of the bone indicates that the lesion is indolent, but it is difficult to tell how the process is related to the underlying metatarsals. The MRI shows that the lesions have no medullary continuity with the underlying metatarsals, eliminating the diagnosis of osteochondroma. Parosteal osteosarcoma presents as an ossific mass arising from the surface of bone, but involvement of

multiple bones would be exceedingly rare, and the mass consists entirely of mature bone without soft tissue component or destruction. This leaves a category of lesions known as reactive lesions of the bone surface, which commonly occur in the hands and feet. Included in this category are florid reactive periostitis, BPOP, and acquired osteochondroma (Turret exostosis). Radiographically, these lesions may be indistinguishable from one another. Pathologic distinction is based on the amount and character of reactive spindle cells, cartilage, and bone formation.

These lesions are related to myositis ossificans and are thought to occur as a result of trauma. Patients are typically 20 to 40 years old. The middle and proximal phalanges of the hand are most commonly affected. The chief radiologic differential is osteochondroma, which is not surprising, since these lesions often have a metaplastic cartilage cap. The lack of cortical and medullary continuity on cross-sectional imaging excludes the diagnosis, as mentioned earlier. BPOP pathologically consists of prominent bone and cartilage formation with atypical cells in both cell lines, leaving the pathologist vulnerable to the erroneous microscopic diagnosis of malignancy if the radiographic appearance is not considered [84–86]. BPOP is a benign disease with low likelihood of recurrence after resection. CT is also an excellent method of examining diseases that involve the cortex and extensive mineralization, and in these situations, CT may be preferable to MRI.



FIGURE 8.46A



FIGURE 8.46B

**FINDINGS** Radiographs of the great toe show asymmetric cartilage space narrowing, subchondral sclerosis, and prominent osteophytes at the first MTP joint. Alignment of the great toe and first ray is normal.

**DIFFERENTIAL DIAGNOSIS** None.

**DIAGNOSIS** Hallux rigidus (hallux limitus).

**DISCUSSION** Hallux rigidus is characterized by restriction of motion at the first MTP joint. The condition is also called hallux limitus, because the range of motion is very limited. This limitation in motion is usually in the dorsal direction and is most commonly associated with a mechanical block caused by periarticular osteophytes [92]. These osteophytes tend to form a horseshoe-shaped collar of hypertrophic bone around the medial, dorsal, and lateral aspects of the

first metatarsal following the articular margin, often with matching bony hypertrophy of the proximal phalanx. The condition follows the natural history of osteoarthritis and has a prevalence of about 2% in individuals older than 50. Various conditions may result in hallux rigidus, including generalized, idiopathic osteoarthritis, posttraumatic osteoarthritis, metabolic disorders such as crystal arthropathies, and congenital disorders such as a long first ray or abnormal gait. Most patients present with chronic pain, but fracture of an osteophyte or presence of a new loose body may result in an acute exacerbation. Mechanical symptoms from impingement of the dorsal bony hypertrophy on shoes may occur, and impingement of the dorsal digital nerve as it passes over the bony hypertrophy may cause burning pain or paresthesias. Females are affected twice as often as males, and most symptomatic patients are in the adolescent or elderly age groups.

**CLINICAL HISTORY** *A 45-year-old woman with painful feet.*



FIGURE 8.47A



FIGURE 8.47B

**FINDINGS** (A, B) AP and oblique radiographs of the left foot show lateral deviation of the great toe and medial deviation of the first metatarsal. The articular surface of each first metatarsal head is 50% uncovered. The lateral sesamoid is subluxated laterally from beneath the first metatarsal head. The great toe is slightly rotated externally along its long axis. Soft tissue prominence is present over the medial aspect of the first metatarsal head.

**DIFFERENTIAL DIAGNOSIS** Bunion, gout, rheumatoid arthritis, SLE.

**DIAGNOSIS** Bunion.

**DISCUSSION** The presence of a soft tissue lump at the first MTP joint suggests tophaceous gout, but the absence of erosions would be inconsistent. The lateral deviation of the great toe and the medial deviation of the first metatarsal (hallux valgus, metatarsus primus varus) define a bunion, also called hallux valgus. The soft tissue lump represents a distended bursa covering the medial prominence of the metatarsal head. Osteoarthritis is commonly associated with bunions but is a secondary feature. Bunions are also a common feature of rheumatoid arthritis, but in this case, there are no other findings to suggest that diagnosis.

Foot problems are common in the United States and other well-heeled societies; perhaps 12% of Americans, most of them women, have had an operation on the foot. As many as 80% of adult American women experience pain while wearing shoes, and the prevalence of bunions is approximately 50% [87]. Shoes that are too tight in the forefoot have been implicated as a principal cause of bunions [88]. Familial factors are also important, particularly in children and adolescents [89].

The first MTP joint has a strong plantar capsule and sesamoid mechanism, and a thin dorsal capsule. The extensor

hallucis longus and brevis tendons pass through a hood mechanism over the dorsal aspect of the first MTP joint to insert on the toes. The two heads of the flexor hallucis brevis incorporate sesamoid bones and have separate shallow grooves in which to run. The abductor hallucis inserts on the plantar medial aspect of the proximal phalanx, and the adductor hallucis anchors the sesamoid mechanism and inserts on the plantar lateral aspect of the proximal phalanx. As the great toe deviates laterally and the first metatarsal deviates medially (the causal relationship between these two processes is incompletely understood), the first MTP joint subluxates laterally. The first metatarsal head slides medially off the sesamoids, which are tethered by the adductor hallucis, and secondary degenerative changes occur at the sesamoid articulations as they are pulled out of their grooves. The abductor hallucis tendon displaces to the plantar aspect, pronating the proximal phalanx, and the flexor and extensor tendons act as a bowstring to worsen the deformity. In advanced cases, the great toe may deviate so far that it crosses underneath the second toe.

The severity of a bunion deformity may be assessed by the degree of great toe deviation, the angle between the first and second metatarsals, and the amount of lateral subluxation of the sesamoids. These measurements should be made on weight-bearing radiographs. When surgical treatment is called for, a wide variety of operations are possible, consisting generally of combinations of osteotomies to realign the bones, and soft tissue repairs to maintain the reduction [90]. Other common foot deformities that occur in the lesser toes include the claw toe (extension at the MTP joint, flexion at the PIP and DIP joints), the hammer toe (extension at the MTP joint, flexion at the PIP joint, hyperextension at the DIP joint), and the mallet toe (isolated flexion at the DIP joint). As if these problems were not enough, women's high-heeled shoes have been implicated in the development of medial and patellofemoral compartment osteoarthritis of the knee [91].


**FIGURE 8.48**

**FINDINGS** AP radiograph of both feet shows severe bilateral abnormalities. Both feet show marked valgus deviation of the great and lesser toes, with lateral subluxations that are most prominent at the great toe MTP joints. The ends of the bones of the MTP joints have been eroded, particularly at the second through fourth toes, with a suggestion of pencil-in-cup deformity at several sites. Erosions and subluxations are present at the IP joints of the great toes. Bone mineralization is normal or perhaps slightly decreased, and soft tissue swelling is relatively modest compared with the severity of the forefoot joint changes. The intertarsal joints are nearly intact, but proliferative bone is present along the medial aspects of the navicular and medial cuneiform bones.

**DIFFERENTIAL DIAGNOSIS** Rheumatoid arthritis, psoriatic arthritis, reactive arthritis, ankylosing spondylitis, neuropathic osteoarthropathy, trauma.

**DIAGNOSIS** Psoriatic arthritis (arthritis mutilans).

**DISCUSSION** The severity of the joint changes fits the descriptive term arthritis mutilans. Although in many cases it is difficult, and perhaps not important, to determine the underlying pathophysiology, the exercise is worthwhile because the diagnostic reasoning is similar in early, subtle disease. There is obvious bilateral, symmetric polyarticular disease. The central, intra-articular erosions suggest a spondyloarthropathy as the underlying disease rather than rheumatoid arthritis, because the erosions in rheumatoid arthritis tend to occur at the margins of the joint. Erosions in rheumatoid arthritis are unlikely to assume a pencil-in-cup morphology. Radiographic changes in reactive arthritis are typically rather mild, and proliferative rather than erosive changes predominate. The severity of these changes would be unusual for ankylosing spondylitis. Neuropathic osteoarthropathy and posttraumatic osteoarthritis may involve the feet bilaterally, but in those entities one would expect reactive bone formation and osseous debris, both of which are lacking in this case.



FIGURE 8.49

**FINDINGS** AP radiograph of the great toe. The articular ends of the IP joint have been eroded. Bone mineral density is maintained, and there is marked periosteal reaction about the joints.

**DIFFERENTIAL DIAGNOSIS** Psoriatic arthritis, reactive arthritis, ankylosing spondylitis, rheumatoid arthritis, septic arthritis, resection arthroplasty.

**DIAGNOSIS** Psoriatic arthritis.

**DISCUSSION** Severe erosions of the IP joint suggest an inflammatory process, but one that has not progressed to

ankylosis. The periosteal new bone formation is fluffy (the morphology associated with periostitis), rather than linear (the morphology that would be associated with infection). The lack of osteoporosis argues against rheumatoid arthritis, but osteoporosis in the feet of rheumatoid patients is often less striking than osteoporosis in the hands and upper limbs. Foot surgery actually has a greater prevalence than inflammatory arthritis among adults in the United States, so postsurgical change is always a consideration when a joint is missing. The age of the patient is more suggestive of psoriatic arthritis than reactive arthritis.



FIGURE 8.50A

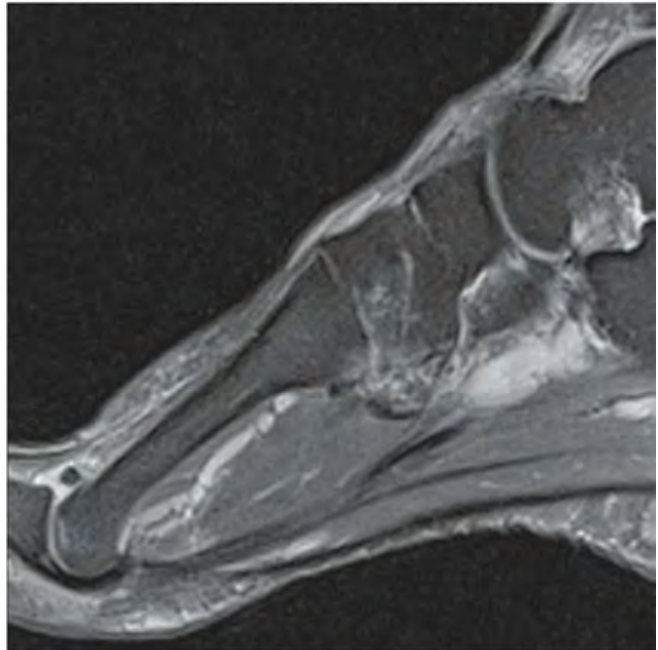


FIGURE 8.50B

**FINDINGS** (A) AP radiograph of the foot (detail of toes) and (B) sagittal proton density fat-suppressed MRI of the left foot. The head of the second metatarsal is broad, flat, and dense. MRI shows a subchondral low density at the head of the second metatarsal representing a subchondral fracture with minimal edema.

**DIFFERENTIAL DIAGNOSIS** Subchondral fracture, post-traumatic osteoarthritis, postinflammatory osteoarthritis, Freiberg infraction.

**DIAGNOSIS** Subchondral fracture.

**DISCUSSION** Subchondral fractures of metatarsal heads are believed to occur secondary to overuse or in patients with underlying conditions predisposing to insufficiency

fractures. The location and radiographic appearance of metatarsal head subchondral fractures are similar to those seen in Freiberg infraction. Although Freiberg infraction affects adolescents (12 to 18 years) and metatarsal head subchondral fractures are seen in adults, both entities likely share a cause that combines mechanical stress, subchondral fracture, vascular injury, and subsequent osteonecrosis. On MR, two types of MRI findings may be noted. In the early stage, there are subchondral fractures with severe bone marrow edema-like pattern that extended into the periarticular soft tissues. In the late stage, there is metatarsal head flattening with subchondral sclerosis and mild or absent marrow edema-like pattern. The treatment of metatarsal head subchondral fractures and Freiberg infraction includes modification of activities, orthotics, and surgical intervention [93].



FIGURE 8.51

**FINDINGS** AP radiograph of the forefoot with attention to the first MTP joint shows transverse fractures of the medial (tibial) and lateral (fibular) sesamoids. The fracture fragments are distracted by several millimeters.

**DIFFERENTIAL DIAGNOSIS** None.

**DIAGNOSIS** Sesamoid fracture.

**DISCUSSION** Traumatic fractures of the sesamoid bones of the great toe may occur with dorsal dislocation of the first MTP joint. The medial and lateral heads of the flexor hallucis brevis attach to the medial and lateral sesamoid bones, respectively, which then attach to the proximal plantar aspect of the proximal phalanx of the great toe through the plantar capsule. Dorsal dislocation of the great toe at the MTP joint produces severe tensile loading of the sesamoid mechanism and is the basis for these distracted transverse fractures. Alternatively, the plantar capsule may rupture distal to the sesamoids. These injuries are typically sustained when force

is applied to the dorsiflexed great toe in activities such as football, motor vehicle accidents, equestrian stirrup injuries, and falls from heights. The term “turf toe” refers to the higher frequency of these injuries in football players who play on artificial turf as opposed to grass [94].

Stress fractures of the sesamoids are more common injuries than traumatic fractures, and they occur in various athletic activities, including dance and distance running. Because the flexor hallucis brevis tends to distract the fragments, nonunion is a common complication. Although resection of the sesamoid fragments is the most common operative treatment for such nonunions, bone grafting may be successful [95]. Stress fractures occur more commonly in the medial sesamoid [96], whereas traumatic fractures occur more commonly in the lateral sesamoid. Sesamoid fractures may be distinguished radiographically from bipartite sesamoids by the absence of rounded contours and circumferential cortical margins. MRI can differentiate between nondisplaced sesamoid fractures and other causes of sesamoid pain including sesamoiditis, osteonecrosis, osteomyelitis, arthritis, and bursitis [97].

**CLINICAL HISTORY** A 33-year-old woman soccer player with great toe pain.

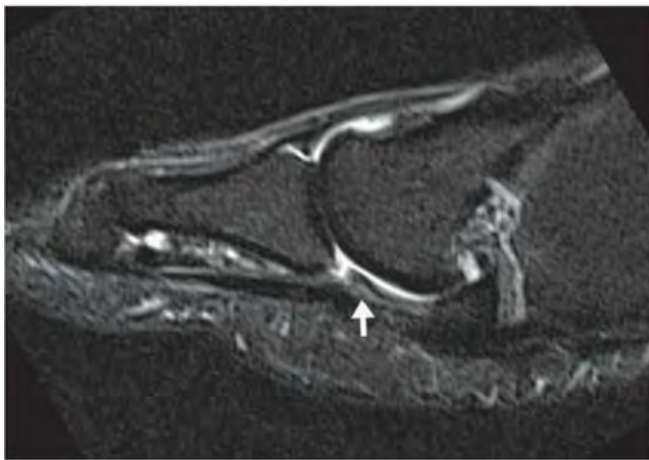


FIGURE 8.52A

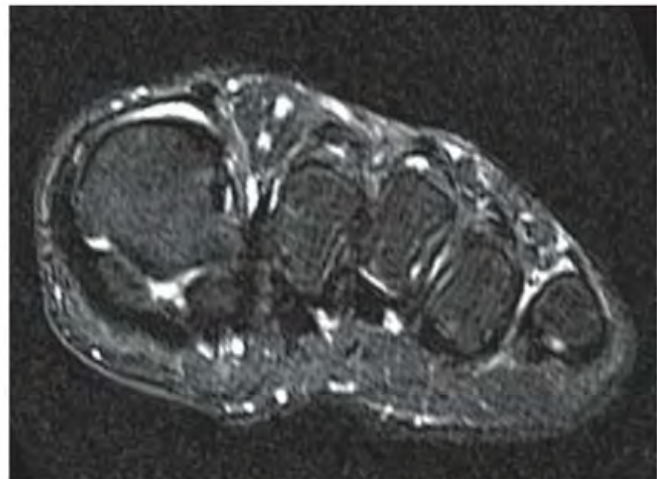


FIGURE 8.52B



FIGURE 8.52C

**FINDINGS** Sagittal inversion recovery (A, C), and axial T2-weighted, fat-suppressed MRI (B) through the first metatarsophalangeal (MTP) joint shows the plantar plate with intermediate signal intensity (*arrows* in A). There is no partial or complete disruption of the plantar plate. Both sesamoids are well contained under the first metatarsal head, and the flexor hallucis longus is well situated in the groove. Parasagittal image (C) demonstrates small subchondral edema in the first metatarsal head.

**DIFFERENTIAL DIAGNOSIS** None.

**DIAGNOSIS** Turf toe (Grade I plantar plate injury).

**DISCUSSION** The plantar plate is a fibrocartilaginous thickening of the plantar aspect of the capsule of the first MTP joint. It has a very strong distal attachment along the plantar

aspect of the base of the proximal phalanx and a weaker attachment proximally through the capsule to the plantar aspect of the first metatarsal neck. The plantar plate extends both medially and laterally to contain the tibial and fibular sesamoids, and it prevents hyperextension of the first MTP joint. The term “turf toe” has been used to describe various soft tissue injuries about the first MTP joint. However, it is strictly defined as a plantar capsular ligament injury of the first MTP joint. Turf toe was first described in athletes playing American football on artificial turf. The incidence of injury has increased with the widespread use of new artificial playing surfaces combined with lighter and more flexible footwear designed for these surfaces, which typically provide less support to the MTP joints [98].

MR imaging is ideal for grading the extent of plantar plate injury, which is usually best depicted on sagittal and short-axis axial T2-weighted images through the first MTP joint. Normally, the plantar plate shows homogeneous signal intensity in all sequences. With MR arthrography, a small central distal recess is identified between both lateral insertions of the plantar plate in the proximal phalanx. This recess should not be misinterpreted as evidence of a tear [99]. Grade I injury demonstrates soft tissue edema and swelling along the plantar aspect of the first MTP joint. There may be mild thickening and edema within the plantar capsular structures. Grade II injury reveals a partial-thickness tear/disruption of the plantar capsule, and a Grade III injury manifests as a complete disruption of the plantar capsular structures and may demonstrate associated sesamoid pathology. Associated osteochondral lesions of the dorsal metatarsal head may also be demonstrated [99]. Turf toe is usually treated successfully with conservative management, and surgery is reserved for refractory or complicated cases.



FIGURE 8.53

**FINDINGS** AP radiograph of both feet demonstrates extensive bony resorption of the phalanges, with lace-like destruction. Margins of the bone resorption are corticated. There are no joint changes. Cyst-like lesions are best seen at the left great toe.

**DIFFERENTIAL DIAGNOSIS** Thermal injury, leprosy, sarcoidosis, gout.

**DIAGNOSIS** Sarcoidosis.

**DISCUSSION** Sarcoidosis is a multisystemic granulomatous disease of unknown etiology commonly encountered in young adults affecting the lungs, skin, and eyes. Skeletal

involvement is seen in 5% to 10% of patients with sarcoidosis, and the disease most frequently affects the phalanges of the hands and feet, although involvement of the vertebral bodies can occur. Radiologic features may include cyst-like radiolucent areas, a lace-like honeycomb appearance, or extensive bone erosion with pathologic fractures [100]. The articular spaces are usually intact, unless extensive neuropathic lesions develop. A subcutaneous soft tissue mass or tenosynovitis may also be present. The natural history of sarcoid bone lesions is variable, ranging from rare cases of recovery to gradual progression and eventual auto-amputation. Treatment with systemic corticosteroids may result in improvement or stabilization of bone lesions, but bone usually does not return to normal.

## SOURCES AND READINGS

- Churchill RS, Sferra JJ. Posterior tibial tendon insufficiency. Its diagnosis, management, and treatment. *Am J Orthop*. 1998;27:339–347.
- Anderson MW, Kaplan PA, Dussault RG, Hurwitz S. Association of posterior tibial tendon abnormalities with abnormal signal intensity in the sinus tarsi on MR imaging. *Skeletal Radiol*. 2000;29:514–519.
- Crawford AH. Ankle fractures in children. *Instr Course Lect*. 1995;44:317–324.
- Karrholm J. The triplane fracture: four years of follow-up of 21 cases and review of the literature. *J Pediatr Orthop B*. 1997;6:91–102.
- El-Karef E, Sadek HI, Nairn DS, Aldam CH, Allen PW. Triplane fracture of the distal tibia. *Injury*. 2000;31:729–736.
- Barnada A, Gaynor T, Mubarak SJ. Premature physal closure following distal tibia physal fractures: a new radiographic predictor. *J Pediatr Orthop*. 2003;23:733–739.
- Marchevsky AM, Damsker B, Green S, Tepper S. The clinicopathological spectrum of non-tuberculous mycobacterial osteoarticular infections. *J Bone Joint Surg Am*. 1985;67:925–929.
- Hirsch R, Miller SM, Kazi S, Cate TR, Reveille JD. Human immunodeficiency virus-associated atypical mycobacterial skeletal infections. *Semin Arthritis Rheum*. 1996;25:347–356.
- Granowetter L, West DC. The Ewing's sarcoma family of tumours: Ewing's sarcoma and peripheral primitive neuroectodermal tumor of bone and soft tissue. *Cancer Treat Res*. 1997;92:253–308.
- Kransdorf MJ, Murphey MD. *Imaging of Soft Tissue Tumors*. Philadelphia, PA: Saunders; 1997:264–269.
- Kimber C, Michalski A, Spitz L, Pierro A. Primitive neuroectodermal tumours: anatomic location, extent of surgery, and outcome. *J Pediatr Surg*. 1998;33:39–41.
- Brodie JT, Dormans JP, Gregg JR, Davidson RS. Accessory soleus muscle. A report of 4 cases and review of literature. *Clin Orthop Relat Res*. 1997;180–186.
- Doda N, Peh WC, Chawla A. Symptomatic accessory soleus muscle: diagnosis and follow-up on magnetic resonance imaging. *Br J Radiol*. 2006;79:e129–e132.
- Sookur PA, Naraghi AM, Blealney RR, Jalan R, Chan O, White LM. Accessory muscles: anatomy, symptoms, and radiologic evaluation. *Radiographics*. 2008;28:481–499.
- Helgason JW, Chandnani VP. MR arthrography of the ankle. *Radiol Clin North Am*. 1998;36:729–738.
- Chandnani VP, Harper MT, Ficke JR, et al. Chronic ankle instability: evaluation with MR arthrography, MR imaging, and stress radiography. *Radiology*. 1994;192:189–194.
- Levine SM, Lambiase RE, Petchprapa CN. Cortical lesions of the tibia: characteristic appearances at conventional radiography. *Radiographics*. 2003;23:157–177.
- Rhys R, Davies AM, Mangham DC, Grimer RJ. Sclerotome distribution of melorheostosis and multicentric fibromatosis. *Skeletal Radiol*. 1998;27:633–636.
- Donath J, Poor G, Kiss C, Fornet B, Genant H. Atypical form of active melorheostosis and its treatment with bisphosphonate. *Skeletal Radiol*. 2002;31(12):709–713.
- Rodriguez-Merchan EC. Management of the orthopaedic complications of haemophilia. *J Bone Joint Surg Br*. 1998;80:191–196.
- Smith JA. Bone disorders in sickle cell disease. *Hematol Oncol Clin North Am*. 1996;10:1345–1356.
- Rifai A, Nyman R. Scintigraphy and ultrasonography in differentiating osteomyelitis from bone infarction in sickle cell disease. *Acta Radiol*. 1997;38:139–143.
- Sadat-Ali M, al-Uman R, al-Habdan I, al-Mulhim F. Ultrasonography: can it differentiate between vasoocclusive crisis and acute osteomyelitis in sickle cell disease? *J Pediatr Orthop*. 1998;18:552–554.
- Al-Nakshabandi NA, Ryan AG, Choudur H, et al. Pigmented villonodular synovitis. *Clin Radiol*. 2004;59:414–420.
- Baker ND, Klein JD, Weidner N, Weissman BN, Brick GW. Pigmented villonodular synovitis containing coarse calcifications. *AJR Am J Roentgenol*. 1989;153:1228–1230.
- Cobby MJ, Adler RS, Swartz R, Martel W. Dialysis-related amyloid arthropathy: MRI findings in 4 patients. *AJR Am J Roentgenol*. 1991;157:1023–1027.
- Kalil RK, Unni KK. Malignancy in pigmented villonodular synovitis. *Skeletal Radiol*. 1998;27:392–395.
- Bertoni F, Unni KK, Beabout JW, Simm FH. Malignant giant cell tumor of the tendon sheaths and joints (malignant pigmented villonodular synovitis). *Am J Surg Pathol*. 1997;21:153–163.
- Maillard SM, Jones R, Owens C, et al. Quantitative assessment of MRI T2 relaxation time of thigh muscles in juvenile dermatomyositis. *Rheumatology (Oxford)*. 2004;43:603–608.
- Lofberg M, Liewendahl K, Lamminen A, Korhola O, Somer H. Antimyosin scintigraphy compared with magnetic resonance imaging in inflammatory myopathies. *Arch Neurol*. 1998;55:987–993.
- Ly JQ, LaGatta LM, Beall DP. Calcaneal chondroblastoma with secondary aneurysmal bone cyst. *AJR Am J Roentgenol*. 2004;182:130.
- Lektrakul N, Chung CB, Lai Ym, et al. Tarsal sinus: arthrographic, MR imaging, MR arthrographic, and pathologic findings in cadavers and retrospective study data in patients with sinus tarsi syndrome. *Radiology*. 2001;219:802–810.
- Lektrakul N, Chung CB, Lai Ym, et al. Tarsal sinus: arthrographic, MR imaging, MR arthrographic, and pathologic findings in cadavers and retrospective study data in patients with sinus tarsi syndrome. *Radiology*. 2001;219:802–810.
- Rosenberg ZS, Beltran J, Bencardino JT. MR imaging of the ankle and foot. *Radiographics*. 2000;20(Spec No):S153–S179.
- Oloff LM, Schulhofer SD, Bocko AP. Subtalar joint arthroscopy for sinus tarsi syndrome: a review of 29 cases. *J Foot Ankle Surg*. 2001;40:152–157.
- Delanois RE, Mont MA, Yoon TR, Mizell M, Hungerford DS. A traumatic osteonecrosis of the talus. *J Bone Joint Surg Am*. 1998;80:529–536.
- Inokuchi S, Ogawa K, Usami N, Hashimoto T. Long-term follow up of talus fractures. *Orthopedics*. 1996;19:477–481.
- Bohay DR, Manoli A II. Subtalar joint dislocations. *Foot Ankle Int*. 1995;16:803–808.
- Goldner JL, Poletti SC, Gates HS III, Richardson WJ. Severe open subtalar dislocations: long-term results. *J Bone Joint Surg Am*. 1995;77:1075–1079.
- Drennan JC. Tarsal coalitions. *Instr Course Lect*. 1996;45:323–329.
- Liu PT, Roberts CC, Chivers FS, et al. "Absent middle facet": a sign on unenhanced radiography of subtalar joint coalition. *AJR Am J Roentgenol*. 2003;181:1565–1572.
- Drennan JC. Congenital vertical talus. *Instr Course Lect*. 1996;45:315–322.
- Greene WB. Metatarsus adductus and skewfoot. *Instr Course Lect*. 1994;43:161–177.
- Reilly PA, Evison G, McHugh NJ, Maddison PJ. Arthropathy of hands and feet in systemic lupus erythematosus. *J Rheumatol*. 1990;17:777–784.
- Mizuntani W, Quismorio FP Jr. Lupus foot: deforming arthropathy of the feet in systemic lupus erythematosus. *J Rheumatol*. 1984;11:80–82.
- Calamia KT, Balabanova M. Vasculitis in systemic lupus erythematosus. *Clin Dermatol*. 2004;22:148–156.
- Gonzalez JV, Stuck RM, Streit N. Intraosseous lipoma of the calcaneus: a clinicopathologic study of three cases. *J Foot Ankle Surg*. 1997;36:306–310.
- Greaney RB, Gerber FH, Laughlin RL, et al. Distribution and natural history of stress fractures in U.S. Marine recruits. *Radiology*. 1983;146:339–346.
- Cohen PA, Job-Deslandre CH, Lalande G, Adamsbaum C. Overview of the radiology of juvenile idiopathic arthritis (JIA). *Eur J Radiol*. 2000;33:94–101.
- Johnson K, Gardner-Medwin J. Childhood arthritis: classification and radiology. *Clin Radiol*. 2002;57(1):47–58.
- DeMaio M, Paine R, Mangine RE, Drez D Jr. Plantar fasciitis. *Orthopedics*. 1993;16:1153–1163.

52. Ozdemir H, Ozdemir A, Soyucu Y, Urguden M. The role of bone scintigraphy in determining the etiology of heel pain. *Ann Nucl Med*. 2002;16:395–401.
53. Morrison WB. Magnetic resonance imaging of sports injuries of the ankle. *Top Magn Reson Imaging*. 2003;14:179–197.
54. Gerster JC, Vischer TL, Bennani A, Fallet GH. The painful heel. Comparative study in rheumatoid arthritis, ankylosing spondylitis, Reiter's syndrome, and generalized osteoarthritis. *Ann Rheum Dis*. 1977;36:343–348.
55. Kiryu H, Tsuneyoshi M, Enjoji M. Myofibroblasts in fibromatoses. An electron microscopic study. *Acta Pathol Jpn*. 1985;35:533–547.
56. Sundaram M, McGuire MH, Schajowicz F. Soft tissue masses: histologic basis for decreased signal intensity (short T2) on T2-weighted MR images. *AJR Am J Roentgenol*. 1987;148:1247–1250.
57. Yacoe ME, Bergman AG, Ladd AL, Helman BH. Dupuytren's contracture: MR imaging findings and correlation between MR signal intensity and cellularity of lesions. *AJR Am J Roentgenol*. 1993;160:813–817.
58. Pasternack WA, Davison GA. Plantar fibromatosis: staging by magnetic resonance imaging. *J Foot Ankle Surg*. 1993;32:390–396.
59. Morrison WB, Schweitzer ME, Wapner KL, Lachman RD. Plantar fibromatosis: a benign aggressive neoplasm with a characteristic appearance on MR images. *Radiology*. 1994;193:841–845.
60. Hayes CW, Conway WF. Calcium hydroxyapatite deposition disease. *Radiographics*. 1990;10:1031–1048.
61. Secundini R, Scheines EJ, Gusis SE, Riopedre AM, Citera G, Maldonado Cocco JA. Clinico-radiological correlation of enthesitis in seronegative spondyloarthropathies (SNSA). *Clin Rheumatol*. 1997;16:129–132.
62. Tan PL, Teh J. MRI of the diabetic foot: differentiation of infection from neuropathic change. *Br J Radiol*. 2007;80:939–948.
63. Takao M, Ochi M, Uchio Y, Naito K, Kono T, Oae K. Osteochondral lesions of the talar dome associated with trauma. *Arthroscopy*. 2003;19:1061–1067.
64. Barnes CJ, Ferkel RD. Arthroscopic debridement and drilling of osteochondral lesions of the talus. *Foot Ankle Clin*. 2003;8:243–257.
65. Reade B, Atlas G, Distasio J, Kruljac S. Mueller-Weiss syndrome: an uncommon cause of midfoot pain. *J Foot Ankle Surg*. 1998;37:535–539.
66. Haller J, Sartoris DJ, Resnick D, et al. Spontaneous osteonecrosis of the tarsal navicular in adults: imaging findings. *AJR Am J Roentgenol*. 1988;151:355–358.
67. Kramer J, Recht M, Deely DM, et al. MR appearance of idiopathic synovial osteochondromatosis. *JCAT*. 1993;17:772–776.
68. Kitagawa Y, Ito H, Amano Y, Sawaizumi T, Takeuchi T. MR imaging for preoperative diagnosis and assessment of local tumor extent on localized giant cell tumor of tendon sheath. *Skeletal Radiol*. 2003;32:633–638.
69. Middleton WD, Patel V, Teefey SA, Boyer MI. Giant cell tumors of the tendon sheath: analysis of sonographic findings. *AJR Am J Roentgenol*. 2004;183:337–339.
70. Goiney RC, Connell DG, Nichols DM. CT evaluation of tarso-metatarsal fracture-dislocation injuries. *AJR Am J Roentgenol*. 1985;144:985–990.
71. Otis JC, Deland JT, Lee S, Gordon J. Peroneus brevis is a more effective evorter than peroneus longus. *Foot Ankle Int*. 2004;25:242–246.
72. Rosenberg ZS, Beltran J, Cheung YY, Colon E, Herraiz E. MR features of longitudinal tears of the peroneus brevis tendon. *AJR Am J Roentgenol*. 1997;168:141–147.
73. Dombek MF, Lamm BM, Saltrick K, Mendicino RW, Catanzariti AR. Peroneal tendon tears: a retrospective review. *J Foot Ankle Surg*. 2003;42:250–258.
74. Williams BA, Morris LL, Toogood IR, Penfold JL, Foster BK. Limb deformity and metaphyseal abnormalities in thalassemia major. *Am J Pediatr Hematol Oncol*. 1992;14:197–201.
75. Giuzio E, Bria M, Bisconte MG, et al. Skeletal changes in thalassemia major. *Ital J Orthop Traumatol*. 1991;17:269–275.
76. Johanson NA. Musculoskeletal problems in hemoglobinopathies. *Orthop Clin North Am*. 1990;21:191–198.
77. Brasch RC, Wesbey GE, Gooding CA, Koerper MA. MRI of transfusional hemosiderosis complicating thalassemia major. *Radiology*. 1984;150:767–771.
78. Levin TL, Sheth SS, Ruzal-Shapiro C, Abramson S, Piomelli S, Berdon WE. MRI marrow observations in thalassemia: the effects of primary disease, transfusional treatment, and chelation. *Pediatr Radiol*. 1995;25:607–613.
79. Steinbach LS, Johnston JO, Tepper EF, Honda GD, Martel W. Tumoral calcinosis: radiologic-pathologic correlation. *Skeletal Radiol*. 1995;24:573–578.
80. Eisele SA, Sammarco GJ. Fatigue fractures of the foot and ankle in the athlete. *Instr Course Lect*. 1993;42:175–183.
81. Brower AC. The osteochondroses. *Orthop Clin North Am*. 1983;14:99–117.
82. Sun TC, Swee RG, Shives TC, Uni KK. Chondrosarcoma in Maffucci's syndrome. *J Bone Joint Surg Am*. 1985;67:1214–1219.
83. Lewis RJ, Ketcham AS. Maffucci syndrome: functional and neoplastic significance. Case report and review of the literature. *J Bone Joint Surg Am*. 1973;55:1465–1479.
84. Nora EF, Dahlin DC, Beabout JW. Bizarre parosteal osteochondromatous proliferations of the hands and feet. *Am J Surg Pathol*. 1983;7:245–250.
85. Bandiera S, Bacchini P, Bertoni F. Bizarre parosteal osteochondromatous proliferation of bone. *Skeletal Radiol*. 1998;27:154–156.
86. Meneses MF, Unni KK, Swee RG. Bizarre parosteal osteochondromatous proliferation of bone (Nora's lesion). *Am J Surg Pathol*. 1993;17:691–697.
87. Thompson GH. Bunions and deformities of the toes in children and adolescents. *Instr Course Lect*. 1994;45:355–367.
88. Coughlin MJ, Thompson FM. The high price of high-fashion footwear. *Instr Course Lect*. 1995;44:371–377.
89. Frey CC. Trends in women's footwear. *Instr Course Lect*. 1995;44:385–387.
90. Coughlin MJ. Hallux valgus. *J Bone Joint Surg Am*. 1996;78:932–966.
91. Kerrigan DC, Todd MK, Riley PO. Knee osteoarthritis and high-heeled shoes. *Lancet*. 1998;351:1399–1401.
92. Shereff MJ, Baumhauer JF. Hallux rigidus and osteoarthritis of the first metatarsophalangeal joint. *J Bone Joint Surg Am*. 1998;80:898–908.
93. Torriani M, Thomas BJ, Bredella MA, Ouellette H. MRI of metatarsal head subchondral fractures in patients with forefoot pain. *AJR Am J Roentgenol*. 2008;190:570–575.
94. Rodeo SA, O'Brien S, Warren RF, Barnes R, Wickiewicz TL, Dillingham MF. Turf-toe: an analysis of metatarsophalangeal joint sprains in professional football players. *Am J Sports Med*. 1990;18:280–285.
95. Richardson EG. Hallux sesamoid pain: causes and surgical treatment. *J Am Acad Orthop Surg*. 1999;7:270–278.
96. Biedert R, Hintermann B. Stress fractures of the medial great toe sesamoids in athletes. *Foot Ankle Int*. 2003;24:137–141.
97. Karasick D, Schweitzer ME. Disorders of the hallux sesamoid complex: MR features. *Skeletal Radiol*. 1998;27:411–418.
98. Sanders TG, Rathur SK. Imaging of painful conditions of the hallux sesamoid complex and plantar capsular structures of the first metatarsophalangeal joint. *Radiol Clin North Am*. 2008;46(6):1079–1092.
99. Theumann NH, Pfirrmann CW, Mohana Borges AV, Trudell DJ, Resnick D. Metatarsophalangeal joint of the great toe: normal MR, MR arthrographic, and MR bursographic findings in cadavers. *J Comput Assist Tomogr*. 2002;26(5):829–838.
100. Koyama T, Ueda H, Togashi K, Umekoka S, Kataoka M, Nagai S. Radiologic manifestations of sarcoidosis in various organs. *Radiographics*. 2004;24:87–104.



# A

Accessory soleus muscle  
ankle  
lateral radiograph, 489  
MRI, 489  
Accident. *See* Automobile accident;  
Motorcycle accident; Motor  
vehicle accident  
Acetabular dysplasia, 220  
Acetabular fractures, 221  
Achilles tendon rupture  
MRI  
basketball, 478  
sonography  
ankle, 476–477  
Achondroplasia  
AP radiograph  
lower leg, 423  
lumbar spine, 202  
Acquired osteochondroma (Turret exos-  
tosis), 538  
Acromegaly  
with carpal tunnel syndrome, 26  
hands, 26  
Acromioclavicular separation (grade 2)  
AP radiograph, 119  
shoulder, 119  
Acromioclavicular subluxation, 118  
Acute brachial neuritis, 99  
Acute osteomyelitis  
shoulder, 95  
Adamantinoma  
lower leg  
AP radiograph, 436–437  
lateral radiograph, 436–437  
Albers-Schonberg disease, 419  
Amyloidosis  
thigh, 272–273  
Anemia  
CT  
pelvis, 244  
Aneurysmal bone cysts (ABCs)  
AP radiograph, 312–313  
hip pain, 312–313  
MRI, 312–313  
lower limbs, 472–473  
Angiomatosis  
cystic, 246  
Ankle  
AP radiograph  
accessory soleus muscle, 489  
atypical mycobacterium osteomyelitis,  
486–487  
football injury, 545–546  
hemophilic pseudotumor, 493  
motorcycle accident, 503  
osteonecrosis, 502  
pain, 497, 502  
pigmented villonodular synovitis  
(PVNS), 496–497  
Salter type IV fracture, 483  
CT  
hemophilic pseudotumor, 493  
tripplane fracture, 484–485

lateral radiograph  
atypical mycobacterium osteomyelitis,  
486–487  
calcaneal fatigue fracture, 512–513  
football injury, 545–546  
hydroxyapatite deposition disease, 515  
motorcycle accident, 503  
osteonecrosis, 502  
osteonecrosis in sickle cell disease,  
494  
pain, 489, 494  
pigmented villonodular synovitis  
(PVNS), 496–497  
reactive arthritis, 518  
subtalar dislocation, 503  
Maisonneuve fracture of, 432  
mortise radiograph  
osteonecrosis, 494, 502  
pain, 494  
pigmented villonodular synovitis  
(PVNS), 496–497  
MRI  
accessory soleus muscle, 489  
atypical mycobacterium osteomyelitis,  
486–487  
basketball, 478, 522  
calcaneal fatigue fracture, 512–513  
dermatomyositis, 498  
extraskeletal primitive neuroectoder-  
mal tumor (PNET), 488  
lateral ankle ligament tear, 490–491  
marrow infarction, 495  
osteochondral lesion of the talus, 521  
peroneus brevis tendon split tear, 529  
pigmented villonodular synovitis  
(PVNS), 496–497  
PTT longitudinal split tear, 482  
sinus tarsi syndrome, 499  
swollen, 472–473  
oblique radiograph  
basketball, 522  
bunion, 540–541  
chronic foot swelling, 531  
idiopathic tumoral calcinosis, 531  
osteochondral lesion of the  
talus, 522  
sonography  
rugby, 476–477  
Ankylosing spondylitis  
automobile accident, 184–185  
back pain, 234–235  
cervical spine, 148–149  
with fracture, 148–149  
with fracture dislocation  
lumbar spine, 184–185  
hip pain, 241  
pelvis, 234–235, 241  
ulcerative colitis, 234–235  
Anterior cruciate ligament (ACL) sprain  
knee  
AP radiograph, 392–393  
MRI, 384–385, 392–394  
Anterior hip dislocation, 226  
Anterior shoulder dislocation, 108–109

Anteroposterior (AP) radiograph  
ankle  
atypical mycobacterium osteomyelitis,  
486–487  
football injury, 545, 546  
hemophilic pseudotumor, 493  
metatarsus adductus, 507  
osteonecrosis, 483  
pain, 493, 496–497, 502  
pigmented villonodular synovitis  
(PVNS), 496–497  
Salter type IV fracture, 483  
tripplane fractures, 484–485  
arms  
bone cyst, with pathologic  
fracture, 89  
juxtacortical chondroma, 86–87  
cervical spine  
Klippel-Feil syndrome, 142–143  
osteopetrosis, 157  
retinoid toxicity, 158–159  
elbows, 72  
medial epicondyle avulsion fracture,  
75  
osteochondrosis of the capitellum, 74  
posterior dislocation, 68  
posterior elbow dislocation, 76  
radial head subluxation, 69  
foot  
anemia, 530  
classic clubfoot (talipes equinovarus),  
505  
diabetes, 520–521  
football player, 545  
freiberg infraction, 533  
intraosseous lipoma, 474–475,  
510–511  
Lisfranc fracture dislocation, 528  
mass, 426–427, 538  
melorheostosis, 492  
motor vehicle accident, 503, 528  
Mueller-Weiss syndrome, 523  
multiple enchondromatosis, 537  
neuropathic osteoarthropathy,  
520–521  
pain, 492, 499–501, 510–511,  
520–521, 523, 532, 533, 544  
polyarticular arthritis, 509, 536  
rash, 542  
rheumatoid arthritis, 536  
swelling, 519  
systemic lupus erythematosus (SLE),  
508  
thalassemia, 530  
topaceous gout, 519  
humerus, 89  
knee  
anterior cruciate ligament (ACL)  
sprain, 392–393  
articular chondroma, 338–339  
battered child, 401  
calcified medullary infarcts with sub-  
chondral collapse of the tibial  
articular surface, 364–365

## Anteroposterior (AP) radiograph

(Continued)

- calcium pyrophosphate dihydrate (CPPD), 369
- Gaucher disease, 360–361
- giant cell tumor, 340–341
- hemophilic knee, 356–357
- horizontal intercondylar dislocation of the patella, 400
- inflammatory arthritis, 364–365
- juvenile idiopathic arthritis, 372–375
- leg-length discrepancy, 380
- lymphoma, 352–353
- malignant fibrous histiocytoma (MFH), 350–351
- mass, 346–347
- medial collateral ligament (MCL) sprain, 396–393
- metallosis, 409
- osteochondromatosis, 376–377
- osteosarcoma, 342, 344–345, 348–349
- Paget's disease, 382–383
- pain, 340–342
- parosteal osteosarcoma, 346–347
- poliomyelitis, 380
- primary lymphoma of bone, 352–353
- pyrophosphate arthropathy, 378
- radiation changes, 366
- recurrent pain, 369, 378
- rheumatoid arthritis, 368
- secondary synovial osteochondromatosis, 376–377
- short stature, 374–375
- sickle cell anemia, 363
- swelling, 338–339, 342, 344–345
- swollen, 356–357
- total knee replacement with failure of tibial polyethylene, 407
- trauma, 400
- lower leg, 445
  - achondroplasia, 423
  - adamantinoma, 436–437
  - Blount's disease, 416
  - bowed, 422
  - Brodie's abscess, 448–449
  - calcific myonecrosis, 462–463
  - chondromyxoid fibroma, 434–435
  - congenital adrenocortical hyperplasia with limb lengthening, 420–421
  - cystic lymphangiomas, 464
  - Ewing's sarcoma, 446–447
  - falls, 432
  - fibrous dysplasia, 424–425
  - foot drop, 462–463
  - hypertrophic osteoarthropathy, 471
  - knee pain, 433
  - knee trauma, 458
  - Maisonneuve fractures, 432
  - mass, 431
  - multiple bone lesions, 464
  - multiple problems, 418
  - NF-1, 417
  - nonossifying fibroma, 433
  - open segmental fracture, 452
  - ossifying fibroma, 442–443
  - osteoblastoma, 431
  - osteochondroma, 430
  - osteogenesis imperfecta, 418
  - osteopetrosis, 419
  - Paget's disease, 445
  - pain, 424–425
  - periosteal osteosarcoma, 440–441
  - physiologic bowing, 422
  - Salter type IV fracture, 458
  - short stature, 420–421, 423
  - stress fracture, 454–455
  - swelling, 430
  - tender, 446–447
  - toddler, 453
  - tuberculous osteomyelitis, 450–451
- lumbar spine
  - achondroplasia, 202
  - ankylosing spondylitis, 184–185
  - hemangioma, 181
  - hemangioma with vertebral collapse, 186–187
  - multiple myeloma, 188–189
  - psoriatic spondyloarthropathy, 194–195
- pelvis
  - anterior hip dislocation, 226
  - back pain, 234–235
  - bilateral hip pain, 241
  - chondrosarcoma, 216–217
  - desmoplastic fibroma, 254–255
  - developmental dysplasia of the hip, 215
  - diffuse breast carcinoma metastases, 251
  - dislocated total hip replacement, 256
  - eosinophilic granuloma, 249
  - episodic pain, 264
  - Ewing's sarcoma, 208–209
  - femoroacetabular impingement, 221
  - fluorosis, 227
  - groin pain, 250
  - hemangiomatosis, 245
  - hip stiffness, 223
  - inguinal mass, 252–253
  - insufficiency fractures, 210–211
  - joint stiffness, 242
  - lung cancer metastasis, 260–261
  - motor vehicle crash, 224–225
  - multiple hereditary exostoses, 247
  - non-Hodgkin's lymphoma, 210–211
  - osteoarthritis, 238–239
  - osteosarcoma, 218–219
  - pain, 230
  - plasmacytoma, 248
  - pubic pain, 216–217
  - rheumatoid arthritis, 240
  - sacroiliac joint pain, 228
  - small fingernails, 243
  - total hip prosthesis, 257
  - total hip replacement, 257
- ribs
  - Brown tumor, 126–127
- shoulder
  - acromioclavicular separation (grade 2), 119
  - acromioclavicular subluxation, 118
  - acute osteomyelitis, 95
  - anterior dislocation, 108–109
  - brachial plexus palsy, 98
  - chondroblastoma, 94
  - chondrosarcoma, 90–91

- Ewing's sarcoma, 93
- lung cancer metastasis, 88
- luxatio erecta, 107
- neuropathic arthropathy, 112
- osteolysis, 118
- osteonecrosis, 97
- pain, 88, 90–91
- posterior dislocation, 110
- pyrophosphate arthropathy, 117
- rheumatoid arthritis, 116
- rotator cuff tear, 104–105
- secondary tumoral calcinosis, 124–125
- telangiectatic osteosarcoma, 92
- spine
  - Scheuermann's disease, 168
- supraspinatus tendon
  - rotator cuff tear, 104–105
- thigh
  - aneurysmal bone cysts, 312–313
  - bisphosphonate-related fracture, 298
  - calcinosis universalis, 311
  - Camurati-Engelmann disease, 323
  - chondrosarcoma, 306–307
  - Erdheim-Chester disease, 328
  - Ewing's sarcoma, 304
  - failure to thrive, 310
  - fibrous dysplasia, 281
  - gait disturbance, 275
  - hip distress, 288–289
  - hip pain, 276–278, 284–286, 312–313
  - hip pain after fall, 290
  - intertrochanteric femur fracture, 290
  - Legg-Calvé-Perthes disease, 282, 286
  - leg pain, 296–297, 301
  - leukemia, 310
  - limb deformity, 281
  - liposclerosing myxofibrous tumor of bone, 314–315
  - malignant fibrous histiocytoma, 331
  - mass, 305–307
  - melorheostosis, 329
  - mixed connective tissue disease, 311
  - multiple epiphyseal dysplasia, 280
  - multiple myeloma, 300
  - muscle weakness, 311, 313
  - non-Hodgkin's B-cell lymphoma, 309
  - osteomalacia, with Looser's zones, 291
  - osteomyelitis, chronic, 296–297
  - osteonecrosis, 274, 276–277
  - osteopoikilosis, 283
  - osteosarcoma with skip metastasis, 301
  - periarticular calcinosis, 299
  - prostate cancer, 283
  - proximal focal femoral deficiency (PFFD), 275
  - renal failure hemodialysis, 299
  - septic arthritis, 288–289
  - slipped capital femoral epiphysis, 284–285
  - stress fracture, 292–293
  - sudden pain, 308–309
  - swelling, 296–297, 304
  - synovial sarcoma, 324–325
  - transient bone marrow edema, 278–279
  - weight loss and fatigue, 300

- thoracic spine  
 eosinophilic granuloma, 167  
 ochronosis, 172–173  
 sickle cell disease, 171  
 tuberculous spondylitis, 164–165  
 thoracolumbar spine  
 ivory vertebra from Paget's disease, 180
- AP. *See* Anteroposterior (AP) radiograph
- A2 pulley rupture  
 volar sonography, 31
- Arms. *See also* Elbow, arm, and shoulder; specific bone  
 AP radiograph  
 bone cyst, with pathologic fracture, 89  
 juxtacortical chondroma, 86–87
- CT  
 juxtacortical chondroma, 86–87  
 lateral radiograph  
 juxtacortical chondroma, 86–87
- MRI  
 complete biceps tendon rupture, 82–83  
 juxtacortical chondroma, 86–87
- Army. *See* Military recruits
- Arthritis, 225. *See also* Inflammatory arthritis; Juvenile chronic arthritis; Juvenile idiopathic arthritis (Still's disease); Monoarticular arthritis; Polyarticular arthritis; Rheumatoid arthritis; Septic arthritis
- aseptic, 70  
 bacterial septic, 70  
 gouty  
 vs. tophaceous gout, 17  
 psoriatic  
 hands, 2, 3  
 psoriatic vs. rheumatoid, 3  
 reactive, 70  
 tuberculous  
 MCP joint, 8
- Arthritis mutilans  
 hands, 2, 3  
 of hands, 3  
 vs. rheumatoid, 3
- Arthrofibrosis  
 knee  
 MRI, 412
- Arthrogryposis, 67  
 vs. carpal coalition, 41
- Articular chondroma  
 knee  
 AP radiograph, 338–339  
 MRI, 338–339  
 with swelling, 338–339
- Aseptic arthritis, 70
- Atlantooccipital dislocation, 132
- Atypical mycobacterium osteomyelitis  
 ankle  
 AP radiographs, 486–487  
 lateral radiographs, 486–487  
 MRI, 486–487
- Automobile accident  
 cervical spine  
 bilateral facet dislocation, 155  
 hyperextension sprain with teardrop fragment, 146–147  
 hyperflexion fractures, 160–161  
 hyperflexion sprain, 133  
 hyperflexion teardrop fracture, 144–145  
 odontoid fracture nonunion, 136–137  
 traumatic C2 spondylolisthesis, 138–139  
 unilateral facet dislocation, 140–141  
 lumbar spine  
 ankylosing spondylitis, 184–185
- Automobile accidents  
 luxatio erecta, 107  
 right sternoclavicular joint dislocation, 123
- Avulsion fractures  
 medial epicondyle, 75  
 UCL tear, 78
- B**
- Back pain  
 AP radiograph  
 ankylosing spondylitis, 234–235  
 eosinophilic granuloma, 167  
 Ewing's sarcoma, 208–209  
 hemangioma, 181  
 with vertebral collapse, 186–187  
 multiple myeloma, 188–189  
 psoriatic spondyloarthropathy, 194–195  
 sarcoma arising in Paget's disease, 230  
 tuberculous spondylitis (Pott's disease), 164–165
- CT  
 bilateral L5 spondylolysis without anterolisthesis, 198–199  
 with chronic lymphocytic leukemia, 214  
 cystic angiomas, 246  
 multiple myeloma, 188–189  
 osteoblastoma, 150  
 psoriatic spondyloarthropathy, 194–195  
 reactive arthritis, 231  
 tuberculous spondylitis (Pott's disease), 164–165
- lateral radiograph  
 Cushing's disease, 170  
 degenerative disc disease, 191  
 hemangioma, 181  
 with vertebral collapse, 186–187  
 involutional osteoporosis, 169  
 multiple myeloma, 188–189  
 pyogenic diskitis, 162–163
- MRI  
 chordoma, 206  
 with chronic lymphocytic leukemia, 214  
 cystic angiomas, 246  
 eosinophilic granuloma, 167  
 Ewing's sarcoma, 208–209  
 hemangioma, 181  
 with vertebral collapse, 186–187  
 herniated nucleus pulposus, 192–193  
 sarcoma arising in Paget's disease, 230  
 tuberculous spondylitis (Pott's disease), 164–165
- Bacterial septic arthritis, 70
- Baker's cyst rupture, 386
- Baseball  
 elbows, 78
- Basic training. *See* Military recruits
- Basketball  
 ankle  
 MRI, 478
- Battered child  
 with corner fractures  
 AP radiograph, 401
- Benign exostoses. *See* Osteochondroma
- Biceps tendons  
 MRI, 82–83  
 rupture of, 82–83
- Bilateral facet dislocation  
 automobile accident, 155  
 cervical spine, 155
- Bilateral L5 spondylolysis  
 without anterolisthesis  
 lumbosacral junction, 198–199  
 motor vehicle accident, 198–199
- Bilateral Madelung deformity  
 PA radiograph  
 wrist, 57
- Bisphosphonate-related fracture  
 AP radiograph, 298  
 MRI, 298
- Blount's disease (tibia vara)  
 AP radiograph  
 lower leg, 416  
 lateral radiograph, 416
- Bone cyst  
 MRI  
 aneurysmal, 472–473  
 lower leg, 429  
 with pathologic fracture, 88, 89
- Bone dysplasia, 40
- Bone marrow  
 transient edema, 278–279
- Bone scan. *See* Radionuclide bone scan
- BPOP (Nora's lesion)  
 AP radiograph, 538  
 MRI, 538
- Brachial plexus palsy, 98
- Breast cancer  
 Paget's disease, 190
- Brodie's abscess  
 lower leg  
 AP radiograph, 448–449  
 lateral radiograph, 448–449  
 MRI, 448–449
- Brodie's abscess, 175
- Brown tumor  
 AP radiograph, 126–127  
 CT, 126–127  
 ribs, 126–127
- Bucket-handle tear  
 MRI  
 knee, 390
- Bunion deformity, 540–541
- Burns  
 hands, 13  
 trauma, 13  
 heterotopic ossification after, 72
- Buttock pain, 229
- C**
- Caffey's disease  
 lateral radiograph, 67
- Calcaneal fatigue fracture  
 lateral radiograph, 512–513  
 MRI, 512–513

- Calcification
  - chondroblastoma, 94
  - hands, 14, 27
  - polymyositis, 28
- Calcific myonecrosis
  - lower leg
    - AP radiograph, 462–463
    - CT, 462–463
    - lateral radiograph, 462–463
- Calcific retrocalcaneal bursitis. *See* Hydroxyapatite deposition disease
- Calcific tendinitis
  - hands, 28
- Calcific tendinitis/peri arthritis
  - vs. synovial chondromatosis, 34
  - wrist, 34
- Calcific tendinosis
  - shoulder, 120–121
- Calcified medullary infarcts
  - with subchondral collapse of the tibial articular surface
    - AP radiographs, 364–365
    - CT, 364–365
    - MRI, 364–365
- Calcinosis. *See* Idiopathic tumoral calcinosis
- Calcinosis universalis
  - AP radiographs, 311
  - muscle weakness, 311
  - thighs, 311
- Calcium pyrophosphate dihydrate (CPPD), 173
  - AP radiograph, 369
  - knee, 369
  - PA radiograph
    - pyrophosphate arthropathy, 32
- Camurati–Engelmann disease
  - AP radiographs, 323
  - thigh, 323
- Canoe paddle shaped ribs, 156
- Capitellum osteochondrosis
  - pitchers, 74
- Carpal coalition
  - lateral radiograph
    - wrist, 41
  - PA radiograph
    - wrist, 41
- Carpal tunnel syndrome
  - with acromegaly, 26
- Cervical spine
  - AP radiograph
    - Klippel–Feil syndrome, 142–143
    - osteopetrosis, 157
    - retinoid toxicity, 158–159
- CT
  - ankylosing spondylitis, 148–149
  - bilateral facet dislocation, 155
  - complex C1–C2 fractures, 134–135
  - hyperextension sprain with teardrop fragment, 146–147
  - hyperflexion fractures, 160–161
  - juvenile chronic arthritis, 142–143
  - osteoblastoma, 150
  - retinoid toxicity, 158–159
  - traumatic C2 spondylolisthesis, 138–139
  - unilateral facet dislocation, 140–141
- lateral radiograph
  - ankylosing spondylitis, 148–149
  - atlantooccipital dislocation, 132
  - hyperextension sprain with teardrop fragment, 146–147
  - hyperflexion fractures, 160–161
  - hyperflexion sprain, 133
  - hyperflexion teardrop fracture, 144–145
  - juvenile chronic arthritis, 154
  - Klippel–Feil syndrome, 142–143
  - Morquio’s syndrome, 156
  - odontoid fracture nonunion, 136–137
  - osteopetrosis, 157
  - retinoid toxicity, 158–159
  - rheumatoid arthritis, 152–153
  - traumatic C2 spondylolisthesis, 138–139
  - tuberculous spondylitis, 151
  - unilateral facet dislocation, 140–141
- MRI
  - atlanto-occipital dislocation, 132
  - hyperflexion sprain, 133
  - hyperflexion teardrop fracture, 144–145
  - odontoid fracture nonunion, 136–137
  - tuberculous spondylitis, 151
  - unilateral facet dislocation, 140–141
- Cervical spine fractures
  - complex fractures
    - CT, 134–135
    - lateral radiograph, 134–135
    - MRI, 134–135
- Chance fracture
  - automobile accident, 182–183
  - thoracolumbar spine, 182–183
- Charcot joints
  - shoulder, 112
- Charcot-Marie-Tooth disease, 112
- Cheerio sign, 113
- Children. *See also* Battered child
  - arms
    - juxtacortical chondroma, 86–87
  - elbows
    - AP radiograph, 74, 75
    - oblique radiograph, 70
    - posterior dislocation, 68
    - trauma, 68, 76
  - humerus
    - AP radiograph, 89
  - shoulder
    - AP radiograph, 92, 98
  - upper limb deformity
    - radioulnar synostosis, 67
- Chondroblastoma
  - AP radiograph, 94
  - CT, 94
  - elbow, arm, and shoulder, 94
- Chondroblastoma with secondary aneurysmal bone cyst
  - foot
    - CT, 500–501
    - lateral radiograph, 500–501
    - MRI, 500–501
- Chondrocalcinosis, 32
- Chondroma
  - juxtacortical, 86–87
- Chondromalacia patellae
  - MRI, 367
- Chondromyxoid fibroma
  - lower leg
    - AP radiograph, 434–435
    - lateral radiograph, 434–435
- Chondrosarcoma
  - pelvis
    - AP radiograph, 216–217
    - CT, 216–217, 246
    - MRI, 216–217, 246
    - pubic pain, 216–217
  - shoulder, 90–91
  - thigh
    - AP radiographs, 306–307
    - lateral radiographs, 306–307
    - MRI, 306–307
- Chordoma
  - pelvis
    - back pain, 206
- Chronic recurrent multifocal osteomyelitis
  - whole-body radionuclide bone scan
    - lower leg, 465
- Chronic renal failure, 27
- Chronic sclerosing osteomyelitis
  - PA radiograph
    - hands, 40
  - radionuclide bone scan
    - hands, 40
- Chronic ulnar-sided wrist pain, 44–45
- Chronic wrist pain, 32, 42
- Classic clubfoot (talipes equinovarus)
  - AP radiograph, 505
  - lateral radiograph, 505
- Clavicle
  - fractures of, 98
  - osteolysis, 118
- Clostridial myonecrosis (gas gangrene)
  - lateral radiograph
    - lower leg, 444
- Clostridium perfringens*, 444
- Clostridium septicum*, 444
- Clubfoot
  - deformities, 67
- Coccidioidomycosis
  - with weight loss
    - lumbar spine, 196–197
- College basketball player
  - elbows, 78
- Complete biceps tendon rupture
  - arms, 82–83
- Compression fractures
  - with involutional osteoporosis, 169
- Computed tomography (CT)
  - ankle and foot
    - freiberg infraction, 533
    - hemophilic pseudotumor, 493
    - idiopathic tumoral calcinosis, 531
    - intraosseous lipoma, 474–475, 510–511
    - melorheostosis, 492
    - osteochondromatosis, 524–525
    - swelling, 531
    - synovial osteochondromatosis, 525
    - tarsal coalition, 504
    - tripplane fracture, 484–485
  - back pain
    - with chronic lymphocytic leukemia, 214

- cervical spine
    - ankylosing spondylitis, 148–149
    - bilateral facet dislocation, 155
    - complex C1–C2 fractures, 134–135
    - hyperextension sprain with teardrop fragment, 146–147
    - Klippel–Feil syndrome, 142–143
    - odontoid fracture nonunion, 136–137
    - osteoblastoma, 150
    - retinoid toxicity, 158–159
    - traumatic C2 spondylolisthesis, 138–139
    - unilateral facet dislocation, 140–141
  - elbow, arm and shoulder
    - bilateral posterior shoulder dislocations, seizure disorder, 111
    - brachial plexus palsy, 98
    - Brown tumor, 126–127
    - chondroblastoma, 94
    - chondrosarcoma, 90–91
    - elastofibroma, 128
    - fibromatosis, 84–85
    - juxtacortical chondroma, 86–87
    - secondary tumoral calcinosis, 124–125
    - SLAP, 113
    - sternoclavicular dislocation, 123
    - telangiectatic osteosarcoma, 92
  - femur and thigh
    - chondrosarcoma, 324–325
    - chronic osteomyelitis, 324–325
    - glomus tumor, 332
    - high-grade surface osteosarcoma, 305
    - hip pain, 308–309
    - liposarcoma, 326–327
    - liposclerosing myxofibrous tumor of bone, 314–315
    - malignant fibrous histiocytoma, 331
    - mass, 305–307
    - muscle weakness, 287
    - myositis ossificans, 320
    - non-Hodgkin's B-cell lymphoma, 309
    - osteopoikilosis, 283
    - osteosarcoma, high-grade surface, 305
    - pain worse at night, 316–317
    - polymyositis, 287
    - prostate cancer, 283
    - slipped capital femoral epiphysis, 284–285
    - swelling, 320
    - synovial sarcoma, 324–325
  - hand and wrist
    - osteonecrosis of lunate, 42–43
    - triquetral fracture, 38
    - wood splinter, 52
  - knee
    - calcified medullary infarcts, 364–365
    - inflammatory arthritis, 364–365
    - mass, 346–347
    - metallosis, 408–409
    - Non-Hodgkin's lymphoma, 354–355
    - osteosarcoma, 348–349
    - Paget's disease, 382–383
    - pain, 348–349
    - pain resembling intermittent claudication, 410–411
    - parosteal osteosarcoma, 346–347
    - popliteal artery entrapment syndrome, 410–411
    - primary lymphoma of bone, 352–353
  - lower leg
    - Army privates in basic training, 456
    - calcific myonecrosis, 462–463
    - diabetes mellitus, 468–469
    - fibrous dysplasia, 424–425
    - foot drop, 462–463
    - military recruits, 456
    - muscle weakness, 466–467
    - necrotizing fasciitis, 468–469
    - ossifying fibroma, 442–443
    - pain, 424–425
    - periosteal osteosarcoma, 440–441
    - polymyositis, 466–467
    - stress fractures, 456
    - swelling, 442–443
  - lumbar spine
    - ankylosing spondylitis with fracture dislocation, 184–185
    - multiple myeloma, 188–189
    - psoriatic spondyloarthropathy, 194–195
    - sclerotic prostate cancer metastasis, 176–177
  - lumbosacral junction
    - bilateral L5 spondylolysis without anterolisthesis, 198–199
    - traumatic lumbosacral spondylolisthesis, 200–201
  - muscle weakness, 466–467
  - pelvis
    - anemia, 244
    - anterior hip dislocation, 226
    - chordoma, 206
    - cystic angiomas, 246
    - desmoplastic fibroma, 254–255
    - eosinophilic granuloma, 249
    - femoracetabular impingement, 221
    - groin pain, 250, 258–259
    - hip pain, 236–237
    - iliopsoas bursitis, 258–259
    - insufficiency fractures, 210–211, 250
    - lung cancer metastasis, 260–261
    - lymphoma, 214
    - motor vehicle crash, 224–225
    - myelofibrosis, 244
    - nail-patella syndrome, 243
    - non-Hodgkin's lymphoma, 210–211
    - osteosarcoma, 218–219
    - pigmented villonodular synovitis, 236–237
    - plasmacytoma, 248
    - posterior hip dislocation, 224–225
    - reactive arthritis, 231
    - small fingernails, 243
    - tuberculosis, 252–253
  - polymyositis, 466–467
  - ribs
    - Brown tumor, 126–127
  - shoulder, 92
  - spine
    - ankylosing spondylitis with fracture, 184–185
    - bilateral facet dislocation, 155
    - hyperextension sprain at C5–C6 with teardrop fragment, 144–145
    - hyperflexion fractures of thoracic spine, 160–161
    - ivory vertebra from sclerotic prostate metastasis, 176–177
    - metastatic osteosarcoma, 166
    - osteoblastoma, 150
    - Paget's disease, 190
    - psoriatic spondyloarthropathy, 194–195
    - retinoid toxicity, 158–159
    - traumatic C2 spondylolisthesis, 138–139
    - tuberculous spondylitis, 164–165
    - unilateral facet dislocation, 140–141
  - thoracic spine
    - retinoid toxicity, 158–159
  - thoracolumbar spine
    - chance fracture, 182–183
    - ivory vertebra from Paget's disease, 180
  - wrist
    - bilateral Madelung deformity, 57
    - lunate osteonecrosis, 42–43
    - osteoid osteoma, 46–47
    - triquetral fracture, 38
  - Coned epiphysis, 29
  - Congenital adrenocortical hyperplasia with limb lengthening
    - AP radiograph
      - lower leg, 420–421
  - Congenital scoliosis
    - thoracolumbar spine, 174
  - Congenital syphilis
    - PA radiograph
      - forearm, 56
  - Congenital vertical talus
    - AP radiograph, 506
    - lateral radiograph, 506
  - CPPD. *See* Calcium pyrophosphate dihydrate (CPPD)
  - CT. *See* Computed tomography (CT)
  - Cupped metaphysis, 29
  - Cushing's disease
    - back pain, 170
    - lumbar spine, 170
  - Cystic angiomas, 246
  - Cystic lymphangiomatosis (cystic angiomas)
    - AP radiograph
      - lower leg, 464
- D**
- DDH. *See* Developmental dysplasia of the hip (DDH)
  - Death bringing dwarfism, 202
  - Degenerative disc disease
    - back pain, 191
    - lumbar spine, 191
  - De Quervain tenosynovitis
    - wrist, 51
  - Dermatomyositis
    - AP radiographs
      - knee, 379
    - lateral radiographs
      - knee, 379
  - MRI
    - ankle, 498
  - Desmoid tumor
    - extraabdominal
      - shoulder, 84–85

- Desmoplastic fibroma  
 AP radiograph  
 pelvis, 254–255  
 CT  
 pelvis, 254–255  
 MRI  
 pelvis, 254–255  
 PA radiograph  
 wrist, 54
- Developmental dysplasia of the hip (DDH)  
 AP radiograph, 215
- Diabetes mellitus  
 with acromegaly, 26  
 AP radiograph  
 foot, 520–521  
 lower leg  
 CT, 468–469  
 with tuberculous arthritis, 8
- Dialysis-related amyloidosis  
 hemodialysis, 272  
 MRI, 273
- Diffuse breast carcinoma metastases  
 AP radiograph  
 pelvis, 251
- DIP. *See* Distal interphalangeal (DIP) joint
- Discoid meniscus with complex tear  
 MRI, 362
- Dislocated total hip replacement  
 AP radiograph, 256
- Dislocation  
 shoulder, 110
- Disseminated intravascular coagulopathy,  
 29
- Distal humerus  
 supracondylar fracture of, 73
- Distal interphalangeal (DIP) joint  
 psoriatic arthritis, 2
- Dwarfism  
 thanatophoric (death bringing), 202
- Dysplasia epiphysealis multiplex, 280
- E**
- Effendi classification, 139
- Ehlers-Danlos syndrome, 508
- Elastofibroma  
 shoulder, 128
- Elbow  
 apophyses  
 ossification of, 76  
 AP radiograph, 72  
 children, 69  
 falls, 66  
 medial epicondyle avulsion fracture, 75  
 mountain bike accident, 68  
 pain, 74  
 posterior elbow dislocation, 76  
 trauma, 68, 75, 76  
 axial image, 77  
 coronal image, 77  
 divergent dislocation, 68  
 complications with, 68  
 epiphyses  
 ossification of, 76  
 lateral radiograph, 72  
 falls, 64–66, 73, 80–81  
 mountain bike accident, 68  
 occult distal humerus fracture, 80–81  
 posterior elbow dislocation, 76  
 radioulnar synostosis, 67  
 swelling, 71  
 trauma, 68, 75
- MRI  
 falls, 80–81  
 lateral epicondylitis, 77  
 occult distal humerus fracture, 80–81  
 posterior injury, 79  
 triceps tendon tear with olecranon bursa hemorrhage, 79
- oblique radiograph  
 children, 69  
 radioulnar synostosis, 67  
 septic elbow joint, 70  
 posterior dislocation, 68  
 radial head fracture, 64–65  
 sonography  
 swelling, 71
- Elbow, arm, and shoulder  
 lateral radiograph  
 radial head fracture, 64–65
- MRI  
 college basketball player, 78  
 fibromatosis, 84–85  
 ganglion cyst, 103  
 UCL tear, 78
- Elderly  
 shoulder  
 MRI, 102
- Ellis-van Creveld syndrome  
 vs. carpal coalition, 41
- Embolic disease  
 hands, 29
- Enchondroma  
 hands, 16  
 little finger, 16
- Eosinophilic granuloma (EG), 249  
 AP radiograph, 302–303  
 back pain, 167  
 leg pain, 302–303  
 thoracic spine, 167
- Epicondylitis  
 lateral, 77  
 ultrasonography of, 77
- Epidermoid inclusion cyst  
 finger, 11
- Epiphysis  
 coned, 29
- Erb's palsy, 98
- Erdheim-Chester disease  
 thigh  
 AP radiograph, 328  
 MRI, 328  
 pulmonary symptoms, 328
- Erosive osteoarthritis  
 gull-wing, 5  
 hands, 5  
 vs. psoriatic arthritis, 5
- Ewing's sarcoma  
 AP radiograph, 93, 446–447  
 back pain, 208–209  
 lower leg  
 AP radiograph, 446–447  
 lateral radiograph, 446–447  
 MRI, 446–447  
 pelvis, 208–209  
 shoulder, 93
- thigh  
 AP femur radiograph, 304  
 AP radiograph, 304  
 swelling and pain, 304
- Extensor tendon irritation  
 lateral radiograph  
 wrist, 58–59  
 sonography  
 wrist, 58–59
- Extraabdominal desmoid tumor  
 shoulder, 84–85
- Extraskeletal primitive neuroectodermal tumor (PNET)  
 MRI  
 ankle, 488
- F**
- Facet dislocation  
 bilateral  
 automobile accident, 155  
 cervical spine, 155  
 unilateral  
 automobile accident, 140–141  
 cervical spine, 140–141
- Failure to thrive  
 AP radiograph  
 knee, 401  
 thigh, 310  
 MRI  
 thigh, 310
- Fallen-fragment sign, 89
- Falls  
 complex C1–C2 fractures, 134–135  
 elbow, 64–66, 73  
 lateral radiograph, 64–66  
 Maisonneuve fracture of lower leg, 432
- Fatigue fracture  
 calcaneal  
 lateral radiograph, 512–513  
 MRI, 512–513
- Fat pad sign, 64–65
- Fat-suppressed images, 99
- Femoroacetabular impingement  
 acetabular fracture, 221  
 pelvis, 221
- Femur  
 osteosarcoma with skip metastasis, 301
- Femur radiographs  
 multiple myeloma, 300
- Fibrodysplasia ossificans progressiva (FOP), 223
- Fibroma, 433. *See also* Chondromyxoid fibroma; Desmoplastic fibroma
- forearm  
 PA radiograph, 55
- Fibromatosis  
 shoulder, 84–85
- Fibrous ankylosis  
 with tuberculous arthritis, 8
- Fibrous cortical defect, 433
- forearm, 55
- Fibrous dysplasia  
 AP radiograph, 281  
 limb deformity, 281  
 lower leg  
 AP radiograph, 424–425  
 CT, 424–425

- PA radiograph
  - hands, 15
- Fifth CMC volar dislocation
  - hands, 35
- Finger
  - PA radiograph
    - epidermoid inclusion cyst, 11
    - glomus tumor, 10
- First metacarpophalangeal (MCP) joint
  - lateral radiograph
    - tuberculous arthritis, 8
- Fluorosis
  - pelvis
    - bone pain, 227
    - muscle weakness, 227
- Fong's syndrome
  - pelvis, 243
- Foot
  - AP radiograph
    - anemia, 530
    - classic clubfoot (talipes equinovarus), 505
    - congenital vertical talus, 506
    - diabetes, 520–521
    - football player, 545
    - freiberg infraction, 533
    - Maffucci's syndrome, 534–535
    - mass, 516–517, 526–527, 538
    - melorheostosis, 492
    - metatarsus adductus, 507
    - motor vehicle accident, 503, 528
    - Mueller-Weiss syndrome, 523
    - multiple enchondromatosis, 537
    - neuropathic osteoarthropathy, 520–521
    - pain, 474–475, 492, 520–521, 523, 533, 544
    - polyarticular arthritis, 509
    - rash, 542
    - rheumatoid arthritis, 536
    - subchondral fracture, 544
    - swelling, 515
    - systemic lupus erythematosus (SLE), 508
    - thalassemia, 530
    - tophaceous gout, 519
  - CT
    - freiberg infraction, 533
    - idiopathic tumoral calcinosis, 531
    - intraosseous lipoma, 510–511
    - melorheostosis, 492
    - pain, 474–475, 492, 499–501, 510–511, 533
    - swelling, 531
    - synovial osteochondromatosis, 524–525
    - tarsal coalition, 504
  - lateral radiograph
    - chondroblastoma with secondary aneurysmal bone cyst, 500–501
    - classic clubfoot (talipes equinovarus), 505
    - congenital vertical talus, 506
    - diabetes, 520–521
    - idiopathic tumoral calcinosis, 531
    - intraosseous lipoma, 510–511
    - juvenile idiopathic arthritis, 509
    - metatarsus adductus, 507
    - motor vehicle accident, 503, 528
- Mueller-Weiss syndrome, 523
- neuropathic osteoarthropathy, 520–521
- pain, 474–475, 500, 501, 510–511, 520–521, 523
- plantar fasciitis, 514
- polyarticular arthritis, 509
- swelling, 518, 531, 534–535
- synovial osteochondromatosis, 525
- systemic lupus erythematosus (SLE), 508
- tarsal coalition, 504
- MRI
  - chondroblastoma with secondary aneurysmal bone cyst, 500–501
  - giant cell tumor of the tendon sheath, 527
  - lisfranc fracture dislocation, divergent type, 528
  - mass, 516–517, 526–527, 538
  - pain, 499–501, 520–521, 532, 544
  - plantar fasciitis, 514
  - plantar fibromatosis, 516–517
  - swelling, 488, 496–497
- oblique radiograph
  - basketball injury, 522
  - idiopathic tumoral calcinosis, 531
  - osteochondral lesion, 522
  - swelling, 531
- radionuclide bone scan, 495, 514
- whole-body radionuclide bone scans, 495
- Football injury
  - ankle
    - AP radiograph, 545–546
    - lateral radiograph, 545–546
- FOP. *See* Fibrodysplasia ossificans progressiva (FOP)
- Forearm
  - PA radiograph
    - congenital syphilis, 56
    - nonossifying fibroma, 55
- Fourth metacarpal fracture
  - lateral radiograph
    - hands, 35
  - PA radiograph
    - hands, 35
- Fracture nonunion
  - trauma, 96
- Fractures. *See also* Stress fractures
  - hangman's, 138–139
  - hyperflexion
    - thoracic spine, 160–161
  - hyperflexion teardrop
    - cervical spine, 144–145
  - lower leg, 432
- Maisonneuve
  - AP radiograph, 432
- Salter type IV
  - lower leg, 458
- tibia
  - AP radiograph, 453
- toddler, 453
- triquetral
  - wrist, 38
- trough, 111
- Freiberg infraction
  - AP radiograph, 533
  - CT, 533
  - pain, 533
- G
  - Gait disturbance
    - AP radiograph, 275
  - Galeazzi's fracture dislocation
    - lateral radiograph
      - wrist, 60
    - PA radiograph
      - wrist, 60
  - Ganglion cyst
    - elbow, arm, and shoulder, 103
    - hands, 39
    - peroneal nerve, 460–461
    - spinoglenoid notch, 103
  - Gas gangrene
    - lateral radiograph
      - lower leg, 444
  - Gaucher disease
    - AP radiograph, 360–361
    - knee, 360–361
    - MRI, 360–361
  - Giant cell reparative granuloma
    - hands, 18
  - Giant cell tumor, 54
    - knee
      - AP radiographs, 340–341
      - lateral radiographs, 340–341
    - tendon sheath
      - MRI, 30, 526–527
  - Glenohumeral joint, 108–109
  - Glomus tumor
    - hands, 10
    - thigh
      - CT, 322
      - MRI, 322
  - Gluteus medius tendon tear, 229
  - Gouty arthritis
    - vs. tophaceous gout, 17
  - Graves' disease, 25
  - Greenstick fractures, 73
  - Groin pain
    - pelvis
      - AP radiograph, 250
      - CT, 250, 258–259
      - MRI, 250, 258–259
  - Growth hormone, 26
  - Growth plate fracture (Salter type I)
    - wrist, 49
  - Gull-wing appearance
    - hands, 5
  - Gymnasts
    - capitellum osteochondrosis, 74
- H
  - Hallux rigidus (hallux limitus), 539
  - Hamstrings tear with associated hematoma
    - axial STIR image, 271
  - Hands
    - acromegaly, 26
    - arthritis mutilans, 2, 3
    - burns, 13
    - calcification, 14, 27
    - chronic sclerosing osteomyelitis, 40
    - embolic disease, 29
    - enchondroma, 16
    - erosive osteoarthritis, 5
    - ganglion cyst, 39
    - giant cell reparative granuloma, 18
    - gull-wing appearance, 5

Hands (*Continued*)

- honeycomb appearance, 12
  - hyperparathyroidism, 27
  - juvenile idiopathic arthritis, 24
  - lace-like appearance, 12
  - lateral radiograph
    - fourth metacarpal fracture, 35
    - osteoarthritis, 4
    - polymyositis, 28
    - scleroderma, 14
    - tuberculous arthritis, 8
  - MRI
    - giant cell tumor of tendon sheath, 30
    - osteomyelitis, 6–7
  - multicentric reticulohistiocytosis, 19
  - oblique radiograph
    - thyroid acropachy, 25
  - osteoarthritis, 4
  - osteomyelitis, 6–7
  - osteoporosis, 13, 24
  - PA radiograph
    - acromegaly, 26
    - burns, 13
    - chronic sclerosing osteomyelitis, 40
    - congenital syphilis, 56
    - embolic disease, 29
    - enchondroma, 16
    - erosive osteoarthritis, 5
    - fourth metacarpal fracture, 35
    - giant cell reparative granuloma, 18
    - glomus tumor, 10
    - hemochromatosis, 33
    - hyperparathyroidism, 27
    - juvenile idiopathic arthritis, 24
    - multicentric reticulohistiocytosis, 19
    - osteoarthritis, 4
    - polymyositis, 28
    - polyostotic fibrous dysplasia, 15
    - psoriatic arthritis, 2, 3
    - pyrophosphate arthropathy, 32
    - rheumatoid arthritis, 21–23
    - sarcoidosis, 12
    - scleroderma, 14
    - systemic lupus erythematosus, 20
    - thyroid acropachy, 25
    - tophaceous gout, 17
  - periarticular osseous excrescences, 13
  - periostitis, 2, 3, 13, 24
  - polyarthritis, 3
  - polyarticular arthritis, 4
  - polymyositis, 28
  - polyostotic fibrous dysplasia, 15
  - postmenopausal women, 5
  - pseudoclubbing, 12
  - psoriatic arthritis, 2, 3
  - pyrophosphate arthropathy, 4
  - radionuclide bone scan
    - chronic sclerosing osteomyelitis, 40
  - rheumatoid arthritis, 21–23
  - sacroiliitis, 3
  - sarcoidosis, 12
  - scleroderma, 14
  - spondylitis, 3
  - subperiosteal bone resorption, 27
  - systemic lupus erythematosus, 20
  - thyroid acropachy, 25
  - tophaceous gout, 17
- Hangman's fractures, 138–139
- Healing rickets
  - wrist, 48
- Hemangioma
  - back pain, 181
  - lower leg
    - lateral radiograph, 438–439
    - MRI, 438–439
  - lumbar spine, 181
  - with vertebral collapse, 186–187
- Hemangiomatosis
  - AP radiograph
    - pelvis, 245
- Hematoma
  - MRI
    - pelvis, 263
- Hemochromatosis
  - metacarpals, 33
  - oblique radiograph
    - hands, 33
  - PA radiograph
    - hands, 33
- Hemophilic pseudotumor
  - ankle
    - AP radiograph, 493
    - CT, 493
- Hemophilic knee
  - AP radiographs, 356–357
  - lateral radiograph, 356–357
- Hepatitis, 70
- Herniated nucleus pulposus, 192–193
- Heterotopic ossification after burns
  - elbow, 72
- Hill-Sachs lesion, 108–109
- Hip
  - anterior dislocation, 226
  - AP radiograph
    - developmental dysplasia of, 215
- Histiocytoma. *See* Malignant fibrous histiocytoma
- HIV. *See* Human immunodeficiency virus (HIV)
- HLA-B27. *See* Human leukocyte antigen (HLA-B27)
- Holt–Oram syndrome, 67
  - vs. carpal coalition, 41
- Honeycomb appearance
  - hands, 12
- Horizontal intercondylar dislocation of the patella
  - knee
    - AP radiographs, 400
    - lateral radiographs, 400
- Human immunodeficiency virus (HIV)
  - with tuberculous arthritis, 8
- Human leukocyte antigen (HLA-B27), 232
- Humerus
  - AP radiograph, 89
  - distal supracondylar fracture of, 73
  - fracture nonunion, 96
- Hydroxyapatite crystal deposition disease (calcific tendinitis), 28
- Hydroxyapatite deposition disease (calcific retrocalcaneal bursitis)
  - lateral radiograph, 515
- Hydroxyapatite deposition disease (calcific tendinitis/periartthritis)
  - vs. synovial chondromatosis, 34
  - wrist, 34
- Hyperbaric oxygen
  - for clostridial myonecrosis, 444
- Hyperextension sprain
  - with teardrop fragment
    - automobile accident, 146–147
    - cervical spine, 146–147
- Hyperflexion fractures
  - thoracic spine
    - automobile accident, 160–161
- Hyperflexion sprain
  - automobile accident, 133
  - cervical spine, 133
- Hyperflexion teardrop fracture
  - automobile accident, 144–145
  - cervical spine, 144–145
- Hyperparathyroidism
  - hands, 27
- Hypertension
  - with acromegaly, 26
- Hypertrophic osteoarthropathy
  - wrist, 53
- Hypertrophic osteoarthropathy (HOA)
  - AP radiograph
    - lower leg, 471
- Hypocalcemia, 27
- I**
- Idiopathic tumoral calcinosis
  - foot
    - CT, 531
    - lateral and oblique radiographs, 531
    - oblique radiograph, 531
- Iliopsoas bursitis
  - groin pain, 258–259
  - pelvis, 258–259
- Index finger
  - lateral radiograph
    - polymyositis, 28
  - PA radiograph
    - polymyositis, 28
- Inferior glenohumeral dislocation, 107
- Inflammatory arthritis
  - knee
    - AP radiograph, 364–365
    - CT, 364–365
    - MRI, 364–365
- Insufficiency fractures, 250
- Intertrochanteric femur fracture
  - AP radiograph, 290
  - hip pain after a fall, 290
- Intramuscular lipoma
  - MRI, 102
  - shoulder, 102
  - subcutaneous lipoma, 102
- Intramuscular myxoma
  - pelvis
    - CT, 222
- Intraosseous lipoma
  - foot
    - AP radiograph, 474–475
    - CT, 474–475, 510–511
    - lateral and harris view radiographs, 510–511
    - lateral radiograph, 474–475
- Intravenous drug use
  - with tuberculous arthritis, 8
- Involutional osteoporosis
  - with compression fractures, 169
  - thoracic spine, 169

- J**
- Joint stiffness
    - pelvis, 242
  - Juvenile chronic arthritis
    - cervical spine
      - CT, 142–143
      - lateral radiograph, 154
  - Juvenile idiopathic arthritis (Still's disease), 154, 242
  - foot
    - lateral radiograph, 509
  - hands, 24
  - knee
    - AP radiographs, 372–375
    - lateral radiographs, 372–375
  - Juxta-articular osteoporosis, 70
  - Juxtacortical chondroma, 86–87
  - Juxtacortical osteosarcoma. *See* Parosteal osteosarcoma
- K**
- Kienböck's disease
    - wrist, 42–43
  - Klippel–Feil syndrome
    - cervical spine, 142–143
    - motor vehicle accident, 142–143
  - Klippel–Trenaunay syndrome
    - MRI, 332–333
  - Klumpke's paralysis, 98
  - Knee. *See also* Total knee replacement
    - AP radiograph
      - anterior cruciate ligament (ACL) sprain, 392–393
      - AP radiographs, 356–357
      - articular chondroma, 338–339
      - battered child, 401
      - calcified medullary infarcts with subchondral collapse of the tibial articular surface, 364–365
      - calcium pyrophosphate dihydrate (CPPD), 369
      - dermatomyositis, 379
      - failure to thrive, 401
      - Gaucher disease, 360–361
      - giant cell tumor, 340–341
      - hemophilia, 356–357
      - horizontal intercondylar dislocation of the patella, 400
      - inflammatory arthritis, 364–365
      - injury, 392–393
      - juvenile idiopathic arthritis, 372–375
      - leg-length discrepancy, 380
      - mass, 346–347
      - medial collateral ligament (MCL) sprain, 392–393
      - metallosis, 408–409
      - MFH of bone, 350–351
      - osteosarcoma, 342, 344–345
      - Paget's disease, 382–383
      - pain, 340–345, 348–353, 433
      - parosteal osteosarcoma, 346–349
      - poliomyelitis, 380
      - primary lymphoma of bone, 352–353
      - pyrophosphate arthropathy, 378
      - recurrent pain, 369, 378
      - rheumatoid arthritis, 368
      - secondary synovial osteochondromatosis, 376–377
      - short stature, 374–375
    - anterior cruciate ligament (ACL) sprain, 392–393
    - AP radiographs, 356–357
    - articular chondroma, 338–339
    - battered child, 401
    - calcified medullary infarcts with subchondral collapse of the tibial articular surface, 364–365
    - calcium pyrophosphate dihydrate (CPPD), 369
    - dermatomyositis, 379
    - failure to thrive, 401
    - Gaucher disease, 360–361
    - giant cell tumor, 340–341
    - hemophilia, 356–357
    - horizontal intercondylar dislocation of the patella, 400
    - inflammatory arthritis, 364–365
    - injury, 392–393
    - juvenile idiopathic arthritis, 372–375
    - leg-length discrepancy, 380
    - mass, 346–347
    - medial collateral ligament (MCL) sprain, 392–393
    - metallosis, 408–409
    - MFH of bone, 350–351
    - osteosarcoma, 342, 344–345
    - Paget's disease, 382–383
    - pain, 340–345, 348–353, 433
    - parosteal osteosarcoma, 346–349
    - poliomyelitis, 380
    - primary lymphoma of bone, 352–353
    - pyrophosphate arthropathy, 378
    - recurrent pain, 369, 378
    - rheumatoid arthritis, 368
    - secondary synovial osteochondromatosis, 376–377
    - short stature, 374–375
  - sickle cell anemia, 363
  - swelling, 338–339, 344–345
  - swollen, 356–357, 372–373, 376–377
  - total knee replacement with failure of tibial polyethylene, 407
  - trauma, 352–353
- CT**
- inflammatory arthritis, 364–365
  - mass, 346–347
  - metallosis, 408–409
  - Non-Hodgkin's lymphoma, 354–355
  - osteosarcoma, 348–349
  - Paget's disease, 382–383
  - pain resembling intermittent claudication, 410–411
- fat-saturated images, 346–347, 367
- fat-suppressed images, 362, 371, 389, 391, 394, 396, 397, 399, 403, 405, 406, 412
- lateral radiograph
- dermatomyositis, 379
  - hemophilia, 356–357
  - Horizontal intercondylar dislocation of the patella, 400
  - juvenile idiopathic arthritis, 372–375
  - leg-length discrepancy, 380
  - metallosis, 408–409
  - osteosarcoma, 342, 344–345
  - poliomyelitis, 380
  - pyrophosphate arthropathy, 378
  - recurrent pain, 378
  - secondary synovial osteochondromatosis, 376–377
  - short stature, 374–375
  - swelling, 342–345, 358–359
  - swollen, 356–357, 372–373, 376–377
  - trauma, 400
- MRI**
- acute pain, 367
  - anterior cruciate ligament (ACL) sprain, 384–385, 392–394
  - arthrofibrosis, 412
  - articular chondroma, 338–339
  - bucket-handle tear, 390
  - calcified medullary infarcts with subchondral collapse of the tibial articular surface, 364–365
  - chondromalacia patellae, 367
  - chronic pain, 348–349
  - effusion, 390
  - Gaucher disease, 360–361
  - giant cell tumor, 340–341
  - headache, 343
  - inflammatory arthritis, 364–365
  - lateral tibial plateau fracture, 387
  - lipoma arborescens, 402–403
  - mass, 346–347
  - medial collateral ligament (MCL) sprain, 384–385
  - medial meniscal tear, 388
  - Non-Hodgkin's lymphoma, 354–355
  - osteochondral fracture, 399
  - osteosarcoma, 344–345
  - Paget's disease, 382–383
  - pain, 340–341, 344–345, 350–353, 362, 367, 370–371, 382–383, 386, 387, 398–399
  - pain resembling intermittent claudication, 410–411
- parosteal osteosarcoma, 346–347
- PCL sprain, 395
- pes anserinus bursitis, 404–405
- pigmented villonodular synovitis (PVNS), 370–371
- polycythemia vera, 343
- positive posterior drawer test, 395
- primary lymphoma of bone, 352–353
- Radial tear of the lateral meniscus, 391
- ruptured baker cyst, 386
- Salter type II fracture, 381
- Sinding–Larsen–Johansson (SLJ) disease, 397
- sports injury, 381
- subchondral insufficiency fracture of the knee (SIFK), 406
- swelling, 338–339
- transient lateral patellar dislocation, 396
- twisted, 394
- Kyphosis**
- with involutional osteoporosis, 169
- L**
- Lace-like appearance
- hands, 12
- Lateral ankle ligament tear
- ankle sprain, 490–491
- Lateral cervical spine
- polyarticular arthritis, 152–153
  - rheumatoid arthritis, 152–153
- Lateral epicondylitis, 77
- Lateral radiograph, 444
- ankle
- accessory soleus muscle, 489
  - atypical mycobacterium osteomyelitis, 487
  - calcaneal fatigue fracture, 512–513
  - football injury, 545
  - hydroxyapatite deposition disease, 515
  - metatarsus adductus, 507
  - motorcycle accident, 503
  - osteonecrosis, 502
  - osteonecrosis in sickle cell disease, 494
  - pain, 489, 494, 502
  - pigmented villonodular synovitis (PVNS), 496–497
  - reactive arthritis, 518
  - subtalar dislocation, 503
  - tripplane fracture, 584–585
- arms
- juxtacortical chondroma, 86–87
- cervical spine
- ankylosing spondylitis, 148–149
  - atlantooccipital dislocation, 132
  - hyperextension sprain with teardrop fragment, 146–147
  - hyperflexion fractures, 160–161
  - hyperflexion sprain, 133
  - hyperflexion teardrop fracture, 144–145
  - juvenile chronic arthritis, 154
  - Klippel–Feil syndrome, 142–143
  - Morquio's syndrome, 156
  - odontoid fracture nonunion, 136–137
  - osteopetrosis, 157
  - retinoid toxicity, 158–159
  - rheumatoid arthritis, 152–153

Lateral radiograph (*Continued*)

- traumatic C2 spondylolisthesis, 138–139
- tuberculous spondylitis, 151
- unilateral facet dislocation, 140–141
- elbow, arm and shoulder
  - posterior elbow dislocation, 68
  - radioulnar synostosis, 67
- elbows, 72
  - falls, 64–66, 73, 80–81
  - occult distal humerus fracture, 80–81
  - posterior elbow dislocation, 76
  - radial head fracture, 64–65
  - septic olecranon bursitis, 71
  - supracondylar fracture, 73
- finger
  - epidermoid inclusion cyst, 11
- first metacarpophalangeal (MCP) joint
  - tuberculous arthritis, 8
- foot
  - classic clubfoot (talipes equinovarus), 505
  - congenital vertical talus, 506
  - diabetes, 520–521
  - idiopathic tumoral calcinosis, 531
  - intraosseous lipoma, 474–475, 510–511
  - juvenile idiopathic arthritis, 509
  - Lisfranc fracture-dislocation, 528
  - monoarticular arthritis, 524–525
  - motor vehicle accident, 503, 528
  - Mueller-Weiss syndrome, 523
  - neuropathic osteoarthropathy, 520–521
  - pain, 474–475, 500–501, 510–511, 520–521, 523
  - plantar fasciitis, 514
  - polyarticular arthritis, 509
  - swelling, 496–497, 518, 531, 534–535
  - systemic lupus erythematosus (SLE), 508
- hands
  - enchondroma, 16
  - fourth metacarpal fracture, 35
  - osteoarthritis, 4
  - polymyositis, 28
  - scleroderma, 14
  - tuberculous arthritis, 8
- knee
  - calcified medullary infarcts with subchondral collapse of the tibial articular surface, 364–365
  - chronic Sinding–Larsen–Johansson (SLJ) disease, 397
  - hemophilic knee, 356–357
  - horizontal intercondylar dislocation of the patella, 400
  - juvenile idiopathic arthritis, 372–373
  - leg-length discrepancy, 380
  - lymphoma, 366
  - metallosis, 408–409
  - osteochondromatosis, 376–377
  - osteosarcoma, 342, 344–345
  - poliomyelitis, 380
  - pyrophosphate arthropathy, 378
  - radiation changes, 336
  - recurrent pain, 378
  - rickets, 358–359
  - secondary synovial osteochondromatosis, 376–377

- short stature, 374–375
- swelling, 342, 358–359
- swollen, 356–357, 372–373, 376–377
- trauma, 400
- lower leg, 444
  - adamantinoma, 436–437
  - Army privates in basic training, 456
  - Blount's disease, 416
  - Brodie's abscess, 448–449
  - calcific myonecrosis, 462–463
  - chondromyxoid fibroma, 434–435
  - clostridial myonecrosis, 444
  - Ewing's sarcoma, 446–447
  - foot drop, 462–463
  - hemangioma, 438–439
  - knee pain, 448–449
  - mass, 431
  - multiple problems, 418
  - nonossifying fibroma, 433
  - open segmental fracture, 452
  - osteoblastoma, 431
  - osteochondroma, 430
  - osteogenesis imperfecta, 418
  - pain, 440–441
  - periosteal osteosarcoma, 440–441
  - progressive bowing deformity, 416
  - swelling, 430
  - tender, 446–447
  - tuberculous osteomyelitis, 450–451
- lumbar spine
  - ankylosing spondylitis with fracture dislocation, 184–185
  - Cushing's disease, 170
  - degenerative disc disease, 191
  - hemangioma, 181
  - with vertebral collapse, 186–187
  - multiple myeloma, 188–189
  - renal osteodystrophy with rugger jersey spine, 179
- pelvis
  - acetabular dysplasia, 220
  - dislocated total hip replacement, 256
  - synovial osteochondromatosis, 233
- thigh
  - chondrosarcoma, 306–307
  - increasing girth, 305
  - liposarcoma, 326–327
  - mass, 306–307
  - myositis ossificans, 320
  - slipped capital femoral epiphysis (SCFE), 384–385
  - synovial sarcoma, 324–325
- thoracic spine
  - eosinophilic granuloma, 167
  - involutional osteoporosis, 169
  - Morquio's syndrome, 156
  - ochronosis, 172–173
  - osteopetrosis, 157
  - pyogenic diskitis, 162–163
  - retinoid toxicity, 159
  - sickle cell disease, 171
- thoracolumbar spine
  - ivory vertebra from Paget's disease, 180
- wrist
  - carpal coalition, 41
  - extensor tendon irritation, 58–59
  - Galeazzi's fracture dislocation, 60
  - hydroxyapatite deposition disease, 34

- lunate dislocation, 37
- rotary subluxation, 36
- scapholunate dislocation, 36
- triquetral fracture, 38
- Lateral tibial plateau fracture
  - MRI
    - knee, 387
- Lead bands, 50
- Lead lines, 50
- Lead poisoning
  - wrist, 50
- Legg–Calvé–Perthes disease, 416
  - AP radiograph, 282, 286
  - MRI, 286, 289
- Leukemia
  - AP radiograph, 310
  - MRI, 310
- Lipoma. *See* Intraosseous lipoma
- Lipoma arborescens
  - MRI
    - knee, 402–403
- Lipoma dolorosa, 102
- Liposarcoma
  - thigh
    - CT, 326–327
    - lateral radiograph, 326–327
    - MRI, 326–327
- Liposclerosing myxofibrous tumor of bone
  - AP radiograph, 314–315
  - CT, 314–315
  - hip pain, 314–315
  - MRI, 314–315
- Lisfranc fracture dislocation, divergent type
  - foot
    - AP radiographs, 528
    - lateral radiographs, 528
- Little finger
  - PA radiograph
    - enchondroma, 16
- Little leaguer's elbow, 74
- Lower leg
  - AP radiograph, 445
  - bowed, 422
  - congenital adrenocortical hyperplasia with limb lengthening, 420–421
  - cystic lymphangiomatosis, 464
  - falls, 432
  - foot drop, 462–463
  - hypertrophic osteoarthropathy, 471
  - knee pain, 433, 448–451
  - knee trauma, 458
  - mass, 431, 436–437
  - multiple bone lesions, 464
  - multiple problems, 418, 419
  - NF-1, 417
  - open segmental fracture, 452
  - osteoblastoma, 431
  - osteogenesis imperfecta, 418
  - osteopetrosis, 419
  - pain, 424–425, 440–441
  - progressive bowing deformity, 416
  - runners, 454–455
  - short stature, 420–421, 423
  - swelling, 430, 434–435, 442–443
  - tender, 446–447
  - toddler, 453
- CT
  - Army privates in basic training, 456
  - diabetes, 468–469

- foot drop, 462–463  
knee pain, 448–449  
muscle weakness, 466–467  
pain, 424–425, 440–441  
polymyositis, 466–467  
swelling, 442–443
- lateral radiograph, 445  
Army privates in basic training, 456  
foot drop, 462–463  
knee pain, 433, 450–451  
mass, 431, 436–437  
multiple problems, 418  
open segmental fracture, 452  
osteoblastoma, 431  
osteogenesis imperfecta, 418  
pain, 440–441  
progressive bowing deformity, 416  
swelling, 430, 434–435, 438–439  
tender, 446–447
- MRI**  
Achilles tendon rupture, 478  
ankle swelling, 472–473  
bone cyst, 429  
deep vein thrombosis, 459  
diabetes, 468–469  
knee pain, 448–451  
mass, 428  
Mazabraud syndrome, 426–427  
pain, 440–441, 457  
peroneal nerve ganglion cyst, 460–461  
polymyositis, 466–467  
runners, 454–455  
soleus, 459  
subacute intramuscular hematoma, 459  
swelling, 429, 442–443, 457, 470  
tender, 446–447  
toe dorsiflexion, 460–461
- radionuclide bone scan  
Army privates in basic training, 456  
whole-body radionuclide bone scan, 445  
recurrent pain, 465
- Lumbar spine**  
**AP radiograph**  
achondroplasia, 202  
ankylosing spondylitis with fracture dislocation, 184–185  
chance fracture, 182–183  
hemangioma, 181  
with vertebral collapse, 186–187  
multiple myeloma, 188–189  
psoriatic spondyloarthropathy, 194–195
- CT**  
ankylosing spondylitis with fracture dislocation, 184–185  
multiple myeloma, 188–189  
psoriatic spondyloarthropathy, 194–195  
sclerotic prostate cancer metastasis, 176–177
- lateral radiograph  
ankylosing spondylitis with fracture dislocation, 184–185  
Cushing's disease, 170  
degenerative disc disease, 191  
hemangioma, 181  
with vertebral collapse, 186–187  
multiple myeloma, 188–189
- renal osteodystrophy with rugger jersey spine, 179
- MRI**  
coccidioidomycosis, 196–197  
hemangioma, 181  
with vertebral collapse, 186–187  
herniated nucleus pulposus, 192–193  
psoriatic spondyloarthropathy, 194–195  
sclerotic prostate cancer metastasis, 176–177
- Lumbosacral junction**  
**CT**  
bilateral L5 spondylolysis without anterolisthesis, 198–199  
traumatic lumbosacral spondylolisthesis, 200–201
- Lunate dislocation**  
lateral radiograph  
wrist, 37  
**PA radiograph**  
wrist, 37
- Lunate malacia**  
wrist, 42–43
- Lunate osteonecrosis**  
wrist, 42–43
- Lung cancer metastasis**, 260–261  
shoulder, 88
- Lung carcinoma**  
thumb, 9
- Luxatio erecta**  
shoulder, 107
- Lymphoma. See also Non-Hodgkin's lymphoma; Primary lymphoma of bone**  
pelvis  
CT, 214  
MRI, 214
- Lytic metastasis (lung carcinoma)**  
thumb, 9
- M**  
Madelung deformity, 57  
Madelung's deformity, 67  
Maffucci's syndrome  
AP radiograph, 534–535  
lateral radiograph, 534–535  
MRI, 534–535
- Magnetic resonance imaging (MRI)**  
Achilles tendon rupture  
basketball, 478  
aneurysmal bone cyst, 472–473  
ankle and foot  
accessory soleus muscle, 489  
atypical mycobacterium osteomyelitis, 487  
basketball, 478, 522  
calcaneal fatigue fracture, 512–513  
dermatomyositis, 498  
extraskeletal primitive neuroectodermal tumor (PNET), 488  
giant cell tumor of the tendon sheath, 526–527  
lisfranc fracture dislocation, divergent type, 528  
Maffucci's syndrome, 534–535  
marrow infarction, 495  
mass, 516–517, 526–527, 538  
metatarsal stress fracture, 523
- Nora's lesion, 538  
osteochondral lesion of the talus, 521  
pain, 482, 496, 497, 529  
peroneus brevis tendon split tear, 529  
pigmented villonodular synovitis (PVNS), 496–497  
plantar fasciitis, 514  
plantar fibromatosis, 516–517  
posterior tibial tendon (PTT), 482  
sinus tarsi syndrome, 499  
swelling, 488, 496–497, 515, 518, 534–535  
synovial osteochondromatosis, 524–525
- back pain**  
with chronic lymphocytic leukemia, 214
- bone cyst**  
aneurysmal, 472–473
- cervical spine**  
atlanto-occipital dislocation, 132  
hyperflexion sprain, 133  
hyperflexion teardrop fracture, 144–145  
odontoid fracture nonunion, 136–137  
rheumatoid arthritis, 152–153  
tuberculous spondylitis, 151  
unilateral facet dislocation, 140–141
- elbow, arm, and shoulder**  
calcific tendinitis, 120–121  
chondrosarcoma, 90–91  
clavicle osteolysis, 118  
complete biceps tendon rupture, 82–83  
elastofibroma, 128  
fibromatosis, 84–85  
intramuscular lipoma, 102  
juxtacortical chondroma, 86–87  
lateral epicondylitis, 77  
occult distal humerus fracture, 80–81  
quadrilateral space syndrome, 100–101  
rotator cuff tear, 104–105  
SLAP, 113  
subcutaneous lipoma, 102  
subscapularis rupture, 105, 106  
supracapsular ganglion cyst, 103  
synovial osteochondromatosis, 114–115  
triceps tendon tear with olecranon bursa hemorrhage, 79  
UCL tear, 78
- femur and thigh**  
aneurysmal bone cysts, 312–313  
bisphosphonate-related fracture, 298  
chondrosarcoma, 318–319  
dialysis-related amyloidosis, 272–273  
eosinophilic granuloma, 302–303  
Erdheim-Chester disease, 328  
failure to thrive, 310  
glomus tumor, 322  
hamstrings tear with associated hematoma, 271  
hip distress, 288–289  
hip pain, 276–279  
hip pain after fall, 290  
increasing girth, 305  
intertrochanteric femur fracture, 290  
intertrochanteric hip fracture, 290

# Magnetic resonance imaging (MRI)

(Continued)

- Klippel-Trenaunay syndrome, 332-333
- Legg-Calvé-Perthes disease, 286
- leukemia, 310
- liposarcoma, 326-327
- liposclerosing myxofibrous tumor of bone, 314-315
- malignant fibrous histiocytoma, 318-319, 331
- mass, 305-307
- melorheostosis, 329
- Morel-Lavallée lesion, 334
- neurofibroma, 321
- non-Hodgkin's B-cell lymphoma, 309
- osteoid osteoma, 316-317
- osteonecrosis, 276-277
- pain, 392-393
- pain worse at night, 316-317
- rectus femoris strain, grade 3, 270
- septic arthritis, 288-289
- soft tissue sarcoma, 318-319
- stress fracture, 292-293
- sudden pain, 308-309
- swelling, 296-297
- synovial sarcoma, 324-325
- transient bone marrow edema, 278-279
- hand and wrist
  - osteonecrosis of lunate, 42-43
  - wood splinter, 52
- hands
  - giant cell tumor of tendon sheath, 30
  - osteomyelitis, 6-7
- hemangioma
  - lower leg, 438-439
- hematoma
  - pelvis, 263
- knee
  - acute pain, 367
  - anterior cruciate ligament (ACL) sprain, 384-385, 392-394
  - arthrofibrosis, 412
  - articular chondroma, 338-339
  - bucket-handle tear, 390
  - calcified medullary infarcts, 364-365
  - chondromalacia patellae, 367
  - chronic pain, 397
  - discoid meniscus with complex tear, 362
  - effusion, 390
  - Gaucher disease, 360-361
  - giant cell tumor, 340-341
  - headache, 343
  - inflammatory arthritis, 364-365
  - injury, 354-355
  - lateral tibial plateau fracture, 387
  - lipoma arborescens, 402-403
  - malignant fibrous histiocytoma (MFH), 350-351
  - mass, 346-347
  - medial collateral ligament (MCL) sprain, 392-393
  - medial meniscal tear, 388
  - non-Hodgkin's lymphoma, 354-355
  - osteochondral fracture, 399
  - osteosarcoma, 344-345
  - Paget's disease, 382-383
  - pain, 344-345, 350-353, 362, 367, 386, 387
  - pain resembling intermittent claudication, 410
  - parosteal osteosarcomas, 346-347
  - PCL sprain, 395
  - pes anserinus bursitis, 404-405
  - pigmented villonodular synovitis (PVNS), 370-371
  - polycythemia vera, 343
  - popliteal artery entrapment syndrome, 410-411
  - positive posterior drawer test, 395
  - primary lymphoma of bone, 352-353
  - radial tear of the lateral meniscus, 391
  - ruptured Baker cyst, 386
  - Salter type II fracture, 381
  - Sinding-Larsen-Johansson (SLJ) disease, 397
  - sports injury, 380-381
  - subchondral insufficiency fracture of the knee (SIFK), 406
  - swelling, 338-339
  - transient lateral patellar dislocation, 396
  - trauma, 352-353
- lower leg
  - aneurysmal bone cyst, 472-473
  - ankle swelling, 472-473
  - Blount's disease, 416
  - bone cyst, 429
  - Brodie's abscess, 448-449
  - diabetes mellitus, 468-469
  - Ewing's sarcoma, 446-447
  - knee pain, 448-449
  - mass, 428
  - Mazabraud syndrome, 426-427
  - necrotizing fasciitis, 468-469
  - neurofibromas, 428
  - ossifying fibroma, 442-443
  - pain, 440-441
  - periosteal osteosarcoma, 440-441
  - peroneal nerve ganglion cyst, 460-461
  - plantaris tendon rupture, 457
  - polymyositis, 466-467
  - pyomyositis with abscess, 470
  - runners, 454-455
  - soft tissue hemangioma, 438-439
  - stress fracture, 454-455
  - subacute intramuscular hematoma, 459
  - swelling, 429
  - tender, 446-447
  - tuberculous osteomyelitis, 450-451
- lumbar spine
  - coccidioidomycosis, 196-197
  - hemangioma, 181
  - with vertebral collapse, 186-187
  - herniated nucleus pulposus, 192-193
  - psoriatic spondyloarthropathy, 194-195
  - sclerotic prostate cancer metastasis, 176-177
- mass, 30
- osteomyelitis, 6-7
- pelvis
  - bicycle crash, 263
  - chondrosarcoma, 216-217
  - chordoma, 206
  - cystic angiomas, 246
  - desmoplastic fibroma, 254-255
  - Ewing's sarcoma, 208-209
  - gluteus medius tendon tear, 229
  - groin pain, 250, 258-259
  - hematoma, 263
  - hip pain, 236-237
  - iliopsoas bursitis, 258-259
  - insufficiency fractures, 250
  - intramuscular myxoma, 222
  - IV drug abuse, 232
  - lymphoma, 214
  - nail-patella syndrome, 243
  - osteosarcoma, 218-219
  - pain, 254-255
  - pigmented villonodular synovitis, 236-237
  - prostate cancer, 207
  - radiation change, 207
  - Richter's syndrome, 214
  - sarcoma arising in Paget's disease, 230
  - schwannoma, 212-213
  - septic hip abscess, 262
  - septic sacroiliitis, 232
  - small fingernails, 243
  - synovial osteochondromatosis, 233
  - total hip replacement, 262
  - polymyositis, 466-467
  - shoulder, 100-101
    - acute osteomyelitis, 95
    - osteonecrosis, 97
    - Parsonage-Turner syndrome, 99
    - rotator cuff tear, 104-105
    - secondary tumoral calcinosis, 124-125
  - spinoglenoid notch
    - ganglion cyst, 103
  - supraspinatus tendon
    - rotator cuff tear, 104-105
  - swollen, 472-473
  - tendon sheath
    - giant cell tumor, 30
  - thoracic spine
    - eosinophilic granuloma, 167
    - pyogenic diskitis, 162-163
  - wrist
    - bilateral Madelung deformity, 57
    - ulnar impaction syndrome, 44-45
- Maisonneuve fracture
  - AP radiograph
    - lower leg, 432
- Malignant fibrous histiocytoma (MFH)
  - with knee pain
    - AP radiograph, 330-331
    - CT, 330-331
    - MRI, 330-331
  - MRI, 318-319
  - thigh mass, 318-319
- Malignant fibrous histiocytoma (MFH) of bone
  - AP radiographs
    - knee, 350-351
  - lateral radiographs
    - knee, 350-351
  - MRI
    - knee, 350-351

- Marrow infarction  
whole-body radionuclide bone scans  
foot, 495
- Mazabraud syndrome  
lower leg, 426–427
- MCP. *See* Metacarpophalangeal (MCP) joint
- Medial collateral ligament (MCL) sprain  
knee  
AP radiograph, 392–393  
MRI, 392–393
- Medial epicondyle  
avulsion fracture, 75  
with posterior elbow dislocation, 68, 76
- elbow  
posterior elbow dislocation, 76
- Medial meniscal tear  
MRI, 388
- Melorheostosis  
AP radiographs, 329  
foot  
AP radiographs, 492  
CT, 492  
oblique radiographs, 492  
lateral radiographs, 329  
MRI, 329
- Meningococcemia  
neonatal, 29
- Metacarpals  
hemochromatosis  
oblique radiograph, 33  
PA radiograph, 33
- Metacarpophalangeal (MCP) joint  
lateral radiograph  
tuberculous arthritis, 8  
psoriatic arthritis, 2
- Metallosis  
knee  
AP radiographs, 408–409  
CT, 408–409  
lateral radiographs, 408–409
- Metaphysis  
cupped, 29
- Metastatic calcification, 299
- Metastatic osteosarcoma  
spine, 166
- Metatarsal stress fracture  
radionuclide bone scan pain, 532
- Metatarsus adductus  
AP radiographs, 507  
lateral radiographs, 507
- Migratory pain syndrome, 102
- Military recruits  
lower leg  
CT, 456  
radionuclide bone scan, 456
- Mixed connective tissue disease. *See* calcinosis universalis
- Monoarticular arthritis  
lateral radiograph  
foot, 524–525
- Monteggia fracture dislocation  
elbow, 66
- Morel-Lavallée lesion  
MRI, 334  
STIR, 334
- Morquio's syndrome, 156
- Motorbike accident  
supraspinatus tendon  
rotator cuff tear, 104–105
- Motorcycle accident  
ankle  
AP radiograph, 503  
lateral radiograph, 503
- Motor vehicle accident  
cervical spine  
atlanto-occipital dislocation, 132  
Klippel-Feil syndrome, 142–143  
lumbosacral junction  
bilateral L5 spondylolysis without anterolisthesis, 198–199  
PA radiograph  
Galeazzi's fracture dislocation, 60  
pelvis  
posterior hip dislocation, 224–225
- Mountain bike accident  
elbow, 68
- MRI. *See* Magnetic resonance imaging (MRI)
- MuCune-Albright syndrome, 15
- Mueller-Weiss syndrome  
AP radiographs, 523  
lateral radiographs, 523
- Multicentric reticulohistiocytosis  
hands, 19
- Multiple enchondromatosis (Ollier's disease)  
AP radiograph  
foot, 537
- Multiple epiphyseal dysplasia  
thigh  
AP radiograph, 280  
gait problems, 280
- Multiple hereditary exostoses (MHE), 67, 247. *See also* Osteochondromatosis
- Multiple myeloma  
AP radiograph, 188–189  
AP radiographs, 300  
with fatigue and weight loss, 300  
femur radiographs, 300
- Muscle weakness  
CT  
lower leg, 466–467
- Mycobacterium tuberculosis, 8
- Myelofibrosis, 244
- N**
- Nail-patella syndrome, 69, 243
- Necrotizing fasciitis  
CT  
lower leg, 468–469  
MRI  
lower leg, 468–469
- Neonatal meningococcemia, 29
- Nerve entrapment, 103
- Neuritis  
acute brachial, 99
- Neurofibroma, 212–213  
MRI  
thigh, 321
- Neurofibromas  
lower leg, 428
- Neurofibromatosis (Type 1) (NF-1)  
AP radiograph, 417  
lower leg, 417
- Neuropathic arthropathy (Charcot joint)  
shoulder, 112
- Neuropathic osteoarthritis  
foot  
AP radiographs, 520–521  
lateral radiographs, 520–521
- Non-Hodgkin's B-cell lymphoma  
AP radiograph, 308–309  
CT, 308–309  
hip pain, 308–309  
MRI, 308–309
- Non-Hodgkin's lymphoma, 210–211  
CT, 354–355  
knee, 354–355  
MRI, 354–355
- Nonossifying fibroma (fibrous cortical defect)  
lower leg, 433  
PA radiograph  
forearm, 55  
wrist, 55
- Nora's lesion  
AP radiograph, 538  
MRI, 538
- O**
- Oblique radiograph  
elbow, 70  
radial head subluxation, 69  
elbow, arm and shoulder  
radioulnar synostosis, 67  
enchondroma  
hands, 16  
hands  
thyroid acropachy, 25  
lower leg  
Maisonneuve fracture, 432  
metacarpals  
hemochromatosis, 33  
wrist  
hypertrophic osteoarthritis, 53
- Occult distal humerus fracture  
elbow, 80–81
- Ochronosis  
thoracic spine, 172–173
- Odontoid fracture nonunion  
automobile accident, 136–137  
cervical spine, 136–137
- Ollier's disease. *See* Multiple enchondromatosis
- Open reduction and internal fixation (ORIF), 58–59
- Open segmental fracture  
lower leg  
AP radiograph, 452  
lateral radiograph, 452
- ORIF. *See* Open reduction and internal fixation (ORIF)
- Ossifying fibroma (osteofibrous dysplasia)  
lower leg  
AP radiograph, 442–443  
CT, 442–443  
MRI, 442–443
- Osteitis deformans. *See* Paget's disease
- Osteoarthritis, 238–239  
of hands, 4, 5  
vs. psoriatic arthritis, 5

- Osteoarthritis
  - with acromegaly, 26
- Osteoblastic neoplasms
  - vs. chronic sclerosing osteomyelitis, 40
- Osteoblastoma
  - cervical spine, 150
  - lower leg
    - AP radiograph, 431
    - lateral radiograph, 431
- Osteochondral fracture
  - MRI
    - knee, 399
- Osteochondral lesion of the talus
  - MRI, 522
  - oblique radiograph, 522
- Osteochondritis dissecans. *See* Osteochondral fracture
- Osteochondroma
  - lower leg
    - AP radiograph, 430
    - lateral radiograph, 430
- Osteochondromatosis, 114–115
- Osteochondrosis of the capitellum
  - elbow, 74
- Osteofibrous dysplasia
  - lower leg
    - AP radiograph, 442–443
    - CT, 442–443
    - MRI, 442–443
- Osteogenesis imperfecta
  - lower leg
    - AP radiograph, 418
    - lateral radiograph, 418
  - thoracolumbar spine, 178
- Osteoid osteoma
  - aspirin and nonsteroidal anti-inflammatory drugs, 316–317
  - CT, 316–317
  - MRI, 316–317
  - PA radiograph
    - wrist, 46–47
  - thoracolumbar spine, 175
- Osteolysis
  - causing total hip replacement failure
    - pelvis, 257
  - of distal clavicle, 118
- Osteomalacia
  - AP radiograph of, 291
  - with Looser's zones, 291
  - with metabolic disease, 291
- Osteomyelitis
  - chronic, 294–295
    - leg pain and swelling, 296–297
  - chronic recurrent multifocal
    - lower leg, 465
    - whole-body radionuclide bone scan, 465
  - chronic sclerosing
    - hands, 40
  - vs. chronic sclerosing osteomyelitis, 40
  - MRI
    - hands, 6–7
  - tuberculous
    - AP radiograph, 450–451
    - lateral radiograph, 450–451
    - lower leg, 450–451
    - MRI, 450–451
- Osteonecrosis
  - ankle
    - AP radiographs, 502
  - lateral radiographs, 494, 502
  - mortise radiographs, 502
  - hand and wrist
    - lunate, 42–43
  - shoulder, 97
  - thigh
    - AP radiograph, 274
    - hip pain, 274, 276–277
- Osteonecrosis of the lunate
  - PA radiograph
    - wrist, 42–43
- Osteoonychodysostosis, 243
- Osteopenia
  - with involutional osteoporosis, 169
- Osteopetrosis
  - AP radiograph
    - lower leg, 419
- Osteopoikilosis
  - AP radiographs, 283
  - prostate cancer, 283
- Osteoporosis, 72
  - back pain, 170
  - hands, 13
  - involutional
    - with compression fractures, 169
  - thoracic spine, 169
  - juxta-articular, 70
  - lumbar spine, 170
  - with renal osteodystrophy, 179
- Osteosarcoma, 218–219. *See also* Periosteal osteosarcoma
  - AP radiograph, 301
  - knee, 342, 344–345, 348–349
  - CT
    - knee, 348–349
  - high-grade surface
    - CT, 305
    - MRI, 305
    - thigh mass, 305
  - lateral radiograph
    - knee, 342, 344–345
  - leg pain, 301
  - metastatic
    - spine, 166
  - MRI
    - knee, 344–345
  - with skip metastasis, 301
  - telangiectatic, 92
  - CT, 92
- Osteosclerosis
  - with renal osteodystrophy, 179
- P**
- PA. *See* Posteroanterior (PA) radiographs
- Paget's disease, 244
  - AP radiograph
    - lower leg, 445
  - breast cancer, 190
  - vs. chronic sclerosing osteomyelitis, 40
  - knee
    - AP radiograph, 382–383
    - CT, 382–383
    - MRI, 382–383
  - lateral radiograph
    - lower leg, 445
  - sarcoma arising in, 230
  - back pain, 230
  - whole-body radionuclide bone scan
    - lower leg, 445
- Pain. *See* Back pain; Groin pain
- Palsy
  - brachial plexus, 98
- Panner's disease, 74
- PA radiograph
  - thoracolumbar spine
    - osteogenesis imperfecta, 178
- Paralysis
  - Klumpke's, 98
- Parameniscal cyst
  - coronal, 389
- Parosteal osteosarcoma
  - AP radiographs, 346–347
  - lateral radiographs, 346–347
- Parsonage-Turner syndrome, 99
- PCL sprain
  - MRI
    - knee, 395
- Pelvis
  - acetabular dysplasia, 220
  - AP radiograph
    - anterior hip dislocation, 226
    - back pain, 234–235
    - bilateral deficiency, 275
    - bilateral hip pain, 241
    - chondrosarcoma, 216–217
    - desmoplastic fibroma, 254–255
    - developmental dysplasia of the hip, 215
    - diffuse breast carcinoma metastases, 251
    - dislocated total hip replacement, 256
    - eosinophilic granuloma, 249
    - episodic pain, 264
    - Ewing's sarcoma, 208–209
    - femoroacetabular impingement, 221
    - fluorosis, 227
    - groin pain, 250
    - hemangiomatosis, 245
    - hip stiffness, 223
    - inguinal mass, 252–253
    - insufficiency fractures, 210–211
    - joint stiffness, 242
    - lung cancer metastasis, 260–261
    - motor vehicle crash, 224–225
    - multiple hereditary exostoses, 247
    - non-Hodgkin's lymphoma, 210–211
    - osteoarthritis, 238–239
    - osteosarcoma, 218–219
    - pain, 230
    - plasmacytoma, 248
    - pubic pain, 216–217
    - rheumatoid arthritis, 240
    - sacroiliac joint pain, 228
    - small fingernails, 243
    - total hip prosthesis, 257
    - total hip replacement, 257
  - CT
    - anemia, 244
    - anterior hip dislocation, 226
    - chordoma, 206
    - cystic angiomas, 246
    - desmoplastic fibroma, 254–255
    - eosinophilic granuloma, 249
    - femoroacetabular impingement, 221
    - groin pain, 250, 258–259
    - hip pain, 236–237
    - iliopsoas bursitis, 258–259
    - insufficiency fractures, 210–211, 250

- lung cancer metastasis, 260–261
- lymphoma, 214
- motor vehicle crash, 224–225
- myelofibrosis, 244
- nail-patella syndrome, 243
- non-Hodgkin's lymphoma, 210–211
- osteosarcoma, 218–219
- pigmented villonodular synovitis, 236–237
- plasmacytoma, 248
- posterior hip dislocation, 224–225
- reactive arthritis, 231
- small fingernails, 243
- tuberculosis, 252–253
- joint stiffness, 242
- lateral radiograph
  - dislocated total hip replacement, 256
  - synovial osteochondromatosis, 233
- MRI
  - bicycle crash, 263
  - chondrosarcoma, 216–217
  - chordoma, 206
  - cystic angiomas, 246
  - desmoplastic fibroma, 254–255
  - Ewing's sarcoma, 208–209
  - gluteus medius tendon tear, 229
  - groin pain, 250, 258–259
  - hematoma, 263
  - hip pain, 236–237
  - iliopsoas bursitis, 258–259
  - insufficiency fractures, 250
  - intramuscular myxoma, 222
  - IV drug abuse, 232
  - lymphoma, 214
  - nail-patella syndrome, 243
  - osteosarcoma, 218–219
  - pain, 254–255
  - pigmented villonodular synovitis, 236–237
  - prostate cancer, 207
  - pubic pain, 216–217
  - radiation change, 207
  - Richter's syndrome, 214
  - sarcoma arising in Paget's disease, 230
  - schwannoma, 212–213
  - septic hip abscess, 262
  - septic sacroiliitis, 232
  - small fingernails, 243
  - synovial osteochondromatosis, 233
  - total hip replacement, 262
- Periarticular osseous excrescences
  - hands, 13
- Periosteal osteosarcoma
  - lower leg
    - AP radiograph, 440–441
    - lateral radiograph, 440–441
    - MRI, 440–441
- Periostitis, 72
  - forearm, 56
  - hands, 2, 3, 13
- Peroneal nerve ganglion cyst
  - MRI
    - lower leg, 460–461
- Peroneus brevis tendon split tear
  - pain, 529
- Pes anserinus bursitis
  - MRI
    - knee, 404–405
- PFFD. *See* Proximal focal femoral deficiency (PFFD)
- Physiologic bowing
  - AP radiograph
    - lower leg, 422
- Pigmented villonodular synovitis (PVNS), 236–237
  - ankle
    - AP and mortise radiographs, 496–497
    - lateral radiograph, 497
    - MRI, 497
  - MRI
    - knee, 370–371
- PIP. *See* Proximal interphalangeal (PIP) joint
- Pitchers
  - capitellum osteochondrosis, 74
- Plantar fasciitis
  - lateral radiograph, 514
  - MRI, 514
- Plantar fibromatosis, 516–517
- Plantaris tendon rupture
  - lower leg
    - MRI, 457
- Plasmacytoma, 248
- Plastic bowing, 73
- Poliomyelitis
  - knee
    - AP radiographs, 380
    - lateral radiographs, 380
- Polyarthritis
  - hands, 3, 23
- Polyarticular arthritis
  - foot
    - AP radiograph, 509
    - lateral radiograph, 509
  - hands, 4
- Polycythemia vera
  - MRI
    - knee, 343
- Polymyositis
  - CT
    - lower leg, 466–467
  - hands, 28
  - index finger, 28
  - MRI
    - lower leg, 466–467
    - vs. RA, 28
    - vs. SLE, 28
- Polyostotic fibrous dysplasia
  - hands, 15
- Popliteal artery entrapment syndrome
  - knee
    - CT, 410–411
    - MRI, 410–411
- Posterior elbow dislocation
  - elbow, 68, 76
- Posterior hip dislocation
  - motor vehicle accident, 224–225
- Posterior shoulder dislocation, 110
- Posterior tibial tendon (PTT) tear
  - MRI
    - ankle, 482
- Posteroanterior (PA) radiograph
  - finger
    - epidermoid inclusion cyst, 11
  - forearm
    - congenital syphilis, 56
    - nonossifying fibroma, 55
- hands
  - acromegaly, 26
  - burns, 13
  - chronic sclerosing osteomyelitis, 40
  - congenital syphilis, 56
  - embolic disease, 29
  - erosive osteoarthritis, 5
  - fourth metacarpal fracture, 35
  - giant cell reparative granuloma, 18
  - hemochromatosis, 33
  - hyperparathyroidism, 27
  - juvenile idiopathic arthritis, 24
  - multicentric reticulohistiocytosis, 19
  - osteoarthritis, 4
  - polymyositis, 28
  - polyostotic fibrous dysplasia, 15
  - psoriatic arthritis, 2, 3
  - rheumatoid arthritis, 21–23
  - sarcoidosis, 12
  - scleroderma, 14
  - systemic lupus erythematosus, 20
  - thyroid acropachy, 25
  - tophaceous gout, 17
- index finger
  - polymyositis, 28
- little finger
  - enchondroma, 16
- metacarpals
  - hemochromatosis, 33
- thumb
  - glomus tumor, 10
- wrist
  - bilateral Madelung deformity, 57
  - carpal coalition, 41
  - desmoplastic fibroma, 54
  - Galeazzi's fracture dislocation, 60
  - growth plate fracture, 49
  - healing rickets, 48
  - hydroxyapatite deposition disease, 34
  - lead poisoning, 50
  - lunate dislocation, 37
  - lunate osteonecrosis, 42–43
  - nonossifying fibroma, 55
  - osteoid osteoma, 46–47
  - rotary subluxation, 36
  - scapholunate dislocation, 36
  - SLAC wrist, 32
- Posteroanterior (PA) radiographs
  - shoulder
    - chondrosarcoma, 90–91
- Postmenopausal women
  - hands, 5
- Pott's disease
  - back pain, 164–165
  - cervical spine, 151
  - thoracic spine, 164–165
- Primary lymphoma of bone
  - knee
    - AP radiograph, 352–353
    - MRI radiograph, 352–353
- Progressive bowing deformity
  - lower leg
    - AP radiograph, 416
    - lateral radiograph, 416
- Progressive systemic sclerosis
  - hands, 14
- Prostate cancer
  - MRI, 207
  - pelvis, 207

Proximal femur. *See also* Thigh  
chronic osteomyelitis, 296–297

Proximal focal femoral deficiency (PFFD)  
femurs  
  aplasia, 275  
  AP radiograph, 275

Proximal interphalangeal (PIP) joint  
psoriatic arthritis, 2

Pseudoclubbing  
hands, 12

Psoriatic arthritis  
hands, 2, 3  
  PA radiograph, 2, 3  
  vs. rheumatoid arthritis, 3

Psoriatic arthritis (arthritis mutilans)  
foot  
  AP radiograph, 543

Psoriatic spondyloarthropathy  
back pain, 194–195  
lumbar spine, 194–195

PTT. *See* Posterior tibial tendon (PTT) tear

Pubic pain  
  AP radiograph, 216–217  
  MRI, 216–217

Pulled elbow, 69

PVNS. *See* Pigmented villonodular synovitis (PVNS)

Pyogenic diskitis  
thoracic spine, 162–163

Pyogenic infection, 470

Pyomyositis with abscess  
MRI  
  lower leg, 470

Pyrophosphate arthropathy  
hands, 4  
knee  
  AP radiographs, 378  
  lateral radiographs, 378  
shoulder, 117  
wrist, 32

## Q

Quadrilateral space syndrome, 100–101

## R

Radial head  
fracture  
  elbow, arm, and shoulder, 64–65  
  subluxation, 69

Radial tear  
of the lateral meniscus  
  MRI, 391

Radiation changes  
  AP radiographs, 366  
  lateral radiographs, 366

Radionuclide bone scan  
hands  
  chronic sclerosing osteomyelitis, 40  
lower leg  
  Army privates in basic training, 456  
  military recruits, 456  
  stress fractures, 456  
shoulder  
  lung cancer metastasis, 88

Radioulnar synostosis  
elbow, 67

Raynaud's phenomenon  
with acromegaly, 26

Reactive arthritis, 70  
ankle  
  lateral radiograph, 518  
pelvis  
  back pain, 231  
  Chlamydia-urethritis, 231

Rectus femoris strain, grade 3  
MRI  
  non-contact football injury, 270  
proximal thigh, 270

Renal failure  
chronic, 27

Renal osteodystrophy  
with rugger jersey spine  
  lumbar spine, 179

Retinoid toxicity, 158–159  
  congenital ichthyosis, 158–159

Reverse Hill-Sachs lesion, 110, 111

Rheumatic fever, 70

Rheumatoid arthritis, 240  
hands, 21–23  
polyarthritis, 23  
shoulder, 116

Rheumatoid arthritis (RA)  
AP radiograph  
  knee, 368  
foot  
  AP radiograph, 536

Ribs  
Brown tumor  
  AP radiography, 126–127  
  CT, 126–127  
canoe paddle shaped, 156

Richter's syndrome  
pelvis  
  chronic lymphocytic leukemia (CLL),  
  214

Rickets  
knee, 358–359  
lateral knee radiograph, 358–359  
pelvis  
  sacroiliac joint pain, 228

Right sternoclavicular joint dislocation  
automobile accident, 123

Rotary subluxation  
PA radiograph  
  wrist, 36

Rotator cuff tear, 84–85, 104–105, 117

Rugby, 108–109  
  Achilles tendon rupture  
  sonography, 476–477

Rugger jersey spine  
lumbar spine, 179

Runners  
lower leg  
  runners, 454–455  
  stress fracture, 454–455

Ruptured Baker cyst  
MRI  
  knee, 386

**S**

Sacroiliac joint pain  
  AP radiograph, 228

Sacroiliitis  
hands, 3

Salter type I  
elbow, 75

Salter type I fracture  
wrist, 49

Salter type II fracture  
MRI  
  knee, 381

Salter type IV fracture  
AP radiograph  
  ankle, 483  
  lower leg, 458

Sarcoidosis  
bilateral hand deformities, 12  
foot  
  AP radiograph, 547  
hands, 12

Sarcoma. *See* Ewing's sarcoma; Synovial sarcoma

Sausage-digit soft tissue swelling, 2

Scaphoid  
  rotary subluxation of, 36

Scapholunate advanced collapse (SLAC wrist)  
  pyrophosphate arthropathy, 32

Scapholunate dislocation  
wrist, 36

SCFE. *See* Slipped capital femoral epiphysis (SCFE)

Scheuermann's disease, 168

Scleroderma (progressive systemic sclerosis)  
hands, 14

Sclerosing bone dysplasia  
vs. chronic sclerosing osteomyelitis, 40

Sclerosis, 179

Sclerotic prostate cancer metastasis,  
  176–177  
  ivory vertebra, 176–177

Scoliosis  
congenital  
  thoracolumbar spine, 174  
osteoid osteoma, 175

Secondary synovial osteochondromatosis  
AP radiographs  
  knee, 376–377  
lateral radiographs  
  knee, 376–377

Secondary tumoral calcinosis  
shoulder, 124–125

Seizure disorder  
with shoulder dislocations, 111

Septic arthritis  
  AP radiographs of, 288–289

Septic elbow joint, 70  
elbow, 70

Septic hip abscess  
pelvis, 262

Septic olecranon bursitis  
elbow, 71

Septic sacroiliitis  
pelvis  
  intravenous drug abuse, 232

Sesamoid fracture  
  AP radiograph, 545

Short stature  
  AP radiograph  
  lower leg, 423

Shoulder  
  anterior dislocation, 108–109  
  AP radiograph

- acromioclavicular separation (grade 2), 119
- acromioclavicular subluxation, 118
- acute osteomyelitis, 95
- anterior dislocation, 108–109
- brachial plexus palsy, 98
- chondroblastoma, 94
- chondrosarcoma, 90–91
- Ewing's sarcoma, 93
- lung cancer metastasis, 88
- luxatio erecta, 107
- neuropathic arthropathy, 112
- osteolysis, 118
- osteonecrosis, 97
- osteosarcoma, 92
- posterior dislocation, 110
- pyrophosphate arthropathy, 117
- rheumatoid arthritis, 116
- rotator cuff tear, 104–105
- secondary tumoral calcinosis, 124–125
- bilateral posterior shoulder dislocations, 111
- bilateral posterior shoulder dislocations, seizure disorder, 111
- CT
  - bilateral posterior shoulder dislocations, 111
  - brachial plexus palsy, 98
  - chondrosarcoma, 90–91
  - elastofibroma, 128
  - fibromatosis, 84–85
  - osteosarcoma, 92
  - seizure disorder, 111
  - sternoclavicular dislocation, 123
- dislocation, 110
- fracture nonunion, 96
- idiopathic denervation of, 99
- MRI
  - acute osteomyelitis, 95
  - calcific tendinitis, 120–121
  - chondrosarcoma, 90–91
  - elastofibroma, 128
  - fibromatosis, 84–85
  - intramuscular lipoma, 102
  - osteonecrosis, 97
  - Parsonage-Turner syndrome, 99
  - quadriateral space syndrome, 100–101
  - rotator cuff tear, 104–105
  - SLAP, 113
  - subscapularis rupture, 105, 106
  - synovial osteochondromatosis, 114–115
- PA chest radiograph
  - chondrosarcoma, 90–91
- radionuclide bone scan
  - lung cancer metastasis, 88
- sonography
  - supraspinatus tendon tear, 122
- Sickle cell anemia
  - AP radiograph
    - knee, 363
- Sickle cell disease, 264
  - osteonecrosis
    - ankle, 494
    - lateral and mortise radiographs, 494
    - thoracic spine, 171
- Sinding-Larsen-Johansson (SLJ) disease
  - lateral radiograph
    - knee, 397
- Sinus tarsi syndrome
  - MRI
    - ankle, 499
- SLAC. *See* Scapholunate advanced collapse (SLAC wrist)
- SLAP. *See* Superior labral anterior to posterior (SLAP) tear
- SLE. *See* Systemic lupus erythematosus (SLE)
- Slipped capital femoral epiphysis (SCFE)
  - AP radiograph, 284–285
  - hip pain, 285
- SLJ. *See* Sinding-Larsen-Johansson (SLJ) disease
- Smoking, 82–83, 126–127
- Soft tissue sarcoma. *See* malignant fibrous histiocytoma (MFH)
- Sonography
  - Achilles tendon rupture, 476–477
  - ankle
    - rugby, 476–477
  - A2 pulley rupture, 31
  - elbow
    - septic olecranon bursitis, 71
  - shoulder
    - supraspinatus tendon tear, 122
  - wrist
    - extensor tendon irritation, 58–59
    - wood splinter, 52
- Spine. *See also* Cervical spine; Thoracic spine; Thoracolumbar spine
  - AP radiograph
    - Scheuermann's disease, 168
  - CT
    - metastatic osteosarcoma, 166
    - Paget's disease, 190
  - Spinnaker sail sign, 64–65
- Spinoglenoid notch
  - MRI
    - ganglion cyst, 103
- Spondylitis
  - hands, 3
- Sports injuries. *See* specific sport
- Sprengel deformity
  - with Klippel-Feil syndrome, 142–143
- Standing lateral spine
  - Scheuermann's disease, 168
- Standing PA radiograph
  - thoracolumbar spine
    - congenital scoliosis, 174
    - osteoid osteoma, 175
- Staphylococcus aureus*, 448–449
- Sternoclavicular joint
  - dislocation
    - automobile accident, 123
    - CT, 123
    - shoulder, 123
- STIR image
  - thigh
    - eosinophilic granuloma, 302–303
- Streptococcus*, 470
- Stress fracture
  - AP radiographs, 292
  - distal thigh pain, 292–293
  - MRI of, 292
- Stress fractures
  - lower leg
    - AP radiograph, 454–455
    - CT, 456
    - MRI, 454–455
    - radionuclide bone scan, 456
- Subacute intramuscular hematoma
  - lower leg
    - MRI, 459
- Subchondral fracture
  - foot
    - AP radiograph, 544
- Subchondral insufficiency fracture of the knee (SIFK)
  - MRI
    - knee, 406
- Subcutaneous lipoma, 102
- Subperiosteal bone resorption
  - hands, 27
- Subscapularis rupture, 106
  - MRI, 105
  - shoulder, 105
- Subtalar dislocation
  - ankle
    - AP radiograph, 503
    - lateral radiograph, 503
    - oblique radiograph, 503
- Superior labral anterior to posterior (SLAP) tear, 113
- Superior labrum
  - bucket-handle tear, 113
- Supracondylar fracture
  - elbow, 73
- Suprascapular nerve entrapment, 103
- Supraspinatus tendon
  - rotator cuff tear
    - AP radiograph, 104–105
    - MRI, 104–105
    - sonography, 122
- Symphalangism
  - vs. carpal coalition, 41
- Synovial osteochondromatosis, 114–115, 233
  - foot
    - CT, 524–525
    - lateral radiograph, 524–525
    - MRI, 524–525
  - shoulder, 114–115
- Synovial sarcoma
  - thigh
    - AP radiographs, 324–325
    - CT, 324–325
    - lateral radiographs, 324–325
    - MRI, 324–325
- Syphilis
  - congenital
    - forearm, 56
- Syphilitic osteochondritis
  - forearm, 56
- Systemic lupus erythematosus (SLE)
  - foot
    - AP radiograph, 508
    - lateral radiograph, 508
  - hands, 20
- T
  - Tarsal coalition
    - vs. carpal coalition, 41
  - foot

- Tarsal coalition (*Continued*)  
 CT, 504  
 lateral radiograph, 504
- Telangiectatic osteosarcoma  
 shoulder, 92
- Tendinosis  
 calcific  
 shoulder, 120–121
- Tendon sheath  
 giant cell tumor  
 MRI, 30
- Tenosynovitis  
 De Quervain  
 wrist, 51
- TFCC. *See* Triangular fibrocartilage complex (TFCC)
- Thalassemia  
 AP radiograph  
 foot, 530
- Thanatophoric (death bringing) dwarfism, 202
- Thermal burns, 72
- Thigh  
 AP radiograph  
 bisphosphonate-related fracture, 298  
 calcinosis universalis, 311  
 Camurati–Engelmann disease, 321  
 eosinophilic granuloma, 302–303  
 Erdheim–Chester disease, 328  
 Ewing's sarcoma, 304  
 failure to thrive, 310  
 fibrous dysplasia, 282  
 gait disturbance, 275  
 hip distress, 288–289  
 hip pain, 274, 276–279, 284–286, 308–309, 312–313  
 hip pain after fall, 290  
 intertrochanteric femur fracture, 290  
 Legg–Calvé–Perthes disease, 282  
 leg pain, 296, 301–303  
 leukemia, 310  
 limb deformity, 281  
 liposarcoma, 326–327  
 mass, 306–307  
 melorheostosis, 329  
 multiple epiphyseal dysplasia, 280  
 muscle weakness, 287  
 osteomalacia, with Looser's zones, 291  
 osteonecrosis, 274  
 osteopoikilosis, 283  
 osteosarcoma, high-grade surface, 305  
 periarticular calcinosis, 299  
 prostate cancer, 283  
 renal failure hemodialysis, 272–273  
 septic arthritis, 289  
 stress fracture, 292–293  
 sudden pain, 308–309  
 swelling, 296–297, 304  
 transient bone marrow edema, 278–279  
 weight loss and fatigue, 300
- CT  
 hip pain, 284–285, 308–309  
 liposarcoma, 326–327  
 mass, 305, 322, 326–327  
 muscle weakness, 287, 466–467  
 myositis ossificans, 320  
 osteoid osteoma, 316–317  
 osteomyelitis, chronic, 294–295  
 osteopoikilosis, 283  
 pain worse at night, 316–317  
 prostate cancer, 283  
 swelling, 296–297
- lateral radiograph  
 increasing girth, 305  
 liposarcoma, 326–327  
 mass, 308–309  
 myositis ossificans, 320  
 swelling, 296–297  
 synovial sarcoma, 324–325
- MRI  
 dialysis-related amyloidosis, 272–273  
 Erdheim–Chester disease, 328  
 failure to thrive, 310  
 glomus tumor, 322  
 hamstrings tear with associated hematoma, 271  
 hip distress, 288–289  
 hip pain after fall, 290  
 increasing girth, 305  
 liposarcoma, 326–327  
 malignant fibrous histiocytoma, 318–319  
 melorheostosis, 329  
 neurofibroma, 321  
 osteoid osteoma, 316–317  
 pain worse at night, 316–317  
 rectus femoris strain, grade 3, 270  
 stress fracture, 292–293  
 sudden pain, 308–309  
 swelling, 324–325
- radionuclide bone scan  
 pain, 294–295, 301
- Thoracic spine  
 AP radiograph  
 eosinophilic granuloma, 167  
 ochronosis, 172–173  
 sickle cell disease, 171  
 tuberculous spondylitis, 164–165
- CT  
 retinoid toxicity, 158–159
- hyperflexion fractures  
 automobile accident, 160–161
- lateral radiograph  
 eosinophilic granuloma, 167  
 involutional osteoporosis, 169  
 Morquio's syndrome, 156  
 ochronosis, 172–173  
 osteopetrosis, 157  
 pyogenic diskitis, 162–163  
 retinoid toxicity, 159  
 sickle cell disease, 171
- MRI  
 eosinophilic granuloma, 167  
 pyogenic diskitis, 162–163
- Thoracolumbar spine  
 AP radiograph  
 ivory vertebra from Paget's disease, 180
- CT  
 chance fracture, 182–183  
 ivory vertebra from sclerotic prostate metastasis, 176–177  
 osteoid osteoma, 175
- lateral radiograph  
 ivory vertebra from Paget's disease, 180
- PA radiograph  
 osteogenesis imperfecta, 178
- standing PA radiograph  
 congenital scoliosis, 174  
 osteoid osteoma, 175
- Thumb  
 lytic metastasis, 9
- MRI  
 giant cell tumor of tendon sheath, 30  
 mass, 30
- PA radiograph  
 glomus tumor, 10
- Thyroid acropachy  
 hands, 25
- Tibia  
 fractures  
 AP radiograph, 453  
 toddler, 453
- Tibia vara  
 Blount's disease, 416
- Tobacco, 82–83
- Tophaceous gout  
 AP radiograph  
 foot, 519  
 vs. gouty arthritis, 17  
 hands, 17
- Torus fractures, 73
- Total knee replacement  
 with failure of tibial polyethylene  
 AP radiograph, 407
- Transient bone marrow edema  
 AP radiograph  
 hip pain, 278–279
- Transient lateral patellar dislocation  
 MRI  
 knee, 396
- Trapdoor fragment, 89
- Trauma  
 arms  
 juxtacortical chondroma, 86–87
- burns, 13
- children  
 growth plate fracture, 49  
 medial epicondyle avulsion fracture, 75  
 medial epicondylar avulsion fracture, 68  
 Salter type IV, 458  
 subluxation of radial head, 69  
 supracondylar fracture of distal humerus, 73  
 tibia fracture, 453
- elbow, arm and shoulder  
 bone cyst, with pathologic fracture, 89  
 ganglion cyst, 103
- elbows  
 complete biceps tendon rupture, 82–83  
 lateral epicondylitis, 77  
 medial epicondyle avulsion fracture, 75  
 Monteggia fracture dislocation, 66  
 occult distal humerus fracture, 80–81  
 osteochondrosis of the capitellum, 74  
 posterior elbow dislocation, 68, 76  
 radial head fracture, 64–65

- radial head subluxation, 69
- septic elbow joint, 70
- supracondylar fracture, 73
- triceps tendon tear, 79
- UCL tear, 78
- finger, 11
- foot, 453, 478
- fracture nonunion, 96
- hand and wrist
  - bilateral Madelung deformity, 57
  - carpal coalition, 41
  - De Quervain tenosynovitis, 51
  - desmoplastic fibroma, 54
  - extensor tendon irritation, 58–59
  - Galeazzi's fracture dislocation, 60
  - growth plate fracture, 49
  - healing rickets, 48
  - heterotopic ossification after burns, 72
  - hypertrophic osteoarthropathy, 53
  - lead poisoning, 50
  - osteoid osteoma, 46–47
  - osteonecrosis of the lunate, 42–43
  - rotary subluxation, 36
  - triquetral fracture, 38
  - ulnar impaction syndrome, 44–45
- leg and ankle, 432, 452, 456
- lower leg
  - achondroplasia, 423
  - bone cyst, 429
  - chondromyxoid fibroma, 434–435
  - congenital adrenocortical hyperplasia
    - with limb lengthening, 420–421
  - fibrous dysplasia, 424–425
  - Maisonneuve fracture, 432
  - Mazabraud syndrome, 426–427
  - neurofibromas, 428
  - NF-1, 417
  - nonossifying fibroma, 433
  - osteoblastoma, 431
  - osteochondroma, 430
  - osteogenesis imperfecta, 418
  - osteopetrosis, 419
  - physiologic bowing, 422
- ribs
  - Brown tumor, 126–127
- shoulder
  - acromioclavicular separation (grade 2), 119
  - acromioclavicular subluxation, 118
  - acute osteomyelitis, 95
  - anterior shoulder dislocation, 108–109
  - bilateral posterior shoulder dislocations, 111
  - brachial plexus palsy, 98
  - calcific tendinitis, 120–121
  - chondroblastoma, 94
  - chondrosarcoma, 90–91
  - elastofibroma, 128
  - Ewing's sarcoma, 93
  - fibromatosis, 84–85
  - intramuscular lipoma, 102
  - lung cancer metastasis, 88
  - luxatio erecta, 107
  - neuropathic arthropathy, 112
  - osteolysis, 118
  - osteonecrosis, 97
  - Parsonage-Turner syndrome, 99
  - posterior shoulder dislocation, 110
  - pyrophosphate arthropathy, 117
  - quadrilateral space syndrome, 100–101
  - rheumatoid arthritis, 116
  - rotator cuff tear, 104–105
  - secondary tumoral calcinosis, 124–125
  - SLAP, 113
  - sternoclavicular dislocation, 123
  - subscapularis rupture, 106
  - supraspinatus tendon tear, 122
  - synovial osteochondromatosis, 114–115
  - telangiectatic osteosarcoma, 92
- Traumatic C2 spondylolisthesis (hangman's fracture), 138–139
- Traumatic lumbosacral spondylolisthesis
  - all-terrain vehicle (ATV) crash, 200–201
  - lumbosacral junction, 200–201
- Treponema pallidum*, 56
- Triangular fibrocartilage complex (TFCC)
  - wrist, 44–45
- Triceps tendon tear
  - with olecranon bursa hemorrhage, 79
- Triplane fracture
  - ankle
    - AP radiographs, 484–485
    - CT, 484–485
    - lateral radiographs, 484–485
- Triquetral fracture
  - wrist, 38
- Trough fracture, 111
- Tubercle bacillus, 296–297
- Tuberculosis
  - inguinal mass, 252–253
- Tuberculous arthritis
  - MCP joint, 8
- Tuberculous osteomyelitis
  - lower leg
    - AP radiograph, 450–451
    - lateral radiograph, 450–451
    - MRI, 450–451
- Tuberculous spondylitis (Pott's disease)
  - back pain, 164–165
  - cervical spine, 151
  - thoracic spine, 164–165
- Tumoral calcinosis
  - AP radiograph, 299
- Turf toe (Grade I plantar plate injury)
  - foot
    - MRI, 546
- Turner's syndrome
  - vs. carpal coalition, 41
- Turret exostosis, 538
- U**
- Ulcerative colitis
  - pelvis
    - ankylosing spondylitis, 234–235
- Ulnar collateral ligament (UCL)
  - tear, 78
- Ulnar impaction syndrome
  - MRI
    - wrist, 44–45
- Ulnar nerve
  - damage to, 75
- Unilateral facet dislocation
  - automobile accident, 140–141
  - cervical spine, 140–141
- Upper body strength training, 79
- Upper limb deformity
  - lateral radiograph, 67
  - oblique radiograph, 67
- V**
- Vaccination, 99
- Vertical talus
  - congenital
    - AP radiograph, 506
    - lateral radiograph, 506
- Viral illness, 99
- W**
- Weight loss and fatigue, 300
- Whipple's disease, 235
- Whole-body radionuclide bone scan
  - chronic recurrent multifocal osteomyelitis, 465
- foot
  - marrow infarction, 495
- lower leg, 445, 465
  - recurrent pain, 465
- Paget's disease, 445
- Wood splinter
  - sonography
    - wrist, 52
- Wrist
  - CT
    - lunate osteonecrosis, 42–43
    - triquetral fracture, 38
    - wood splinter, 52
- De Quervain tenosynovitis, 51
- lateral radiograph
  - carpal coalition, 41
  - extensor tendon irritation, 58–59
  - Galeazzi's fracture dislocation, 60
  - hydroxyapatite deposition
    - disease, 34
  - lunate dislocation, 37
  - scapholunate dislocation, 36
  - triquetral fracture, 38
- MRI
  - lunate osteonecrosis, 42–43
  - ulnar impaction syndrome, 44–45
  - wood splinter, 52
- oblique radiograph
  - hypertrophic osteoarthropathy, 53
- PA radiograph
  - bilateral Madelung deformity, 57
  - carpal coalition, 41
  - desmoplastic fibroma, 54
  - Galeazzi's fracture dislocation, 60
  - growth plate fracture, 49
  - healing rickets, 48
  - hydroxyapatite deposition disease, 34
  - lead poisoning, 50
  - lunate dislocation, 37
  - lunate osteonecrosis, 42–43
  - nonossifying fibroma, 55
  - osteoid osteoma, 46–47
  - pyrophosphate arthropathy, 32
  - rotary subluxation, 36
  - scapholunate dislocation, 36
  - SLAC wrist, 32
- sonography
  - extensor tendon irritation, 58–59
  - wood splinter, 52